SOLID MECHANICS AND ITS APPLICATIONS
Volume 139

Series Editor: G.M.L. GLADWELL
Department of Civil Engineering
University of Waterloo
Waterloo, Ontario, Canada N2L 3GI

Aims and Scope of the Series

The fundamental questions arising in mechanics are: *Why?, How?,* and *How much?* The aim of this series is to provide lucid accounts written by authoritative researchers giving vision and insight in answering these questions on the subject of mechanics as it relates to solids.

The scope of the series covers the entire spectrum of solid mechanics. Thus it includes the foundation of mechanics; variational formulations; computational mechanics; statics, kinematics and dynamics of rigid and elastic bodies: vibrations of solids and structures; dynamical systems and chaos; the theories of elasticity, plasticity and viscoelasticity; composite materials; rods, beams, shells and membranes; structural control and stability; soils, rocks and geomechanics; fracture; tribology; experimental mechanics; biomechanics and machine design.

The median level of presentation is the first year graduate student. Some texts are monographs defining the current state of the field; others are accessible to final year undergraduates; but essentially the emphasis is on readability and clarity.

For a list of related mechanics titles, see final pages.

Fracture Mechanics

Inverse Problems and Solutions

by

H. D. BUI
École Polytechnique
Department of Mechanics
Palaiseau, France
and
Research & Development Division,
Electricité de France,
Clamart, France

Springer

A C.I.P. Catalogue record for this book is available from the Library of Congress.

ISBN 10 1 4020 4836 X (HB)
ISBN 13 978 1 4020 4836 4 (HB)
ISBN 10 1 4020 4837 8 (e book)
ISBN 13 978 1 4020 4837 1 (e book)

Published by Springer,
P.O. Box 17, 3300 AA Dordrecht, The Netherlands.

www.springer.com

Printed on acid free paper

Printed in the Netherlands.

This book is dedicated to the memory of my beloved parents

Contents

Preface

This book is an outgrowth of my involvement in two groups of research in solid mechanics, created in 1960 for the French nuclear energy program. At this time, it was decided that France, as a no-oil reservoir country, must be powered by nuclear energy, which represents today 80% of the total national energy supply. Long before the construction of the first nuclear plant at Fessenheim in 1973, Electricité de France (EdF) created its first solid mechanics laboratory, appointed researchers and sent them to the universities or abroad in order to learn about theories and new methods of assessment of the safety of structures. Working at EdF, I was training in Professor Jean Mandel's laboratory at Ecole Polytechnique (LMS), Paris. My friend René Labbens, working at Framatome (the builder of nuclear plants) was training at the Lehigh University, under the guidance of professors G. R. Irwin and G. C. Sih. We had to work hard, both academically at the universities laboratories and performing engineering tasks for our employer. This dual position was a great chance for many of us, since we discovered that real industrial problems are the source of new subjects and research problems to be solved by theoreticians in the universities and conversely we immediately knew if our theoretical work was good or not for applications as revealed in our daily works conducted for our industrial employer.

This book is an attempt to collect together many results obtained by my groups in both laboratories and also by other groups in France or abroad working over decades in the fields of Fracture Mechanics and Inverse problems. Most of the results published in this book are unknown, since many of them were either published in French journals or in industrial reports. This is the reason why I decided to collect them in this book for a larger audience.

The book is intended for under-graduated students and scientists. It is self-contained in that one can find both classical topics and the new material that cannot be found in other books. For example, one can find in Chapter 1 devoted to the fundamentals of Deformation and Fracture, a brief introduction to the mechanics of continuous media, including elasticity and plasticity. This chapter also contains two new subjects: the Tonti

diagram in elasticity dealing with duality and the experimental foundations of metal plasticity.

One can roughly say that Fracture Mechanics deal with the mechanics of either a hypothetical, formal crack, or a real crack observed in the course of a maintenance operation or detected through a Non destructive Testing of materials. The first kind of cracks is studied in theoretical papers aimed at the assessment of structures while the second kind of cracks is considered, for example, in the context of the time-life of a nuclear reactor or a pipe. It turns out that the most important and interesting problems are arising in the maintenance operations: non destructive testing of structures, identification of real internal cracks, determination of the internal thermo-mechanical loads in pipes without inserting a thermocouple (making a hole), the engineering "Leak-Before-Break" problem, which consists in determining a hidden longitudinal crack in a pipe (hidden to the observer by a thick heat insulator) from measurement of the fluid flow rate. They are typically inverse problems or free boundary value problems. The time-life of an nuclear vessel, from the design to the maintenance operation, is parallel to the time-life of a researcher who moves necessarily from direct problems to inverse problems. This is the justification of the book title.

For convenience the book is divided into two parts: Fracture Mechanics (Chaps. 1-8 and Appendices A, B) and Inverse problems & solutions (Chaps. 9-12). However, Inverse problems can be found along many chapters of the first part. For example, given the boundary traction vector and the boundary velocity field, the problem of finding separetely the elastic *and* the kinetic energies in a cracked body can be treated, whenever the crack is *known*, as a direct problem for which one set of boundary datum is superfluous. But when the crack is unknown, this problem becomes an inverse one for which two types of boundary data are necessary and, as it is proved to be, sufficient (Chap. 5). Another example is provided by the earthquake inverse problem in geophysics, which is solved in closed-form in the second part (Chap. 11).

In presenting the first part, we do not go into the details of classical subjects (stress intensity factor, energy release rate, Irwin's formula or the J-integral etc), but we mention instead new subjects or topics which cannot be found in many other books. Chap. 1 introduces the Tonti diagram which reveals in statics and dynamics the duality (or symmetry) of the equations of elasticity. The duality is the key tool to solve many inverse problems, sometimes in closed-form. Then, experimental works on metal plasticity are presented, followed by the Prandt-Reuss theory of plasticity and the

generalized standard material theory. A true path-independent integral for thermo-elasticity is given in Chapter 2, as well as the Lagrangian derivative of the potential energy, leading to the G-theta integral, which is the equivalent to the J-integral, but may be more suitable for numerical computations by the finite element methods. Chap. 3 collects new solutions of cracks problems: kinked crack, damage models in plasticity, frictional interface crack problem with Coulomb's friction law, where the significance of the J-integral has been elucidated. The non uniqueness of solution of frictional crack problem is proved for the first time.

The logarithmic singularity of the temperature field and its relationship with the energy release rate G are established in Chap. 4. Dynamic fracture, dynamic path-independent integrals for moving or stationary cracks and an inverse problem for determining different energies from the measurements of mechanical fields, are given in Chap. 5. We include in Chapter 6 many methods of solutions to three-dimensional crack problems, e.g. planar crack of arbitrary shape in unbounded and bounded solids, edge crack, angular crack etc. This chapter contains some mathematical formulations of 3D elasticity by boundary integrals. It presents closed-form solutions to: the Dirichlet boundary value problem and the Neumann boundary value problem. Ductile fracture may be considered as a theory of porous plasticity, rather than the extension of "linear" fracture mechanics to "nonlinear" materials Two models are then considered: Rousselier's model and Gurson's model of cavities growth. There are many theories of cavitation in solids worked out for example by Ball (1982), Horgan and Pence (1989) and others. Chap. 7 discusses another cavitation model according to Abeyaratne and Hou (1989) for finite strain in elasticity as well as in creeping materials. Finally Chap. 8 introduces the theory of a fluid-filled crack which has many applications in engineering sciences (hydraulic fracturing of rocks, capillary stress-intensity factor, wear mechanics, viscous fluid flow through/parallel to/a crack). It contains also the analysis of the"Leak-Before-Break" engineering inverse problem, with the pressure and the fluid flow rate as the data, to determine a longitudinal through crack length in a pipe.

Chaps. 9-12 are entirely devoted to inverse problems for the identification of cracks and defects, by classical x-rays or gamma-rays tomography. The success of the scanner tomography in medical imaging is due mainly to the works, a century ago, by Radon who invented the corresponding integral transform and its inverse. We remind that Radon's transform assumes that there is no attenuation of the rays in the sound medium. Only in recent years (2001) that the attenuated Radon's transform has been inverted by Novikov (2001) of the Nantes University (France). Also, when

the powerful gamma-rays (for inspection of defects in a nuclear reactor of 30cm thick) are scattered by nearby electrons (by Compton's scattering), the correct transform is called the "conical Radon's transform" which has been recently inverted in closed-form by Mai Nguyen and Truong (2002) of the Cergy-Pontoise University (France). Chap. 9 contains also another discovery by Fink (1997), Fink and Prada (2001) of the Paris University, namely the Time Reversal Mirror TRM.

The problems of identifying planar cracks in solids, using different physical phenomena (acoustic wave, elastic waves, heat diffusion) are solved in closed-form (Chap. 11), by considering the reciprocity gap functional technique, first introduced by Andrieux and Ben Abda (1992) of Electricite de France and the University of Tunis, respectively, and then used by our two research groups at EdF and LMS. In particular, the earthquake inverse problem for identifying a moving sliding fault in an elastic solid from acceleration data measured on the free surface has been recently solved in closed-form by the same technique.

General methods to solve the ill-posed inverse problems are given in Chap. 12. Some particular subjects (residual stresses in Fracture Mechanics, weak interface singularities) are given in appendices A and B, and suggestions of problems and exercices for students in App. C.

Many people have contributed to this book, graduate students, colleagues in France and in the abroad, in the Universities and Industries. Warm thanks to all of them. I am grateful to Jean-Baptiste Leblond, Sylvain Leclercq, Chau & Chuong Nguyen, Hung T. Trinh, Lev Truskinovsky, Abdelbacet Oueslati and Ms Mireille Vermède for their contribution to a careful job of checking the book. I am also very grateful to Xanthippi Markenscoff for her comments and encouragement in the writing of this book.

H.D. Bui

Ecole Polytechnique, Department of Mechanics, Palaiseau,
France and Research & Development Division,
Electricité de France, Clamart, France

Notations

$\mathbf{x} = (x_1, x_2, x_3)$	Position vector at time t and Eulerian coordinates
$\mathbf{X} = (X_1, X_2, X_3)$	Initial position vector and Lagrangian coordinates
$F = \partial\mathbf{x}/\partial\mathbf{X}$	Gradient of the transformation $\mathbf{X} \to \mathbf{x}$
T, T^{τ}	Tensor and transpose tensor
T, T*	Operator and adjoint operator
E_{ij}	Components of the Lagrangian deformation tensor
A_{ij}	Components of the Eulerian deformation tensor
$\mathbf{u}(\mathbf{x})$	Displacement field
$\varepsilon = (\varepsilon_{ij})$	Linearized strain tensor $\varepsilon = \varepsilon[\,\mathbf{u}\,] = \frac{1}{2}(\nabla + \nabla^{\tau})\mathbf{u}$
$\sigma = (\sigma_{ij})$	Cauchy stress
$\theta = (\theta_{ij})$	Unsymmetric Boussinesq-Kirchhoff stress tensor
$\pi = (\pi_{ij})$	Symmetric Piola-Kirchoff stress tensor
R	Left curl operator $RB := -(\partial_k B_{ij})\mathbf{e}^i \otimes (\mathbf{e}^j \wedge \mathbf{e}^k)$
R*	Right curl operator $R^*B := (\partial_k B_{ij})(\mathbf{e}^k \wedge \mathbf{e}^i) \otimes \mathbf{e}^j$
$\mathbf{g} = (g_i)$	Body force
L_{ijhk}	Components of the elastic moduli tensor
$\sigma[\,\mathbf{u}\,]$	Elastic stress $\sigma[\,\mathbf{u}\,] = \mathbf{L}\cdot\varepsilon[\,\mathbf{u}\,]$. (or $\sigma_{ij} = L_{ijhk}\varepsilon_{hk}[\,\mathbf{u}\,]$)
E, ν	Young modulus, Poisson ratio
λ, μ	Lamé's coefficients
W(ε)	Elastic strain energy density
p	Momentum
ρ	Density
$D = -div$	(minus) Divergence operator
D*	Adjoint of D
η,ζ	Incompatibility tensors

Z	Dynamic tensor
B	Beltrami tensor $B = \psi(x_1,x_2)\mathbf{e}^3\otimes\mathbf{e}^3$ (in 2D)
$\psi(x_1, x_2)$	Airy's function
$\alpha = (\alpha_i)$	Internal variables
α	Surface tension in Young-Laplace's law
$\varepsilon^e, \varepsilon^p$	Elastic, plastic strains
$f(\sigma, \alpha)$	Yield function
λ	Plastic multiplier, $\dot{\varepsilon}^p = \lambda \partial f / \partial \sigma$
$s = (s_{ij})$	Stress deviator
$\mathbf{A} = (A_i)$	Generalized force
$A(\mathbf{x})$	Localization tensor in homogenization theory: $\Sigma \rightarrow \sigma(\mathbf{x})$
$D = A_i d\alpha_i/dt$	Dissipation rate
$D = \text{grad}\mathbf{v}(\mathbf{x})$	Deformation rate
D^p	Plastic deformation rate
$[[u]]$	Discontinuity of u
K_I, K_{II}, K_{III}	Stress Intensity Factors in modes I, II, III
$K_i^{(\sigma)}$ (i = I, II, III)	Stress definition of SIF
$K_i^{(u)}$ (i = I, II, III)	Displacement definition of SIF
K_{Ic}	Toughness (in Statics)
K_{dyn}	Dynamic toughness (mode I)
K_I^0	Capillary Stress Intensity Factor (mode I)
G	Energy release rate (isothermal crack propagation)
$\mathcal{G}$	Thermodynamical force (iso-entropic propagation)
F	Freund's flux of energy through a small contour
J	J-integral
G^θ	Lagrangian derivative of the energy
T	Path-independent T-integral in thermo-elasticity
T^n	Stress operator: $\mathbf{u}(\mathbf{x}) \rightarrow \sigma[\mathbf{u}].\mathbf{n}$
$V, \dot{a}$	Crack velocity
c_p, c_s	Dilatational, shear wave speeds
$V_i^k(\mathbf{x}, \mathbf{y})$	Kelvin-Somigliana fundamental tensor

$B_i^k(\mathbf{x}, \mathbf{y}; \mathbf{n}_y)$	Kupradze-Bashelishvili fundamental tensor
$S_i(\mathbf{x})$, $D_i(\mathbf{x})$	Single, double layer potentials
η, $\eta' = \eta/\rho$	Viscosity coefficient, kinematic viscosity
$k = \omega/c$	Wave number corresponding to the velocity c
$F(\hat{\mathbf{x}}; k)$	Far-field
RG(u,v)	Reciprocity Gap functional (pseudo bilinear form)
$R^d(v)$	Boundary RG functional (linear form)
$g_{,t}$ $\partial_t g$ $\partial g/\partial t$ $\dot{g}$	Partial derivative of g with respect to time
$g_{,k} = \partial_k g = \partial g/\partial x_k$	Partial derivative of g with respect to x_k

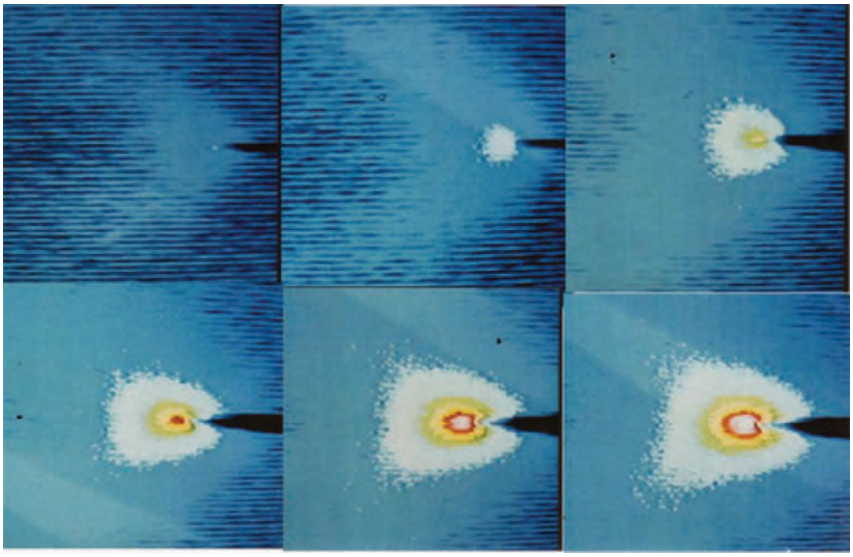

Plate 1. Infrared observation of crack propagation in a sheet of steel of 50mm width; images for six time instances during 6 seconds, each color corresponding to 2°C (Bui, Ehrlacher and Nguyen, 1979, permission of LMS-Ecole Polytechnique).

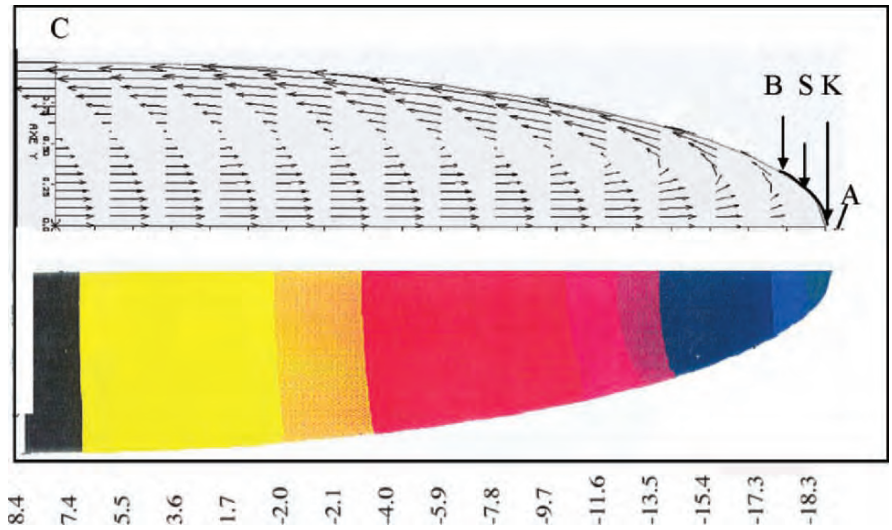

Plate 2. Stream lines of the "fountain" viscous fluid flow near the crack tip. Pressure decreases smoothly at K; Bui, Guyon and Thomas, In: Continuum Thermomechanics, G.A. Maugin et al (Eds.), p. 63, Kluwer Acad. Pub. (2002).

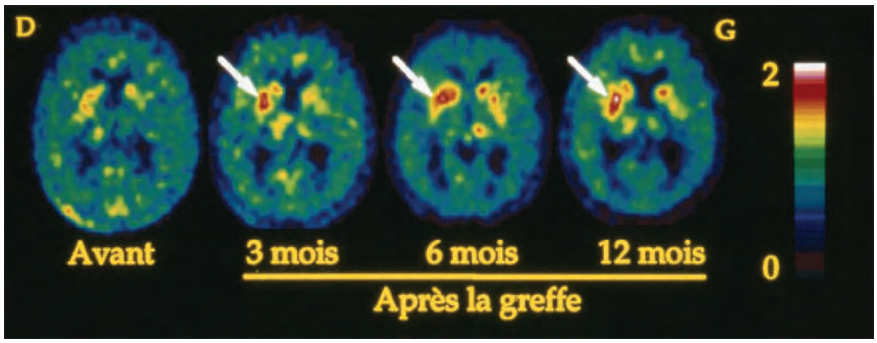

Plate 3. Positon Emission Tomography (PET). A functional tomography using ^{18}Fluoro-Deoxy-Glucose concentrated in living tissue absorbing glucose in the Parkinson desease: before, 3, 6, 12 monthes after the transplant of dopamine neurones, indicating the progressive fixing of ^{18}FDG and thence the viability of the transplant (permission of CEA/SHFJ Orsay, Ph. Remy, Clefs cea, N° 34 Winter 1996-1997.

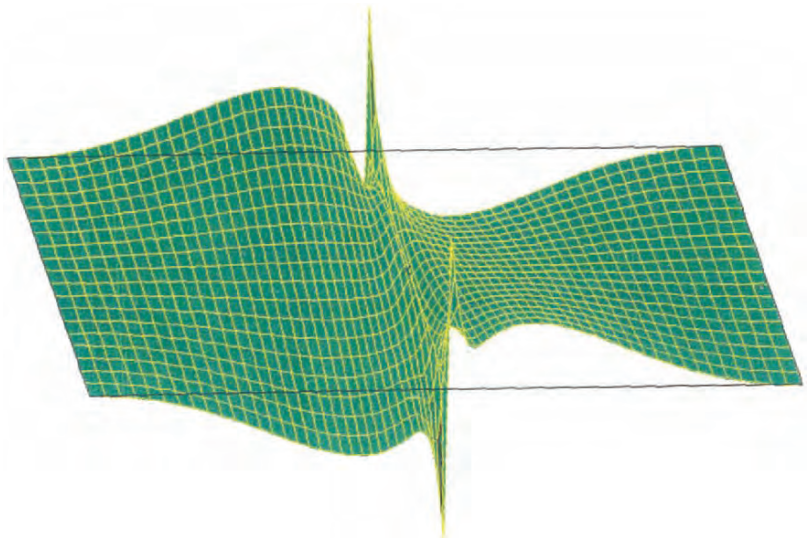

Plate 4. The 'Thorn" singularities of the stress $\sigma_{zz}(r,z)$ at the interface z=0 of a discontinuous thermal strain or radial plastic strain ε^{p}_{rr} in a tube of axis Oz. The wavy surface without thorns is the Love-Kirchhoff shell solution.

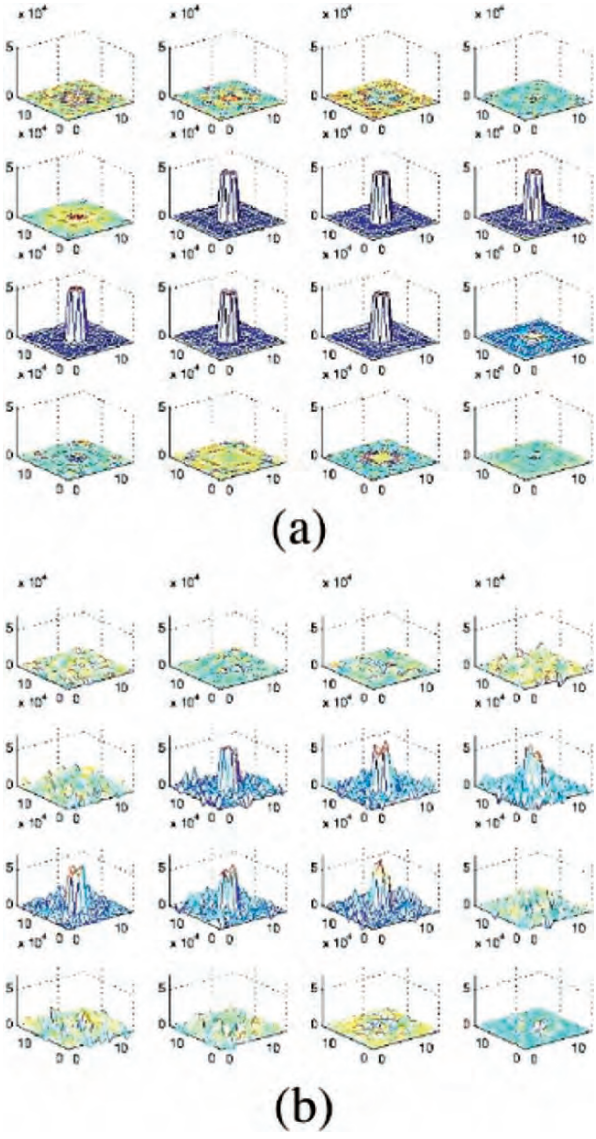

Plate 5. Reconstructed object by conical Radon's transform at different times, using photons in the range $5° < \theta < 175°$, (a) no noise, (b) with noise (S/N=9.7dB, RMSE=8.9%), (Permission Nguyen and Truong, University of Cergy Pontoise).

Chapter 1

Deformation and Fracture

This chapter reminds some fundamentals in Solid Mechanics, mainly for Elasticity, Plasticity and Fracture.

The mechanical behavior of materials is observed at the macroscopic scale of usual experiments and thus supposes some macro-homogeneity of the media which cannot be rigorously quantified. When dealing with continuous media, we consider a macroscopic scale to describe the motion of a Representative Volume Element (RVE), for instance containing 125 crystalline grains ($125 = 5^3$). The RVE will be identified as the material *point*, regardless of what actually happens inside the RVE. Microscopic aspects of phenomena inside the RVE are not considered in this book. However the underlying microscopic or sub-microscopic mechanisms at the scale of a grain size or at the atomic scale are always present. They explain the transition from elasticity to plasticity and from plasticity to fracture. The transition from plasticity to ductile fracture or to damage fracture for example can be understood in the following manner. At some critical stress state, the RVE loses its status of a representative volume for the description of a macroscopic material point. Magnifying the RVE, one can observe microcracks, cavities, or delaminations at the interface between metallic crystals etc, whose sizes are of the same order of the RVE size. Growth of microscopic cavities is followed by the coalescence between these cavities. The coalesced cavities result first from a shear band joining two neighbouring cavities, then from the propagation of a shear crack inside the shear band which finally becomes an opening crack visible to the naked eye. This is a physical description of ductile fracture. Damage begins gradually at the earlier stage of the deformation by a continuous formation of isolated cavities. The mean density ρ_m over some RVE decreases resulting in a macroscopic cavity. These considerations show that there is *no* simple constitutive laws at a macroscopic scale which take account of all these phenomena. Solid Mechanics for Engineering sciences consider some compromise between the understanding of complex phenomena at different scales and a suitable description of phenomena acceptable for computations and applications.

This compromise is called a *model.*

1.1. Deformation

1.1.1 Geometric transforms

The deformation of a solid from its natural state is characterized by the motion of each material point from the position vector $\mathbf{X} = (X_1, X_2, X_3)$ at time $t = 0$ to the position vector $\mathbf{x} = (x_1, x_2, x_3)$ at time t. Coordinates are given with respect to the same reference frame, with fixed orthonormal basis vectors $\mathbf{e}^1$, $\mathbf{e}^2$, $\mathbf{e}^3$. One assumes that functions $(\mathbf{X}, t)\rightarrow(\mathbf{x}, t)$ or $(\mathbf{x}, t)\rightarrow(\mathbf{X}, t)$ are one-to-one mappings, continuously differentiable with respect to variables in their respective domains $(\Omega_0$ or $\Omega) \times [0, t]$. The displacement field $\mathbf{u} = \mathbf{x} - \mathbf{X}$ can be measured with either Lagrangian variables X_i or Eulerian variables x_i. There are two possible descriptions of deformation according to the choice of variables in $\mathbf{u}(\mathbf{X}, t)$ or $\mathbf{u}(\mathbf{x}, t)$. The deformation in solids is characterized by a distance change between two neighbouring points, from the natural state to the current one. Let $F \equiv \partial\mathbf{x}/\partial\mathbf{X}$ be the gradient tensor of components

$$F_{ij} = \frac{\partial x_i}{\partial X_j} \tag{1.1}$$

and $G \equiv \partial\mathbf{X}/\partial\mathbf{x}$ be its inverse with components

$$G_{ij} = \frac{\partial X_i}{\partial x_j} \tag{1.2}$$

The Variation of the square of a small arc is a quadratic form in $d\mathbf{X}$ or $d\mathbf{x}$,

$$ds^2 - ds_0^2 = 2E_{ij}dX_idX_j = 2A_{ij}dx_idx_j \tag{1.3}$$

where

$$A_{ij} = \frac{1}{2}(\delta_{ij} - \frac{\partial X_k}{\partial x_i}\frac{\partial X_k}{\partial x_j}) \tag{1.4}$$

$$E_{ij} = \frac{1}{2}(\frac{\partial x_k}{\partial X_i}\frac{\partial x_k}{\partial X_j} - \delta_{ij}) \tag{1.5}$$

$E = (F^{\tau}F - I)/2$ and $A = (I - G^{\tau}G)/2$ are called the Lagrangian and the Eulerian strain tensors respectively and I is the identity tensor.

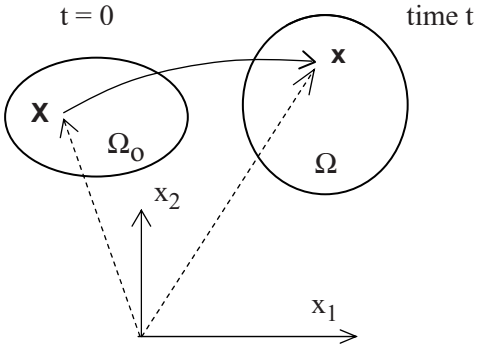

Figure 1.1: Geometric transform of Ω_O from the initial state at t = 0 to Ω at time t. Point **x** in Ω at time t corresponds to point **X** in Ω_O at t = 0

The components of the Eulerian deformation tensor (also called the Almansi-Euler tensor) are given in terms of displacement **u** by

$$A_{ik} = \frac{1}{2}\left(\frac{\partial u_i}{\partial x_k} + \frac{\partial u_k}{\partial x_i} - \frac{\partial u_h}{\partial x_i}\frac{\partial u_h}{\partial x_k}\right) \tag{1.6}$$

By introducing the mass density $\rho(\mathbf{x})$, the continuity of the body can be expressed as $\rho(\mathbf{x})\det F = \rho_0(\mathbf{X})$, known as the conservation of mass.

1.1.2 Small strain

The small strain assumptions are based on the following experimental fact. For most materials and structures, Engineering designs as well as criteria for the validity of the behavior laws of materials considered impose some limitations on the magnitude of the gradient $|\partial\mathbf{u}/\partial\mathbf{x}|$ less than 10% for example. The non-linear term in Eq.(1.6) has then the magnitude 1% which can be neglected compared with the linear terms.

Moreover one generally deals with deformation in which the displacement itself $|\mathbf{u}|$ is small compared to the solid size. Since in quasi-statics, the displacement is defined up to a rigid motion $\mathbf{r} = \mathbf{a} + \boldsymbol{\omega}\wedge\mathbf{X}$, the smallness of the displacement is measured with respect to some transported configuration of Ω_0 by **r**.

It should be noted that the smallness of **u** is not assumed in dynamics. These two assumptions greatly simplify the analyses in Solids Mechanics. One then makes the approximations $\mathbf{X} \cong \mathbf{x}$, $\partial/\partial\mathbf{x} \cong \partial/\partial\mathbf{X}$ and

$$E_{ik} \cong A_{ik} = \frac{1}{2}\left(\frac{\partial u_i}{\partial x_k} + \frac{\partial u_k}{\partial x_i}\right) \tag{1.7}$$

Eq. (7) defines the linearized strain tensor

$$\varepsilon_{ik} \coloneqq \frac{1}{2}\left(\frac{\partial u_i}{\partial x_k} + \frac{\partial u_k}{\partial x_i}\right) \tag{1.8}$$

or in a compact notation $\varepsilon = (\nabla\mathbf{u}+\nabla^{\tau}\mathbf{u})/2$ irrespective of the coordinates used x_i or X_i. Both tensors E and A coincide with ε. The mass conservation law reduces to $\rho(\mathbf{x})(1 + tr\varepsilon) = \rho_0(\mathbf{x})$. A strain tensor Eq. (1.8) is called a *compatible strain* when there exists a differentiable displacement field $\mathbf{u}(\mathbf{x})$ satisfying Eq. (1.8).

1.1.3 Compatibility conditions

Let us recall without proofs the compatibility conditions for the linearized strain ε in some simply-connected region Ω to be the symmetric part of the gradient of function $\mathbf{u}(\mathbf{x})$ continuous and continuously differentiable in Ω. Mathematically, a compact form of the compatibility equations can be obtained with the use of differential operators R and its adjoint R* defined hereafter. The proofs can be found in classical Course on the Mechanics of continuous media. Let $B(\mathbf{x})$ be a symmetric second order tensor field $B(\mathbf{x}) = B_{ij}(\mathbf{x})\mathbf{e}^i\otimes\mathbf{e}^j$. We make use of the short notations $\partial_k \equiv \partial/\partial x_k$ and define the operator R (rot, curl in many books) and its adjoint operator R* (or rot*, curl*) by

$$RB := -(\partial_k B)\wedge \mathbf{e}^k = -(\partial_k B_{ij})\mathbf{e}^i \otimes (\mathbf{e}^j \wedge \mathbf{e}^k) \tag{1.9}$$

$$R^*B := \mathbf{e}^k \wedge (\partial_k B) = (\partial_k B_{ij})(\mathbf{e}^k \wedge \mathbf{e}^i) \otimes \mathbf{e}^j \tag{1.10}$$

The operator R is called the *left curl* while its adjoint R* is the *right curl* operator. The operator RR* is self-adjoint. The compatibility conditions for the small strain can be written as

$$RR^*\,\varepsilon = 0 \tag{1.11}$$

These are second order differential equations on the strain components. The 6 equations (1.11) are necessary for the existence of continuous and continuously differentiable $\mathbf{u}(\mathbf{x})$ satisfying Eq. (1.8). They are sufficient conditions for a simply-connected domain in the sense that any closed loop inside the domain can be reduced to a zero circuit by a continuous defor-

mation of the loop. Otherwise, with n irreductible connexions (annulus and toroidal cavities in 3D, or holes and internal cracks in 2D), one has to satisfy $6(n-1)$ *closing* conditions for displacement continuity in 3D or $3(-1)$ closing conditions in 2D. These conditions express the continuity and uniformity of the displacement around a connexion. A domain with an edge crack is simply-connected. The two faces of the crack belongs to $\partial\Omega$ where the displacement is discontinuous.

1.1.4 Stress

Let us recall some fundamentals on stress and introduce some notations. There are many definitions of the stress tensors, according to the choice of space variables. A distinction between stress tensors is important in non-linear theories. Consider a small area element dS of material points with unit normal $\mathbf{n}$ which is subjected to the contact force $\mathbf{T}dS$ by particles on the normal side. At time t, the area element dS corresponds to the area element dS_0 with normal $\mathbf{n}_0$ at initial time $t = 0$. A material vector $d\mathbf{x}_0$ on dS_0 becomes $d\mathbf{x}$ on dS, $d\mathbf{x} = Fd\mathbf{x}_0$. Three stress tensors can be defined by the following mappings

$\sigma : \mathbf{n}dS \rightarrow \mathbb{T}dS$ (Symmetric Cauchy stress σ, $\mathbf{T} = \sigma.\mathbf{n}$),

$\theta : \mathbf{n}_0 dS \rightarrow \mathbf{T}dS$ (Unsymmetric Boussinesq-Kirchhoff stress θ, $\mathbf{T} = \theta.n_0$),

$\pi : \mathbf{n}_0 dS_0 \rightarrow \mathbf{T}dS$ (Symmetric Piola-Kirchhoff stress π).

Different stress tensors are related together by $\theta = F.\pi$ and $\sigma \det F = \theta.F^{\tau}$ (τ denotes the transposition). Conservation laws of momentum can be expressed either with Lagrangian variables $\mathbf{X}$

$$\frac{\partial \theta_{ik}}{\partial X_k} + \rho_0(\mathbf{X})(g_i - \frac{\partial^2 u_i}{\partial t^2}) = 0 \text{ in } \Omega_0 \tag{1.12}$$

or with Eulerian variables $\mathbf{x}$

$$\frac{\partial \sigma_{ik}}{\partial x_k} + \rho(\mathbf{x})(g_i - \frac{\partial}{\partial t} v_i - v_h \frac{\partial^2 v_i}{\partial x_h}) = 0 \tag{1.13}$$

The body force $\mathbf{g}$ per unit mass at point in the initial configuration, Eq. (1.12) is not generally considered in Fracture Mechanics and $-\rho_0 \ddot{\mathbf{u}}$ is the

inertial force (the double dot denotes $\partial^2/\partial t^2$ or $\partial_t\partial_t$), while **g** in Eq. (1.13) is the body force per unit mass evaluated in the current configuration.

In the linearized theory, all stress tensors are equivalent. We consider **g** = **0** in the book so that Eq. (1.13) can be written as

$$-\mathrm{div}\sigma + \mathbf{p} = 0 \tag{1.14}$$

$$\mathbf{p} = \rho\frac{\partial \mathbf{v}}{\partial t} \tag{1.15}$$

with **p** being the momentum. It should be noted that Eq. (1.14), called the *equation of motion*, is independent of the material considered, while Eq. (1.15) depends on the material property ρ. Therefore we consider Eq. (1.15) as the *constitutive law* linking the momentum **p** to the particle acceleration $\partial\mathbf{v}/\partial t$, via the density ρ. In the *equilibrium* case, Eq. (1.14) reduces to $\mathrm{div}\sigma = 0$.

1.2. Elasticity

1.2.1 Constitutive laws

In the previous Sect. 1.1.3 it has been considered that $\mathbf{p} = \rho\partial\mathbf{v}/\partial t$ is an universal constitutive law for any material. In Elasticity, the stress-strain law is specific to each material and can be defined by a relation of the form $\sigma = \sigma(\varepsilon)$ or its inverted form $\varepsilon = \varepsilon(\sigma)$. Let us consider here the isothermal behavior of hyperelastic materials. The elastic constitutive law derives from a strain energy density $W(\varepsilon)$, a convex function of the strain which gives the stress as

$$\sigma_{ij} = \frac{\partial W}{\partial \varepsilon_{ij}} \tag{1.16}$$

or shortly $\sigma = \partial W/\partial\varepsilon$We recall that a (strictly) convex function f(x) of x in some space satisfies $f(\alpha x + (1-\alpha)y) < f(x) + (1-\alpha)f(y)$ for any x, y. In linear elasticity the strain energy density is a quadratic function of the strain components

$$W(\varepsilon) = a_{ij}\varepsilon_{ij} + \tfrac{1}{2} L_{ijhk}\varepsilon_{ij}\varepsilon_{hk} \tag{1.17}$$

where the elastic moduli possess the symmetry properties, which can be justified experimentally.

$$L_{ijhk} = L_{hkij} = L_{jihk} \tag{1.18}$$

For stability reasons and uniqueness of solutions in statics, one assumes that L is positive definite, $\varepsilon.L.\varepsilon > 0$. This is true in linear isotropic elasticity

$$L_{ijhk} = \lambda\delta_{ij}\delta_{hk} + \mu(\delta_{ih}\delta_{jk} + \delta_{ik}\delta_{jh}) \tag{1.19}$$

$\mu > 0$, $3\lambda + 2\mu > 0$. The elastic law $\sigma = L.\varepsilon$ can be inverted as $\varepsilon = M.\sigma$ with the compliance moduli tensor $M_{ijhk} = (1 + \nu)\delta_{ij}\delta_h /E - tr(\sigma)I_{ihjk}$, $I_{ihjk} = (\delta_{ih}\delta_{jk} + \delta_{jh}\delta_{ik})/2$. The strain components are

$$\varepsilon_{ij} = \frac{1+\nu}{E}\sigma_{ij} - \frac{1}{E}tr(\sigma)\delta_{ij} \tag{1.20}$$

with E the Young modulus and ν the Poisson coefficient.

1.2.2 Tonti's diagram in elasticity

Tonti (1975) has discovered the symmetry in equations of Physics, including elastic rods and beams theory which reflects a profound symmetry existing in Nature. The same symmetry or more precisely *duality* exists for example in Electromagnetics (Bossavit, 1988) and in three-dimensional Elasticity (Bui 1992).

Hereafter we remind only recent results for duality in Elasticity. Let us write the small strain tensor, Eq. (1.8), shortly as $\varepsilon = D^*\mathbf{u}$, with $D^* = (1/2)(\nabla+\nabla^\tau)$, where precisely D* is the adjoint of the differential operator $D = -\text{div}$. To verify the duality between operators D, D*, in a mathematical sense, we recall the symmetry of stress and introduce an arbitrarily regular differentiable field **w** in Ω, such that the gradient ∇**w** is square integrable and $\mathbf{w} = \mathbf{0}$ on ∂Ω. We consider the Green-Gauss identity

$$\int_\Omega -\text{div}\sigma.\mathbf{w}d\Omega \equiv -\int_{\partial\Omega}\mathbf{n}.\sigma.\mathbf{w}dS + \int_\Omega \tfrac{1}{2}\sigma.(\nabla + \nabla^t)\mathbf{w}d\Omega$$

The first volume integral can be written as $<D\sigma, \mathbf{w}>$, the second integral over ∂Ω vanishes and the third volume integral can be written as $<\sigma, D^*\mathbf{w}>$. We then obtain the duality relation

$$<D\sigma,\mathbf{w}> = <\sigma,D^*\mathbf{w}>$$

$(-\int_{\partial\Omega}\mathbf{n}.\sigma.\mathbf{w}dS = 0)$, which justifies the notation D and D*.

Kinematics of Elasticity

Consider the 2×1 matrix operator C and the 2×2 matrix operator S

$$C = \begin{bmatrix} \partial_t \\ D^* \end{bmatrix}, \qquad S = \begin{bmatrix} -D^* & \partial_t \\ 0 & RR^* \end{bmatrix} \tag{1.21}$$

Applying C to $\mathbf{u}$ we obtain

$$\mathbf{v} = \partial_t \mathbf{u} \tag{1.22}$$

$$\varepsilon = D^* \mathbf{u}. \tag{1.23}$$

Applying S to C$\mathbf{u}$ we then obtain two *incompatibility* tensors respectively

$$\eta = -D^* \mathbf{v} + \partial_t \varepsilon \tag{1.24}$$

$$\zeta = RR^* \varepsilon \tag{1.25}$$

The incompatibility tensor ζ is well-known in the theory of dislocations. The first compatibility equation $\eta = 0$ indicates that the strain rate is the symmetric part of the velocity gradient,

$$-D^* \mathbf{v} + \partial_t \varepsilon = 0 \tag{1.26}$$

The second compatibility equation $\zeta = 0$ is nothing but the compatibility equation of the strain

$$RR^* \varepsilon = 0 \tag{1.27}$$

Dynamics of Elasticity

Consider a matrix $M(2 \times 1)$ of elements $Z(\mathbf{x})$ and $B(\mathbf{x})$, which are symmetric second order tensor fields, which we term *dynamic tenso* · and *Beltrami's tensor,* respectively $M^\tau = (Z, B)$. Applying the adjoint S* to M, we then obtain the representation of the momentum $\mathbf{p}$ and the stress σ

$$\mathbf{p} = -DZ \tag{1.28}$$

$$\sigma = \partial_t Z + RR^* B \tag{1.29}$$

In dynamics, because of $DR \equiv 0$, the representations of the momentum and the stress Eqs. (1.28), (1.29) satisfy identically the equation of motion,

$$\partial_t \mathbf{p} + D\sigma = -\partial_t DZ + D(\partial_t Z + RR^* B) = -\partial_t DZ + D(\partial_t Z) = 0 \tag{1.30}$$

In statics, the Beltrami representation of the equilibrium stress $\sigma = RR^*B$ is well-known. In two-dimensions the Beltrami tensor $B(\mathbf{x}) = \psi(x_1,x_2)\mathbf{e}^3\otimes\mathbf{e}^3$ can be expressed in terms of the Airy function ψ. The Tonti diagram in Elasticity clearly shows vertically two diagrams, the kinematics and the dynamics of continuous media and a horizontal link by two constitutive physical laws $\mathbf{p} = \rho\mathbf{v}$ and $\sigma = L.\varepsilon$. Operators C, S* in the kinematic diagram are the adjoint operators of C*, S in the dynamic diagram. The Tonti diagram was originally introduced in the theory of Boundary Integral Equations for symmetrization purposes (Bui, 1992). Generally, in BIE methods one deals with unsymmetric systems of equations, starting from the displacement to the strain, then to the constitutive laws and finally to the equation of motion (or equilibrium equation).

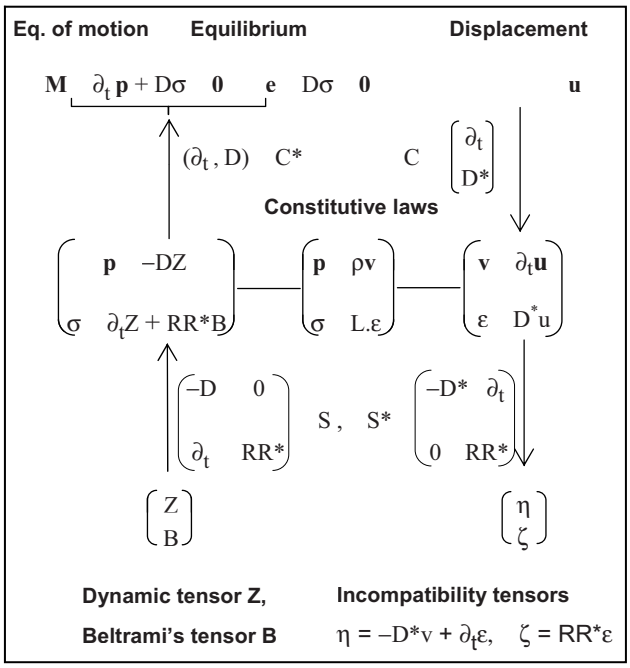

Figure 1.2: Tonti's diagram in Elasticity. The kinematic chart goes down from the displacement field **u** to the incompatibility tensors η, ζ , with the operators C and S*. The dynamic chart goes up from the dynamic symmetric 2^{nd} order tensor Z and the symmetric 2^{nd} order Beltrami tensor B. Operators C* and S are adjoint to operators C and S*. They gives rise to the equation of motion $\mathbf{m} = \mathbf{0}$ or the equiibrium equation $\mathbf{e} = \mathbf{0}$. The link between kinematic and dynamic charts is established by the constitutive laws, for momentum and elasticity (Bui 1992)

It is shown that the symmetry in BIE can be restored by considering the symmetry between the stress and the strain, in time domain as well as in frequency domain

1.3. Plasticity

1.3.1 Experimental yield surfaces

We consider metallic materials for describing some experimental evidence at the basis of the plasticity theory. Elasticity law holds true for the magnitude of stress or strain below some *threshold* value called the yield stress σ_0.

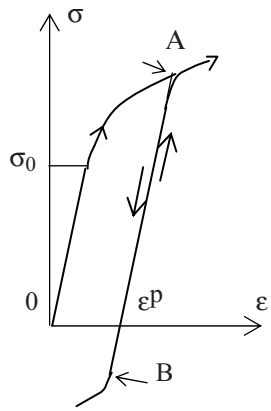

Figure 1.3: Stress-strain curve in uniaxial loadings

For higher stress one observes a plastic deformation ε^p. Unloading then loading are elastic, with the same Young modulus for the *variations* of stress and strain,
Plasticity is then characterized by three features:

i) The stress and elastic strain *rates* obey the elastic law $\partial\sigma/\partial t = L_{\circ}\partial\varepsilon^e/\partial t$,

ii) After plastic deformation, the new elastic domain BA, Fig. 1.3, depends on the plastic strain, more generally on some set of unknown internal parameters α in a complex manner.

iii) Unloading at A is elastic and reloading at A is plastic with the same plastic strain rates $\partial\varepsilon^p/\partial t$ as that prevails before unloading.

Let us consider a thin tube along Ox_2 subjected to tension σ (compression) and shear τ (by torsion). Yield surfaces in the stress space (σ, τ) have been obtained experimentally on copper, Armco iron, aluminium, Fig. 1.4. The initial yield surface is nearly the V. Misès ellipse, but subsequent convex yield surfaces deviates significantly from known criteria: isotropic hardening (isotropic expansion) or kinematic hardening (translation of surfaces). The initial Mises criterion $s_{hk}s_{hk} = Cte$ can be explained by microscopic considerations on the yield shear stress in polycrystals. The shear stress, along planes with normal **n** in the direction **m** of the slip plane, $\tau = \sigma_{hk}(n_h m_k + m_k n_h)/2$ is a deviatoric stress. If the initial shear stress is constant for any **n**, **m**, then the distance of σ to the hydrostatic vector of the stress space should be a deviatoric stress with constant norm, i.e $s_{hk}s_{hk} = Cte$. Experiments show only an approximate coincidence with this theory of crystal plasticity. There is a round nose in subsequent yield surfaces which are the reminiscence of the vertex of yield surfaces in monocrystals. Experiments also suggest that the yield surface in the stress space may depend on some set of internal variables α in a complex manner so that it is practically impossible to determine exactly the function $f(\sigma, \alpha)$. The reasons are twofold: firstly internal variables α are yet unknown and secondly the inverse problem to identify functions $f(\sigma, \alpha)$ from experimental data is underdetermined by a finite number of possible experiments, generally two types of experiments (traction or compression and torsion on thin tubes), exceptionnally three parameters with an internal pressure.

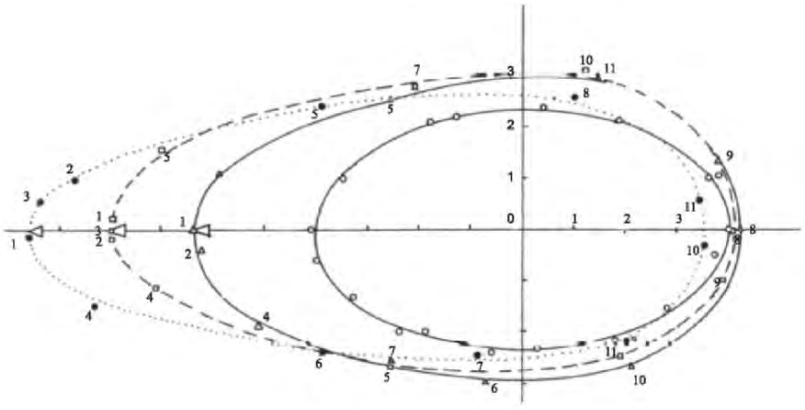

Figure 1.4: Yield surfaces in the stress space (σ, τ) for aluminium 99.5%. The initial yield surface is nearly the Misès ellipse. Subsequent yield surfaces deviates from known criteria: isotropic hardening (expansion) or kinematic hardening (translation) (Bui, 1964)

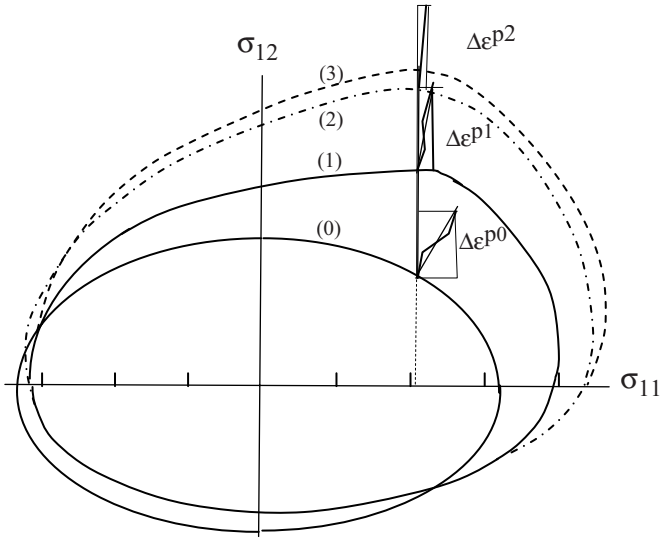

Figure 1.5: Incremental plastic vectors ($\Delta\varepsilon_{11}$, $2\Delta\varepsilon_{12}$) are normal to subsequent yield surfaces in the (σ_{11}, σ_{12})-space, justifying the *normality law* (Bui, 1964)

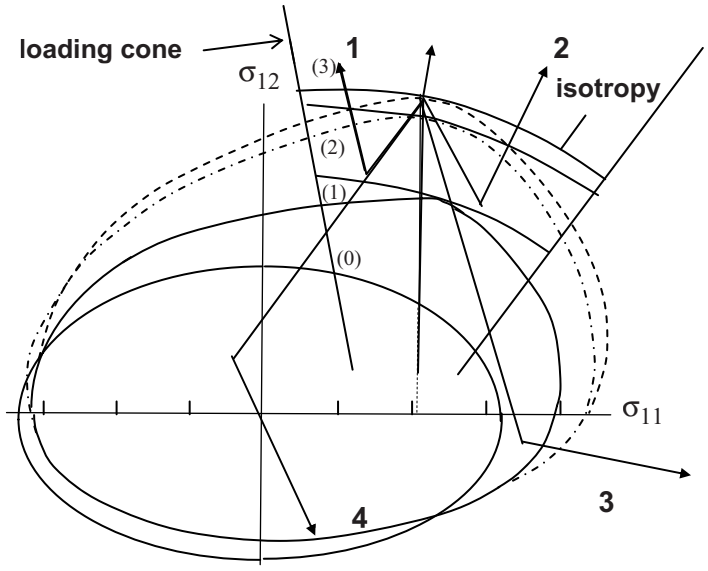

Figure 1.6: Isotropic hardening theory is an approximation for pathes 1 and 2 lying in some loading cone. This is true for the Deformation theory of Plasticity (Hencky's theory). The yield surface to be considered for pathes 3 and 4 may be a mixed theory of isotropic and kinematic hardening (Bui, 1964)

One cannot determine neither the nature of internal parameters nor the manner they influence the subsequent yield surfaces geometry. Therefore macroscopic Plasticity theory is based necessarily on approximations which are not always stated with clarity in the literature. Based on some experiments on tubes which offer simple means to test two independent loads, we can drawn some useful conclusions on yield surfaces:

1. Unloadings at the current point **0** are elastic. The yield surfaces after a partially elastic unloading then plastic reloadings **1** and **2**, for load pathes lying within some cone, correspond approximately to the isotropy criterion (heavy line curves). The stress pathes inducing plastic deformation should not deviate too much from this loading cone. This is true for proportional loadings starting from the zero stress state as considered in the Deformation theory of plasticity called the *Hencky theory*.

2. The plasticity criterion for pathes **3** or **4** corresponds to rather some mixed isotropic and kinematic hardening, or perfect plasticity for load **4**.

3. The plastic rate obeys the *normality law* $\partial_t \varepsilon^p = \gamma \partial f/\partial \sigma$, with a positive multiplier $\gamma > 0$.

Remarks. In an uncoupled or coupled theory of thermo-elasticity, the stress fields depend on both mechanical loading and thermal loading conditions. The loading cone condition may be satisfied by the overall stress. This condition must be checked a posterirori to ensure the validity of the hardening theory considered (perfect plasticity, isotropic hardening, kinematic hardening). Very often, thermal loadings induce reverse compressive stresses which must be in the current elastic domain

1.3.2 Prandtl-Reuss equations

The convex elastic domain C_α in the stress space is defined by $f(\sigma, \alpha) \leq 0$. Some popular criteria are given by functions

$$f(\sigma, \alpha) \equiv f(\sigma - k_0 \text{ (Perfect plasticity)} \tag{1.31}$$

$$f(\sigma, \alpha) \equiv f(\sigma) - k(\alpha) \text{ (Isotropic hardening)} \tag{1.32}$$

$$f(\sigma, \alpha) \equiv f(\sigma - c.\alpha) - k_0 \text{ (Kinematic hardening)} \tag{1.33}$$

The strain rates is decomposed into elastic and plastic rates

$$\dot{\boldsymbol{\varepsilon}} = \dot{\boldsymbol{\varepsilon}}^e + \dot{\boldsymbol{\varepsilon}}^p \tag{1.34}$$

- For strain hardening materials the normality law is:

$$\dot{\varepsilon}^p = \gamma \frac{\partial f}{\partial \sigma}, \ \gamma \geq 0 \ \text{ for } f = 0 \text{ and } f^* > 0 \tag{1.35}$$

$$\dot{\varepsilon}^p = 0, \ \text{ for } f < 0 \text{ or } f^* \leq 0 \tag{1.36}$$

- For perfect plasticity:

$$\dot{\varepsilon}^p = \gamma \frac{\partial f}{\partial \sigma}, \text{ arbitrary } \gamma > 0 \text{ for } f = 0 \ \text{ and } \ \dot{f} = 0 \tag{1.37}$$

$$\dot{\varepsilon}^p = 0, \ \text{ for } f < 0 \text{ or } \dot{f} < 0 \tag{1.38}$$

where $f^* = (\partial f/\partial\sigma)\mathbf{:}\partial_t\sigma$ the rate of f at fixed α. Eqs. (1.34)-(1.38) are called Prandtl-Reuss's equations of plasticity. We follow Mandel's work to present some experimental facts in plasticity (Mandel et al, 1962; Mandel, 1966). To complete the normality law, one should have to introduce a function $q(\sigma, \alpha) \neq 0$ which characterizes the evolution of internal parameter as $\partial_t\alpha = \gamma q(\sigma, \alpha)$ with the same multiplier $\gamma > 0$, which can be shown in the hardening case $(\partial f/\partial\sigma)\mathbf{:}q \neq 0$ to be the ratio $g = f^*/\{(\partial f/\partial\sigma)\mathbf{:}q\}$.

An approximate theory of plasticity, valid for loading cone condition in the sense stated in Sect. 1.3.1, is based on the plastic potential $f = s_{hk}s_{hk}/2 - k^2(\alpha)$, where s is the stress deviator, $s = \sigma - tr(\sigma)I_2/3$. In a radial loading, one considers that $q(\sigma,\alpha)$ is simply a function of the equivalent deviatoric strain $e_e = (e_{ij}e_{ij})^{1/2}$ or equivalent stress $e_e = (s_{ij}s_{ij})^{1/2}$, since the relationship between these quantities is one-to-one. Instead of the rate f^* let us consider the increments $\delta f = s_{ij}\delta s_{ij} = s_e\delta s_e$ and write

$$\delta e_{ij} = (1/2\mu)\delta s_{ij} + s_{ij}q(s_e^2/2)s_e\delta s_e = (1/2\mu)\delta s_{ij} + \{s_{ij}/s_e\}\, q(s_e^2/2)s_e^2\delta s_e$$

In radial or proportional loadings the ratio $\{s_{ij}/s_e\}$ is constant during the load so that an integration from the initial state to the current one gives the Hencky theory of plasticity

$$e_{ij} = \frac{1}{2\mu} s_{ij} + \frac{s_{ij}}{s_e} h(s_e) \tag{1.39}$$

In neglecting the elastic term $(1/2\mu)s_{ij}$, one gets the Mises theory of plasticity. In Eq. (1.39), function $h(s_e)$ may be determined experimentally by simple loadings (traction, traction+torque, traction+torque+internal pressure on tube).

From Eq. (1.39) the equivalent deviatoric strain and stress are related by $e_e = s_e/2\mu + h(s_e)$.

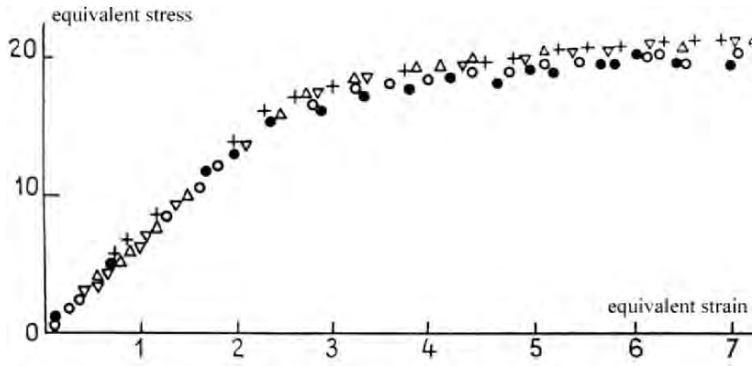

Figure 1.7: Relation between deviatoric equivalent stress and deviatoric equivalent strain $e_e = s_e/2\mu+h(s_e)$ determined in Osgood's experiments. (h = shear stress/normal stress) △ (h = 0); **o**(h = 0.5); ▽(h = 1); •(h = 2); +(h = ∞), (Mandel, 1966)

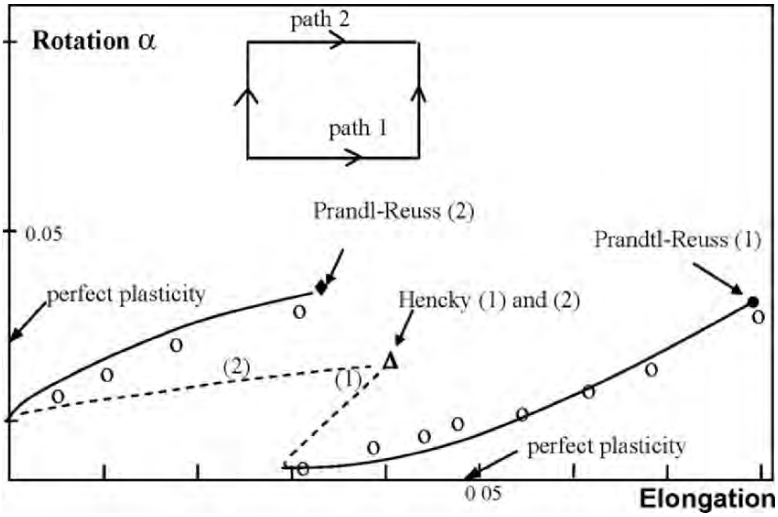

Figure 1.8: Comparison between Hencky's theory and Prandtl-Reuss's theory of plasticity, for two stress pathes (1) and (2) ending at the same point. Hencky's theory in doted lines with the same strain end point (△); Prandtl-Reuss's theory in continuous lines with different end points (•, ♦); For perfect plasticity, the plastic strain of path (1) continues without rotation while the plastic strain of path (2) continues without elongation. Experiments (**o**). (Mandel et al, 1962)

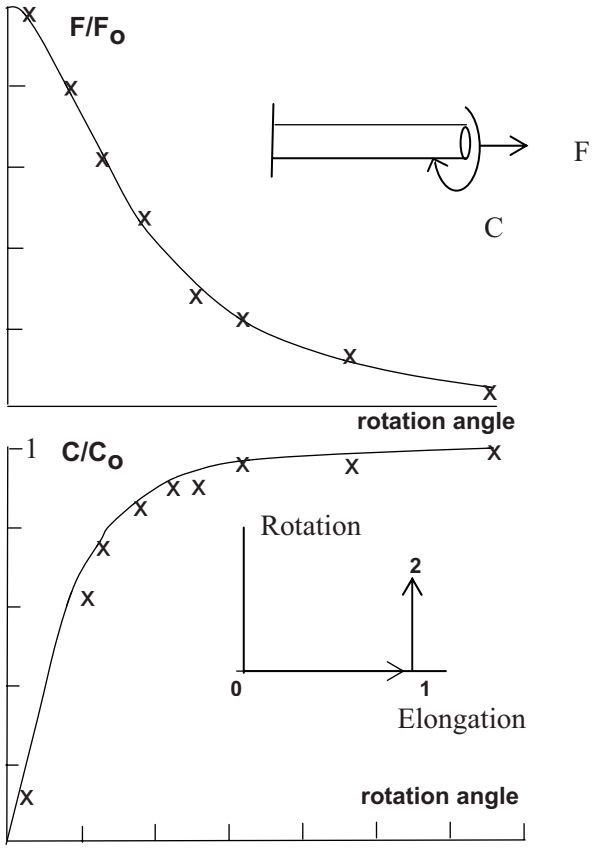

Figure 1.9: Experiments on a long cylinder subject to strain pathes; First phase 0→1 (elongation in the plastic domain) and second phase 1→2 (rotation); Mises's theory predicts a sudden decrease of F/F_O to zero and a sudden increase of C/C_O to 1. Prandt-Reuss's theory predicts smooth variations of force and torque (Mandel et al, 1962)

Osgood's experiments on tubes, for the ratio torque/traction ranging from zero to infinity, show a good coincidence for functions h or q, even for non proportional loadings, subjected only to the loading cone condition ($0 < \theta < 90°$) Fig. 1.6. Experiments shown in Fig. 1.7 indicates a moderate discrepancy between results from different loading pathes. They do not mean that Hencky's theory (1.39) is good for non proportional loadings. To compare theories for non proportional loadings, experiments have been performed on aluminium tubes subjected to loading pathes traction + torque (path 1) or torque+traction (path 2) ending at the same point.

Hencky's theory predicts the same final response in the strain space (point ▵) while the incremental Prandtl-Reuss theory predicts different responses (points • ♦) according the loading path considered, Fig. 1.8.

Another experiment on long cylindrical specimen of aluminium of initial length l_o has been performed for a comparison between Mises's theory (elastic strain neglected) and Prantlt-Reuss's theory (Mandel et al, 1962).

They consist in considering different *strain paths*: First we elongate significantly the specimen up to the length $l_o(1 + e_1)$ with large plastic strain so that the elastic strain is negligible. The plastic strain is thus e_1. Now fixing the specimen length, $l = l_o + e_1$, we then apply an increasing rotation angle $\alpha \to \infty$. Both theories agree in the first phase of the elongation of the cylinder (proportional loading). In the second phase Mises's theory predicts a sudden drop of the force $F/F_o = 0$ and a sudden increase of the torque to $C/C_o = 1$ while Prandt-Reuss's theory predicts smooth variations of $F(\alpha)$ and $C(\alpha)$ as shown in Fig. 1.9. For detailed calculations of $F(\alpha)$ and $C(\alpha)$ the readers can refer to (Mandel, 1966; Mandel et al, 1966).

1.3.3 Generalized Standard Materials

Halphen and Nguyen (1975) developed a mathematical theory of plasticity which incorporates strain energy and dissipation energy in an unified manner. Some specific aspects of dissipation including experimental justifications will be considered in Chap. 4. Here, we consider some general aspects of constitutive laws in Plasticity in isothermal small strain and quasi-static conditions. State variables are the pair (ε, α) of strain ε and internal variables $\alpha = (\varepsilon^p, \beta)$, which consists of observable plastic deformation ε^p and hidden variables $\beta = (\beta_1, \beta_2$ One introduces the free energy per unit volume $W(\varepsilon,\alpha)$ and the pseudo-dissipation potential $\Phi(\partial_t\alpha)$, which are convex and differentiable functions of their arguments so that stress σ and generalized forces **A** are given respectively by

$$\sigma = \frac{\partial W}{\partial \varepsilon}, \qquad \mathbf{A} = -\frac{\partial W}{\partial \alpha} = \frac{\partial \Phi}{\partial \dot{\alpha}} \tag{1.40}$$

and the dissipation is

$$D = \mathbf{A}.\dot{\alpha} \geq 0 \tag{1.41}$$

The second form of A, Eq. (1.40) defines the evolution law of internal parameters. An explicit form of the evolution law is given by normality law

$$\dot{\alpha} = \frac{\partial \Psi}{\partial \mathbf{A}} \tag{1.42}$$

Function Ψ is related to Φ by duality in the sense of Legendre's transform

$$\Phi(\dot{\alpha}) = \sup_{A \in V} \left\{ \dot{\mathbf{A}}.\dot{\alpha} - \Psi(\mathbf{A}) \right\} \tag{1.43}$$

where V is some convex set. If convex V has vertex points, differentiation in (1.42) has to be replaced by the notion of sub-differential, (Moreau, 1975). We do not consider vertex points since experiments only show rounded noses.

1.4. Fracture

1.4.1 Introduction to fracture mechanics

Fracture in solids means the appearance of a surface of discontinuity S in the medium, separating locally the solid into two parts, S with the unit outward normal **n**, S^+ with opposite normal –**n**. The surface S is called a crack. When the solid is subject to loads there is a jump of the displacement

$$[[u_i]] = u_i^+ - u_i \tag{1.44}$$

The normal jump is non negative, $[[u_n]] \geq 0$. This condition makes crack problems resembling the non linear Signorini contact problems in solids mechanics. Generally, this condition is discarded in the literature because most problems in Fracture Mechanics involve tensile loads which open the crack. We will see in Chap. 3 that condition $[[u_n]] \geq 0$ must be considered in some interface crack problems in order to avoid overlapping phenomena. Contact problems are very important in vibrations of structures. If one neglects contact problems, the response of the structure is linear. Contact problems introduce non-linearity which can be observed in the frequency spectrum, which becomes the signature of the cracked system. When the normal crack discontinuity is positive, the stress vector $\mathbf{T} = \sigma.\mathbf{n}$ vanishes on the crack.

$$T_i \equiv \sigma_{ij} n_j = 0 \tag{1.45}$$

The crack surface S generally posesses a crack front F sufficiently smooth enough for the introduction of local Cartesian frame, Ox_3 tangent to F, Ox_1x_2 normal to the crack front and Ox_1 on the crack. The deformed configurations near the crack front are displayed in three modes according to three components of the displacement discontinuity:

Opening mode I: $[[u_2]] \geq 0$

In-plane shear mode II: $[[u_1]] \neq 0$

Anti-plane shear mode III: $[[u_3]] \neq 0$.

Mode I is often observed in metallic structures, while mode II and mode III could be possible for cracks under compressive stresses in underground rocks, or in earthquake for example. Mode II is observed in the delamination of composites, or generally on weak interfaces of solids which canalize crack propagations under compression and high shear stresses. In these shear modes of fracture, stress free conditions Eq. (1.45) are no longer va-lid. Modelling the stress boundary conditions on an earthquake fault is probably the most difficult problem arising in Geophysics. Cracks appearing in solids by a true fracture inside a sound solid, or crack like surface of discontinuity at the interface of two contacting solids which move by a relative slip, in the stick-slip phenomena for example, can be analysed by methods of Fracture Mechanics. The physics of these phenomena may be different from an energetic point of views. Their mathematical analyses are practically the same

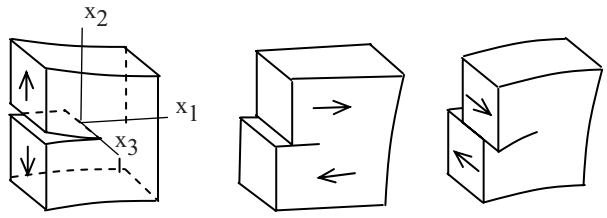

Figure 1.10: Fracture modes I (opening), II (in-plane shear), III (anti-plane shear)

1.4.2 Stress intensity factors

A fracture criterion is given by some relationship between parameters p_i which characterize the mechanical state of the crack tip zone, $f(p_1, p_2,.) = 0$ or more generally $f(p_i, dp_i/dt) = 0$ for time dependent fracture, dynamic

fracture or fatigue crack propagation. In linear elastic medium, all parameters are equivalent to the Stress Intensity Factors (SIF) governing the singular stress fields at the crack tip. The SIF are defined with respect to the orthonormal coordinates $Ox_1x_2x_3$ shown in Fig. 1.10 (I), with Ox_3 parallel to the crack front, which must be regular at the origin O. In the plane Ox_1x_2, with a cut along negative Ox_2, we search a solution of the elastic equilibrium equations $\mathrm{div}(\sigma(u)) = 0$ for the Cartesian coordinates of the displacement field u in the form $u_i = r^{\alpha} g_i(\theta)$, i = 1,2 with polar coordinates r, θ, satisfying the boundary conditions $T_i = 0$. By selecting square integrable stress fields, we get the highest singular eigensolutions with the eigenvalue $\alpha = 1/2$ for the displacements

$$u_1 = \frac{K_I}{2\mu}\sqrt{\frac{r}{2\pi}}\cos\frac{\theta}{2}(\kappa - \cos\theta) + \frac{K_{II}}{2\mu}\sqrt{\frac{r}{2\pi}}\sin\frac{\theta}{2}(\kappa + \cos\theta + 2) \tag{1.46}$$

$$u_2 = \frac{K_I}{2\mu}\sqrt{\frac{r}{2\pi}}\sin\frac{\theta}{2}(\kappa - \cos\theta) - \frac{K_{II}}{2\mu}\sqrt{\frac{r}{2\pi}}\cos\frac{\theta}{2}(\kappa + \cos\theta - 2) \tag{1.47}$$

and for the stresses

$$\sigma_{11} = \frac{K_I}{\sqrt{2\pi r}}\cos\frac{\theta}{2}\left(1 - \sin\frac{\theta}{2}\sin\frac{3\theta}{2}\right) - \frac{K_{II}}{\sqrt{2\pi r}}\sin\frac{\theta}{2}\left(2 + \cos\frac{\theta}{2}\cos\frac{3\theta}{2}\right) \tag{1.48}$$

$$\sigma_{12} = \frac{K_I}{\sqrt{2\pi r}}\cos\frac{\theta}{2}\sin\frac{\theta}{2}\cos\frac{3\theta}{2} + \frac{K_{II}}{\sqrt{2\pi r}}\cos\frac{\theta}{2}\left(1 - \sin\frac{\theta}{2}\sin\frac{3\theta}{2}\right) \tag{1.49}$$

$$\sigma_{22} = \frac{K_I}{\sqrt{2\pi r}}\cos\frac{\theta}{2}\left(1 + \sin\frac{\theta}{2}\sin\frac{3\theta}{2}\right) + \frac{K_{II}}{\sqrt{2\pi r}}\sin\frac{\theta}{2}\cos\frac{\theta}{2}\cos\frac{3\theta}{2} \tag{1.50}$$

with $\kappa = 3 - 4\nu$ in plane strain. Formulae for plane strain are exact. We recall the value $\kappa = (3 - \nu)/(1 + \nu)$ for plane stress which is generally considered for thin plate. However the corresponding formulae in plane stress, as shown in Chap. 3, are not exact. One may consider the formal solutions in plane stress as approximate solutions for non metallic medium. An evaluation of the approximation in plane stress can only be made by a comparison with a three-dimensional solution. For metallic materials, plane stress condition is questioned because there are often plastic deformations through the thickness of the specimen concentrated in inclined shear bands which violate the elasticity assumption. In the anti-plane strain case, the asymptotic solution is given by formulae

$$u_3 = \frac{2K_{III}}{\mu}\sqrt{\frac{r}{2\pi}}\sin\frac{\theta}{2} \tag{1.51}$$

$$\sigma_{13} = -\frac{K_{III}}{\sqrt{2\pi r}}\sin\frac{\theta}{2} \tag{1.52}$$

$$\sigma_{13} = \frac{K_{III}}{\sqrt{2\pi r}}\cos\frac{\theta}{2} \tag{1.53}$$

From the asymptotic solutions in modes I, II, III, one can define the SIF either by

$$K_I = \lim_{r\to 0}\sigma_{22}(r,\theta=0)\sqrt{2\pi r} \tag{1.54}$$

$$K_{II} = \lim_{r\to 0}\sigma_{21}(r,\theta=0)\sqrt{2\pi r} \tag{1.55}$$

$$K_{III} = \lim_{r\to 0}\sigma_{23}(r,\theta=0)\sqrt{2\pi r} \tag{1.56}$$

or by

$$K_I = \frac{\mu}{\kappa+1}\lim_{r\to 0}[[u_2]](r)\sqrt{2\pi/r} \tag{1.57}$$

$$K_{II} = \frac{\mu}{\kappa+1}\lim_{r\to 0}[[u_1]](r)\sqrt{2\pi/r} \tag{1.58}$$

$$K_{III} = \frac{\mu}{4}\lim_{r\to 0}[[u_2]](r)\sqrt{2\pi/r} \tag{1.59}$$

Formulae (1.50)-(1.52) are the stress definitions of SIF while formulae (1.53)-(1.55) are the kinematic definitions of SIF. Both definitions are equivalent in quasi-statics, but they give different results in elastodynamics for values of the crack speed higher than 60% of Rayleigh's wave c_R.

1.4.3 On the physics of separation

Let us briefly mention some underlying physics behind fracture at different scales, from a macroscopic scale to the atomic one, by considering some examples.

1. **A mechanical model**. Consider a simple mechanical system consisting of a linear spring of stiffness k attached to a rigid piston which moves inside a fixed hollow tube of length l, Fig. 1.11. For a piston displacement y, the resistance force τ by the cylinder is assumed to be proportional to the remaining frictional contact zone (l–y) so that the displacement of the spring x is $x - y = \tau/k = \alpha(l-y)/k$. The force-displacement curve $\tau(x)$ is then defined parametrically by $\tau = \alpha(l-y)$ and $x = y+\alpha(l-y)/k$, where y is the internal parameter. This curve is a straight line of negative slope for $0 < x < l$, beyond which the piston is getting out of the cylinder, and no force could exist for $x \geq l$. This simple model of fracture, consisting in the separation of the spring from the hollow cylinder, makes it possible to analyse the energy dissipated by friction in the process zone inside the tube. A generalization of the model accounting for threshold resistance and/or viscosity is left to the readers.

2. **The adhesive tape on a rigid substrate**. Next example is given by the pull-out of a scotch tape in common use at home or school. Here the cohesive force is given by the glue layer whose long molecules act as pistons inside hollow cylinders, at the nanoscale of the molecules. See Exercice for evaluating the fracture energy.

3. **Surface force between solid and fluid**. Consider a spherical ball lying on a rigid surface with a liquid interface and a concave meniscus of

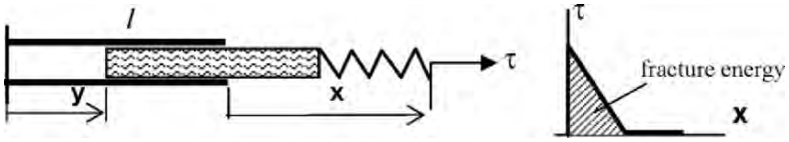

Figure 1.11: A mechanical model of fracture : a spring is attached to the piston moving with friction inside a fixed hollow tube. The total supplied energy for getting the piston outside the cylinder is called a fracture energy

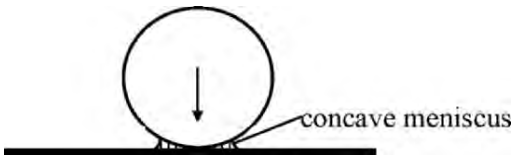

Figure 1.12: Capillary force in the fluid-solid system with concave meniscus pulling back solids together

radius R. The depressure $-p = \alpha/R$, where α is the surface tension, pulling back the spherical ball to the substrate is responsible for the cohesion of wet sands in the beach. Here the cohesive force is due to surface force or capillary force. In the convex meniscus case, the repelling force (positive pressure) sustains the heavy ball which can be easily removed from the substrate without energy other than that is necessary against gravity work.

4. **Adhesion between solids**. Van der Vaals weak attracting forces between solids are responsible for the adhesion of solids. Replacing the liquid of Fig. 1.12 by the VdV forces between solids, we obtain the model of adhesion which is worked out by Maugis and Barquins (1980) who made a perfect parallel between the separation of adhesive solids and the fracture of solids.

5. **Atomic forces**. We simply mention the force between two atoms, which is a repelling force at very short distance, then an attracting force beyond this distance. The variation around the equilibrium distance is at the origin of elasticity. Far beyond some maximum value of the attracting force, atoms are not longer tied together. This atomic description is considered in the theory of dislocations. When generalized to an array of atoms in the Peierls model of crystals, the dislocation theory explains the origin of plasticity then fracture. The origin of atomic forces may be found in electronic interactions.

1.4.4 Different types of fracture

Macroscopic observations of fracture in solids shows a variety of features which convince us that their physical mechanisms should be different. The fracture of a car glass is a well known phenomenon for drivers, but the mechanisms of the chain breaking of glass into small and regular pieces like a puzzle are not well understood. Here the driving force is the release of residual stresses induced previously by a thermal treatment, which is not

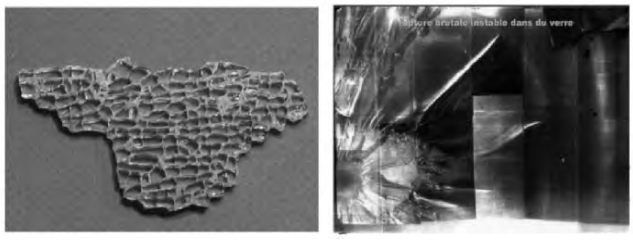

Figure 1.13: Dynamic fractures of glass (Courtesy of L. Malinsky and H. Maigre, LM.S, Ecole Polytechnique)

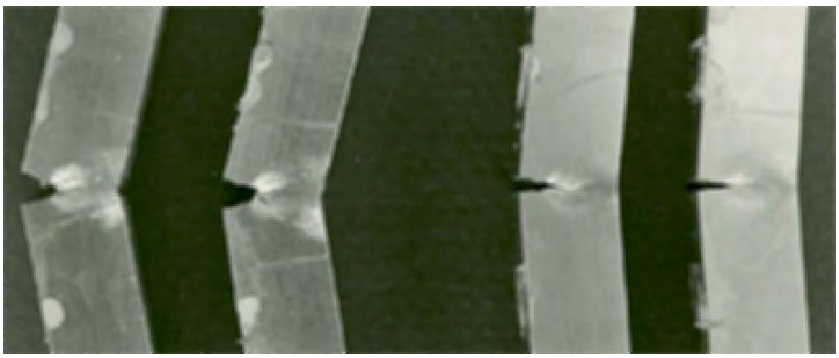

Figure 1.14: A stainless steel specimen with a fatigue crack subject to a three points bending. From the right to the left: No visible crack propagation under bending loads in photos 1 and 2. A crack deviation is observed in photo 3, inside the shear stress zone, which can be described by the slip lines fields of the theory of rigid perfect plasticity (dotted lines in the upper part of the photo 3) (Courtesy of EDF, Etudes des materiaux Department)

completely analysed. A similar phenomenon called a *thermal striping* is observed on the surface of a solid subject to cyclic loads. Another complex phenomenon is the star shaped cracking of a multi-layered glass which resists to dynamic impacts, Fig. 1.13b. There are spectacular fractures like the breaking of the Liberty ship in the 50's, at the weld zone weakened by low temperature. Another example of a spectacular fracture is the wavy shaped crack over kilometers long in a pressurized pipe under cold environment. The common feature in all these phenomena is called a *brittle fracture*. We remind the catastrophic failure of an aircraft in the 50's due to a phenomenon called a *fatigue* crack propagation. To avoid either brittle fracture or fatigue crack, one designs nuclear vessels with stainless steel which requires much more energy for propagating a crack. Crack propagations in such materials are studied in *ductile fracture* mechanics, with methods completely different from those considered in brittle fracture or in fatigue. In brittle fracture, crack generally propagates under mode I. In ductile fracture, as shown in photo 3 of Fig. 1.14, crack can propagate in mode II, in the shear stress zone. Fatigue crack propagation also exists in mode II, for a short while AB, Fig. 1.15.

A classification of different types of fracture can be made by comparing the magnitude of plastic deformation. Brittle fracture is characterized by the quasi-absence of plasticity in the load-displacement curve up to the rupture point. On the contrary, the curve for ductile fracture shows a non-

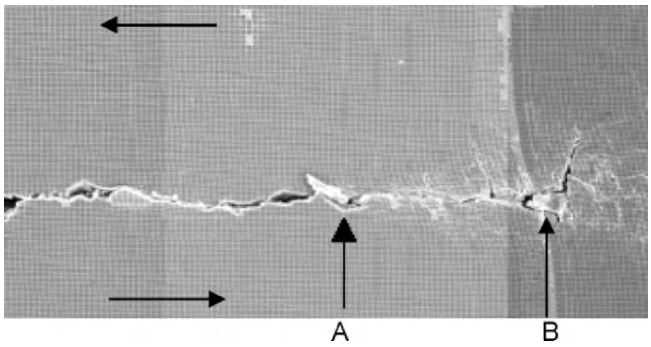

Figure 1.15: Fatigue propagation in metals in shear mode $K_{II} < 0$. Crack tip A is first obtained by a mode I fatigue. AB is the fatigue crack propagation in mode II. At B, crack deviates in a direction predicted by brittle fracture mechanics (Courtesy of Ch. Pinna and V. Doquet (1999), CNRS/LMS/Ecole Polytechnique)

linear behavior, with a large plastic deformation before the appearance of crack propagation. Most of the supplied energy is dissipated by plasticity inside the specimen. The load-displacement curve of a three-points bending specimen in stainless steel shows a large plastic deformation before crack propagation by intense shear loads. Very often, a cracked bending specimen of stainless steel undergoes a larger plastic deformation than that shown in Fig. 1.14, without ensuing crack propagation.

Fatigue crack propagation under cyclic loadings is characterized by two phenomena. Outside a thin zone near the crack faces of the order of some grain size, there is no observable plastic deformation. In a thin zone, near the crack faces, microscopic observations indicate that the *cumulated* plastic deformations p during N cycles

$$p = \sum_{i=1}^{N} \left| \varepsilon^p(i) \right| \tag{1.60}$$

should be very high, while the total plastic deformation at each material point could be negligible $\sum_{I\ 1,N} \varepsilon^p(i) = 0$. This is the microscopic counterpart of a phenomenon observed at the macroscopic scale of a specimen subject
to cyclic loadings, called a *plastic shakedown*. The mean plastic strain at plastic shakedown does not change significantly while the cumulated plastic strain increases with the number of cycles N.

For a higher cyclic load, plastic shakedown progressively becomes a *racheting* phenomenon with the increase of both the mean value of plastic deformation and the cumultated one. Plastic shakedown and rachetting

phenomenon explains the rate form of the fatigue crack propagation and its acceleration. A log-log plot of da/dN (crack growth per cycle) versus ΔK_I (the variation of the SIF during the cycle) typically shows three phases. The first phase is characterized by a fatigue crack initiation above a threshold value. The second phase corresponds to a stable propagation, known as the *Paris law* with m between 2 to 5 for steel

$$\frac{da}{dN} = C\,\Delta K^{m} \qquad (1.61)$$

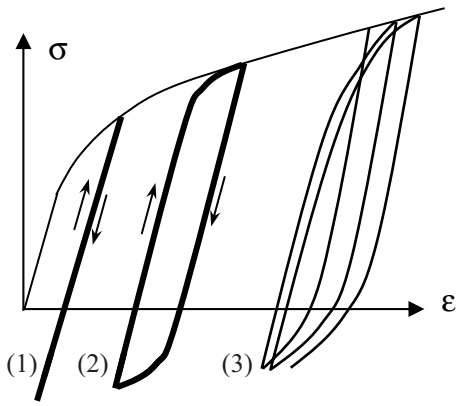

Figure 1.16: Cyclic loadings on a metallic specimen: (1) elastic shakedown; (2) plastic skakedown; (3) rachetting

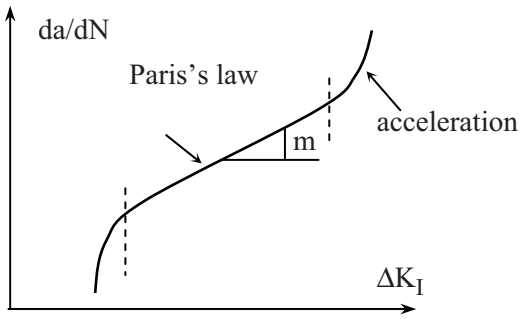

Figure 1.17: Fatigue crack propagation. A log-log plot of da/dN function of the load ΔK_I

The third phase indicates an acceleration of the fatigue crack propagation. The Paris law (1.61) does not apply to short cracks initiated at the free surface of the body. Perhaps, for short cracks under fatigue loadings plastic dissipation mechanisms may be considered, as in *Cherepanov's model* (1968).

Fatigue of metals under applied cyclic loadings with maximum stress amplitude S is characterized by the S-N curve, relating the number of cycles at rupture under S, Fig. 1.18. Below some threshold stress S_0, there is practically no rupture. The S-N curve obtained by a tension test specimen is not actually an intrinsic material property. By changing both the magnitude of the stress S and the mean applied stress σ_m one observes different threshold stress S_0. *Dang Van's criterion* (1999) is based on a local approach to fatigue rupture, Fig. 1.19

$$\max_t \left[\tau(t) + a\sigma_m(t)\right] < b \tag{1.62}$$

where a and b are simply determined by two different tests, $\tau(t)$ is the maximun shear stress at point **x**. In the (σ_m, $\tau > 0$) half-plane the actual loading curve ($\sigma_m(t)$, $\tau(t)$) of any structure can be compared with the safety criterion at different point **x**.

Dang Van's criterion requires numerical calculation of the structure under thermo-mechanical cyclic loads. New methods of asymptotic solutions (for $t \to \infty$), or large time increment, are particularly suitable for the application of Dang Van's criterion to real structures. (See Maitournam et al (2002) for a direct calculation of the limit cycle and Ladevèze (1998) for a rapid solution by the method of large time increment).

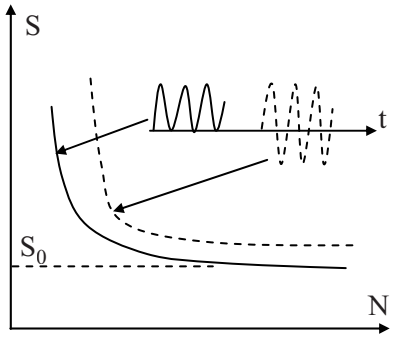

Figure 1.18: The S-N curve in high cyclic fatigue; S-N curve is sensitive to specimen geometry and cyclic loadings

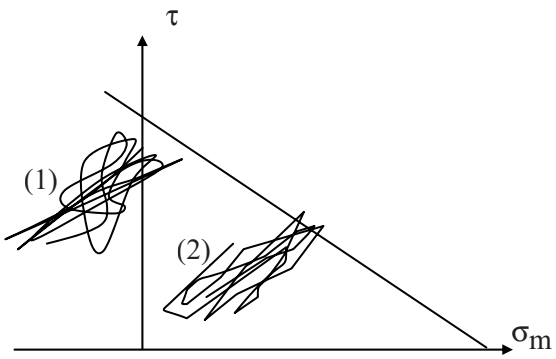

Figure 1.19: Dang Van's criterion in high cyclic fatigue; (1) safe cyclic load history; (2) unsafe cyclic load history

1.4.5 Brittle fracture criterion

In mode I, most theories predict a brittle fracture at a critical value of SIF, $K_I = K_{Ic}$.The constant K_{Ic} is the *toughness* of the material. The experimental determination of the toughness follows some normalized procedure given in ASTM codes which define the geometry of the specimen (Compact Tension Specimen) and the loading conditions. The specimen must have some valid thickness $B > B_0 = 2.5(K_{Ic}/\sigma_0)^2$, for which the plastic zone at the crack tip can be neglected, Fig. 1.18. Below a minimum value B_0, experimental K_I are not constant, much more higher than the plateau value. There are some reasons for this feature: first a thin specimen cannot be in plane strain state, second there is a plastic deformation by inclined shear slips through the specimen. In linear elasticity, for a given crack geometry, the stress or displacement fields, and thus the SIF are linear with respect to the load, but *non linear* with respect to the crack length. It should be noted that words like "linear fracture mechanics" are not adequate since fracture in linear elastic material is essentially a non linear phenomenon. A dimensional analysis shows that K_α has the dimension of a stress times the square root of a length. Typical values of K_{Ic} for steel are about 50-200MPa$\sqrt{m}$. There is another condition for the validity of brittle fracture. It is concerning the crack length l and the radius R of the plastic zone at the crack tip which must be small $R << l$ (*small scale yielding* assumption). Experiments suggest the condition $2.5(K_{Ic}/\sigma_0)^2 < l$.

Chapter 2

Energetic Aspects of Fracture

Griffith was the first to consider fracture in solids as a physical process which requires energy to create additional crack surface. This chapter examines some macroscopic consequences of Griffith's model. Consider a cracked solid Ω subject to some loads on its external boundary S_{ext}. As illustrated by some examples in Chap. 1, fracture can be obtained by applying some internal forces between crack surfaces $S^{\pm}$ to be created from the initial configuration to the final one, when a complete separation of particles occurs. In the macroscopic point of view, the details of what happens between $S^{\pm}$ are not essential. Only some energetic aspects of relevant features in $S^{\pm}$ are important for modelling fracture.

The separation energy averaged over the fracture surface per unit is called a *surface energy*.

2.1 Griffith's theory of fracture

During a crack advance of the area amount δS, the supply of energy for fracture being δW_S, the solid geometry changes as well as stored elastic strain energy δW_{elast}, kinetic energy δW_{kin}, potential energy of external loads δW_{ext} (equal to minus the work done by the external force $-\int \mathbf{F}.\delta\mathbf{u}$). Griffith postulated that $\delta W_S = 2\gamma\delta S$ and that the total energy does not change

$$\delta W_{tot} \equiv \delta W_{elast} + \delta W_{kin} + \delta W_{ext} + \delta W_S = 0 \tag{2.1}$$

Suppose that an equilibrium state is reached for a stationary crack S, with the external load **F** so that any infinitesimal change of the equilibrium state with $\delta S > 0$ under $\delta W_{kin} = 0$ implies

$$\delta W_{elast} + \delta W_{ext} + 2\gamma\delta S = 0 \tag{2.2}$$

This is the criterion of crack initiation at the equilibrium state of the solid at rest just at some critical load.

$$-\frac{\delta}{\delta S}\{\quad_{elast}+\quad_{ext}\}=2\gamma \tag{2.3}$$

Defining the quasi-static *energy release rate* by $G = -\delta(W_{elast}+W_{ext})/\delta S$, one gets the crack initiation criterion as $G = 2\gamma$. Crack propagation under $\delta W_{kin} = 0$ is called a controlled or stable propagation.

Suppose now that during a crack propagation $W_{kin} > 0$, one wishes to know whether the propagation is globally stable or not, in the sense that whether $\delta W_{kin} < 0$ or $\delta W_{kin} > 0$. A decrease or an increase of kinetic energy δW_{kin} should indicate the stability or instability of the whole cracked system, which is more or less under control, at least at the beginning of crack propagation. The global criterion of stability adopted here is different from a local stability criterion, for instance in a two-dimensional problem, which involves the rate of change of the crack velocity da/dt.

Local instability or stability means acceleration or deceleration of the crack.

In a three-dimensional problem, another kind of stability may be considered for the crack shape front which may have either a regular geometry or a wavy shaped geometry, both geometries being two possible responses of the cracked solid under the same global energy release rate. Such kind of geometric instability is considered in bifurcation problems related to second derivatives of the potential energy, $\delta G/\delta S = 0$ with respect to governing parameters of S. Therefore, there may be different points of views when one deals with stability in fracture mechanics. Here global instability criterion considered is related to the excess of energy release rate over 2γ

$$G > 2\gamma \qquad \Rightarrow \qquad \delta W_{kin} > 0 \tag{2.4}$$

which can be transformed in either kinetic energy or fracture energy to provide an additional propagation or both energies. Further analyses of energies by Berry (1960) show how global and local stability or instability are related to each other. In dynamic fracture, kinetic energy is so important an energy that the balance equation of energy leads to another definition of the energy release rate including the kinetic energy, as the *flux of energy*, (Freund, 1990)

$$F = -\frac{d}{dt}\{\quad_{elast}+\quad_{ext}+W_{kin}\} \tag{2.5}$$

The balance of equation reads $F = D$, where the *fracture dissipation rate* is $D = 2\gamma da/dt$ in Griffith's theory and $F = Gda/dt$ (two-dimensional problems). Eq. (2.5) is related to the rate of energy change of the cracked solid, outside the process zone, while D is the relevant feature of the inside of the

process zone. The new point of views enables us to consider different theories of three-dimensional fracture in which dissipation rate D(φ) depends on the crack front velocity φ which may be different from Griffith's model.

2.2 Some expressions of G in quasi-statics

Consider states of plane strain for analysing energy in quasistatic crack propagation. Further analyses will focus on dynamic crack propagation (Chap. 5). The external boundary consists of two parts, S_T where the stress vector $\mathbf{T}^d$ is prescribed and S_u where the displacement $\mathbf{u}^d$ is prescribed. We look at the change of stored elastic energy and works done by forces when the crack length changes by an amount da, not necessarily in the same direction of the main crack.

The energy release rate per unit thickness of the solid is

$$G = -\frac{d}{da}\int_\Omega W(\varepsilon)d\omega + \int_{S_T} T_i^d \frac{du_i}{da} ds = -\frac{d}{da} P \tag{2.6}$$

with P the *potential energy*. The derivative of the strain energy is given by

$$\frac{d}{da}\int_\Omega \tfrac{1}{2}\sigma_{ij}\varepsilon_{ij}d\omega = \tfrac{1}{2}\int_S \{T_i \frac{du_i}{da} + u_i \frac{dT_i}{da}\} ds$$

Combining the above equations, taking account of $du_i/dt = 0$ on S_i, one obtains the energy release rate as

$$G = \tfrac{1}{2}\int_S \{T_i \frac{du_i}{da} - u_i \frac{dT_i}{da}\} ds$$

$$G = \tfrac{1}{2}\int_{S_T} T_i^d \frac{du_i}{da} ds - \tfrac{1}{2}\int_{S_u} u_i^d \frac{dT_i}{da} ds \tag{2.7}$$

Eq. (2.7) derived for a stress free crack is also valid for a frictionless contact crack. The reasons are the following ones. In contact zones, normal and shear stresses are continuous so that stress vectors on $S^\pm$ are opposite to each other, $\mathbf{T}^+ = -\mathbf{T}^-$. Among contributions to G from δΩ there are terms from the crack surface S, for instance

$$\mathbf{T}^+.d\mathbf{u}^+/da + \mathbf{T}^-.d\mathbf{u}^-/da = T_t^+ d(u_t^+ - u_t^-)/da + T_n^+ d(u_n^+ - u_n^-)/da$$

which vanishes because of the frictionless contact $T_t^+ = 0$ and the contact condition $[[u_n]] = u_n^+ - u_n^- = 0$.

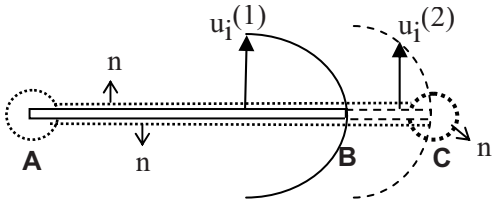

Figure 2.1: Path integration along the crack avoiding crack tips A and C by small circles, with inward normal **n**; Displacement $\mathbf{u}^{(1)}$ near tip B prior to crack propagation; Displacement $\mathbf{u}^{(2)}$ near tip B, after crack advance d*l*; Crack tip A is fixed

2.3 Irwin's formula

Let us consider another formula equivalent to Eq. (2.7). First, consider the Betti reciprocal theorem for any pair of elastic fields (**u**,**T**) and (**u***,**T***) which can be expressed by the zero-valued of the integral

$$\oint(\mathbf{T}.\mathbf{u}^* - \mathbf{T}^*.\mathbf{u})ds = 0 \tag{2.8}$$

for any closed curve S. Therefore, considering the rate fields (d**u**/da, d**T**/da) as the star fields, we can change the integral over S in the one involving any other contour encircling the crack with inward normal **n** to the elastic domain. One contour may be of interest for the calculation of G. It consists of the limiting contour along the crack faces and two small circles around the crack tips A and C.

Consider the incremental form of G with the latter contour

$$G\delta a = \tfrac{1}{2}\int(\ {}_i\delta u_i - u_i\delta T_i)ds \tag{2.9}$$

Using the singularities of stress and displacement before (state 1) and after crack advance (state 2), it is not difficult to show that the only non zero contribution to the latter integral comes from terms along $(BC)^+$ $(BC)^-$

$$G\delta a = \tfrac{1}{2}\int_{BC} T_i^{+(1)}(u_i^{(2)+} - u_i^{(2)-})ds = \int_{BC} T_i^{+(1)}[[u_i^{(2)}]]ds \tag{2.10}$$

G given by Eq. (2.10) can be evaluated using the stress and displacement fields near the crack tip given in Chap. 1, with the stress intensity factors of states (1) and (2).

In mode I, with coordinate axes at tip B, the asymptotic expressions of normal stress and displacement at S^+ to be considered are

$$\sigma_{22}^{(1)}(x_1) \cong K_I \frac{1}{\sqrt{2\pi x_1}} \qquad (x_1 > 0)$$

$$u_2^{(2)}(x_1) \cong K_I \frac{\kappa+1}{2\mu\sqrt{2\pi}} \sqrt{2\pi(dl - x_1)} \qquad (x_1 < dl)$$

In plane strain mode I, Eq. (2.10) yields the Irwin formula

$$G = \frac{1-\nu^2}{E} K_I^2 \tag{2.11}$$

In mixed modes I +II+III the Irwin formula is

$$G = \frac{1-\nu^2}{E}(K_I^2 + K_{II}^2) + \frac{1}{2\mu} K_{III}^2 \tag{2.12}$$

Brittle fracture, in plane strain mode I, is characterized by the toughness K_{Ic} which is related to the Griffith surface energy by

$$K_{Ic} = \sqrt{\frac{2\gamma E}{1-\nu^2}} \tag{2.13}$$

It should be noted that modes I and II appear in Eq. (2.12) symmetrically. However, physically at a macroscopic scale, mode I fracture is generally observed in a homogeneous metallic solid, except when there are concentrate symmetric shear bands starting from the crack tip.

For instance in a three-point bending specimen, crack propagation in a symmetrical mode I requires much more energy than a dissymmetric propagation in mode II observed along shear bands, as shown in Fig. 1.14, Chap. 1.

Mode II fracture is observed along shear slip planes in crystals, Fig. 2.2, and also in fatigue crack propagation as observed by Pinna and Doquet (1999), Fig. 1.15.

Except these particular cases of mode II fracture, an existing crack in mode II loading generally deviates from its original direction and then propagates in a direction which corresponds to the opening mode I fracture. This is true for brittle fracture. Therefore, it is important to derive formulae to calculate stress intensity factors *after* deviation from stress intensity factors *before* deviation, which are not the same. Stress intensity factors are defined with respect to axes along the crack. After deviation, the new axes has to be considered to evaluate displacement and stress components.

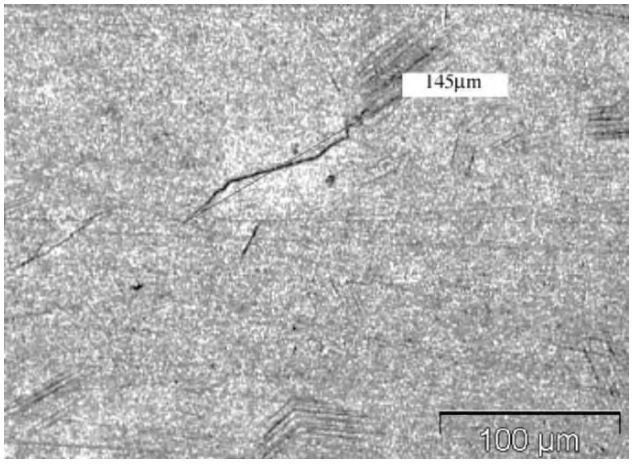

Figure 2.2: A shear mode II crack joining microcracks initiated along slip planes in Fe. Multiple slips at the bottom of the figure (Courtesy of S. Taheri, EDF)

2.4 Barenblatt's cohesive force model

Consider a crack propagation under constant $K_I = K_{Ic}$. Upon magnifying the process zone, Barenblatt considered that the separation of particles occurs in a very short distance $d \ll a$, under non linear attractive cohesive force $F([[u_n]])$. In moving coordinate, force F first increases then decreases to zero. A constant K_I implies one of the following equivalent models:

i). Constant asymptotic near fields, or Griffith-Irwin's model

ii). In moving coordinates with the crack tip M = (0, 0), existence of an *autonomous* function $F(x_1)$ in the cohesive zone $-d < x_1 < 0$, with fixed d. By introducing Bueckner's weight function $k(x_1, M)$ which determines the SIF at the crack tip M, by a pair of opposite unit point loads at x_1, one gets the stress intensity at the crack tip M as ($\phi = [[u_n]]$)

$$K_I(M) = \int_0^d k(x_1, M) F(\phi(x_1)) = K_{Ic}.$$

This model has been introduced by Barenblatt (1962) in order to remove stress singularity.

iii). In fixed coordinate axes, suppose that $\delta a \gg d$, the work done by cohesive forces per unit crack propagation length is constant

This is the model introduced by Willis (1967) who showed that it implies G = const. The latter equation results from Eq. (2.10) where the right hand side of the equation is replaced by the stress working by cohesive forces on δa, thus equal to

$$\int_{[0,d]} \mathrm{F}([[\mathrm{u_n}]])d[[\mathrm{u_n}]] = const.\delta \mathrm{a} \ .$$

2.5 Berry's interpretation of energies

Consider a cracked elastic solid with the crack length l, subject to a 1D-parameter loading. Let Q-q be the quasi-static load-displacement curve. The curve Q-q is a straight line as long as $K_I(l) < K_{Ic}$. The domain of the (Q,q) plane defined by $K_I(l) < K_{Ic}$ is bounded by a curve Γ parameterized by l which is called an *equilibrium curve*. The larger the crack length, the lower the slope Q/q. The equilibrium curve shape depends on the geometry of the cracked solid and on the toughness. Typically, as shown by Bazant and Cedolin (1991), the system consisting of a cracked solid and an elastic spring representing the testing machine has a monotonically decreasing equilibrum curve when the machine is stiff. The equilibrium curve can have a snap-back when it is soft.

What happens when the loading curve Q-q is going beyond the equilibrium curve Γ at some point?

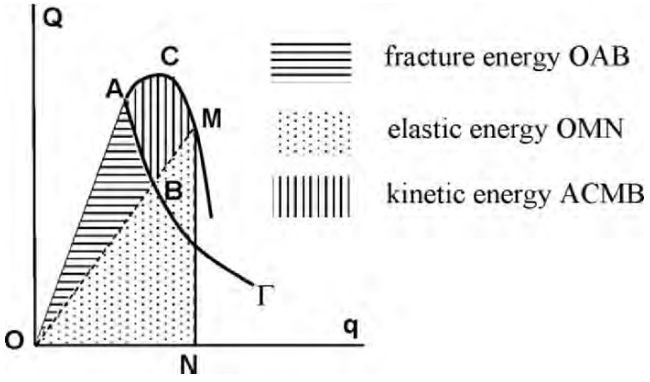

Figure 2.3: The equilibrium curve Γ is defined by the quasi-static criterion $K_I(l) = K_{Ic}$. Stiffness OA is associated to the initial crack length l_0. Stiffness OB is associated to a larger crack length l. The loading path ACM is associated to a propagating crack with the crack length l corresponding to the stiffness OB

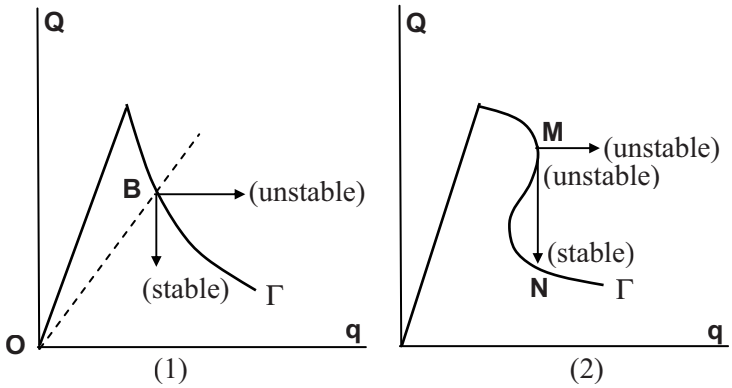

Figure 2.4: The equilibrium curve Γ for a stiff system (1) and for a soft one (2) showing a snap-back, (Bazant and Cedolin, 1991). Prescribed loading Q = const at B or M is fundamentally unstable because of unlimited increase of kinetic energy. Prescribed displacement q = const at B is stable. Prescribed displacement at M is first unstable then, after a snap-through, becomes stable at point N

The equilibrium state with the initial stationary crack length l_0 is no longer valid beyond Γ. Therefore, either crack propagates or kinetic energy has to be considered, or both cases are possible. Only a dynamic analysis of the cracked solid, with a known or given crack history l(t), can determine different energies in a crack propagation.

We shall consider in Sect. 2.6 the *inverse energetic problem* for a stationary unknown crack and the case of dynamic crack propagating will be considered in Chap. 5. Here, we focus on Berry's model which provides an approximate but useful interpretation of energies involved in the case where the loading point (Q, q) is beyond the equilibrium curve, under some assumption on the crack history. First, consider a quasi-static loading Q-q such that crack propagates from l_0 (point A) to l (point B) so that the loading point (Q, q) is along the equilibrium curve Γ. Eq. (2.9) shows that $G(l - l_0)$ is nothing but the area of the shadowed curved triangle OAB.

Second, suppose that a load-displacement curve is along OACM, Fig. 2.3. Assume that the crack length at point M is given by the one which corresponds to the stiffness OB of the equilibrium curve Γ . Energy considerations and the balance equation of energy show that:

1) OACMN is the total energy provided by the external load,

2) OMN is the stored elastic energy by the cracked system with the crack length l(B),

3) OABO is the total Griffith surface energy

4) ACMB is the total kinetic energy at M.

Berry's model provides a simple stability analysis of crack propagation just after crack initiation.

Unstability considered here corresponds to the unlimited increase of kinetic energy, as explained in Fig. 2.4.

2.6 Stability analysis of multiple cracks

In fatigue cracking of metals under mechanical and thermal cycles, there is a phenomenon called a thermal striping which consists of a series of edge cracks of equal length, spaced at nearly equal interval 2b.

To understand thermal striping, let us consider a simple experiment of fracture (which can be performed in a class-room) on a sheet of a A4 paper of width 5 cm. Make first a symmetric cut A of 2 cm at 6 cm from one end, then two other cuts B and C of the same length 2 cm at respectively 6.5 cm and 6 cm from the other end. Second pull the sheet apart and observe its fracture. At first sight, fracture should occur at the weakest zone, near B and C, but it actually occurs at A, because brittle fracture predicts a stress intensity factor higher at A than the ones at B, C.

The interaction between cracks B and C mutually lowers the stress in the vicinity of each crack tip. The higher the number of cracks, the lower the stress intensity factor, for the same crack length.

The number of cracks per unit length on the stress free surface is $N \propto a/2b$. The number N is the entire part of the ratio $N = a/2b$. Assume that the cracks have the same depth a and that an uniform tensile stress σ_{22} is applied at infinity, Fig. 2.5b.

The solution for the stress intensity factor has been given by Bowie (1973), Sih (1973) as $K_I(a/2b) = f(a/2b)\sigma(\pi a)$, where the function f(.) has been numerically evaluated. From their numerical solution, for a fixed crack length a, we get the limiting values at low b

$$f^2(a/2b) \to \frac{\pi b}{a} \qquad (\text{as } b \to 0) \tag{2.14}$$

and at large b

$$f^2(a/2b) \to (1.12)^2 \quad (\text{as } b \to \infty) \tag{2.15}$$

This limit value corresponds to that of an isolated edge crack for which the stress intensity factor is $K_I = 1.12\sigma\sqrt{(\pi a)}$.

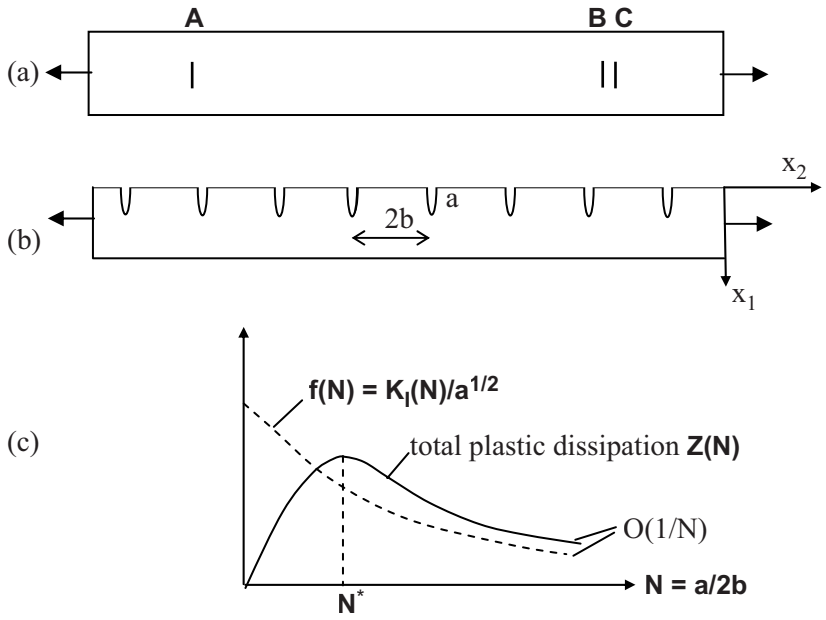

Figure 2.5: (a) A sheet of paper with three cuts A, B, C. The weakest zone seems to be at B and C. Surprisingly, fracture occurs at A; (b) N(= a/2b) edge cracks per unit length spaced at the same interval; (c) Bowie's functions $f(N) \equiv K_I/\sqrt{(\pi a)}$ in dotted line, the total plastic dissipation per unit length is Z(N), in continuous line

Thermal striping deals with very short cracks for which Griffith's criterion does not apply to metals without some modification. One can consider first plastic dissipation for one crack, then for the system of N cracks. Some models exist for describing the mechanisms of dissipation, for instance Cherepanov's model (1968), Bui and Ehrlacher's model (1981). The last model, using a damage theory in plasticity confirms the former one. Cherepanov's model is based on some estimation of plastic dissipated energy dW_p and fracture energy dW_F. For a crack advance da, the first term dW_p should be proportional to the variation of the active plastic zone area

$$dW_p \propto d(\pi R^2),$$

with the radius of the circular plastic zone R proportional to K_I^2 (take R satisfying $K_I = \sigma_0\sqrt{(\pi R)}$)

$$dW_p \propto AK_I^3\, dK_I \qquad (2.16)$$

The second term should be proportional to the area of the wake plastic zone 2Rda or

$$d_F \propto BK_I^2\, da \tag{2.17}$$

Eqs. (2.16) and (2.17) will be justified by an analytical model of plasticity and damage, Chap. 4. Thus Griffith's model is generalized by Cherepanov (1968) as $dW_p + dW_F = 2\gamma da$. Using Eqs. (2.16), (2.17) one gets a differential equation which, upon an integration, provides the *resistance curve* $a(K_I)$

$$a - a_0 = -\frac{AK_I^2}{2B} - \frac{A\gamma}{B^2}\log\{1-\frac{BK_I^2}{2\gamma}\} \tag{2.18}$$

For an edge crack initiated at the free surface $a_0 = 0$, because of small crack length, K_I is small. Thus, according to Eq. (2.18), the fatigue crack propagation law of short crack takes the form

$$a \cong \frac{A}{8\gamma}K_I^4 \tag{2.19}$$

This equation explains why nothing happens to a structure during a fatigue loading during almost its lifetime and that only a visible edge crack is observed long time after loading. Remark that, in a small scale yielding, by replacing K_I by ΔK_I and $(a-a_0)$ or more generally $a_n - a_{n-1}$ in Eq. (2.18) by da/dN (crack advance per cycle) we recover the Paris law of fatigue with m = 4. Also some model based on the so-called Weibull statistics predicts a probability of fracture $P \cong K_I^4$, Pineau (1992). Therefore, Cherepanov's model (2.18) can be considered either a resistance curve without threshold, or a fatigue law. From (2.16), the total energy dissipated by plasticity for one crack is $_{plast} \cong K_I^4$. Therefore for N cracks, it is $Z(N) \propto \sigma^4\pi^2a^2Nf^4(N)$. For large N (as $b \to 0$), Eq. (2.14) shows that $f^2(N) \propto 1/N$, hence function Z(N) behaves like 1/N

$$Z(N) \propto O(\frac{1}{N}) \quad \text{(large N)}$$

while for small N, according to Eq. (2.15), $f^2(N) \propto$ const, hence Z is a linear function of N

$$Z(N) \propto O(N) \quad \text{(small N)}$$

The curve Z(N) shown in Fig. 2.5c indicates that there is a maximum of energy dissipated per unit length corresponding to some N^*. This model supports the idea following which the observed multiple crack configuration

corresponds to the maximum of dissipation of energy, or the minimum of the total free energy of the system (per unit length). The model justifies an equilibrium configuration of identical cracks spaced at the same interval $2b^* = N^*a$, for fixed a and σ, $-\partial P/\partial b = 0$. However it does not tell us about the stability of the system, when b^* is fixed. Stability considerations of the multiple cracks configuration, as done in (Nemat-Nasser et al, 1980; Nguyen 1984, 2000; Nguyen et al, 1990; Stolz, 1990; Suo and Combescure, 1989), require the knowledge of *second derivatives* of the potential energy $-\partial^2 P/\partial l_i \partial_j$. This derivative indicates the influence of the propagating crack (j) on the energy release rate in the crack (i) propagation. A negative value of the second derivative $-\partial^2 P/\partial l_i \partial_j$ means that crack propagation (j) inhibes crack (i) and vice versa since the second derivative is symmetric. The observed stable configuration of multiple cracks is that corresponds to $-\partial^2 P/\partial l_i \partial_j = 0$ for any (i), (j). Probably for uniform stress σ_{22} in a semi-infinite half-plane $x_1 > 0$, the multiple crack system is unstable. Nguyen et al (1990) found that a system of two cracks in a strip subjected to uniform tension is unstable, in the sense that when $-\partial^2 P/\partial l_1 \partial_1 > 0$ it implies $-\partial^2 P/\partial l_1 \partial_2 < 0$ and vice versa. When the applied stress decreases with increasing depth ($d\sigma_{22}/dx_1 < 0$), one can expect that the system of multiple cracks becomes stable when the crack lengthes reach a compressive stress zone. Suo and Combescure (1992) considered an infinite periodic system of cells containing two cracks in each cell, subject to uniform tension. They got the same instability result.

2.7 An inverse energetic problem

The problem of determining stored elastic and kinetic energies, for a stationary crack is now considered for a three-dimensional elastic solid, with a frictionless stationary crack. When the crack is *known*, as well as prescribed loads, the initial boundary value problem is a well-known forward one whose solution determines both mechanical fields and energies, thus nothing is new. Perhaps, a novelty should be on the consideration and treatment of dynamic frictionless contact crack. But we do not consider this contact problem, even if it is very important for applications. The problem examined here is to determine stored and kinetric energies when the crack is *unknown*. This is an inverse energetic problem, in the usual terminology of applied mathematics, which requires additional data for the solution. Those are the pair of boundary data $(\mathbf{T}, \dot{\mathbf{u}})$, prescribed loads $\mathbf{T}$ *and* measured velocity $\dot{\mathbf{u}}$ on $S_{ext} \times [0,t]$.

When the solid is subject to dynamic loads, it is sometimes important to know the ratio kinetic energy/stored elastic energy which is a function of time. In some industrial applications, for instance for saving energy, one wishes to control the process in order to minimize the kinetic energy lost by heating and heat conduction. Conversely, in some applications one maximizes the kinetic energy of fracture debris. Let us show how to solve the energetic inverse problem.

We follow the work of Brun (1969) who solved the same problem in an uncracked solid and we apply his results to a cracked system. The unknown frictionless crack is S. The elastic energy and kinetic energy are respectively

$$W_{elast} = \tfrac{1}{2} \int_{\Omega} \sigma_{ij} \varepsilon_{ij} d\omega \tag{2.20}$$

$$W_{kin} = \tfrac{1}{2} \int_{\Omega} \rho \dot{u}_i \dot{u}_i d\omega \tag{2.21}$$

Conservation of energy is written as

$$W_{elast} + \quad _{kin} = \int_{S_{ext}} \int_0^t T_i(\mathbf{x}, \tau) \dot{u}_i(x, \tau) dS d\tau \tag{2.22}$$

The conservation law (2.22) is also valid for a frictionless contact crack, because either $\mathbf{T} = \mathbf{0}$ in the opening zone, or $T_t^+ = 0$ (tangential stress) and $[[u_n]] = u_n^+ - u_n = 0$ in the frictionless contact zone.

To calculate the energies separately we need another independent equation. Let us consider *causal* continuous functions of time f(t), which are identically zero for time $t \leq 0$. For any causal function f(t) let us introduce the time integral operator

$$\int_t (.) d\tau := \int_0^t (.) d\tau - \int_t^{2t} (.) d\tau \tag{2.23}$$

which is the difference between two integrals over different time intervals. The following identities can easily be checked

$$\int_t f(2t - \tau) f(\tau) d\tau = 0 \tag{2.24}$$

$$\int_t f(2t - \tau) \dot{f}(\tau) d\tau \equiv f^2(t) \tag{2.25}$$

$$\int_t \dot{g}(2t - \tau) g(\tau) d\tau \equiv -g^2(t) \tag{2.26}$$

To obtain $g^2(t)$ defined by the right hand side of Eqs. (2.25), (2.26), in the time interval [0, t] one needs function $f(\tau)$ defined in the *double* time interval [0, 2t]. In what follows, for simplicity, we omit variables **x** in causal functions $g(\mathbf{x}, t)$.

Multiplying the equation of motion of the first field $\mathbf{u}^{(1)}(t_1)$ at time t_1 by the velocity of the second field $\mathbf{u}^{(2)}(t_2)$ at time t_2, we obtain

$$\int_\Omega u^{(1)}_{i,j}(t_1) L_{ijhk} \dot{u}^{(2)}_{h,k}(t_2) d\omega + \int_\Omega \rho \ddot{\mathbf{u}}^{(1)}(t_1).\dot{\mathbf{u}}^{(2)}(t_2) d\omega =$$

$$= \int_{S_{ext}} \mathbf{T}^{(1)}(t_1).\dot{\mathbf{u}}^{(2)}(t_2) dS \tag{2.27}$$

First we take the same function $\mathbf{u}(\tau)$ at different times $t_1 = 2t-\tau$, $t_2 = \tau$, second we apply the integral operator $\int_t$ to (2.27). Using Eq. (2.25) and the symmetry of the moduli tensor, we can express the first term of (2.27) as

$$\int_\Omega d\omega \int_t u_{i,j}(2t-\tau) L_{ijhk} \dot{u}_{h,k}(\tau) d\tau \equiv$$

$$\equiv \tfrac{1}{2} \int_\Omega d\omega L_{ijhk} \int_t \{u_{i,j}(2t-\tau)\dot{u}_{h,k}(\tau) + u_{h,k}(2t-\tau)\dot{u}_{i,j}(\tau) d\tau =$$

$$= \int_\Omega L_{ijhk} u_{i,j}(t) u_{h,k}(t) d\omega = 2 \quad _{elast} \tag{2.28}$$

and using (2.26), we can express the second term of (2.27) as

$$\int_\Omega d\omega \int_t \rho \ddot{\mathbf{u}}(2t-\tau).\dot{\mathbf{u}}(\tau) d\tau = -\int_\Omega \rho \dot{\mathbf{u}}\,\acute{}\,t\grave{}\,.\dot{\mathbf{u}}(t) dS = -2W_{kin}$$

Finally, applying the integral operator $\int_t$ to Eq. (2.27) we obtain

$$W_{elast} - W_{kin} = \tfrac{1}{2} \int_{S_{ext}} \{\int_0^t - \int_t^{2t}\} \mathbf{T}(\mathbf{x}, 2t-\tau).\dot{\mathbf{u}}(\mathbf{x}, \tau) dS d\tau \tag{2.29}$$

Eqs. (2.22), (2.29) solve the inverse energetic problem. Eq. (2.29) is valid for a frictionless contact crack too. Given external boundary data **T**, $\dot{\mathbf{u}}$ in the time interval [0,T], one can calculate the elastic energy $W_{elast}(t)$ and the kinetic energy $W_{kin}(t)$ of the solid Ω containing an unknown crack, separately, in the half time interval $[0, \frac{1}{2}T]$

$$W_{elast}(t) = \tfrac{1}{2} \int_{S_{ext}} \int_0^t \mathbf{T}(\mathbf{x}, \tau).\dot{\mathbf{u}}(\mathbf{x}, \tau) dS d\tau -$$

$$- \tfrac{1}{4} \int_{S_{ext}} \{\int_0^t - \int_t^{2t}\} \mathbf{T}(\mathbf{x}, 2t-\tau).\dot{\mathbf{u}}(\mathbf{x}, \tau) dS d\tau \tag{2.30}$$

$$W_{kin}(t) = \tfrac{1}{2} \int_{S_{ext}} \int_0^t \mathbf{T}(\mathbf{x}, \tau).\dot{\mathbf{u}}(\mathbf{x}, \tau) dS d\tau +$$

$$+ \tfrac{1}{4} \int_{S_{ext}} \{ \int_0^t - \int_t^{2t} \} \mathbf{T}(\mathbf{x}, 2t - \tau).\dot{\mathbf{u}}(\mathbf{x}, \tau) dS d\tau \qquad (2.31)$$

Eqs. (2.30), (2.31) has been derived by Brun (1969) for an uncracked elastic body. We have shown that Brun's theorem is valid for stress free cracks as well as for frictionless contact cracks. The generalization of (2.30), (2.31) to dynamic crack propagation has been given by Bui and de Langre (1988), see Chap. 5.

2.8 Path-independent integrals in quasi-statics

Path-independent integrals have many interesting applications in computational fracture mechanics. The main reason is that stress-intensity factors are defined by the near tip fields of stress or displacement which are unaccurate in numerical computations. Therefore, to transfer informations on the stress singularity at the crack tip to the external surface of the cracked solid where numerical solutions can be obtained with a better accuracy, and vice versa, we consider path-independent integrals which are the right tools to work with for the calculation of G or K. In Sect. 2.3 an example of a path-independent integral for the calculation of G has been given. There are other path-independent integrals derived from *conservation laws* such as

$$\mathrm{div} A + \mathbf{B} = 0 \qquad (2.32)$$

with a second order tensor (or vector) A and a vector (or scalar) **B** which are related to physical quantities and their derivatives. If the source term $\mathbf{B} = \mathbf{0}$ vanishes in a domain Δ, then the flux of $A.\mathbf{n}$ across $\partial\Delta$ vanishes too

$$\int_{\partial\Delta} A.\mathbf{n}\, ds = 0. \qquad (2.33)$$

Assume that $\mathbf{B} = \mathbf{0}$ in the entire solid and that $A.\mathbf{n} = 0$ along the crack faces, then Eq. (2.33) can be written as

$$\int_{\Gamma_1} A.\mathbf{n}\, ds = \int_{\Gamma_2} A.\mathbf{n}\, ds$$

for open pathes Γ_1 and Γ_2 with end points on $S^{\pm}$.

The above equation defines the path-independent integral

$$C = \int_{\Gamma} A.\mathbf{n}\, ds \qquad (2.34)$$

for an arbitrary contour surrounding the crack tip. The integral C does not vanish only if A is singular as O(1/r).

To summarize, three conditions may be necessary and sufficient for path-independent integrals: a conservation law without source term $\mathbf{B} = \mathbf{0}$; vanishing flux $\mathbf{A}.\mathbf{n} = \mathbf{0}$ on the crack faces; and singularity of $A \cong O(1/r)$.

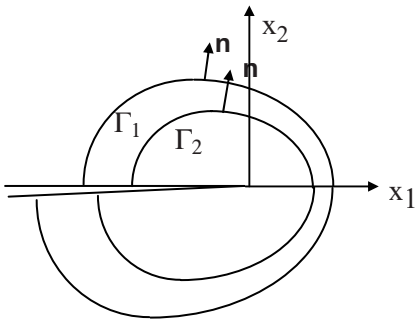

Figure 2.6: Path-independent integral along path Γ, with two end points on the stress free crack faces

2.8.1 The path-independent J-integral

The J-integral discovered independently by Rice (1968) and Cherepanov (1968) originated from a conservation law given by Eshelby (1951) who introduced an integral having the meaning of a generalized force on an elastic singularity in a continuum lattice.

The Eshelby law is a source free conservation law, div $A = 0$, with $A = W(\varepsilon)I - (\text{grad } u)^{\tau}.\sigma$

$$A_{ik} = W(\varepsilon)\delta_{ik} - \sigma_{jk}\, u_{j,i} \tag{2.35}$$

(We recall the notation $_{j,i} = \partial u_i/\partial x_i$) Eshelby's terminology for A is the *energy momentum tensor*. In Eq. (2.35) $W(\varepsilon)$ is the quadratic elastic strain energy ergy density $W = \frac{1}{2}\varepsilon_{ij}L_{ijhk}\varepsilon_{hk}$. For a crack, the tensor A has the right singularity as O(1/r). The Eshelby force on the elastic singularity is $F_i = \int_\gamma A_{ik} n_k\, ds$ where γ is any closed contour encircling the singularirty. The path-independent J-integral is defined with a open path Γ, with end points on the stress free crack line, along negative Ox_1, encircling the crack tip

$$J = \int_\Gamma \{W(\varepsilon) n_1 - \sigma_{ij} n_j u_{i,1}\}\, ds \tag{2.36}$$

It is the first component of the Eshelby generalized force. When the contour Γ is a circle around the crack tip with a vanishing radius, the J-integral can be easily evaluated as

$$J = \frac{1-\nu^2}{E}(K_I^2 + K_{II}^2) \quad \text{(in plane strain state)} \tag{2.37}$$

$$J = \frac{1}{2\mu}K_{III}^2 \qquad \text{(antiplane strain state)} \tag{2.38}$$

Comparing Eqs. (2.37) and (2.38) with Eq. (2.12) one concludes that J is idendical to the energy release rate in linear fracture mechanics, $J \equiv G$, and that J-integral is also equal to minus the derivative of the potential energy

$$J = -\frac{dP}{dl} \tag{2.39}$$

It can be shown that Eq. (2.39) is true for path-independent J-integrals in non-linear elasticity, where the elastic strain energy density $W(\varepsilon)$ is not necessarily quadratic in ε. Rice (1968) defined his J-integral for the sress working density (see the proof in Exercices)

$$W(\varepsilon) = \int_0^{\varepsilon} \sigma_{ij}(\varepsilon)\, d\varepsilon_{ij} \tag{2.40}$$

Remarks. The path-indepedent dual I-integral, (Bui, 1974), is defined by the stress density energy $U(\sigma)$, $\varepsilon = \partial U/\partial\sigma$ and

$I = -dQ/dl$,

Q is the complementary potential energy (Exercices).

2.8.2 Associated J-integrals for separating mixed modes

The J-integral (2.36) is equal to the quadratic form of stress intensity factors (2.37). For pure mode I or pure mode II, the J-integral allows for the calculation of the stress intensity factor K_I or K_{II}, but in mixed mode, it does not allows K_I and K_{II} to be separately calculated. Chen and Shield (1977) proposed a method for separating mixed modes, based on the path-independent integral $M_1(\mathbf{u}^{(1)}, \mathbf{u}^{(2)})$ which is a bilinear and symmetric form of two independent fields $\mathbf{u}^{(1)}$ and $\mathbf{u}^{(2)}$. Introduce the bilinear form of the energy density $B(\mathbf{u},\mathbf{v}) := \nabla\mathbf{u}.\mathbf{L}.\nabla\mathbf{v}$. Chen and Shield's integral is defined by

$$M(\mathbf{u}^{(1)},\mathbf{u}^{(2)}) = \int_{\Gamma} \{B(\mathbf{u}^{(1)},\mathbf{u}^{(2)}) - \mathbf{n}.\frac{\partial B}{\partial(\nabla \mathbf{u}^{(1)})}.\frac{\partial \mathbf{u}^{(2)}}{\partial x_1}$$

$$-\mathbf{n}.\frac{\partial B}{\partial(\nabla \mathbf{u}^{(2)})}.\frac{\partial \mathbf{u}^{(1)}}{\partial x_1}\} ds \tag{2.41}$$

Let the first field be the actual field $\mathbf{u}^{(1)} = \mathbf{u}$ and the second field be any displacement field in the same cracked solid $\mathbf{u}^{(2)} = \mathbf{v}$, with known stress intensity factors $K_I(\mathbf{v})$, $K_{II}(\mathbf{v})$. Thus the M-integral provides the second equation for determining K_I and K_{II} as

$$M(\mathbf{u},\mathbf{v}) = \frac{2(1-\nu^2)}{E}\{K_I(\mathbf{u})K_I(\mathbf{v}) + K_{II}(\mathbf{u})K_{II}(\mathbf{v})\} \tag{2.42}$$

The conservation law (2.9) provides another means for separating mixed mode. Consider the path-independent integral

$$F = \tfrac{1}{2}\int_{\Gamma} \{\mathbf{n}.\sigma(\mathbf{u}).\mathbf{u}^* - \mathbf{n}.\sigma(\mathbf{u}^*).\mathbf{u}\} ds \tag{2.43}$$

By taking the field $\mathbf{u}^* = -\partial \mathbf{u}^S/\partial x_1$, where $\mathbf{u}^S$ is the solution of the semi-infinite crack in mode I with the stress intensity factor $K_I(\mathbf{u}^S)$, we get

$$K_I = \frac{E}{(1-\nu^2)K_I(\mathbf{u}^S)}\int_{\Gamma} \{-\mathbf{n}.\sigma(\mathbf{u}).\frac{\partial}{\partial x_1}\mathbf{u}^S + \mathbf{n}.\sigma(\mathbf{u}^S).\mathbf{u}\} ds \tag{2.44}$$

For calculating K_{II} we take the field $\mathbf{u}^* = -\partial \mathbf{u}^A/\partial x_1$ where $\mathbf{u}^A$ is the solution of the semi-infinite crack in mode II, with $K_I(\mathbf{u}^A)$. Thus

$$K_I = \frac{E}{(1-\nu^2)K_I(\mathbf{u}^A)}\int_{\Gamma} \{-\mathbf{n}.\sigma(\mathbf{u}).\frac{\partial}{\partial x_1}\mathbf{u}^A + \mathbf{n}.\sigma(\mathbf{u}^A).\mathbf{u}\} ds \tag{2.45}$$

Ishikawa et al (1979) introduced a different method for the extraction of stress intensity factors.

Consider a mixed mode loading on the cracked body Ω. Let Ω' be the mirror image of Ω by a symmetry with respect to the crack line and $V = \Omega \cup \Omega'$. Any displacement field **u** defined in V can be splitted into the symmetric part $\mathbf{u}^I$ and antisymmetric part $\mathbf{u}^{II}$ by

$$\begin{aligned} u_1^I(x_1, x_2) &= \tfrac{1}{2}\{u_1(x_1,x_2) + u_1(x_1,-x_2)\} \\ u_2^I(x_1, x_2) &= \tfrac{1}{2}\{u_2(x_1,x_2) - u_2(x_1,-x_2)\} \end{aligned} \tag{2.46}$$

$$u_1^{II}(x_1,x_2) = \tfrac{1}{2}\ \{u_1(x_1,x_2) - u_1(x_1,-x_2)\}$$

$$u_1^{II}(x_1,x_2) = \tfrac{1}{2}\ \{u_1(x_1,x_2) - u_1(x_1,-x_2)\} \tag{2.47}$$

By taking a contour Γ of the J-integral belonging to V, Ishikawa et al (1979) made use of the decompositions $\mathbf{u} = \mathbf{u}^I + \mathbf{u}^{II}$, $\sigma = \sigma^I + \sigma^{II}$ and obtain four terms $J = J_{(I,I)} + J_{(II,II)} + J_{(I,II)} + J_{(II,I)}$ the crossed terms being equal to zero. Bui (1983) did not consider $\sigma = \sigma^I + \sigma^{II}$ and replaced $\mathbf{u}$ by $\mathbf{u}^I$ (or $\mathbf{u}^{II}$) directly in the J-integral to obtain the mixed mode separation

$$J_I = \int_\Gamma \{W(\nabla u^I)n_1 - \sigma_{ij}(u^I)n_j u^I_{i,1}\}\,ds \tag{2.48}$$

$$J_{II} = \int_\Gamma \{W(\nabla u^{II})n_1 - \sigma_{ij}(u^{II})n_j u^{II}_{i,1}\}\,ds \tag{2.49}$$

2.8.3 The T-integral in linear thermo-elasticity

In classical linear uncoupled thermo-elasticity, a conservation law of the form $\mathrm{div}A + \mathbf{B} = 0$ exists, with a non vanishing source term. Let $W(\varepsilon, \tau)$ be the free energy density, function of the strain and the temperature variation

$$W(\varepsilon,\ \tau) = \tfrac{1}{2}\lambda(\varepsilon_{kk})^2 + \mu\varepsilon_{ij}\varepsilon_{ij} - (3\lambda + 2\mu)\alpha\tau\varepsilon_{kk} + \tfrac{1}{2}b\tau^2 \tag{2.50}$$

where α is the thermal expansion coefficient. Stress and volumic entropy are given by $\sigma_{ij} = \partial W/\partial\varepsilon_{ij}$ and $S = -\partial W/\partial\tau$. Assume that the conductivity coefficient k is constant ($\mathbf{q} = -k\,\mathrm{gra}\ \tau$), the thermal equation is $\mathrm{divgra}\ \tau = 0$. The conservation law in thermoelasticity is well known

$$\frac{\partial}{\partial x_k}\{W(\varepsilon,\tau)\delta_{ik} \quad \sigma_{jk}\partial_i u_j\} + \frac{\partial W}{\partial\tau}\,\mathrm{grad}\,\tau = 0 \tag{2.51}$$

Under either adiabatic condition $S = 0$ or uniform temperature $\mathrm{grad}\,\tau = 0$, the source term B vanishes. Otherwise, the thermo-elastic J-integral contains an area integral over the surface $A(\Gamma)$ enclosed by the contour Γ

$$J = \int_\Gamma \{W(\varepsilon,\ \tau)n_1 - \sigma_{ij}n_j\partial_1 u_i\}\,ds + \int_{A(\Gamma)} S\tau_{,1}\,dA \tag{2.52}$$

It can be shown that the area integral can be transformed into a path integral over Γ in very restrictive cases, for instance:

i) the gradient gradτ is parallel to the crack line, as assumed in (Bui, 1977); ii) the fields $\tau u_{1,2}$ and $u_1\tau_{,2}$ are continuous across the crack line, as assumed in (Gurtin, 1979).

Let us recall, for later use, the equations in thermo-elasticity

$$\sigma_{ij} = \mu(u_{i,j} + u_{j,i}) + \lambda\delta_{ij}u_{k,k} - (3\lambda + 2\mu)\alpha\tau\delta_{ij} \quad \text{in } \Omega \tag{2.53}$$

$$\sigma_{ij,j} = 0 \quad \text{in } \Omega \tag{2.54}$$

$$\tau_{,kk} = 0 \quad \text{in } \Omega \tag{2.55}$$

$$\sigma_{ij}n_j = 0 \text{ on } S^{\pm} \tag{2.56}$$

$$\tau_{,j}n_j = 0 \text{ on } S^{\pm} \tag{2.57}$$

The path independent T-integral

A true path-independent integral in linear thermo-elasticity has been derived by Bui (1984), Bui and Proix (1984) who introduced a new conservation law in thermo-elasticity *without* source terms. The conservation law makes use of adjoint thermo-mechanical fields. Consider a set of auxiliary or adjoint fields ($\mathbf{u}^*$, σ^*, w^*) such that ($\mathbf{u}^*$, σ^*) is an elastic field in the same cracked body with known stress-intensity factors K_I^*, K_{II}^*, for instance the exact asymptotic solution for a semi-infinite crack subject to mechanical loading. No body forces are assumed for both fields σ and σ^*, $\mathrm{div}\sigma = \mathbf{0}$, $\mathrm{div}\sigma^* = \mathbf{0}$.

The adjoint stress satisfies the stress free condition on the crack faces, $\sigma^*.\mathbf{n} = \mathbf{0}$. The scalar field w^* is assumed to be harmonic

$$\mathrm{div}\,\mathrm{grad}w^* = 0 \quad \text{in } \Omega \tag{2.58}$$

and to satisfy the boundary condition on the crack faces

$$\frac{\partial w^*}{\partial n} = \frac{\partial u_1^*}{\partial n} \qquad \text{on } S^{\pm} \tag{2.59}$$

The components of the adjoint fields are explicitly given by the formulae

$$u_1^* = \frac{K_I^*}{\mu}\left(\frac{r}{2\pi}\right)^{1/2}\cos(\frac{\varphi}{2})\{1 - 2\nu + \sin^2(\frac{\varphi}{2})\} +$$

$$+ \frac{K_{II}^*}{\mu}\left(\frac{r}{2\pi}\right)^{1/2}\sin(\frac{\varphi}{2})\{2 - 2\nu + \cos^2(\frac{\varphi}{2})\} \quad (2.60)$$

$$u_2^* = \frac{K_I^*}{\mu}\left(\frac{r}{2\pi}\right)^{1/2}\sin(\frac{\varphi}{2})\{2 - 2\nu - \cos^2(\frac{\varphi}{2})\} +$$

$$+ \frac{K_{II}^*}{\mu}\left(\frac{r}{2\pi}\right)^{1/2}\cos(\frac{\varphi}{2})\{2\nu - 1 + \sin^2(\frac{\varphi}{2})\} \quad (2.61)$$

$$\sigma_{11}^* = K_I^*\frac{1}{\sqrt{2\pi r}}\cos(\frac{\varphi}{2})\{1 - \frac{3}{}\sin(\frac{\varphi}{2})\sin(\frac{}{2})\} -$$

$$- K_{II}^*\frac{1}{\sqrt{2\pi r}}\sin(\frac{\varphi}{2})\{2 + \cos(\frac{\varphi}{2})\cos(\frac{3\varphi}{2})\} \quad (2.62)$$

$$\sigma_{12}^* = K_I^*\frac{1}{\sqrt{2\pi r}}\cos(\frac{\varphi}{2})\sin(\frac{\varphi}{2})\cos(\frac{3\varphi}{2}) +$$

$$+ K_{II}^*\frac{1}{\sqrt{2\pi r}}\cos(\frac{\varphi}{2})\{1 - \sin(\frac{\varphi}{2})\sin(\frac{3\varphi}{2})\} \quad (2.63)$$

$$\sigma_{22}^* = K_I^*\frac{1}{\sqrt{2\pi r}}\cos(\frac{\varphi}{2})\{1 + \sin(\frac{\varphi}{2})\sin(\frac{3\varphi}{2})\} +$$

$$+ K_{II}^*\frac{1}{\sqrt{2\pi r}}\sin(\frac{\varphi}{2})\cos(\frac{\varphi}{2})\cos(\frac{3\varphi}{2}) \quad (2.64)$$

The harmonic function w* satisfying the boundary conditions (2.59) is given by

$$w^* = \frac{2K_I^*}{\mu}\left(\frac{r}{2\pi}\right)^{1/2}(1 - \nu)\cos(\frac{\varphi}{2}) \quad (2.65)$$

It should be noted that (**u***, σ*, w*) is *not* a thermo-elastic field. The actual thermo-elastic field (**u**, σ, τ) satisfies the strong coupling (2.53) while only a weak coupling exists between the harmonic field w* and the displacement field **u***. The thermo-elastic conservation law without source terms is given by

$$\frac{\partial}{\partial x_j}\{\frac{1}{2}u_i\sigma^*_{ij,1} - \frac{1}{2}u^*_{i,1}\sigma_{ij} - \gamma\tau(u^*_{1,j} - w^*_{,j}) + \gamma(u^*_1 - w^*)\tau_{,j}\} = 0 \quad (2.66)$$

where $\gamma = -\frac{1}{2}\alpha\mu(3\lambda + 2\mu)/(\lambda + \mu)$. Eq. (2.66) can be directly checked by considering the symmetry of the moduli tensor, the equilibrium equations $\mathrm{div}\sigma = 0$, $\mathrm{div}\sigma^* = 0$, $\mathrm{divgrad}w^* = 0$ and the first component of the equilibrium equation for $\mathbf{u}^*$,

$$\frac{\partial}{\partial x_1}\mathrm{div}\,\mathbf{u}^* + \frac{\mu}{\mu+\lambda}\mathrm{div}\,\mathrm{grad}\,u^*_1 = 0\,.$$

The conservation law (2.66) allows us to define a *true* path-independent integral for thermo-elasticity, as follows

$$T = \int_\Gamma \{\frac{1}{2}u_i\sigma^*_{ij,1}n_j - \frac{1}{2}u^*_{i,1}\sigma_{ij}n_j - \gamma\tau(u^*_{1,n} - w^*_{,n}) + \gamma(u^*_1 - w^*)\tau_{,n}\}ds \tag{2.67}$$

The path-independence property of T results from (2.66), the stress free conditions $\sigma.\mathbf{n} = \mathbf{0}$, $\sigma^*.\mathbf{n} = \mathbf{0}$ on the line crack, conditions (2.57) and (2.59). For a vanishing contour around the crack tip, the third and fourth terms of the latter integral are more regular than the first two terms. Thus the T-integral can be easily calculated by means of the near tip fields. We obtain

$$T = \frac{(1-\nu^2)}{E}(K_I K_I^* + K_{II}K_{II}^*) \tag{2.68}$$

2.8.4 Lagrangian derivative of energy and the G-theta integral

So far, the focus has been on path-independent integrals for use in numerical computations of G or K_i, with a contour Γ of sufficiently large radius to avoid the crack tip. Numerical computations by the finite elements methods, however, provide mechanical fields inside the elements, rather than on the edges of the elements which define the contour Γ. Thus methods based on path-independent integrals need some interpolation procedure between elements at both sides of the contour. A new method called *Lagrangian derivative* of energy has been proposed by Otsuka (1981), de Lorenzi (1981), Destuynder and Djaoua (1981) which still considers the advantage of conservations laws for the calculation of the G or K_i with the relevant field quantities far from the crack tip, but avoids the above mentioned difficulty. That is the Lagrangian derivative of the potential energy defined by an arbitrarily chosen area integral.

Consider the cracked solid Ω, subject to displacement $\mathbf{u}^d$ on $S_u \equiv S_{ext}$.

Let $L(\mathbf{u})$ be the Lagrangian $L(\mathbf{u}) = \int_\Omega W(\mathbf{u})d\omega$. We wish to calculate the infinitesimal change of $L(\mathbf{u}(\Omega)) \rightarrow L'(\mathbf{u}'(\Omega')) = L + \delta L$ in the crack tip advance $\delta\eta$. The domain Ω changes to Ω' as well as variable $\mathbf{x} \rightarrow \mathbf{x}'$ and field $\mathbf{u} \rightarrow \mathbf{u}'$. Let us consider the transforms of both variable and field, with a small parameter η

$$\mathbf{x} \rightarrow \mathbf{x}' = \mathbf{x} + \eta\theta(\mathbf{x}) \tag{2.69}$$

$$\mathbf{u} \rightarrow \mathbf{u}' = \mathbf{u} + \eta\gamma(\mathbf{x}) \tag{2.70}$$

The Lagrangian derivative of the energy is

$$\frac{\delta L}{\delta \eta}\Big|_{\eta=0} = \int_\Omega \frac{\partial}{\partial x_h}\{W\theta_h + \frac{\partial W}{\partial u_{i,h}}(\gamma_i - u_{i,k}\theta_k)\}d\omega$$

Taking into account $\gamma(\mathbf{x}) = 0$ on S_{ext} (both $\mathbf{u}$ and $\mathbf{u}'$ satisfy the same boundary condition), the equilibrium equation $\partial(\partial W/\partial u_{i,h})/\partial x_h = 0$ we obtain

$$\int_\Omega \sigma_{ij}\gamma_{i,j}d\omega \equiv \int_{\partial\Omega} \sigma_{ij}n_j\gamma_i dS = 0$$

$$\int_\Omega \frac{\partial}{\partial x_h}\{W\theta_h + \frac{\partial W}{\partial u_{i,h}}(\gamma_i - u_{i,k}\theta_k)\}d\omega = \int_\Omega (W \operatorname{div}\theta - \sigma_{ij}u_{i,k}\theta_{k,j})d\omega$$

Let us take a continuous transform field $\theta(\mathbf{x})$ such that $(\theta_1 = 1, \theta_2 = 0)$ near the crack tip, $(\theta_1 = 0, \theta_2 = 0)$ near the external boundary, so that $\operatorname{div}\theta \neq 0$, $\nabla\theta \neq 0$ only in a ring shaped area domain C, thus the energy release rate is

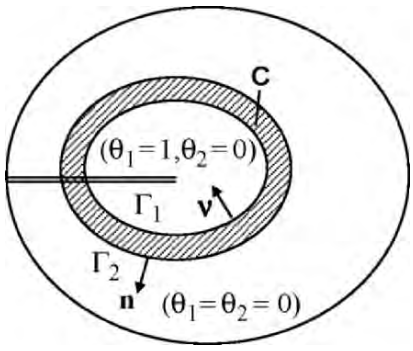

Figure 2.7: The ring shaped area domain C for the Lagrangian derivative of energy, bounded by Γ_1, with inward normal ν, and Γ_2, with outward normal $\mathbf{n}$

expressed by an arbitralily chosen area integral which avoids the crack tip, as shown in Fig. 2.7

$$G^{\theta} = -\int_C (W \operatorname{div} \theta - \sigma_{ij} u_{i,k} \theta_{k,j}) d\omega \tag{2.71}$$

The G^{θ}-integral has been independently given by Otsuka (1981), de Lorenzi (1981), Destuynder and Djaoua (1981). It should be noted that a discontinuous θ -field, ($\theta_1 = 1$, $\theta_2 = 0$) inside a contour Γ and ($\theta_1 = \theta_2 = 0$) outside Γ, yields the J-integral as the limit when contours Γ_1 and Γ_2 coincide with Γ. Therefore Eq. (2.71) is the area version of the J-integral. In thermo-elasticity, it can be shown that the T-integral is equal to the area-independent A-integral, given in (Bui, 198; Bui and Proix, 1983) as

$$A = \int_C \{ -\frac{1}{2} u_i \sigma^*_{ij,1} + \frac{1}{2} u^*_{i,1} \sigma_{ij} + \gamma \tau (u^*_{1,j} - w^*_{,j}) -$$

$$- \gamma (u^*_1 - w^*) \tau_{,j} \} \varphi_{,j} ds \tag{2.72}$$

for any continuously differentiable scalar field $\varphi(\mathbf{x})$ such that $\varphi(\mathbf{x}) = 0$ on Γ_2 and $\varphi(\mathbf{x}) = 1$ on Γ_1. This result can be checked by using the Green-Gauss theorem. By taking account of $\varphi(\mathbf{x}) = 0$ on Γ_2 we can transform (2.64) into a path-independent integral over Γ_1(ν is the inward normal)

$$A = \int_{\Gamma_1} \{ -\frac{1}{2} u_i \sigma^*_{ij,1} \nu_j + \frac{1}{2} u^*_{i,1} \sigma_{ij} \nu_j + \gamma \tau (u^*_{1,j} - w^*_{,j}) \nu_j -$$

$$- \gamma (u^*_1 - w^*) \tau_{,j} \nu_j \} ds$$

This is nothing but the T-integral (with outward normal $\mathbf{n} = -\nu$)

$$A = \int_{\Gamma_1} \{ \frac{1}{2} u_i \sigma^*_{ij,1} n_j - \frac{1}{2} u^*_{i,1} \sigma_{ij} n_j - \gamma \tau (u^*_{1,j} - w^*_{,j}) n_j -$$

$$+ \gamma (u^*_1 - w^*) \tau_{,j} n_j \} ds \equiv T \tag{2.73}$$

2.9 Generalization of Griffith's model in three dimensions

The fatigue crack propagation and brittle fracture of cracks in three dimensions have been observed in the failure of pressurized cylinders in operation

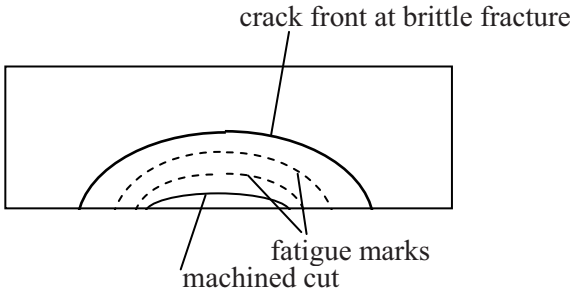

Figure 2.8: Fatigue crack propagation from a machined cut in metal; fatigue marks by overloads (discontinuous lines); crack front at brittle fracture (continuous line). Crack shapes are nearly semi-elliptical curves, along which $K_I(s)$ is not constant

on or in testing specimens for the validation purposes etc. To study crack propagation, the solid is subject to overloads which mark the crack front at different times. To identify the crack propagation law, an inverse analysis based on a postmortem interpretation of crack propagation can be performed, using three-dimensional numerical computations of stress intensity factors $K_I(s)$. Fatigue crack propagation can be described by the Paris law in the local form $\varphi(s) = Cte.(\Delta K_I(s))^m$, with $\varphi(s) \geq 0$ being the crack propagation velocity at point s of the crack front and $\Delta K_I(s)$ the local stress intensity factor variation. It should be noted that the exponent m is different from the one measured in two-dimensional fatigue for the same material and that m becomes infinite at brittle fracture, Lazarus (2003). Labourdette and Baudin (1981) measured $m \propto 2$ in aluminium. Some other results reported in the literature indicate $m \propto 4$. Models based on Weibull's statistics predict a propagation law in the form $\varphi(s) \propto K_I^4(s)$, (Pineau, 1992).

It turns out that three-dimensional crack propagation problems – fatigue or brittle fracture – is not yet a well known and widely accepted subject. One main reason is that experiments in three-dimensions are difficult to analyse. Crack advance measured between two overload marks is rather a large increment than an infinitesimal one. Hovewer, it is found that the crack front marks during fatigue and the one just at brittle fracture under the last overload are generally very similar. It is likely that the transition from fatigue to brittle fracture is very sharp with an acceleration rate which corresponds to the increase of the exponent m up to infinity. Such acceleration behavior has been already observed in two-dimensional fatigue propagation. The transition model using the change on coefficient m has

been considered by Lazarus (2003). An inverse numerical analysis given by Labourdette and Baudin (1981), which agrees well with experiments, suggests that $K_I(s)$ is not constant along the fatigue crack front, $K_I(s) \neq K_{Ic}$. Consider an elliptical crack in a solid subject to tensile load. For a small crack, the solution of an elliptical crack in an infinite elastic body is quite good for the analysis, Sih (1973). The stress intensity factor $K_I(s)$ varies along the crack front, with maximum values at the major axis points. Therefore, brittle fracture in three-dimensions seems to be not governed by a local criterion – which should imply a crack propagation at isolated points of maximum K_I – for instance

$$\max_s K_I(s) = K_{Ic}\,, \tag{2.74}$$

The criterion (2.66) yields a critical applied stress too low with respect to the experimental ones.

2.9.1 A local model of viscous fracture

Let us reconsider the balance equation of energy in three-dimensional mode I

$$G\ \varphi) \equiv \frac{1-\nu^2}{E} \int_\Gamma K_I^2(s\ \varphi(s) ds = D(\varphi, K_I)$$

where $D(\varphi, K_I)$ is the global dissipation. Take a dissipation which consists of two terms $D(\varphi, K_I) = D_1(\varphi)+D_2(K_I)$, the first one $D_1(\varphi)$ being homogeneous of degree one, $D_1(\chi\varphi) = \chi D_1(\varphi)$, $(\chi > 0)$, and the second one $D_2(K_I)$ being nearly independent of the propagation rate φ. To justify this assumption, let us consider an analogy with the visco-plastic dissipation rate in metals which consists of two terms, the plastic rate $\sigma{:}\partial_t\varepsilon^p$ and the viscous dissipation rate $\sigma{:}\partial_t\varepsilon^v$, with the Norton-Hoff viscous power law, $J(\sigma) = \frac{1}{2}\, s_{i\text{-}j}s_{ij}$, $s = dev(\sigma)$ is the stress deviator, J_0 is the threshold, $< \mathbf{.} >_+$ is the positive part of function $D = \sigma{:}\partial_t\varepsilon^p + C < J(\sigma) - J_0 >_+^n dev(\sigma){:}\sigma$.
Considering this analogy, dropping the coefficient $(1-\nu^2)/E$ we obtain a *viscous fracture* model

$$\int_\Gamma K_I^2(s\ \varphi(s) ds = \int_\Gamma K_c^2 \varphi(s) ds + \int_\Gamma \overline{D_2(s)}\, \pi r_{vp}^2(s) ds \tag{2 75}$$

In the second term of the right hand side of Eq. (2.67), $\overline{D_2(s)}$ denotes the mean value of viscoplastic dissipation per unit volume of the torus

process zone, with the radius $r_{vp} \propto C K_I^2(s)$. Assume that this mean value proportional to $< K_I^2(s) - K_c^2(s) >_+^{1+(m/2)}$ we get the model equation

$$\int_\Gamma \{(K_I^2(s) - K_c^2)\varphi(s) - C < K_I^2(s) - K_c^2(s) >_+^{1+(m/2)}\} ds = 0 \tag{2.76}$$

Thus, a local criterion of fracture which identically satisfies (2.76) is given by the crack propagation law,

$$\varphi(s) = C(K_I^2(s) - K_c^2)^{m/2}, \quad \text{if } K_I^2(s) - K_c^2 \geq 0$$
$$\varphi(s) = 0, \text{ otherwise} \tag{2.77}$$

There is a threshold value of the local stress intensity factor below which the crack propagation rate φ(s) vanishes. The model (2.77) bears a resemblance with the Weibull statistics giving the probability of fracture in the form (Pineau 1992)

$$p_R(K_1) = 1 - \exp\{-B(K_1 - K_{min})^4 / (K_0 - K_{min})^4\}$$

where B, $_{min}$, K_0 are some constants. When there is no threshold $K_{min} = 0$, for small K_I, one obtains a power law with m = 4 which agrees with (2.77). The model without threshold is nothing but the local crack propagation law considered in many works, (Lazarus, 2003)

$$\varphi(s) = C K_I^m(s) \tag{2.78}$$

Local model (2.78) is suitable for fatigue crack propagation, φ being replaced by the crack advance da/dN in the normal direction of the crack front per cycle.

The underlying physics of viscosity in crack propagation is the rachetting phenomena which is a progressive plastic deformation in cyclic loads. Also, the balance equation of energy confirms the viscosity model.

2.9.2 A non local model of fracture

Now, let us consider a global criterion with a dissipation rate D(φ) (homogeneous of degree one in φ) without the term $D_2(K_I)$, so that we can normalize D to unity since φ(s) is only defined to within a scalar factor.

$$G(\varphi) := \frac{1-\nu^2}{E}\int_\Gamma K_I^2(s)\,\varphi(s)ds$$

$$\varphi(s) = \arg\{\max_{\varphi \geq 0} G(\varphi)\} := \varphi^*(s) \qquad (2.79)$$

$$D(\varphi^*) = 1$$

The criterion (2.79) satisfies the global balance equation of energy for the optimal solution $G(\varphi^*) = D(\varphi^*)$. The maximum dissipation principle in (2.79) is very similar to the Hill "maximum of plastic work" in plasticity and makes it possible to choose the optimal rate φ. This model was proposed by Bui and Dang Van (1979).

The solution of (2.79) yields both the crack front velocity $\varphi^*(s)$ and the load defined implicitly by $G = D = 1$. The actual velocity $\varphi^*(s)$ should maximize the global energy release rate, for an unit dissipation rate. If we consider Griffith's criterion $D(\varphi) = \int 2\gamma\varphi(s)ds$, we find that the actual crack front Γ should be a constant K_{Ic}-curve, with $K_{Ic} = \{2\gamma E/(1-\nu^2)\}^{1/2}$.

As a matter of fact, Eq. (2.79) can be relaxed by two methods:

i) Define subspaces V of non negative $\varphi(s) \geq 0$ for searching the solution $\varphi^*(s) \in V$. For instance, when dealing with elliptical cracks, one generally assumes that cracks always propagate in an elliptical shape, with two parameters $a > a_0$, $b > b_0$ (the ellipse semi-axes) to be determined.

ii) Introduce a dissipation rate $D(\varphi)$ which differs from the Griffith model.

2.9.3 A dissipation rate model for non local brittle fracture

In Sect. 2.6, Cherepanov's model of fatigue crack propagation underlines the importance of plastic dissipation near the crack tip which modifies the balance equation of energy.

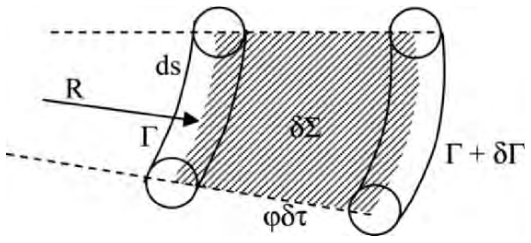

Figure 2.9: Propagation of the crack front; with a new crack area $\delta\Sigma = \varphi(s)\delta\tau ds$, an increment of the crack front length $|\delta\Gamma| = \varphi(s)\delta\tau ds/|R|$ and an increment of the curvature $-(\varphi'' + \varphi/R^2)\delta\tau$

As long as small scale assumption is still a reasonnable one for applications, the energy release rate is still calculated in the framework of elasticity, governed by the term K_I^2. Cherepanov's model modified the Griffith dissipation rate. In three-dimensional brittle fracture, we shall consider a similar model. Fig. 2.9 shows elements of the crack front Γ at time t and of the crack front $\Gamma + \delta\Gamma$ at time $t + \delta t$. Active plastic deformation is assumed to be restricted inside a torus along $\Gamma + \delta\Gamma$, while the incremental wake plastic zone is lying between Γ and $\Gamma + \delta\Gamma$. Griffith's model only considers the dissipation $2\gamma\delta\Sigma$ as proportional to the area increment $\delta\Sigma$ with a constant *surface* energy γ. This part of dissipation can be considered, as in Cherepanov's model, as the contribution of the wake plastic zone. Active plastic dissipation changes when the crack front geometry changes – a feature which does not exist in two-dimensional problems. To account for this, we consider two kinds of variations: the first one being associated to the length change $|\delta\Gamma|$ of the crack front, the second one being associated to the curvature change of the crack front. The first term accounts for the *tensile* plastic work along the crack front, while the second term corresponds to the plastic *bending* of the crack front. The changes of area, length and curvature are the only possible geometric ones to be considered in three-dimensional fracture.

The model of dissipation introduced by Bui and Dang Van (1979) is defined by

$$D(\varphi) := \int_\Gamma \{2\gamma \quad (s) + \alpha \frac{\varphi(s)}{|R(s)|} + \beta \left| \frac{\varphi(s)}{R^2(s)} + \varphi''(s) \right| \} ds \tag{2.80}$$

where α, β, γ are positive constants and $1/R$ is the curvature. The presence of the term φ'' demands that the crack front be smooth. The rate $D(\varphi)$ is a positively homogeneous functional of degree 1 in φ. In two-dimensional fracture mechanics, $R = \infty$ and $\varphi'' = 0$, thus the rate (2.80) coincides with that of Griffith's model.

Another possible model consists in dropping the absolute value symbols $|.|$ in Eq. (2.80) and demanding that the overall dissipation be positive for every non negative $\varphi(s)$. In what follows we discuss the model (2.80).

2.9.4 Convex analysis of three-dimensional brittle fracture

Let us remark that the set $D(\varphi) = 1$ is not a convex set. Since the absolute value of functions $\varphi'' + \varphi/R^2|$ has been considered, the set $D(\varphi) = 1$ may contain many separated convex subsets(*). However, one can mathematically

replace the constraint $D(\varphi) = 1$ by the constraint $D(\varphi) \le 1$ without changchanging the solution of (2.79) because it belongs to the boundary of the convex domain $D(\varphi) \le 1$. Introduce the loading F, so that $K_I(s)/F = k_I(s)$ with the stress intensity factor $k_I(s)$ per unit load. Problem (2.79) becomes a classical non linear and non differentiable convex analysis, similar to the one encountered in the limit analysis of plasticity, (Hill, 1950; Mandel, 1966; Salençon, 1977)

$$G(\varphi) := \frac{1-\nu^2}{E} F^2 \int_\Gamma k_I^2(s)\,\varphi(s)\,ds$$
$$\varphi(s) = \arg\{\max_{\varphi} G(\varphi)\} := \varphi^*(s),\ \varphi \ge 0,\ D(\varphi) \le 1 \tag{2.81}$$

The optimal solution determines both the crack propagation rate φ^* and the critical load F_c by equating G and D

$$\frac{1-\nu^2}{E} F_c^2 \int_\Gamma k_I^2(s)\varphi^*(s)\,ds = D(\varphi^*) = 1 \tag{2.82}$$

Let $g(\varphi) := ((1-\nu^2)/E)\int_\Gamma k_I^2(s)\,\varphi(s)\,ds$.

According to the convex analysis theory, (Ekeland and Temam, 1974), we can write down the following results. The *primal* problem consists in finding the optimal solution φ^* of the problem:

$$\max_{\varphi} F^2\, g(\varphi)$$
$$\varphi \ge 0 \text{ and } D(\varphi) \le 1 \qquad \text{(primal problem)}$$

Consider the Lagrange multiplier λ of the constraint $D(\varphi)-1 = 0$ and introduce the Legendre-Fenchel transform

$$f(\lambda) = \sup_{\varphi} \{g(\varphi) - \lambda(D(\varphi) - 1)\} \tag{2.83}$$

The *dual* problem consists in finding the optimal Lagrangian multiplier λ^* of the problem:

(*) For instance the set $|x| = 1$ in $\mathbb{R}$ is not convex. It consists of two isolated points $\{-1, +1\}$, which are disjoint convex subsets $\{-1\}, \{1\}$, but the set $|x| \le 1$ is convex. The solution in the set $x = 1$ belongs to the boundary of the set $|x| \le 1$.

$\min_{\lambda} F^2 f(\lambda)$ (dual problem)

$\lambda \geq 0$, $f(\lambda) < +\infty$

Since $g(\varphi) \leq g(\varphi^*) = f(\lambda^*) \leq f(\lambda)$, one gets the *lower* bound $1/f^{1/2}(\lambda)$ and the *upper* bound $1/g^{1/2}(\varphi)$ for the critical load F_c

$$\frac{1}{f(\lambda)} \leq \frac{1}{f(\lambda^*)} = F_c^2 = \frac{1}{g(\varphi^*)} \leq \frac{1}{g'(\varphi)} \tag{2.84}$$

The main interest of Convex Analysis is to derive *exact* bounds of the critical load, from the approximate primal solution $1/g(\varphi)$ and the dual one $1/f(\lambda)$. The smaller the difference between the bounds, the better the critical load.

Chapter 3

Solutions of Crack Problems

In this chapter we will give methods of solution to crack problems in two-dimensional isotropic linear elasticity or plasticity. Most examples are classical and can be found in textbooks. Some others are new problems solved in closed-form. They are selected for their teaching character and applications in Fracture Mechanics. It is found that some crack problems may be considered and solved as inverse problems.

3.1. Mathematical problems in plane elasticity

3.1.1 Plane strain and antiplane strain

Plane elasticity is based on different types of assumptions:

i) Displacement fields $u_1(x_1, x_2)$, $u_2(x_1, x_2)$, $u_3(x_1, x_2)$ depend only on x_1, x_2. The case where $u_3 = 0$ is called *plane strain* problem. The case where $u_1(x_1, x_2) = u_2(x_1, x_2) = 0$ is called *anti-plane strain* problem.

ii) Stress fields reduce to $\sigma_{11}(x_1, x_2)$, $\sigma_{22}(x_1, x_2)$, $\sigma_{21}(x_1, x_2)$, $\sigma_{33}(x_1, x_2)$, $\sigma_{23} = \sigma_{13} = 0$. Case $\sigma_{33} = 0$ is called a *plane stress* problem. In plane problems the small strain tensor components reduce to : $\varepsilon_{11}(x_1, x_2)$, $\varepsilon_{22}(x_1, x_2)$, $\varepsilon_{12}(x_1, x_2)$, $\varepsilon_{33}(x_1, x_2)$, $\varepsilon_{32} = \varepsilon_{31} = 0$. In an anti-plane strain problem, the strain components are $\varepsilon_{31}(x_1, x_2)$ and $\varepsilon_{32}(x_1, x_2)$. The compatibility equation is required in any case, $RR^*\varepsilon = 0$ (Chap. 2).

In Cartesian coordinates, the compatibility equation is written as

$$\varepsilon_{ij,kl} + \varepsilon_{kl,ij} - \varepsilon_{ik,jl} - \varepsilon_{jl,ki} = 0 \tag{3.1}$$

For example, strain $\varepsilon_{33}(x_1, x_2)$ must satisfy three compatibility equations

$$\varepsilon_{33,11} = \varepsilon_{33,22} = \varepsilon_{33,12} = 0 \tag{3.2}$$

That is strain $\varepsilon_{33}(x_1, x_2)$ is a linear function of the coordinates

$$\varepsilon_{33}(x_1, x_2) = a + bx_1 + cx_2 \tag{3.3}$$

The transverse displacement component is then obtained by integrating Eq. (3.3) as $u_3 = (a + bx_1 + cx_2)x_3$. Since $\varepsilon_{32} = \varepsilon_{31} = 0$, constants b,c are necessarily the coefficients in the expressions of other components $u_1 = f_1(x_1, x_2) - bx_3^2/2$ and $u_2 = f_2(x_1, x_2) - cx_3^2/2$. In plane strain, the condition $\varepsilon_{33} = 0$ implies $a = b = c = 0$.

3.1.2 Plane stress condition revisited

Plane stress condition implies that the stress tensor components reduce to: $\sigma_{11}(x_1, x_2)$, $\sigma_{22}(x_1, x_2)$, $\sigma_{12}(x_1, x_2)$, $\sigma_{33}(x_1, x_2)$, $\sigma_{32} = \sigma_{31} = 0$. Case $\sigma_{33} = 0$ is called the *plane stress* problem. Example of plane stress condition can be found in the problems of a thin plate under in-plane loadings.

Let us complete the equations by considering the physical link between stress and strain. One assumes linear isotropic elasticity (Hooke's law) which is written shortly as $\sigma = \sigma(\varepsilon)$ with λ, μ being the Lamé constants or in the inverse form $\varepsilon = \varepsilon(\sigma)$ with Poisson's coefficient ν and Young's Modulus E (for real solid, the conditions $0 < \nu < 1/2$, $E > 0$ ensure the definite positiveness of the strain energy $W(\varepsilon)$),

$$\sigma_{ij} = \lambda\varepsilon_{kk}\delta_{ij} + 2\mu\varepsilon_{ij} \tag{3.4}$$

$$\varepsilon_{ij} = -\nu\sigma_{kk}\delta_{ij}/E + (1 + \nu)\sigma_{ij}/E \tag{3.5}$$

In plane strain, the in-plane components of the stress are given by Eq. (3.4). The remaining components are $\sigma_{33} = \lambda(\varepsilon_{11} + \varepsilon_{22})$, $\sigma_{31} = \sigma_{32} = 0$. In plane stress, the in-plane strain components are calculated from (5) and the transverse strain is given by

$$\varepsilon_{33} = -\nu(\sigma_{11} + \sigma_{22})/E \quad \text{(plane stress)} \tag{3.6}$$

Comparing (3.6) with (3.3), we conclude that the plane stress state in elasticity exists only if the in-plane trace $\mathrm{tr}(\sigma) = (\sigma_{11} + \sigma_{22})$ is a *linear* function of the coordinates. If not, even when in-plane stresses $\sigma_{11}(x_1, x_2)$, $\sigma_{22}(x_1, x_2)$, $\sigma_{12}(x_1, x_2)$ satisfy the equilibrium equation $\mathrm{div}(\sigma) = 0$, the problem is always three-dimensional so that transverse components σ_{31}, σ_{32}, σ_{33} do not vanish. Therefore, the compatibility condition (3.3) for a plane stress state is a very restrictive one. In linear Fracture Mechanics, near the crack tip the stress is singular as $O(r^{-1/2})$. Therefore, the singularity of trace $(\sigma_{11} + \sigma_{22})$ implies the singularity of strain $\varepsilon_{33} = -\nu(\sigma_{11} + \sigma_{22})/E$ as $O(1/\sqrt{r})$ so that the compatibility equation (3.1) is violated.

The compatibility condition for ε_{33} may be approximately satisfied in region far from the crack tip, but near the crack tip zone the solution is three-dimensional. We conclude that the use of plane stress model in linear Fracture Mechanics is questionable. Perhaps, the plane stress condition should be an approximate model for thin plate only when the stress field is is finite. That is the case for perfect plasticity in non-linear Fracture Mechanics.

3.1.3 Complex variables in elasticity

Let us recall the Beltrami representation of equilibrium stress by $\sigma = RR^*B$ which satisfies identically $\mathrm{div}(\sigma) = 0$

$$B = \psi(x_1, x_2)\, \mathbf{e}^3 \otimes \mathbf{e}^3 \tag{3.7}$$

where ψ is the Airy function. The stress components are

$$\sigma_{11} = \psi_{,22}, \quad \sigma_{22} = \psi_{,11}, \quad \sigma_{12} = -\psi_{,12} \tag{3.8}$$

Express the compatibility for the in-plane strain components, Eq. (3.1), in terms of the stress (3.8), to obtain the equation $\Delta\Delta\psi = 0$. Harmonic functions and biharmonic functions are more conveniently studied with the aid of complex variables $z = x_1 + ix_2$.

Plane elasticity has been developped in complex variables by Kolosov (1090) and Muskhelishvili (1977), as a powerful tool for obtaining closed-form solutions of many important problems in Elasticity, particularly in Fracture Mechanics. For further use in the book, we recall the theory without justification.

Let us introduce the complex conjugate variable $\bar{z} = x_1 - ix_2$. A complex valued function $f(x_1, x_2) \equiv P(x_1, x_2) + iQ(x_1, x_2)$ with real part P and pure imaginary part iQ can be expressed in terms of z and $\bar{z}$ as $f(z, \bar{z})$ by a simple change of variables. The function f is *analytic* when it depends only on z or $\partial f/\partial \bar{z} = 0$, where

$$\partial/\partial \bar{z} = (\partial/\partial x_1 + i\, \partial/\partial x_2)/2 \tag{3.9}$$

Expliciting $\partial f/\partial \bar{z} = 0$ one gets the Cauchy relations $P_{,1} - Q_{,2} = 0$ and $P_{,2} + Q_{,1} = 0$. Therefore any analytic function f(z) has its real and imaginary parts as harmonic functions, $\Delta P = 0$, $\Delta Q = 0$.

A biharmonic function W ($\Delta\Delta W = 0$) has the complex representation formula

$$W = \mathrm{Re}\left\{\bar{z}\phi(z) + \int \psi(z) dz\right\} \tag{3.10}$$

Stress and displacement components are given by Mukhelishvili's formulae

$$\sigma_{11} + \sigma_{22} = 2\left\{\phi'(z) + \overline{\phi'(z)}\right\} \tag{3.11}$$

$$\sigma_{22} - \sigma_{11} + 2i\sigma_{12} = 2\left\{\bar{z}\phi''(z) + \psi'(z)\right\} \tag{3.12}$$

$$u_1 + i\,u_2 = \frac{1}{2\mu}\left\{\kappa\,(z) - z\overline{\phi'(z)} - \overline{\psi(z)}\right\} \tag{3.13}$$

In Eq. (3.13) constant κ considered in *plane strain* is

$\kappa = 3–4\nu$.

The equations for plane strain are exact. It will be shown in Chap.6 that the field solution near a crack front in a three-dimensional problem shows the same type of singularity as observed in plane strain with the constant $\kappa = 3–4\nu$.

In *plane stress*, the constant is $\kappa = (3 - \nu)/(1 + \nu)$.

For the applications of formulae (3.11)-(3.13) to Fracture Mechanics, we do not consider the plane stress condition. The reasons have been mentioned above. Let us remark that the coefficient κ is not involved in Muskhelishvili's formulae (3.11) and (3.12) for the stresses. The in-plane components in plane stress problems, solutions of the boundary value problem with prescribed tractions, provide a "good approximation" for thin plate, except near the crack tip zone. The reason is that in a plane stress model the strain is partially compatible, namely the in-plane components of the strain. Therefore the solution for thin cracked plate may always be considered as a three-dimensional problem.

Many workers (Benthem, 1976; Bazant and Estenssoro, 1979) showed that the boundary conditions $\sigma_{3k}(x_1, x_2, x_3 = \pm h) = 0$ (k = 1, 2, 3) on lateral stress free surfaces do not imply $\sigma_{3k}(x_1, x_2, x_3) \equiv 0$ throughout the plate. There exists a *boundary layer* with a high normal gradient which disappears far from the crack tip region (a similar phenomenon exists near an interface intersecting a free surface). In *anti-plane strain* case, the non zero displacement component is $u_3(x_1, x_2)$. Displacement and stress components are then expressed by means of one function f(z)

$$\sigma_{31} - i\,\sigma_{32} = 2f'(z) \tag{3.14}$$

$$u_3 = (1/\mu)\,\mathrm{Re}\, f(z) \tag{3.15}$$

Boundary conditions

1. *Finite solid*. On the boundary S with outward unit normal n, the tractions $T_1 ds$, $T_2 ds$ on an arc of length ds, $\mathbf{T} = \sigma.\mathbf{n}$ with normal **n** is given by for plane strain problems by

$$(T_1 + iT_2)ds = -i\,d\left\{\phi(z) + z\overline{\phi'(z)} + \overline{\psi(z)}\right\}. \tag{3.16}$$

2. *Infinite solid*. One assumes that curve S where the traction vectors are prescribed is finite. This is the case for an infinite medium with a cavity under pressure, or a crack with loads on the crack faces. One generally assumes that there is no rotation at infinity. Let the total force on a cavity or a crack be X, Y in Cartesian coordinates. At infinity, the principal stresses and orientation of the first principal stress with respect to Ox_1 at infinity are denoted respectively by N_1, N_2, α. The asymptotic behaviors of functions at infinity are (Muskhelishvili, 1977)

$$\phi'(z) = \Gamma_0 - \frac{X+iY}{2\pi(1+\kappa)}\frac{1}{z} + O(1/z^2) \tag{3.17}$$

$$\psi'(z) = 2\Gamma + \frac{\kappa(X-iY)}{2\pi(1+\kappa)}\frac{1}{z} + O(1/z^2) \tag{3.18}$$

$$\Gamma_0 = \frac{1}{4}(N_1 + N_2) \tag{3.19}$$

$$\Gamma = -\frac{1}{4}(N_1 - N_2)\exp(-2i\alpha)$$

3. *Semi-infinite medium*. The asymptotic behavior of functions are

$$\phi'(z) = -\frac{X+iY}{2\pi}\frac{1}{z} + O(1/z^2) \tag{3.20}$$

$$\psi'(z) = \frac{X-iY}{2\pi}\frac{1}{z} + O(1/z^2) \tag{3.21}$$

where X and Y are the total force on infinite boundary S

3.1.4 The Hilbert problem

Some notions of mathematics and some theorems are needed for deriving the solutions of crack problems. For a complete justification and proof, we

refer to the book (Muskhelishvili, 1977). Let L be an oriented line or closed curve drawn in the complex plane z. We shall not make the distinction between a geometrical point t and its complex representation $t = t_1 + it_2$. Line L or *cut* separates the complex plane locally into two parts, (+) side on the left and (–) side on the right of the curve. A regular function in some region of the complex plane, regular in the sense that it is indefinitely differentiable, is called *analytic* function. Analytic function at region near L can be discontinuous across the curve when it is not *singled-valued* in the region considered. This is the case for the multiple-valued function log(z), which becomes single-valued n the complex plane when a cut is made along the positive axis (In this chapter, we write log(.) instead of ln(.)).

We define the limit of log(z), when z approaches the point $z^+ = x + i0$ in the upper plane by $\log(z^+) := \log(x)$. Then the limit at point $z^- = x - i0$ on the lower face of the cut is $\log(z^-) = \log(x) + i\pi$. In the complex plane outside the cut, the analytic function log(z) becomes *holomorphic* (regular and single-valued).

Another example is given by the multiple-valued function $f(z) = z^{1/2}$ ($z = e^{i\theta}$, $f(z) = r^{1/2}e^{i\theta/2}$) which becomes holomorphic in the complex plane with a cut L along any branch curve drawn in the plane starting from the origin and going to infinity. Function $f(z) = (z^2 - a^2)^{1/2}$ is holomorphic in the complex plane with a cut along any finite curve with end points $z = \pm a$. For discontinuous function f(t) at point $t_0 \in L$, there are two limits $f(t_0^+)$ and $f(t_0^-)$, from one or another side of the curve. Consider for example Cauchy's integral

$$f(z) = \frac{1}{2i\pi}\int_L h(t)\frac{dt}{t-z} \tag{3.22}$$

where h(t) is complex valued function, sectionnally continuous on L or satisfying the Hölder condition in some region G, $|h(t_2) - h(t_1)| \le A\,|t_2 - t_1|^{\mu}$, $\forall t_2, t_1$ in G, with the Hölder constant A and index μ, $0 < \mu \le 1$ for any t_2, t_1 in G.

The limits, $f(t_0^+)$ and $f(t_0^-)$ at regular part of L, outside the end points of L and points of discontinuous g(t), are given by the following *Plemelj formulae*, for the difference

$$f(t_0^+) - f(t_0^-) = h(t_0) \tag{3.23}$$

and for the sum

$$f(t_0^+) + f(t_0^-) = \frac{1}{i\pi}(pv)\int_L h(t)\frac{dt}{t-t_0} \tag{3.24}$$

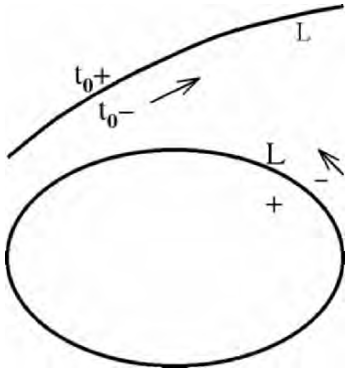

Figure 3.1: Cuts in the complex z-plane : (+) side on the left, (–) on the right of L

where the integral is understood in the principal value (pv) sense, i.e the integral over L outside a symmetric line segment centered at t_0 of vanishing length.

By combining (3.23) and (3.24) one obtains separately $f(t_0^+)$ and $f(t_0^-)$

$$f(t_0^+) = \frac{1}{2}h(t_0) + \frac{1}{2i\pi}(pv)\int_L h(t)\frac{dt}{t-t_0} \tag{3.25}$$

$$f(t_0^-) = -\frac{1}{2}h(t_0) + \frac{1}{2i\pi}(pv)\int_L h(t)\frac{dt}{t-t_0} \tag{3.26}$$

For given $g(t) \neq 0$ and h(t) on L, the *Hilbert problem* consists in finding f(z) satisfying the discontinuity equation on L, except at end points

$$f^+(t) - g(t)f^-(t) = h(t) \quad \text{on } L\backslash\{\text{end points}\} \tag{3.27}$$

Here we denote simply by $f^+(t)$ and $f^-(t)$ the two limits of f(t) on L. We shall only consider a simple curve with two end points a, b. For a constant valued function g(t) = g, which is the case considered in this book, the solution is given by

$$f(z) = \frac{X_0(z)}{2i\pi}\int_L h(t)\frac{dt}{X_0^+(t)(t-z)} + X_0(z)P(z) \tag{3.28}$$

$$X_0(z) = (z-a)^{-\gamma}(z-b)^{\gamma-1} \tag{3.29}$$

$$\gamma = \frac{1}{2i\pi}\log g = \frac{1}{2i\pi}\log|g| + \frac{\arg g}{2\pi} \equiv \alpha + i\beta \tag{3.30}$$

Argument $\theta := \arg(g)$ is chosen in such a manner that $0 \le \theta < 2\pi$, thus $0 \le \alpha < 1$. P(z) is an arbitrary polynomial whose degree is chosen so as to satisfy conditions at infinity of each problem.

The solution (3.29) is unbounded at end points like $|z-a|^{-\alpha}$, $|z-b|^{\alpha-}$ respectively. To obtain a bounded solution f(z) at one end point, z = a or b, one replaces function $X_0(z)$ by

$X_a(z) = X_0(z)(z-a)$

$X_b(z) = X_0(z)(z-b)$

respectively. For function bounded f(z) at all end points, the function considered is $X_{ab}(z) = X_0(z)(z-a)(z-b)$.

It should be noted that *no* solution exists for function X(z), bounded at some end point which does not vanish at this point. Therefore, at end points, function X(z) is either zero or infinite. Let us recall some formulae for further use.

The integral in Eq. (3.28) can be explicitly derived for polynomial h. Making the expansion of h(t)/X(t) at infinity $|t| \to \infty$ one then obtains Eq. (3.32) which gives an explicit result.

For most applications it is sufficient to consider function h(t) which can be approximated by polynomial. Eqs. (3.31), (3.32) then give a closed-form solution.

$$\frac{h(t)}{X(t)} \cong \alpha_q t^q + \alpha_{q-1} t^{q-1} + \ldots + \alpha_1 t + \alpha_0 + \ldots \tag{3.31}$$

$$\frac{1}{i\pi}\int_L h(t)\frac{dt}{X^+(t)(t-z)} = \frac{2}{1-g}\left\{\frac{h(z)}{X(z)} - \alpha_q t^q - \alpha_{q-1} t^{q-1} \ldots - \alpha_1 t - \alpha_0\right\} \tag{3.32}$$

3.2 The finite crack in an infinite medium

This is an important problem in Fracture Mechanics. We show how the solution is derived.

Consider a line crack of finite length, in an infinite medium, with uniform loads at infinity by the remote stresses $\tau = \sigma_{21}^{\infty}$, $\sigma = \sigma_{22}^{\infty}$ and the stress free condition on the crack, lying on the real axis along [a, b].

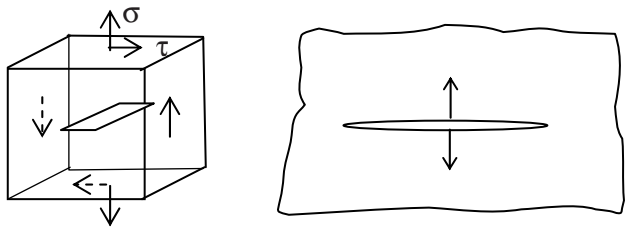

Figure 3.2: (a).The finite crack in an infinite medium under remote loads σ, τ;(b). The auxiliary problem with loads ± $\sigma^0_{2k}(\mathbf{x})$ on the crack faces

3.2.1 The auxiliary problem

The solution is obtained by the superposition of the constant stress field ($\sigma_{11}^{\infty} = 0, \sigma_{12}^{\infty}, \sigma_{22}^{\infty}$) and the *auxiliary* field with opposite $\mathbf{T}^{+} = (\sigma_{12}^{\infty}, \sigma_{22}^{\infty})$ applied to the upper face and $\mathbf{T}^{-} = (-\sigma_{12}^{\infty}, -\sigma_{22}^{\infty})$ applied to the lower face of the crack and no stress at infinity.

For further use, let us consider a more general auxiliary problem in which the tractions on the crack faces is *not* uniform, denoted hereafter by $\sigma^0_{2k}(x_1)$ instead of σ^{∞}_{2k} the conditions for the auxiliary field are

$$\sigma_{2k} = -\sigma^0_{2k}(x_1) \qquad \text{on L} \tag{3.33}$$

$$\sigma_{2k} \to 0 \qquad z \to \infty \tag{3.34}$$

According to Eq.(3.11) and Eq.(3.12), we have

$$\sigma_{22} - i\sigma_{21} = \phi'(z) + \overline{\Omega'(z)} + (z - \bar{z})\overline{\phi''(z)} \tag{3.35}$$

$$\Omega(z) = z\,\phi'(z) + \psi(z) \tag{3.36}$$

The method of solution consists in replacing conjugate values of functions $\overline{F(z)}$ (which are not analytic functions) by analytic functions G(z) in another domain, but having the same value in the real axis $z^{+} = x$, $\overline{F(z^{+})} = G(x)$. Consider for example function F(z) = z, its conjugate value is $\bar{z}$, thus $\partial(\bar{z})/\partial\bar{z} = 1$. The non zero partial derivative with respect to $\bar{z}$ indicates that the function $\bar{z}$ considered is not analytic in z. Now to any function holomorphic F(z) in the upper half plane P^{+} we define function $G(z) \equiv \overline{F}(z) \coloneqq \overline{F(\bar{z})}$ which is holomorphic in the lower half plane P^{-}, and

vice versa. On the real axis, one has $\bar{z} = z$, so that the limit of $\bar{F}(z^-)$ on the real axis is equal to $\bar{F}(z^-) = \overline{F(z^+)}$. The conjugate transform of function has another important property, namely $\partial\bar{F}(z)/\partial z = \overline{\partial F(-)/\partial z}$.

The boundary conditions on the crack can be written in either of the two forms

$$\phi'(t^+) + \bar{\Omega}'(t\ ) = -\sigma_{22}^0(t) + i\sigma_{21}^0(t)$$

$$\phi'(t^-) + \bar{\Omega}'(t^+) = -\sigma_{22}^0(t) + i\sigma_{21}^0(t)$$

Combining these equations we find that function $[\phi' - \bar{\Omega}']$ is continuous across the real axis

$$\left[\phi'(t^+) - \bar{\Omega}'(t^+)\right] - \left[\phi'(t^-) - \bar{\Omega}'(t^-)\right] = 0 \tag{3.37}$$

According to a theorem, a holomorphic function in both the upper half plane and the lower half plane, and continuous across the real axis, must be a constant C, equal to zero by considering the boundary condition at infinity. Finally we obtain the equations

$$\bar{\Omega}'(z) = \phi'(z), \qquad \Omega'(z) = \bar{\phi}'(z) \tag{3.38}$$

Boundary conditions (3.33) with (3.35) can be re-written in the form

$$\phi'(t^+) + \phi'(t^-) = -\sigma_{22}^0(t) + i\sigma_{21}^0(t) \text{ on L} \tag{3.39}$$

This is a Hilbert problem, with g = –1 whose solution is (see Eq.(3.28))

$$\phi'(z) = \frac{X(z)}{2i\pi}\int_L \left\{-\sigma_{22}^0(t) + i\sigma_{21}^0(t)\right\}\frac{dt}{X^+(t)(t-z)} + CX_0(z) \tag{3.40}$$

$$X(z) = (z-a)^{-1/2}(z-b)^{-1/2}$$

$$\psi'(z) = \bar{\phi}'(z) - \phi'(z) - z\phi''(z)$$

The stress intensity factors at the crack tip z_0 are given by

$$K_I(z_0) - iK_{II}(z_0) = 2\sqrt{2\pi}\lim_{z\to z_0}\left\{(z-z_0)^{1/2}\phi'(z)\right\} \tag{3.41}$$

There are different SIF formulae for the crack [a, b], at the right crack tip

$$K_I(b) - iK_{II}(b) = \left[\frac{2}{\pi(b-a)}\right] \int_a^b \left\{\sigma_{22}^0(t) - i\sigma_{21}^0(t)\right\} \left[\frac{t-a}{b-t}\right]^{1/2} dt \qquad (3.42)$$

and at the left crack tip

$$K_I(a) - iK_{II}(a) = \frac{2}{\pi(b-a)} \int_a^b \left\{\sigma_{22}^0(-t) - i\sigma_{21}^0(-t)\right\} \left(\frac{b-t}{t-a}\right)^{1/2} dt \qquad (3.43)$$

Crack under remote uniform loading

Since $\phi'(z) \cong O(1/z^2)$ (no total force at infinity in the auxiliary problem) constant C is equal to zero. For constant stress $-\sigma_{12}^{\infty}, -\sigma_{22}^{\infty}$ on the crack $[-l, +l]$ the solution of the auxilary is

$$\phi'(z) = \frac{1}{2}(\sigma_{22}^{\infty} - i\sigma_{21}^{\infty})\left\{z(z^2 - l^2)^{-1/2} - 1\right. \cdot \qquad (3.44)$$

$$\psi'(z) = \frac{1}{2}(\sigma_{22}^{\infty} - i\sigma_{21}^{\infty}) z l^2 (z^2 - l^2)^{-3/2} + i\sigma_{21}^{\infty} \left\{z(z^2 - l^2)^{-1/2} - 1\right\} \qquad (3.45)$$

Stress intensity factors at crack tips $z_0 = \pm l$ are calculated from the singularities of the auxiliary problem by formulae

$$K_I(z_0) - iK_{II}(z_0) = 2\sqrt{2\pi} \lim_{z \to z_0} \left\{(z - z_0)^{1/2} \phi'(z)\right\} \qquad (3.46)$$

One obtains the same values at both crack tips

$$K_I = \sigma_{22}^{\infty}\sqrt{\pi l}, \quad K_{II} = \sigma_{21}^{\infty}\sqrt{\pi l} \qquad (3.47)$$

Crack under remote bending stress

Under non uniform stresses at infinity, formulae for the right SIF and the left SIF given by Eqs. (3.42), (3.43) can be negative at one tip. In order to

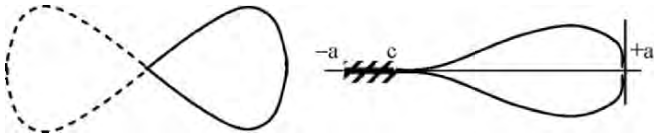

Figure 3.3: The crack overlapping in bending stress and corrections by frictionless contact conditions in [−a, c]

avoid *overlapping*, these formulae must be modified to take into account the condition of positive normal crack opening displacement or $K_I > 0$. Consider the case where the load $\sigma^0_{21}(t) = 0$, $\sigma^0_{22}(t) = \beta t$ is antisymmetric on the crack [−a, +a]. Clearly Eq.(3.42) and Eq.(3.43) with $\beta > 0$ give opposite values of the stress intensity factors at $z = a$ and $z = -a$. To avoid overlappings of the crack faces, we consider the Signorini contact problem and introduce a *contact* zone [−a, c] between the crack faces. The transition point c of the contact zone is an unknown to be determined by the conditions of smooth crack opening and zero contact stress; thus c is determined by the condition that the left SIF at z = c vanishes. The stress intensity factor at c is calculated with the effective crack [c, a]. The condition $K_I(c) = 0$ is written as

$$K_I(c) = 0 \quad \Rightarrow \int_c^a \sigma^0_{22}(-t)\left[\frac{a-t}{t-c}\right]^{1/2} dt = 0 \tag{3.48}$$

Eq.(3.48) determines the contact point c. Having the contact point c, the SIF at z = a is then given by formula for SIF at the right crack tip

$$K_I(a) = \left[\frac{2}{\pi(a-c)}\right]^{1/2} \int_c^a \sigma^0_{22}(t)\left[\frac{t-c}{a-t}\right]^{1/2} dt \tag{3.49}$$

3.2.2 Dugdale-Barenblatt's model

The model considers line zones of concentrated plastic deformation called the *cohesive zone* along [−c,−a] and [a, c], under constant normal stress $\sigma_{22} = \sigma_0$. The length R = c−a has to be determined. The true crack is on [−a, a], but to derive the solution, one considers the effective crack [−c, +c] and solves the auxiliary problem with boundary conditions

$$\sigma^0_{22}(x_1) = \begin{cases} -\sigma^\infty_{22} & |x_1| < a \\ -\sigma^\infty_{22} + \sigma_0 & a < |x_1| < c \end{cases} \tag{3.50}$$

with $\sigma \cong O(1/|z|^2)$ at infinity. The solution is given by (Dugdale, 1960; Barenblatt, 1962)

$$\phi'(z) = \frac{1}{2i\pi}(z^2 - c^2)^{-1/2} \int_{-c}^{+c} \sigma^0_{22}(t) \frac{dt}{-i(c^2 - t^2)^{-1/2}(t - z)} \tag{3.51}$$

In Dugdale-Barenblatt's model, there is another implicit condition that the stresses in front of an effective crack tip are regular. This condition is

$K_I(\pm c) = 0$ or

$$\int_{-c}^{+c} \sigma_{22}^{0}(t) \frac{dt}{(c^2 - t^2)^{1/2}(t - c)} = 0 \tag{3.52}$$

$$\Rightarrow R = c - a = a\left\{\frac{1}{\cos\ \pi\sigma^{\infty} / 2\sigma_0)} - 1\right\} \tag{3.53}$$

The crack-opening displacement COD at x = a, the end of the stretching of the cohesive zone, can be calculated as

$$\delta = u_2^{+}(a) - u_2^{-}(a) = \frac{\kappa + 1}{\pi\mu} \sigma_0 a \log\left\{\frac{1}{\cos(\pi\sigma^{\infty} / 2\sigma_0)}\right\} \tag{3.54}$$

For small σ^{∞}/σ_0 the COD is $\delta \cong (\kappa+1)a\pi(\sigma^{\infty})^2/8\mu\sigma_0$. In plane stress one obtains $\delta \cong a\pi(\sigma^{\infty})^2/E\sigma_0$.

It should be noted that Dugdale-Barenblatt's model does not involve stress singularity so that the plane stress condition may be a good model for thin plate, while it is inconsistent for cracks in elasticity. Another reason is that plasticity appears in thin plate as an inclined shear band through the thickness, thus justifies a localized plastic zone or a thin cohesive zone. Dugdale-Barenblatt's model can be generalized to the anti-plane mode III, (Kostrov and Nikitin, 1967).

3.3 The kinked crack in mixed mode

Consider a line crack along the segment [–a, a] under a mixed mode K_I, K_{II}. Experiments show that when the load increases at some critical value, the crack does not propagate in its direction but rather deviates by some angles. The deviation angle is generally well predicted by theories which consider the maximun hoop stress criterion, with $\sigma_{\theta\theta}$ calculated in the configuration *before* deviation. Most theories consider that the deviation angle θ^* is the solution of the problem:

$$\theta^* = \arg\max_{\theta} \sigma_{\theta\theta} \tag{3.55}$$

Mandel (1974) proposed the zero shear stress criterion

$$\sigma_{r\theta}(\theta^*) = 0 \tag{3.56}$$

with the stress components

$$4\sigma_{\theta\theta}/\sqrt{2\pi r}_0 = K_I(3\cos\frac{\theta}{2}+\cos\frac{3\theta}{2}) - 3K_{II}(\sin\frac{\theta}{2}+\sin\frac{3\theta}{2}) \tag{3.57}$$

$$4\sigma_{\theta r}/\sqrt{2\pi r}_0 = K_I(\sin\frac{\theta}{2}+\sin\frac{3\theta}{2}) + K_{II}(\cos\frac{\theta}{2}+3\cos\frac{3\theta}{2}) \tag{3.58}$$

In the pure mode II, Eqs.(3.55) and (3.56) give the same result, about $\theta^* = -71°$, which is the solution of $\cos(\theta^*/2) + 3\cos(3\theta^*/2) = 0$. These theories predict reasonably the deviation angle, but are not able to predict the critical load at propagation in the new branching direction.

The consistency with linear Fracture Mechanics should require the knowledge of the stress intensity factors with respect to new axes, Ox_1' along the branched crack, k_1^* and k_2^*, in the crack configuration *after* deviation.

These new SIF provide possible criterions in terms of k_1^*, k_2^*, or G^* using the same material constant such as the toughness K_{1c} for example. In pure applied mode K_{II} before kinking, the new SIF are functions of K_{II}. Crack deviation occurs when $k_2^* = 0$ and $k_1^*(K_{II}) = K_{1c}$.

3.3.1 An integral equation of the kinked crack problem

The kinked problem with a main crack $[-l, +l]$ and a finite kink of length s is first studied in (Hussain et al, 1974). This problem leads to an integral equation which is solved by numerical methods. Hereafter we consider the same problem, by first making an asymptotic analysis of the integral equation when the kink length goes to zero and then solving the asymptotic problem in a closed form.

Let the infinite body containing a stress-free crack be loaded at infinity by stress $S = \sigma_{22}^{\infty} - i\sigma_{21}^{\infty}$ for which the SIF is $K_I - iK_{II} = S(\pi l)^{1/2}$.

Using standard notations (Dudukalenko and Romalis, 1973), we consider function $z = \omega(\xi)$ which maps the exterior Ω^- of unit circle $|\xi| = 1$ onto the physical plane. A cut is made along the kinked crack, with the deviation angle $m\pi$ between the two branches. The mapping function $\omega(\xi)$ is obtained by the Schwarz-Christoffel transform

$$z = \omega(\xi) := Re^{im\alpha}(\xi - e^{i\alpha})(\xi - e^{-i\alpha})\xi^{-1}\left[(\xi - e^{-i\alpha})/\ \xi - e^{i\alpha})\right]^m \tag{3.59}$$

$$l = 2R[\cos(\frac{\alpha+\beta}{2})]^{1-m}[\cos(\frac{\alpha-\beta}{2})]^{1+m}$$

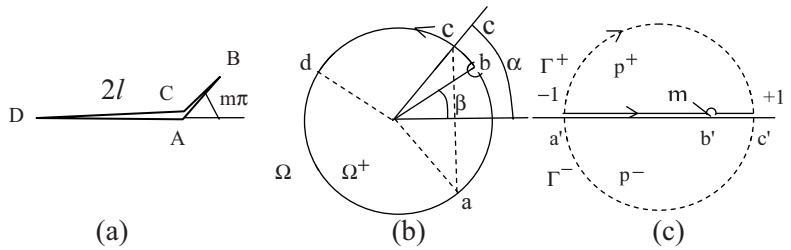

Figure 3.4: The physical plane (a) of a crack with the main length 2*l* and a kink of length s = AB in the direction mπ ; Transform z = ω(ξ) in the ξ-plane (b); Transform ξ(t) in the t-plane (c). Points b, m are indented by semi-circles clockwise

$$s = 4\mathrm{R}[\sin(\frac{\alpha+\beta}{2})]^{1+\mathrm{m}}[\sin(\frac{\alpha-\beta}{2})]^{1-\mathrm{m}}$$

$$\sin\beta = \mathrm{m}\,\sin\alpha$$

Crack tips B, D and corners A, C are mapped into points b, d, a, c of the circle, Fig. 3.4. From complex potentials of Muskhelishvili Φ(z), Ψ(z), we define new complex potentials $\phi(\xi) := \Phi(\omega(\xi))$, $\psi(\xi) := \Psi(\omega(\xi))$.

In Muskhelishvili's book, a method of solution by an integral equation for ϕ(ξ) can be found. This equation has been given by Hussain et al, (1974)

$$\phi(\xi) - \frac{1-e^{2i\pi\mathrm{m}}}{2i\pi}\int_{C_1}\frac{(\sigma-e^{i\alpha})(\sigma-e^{-i\alpha})\overline{\phi'(\sigma)}}{\sigma(\sigma+e^{-i\beta})(\sigma-e^{i\beta})(\sigma-\xi)}d\xi$$

$$= \Gamma\xi e^{\mathrm{im}\alpha} - (\frac{\Gamma+\overline{\Gamma'}}{\xi})\mathrm{R}e^{-\mathrm{im}\alpha} \qquad (3.60)$$

where $\Gamma = \mathrm{S}/4, 2\Gamma + \overline{\Gamma'} = S$, $\mathrm{a} = \mathrm{e}^{-\mathrm{i}\alpha}$, $\mathrm{d} = \mathrm{e}^{\mathrm{i}(\pi-\mathrm{i}\beta)}$, $\mathrm{c} = \mathrm{e}^{\mathrm{i}\alpha}$. Points ξand $\mathrm{b} = \mathrm{e}^{\mathrm{i}\beta}$ are on the circle from the outside Ω^- (point b is unsderstood as b^- or equivalently the contour C_1 is indented by a small clockwise contour around point $\mathrm{b} = \mathrm{e}^{\mathrm{i}\beta}$ as shown in Fig. 3b. The stress intensity factors at the tip B are defined by

$$\mathrm{k}_1(\mathrm{s}, \pi\mathrm{m}) - \mathrm{i}\mathrm{k}_2(\mathrm{s}, \pi\mathrm{m}) = 2\sqrt{\pi}\ \phi'(e^{i\beta})[e^{i\pi\mathrm{m}}\omega''(e^{i\beta})]^{-1/2} \qquad (3.61)$$

First one solves (3.60), then one takes the limit of (3.61) as $\mathrm{s}\to 0$, to determine the initial SIF at kinking $\mathrm{k}_1^* = \mathrm{k}_1(\mathrm{s}\to 0)$, $\mathrm{k}_2^* = \mathrm{k}_2(\mathrm{s}\to 0)$. This

method as given in many works is less attractive than the one considered below which consists in inverting the procedure.

3.3.2 The asymptotic equation

Since $\alpha \to 0$ as $s \to 0$, we make use of a *double scale* technique which magnifies both the variable and the function

$$\xi \;\to\; t = \frac{1}{i\alpha}\log\xi, \quad (\xi = e^{i\alpha t}), \qquad t \in [-1,+1]$$

$$\phi(\xi) \;\to\; g(t) = \frac{1}{i\alpha l}\left\{\phi(\xi(t)) + \overline{\Gamma'}\frac{l}{2}\right\}$$

Inserting these changes of variable and function into Eq.(60) and dropping terms of orders higher than $O(\alpha)$ we then obtain the asymptotic equation in the form

$$g(t) = \frac{1-e^{2i\pi m}}{2i\pi}\int_{-1}^{+1}\frac{(\lambda^2-1)\overline{g'(\lambda)}}{(\lambda-m)(\lambda-t)}d\lambda + S\frac{t+m}{2} \tag{3.62}$$

where real points $\{t, m\}$ are understood as $\{t^-, m^-\}$ of the lower half plane. It is convenient to deal with analytic functions by introducing the conjugate transform of functions by defining

$$\bar{g}(\lambda) := \overline{g(\bar{\lambda})} \;\Rightarrow\; \bar{g}'(\lambda) = \overline{g'(\bar{\lambda})}.$$

The term $\overline{g'(\lambda)}$ in (3.62) is replaced by $\bar{g}'(\lambda)$, which is holomorphic in the upper half plane P^+ and thus allows us to change the indented clockwise contour around point m^- by the clockwise semi-circle Γ^+. By introducing $h(t) = (t^2-1)g'(t)$ we then obtain

$$h(t) = \frac{(t^2-1)(1-e^{2i\pi m})}{4i\pi}\int_{\Gamma^+}\frac{\bar{h}(\lambda)}{(\lambda-m)(\lambda-t)^2}d\lambda + S\frac{(t^2-1)}{2} \tag{3.63}$$

This equation is the same as that of Wu (1978) obtained by a different limiting process.

The SIF is derived from Eq.(3.61) as

$$k_1^*(\pi m) - ik_2^*(\pi m) = 2\sqrt{\pi l}e^{-i\pi m}\left\{(1-m)/(1+m)\right\}^{m/2} g'(m) \tag{3.64}$$

Solution of the integral equation

Let us write Eq. (3.63) in the form $h(t) = Lh(t) + h_0(t)$ where L is an integral operator, $t \in \Gamma^-$ and $h_0(t) = S(t^2-1)/2$. We introduce the norm of uniform convergence over Γ . It can be shown that operator L is bounded, Amestoy et al (1979)

$$\|Lh\| \leq \frac{\sin \pi m}{\pi(1-m)} \|h\| \tag{3.65}$$

For $0 \leq m < 1$, constant $A = (\sin\pi m)/\pi(1 - m)$ is less than 1.
The majoration (3.65) shows that L is a *contracting operator* and thus the solution of Eq. (3.63) is given by the strong convergence of the series using iterated operators L^n with the $C(\Gamma)$ norm

$$h = h_0 + L\, h_0 + L^2\, h_0 + L^3\, h_0 \ \ldots \tag{3.66}$$

After finding the solution along the lower semi-circle, and determining h(m) from Eq. (3.63) and g'(m), we then obtain the SIF as

$$\begin{pmatrix} k_1^* \\ k_2^* \end{pmatrix} = \begin{bmatrix} K_{11} & K_{12} \\ K_{21} & K_{22} \end{bmatrix} \begin{pmatrix} K_I \\ K_{II} \end{pmatrix} \tag{3.67}$$

where K_{hk}'s depends on the kink angle. Numerical computations of the series (3.66) show rapid convergence after 5 terms. Table I gives the computed values of the matrix components K_{hk}. The energy release rate in plane strain is given by $G^* = (1 - \nu^2)(k_1^{*2} + k_2^{*2})/E$.
Two possible criteria can be proposed:

i) the crack branching angle corresponds to maximun G*.

ii) a kinked crack starts propagating in the pure local mode 1, ($k_2^* = 0$).

In the pure mode II before kinking, the first criterion $\partial_m G^*(\theta^*) = 0$ gives $\theta^* \cong -76.6°$, while the second criterion $k_2^*(\theta^*) = 0$ gives $\theta^* \cong -77.3$.

Table I

kink angle	k_{11}	k_{21}	k_{12}	k_{22}	kink angle	k_{11}	k_{21}	k_{12}	k_{22}
0°	0	0	0	1	50	0.7479	0.3431	−1.0665	0.4872
10	0.9886	0.0864	−0.2597	0.9764	60	0.6559	0.3696	−1.1681	0.3077
20	0.9552	0.1680	−0.5068	0.9071	70	0.5598	0.3788	−1.2220	0.1266
30	0.9018	0.2403	−0.7298	0.7972	80	0.4640	0.3718	−1.2293	−0.0453
40	0.8314	0.2995	−0.9189	0.6540	90	0.3722	0.3507	−1.1936	−0.1988

These angles are different compared with values predicted by theories based on the stress fields before kinking. The results on kinked angles are similar to those given in many works, (Bilby and Cardew, 1975). Crack kinking under constant cohesive force in the kink branch has been worked out by Li (1997).

3.4 Crack problems in elastoplasticity

Problems in plasticity are difficult to solve for many reasons : non linearity of the stress-strain laws which physically obey Prandtl-Reuss's law, incremental nature of the elastic-plastic law, existence of threshold stress or yield surface, fundamental difference between loading and unloading, criteria of crack propagation not yet established etc. Moreover experimental facts indicate that crack initiation and crack propagation occur at *large* strain and that ductile fracture and damage are the main phenomena.

Can we have a good mathematical model of ductile fracture and damage within the framework of linearized small strain?

Brittle Fracture mechanics has been faced with the same question, but the problem has been solved in the sense that the square root singularity at a crack tip is considered as the *outer* field solution when we approach the crack tip zone, whose field solution, called the *inner* field, depends on the physics of the process zone, with possibly the finiteness of the stress field in perfect plasticity. Only a possible matching between the outer and inner asymptotic solutions is of interest for applications.

To match asymptotic solutions, one writes the condition $f^{out}(r \to 0) = f^{in}(r \to \infty)$. To our knowledge, there is no general methods for matching solutions. Most solutions are only approximate ones in the sense that some important features are considered, not all. For a fully complete solution in plasticity, with threshold stress, matching is different in that the boundary C between elastic and plastic zones has to determined. This is typically an inverse geometric problem in Fracture Mechanics. Yield criterion and continuity of stress vector and displacement must be satisfied along C. The stress field of the inner solution, for $r \to 0$, is finite for a non hardening material (perfect plasticity) or singular for hardening materials obeying a power law as illustrated by the HRR solution, established simultaneously in two papers (Hutchinson, 1968; Rice and Rosengren, 1968).

Another class of solution, discussed in Sect. 4.2, is related to the small scale yielding assumption, where plasticity is confined to the near tip region and where the outer field is governed by the asymptotic field $f^{out} \cong K_I g(\theta) r^{-1/2}$ (in mode I).

3.4.1 Matching asymptotic solutions

Consider the Ramberg-Osgood stress-strain law for monotonic loading in plane stress

$$\varepsilon_{hk} = \frac{1+\nu}{E}\sigma_{hk} - \frac{\nu}{E}\sigma_{ii}\delta_{hk} + C(\frac{\sigma_e}{\sigma_0})^{n-1} s_{hk} \tag{3.68}$$

where σ_0 is some reference stress (not the yield stress) and $s_{hk} := \sigma_{hk} - \sigma_{ii}\delta_h /3$ is the stress deviator. Since unloading is not allowed, asymptotic models using this law describe stationary cracks only. Some models generalize Eq. (3.68) to viscoplastic materials obeying the strain rate law $\partial_t\varepsilon = L.\partial_t\sigma + C(\sigma_e/\sigma_0)^{n-1}s$ to model a crack propagation (Hui and Riedel, 1981). In the wake plastic zone, there is a stress unloading which cannot be described by the Hencky theory of plasticity, even in the rate form. Therefore, we restrict ourselves to stationary cracks and outline a method of matching solutions, without entering into the details. In elasticity, the asymptotic stress function ψ can be derived by expanding the exact solution near the crack, via the complex variables. It has been done by (Williams, 1957) for example for the first k + 1 terms

$$\psi^e = r^{3/2}h_{eo}(\theta) + r^2 h_{e1}(\theta) + ... + r^{(k+3)/2}h_{ek}(\theta) \tag{3.69}$$

The first term of Eq. (3.69) corresponds to the square root stress singularity, the second term corresponds to the constant T-stress etc... It has been proposed in (Li, 1997) that the stress function ψ^{ep} of the elasto-plastic zone can be expanded in the same manner by

$$\psi^{ep} = r^{(2n+1)/(n+1)}h_{HRR}(\theta) + r^{s_1}h_1(\theta) + ... + r^{s_p}h_p(\theta) \tag{3.70}$$

The first term of Eq. (3.70) is the HRR field (Hutchinson-Rice-Rosengren's solution), with the function $h_{HRR}(\theta)$ determined by considering the compatibility equations for the strain, then solving numerically the nonlinear differential equation for the angular function with some boundary conditions. The exponent (2n + 1)/(n + 1) has been obtained independently by using the J-integral. In Eq. (3.70) many other terms, but not all, can be derived by the same procedure. However, it is more convenient to consider all exponents s_1, s_2, .. and angular functions $h_1(\theta)$, $h_2(\theta)$ as unknowns. For the continuity reason of the stress and displacement, the matching at some arbitrarily chosen radius R is determined by the conditions that all derivatives of different orders of ψ^e and ψ^{ep} are equal. The set of unknowns is denoted by $X = \{s_1, s_2, .h_1(\theta), h_2(\theta), ., R\}$. The matching proposed by Li (1997) consists in the minimization, with respect to

parameters and functions in X of the *complementary* potential $U = \int \underline{u}(\sigma) d\Omega$ with the density $\underline{u}(\sigma)$ from which the strain ε, Eq. (3.68), is derived $\varepsilon = \partial \underline{u}/\partial\sigma$. Numerical results of Li (1997) are in good agreement numerical with the finite element method solutions (Sharma and Aravas, 1991).

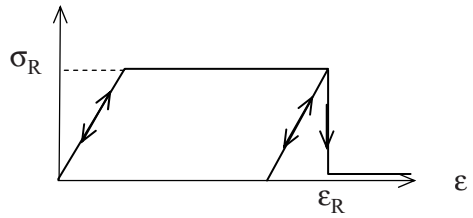

Figure 3.5: Elastic-plastic damage law with the critical strain ε_R. The stress vanishes for strain larger than ε_R

3.4.2. A complete solution in plasticity and damage

We consider an elastic-plastic-brittle law described in Fig. 3.5.
For equivalent strain ε_e less than a critical value $\varepsilon_e < \varepsilon_R$ the stress-strain law is the classical one. For larger equivalent strain $\varepsilon_e > \varepsilon_R$, damage takes place so that the stress decreases with increasing strain. A strain-softening behavior in the uniaxial tension case of the form $\sigma = C\varepsilon(\mu + n\varepsilon/\varepsilon_e)^{-1-1/n}$, $\varepsilon_e > \varepsilon_R$, and $\sigma = C\varepsilon$, $\varepsilon_e < \varepsilon_R$, has been considered by Gao and Bui (1995).

In what follows, we consider the simplest possible model which consists in assuming $\sigma \equiv 0$ for $\varepsilon_e > \varepsilon_R$. In perfect plasticity, the yield stress in anti-plane strain coincides with stress σ_R just at $\varepsilon_e = \varepsilon_R$.

When $\varepsilon_e > \varepsilon_R$ in a solid, according to the model, there exist a fully damaged zone with some finite thickness 2h, a damage front BB', a plastic zone and an elastic-plastic boundary.

The determination of different zones, damaged and plastic zones, is an inverse geometric problem in plasticity. In numerical computations, the inverse problem is generally solved by a shape optimization procedure, using some sensitivity techniques for the corrections or updating of geometries. Since the boundary of the damaged zone is stress free, the *inverse problem* considered is also a sort of free boundary value problem very often encountered in fluid mechanics.

Now we show that this inverse problem is solved in closed form for an anti-plane strain loading.

Elastic solution

Consider first the quasi-static problem in elasticity solved by Bui and Ehrlacher (1979). The remote outer field in mode III, with a complex stress representation, is given by $\tau \cong K_{III}/(2\pi r)^{-1/2}$, $\tau = \sigma_{32} + i_{31}$ (Note that the real variable is σ_{32}). For simplicity we write K instead of K_{III}.

The field solution in the physical plane $\tau(z)$ in equilibrium with the remote outer stress field is searched in its *inverted* form $z(\tau)$. Point B ($z = ih$) is mapped into point $\tau = i\sigma_R$.

$$z\ \tau) = (K^2/2\pi\tau^2) - (2h/\pi)\ln(\tau/\sigma_R) + \text{real constant} \tag{3.71}$$

$$u_3 = \text{Im}\left\{K^2(\sigma_R - \tau)/\pi\mu\tau\sigma_R - 2h(\tau - \sigma_R)/\pi\mu\right\} \tag{3.72}$$

Eqs.(3.71), (3.72) can be easily checked. We arbitrarily fix the real constant so that $x_1(B) = 0$. Thus the equation of the damaged front is

$$\left.\begin{aligned} X_1(\theta) &= (h/\pi)(\cos 2\theta + 1) \\ X_2(\theta) &= -(h/\pi)(\sin 2\theta + 2\theta) \end{aligned}\right\} -\pi < \theta < +\pi \tag{3.73}$$

The damaged front BNB' has the shape of a *cusped* cycloid. The energy release rate in the elastic-brittle damage model is given by the J-integral along BB', with the elastic strain energy density

$$J = \int_{BB'} W(\varepsilon^e)dx_2 = h\sigma_R^2/\mu \tag{3.74}$$

Taking account of J, calculated from the remote field $J = K^2/2\mu$, we obtain

$2h = K^2/\sigma_R^2$.

In the case of infinite stress σ_R, the thickness 2h vanishes so that we recover the crack model as the limiting case $\sigma_R \to \infty$ of the fully damage model. It should be noted that the dissipation rate (with respect to unit length advance of the damage zone) is equal to the total *elastic* energy released by particules along BB' when they move into the damaged zone.

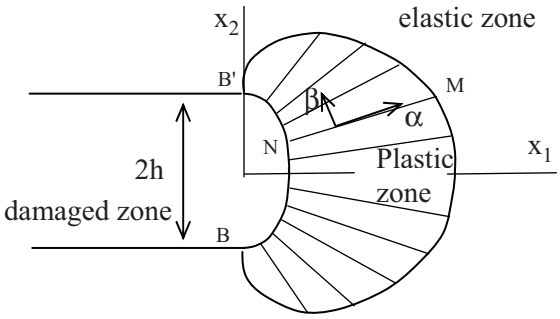

Figure 3.6: Damaged zone, plastic zone and elastic zone. The damage front BB' (point N) is a curled cycloid, Eq. (3.73). The elastic-plastic boundary (point M) is a cusped cycloid, Eq. (3.81)

This rate of energy will be lost by thermal conduction or vibrations etc. This is the reason why it is called the dissipation rate of energy D_R by rupture. The dissipation rate with respect to time is defined by

$$D_R := l \int_{BB'} W(\boldsymbol{\varepsilon}^e) dx_2 \tag{3.75}$$

The elastic-brittle damage model in quasi-statics has been generalized to dynamic elasticity by Ehrlacher (1985).

Remarks. A numerical approach to solve the inverse geometric problems consists of three steps:

i) Having determined the thickness h, by $2h = K^2/\sigma_R^2$, the damage front BB' is defined by a N-dimensional parameter **p**. One solves the elastic equilibrium problem with the remote stress $\sigma \cong K/\sqrt{(2\pi r)}$ and the stress free condition on the damage front.

ii) One calculates the stress $\sigma_{3\beta}$ along BB' which depends on parameters **p**.

iii) One searches the optimal **p** solution of

$$\min_{\mathbf{p} \in \mathcal{P}^N} \left(\int_{BB'} [\sigma_{3\beta}(\mathrm{p}) - \sigma_{\mathrm{R}}]^2 ds \right).$$

Such a minimization problem is generally ill-conditionned (matrix determinant of the linear system is nearly equal to zero) and required regularization methods, see Chap. 12. Historically, the damage front BB' has been

obtained by numerical "experiments", then it has been proved that it is a cusped cycloid (Bui and Ehrlacher, 1979).

Elasto-plastic solution

Now consider the case $\sigma_R/2\mu \le \varepsilon < \varepsilon_R$ for the sound solid. The critical strain ε_R is first reached along the boundary of the damaged zone. We search an elasto-plastic solution with:

- condition $\varepsilon_e = \varepsilon_R$ along the unknown damage front BB',
- stress-free condition along the boundary BB',
- a plastic zone ahead the front BB' where $\sigma_e = \sigma_R$,
- an elastic-plastic boundary defined by three conditions : $\varepsilon_e = \sigma_R/2\mu$, Continuous displacement and continuous stress vector

This is typically an inverse geometric problem, where the outer elastic field is prescribed. At first sight, this problem seems to be more complex than that of finding a stress-free crack in an elastic solid, encountered in the evaluation of materials (Non Destructive Testing of Materials). In fact the problem in anti-plane strain condition can be solved in closed form. The solution in the elastic zone is given by formulae

$$z\ \tau) = (K^2/2\pi\tau^2) - (2h/\pi)\ln(\tau/\sigma_R) + (K^2/2\pi\sigma_R^2) \tag{3.76}$$

$$u_3 = \mathrm{Im}\left\{K^2(\sigma_R - \tau)/\pi\mu\tau\sigma_R - 2h(\tau - \sigma_R)/\pi\mu\right\} \tag{3.77}$$

where τ lies inside the semi-circle $|\tau| \le \sigma_R$, $-\pi/2 \le \theta \le \pi/2$, for $\sigma_R/2\mu \le \varepsilon < \varepsilon_R$. The latter conditions correspond to the load K

$$K_R^2 \le K^2 \le 2h\sigma_R(4\mu\varepsilon_R - \sigma_R) \tag{3.78}$$

with $K_R^2 = 2h\sigma_R^2$. Eq.(3.78) defines a limit load K_∞ ($K_R < K < K_\infty$)

$$K_\infty = \{2h\sigma_R(4\mu\varepsilon_R - \sigma_R)\}^{1/2} \tag{3.79}$$

the circle $|\tau| = \sigma_R$ in the τ-plane is mapped into the elastic-plastic boundary whose equations are

$$\left.\begin{aligned} M_1(\theta) &= (K^2/2\pi\sigma_R^2)(\cos 2\theta + 1) \\ M_2(\theta) &= -(K^2/2\pi\sigma_R^2)\sin 2\theta + (2h\theta/\pi) \end{aligned}\right\} -\pi < \theta < +\pi \tag{3.80}$$

The elastic-plastic boundary (point M) is a *curled cycloid* (Bui and Ehrlacher, 1981). Now a solution is searched in the plastic zone with the flaw rule $\dot{\varepsilon}^{p}_{3i} = \lambda\sigma_{3i}$ (λ is a positive multiplier).

An approximate solution is derived by neglecting elastic strain in the plastic zone and assuming that one family of characteristic lines consists of straight α-lines (β = const), in which according to the theory of plasticity, the stress components $\sigma_{3\alpha}$, $\sigma_{3\beta}$ are constant $\sigma_{3\beta} = \sigma_R$, $\sigma_{3\alpha} = 0$, as well as the displacement u_3 on the α-line (constant θ)

$$u_3(M) = -(1/\mu\pi)\left\{(K^2/\sigma_R^2) + 2h\sigma_R\right\}\sin\theta \tag{3.81}$$

There exists a particular β-line for load $K = K_R$ or $K_R^2 = 2h\sigma_R^2$ when plasticity just appears at BB'. This line is the locus of points N

$$\left.\begin{aligned} N_1(\theta) &= (h/\pi)(\cos 2\theta + 1) \\ N_2(\theta) &= -(h/\pi)\sin 2\theta + (2h\theta/\pi) \end{aligned}\right\} \quad \pi < \theta < +\pi \tag{3.82}$$

The curve (3.82) is the same *cusped cycloid* as that of Eq. (3.73). It should be noted that for $\varepsilon_R \to \infty$ the cusped cycloid BNB' reduces to the crack tip while the curled cycloid BMB' becomes a circle, tangent to the Ox_2 axis. We recover the circular plastic zone ahead the crack tip given in earlier works, (Hult and McClintock, 1957; Rice, 1986).

Rice's paradoxical result recovered by a damage model theory

Rice (1966) observed that a balance equation of energy in perfect plasticity applied to a small zone around the moving crack tip leads to G = 0. This is the paradoxical result in plasticity : no driving force for crack propagation in plastic materials. It has been shown in (Bui, 1987) that $G = D_R = 0$ for a large class of materials having a parabolic strain-hardening law $\sigma = \Lambda\varepsilon + C\varepsilon^n \cong C\varepsilon^n$, $0 < n < 1$. To show this, let us make use of the estimate $\sigma{:}\varepsilon \cong O(1/R)$ along a stress-free notch of radius R. In the fully damaged model, we have R = O(h). Thus, the total elastic energy dissipated along the damaged front BB' vanishes

$$2hW_R \cong 2h(\sigma_R)^2 = 2hC^2(\varepsilon_R)^{2n} \cong 2C(\varepsilon_R)^{n-1} \to 0$$

as $\varepsilon_R \to \infty$. In other words, the J-integral, with the elastic strain energy density (instead of the stress working $\int\sigma{:}d\varepsilon$) around a small contour around the crack tip, vanishes in the limiting damage model.

Over many decades, like the conquest of the Graal, workers have been searching unsuccessfully a characteristic crack parameter for non-linear Fracture Mechanics, putting so much hope on energetic parameters which unfortunately do not provide a criterion of ductile fracture. Very accurate numerical calculation of $J_{tip}= \int_{\Gamma(\eta\to 0)} W(\varepsilon-\varepsilon^p)dx_2 = 0$ for vanishing contour radius confirms the result $(da/dt)J_{tip} = D_R = 0$.

3.4.3. A review of non linear asymptotic solutions

Let us mention some models, without entering into their detailed derivations which are very technical. These models are important for the construction of inner solutions in view of the matching with the outer elastic field for example. Unfortunately, such matchings are scarce, except for two cases:

1. Li's matching solution with the HHR field in the Henky theory of plasticity for a stationary crack (Li, 1997).
2. The possible matching for a moving crack of field based on the elasto-visco-plasticity law without a threshold, using the technique of (Li, 1997)

$$\dot{\varepsilon} = A\dot{\sigma} + B\sigma_e^{n-1}s \qquad (n>3) \tag{3.83}$$

The mode III problem has been investigated in (Kachanov, 1978) where a non-linear equation for the stress function $\psi(x_1, x_2)$ is derived in the form

$$-\dot{a}\Delta\left(\frac{\partial\psi}{\partial x_1}\right) + \gamma \operatorname{div}\{|\operatorname{grad}\psi|^{n-1}\operatorname{grad}\psi\} = 0 \tag{3.84}$$

$\gamma = 2\mu B 3^{(n-1)/2}$. Eq. (3.84) has been numerically solved by (Hui and Riedel, 1981). The solution is $\psi = Cr^{(n-2)/(n-1)}f(\theta)$ where $f(\theta)$ is entirely determined as well as factor C. The striking Hui& Riedel's result is that factor C is completely determined by the crack speed as $C = (\dot{a}/\gamma)^{1/(n-1)}$. There is free ajustable parameter other than the velocity. The words *viscoplastic soliton* have been coined by (Bui, 1994) for the solution (3.84). Indeed C corresponding to the solution (3.84) satisfies a relation of the form $aC + bC^n = 0$. If a free parameter like the SIF in linear Fracture Mechanics exists, $K = hC$ for arbitrary factor h, it would mean that $ahC(1-h^{n-1}) = 0$, so that multiplier h equals either 0 or 1. No free parameter other than C exists for the adjustment with the outer field. In fact the inner field with singular part

$$\psi = (\dot{a}/\gamma\mu)^{1/(n-1)} r^{(n-2)/(n-1)} f(\theta)$$

must be matched with the outer elastic field

$\psi_{out} = K_{III} r^{3/2} h\ \theta)$.

Assuming that such a matching exists, we then obtain some relationship between factors K_{III} and $C = (\dot{a}/\gamma\mu)^{1/(n\ 1)}$ which explains the dependence of K_{III} on crack velocity. In mode I, such a velocity dependence of the toughness has been observed experimentally. The toughness of materials depends on the viscous properties of the process zone, even in the case of brittle materials. Let us finally mention some other asymptotic models. For a stationary crack in perfect plasticity with V. Mises's criterion, the slip lines theory of plasticity applies to a crack problem, (Hult and McClintock, 1957; Rice and Tracey, 1974). In pur mode I, there are two homogeneous stress field sectors and a centered fan stress field, Fig. 3.6 a)

- Sector (I) $0< \theta < 45°$: $\sigma_{22} = \sigma_0$, $\sigma_{11} = \sigma_{12} = 0$ (homogeneous stress)
- Sector (II) $45° < \theta < 135°$: $\sigma_{r\theta} = \sigma_0/\sqrt{2}$, $\sigma_{rr} = 0$, (centered fan)
- Sector (III) $135° < \theta < 180°$: $\sigma_{22} = 0$, $\sigma_{11} = -\sigma_0$ (homogeneous stress).

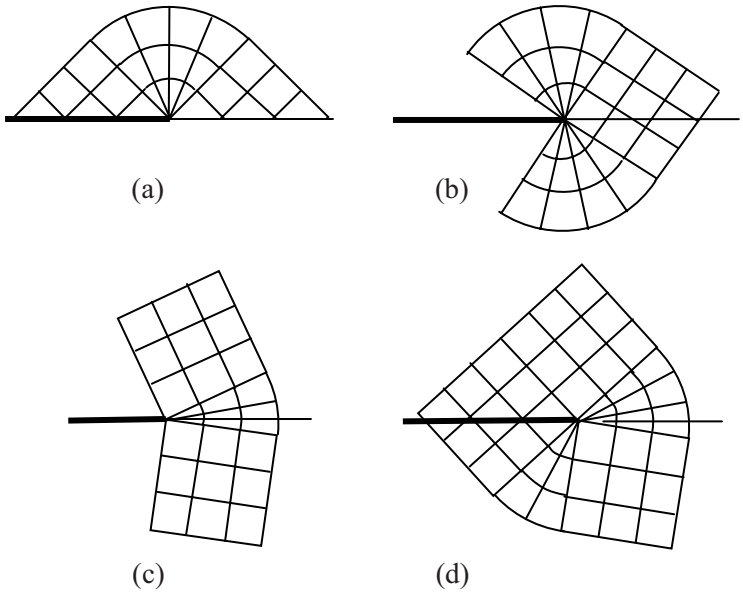

Figure 3.7: Asymptotic solutions in perfect plasticity: (a) fully plastic mode I (Hult and McClintock, 1957); (b) mixed mode I + II with elastic zone (Gao, 1980); (c) mixed mode I + II with elastic zone; (d) fully plastic zone (Gao, 1980)

In the mixed mode I + II of perfect plasticity, Shih (1974) proposed a singular stress field which has a discontinuity line. Gao (1980)* considered the V. Mises criterion and found a continuous stress field with an elastic zone, Figs. 3.7 (b) and (c), which cannot be determined by the asymptotic fields only.

The elastic sector angle is undetermined by an asymptotic analysis. The elastic sector has been confirmed by the finite element method, (Saka et al, 1986; Dong and Pan, 1990).

The asymptotic solution for a stationary crack does not apply to a moving crack. The asymptotic solution for a moving crack contains an elastic unloading sector (IV), $115° < \theta < 163°$, between the fan sector (II), $45° < \theta < 115°$, and the wake plastic sector (III), $163° < \theta < 180°$, near the stress free crack (Gao, 1980; Rice, 1982). An asymptotic solution for a stationary crack in softening material, with a threshold stress has been given by (Gao and Bui, 1995)

$$\sigma = \begin{cases} E\varepsilon, & \varepsilon < \varepsilon_0 \\ \\ E\varepsilon\left[(\mathrm{n}\varepsilon/\varepsilon_0 + \mu)/(\mathrm{n}+\mu)\right]^{-1-1/\mathrm{n}}, & \varepsilon \geq \varepsilon \end{cases} \tag{3.85}$$

There is a damage sector $\beta < \theta < \alpha$ with free angles β, α which cannot be determined without performing the complete matching between inner and outer solutions.

3.5 Inverse geometric problem with Coulomb's friction

The delamination problem in composites is typically an inverse geometric problem in Fracture Mechanics. We look at a simpler problem of frictional delamination at the interface between elastic and rigid bodies solved in (Bui and Oueslati, 2005).

Classical problems consider a *given* crack in homogeneous body or a given interface crack under applied loads. Here, delamination at the interface of composite layers appears *somewhere* under existing localized stress state at the interface. It is expected that crack grows at points of highest shear stress, then propagates towards its final location.

* Gao's paper published in Chinese, in Acta Mechanica Solida Sinica, 1 (1980) was presented to a seminar in France during his sabbatical stay in Electricité de France.

To solve this problem, we first determine the solution for a given crack, then examine how to modify its geometry and location in order to satisfy all physical and mathematical constraints such as : square integrable stress fields, continuous displacements (neither dislocation nor dislocation dipole). The methodology is exactly the same as the one considered in Inverse Problems, based on the Control theory of distributed parameters or fields (infinite dimensions) (Lions, 1971) or Optimisation of finite dimensional parameters.

We consider the frictional contact problem with Coulomb's law and constant friction coefficient f. Before delamination, we assume that there exists a compressive stress state $\sigma^0_{22}(x_1, 0) < 0$ and a shear $\sigma^0_{12}(x_1, 0) < 0$, acting on the interface $x_2 = 0$ between a semi-infinite elastic body Ω^+ $(x_1 > 0)$ and a rigid one Ω $(x_2 < 0)$. The stress field $\sigma_{hk}(x_1, x_2)$ is put as the sum $\sigma^0_{hk}(x_1, x_2) + \theta_{hk}(x_1, x_2)$, where $\theta(\mathbf{x})$ is the auxiliary stress field to be determined, subjected to condition $\theta \to 0$ at infinity. It is assumed that loading conditions are such that only tangential displacement takes place on the whole crack $[[u_2]] = 0$. The case where $[[u_2]] \neq 0$ on some part of the crack has been considered in (Bui and Oueslati, 2004).

3.5.1 Non-uniqueness of solution

Analyses of frictional crack are rather complex because the solution is not generally unique when no information is available on the crack history. Let us consider a classical example of a frictional crack of length 2a in a homogeneous elastic body under remote uniform compression $\sigma^\infty_{22} < 0$ and uniform shear σ^∞_{12}.

The frictional contact condition can be expressed by either $[[u_1]](\sigma_{12} - f\sigma_{22}) = 0$ or $[[u_1]](\sigma_{12} + f\sigma_{22}) = 0$, depending on the sign of relative slip near the crack tip. The solution for mode II is classical, (Bui, 1978, p. 16).

Case 1 : $|\sigma^\infty_{12}| > -f\sigma^\infty_{22}$

$K_{II}(a) = (\sigma^\infty_{12} + f\sigma^\infty_{22})\sqrt{(\pi a)}$, if $\sigma^\infty_{12} > 0$

$K_{II}(a) = (\sigma^\infty_{12} - f\sigma^\infty_{22})\sqrt{(\pi a)}$, if $\sigma^\infty_{12} < 0$.

Case 2 : $|\sigma^\infty_{12}| < -f\sigma^\infty_{22}$

The applied shear is not high enough for a slip to occur under pressure, thus the first solution corresponds to the "no delamination" case $[[\mathbf{u}]] = 0$. Now consider the formal solution given by formulae derived in Case 1 which provide *negative* $K_{II}(a)$ at the right tip under remote *positive* shear stress. Such a solution can be reached experimentally as follows. First apply opposite arbitrary shear loads $\pm\sigma_{12}{}^*(\sigma_{12^*} < 0)$ on the crack faces so that

$K_{II}(a) = \sigma_{12}^* \sqrt{(\pi a)} < 0$, then apply the compression σ^{∞}_{22} sufficiently high to prevent further reverse slip to occur. Next release the additional shear stress $\mp \sigma_{12}^*$ then apply $\sigma^{\infty}_{12} > 0$ to obtain the second solution: negative $K_{II}(a)$ at the right tip under remote positive $\sigma^{\infty}_{12} > 0$.

As shown by this example, non uniqueness of solutions in frictional contact problems is expected, since a full loading history is missing to solve a non-linear problem.

3.5.2 Frictional crack problem without opening

We do not repeat here the method of solution which has been outlined in (Bui and Oueslati, 2005). We first assume that the current stresses as well as displacements satisfy the conditions: $\sigma_{12} < 0$, $\sigma_{22} < 0$, $u_1 < 0$, $u_2 = 0$, called *admissible* conditions (A) for expressing the friction law in the form $\sigma_{12} = \sigma_{22}$. Let us denote the auxiliary displacement and the associated complex potentials by $\mathbf{q}(\mathbf{x})$, $\Theta(z)$, $\Xi(z)$ respectively. Only $\sigma^0_{2i}(x_1, 0)$ is prescribed on the crack, while $\sigma^{\infty}(\mathbf{x})$ is not yet prescribed for a mixed boundary value, $\mathbf{u} = \mathbf{0}$ outside the crack. Owing to this arbitrariness we do not impose strict behavior $1/z^2$ at infinity for $\Theta'(z)$.

To investigate the behavior of solution near the crack, we search a solution behaving as $\Theta'(z) \cong O(1/z)$ at infinity and satisfying the Hilbert problem

$$\Theta'(t^+) - g\Theta'(t^-) = E^0(t^+) \text{ on } [b, a] \tag{3.86}$$

$$E^0(x_1) = -\{\sigma^0_{22}(x_1, 0) - \sigma^0_{12}(x_1, 0)\} \frac{2i}{(\kappa+1) - i\,\mathrm{f}\,\kappa - 1)} \tag{3.87}$$

$$g = -\frac{(\kappa+1) + i\mathrm{f}(\kappa-1)}{(\kappa+1) - i\mathrm{f}(\kappa-1)} \tag{3.88}$$

Even if the physical field solution is defined only in Ω^+, we consider its mathematical continuation in Ω^-, the whole complex plane being cut along the crack [b, a]. The solution of the Hilbert problem, Eq. (3.86), is given by Cauchy's integral

$$\Theta'(z) = \frac{X(z)}{2i\pi} \int_b^a \frac{E^0(t)dt}{X(t^+)(t-z)} + P(z)X(z) \tag{3.89}$$

$$X(z) = (z-b)^{(1/2)-\alpha}(a-z)^{(-3/2)+\alpha} \tag{3.90}$$

$$\tan(\pi\alpha) = \mathrm{f}\ \kappa - 1)/(\kappa + 1) \tag{3.91}$$

for arbitrary rational function P(z). We also have $g = \exp\{2i\pi(\alpha + (1/2))\} = -\exp(2i\pi\alpha)$. For $\kappa = 3 - 4\nu$ (plane strain), we have $0 \le \alpha < 0$. In Eq. (3.89), X(z) is a solution of the homogeneous Hilbert equation with adequate singularities.

Kinematically, the displacement field near the crack tip is described in Fig. 3.8. For negative shear stress, the kinematic at the left tip z = b is called the *pull-out* type singularity ($-\alpha$ in the exponent in Eq. (3.90)), while that corresponding to the right tip is called the *push-in* type singularity ($+\alpha$ in the exponent).

The displacement shown in Fig. 3.8 corresponds to the one of the auxiliary field, $\mathbf{q}(x_1,0)$, which coincides with $\mathbf{u}(x_1, 0)$ on the interface. P(z) is determined by the condition $\Theta'(z) \to 0$. Let us fix arbitrarily the left tip z = b for which function $X(z) \cong (z - b)^{(1/2)-\alpha}$ is regular, for both stress and displacement. The singularity of X(z) at z = a is strongly singular as $X(z) \cong (a - z)^{-(3/2)+\alpha}$ so that unbounded stress and discontinuous displacement should have arisen and thus are not acceptable. Two constants have to be determined, namely a and C, by two conditions: bounded stress and continuous displacement. On taking the constant C which cancels the r.h.s. of Eq.(3.89) at z = a, we then obtain a bounded solution $\Theta'(z)$ at both crack tips (regular stress and bounded displacement) and vanishing at infinity

$$\Theta'(z) = \frac{X(z)}{2i\pi}\left\{\int_b^a \frac{E^0(t)dt}{X(t^+)(t-z)} - \int_b^a \frac{E^0(t)dt}{X(t^+)(t-a)}\right\} \tag{3.92}$$

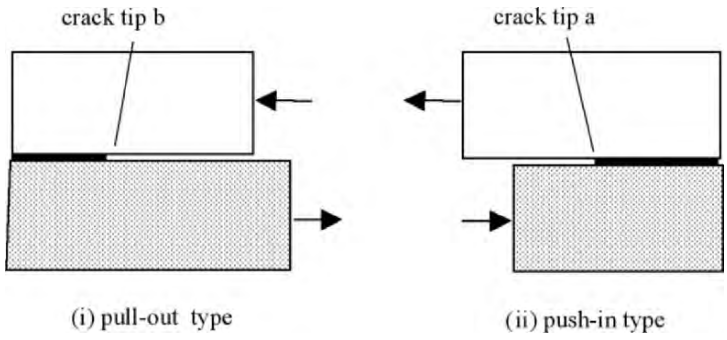

Figure 3.8: (i) The pull-out singularity at z = b; (ii) the push-in singularity at the z = a

Now let us integrate the strain to obtain the displacement as

$$2\mu(q_1(t)+iq_2(t))=\kappa\int_b^{t^+}\{\Theta'(t^+)-\Theta'(t^-)\}dt$$

We thus obtain the compatibility equation at z = a

$$\int_b^a\{\Theta'(t^+)-\Theta'(t^-)\}dt=0 \tag{3.93}$$

This is the compatibility equation to determine the relation f(a, b) = 0.
The curve f(a, b) given by Eq. (3.93) has been calculated for normalized polynomial (Bui and Oueslati, 2005)

$E^0(t)=(1-t^2)$.

Delamination is expected to occur in interval $x_1\in[-1,1]$. As a matter of fact, the quasi-elliptical curve in the (b, a)-plane, contains the points N = (−1,−1) and M = (+1,+1), Fig. 3.9.

It has been found that the admissible conditions (A) for stresses and displacement are satisfied on the curve. Thus the solution to the frictional interface crack problem is *not unique*.

This is the first example of non-uniqueness of solutions encountered in frictional contact problems with Coulomb's law.

To ensure uniqueness, we need other considerations taking the place of unspecified loading history.

It should be noted that the singulatities at tips {b, a} agree with those found by (Deng, 1994) in his analysis of a semi-infinite crack.

The analysis of a finite crack enables us to discuss energetic aspects which cannot be done in the infinite crack case. Finally, this exact solution is a counter-example of a non-ocillatory solution in an interface crack problem with friction.

It is found in many works that the oscillatory solutions which present overlapping in a very small zone of atomic size for the opening mode does not exist in our solution of a frictional contact crack. The oscillatory solution can be observed in other problems involving contact stress. It was discovered by Abramov (see Muskhelishvili, p. 488, 1977) in the punch problem where two components of the displacement are prescribed on the punch, and the stress free condition outside the contact zone. It is a general property of a *mixed* boundary value problem in elasticity. In the punch problem, the oscillations with amplitude $O(r^{1/2})$ appear outside the punch and has no consequence for the stress free boundary which can be freely deformed, contrary to the crack case where the overlapping of cracks faces violates the condition $[[u_n]]\geq 0$.

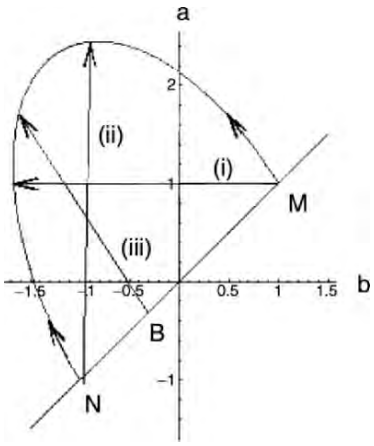

Figure 3.9: The quasi-elliptical curve f(b,a) = 0 above the line a = b. Each point (b, a) provides a solution for the.crack geometry. The curve contains two starting delamination points M (a = b = 1) and N(a = b = −1)

3.5.3 The energy release rate of a frictional interface crack

As noted in many works, J-integral loses it meaning when the path has its end points on the frictional contact zone. The path-independence property of J generally comes from the stress free condition together with the fact that $n_1 = 0$ on the line crack. Let us denote the actual load at time t_1 by $P(t_1)$. When the load increases from the zero load (0) to the load $P(t_1)$, delamination grows from the initial point geometry [0, 0] to the intermediate one [b(τ), a(τ)] at time τ, then to the actual geometry [b, a]. Rice's integral defined with a large contour Γ embrassing the whole crack [b(τ), a(τ)] (a semi-circle with center on the crack and with large radius for example) and with the end points on the unbroken zone, is path-independent (since $n_1 = 0$ and $\mathbf{u} = \mathbf{0}$ on the crack line). Such a nice property does not hold for semi-infinite crack. Thus, assuming that the crack tip b, being in a lower stress state, does not propagate, Jδa still has the classical interpretation of the increment of energy provided by the elastic region *ouside* Γ for an incremental delamination δa at the right tip. Thermodynamically, Jδa can also be interpreted as the increment of the energy *dissipated inside* Γ. There are two kinds of dissipation, $J\delta a = \delta D_R + \delta D_F$, one possibly at the crack tip due to the rupture process δD_R, and another one due to friction $\delta D_F > 0$ along the slipping surface. A glance at the solution Eq. (3.92) shows that $\Theta'(z) \cong (a - z)^{-(1/2)+\alpha}$ has a singularity weaker than $r^{-1/2}$, thus $\delta R_R = 0$, or $G = J_{tip}(\Gamma \to 0) = 0$. (Fig. 3.10).

We recover the same paradoxical result as the one observed in plasticity (no driving force at the tip).

J-integral with a contour encircling completely the crack has the meaning of the rate of energy fully dissipated by friction. The latter result enables us to introduce the following additional assumption to obtain uniqueness of the solution to the frictional interface crack problem: Delamination evolves in such a manner to minimize the energy stored in the system, or to maximize the dissipation by friction. This assumption is related to stability considerations of the cracked system.

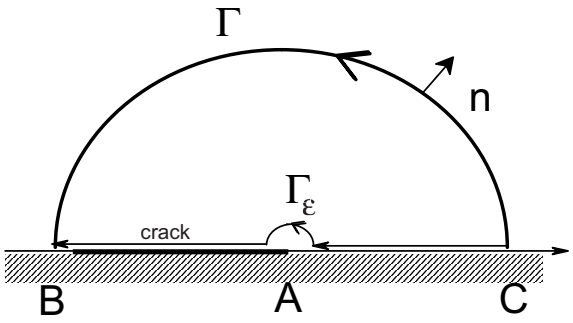

Figure 3.10: Path Γ to define J-integral for frictional interface cracks. The J-integral is path independent whenever B and C are outside the crack. The J_{tip}-integral for a path aroung the crack tip A of vanishing radiius ε, is equal to $D_R = 0$

3.5.4 The frictional interface crack problem with an opening zone

Considering the same loading condition for the auxiliary problem (3-86), (3.87) we want to analyse the structure of mechanical fields near the interface crack, when there is an opening crack [c, d] ($b < c < d < a$) where $\sigma_{22} - i\sigma_{12} = 0$ and $u_2 \geq 0$. On [b, c] and [d, a] conditions of frictional contact still holds, $u_2 = 0$ and $\sigma_{12} - f\sigma_{22} = 0$, assuming that $\sigma_{12} < 0$, $f\sigma_{22} < 0$. The auxiliary stress θ must satisfy $\theta_{22} - i\theta_{12} = -\sigma^0_{22}(x_1, 0) + i\sigma^0_{22}(x_1, 0)$ on the crack and the corresponding displacement $\mathbf{q} = \mathbf{0}$ outside the crack. This is a mixed boundary value problem on real axis, with an incomplete data at infinity. The idea is to search a solution in the form

$$\Theta'(z) = F(z)X_0(z) \tag{3.94}$$

with function $X_0(t^+) = (z-b)^{(1/2)-\alpha}(a-z)^{(1/2)+\alpha}$ regular at z = b, strongly singular at z = a. Function $X_0(z)$ satisfies the homogeneous equation, $X_0(t^+) - X_0(t^+) = 0$ for any holomorphic function F(z) in complex plane with a cut along [c, d]. Function F(z) is thus continuous across [b, c] and [d, a] so that, owing to $X_0(z)$, the frictional contact conditions $u_2 = 0$ and $\sigma_{12} - f\sigma_{22} = 0$ are satisfied on these zones. Expressing the physical stress free condition $\sigma_{12} - f\sigma_{22} = 0$ along [c, d] by

$$\Theta'(z^+) + \kappa\Theta'(z^-) = \{-\sigma^0{}_{22}(x_1,0) + i\sigma^0{}_{22}(x_1, 0)\} = h(x_1)\ ,\ c < z^+ < d \qquad (3.95)$$

taking into account of $X_0(z^+) = gX_0(z^-)$, we are arriving at the Hilbert equation

$$F(t^+) + \frac{\kappa}{g}F(t^-) = \frac{h(t)}{X_0(t^+)} \qquad (3.96)$$

The solution of the Hilbert equation (3.96) is derived by Muskhelishvili's standard method by considering the solution Z(z) of the homogeneous equation $Z(z^+) = -(\kappa/g)Z(z^-)$. Let $-(\kappa/g) = e^{2i\pi\beta}$, $\beta = \alpha - (i/2\pi)\log\kappa$.

Solution of the homogeneous equation, regular at z = c and weakly singular at z = d is

$$Z_1(z) = (z-c)^{+\alpha+(i/(2\pi))\log\kappa}(d-z)^{-\alpha-(i/(2\pi))\log\kappa} \qquad (3.97)$$

Solution of the homogeneous equation, regular at both points c, d is

$$Z_0(z) = (z-c)^{+\alpha+(i/(2\pi))\log\kappa}(d-z)^{1-\alpha-(i/(2\pi))\log\kappa} \qquad (3.98)$$

Before selecting a function for solving frictional interface crack problem, with an opening zone, let us remark that solution in the contact zone, [d,a] for example, resembles a flat punch problem in the presence of friction.

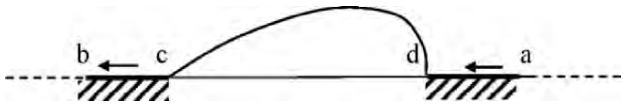

Figure 3.11: Frictional interface crack with sliding contact zones [b, c], [d, a] and opening zone [c, d]

Therefore a stress singularity at the end point of the punch z = d (or z = c) could be possible. Hovewer, we rather search a solution without stress singularity at z = c and d, so that function $Z_0(z)$ may be selected.

$$\Theta'(z) = \frac{X_0(z)Z_0(z)}{2i\pi}\int_c^d \frac{h(t)dt}{Z_0(t^+)X_0(t^+)(t-z)} + QX_0(z)Z_0(z) \tag{3.97}$$

Since $X_0(z)Z_0(z) \cong O(z)$, we must take Q=0 for vanishing $\Theta'(z)$ at infinity

$$\Theta'(z) = \frac{1}{2i\pi}\, X_0(z)Z_0(z)\int_c^d \frac{h(t)dt}{Z_0(t^+)X_0(t^+)(t-z)} \tag{3.98}$$

Solution $\Theta'(z)$ is bounded at points b, c, d and weakly singular at z = a, The last condition to be examined is the regularity at infinity. For $z \to \infty$, regular solution at infinity exists only if h(t) satisfies the condition

$$\int_c^d \frac{h(t)dt}{Z_0(t^+)X_0(t^+)} = 0 \tag{3.99}$$

Subject to the above condition, function $\Theta'(z)$ gives bounded stress at any point except at z = a, where stress is square integrable. It remains to examine continuity conditions of **q**. Let us fix arbitrarily b. Displacement $q_1(t) + iq_2(t)$ is obtained by integrating $\{\Theta'(t^+) - \Theta'(t^-)\}$ as

$$2\mu(q_1(t) + iq_2(t)) = \kappa\{\int_b^t \{\Theta'(t^+) - \Theta'(t^-)\}dt\}.$$

On [b, c], condition $q_2(c) = 0$ is implicitly fulfilled by the contact condition since the latter integral is real on frictional contact zone. We have to write the first compatibility condition for the normal component at z = d with an integration beginning at z = c

$$2\mu q_2(d) = \kappa\,\mathrm{Im}\int_c^d \left\{\Theta'(t^+) - \Theta'(t^-)\right\}dt = 0 \tag{3.100}$$

The second compatibility condition for the tangential component at z = a, can be written as (an integration over the whole crack [b, a])

$$2\mu q_1(a) = \kappa\,\mathrm{Re}\int_b^a \left\{\Theta'(t^+) - \Theta'(t^-)\right\}dt = 0 \tag{3.101}$$

The frictional interface crack problem is basically *underdetermined*, since there are 3 equations, (3.99), (3.100), (3.101), for 4 unknowns a, b, c, d. The solution is *not* unique. One of the unknowns, the parameter b for example, may be arbitrarily selected in its admissibility domain defined by conditions $\sigma_{12}(x_1, 0; b) < 0$, $\sigma_{22}(x_1, 0; b) < 0$ for any x_1 on frictional contact zones.

Chapter 4

Thermodynamics of Crack Propagation

4.1 An elementary example

Consider a simple rheological solid system consisting of a series of linear elastic parallel springs, assembled to two rigid bars and subjected to prescribed displacement δ. Now we consider the evolution of the system when, just after the loading, the first spring breaks suddenly at its middle point under fixed grip bars. Since the rigid bars are fixed after the loading, there is no additional supply of mechanical energy, $\delta W_{ext} = 0$. When the stress is fully released in the broken string, the stored energy of the latter is *released* by the amount $\delta W_{elast} < 0$. According to its definition, the dissipation of energy by the rupture process is $\delta D_R := \delta W_{ex} - \delta W_{elast} = -\delta W_{elast} > 0$. What happens physically? After rupture, the spring evolves *dynamically*; the sum of its stored elastic energy and kinetic energy is alsways conserved, the elastic spring oscillates indefinitely in its own direction. Therefore, the quantity $\delta W_{ext} - \delta W_{elast}$ can also be interpreted as the maximum of kinetic energy δW_{kin} of the vibrating spring when it recovers its original length or when the stress is fully released. In real experiments, the broken spring movement should be chaotic, in different directions of the space, and dissipates energy by collisions, frictional contact with neighbouring springs, or internal dissipative phenomena like plasticity, viscoplasticity etc. Such damping mechanisms will finally slow down the spring.

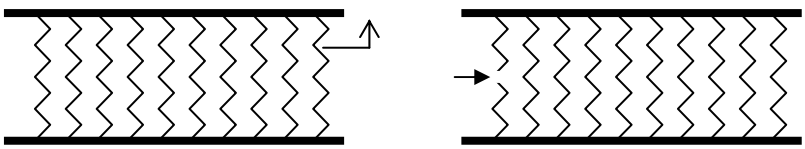

Figure 4.1: Parallel springs fixed to rigid bars under displacement control; The first spring breaks at its middle point; its elastic energy is released and finally dissipated by vibrations and heat conduction through the rigid grips

If the system is not thermally isolated, then thermal conduction through the grips is another cause of damping of the parallel springs system. Thus we conclude that fracture is essentially a dissipative phenomenon.

Thermal conduction mechanisms give us the interpretation of the quantity $\delta D_R \equiv \delta W_{ext} - \delta W_{elast}$ as a dissipated energy. Let us consider another interpretation, by isolating a small region of the first spring containing the broken point and consider that the first spring consists of two parts held together by "internal force" or *cohesion force* F, which is the analogue of atomic force models in metallic solids. The work done δW_F by the cohesion force F(t) from the beginning at equilibrium state, $F(0) = 0$, to the critical state $F = F_{max}$, just before breaking, is equal to $\delta W_F = \delta W_{ext} - \delta W_{elast}$. In the literature, δW_F is called the "stress working" by cohesive force. In models of brittle fracture by cohesive force, the force-displacement curve F(u) is schematically shown in Fig. 4.2.

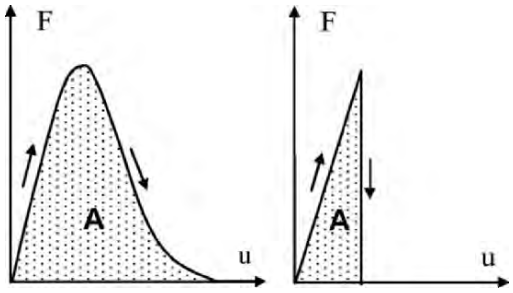

Figure 4.2: Cohesive force models: (a) atomic force; (b) brittle spring

The work done by cohesive force, in a crack propagation per unit length, is equal to the area A under the curve, as shown by Willis (1967). In quasi-statics, Griffith's theory of fracture is based on the assumption that the *energy relase rate,* per unit crack length advance, is the constant 2γ

$$G = -\frac{\delta P}{\delta a} = 2\gamma \tag{4.1}$$

where P is the potential energy

$$P = W_{elast} - W_{ext} \tag{4.2}$$

for prescribed displacement on the external boundary S_{ext} of the elastic body. For general loading on a continuous medium with a crack, with prescribed displacement u^d on the part S_u of the external boundary S_{ext} and prescribed traction T^d on the complementary part S_T, the quasi-static energy release rate is given by

$$G = -\left\{ \frac{\delta}{\delta a} \int_{\Omega} W(\varepsilon) d\omega - \int_{S_T} T_i^d \frac{\delta u_i}{\delta a} ds \right\} \tag{4.3}$$

with the energy density for linear material

$$W(\varepsilon) = \frac{1}{2} \varepsilon_{ij} L_{ijhk} \varepsilon_{hk} \tag{4.4}$$

We recall that Griffith's theory $G = 2\gamma$ is equivalent to the cohesive force model with the area $A = 2\gamma$, when a *self-similarity* of the crack opening displacement near the crack tip region has been assumed. This is also called an *autonomous* crack tip field. The geometry of the crack opening displacement near the tip is unchanged during crack propagation.

4.2 Dissipation analysis

We consider the dynamic evolution of a cracked body in a solid and adopt through out the book the small strain description, $\varepsilon = (\nabla \mathbf{u} + \nabla^{\tau} \mathbf{u})/2$, even if singularities of strain may appear in some analysis. The considered solid can be defined by its free energy $W(\varepsilon, \alpha, T)$, function of the state variables ε, $\alpha = (\alpha_1, \alpha_2, ...)$ with internal variables α_i and temperature T. The first variable ε is directly observable in simple experiments while the second ones are generally not. They are called *hidden* variables, which can be sometimes observed by indirect experiments. The volumic entropy is defined by

$$S = -\frac{\partial W}{\partial T} \tag{4.5}$$

The conjugate (dual) variables to ε, ω are called by Halphen and Nguyen (1975) respectively *reversible stress* σ_{rev} and *generalized force* $\mathbf{A} = (A_i)$

$$\sigma_{rev} = \frac{\partial W}{\partial \varepsilon} \quad \text{(reversible stress)} \tag{4.6}$$

$$\mathbf{A} = -\frac{\partial W}{\partial \alpha} \quad \text{(generalized force)} \tag{4.7}$$

The solid receives the rate of reversible stress working, defined by the quantity $(\partial W/\partial\varepsilon)\mathbf{:}\partial_t\varepsilon + (\partial W/\partial\alpha)\mathbf{.}\partial_t\alpha = (\partial W/\partial\varepsilon)\mathbf{:}\partial_t\varepsilon - A\mathbf{.}\partial_t\alpha$. The volumic intrinsic dissipation rate including thermal dissipation, is defined by

$$D = \sigma : \dot{\varepsilon} - \sigma_{rev} : \dot{\varepsilon} + \mathbf{A}.\dot{\alpha} + T\mathbf{q}.\nabla(\frac{1}{T}) \geq 0 \tag{4.8}$$

where **q** is the heat flux. For example, in classical isothermal plasticity, considering only the plastic deformation ε^p as internal variable and the free energy $W(\varepsilon-\varepsilon^p)$ as function of the elastic strain $\varepsilon^e = \varepsilon - \varepsilon^p$, one has $\sigma = \partial W/\partial\varepsilon^e - \partial W/\partial\varepsilon^p = \partial W/\partial\varepsilon = \sigma_{rev}$, hence $D = \sigma\mathbf{:}\partial_t\varepsilon^p$. This too simple model of plasticity does not describe correctly strain hardening or softening of the material. Adequate internal variables must be introduced for modelling more complex behaviors, (Nguyen, 1977; Maugin, 1992)

Now let us consider crack propagation in elastic or elasto-plastic solid. The solid domain with a moving crack a(t) is denoted by $\Omega(t)$ including the crack tip C, or by $\Omega^*(t)$ if one deletes a small circular region V_η centered at the moving crack tip, with boundary Γ_η and with vanishing radius $\eta \to 0$, $\Omega^*(t) = \Omega(t)\backslash V_\eta$. The dissipation analysis of the domain $\Omega^*(t)$ is analogous to the one given in the example of the elastic spring, outside the small region containing the broken point. Materials inside V_η are very similar to the broken elastic spring. The dissipation rate of the body consists of two parts, the first one due to the intrinsic dissipation D in the domain $\Omega^*(t)$, the another one due to the exchange of thermal energy on the boundary Γ_η which can be denoted by and interpreted as the "dissipation rate by fracture" $D_R = G\dot{a}/dt$. The overall dissipation becomes

$$D_{tot} = G\dot{a} + \int_\Omega D d\omega = \int_\Omega \{D + G\dot{a}\delta(C)\} d\omega \tag{4.9}$$

where $\delta(C)$ means the Dirac delta function $\delta(x - a(t), 0)$ concentrated at the moving crack tip C, in fixed coordinates x,y and *G* is the *energy release rate* (italic *G*)

$$G = \lim_{\eta\to 0} \int_{\Gamma\eta} \{(e+(1/2)\rho\dot{\mathbf{u}}.\dot{\mathbf{u}})n_1 - \mathbf{n}.\sigma.\mathbf{u}_{,1}\} ds \tag{4.10}$$

where $e = W + TS$ is the volumic internal energy, S the volumic entropy. In elastodynamics, without considerations on thermomechanical aspects, the right hand side of Eq. (4.10) is written with W instead of e, and is known as Freund's integral (Freund, 1972).

The parameter *G* is the thermodynamical force associated to *isoentropi*c evolution, while G is associated to *isotherma*l evolution. In practice, the difference between G and *G* is not significant. As we shall see later, both

energy release rates are expressed in terms of stress intensity factors by the same generalized Irwin formulae. The only change is found on elastic coefficients, the Lamé coefficients in isothermal evolution λ, μ being replaced by λ', μ', for isoentropic evolution, with $\lambda' = \lambda + k^2T_0/(\rho c)$ and $\mu' = \mu$ (see Mandel, 1966, p. 587). For steel, at the room temperature T=300°K, $\lambda' \cong 1.03\lambda$. Thus there is only a slight difference between *G* and G.

4.3 Thermal aspects of crack propagation

Experiments performed on an uncracked elastic body, subjected to cycles of loading and unloading, show some well known features.

When there is no heat supply to the elastic system, under adiabatic evolution, the thermo-elastic response of a specimen shows a decrease of temperature in the loading and an increase of temperature in the unloading. Figure 4.3 shows the response of the temperature in the thermo-elastic range and in the thermoplastic range which corresponds to a rapid increase of T. The response in the thermo-elastic range can be analysed as follows.

We consider linear isotropic elastic materials, with constant volumic heat c and thermoelastic coefficients $l_{ij} = -3K\alpha\delta_{ij}$, with the bulk modulus $K = (3\lambda + 2\mu)/3$, Lamé's coefficients λ, μ and the thermal expansion coefficient α

The free energy becomes

$$W(\varepsilon, T) = \tfrac{1}{2}(\lambda\varepsilon_{ii}\varepsilon_{jj} + 2\mu\varepsilon_{ij}\varepsilon_{ij}) - 3K\alpha(T - T_0)\varepsilon_{jj} - cT\ln(\frac{T}{T_0}) - (S_0 - c)T + W_0$$

By linearization at T_0 ($\theta = T - T_0$) and taking $S_0 = 0$, $W_0 = -cT$, the free energy has the quadratic form

$$W(\varepsilon, \theta) = \frac{1}{2}(\lambda\varepsilon_{ii}\varepsilon_{jj} + 2\mu\varepsilon_{ij}\varepsilon_{ij}) - 3K\alpha\theta\varepsilon_{jj} - \frac{c}{2T_0}\theta^2 \tag{4.11}$$

The volumic entropy is $S = 3K\alpha\varepsilon_{ii} + c\theta/T_0$. In a pure tension test, with Poisson ratio $\nu < 1/2$, the trace $\varepsilon_{ii} = \varepsilon_{11}(1 - 2\nu)$ is positive. Under adiabatic condition (S = 0) an increase (or decrease) of the trace ε_{ii} results in the decrease (or increase) of the temperature θ. This is the well known thermoelastic effect.

Experiments have been performed in the elastic and plastic domains in metals (copper, aluminium, iron). A specimen is subjected to some cycles of loadings and unloadings with a variable amplitude in the elastic range.

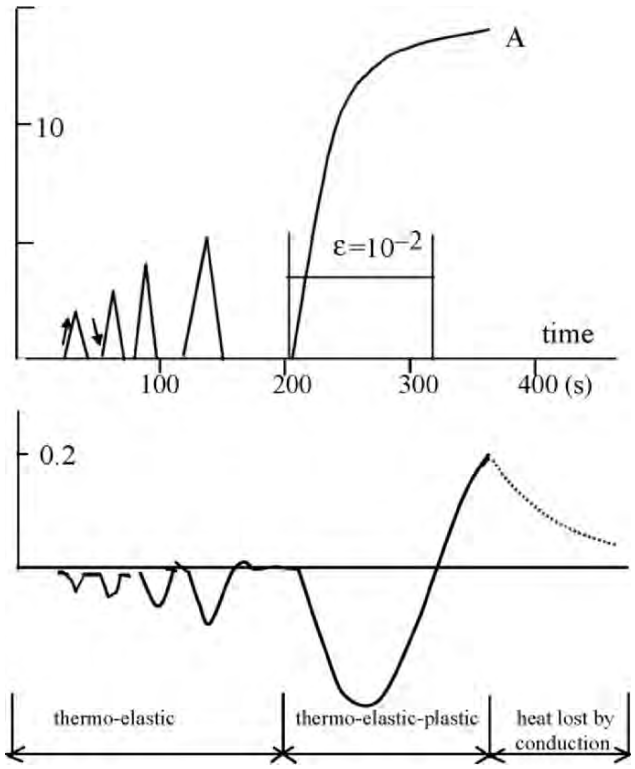

Figure 4.3: Temperature measurements in cycles of loading-unloading in thermo-elastic domain and in thermo-elasto-plasticity (Bui, 1965)

Cooling is observed in loading and vice versa, heating is observed in unloading. In the elastic-plastic range, the thermo-elastic cooling is overwhelmed by the heating due to plastic deformation, Fig. 4.3. At the arrest point A, temperature decreases by heat conduction through the grips. In analysing the heat source by plastic deformation, it is important to make a temperature correction which takes into account the thermal dissipation by conduction.

The thermal analysis of a crack propagation in elastic body (under adiabatic conditions) leads to wrong result if one ignores the dissipation nature of the moving crack. As a matter of fact, in pure dynamic mode I ($K_I > 0$), the trace $tr(\varepsilon)$ ahead a stationary crack tip is positive and singular as $(r)^{-1/2}$. According to the relation $S = 3K\alpha\varepsilon_{jj} + c\theta/T_o = 0$, the temperature variation θ should be negative. If one still considers the last relation for a moving crack tip, one should have a heat *sink* at the crack tip. This is in

contradiction with experimental evidence of a hot point emitting light in fracture of glass, (Weichert and Schönert, 1974). To analyze correctly the temperature response during crack propagation, we must take into account the dissipation inside V_Γ, which comes from the energy release at the process zone. We recall that intuitively a release of stress implies a heating like in what happens in the example of a broken spring. The same feature happens in crack propagation.

Now we show that the dissipation in V_Γ, is equivalent to a moving *point heat source* exterior to the system $\Omega^*(=\Omega\backslash V_\Gamma)$. We assume that there is no exchange of heat along the outer surface S_{ext} and that the exchange of heat through the crack surface is globally zero.

The first and the second principles of thermodynamics lead to

$$\dot{U} + \dot{W}_{kin} = \int_{\partial\Omega_\Gamma} \mathbf{T}.\dot{\mathbf{u}}\, ds + P_{th} \tag{4.12}$$

$$P_{th} = \int_{\Omega_\Gamma} T\dot{S} d\omega - \int_{\Omega_\Gamma} D d\omega - G\dot{a} \quad , \quad D \geq 0 \tag{4.13}$$

where

$$D = \boldsymbol{\sigma}.\dot{\boldsymbol{\varepsilon}} - \boldsymbol{\sigma}_{rev}.\dot{\boldsymbol{\varepsilon}} + \mathbf{A}.\dot{\alpha} + T\mathbf{q}.\nabla(1/T) \geq 0 \,,$$

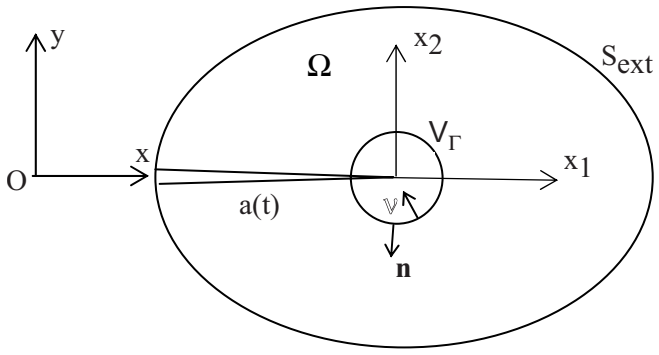

Figure 4.4: Geometry of the solid Ω, with crack length a(t). Fixed axes Ox, y and moving axes O'x_1, x_2. Solid outside a small circular area V_Γ is denote by Ω^*

$$U = \int_{\Omega_\Gamma} (W + TS) d\omega .$$

We assume that the solid has no thermal energy exchange with the exterior, $P_{th} = 0$. We can rewrite the second principle of thermodynamics on Ω_Γ with outward normal ν (opposite to **n** on Γ)

$$\int_\Gamma \mathbf{q}.\nu ds + \int_{\Omega_\Gamma} T\dot{S} d\omega - \int_{\Omega_\Gamma} D d\omega = 0 \qquad (4.14)$$

A comparison between Eqs. (4.13) and (4.14) shows that, when there is no energy exchange with the exterior ($P_{th} = 0$), the energy release rate $G\dot{a}$ is equal to the rate of heat source concentrated at the moving crack tip, (Bui et al, 1980)

$$G\dot{a} = -\lim_{\Gamma \to 0} \int_\Gamma \mathbf{q}.\nu ds = \lim_{\Gamma \to 0} \int_\Gamma \mathbf{q}.\mathbf{n} ds \qquad (4.15)$$

This is a fundamental result which makes a link between energetic aspects of crack propagation with the G concept and thermal aspects with the heat flux **q**. It should be noted that for a stationary crack da/dt = 0 there is no point heat source. For non elastic material, G = 0 for stationary and moving crack; hence there is no point heat source either. For such a material, including plastic one, the hot region observed near the crack tip is due to inelastic dissipation distributed over a small, but non vanishing area around the moving crack tip, rather than a true point heat source.

Evidence of a hot point at the moving crack tip in glass has been reported by Weichert and Schönert (1974). Experiments on thermal aspect of fracture of a thin sheet of steel have been performed by using Infra-red camera. Fig. 4.5 shows a series of images of the deformation of a thin sheet of steel with a circular hole. Images 1-3 correspond to the cooling phenomenon in thermo-elasticity. Plastic heating begins at image 4 and continues up to image 16. Crack initiation and ductile fracture appear suddenly between images 16 and 17. The mechanism of crack initiation has been identified as plastic instability by a necking phenomenon at the highly stressed points at the circular cavity. It should be noted that plastic deformation is very large before the appearance of instability, so that it is very difficult to have an adequate theory based on the small strain assumption which agrees with these experiments.

The same kind of experiments have been performed on a cracked sheet, Fig. 4.6. Ductile fracture occurs since the beginning with a characteristic hot circular region centred at the crack tip and soon after a localized plastic zone is observed ahead the crack tip, which may be explained by a lateral

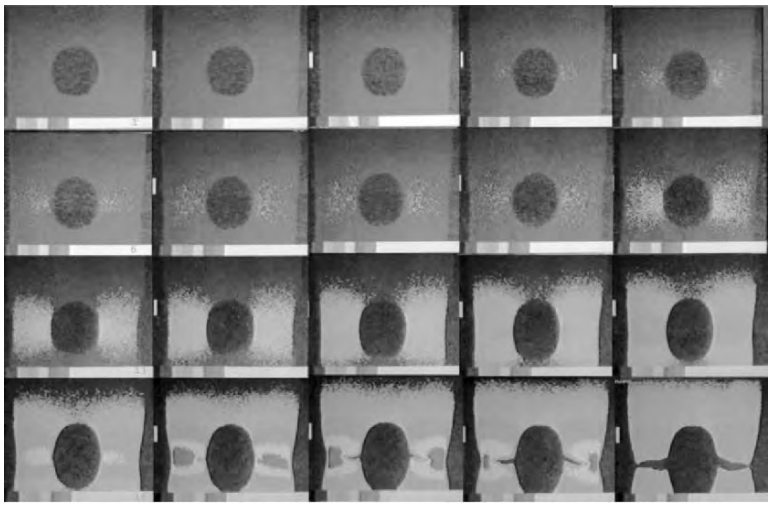

Figure 4.5: Deformation in a thin plate with a circular hole for twenty time instances during 20 seconds. Images 1-3 correspond to thermo-elastic cooling. Plastic heating begins at image 4 and continues up to image 16. Crack initiation and ductile fracture appear suddenly between images 16 and 17, (Bui, Ehrlacher and Nguyen, from an unpusblished report 1979, Ecole Polytechnique)

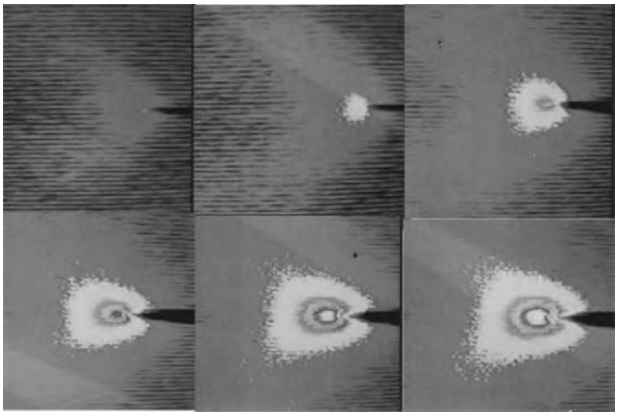

Figure 4.6: Infrared observation of crack propagation in a sheet of steel of 50mm width; images for six time instances during 6 seconds, each color corresponding to 2°C (Bui, Ehrlacher and Nguyen, 1980, permission of LMS-Ecole Polytechnique), (See Plate 1)

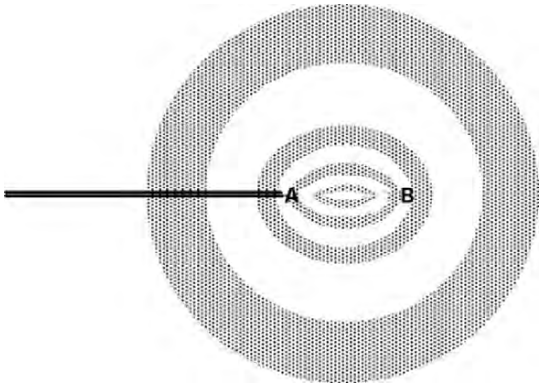

Figure 4.7: Numerical isothermal curves due to a line heat source along AB ahead the crack tip A

necking in the crack tip region. Numerical simulation of a line heat source of some length is shown in Fig. 4.7. The isothermal curve seems to be in qualitative agreement with images 5 and 6, Fig. 4.6.

4.4 Singularity of the temperature in thermo-elasticity

In what follows, we consider plane strain condition for writing the coupled thermo-mechanical equations, using Fourier's law of conduction

$$\mathbf{q} = -k\nabla T \tag{4.16}$$

$$(\lambda+\mu)\nabla(\varepsilon_{11}+\varepsilon_{22}) + \mu\Delta\mathbf{u} - 3K\alpha\nabla T - \rho\ddot{\mathbf{u}} = 0 \text{ (no body force)} \tag{4.17}$$

$$k\Delta T - c\dot{T} - 3K\alpha T(\dot{\varepsilon}_{11}+\dot{\varepsilon}_{22}) + G\dot{a}\,\delta(C) = 0 \tag{4.18}$$

Here the coupling arises at two levels :

i) the classical coupling between the strain and the temperature, as already known in classical thermo-elasticity, Eq. (4.17)

ii) a new coupling exists between the temperature field and the mechanical energy release rate arising in crack propagation, Eq. (4.18).

For a stationary crack, no such a coupling exists since $\dot{a} = 0$. Physically, one needs to supply energy to the process zone for breaking some cohesive forces (in atomic models for example). Such energy comes from the outside region Ω^*, known as the energy release rate. The release of stress at

the process zone is transformed, partially or fully, into heat energy which is dissipated by conduction *back* to Ω*. This is the physical nature for the coupled equations.

The boundary conditions on the opening crack surfaces are

$$\left[u_2\right] = u_2(x,0^+,t) - u_2(x,0^-,t) > 0\,, \qquad x < a(t)$$

$$\sigma_{12}(x,0^{\pm},t) = \sigma_{22}(x,0^{\pm},t) = 0$$

The thermal boundary condition on the crack ($x < a(t)$, $y = 0^{\pm}$) can be taken either as $\partial T/\partial y = 0$ or $[T] = 0$. The dominant singularity of the temperature field T satisfies the equation $k\Delta T + G\dot{a}\,\delta(C)\,;\ 0$ corresponding to the most singular terms of Eq. (4.18). The asymptotic analysis of the temperature field T leads to the dominant *positive* and *logarithmic* singularity which satisfies both boundary conditions

$$T \simeq -\frac{G\dot{a}}{2k\pi}\ln r \tag{4.19}$$

The moving crack tip behaves like a hot point, as observed in Weichert and Schönert's experiments on glass, which is a purely elastic material. Experiments on thin sheet of metal, using an infra-red camera seem to confirm the hot point at the moving crack tip (image 1 of Fig. 4.6). However in metals, as shown in Fig. 4.6, the hot point arising in plastic dissipation rate is rather distributed inside a small circular zone of radius R than concentrated at a point. The higher the yield stress, the smaller the plastic zone. A limiting model with infinite yield stress should corresponds to $R = 0$ and thus the moving point head source (4.19) is reconfirmed. Let us recall that Eq. (4.18) without the point source term $G\dot{a}\delta(C)$ should give rise to a *sink* of heat (negative singular temperature).

4.5 Asymptotic solution of the coupled equations

Now we are going to search asymptotic solutions of (4.17), (4.18) in the basis of functions, involving power r^{β} and compound logarithms $r^{\beta}(\ln r)^{\beta_1}(\ln_m r)^{\beta_m} f(\varphi, t)$, where $\ln_m r \equiv \ln(\ln_{m-1} r)$, $\beta, ..\beta_i$ are real numbers and $f(\varphi,t)$ is twice differentiable on φ, t

$$\mathbf{u} = \mathbf{u}^{(1)} + \mathbf{u}^{(2)} + .. \tag{4.20}$$

$$T = T^{(1)} + T^{(2)} + .. \tag{4.21}$$

the expansion terms are ordered by decreasing singularity. Using such a basis of functions, we search solutions such that different terms in G are integrable. Let us introduce some notations ($x_1 = x - a(t)$, $x_2 = y$, $I = \sqrt{(-1)}$)

$$z = x_1 + ix_2 \equiv re^{i\varphi}$$

$$z_1 = x_1 + i\beta_1 x_2 \equiv r_1 e^{i\varphi_1}$$

$$z_2 = x_1 + i\beta_2 x_2 \equiv r_2 e^{i\varphi_2}$$

where

$$\beta_1 \equiv (1 - \dot{a}^2/c_1^2)^{1/2}$$

$$\beta_2 \equiv (1 - \dot{a}^2/c_2^2)^{1/2}$$

$$c_1 \equiv \sqrt{(\lambda + 2\mu)/\rho} \quad \text{(P-wave velocity)}$$

$$c_2 \equiv \sqrt{\mu/\rho} \quad \text{(S-wave velocity)}$$

The material derivative of any function g twice differentiable in space-time is given by $dg/dt \cong -(da/dt)g_{,1}$ (+ more regular terms). Therefore, dg/dt and $(da/dt)g_{,1}$ have the same order of singularity, d^2g/dt^2 and $(da/dt)2g_{,1}$ have the same order of spatial singularity as well.

It is straighforward to write out the following sequence of equations, by considering terms of the same singularity, which determines successively $T^{(1)}$, $u^{(1)}$, $T^{(2)}$ .. etc, with the stress free condition on the crack for each order

$$k\Delta T^{(1)} + G\dot{a}\delta(C) = 0 \tag{4.22}$$

$$(\lambda + \mu)\nabla(\varepsilon_{11}^{(1)} + \varepsilon_{22}^{(1)}) + \mu\Delta\mathbf{u}^{(1)} - \rho\dot{a}^2\mathbf{u}_{,11}^{(1)} = 0 \tag{4.23}$$

$$k\Delta T^{(2)} + 3K\alpha T^{(1)}\dot{a}(\varepsilon_{11}^{(1)} + \varepsilon_{22}^{(1)})_{,1} = 0 \tag{4.24}$$

Term $T^{(1)}$

We obtain the solution $T^{(1)}$, given previously in Eq. (4.19) as

$$T^{(1)} \simeq -\frac{G\dot{a}}{2k\pi}\ln r \tag{4.25}$$

Term $\boldsymbol{u}^{(1)}$

Eq. (4.23) for displacement field $\mathbf{u}^{(1)}$ is identical to the one derived in isothermal elastodynamics, (Yoffe, 1951; Achenbach and Bazant, 1975). The general solution is given in terms of complex potentials $\Phi_1(z_1)$ and $\Phi_2(z_2)$ by

$$u_1^{(1)} = -\frac{1}{\mu}\mathrm{Re}\left[\Phi_1(z_1)+\frac{1+\beta_2^2}{2}\Phi_2(z_2)\right] \tag{4.26}$$

$$u_2^{(1)} = \frac{1}{\mu}\mathrm{Im}\left[\beta_1\Phi_1(z_1)+\frac{1+\beta_2^2}{2\beta_2}\Phi_2(z_2)\right] \tag{4.27}$$

The singular solution at the crack tip is given by the following potentials

$$\Phi_1(z_1) = \frac{2\sqrt{z_1}}{\left[4\beta_1\beta_2-(1+\beta_2^2)^2\right]\sqrt{2\pi}}\left[-K_I(1+\beta_2^2)+2iK_{II}\beta_2\right] \tag{4.28}$$

$$\Phi_2(z_2) = \frac{2\sqrt{z_2}}{\left[4\beta_1\beta_2-(1+\beta_2^2)^2\right]\sqrt{2\pi}}\left[K_I\frac{4\beta_1\beta_2}{1+\beta_2^2}-2iK_{II}\beta_2\right] \tag{4.29}$$

where K_I and K_{II} are the *dynamic* stress intensity factors derived from the *stress* field $\sigma(\mathbf{u}^{(1)})$ by the same formulae as the ones given in statics

$$K_I^{(\sigma)} = \lim_{r\to 0}\sqrt{2\pi r}\;\sigma_{\varphi\varphi}(r,0) \tag{4.30}$$

$$K_{II}^{(\sigma)} = \lim_{r\to 0}\sqrt{2\pi r}\;\sigma_{\varphi r}(r,0) \tag{4.31}$$

Here we have labelled these stress intensity factors with (σ) to remind their definition based on singular stress fields ahead the crack tip. The expressions of K's based on crack displacement discontinuities behind the crack tip, similar to the ones given in statics, are

$$K_I^{(u)} = \lim_{r\to 0}\frac{\mu}{4(1-\nu)}\frac{\sqrt{2\pi}}{\sqrt{r}}\left[u_2\right] \tag{4.32}$$

$$K_{II}^{(u)} = \lim_{r\to 0}\frac{\mu}{4(1-\nu)}\frac{\sqrt{2\pi}}{\sqrt{r}}\left[u_1\right] \tag{4.33}$$

Factors $K_\alpha^{(u)}$, $(\alpha = I, II)$, are not equivalent to dynamic ones $K_\alpha^{(\sigma)}$.

We can use the terminology of *kinematic* SIF for $K_\alpha^{(u)}$. Both factors are linked together by $K_\alpha^{(u)} = K_\alpha^{(\sigma)} f_\alpha(\dot{a})$, with the universal relations

$$f_I = \frac{\beta_1(1-\beta_2^2)}{(1-\nu)\left[4\beta_1\beta_2 - (1+\beta_2^2)^2\right]} \tag{4.34}$$

$$f_{II} = \frac{\beta_2(1-\beta_2^2)}{(1-\nu)\left[4\beta_1\beta_2 - (1+\beta_2^2)^2\right]} \tag{4.35}$$

Functions f_I and f_{II} increase slowly and monotonically with the crack speed from 1 to infinity as $\dot{a}$ approaches the Rayleigh wave velocity c_R for which the denominator of (4.34) and (4.35) vanishes. For the crack speed less than one half c_R, functions $f_I(\dot{a})$, $_{II}(\dot{a})$ are nearly constant.

The energy release rate, for each order, is given in the literature as

$$G = \frac{1-\nu^2}{E}(K_I^{(\sigma)2} f_I(\dot{a}) + K_{IJ}^{(\sigma)2} f_{II}(\dot{a})) \tag{4.36}$$

The last expression can be written more symmetrically as

$$G = \frac{1-\nu^2}{E}(K_I^{(\sigma)} K_I^{(u)} + K_{IJ}^{(\sigma)} K_{IJ}^{(u)}) \tag{4.37}$$

Eq. (4.37) shows a profound duality between two groups of stress intensity factors, the kinematic and the dynamic ones. In quasi-statics or for vanishing velocity, $f_I(0) = 1$ and $f_{II}(0) = 1$, we recover Irwin's formula.

Term T(2)

Calculating the term $(\varepsilon_{11}^{(1)} + \varepsilon_{22}^{(1)})_{,1}$ from the first order solution $\mathbf{u}^{(1)}$ we find

$$(\varepsilon_{11}^{(1)} + \varepsilon_{22}^{(1)})_{,1} = C_I(\dot{a}) K_I \,\mathrm{Re}(z_1^{-3/2}) + C_I(\dot{a}) K_{II} \,\mathrm{Re}(i z_1^{-3/2})$$

$$C_I(\dot{a}) = -\frac{(1+\beta_2^2)(\beta_1^2 - \beta_2^2)}{2\sqrt{2\pi}(\lambda+\mu)(4\beta_1\beta_2 - (1+\beta_2^2)^2}$$

$$C_{II}(\dot{a}) = -\frac{2\beta_2}{1+\beta_2^2} C_I(\dot{a})$$

The solution is searched in the form $T^{(2)}(r,\theta,t) = \bar{T}(t) + h(\theta,\dot{a}) r^{1/2} \ln r$. Using Eq. (4.24), it has been shown that function h is given by

$$h(\theta,\dot{a}) = A\sin(\frac{\theta}{2}) + \frac{4C_S}{1-\beta_1^2}\left[(\frac{r_1}{r})^{1/2}\cos(\frac{\varphi_1}{2}) - \beta_1\cos(\frac{\theta}{2})\right] -$$

$$-\frac{4C_A}{1-\beta_1^2}\left[(\frac{r_1}{r})^{1/2}\sin(\frac{\varphi_1}{2}) - \sin(\frac{\theta}{2})\right]$$

$$A = \frac{4C_A}{1-\beta_1^2}(1-\sqrt{\frac{1+\beta_1}{2}}),\ r_1/r \equiv \sqrt{\cos^2\theta + \beta_1^2\sin^2\theta},\ \varphi_1 = \arctan(\beta_1\tan\theta)$$

$$C_S = -\frac{3\dot{a}K\alpha G}{2\pi k^2}C_I(\dot{a})K_I, \qquad C_A = \frac{3\dot{a}K\alpha G}{2\pi k^2}C_{II}(\dot{a})K_{II}$$

Finally, the second order temperature field is

$$T^{(2)}(r,\theta) = \overline{T}(t) + \left[C_S R_S(\theta,\dot{a}) + C_A R_A((\theta,\dot{a})\right] r^{1/2}\ln r \qquad (4.38)$$

$$R_S(\theta,\dot{a}) = \frac{4}{1-\beta_1^2}\left[(\frac{r_1}{r})^{1/2}\cos(\frac{\varphi_1}{2}) - \beta_1\cos(\frac{\theta}{2})\right]$$

$$R_A(\theta,\dot{a}) = \frac{4}{1-\beta_1^2}\left[(\frac{r_1}{r})^{1/2}\sin(\frac{\varphi_1}{2}) - \sqrt{\frac{1+\beta_1}{2}}\sin(\frac{\theta}{2})\right]$$

The field $T^{(2)}$ is continuous across the crack line in pure mode I and discontinuous in pure mode II. For steel, functions R_S and R_A depend slighly on the crack velocity, (Bui et al, 1980). The isothermal curves $T^{(1)} + T^{(2)} =$ Cte for steel with constants

$\lambda = \mu = 0.8\ 10^{11}$ N.m^{-2}, $k = 42$ J.m^{-1}.s^{-1}, $\alpha = 1.5\ 10^{-5}$, $K_{Idyn} = 10^7$ N.m$^{3/2}$ are shown in Fig. 4.8, for mode I and in Fig. 4.9 for mode II. It is worth noting that Weichert and Schönert (1974) measured the temperature T = 130°C for steel, at the distance d = 30μm from the crack tip, with velocity $\dot{a}$ =10m.s ^{1}. They conjectured about a higher temperature at the crack tip. On glass, they observed a light emission at $\dot{a}$ =1000 m.s^{-1}, which implies a temperature higher than 1000°K. By filtering the emitted light on different wave lengthes, the temperature T = 3200°K is obtained on glass and 4700°K on quartz.

Most work gives the interpretation of the high temperature by considering plastic deformation on a very small near tip zone. Here, we show that even in pure dynamical thermo-elasticity, the temperature rise is very high for crack propagation.

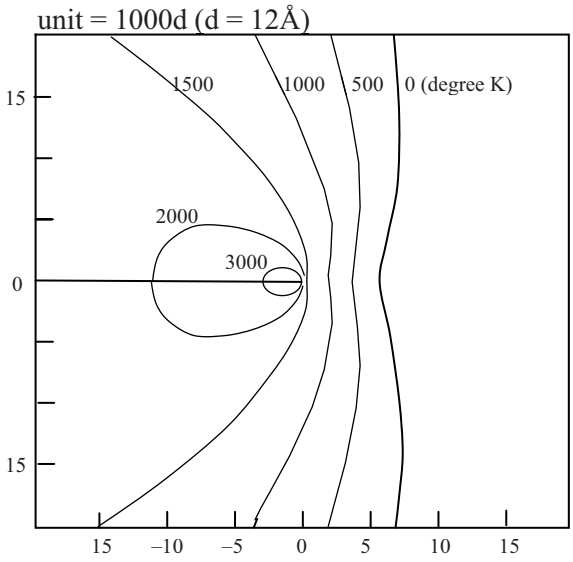

Figure 4.8: Isotherms for steel with da/dt =100m/s, for an insulated mode I crack; (Bui et al, 1980)

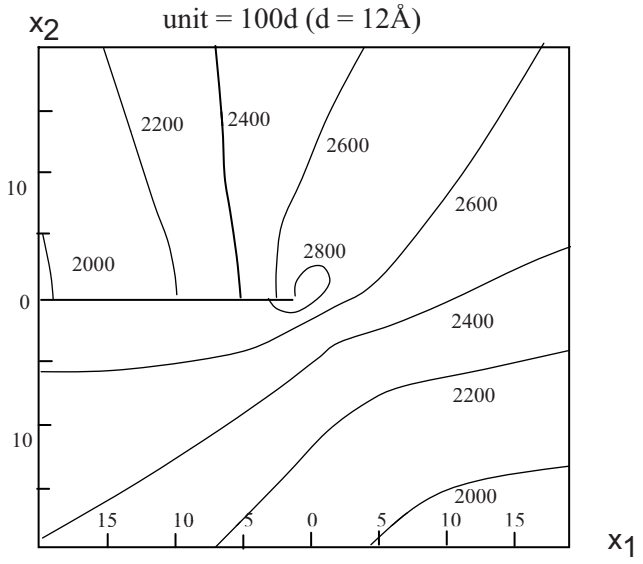

Figure 4.9: Isotherms for steel with da/dt =100m/s, for an insulated mode II crack (Bui et al, 1980).

Chapter 5

Dynamic Fracture Mechanics

5.1 Experimental aspects of crack propagation

When a cracked body at rest for $t < 0$ is subjected to an impulse loading, which is characterized for example by the stress magnitude σ^* and the duration t^*, one observes that the crack is stationary as long as the dynamic stress intensity factor is below some toughness value. Shockley et al (1983) showed that crack initiates at some t^* and above some critical value σ^*. For large t^* it seems that σ^* is constant. Data for the dynamic SIF versus duration t^* show similar features, (Ravi-Chandar and Knauss, 1984). Crack initiation occurs and propagation of crack begins when the dynamic stress intensity factor in mode I reaches some value called *dynamic toughness*. We shall denote the dynamic toughness at propagation by K_{Id}; we use the notation $K_I^{(\sigma)}(t)$ for the mathematical value of SIF for a crack at rest $K_I^{(\sigma)}(t) < K_{Id}$ or at propagation $K_I^{(\sigma)}(t) = K_{Id}$. Such a distinction is necessary because the evaluation of the first paramater $K_I^{(\sigma)}(t)$ as the mechanical response of the cracked body under applied stress loading $\mathbf{T}(t)$ or prescribed displacement $\mathbf{u}(t)$ and *specified* crack length history $a(t)$, is a mathematical problem. As shown later in some examples for particular geometry and loading, this problem is very difficult. It can be overcame by numerical methods (finite element methods) combined with the use of path independent integrals. The second parameter K_{Id} is a *material constant*, which generally depends on the crack velocity. This is an experimental problem, which is much more difficult since it requires, not only accurate methods to calculate the dynamic SIF, but also adequate measurement setups for capturing history of loads, displacements and crack velocity. These reasons explain why difficulties are encountered in dynamic fracture mechanics.

Experiments on dynamic propagation of edge crack, reported by Kalthoff (1985), do not tell us how crack actually initiates. Is the static toughness K_{Ic} equal to K_{Id}? Is the value of SIF the same in crack intiation and in crack arrest? What measurements for SIF's? What formula used for the

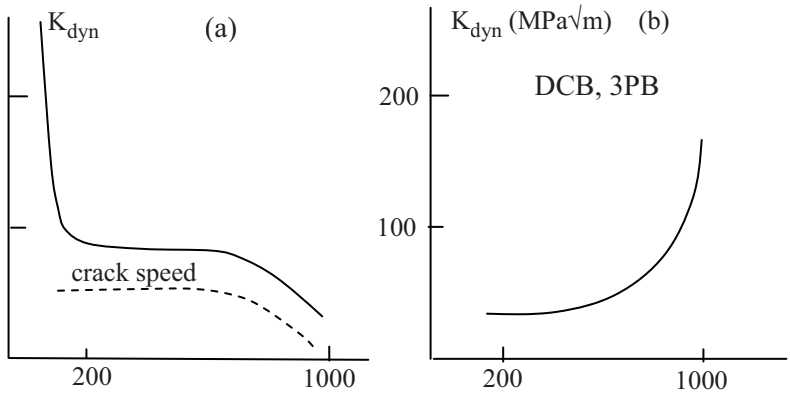

Figure 5.1: Experiments on dynamic Stress Intensity Factors. (a) K_{dyn} function of crack length, (Kalthoff, 1985); (b) K_{dyn} function of crack speed (m/s) determined by DCB or 3-Points-Bending specimens, (Zener and Rosakis, 1989)

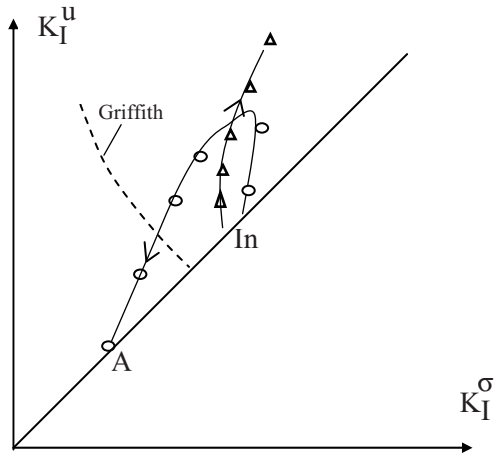

Figure 5.2: Experimental data in the domain $K^\sigma <$ u. (O) (Kalthoff, 1985); (Δ) (Zener and Rosakis, 1989); ---- Griffith (hyperbola); A (Arrest); In (Initiation)

experimental SIF? From the stress, the energy release rate or the crack opening displacement? Some of these questions are still open problems. Results on crack initiation are missing in the crack initation phase because measurements of the crack velocity are performed after some finite propagation. Kalthoff's experiments show a plateau value of SIF corresponding to constant velocity, followed by a decrease of both SIF and velocity. The plateau phase justifies some models of steady state propagation in infinite medium, while the transient phases indicate the geometry dependence and

reflexion of waves. Most works indicate that the dynamic SIF is an increasing function of the crack velocity, (Zener and Rosakis, 1989), Figure 5.2, (b). Different behaviors in crack accelereration and deceleration are often observed. It seems that *no* simple relationship exists between K_{Id} and crack velocity. To describe experiments reported in the literature, we can plot some data available in the ($_I\sigma$, $_I{}^u$) plane (in the sector $45° < \theta < 90°$), rather than in the (K_I, da/dt) plane. The increase of velocity corresponds to the increase of the slope $K_I{}^u/K_I{}^\sigma$. Griffith's criterion with constant 2γ corresponds to an arc of the hyperbola $K_I{}^u/K_I{}^\sigma = 2\gamma E/(1 - \nu^2) = Cte$, starting from the initiation point (In). In Griffith's model, crack initiation (In) and crack arrest (A) correspond to the same point. Kalthoff's experiments corresponds to circles (O) shown in Fig. 5.2, where the plateau value corresponds to the region near the point (P) where crack velocity is stationary and crack arrest corresponds to the point (A). Experiments by Zener and Rosakis (1989) are indicated by triangles (Δ). There are no clear evidence for the initiation point (In) and the arrest point (A) to be the same point on the line $\theta = 45°$ (zero crack speed). It should be expected that strain rates at material points ahead or behind the crack tip are not in the same situation with respect to loading (crack initiation) or unloading (crack arrest). Thus the rate dependence of constitutive laws, which prevails in the process zone, would give different toughness values at initation and crack arrest.

5.2 Fundamental equations

In this chapter, we do not consider thermal effects in the mathematical evaluation of dynamic SIF, because the singular temperature field, Eq. (4.19), does not change significantly the singular stress field. Perhaps, the high temperature field at the moving crack tip has some effects on the material properties inside the process zone, exactly as in the quasi-static toughness of metals when the temperature goes beyond the transition point T_0 from brittle to ductile fracture. Temperature influence on the material property is obvious in slip friction occuring in earth-quake, where energy dissipated by friction causes sometimes melting of rocks.

The fundamental equations of elasto-dynamics for displacement field **u** and stress field σ in plane strain, are given in terms of functions ϕ, ψ on space-time, which are associated respectively to dilatational P-wave and shear S-wave, which propagate with the speeds c_1 or $c_p = \{(\lambda + 2\mu)/\rho\}^{1/2}$, c_2 or $c_s = (\mu/\rho)^{1/2}$ respectively

$$u_x = \phi_{,x} + \psi_{,y} \tag{5.1}$$

$$u_y = \phi_{,y} - \psi_{,x} \tag{5.2}$$

$$\phi_{,xx} + \phi_{,yy} - c_p^{-2}\phi_{,tt} = 0 \tag{5.3}$$

$$\psi_{,xx} + \psi_{,yy} - c_s^{-2}\psi_{,tt} = 0 \tag{5.4}$$

In plane strain case, $u_z = 0$ and u_α ($\alpha = x, y$) is function of (x, y, t). The stress components are given by

$$\sigma_{xx} = (\lambda+2\mu)\phi_{,xx} + \lambda\phi_{,yy} + 2\mu\psi_{,xy} \tag{5.5}$$

$$\sigma_{yy} = (\lambda+2\mu)\phi_{,yy} + \lambda\phi_{,xx} - 2\mu\psi_{,xy} \tag{5.6}$$

$$\sigma_{xy} = \mu(2\phi_{,xy} + \psi_{,yy} - \psi_{,xx}) \tag{5.7}$$

The equations of motion (5.3), (5.4) in the physical domain Ω are given for the case of no body force (except inertial force).

To solve transient problems, we need initial conditions $\mathbf{u}(t \le 0) = \mathbf{0}$ and boundary conditions on $\partial\Omega$.

For infinite medium, when the stresses are not prescribed, one adds the finiteness condition of the total radiated energy E_R through the sphere S defined as

$$E_R = \int_{time}\int_S \sigma_{ij} n_j \ddot{u}_i \, dS dt \tag{5.8}$$

5.3 Steady state solutions

In the steady state case with constant crack velocity, displacement and stress fields depend on time through the combinaison $x_1 = x - \dot{a}\, t$. Let x_1, $x_2(=y)$, be the moving coordinates. This supposes that the applied load is moving with the same crack velocity. In case of finite crack, one crack tip moves with the velocity V and behaves like a source of dissipated energy, while the another one, moving with opposite velocity –V, is a sink of energy. Of course, such a model is not physical; Yoffe (1951) considered her model only for determining the asymptotic behavior of the solution near the moving tip with velocity V.

The complex representation of displacement and stress are given by Radok's formulae

$$u_1 = -\frac{1}{\mu}\mathrm{Re}\left[\phi_1(z_1) + \frac{1+\beta_2^2}{2}\phi_2(z_2)\right] \tag{5.9}$$

$$u_2 = \frac{1}{\mu}\mathrm{Im}\left[\beta_1\phi_1(z_1) + \frac{1+\beta_2^2}{2\beta_2}\phi_2(z_2)\right] \tag{5.10}$$

with $z_1 = x + i\beta_1 y$, $z_2 = x + i\beta_2 y$, $\beta_1 \equiv (1 - \dot{a}^2/c_p^2)^{1/2}$, $\beta_2 \equiv (1 - \dot{a}^2/c_s^2)^{1/2}$. The stress components are

$$\sigma_{11} = -2\mathrm{Re}\left\{\frac{2\beta_1^2 - \beta_2^2 + 1}{2}\phi_1'(z_1) + \frac{1+\beta_2^2}{2}\phi_2'(z_2)\right\} \tag{5.11}$$

$$\sigma_{22} = (1+\beta_2^2)\mathrm{Re}\left\{\phi_1'(z_1) + \phi_2'(z_2)\right\} \tag{5.12}$$

$$\sigma_{12} = 2\mathrm{Im}\left\{\beta_1\phi_1'(z_1) + \frac{1}{4\beta_2}(1+\beta_2^2)^2\phi_2'(z_2)\right\} \tag{5.13}$$

If the prescribed moving load on the crack [a,b] is defined by $\sigma_{12}^d = 0$, $\sigma_{22}^d \neq 0$, then the solution ϕ'_2 is given by

$$\phi_2'(z_2) = -\frac{4\beta_1\beta_2}{(1+\beta_1^2)^2}\phi_1'(z_2) \tag{5.14}$$

for which the bracket in Eq. (5.13) vanishes and $\phi_1'(z_1)$ satisfies

$$\mathrm{Re}\,\phi_1'(x) = \frac{1+\beta_2^2}{(1+\beta_1^2)^2 - 4\beta_1\beta_2}\sigma_y^d(x) := f(x) \tag{5.15}$$

Therefore only *one* function, namely ϕ'_1, has to be determined. The solution of Eq. (5.15) is given by Cauchy's integral ($z = x_1 + ix_2$)

$$\phi_1'(z) = \frac{X(z)}{2i\pi}\int_a^b \frac{2f\,\xi)d\xi}{X(\xi^+)\,\xi - z)} \tag{5.16}$$

$$X(z) = (z - a)^{-1/2}(z - b)^{-1/2}$$

From Eq. (5.16), Yoffe's solution for the crack of length 2a under constant pressure p is given by the function

$$\phi_1'(z_1) = \frac{p(1+\beta_2^2)}{4\beta_1\beta_2 - (1+\beta_2^2)^2}\left\{1 - z_1(z_1^2 - a^2)^{-1/2}\right\} \tag{5.17}$$

The case of a semi-infinite crack $b = 0$, $a = -\infty$, under opposite concentrated unit load at $x_1 = -a$, corresponds to the function

$$\phi_1'(z_1) = \frac{-(1+\beta_2^2)}{\pi\left[4\beta_1\beta_2 - (1+\beta_2^2)^2\right]}\frac{1}{z_1+a}\left(\frac{1}{z_1}\right)^{1/2} \tag{5.18}$$

The Green's function (5.18) allows the determination of the solution for any moving load $\sigma_{22}^{d} \neq 0$ on the crack, for example a constant load $\sigma_{22}^{d} = \sigma$ on [–a, 0] as considered in Cragg's problem

$$\phi_1'(z_1) = \frac{-2\sigma(1+\beta_2^2)}{\pi\left[4\beta_1\beta_2 \quad (1+\beta_2^2)^2\right]}\left[\left(\frac{a}{z_1}\right)^{1/2} - \arctan\left(\frac{a}{z_1}\right)^{1/2}\right] \tag{5.19}$$

It is not difficult to show that dynamic and kinematic SIF are linked by

$$K_I^{(u)} = K_I^{(\sigma)} f_I(\dot{a}), \qquad {}_I(\dot{a}) = \frac{4\beta_1^2(1-\beta_2^2)}{(\kappa+1)\left[4\beta_1\beta_2 - (1+\beta_2^2)^2\right]} \tag{5.20}$$

Similar universal relations hold for modes II and III

$$K_{II}^{(u)} = K_{II}^{(\sigma)} f_{II}(\dot{a}), \qquad {}_{II}(\dot{a}) = \frac{4\beta_2^2(1-\beta_2^2)}{(\kappa+1)\left[4\beta_1\beta_2 - (1+\beta_2^2)^2\right]} \tag{5.21}$$

$$K_{III}^{(u)} = K_{III}^{(\sigma)} f_{III}(\dot{a}), \qquad \tilde{}_{III}(\dot{a}) = \frac{1}{\beta_2} \tag{5.22}$$

5.4 Transient crack problems

In this section we will consider some exact solutions to transient crack problems, a self-similar solution given by Afanasev and Cherepanov (1973).

5.4.1 Symmetric extension of a crack

Let us consider the following problem solved by Afanasev and Cherepanov (1973). A crack of zero initial crack length, is propagating symmet-

rically at constant velocity V at both crack tips, under concentrated impulse load at the origin of fixed coordinates Ox, y $\sigma_{yy}(x, 0, t) = -Q\delta(x)\delta(t)$. To solve the problem, one remarks that the wave equation can be satisfied by any complex function $F(\tau) \equiv f(x, y, t)$ of the Smirnov-Sobolev variable

$$\tau = \tau_x + i\tau_y = \frac{xt - it\left\{(t^2 - c^{-2}(x^2 + y^2)\right\}^{1/2}}{x^2 + y^2} \tag{5.23}$$

This variable is an homogeneous function of (x, y, t) of degree zero, that is, by a scaling of variables $(x, y, t) \rightarrow (ax, ay, at)$, the variable τ is unchanged. The self-similar solution is searched in terms of displacement potentials ϕ, ψ, functions of Smirnov and Sobolev's complex variables z_1, z_2 respectively

$$z_1 = \frac{xt - it\left\{(t^2 - c_p^{-2}(x^2 + y^2)\right\}^{1/2}}{x^2 + y^2}, z_2 = \frac{xt - it\left\{(t^2 - c_s^{-2}(x^2 + y^2)\right\}^{1/2}}{x^2 + y^2} \tag{5.24}$$

An integral transform $f \rightarrow f^*$ is applied to displacements and stresses as

$$u_i^* = \int_0^t u_i(x, y, t)dt \tag{5.25}$$

$$\sigma_{ij}^* = \int_0^t \sigma_{ij}(x, y, t)dt \tag{5.26}$$

The transformed displacement fields are expressed generally in terms of 4 functions $U_1(z_1)$, $U_2(z_2)$, $V_1(z_1)$, $V_2(z_2)$

$$u_x^* = \mathrm{Re}\left\{U_1(z_1) + U_2(z_2)\right\} \tag{5.27}$$

$$u_y^* = \mathrm{Re}\left\{V_1(z_1) + \ _2(z_2)\right\} \tag{5.28}$$

However, the number of independent functions can be reduced. Afanasev and Cherepanov (1973) showed that *one* function, namely W(z), is sufficient for obtaining the solution

$$U_1'(z) = zc_s^2(c_s^{-2} - 2z^2)(c_p^{-2} - z^2)^{-1/2}W'(z) \tag{5.29}$$

$$U_2'(z) = -2zc_s^2(c_s^{-2} - z^2)^{-1/2}W'(z) \tag{5.30}$$

$$V_1'(z) = c_s^2(c_s^{-2} - 2z^2)W'(z) \tag{5.31}$$

$$V_2'(z) = 2z^2 c_s^2 W'(z) \tag{5.32}$$

The transformed stresses are expressed in terms of functions $W(z_1)$ and $W(z_2)$

$$\sigma_{xx}^* = \mu c_s^2 \,\mathrm{Re}\left\{\frac{(c_s^{\,2} - 2c_p^{\,2} + 2z_1^2)(c_s^{\,2} - 2z_1^2)}{c_p^{-2} - z_1^2} W'(z_1)\frac{\partial z_1}{\partial y} - 4z_2^2 W'(z_2)\frac{\partial z_2}{\partial y}\right\} \tag{5.33}$$

$$\sigma_{yy}^* = \mu c_s^2 \,\mathrm{Re}\left\{\frac{(c_s^{\,2} - 2z_1^2)^2}{c_p^{\,2} - z_1^2} W'(z_1)\frac{\partial z_1}{\partial y} + 4z_2^2 W'(z_2)\frac{\partial z_2}{\partial y}\right\} \tag{5.34}$$

$$\sigma_{xy}^* = \mu c_s^2 \,\mathrm{Re}\left\{2(c_s^{\,2} - 2z_1^2)W'(z_1)\frac{\partial z_1}{\partial x} - 2(c_s^{\,2} - 2z_2^2)W'(z_2)\frac{\partial z_2}{\partial x}\right\} \tag{5.35}$$

On the crack, $y = 0$, $z_1 = z_2 = t/x$, $W'(z_1) = W'(z_2)$, hence the condition $\sigma_{xy}^* = 0$ is satisfied. The remaining boundary conditions are: $\sigma_{yy}^* = -Q\delta(x)$ on the crack and $v^*(x, 0, t) = \mathrm{Re}W(z) = 0$ outside the crack. It can be verified that solution of the problem considered corresponds to the function W'

$$W'(\tau) = \frac{\tau\ ^1Q}{2\pi\mu c_s^2(c_s^{-2} - c_p^{-2})}(\tau^2 - V^{-2})^{1/} \tag{5.36}$$

Upon differentiation of u_y^* and σ_{yy}^* with respect to time, one obtains the crack opening displacement $[[u_y]]$ and the normal stress as

$$[[u_y]] = \frac{Qt^{\ 2}}{\pi\ Vc_s^2(c_s^{-2} - c_p^{-2})}(t^2V^2 - x^2)^{1/2},\ (x<Vt) \tag{5.37}$$

$$\sigma_{yy}(x, 0, t) = \frac{-Q\sqrt{V}}{2\pi\sqrt{2}} S(\frac{1}{V})\frac{(V^{-2} - c_p^{-2})^{-1/2}}{c_s^{\,2} - c_p^{-2}}\frac{t^{-3/2}}{(x - Vt)^{1/2}},\ (x>Vt) \tag{5.38}$$

where $S\ \eta) = (c_s^{-2} - 2\eta^2)^2 + 4\eta^2(c_p^{-2} - \eta^2)^{1/2}(c_s^{-2} - \eta^2)^{1/2}$.

Remark that $S = 0$ for $\eta = \pm 1/c_R$ (c_R: Rayleigh's speed) and that the square root singularities are recovered in transient loading of moving crack. Moreover, calculating the kinematic SIF and dynamic SIF, one recovers again the universal relationship $K_I^{(u)} = K_I^{(\sigma)} f_I(da/dt)$ of dynamic crack propagation.

5.4.2 Semi-infinite crack with arbitrary propagation speed

Consider the general case of a finite crack [b(t), a(t)] which propagates at both crack tip db/dt < 0, da/dt > 0. The crack is under opposite normal pressure $p_y(x, t)$ in mode I, shear forces $p_x(x, t)$ in mode II and $p_z(x, t)$ in mode III. The solution of the general mixed mode problem of a finite crack, given by Kostrov (1975), is very complex. Even in simpler case of time independent load, the solution given by Freund (1972) is very complex too.

For simplicity, we consider only mode III crack problem. Let us consider the double Laplace transform of functions f(x, y, t) with respect to x and t, the transformed functions being denoted by the corresponding capital letter F(q, y, p), with argument changes $t \to p$, $x \to q$. Laplace transform's and its inverse transform are

$$f(x, y, t) \rightarrow F(q, y, p) = \int_0^{\infty} e^{-pt} \int_{-\infty}^{+\infty} e^{-qx} f(x, y, t)dxdt$$

$$F(q, y, p) \rightarrow f(x, y, t) = \frac{-1}{4\pi^2} \int_{-i\infty+c}^{+i\infty+c} e^{pt} \int_{-i\infty+c'}^{+i\infty+c'} e^{qx} f(q, y, p)dqdp$$

where c > 0 and c' are chosen so that the integration contour is within the strip $-(1/c_p)Re(p) < Re(q) = c' < (1/c_p)Re(p)$, where F(q, y, p) is regular. After simple calculations, shear wave harmonic equation becomes a second order differential equation in the variable y for the double Laplace transform $U_z(q, y, p)$ which can be solved exactly as

$$U_z(q, y, p) = \frac{-1}{\mu p(c_s^{-2} - q^2 p^{-2})} e^{-|y|(c_s^{-2} p^2 - q^2)} \Sigma(q, p) Sgn(y) \tag{5.39}$$

where Σ(q, p) is the double Laplace transform of the stress, $\sigma_{zx}(x,0,t) = -p(x,t)$ for x > a(t) and $\sigma_{zx}(x, 0, t) = 0$ for x<a(t).
The transforms of stress ahead the crack tip $\Sigma_{zx}(q, 0, p)$ and of the crack jump $W(q, p) = U_z(q,0^+,p) - U_z(q,0^-,p)$, are linked by stress-strain law

$$\Sigma_{zx}(q, p) + pK_3\left(\frac{q}{p}\right) W(q, p) = 0 \tag{5.40}$$

where $K_3(s) = (1/c_s^2 - 1/s^2)^{1/2}/2\mu$. The stress intensity factor $K_{III}(t)$ defined by the limit of $\sigma_{zx}(x, 0, t)(x - a(t))^{1/2}$, $x > a(t)$, $x \to a(t)$, can be calculated after double Laplace inversion of $\Sigma_{zx}(q, 0, p) = -pK_3(q/p)W(q, p)$

$$K_{III}(t) = \frac{\sqrt{2}}{\pi}(1 - \frac{\dot{a}(t)}{c_s})^{1/2} \int_0^{c_s t} p_z(a(t) - x, t - \frac{x}{c_s}) \frac{1}{\sqrt{x}} dx \tag{5.41}$$

Now, suppose that the load $p_z(x)$ does not depend on time and vanishes for $x < a(0)$, then Eq. (5.41) gives the SIF derived by Freund (1972), using a different approach

$$K_{III}(t) = \frac{\sqrt{2}}{\pi}(1 - \frac{\dot{a}(t)}{c_s})^{1/2} \int_{a(0)}^{a(t)} p_z(x) \frac{1}{\sqrt{t - x}} dx \tag{5.42}$$

$$K_{III}(t) = (1 - \frac{a(t)}{c_s})^{1/2} K_{III}^{stat} \tag{5.43}$$

$$K_{III}^{stat} = \frac{\sqrt{2}}{\pi} \int_{a(0)}^{a(t)} p(x) \frac{dx}{(a(t) - x)^{1/2}} \tag{5.44}$$

where K_{III}^{stat} is the SIF calculated as in statics, with the load p(x) given on [a(0), a(t)]. Such a property does not hold for a general transient loading as shown in Eq. (5.41) where the load explicitly depends on time. It should be noted that: i) The SIF (5.43) is a *dynamic* one which vanishes, $K_{III}^{dyn} = 0$, when the crack velocity approaches the shear wave speed c_s, viz, the stress ahead the crack tip becomes regular or finite.
ii) The *kinematic* SIF, $K_{III}^{(u)}(t) = K_{III}^{(\sigma)}(t)(1 - \dot{a}^2(t)/c_s^2)^{1/2}$ as introduced in Bui (1977), can be written for the case of time independent load p(x) on [a(0), a(t)], as follows

$$K_{III}^{(u)}(t) = (1 + \frac{\dot{a}(t)}{c_s})^{-1/2} K_{III}^{stat} \tag{5.45}$$

This means that, as $da/dt \to c_s$, the kinematic SIF approaches a finite value,

$$K_{III}^{(u)}(t) = K_{III}^{stat} / \sqrt{2}$$

5.5 Diffraction of time harmonic plane wave by a crack

This problem arises in the diffraction of time harmonic plane elastic waves in solid for the purpose of crack detection. A steady-state plane wave of direction α impinges the stationary semi-infinite crack, $x < 0$, $y = 0$. The displacement potentials with time factor $\exp(-i\omega t)$ are ($k_{p,s}^2 = \omega^2 / c_{p,s}^2$)

$$\phi^{(in)} = a\exp(-ik_p x\cos\alpha - ik_p y\sin\alpha) \tag{5.46}$$

$$\psi^{(in)} = b\exp(-ik_s x\cos\alpha - ik_s y\sin\alpha) \tag{5.47}$$

Now we show how to derive the solution with the Wiener-Hopf technique, (Noble, 1958).

Wiener-Hopf technique

Here, the Fourier transform of function f(x, y) with respect to x is used $f(x, y)\rightarrow F(s, y)$ with complex s

$$F(s, y) = \frac{1}{\sqrt{2\pi}}\int_{-\infty}^{+\infty} f(x,y)e^{isx}dx \tag{5.48}$$

$$f(x, y) = \frac{1}{\sqrt{2\pi}}\int_{-\infty}^{*+\infty} F(s,y)e^{-isx}ds \tag{5.49}$$

The star (*) in the second integral indicates that the real axis of the s-plane must be appropriately indented, above or below of branch cut points of F. The total field solution is sought in the form $\phi^{(t)} = \phi^{(in)} + \phi$, $\psi^{(t)} = \psi^{(in)} + \psi$, with the stress free condition on the crack. Define the left and right Fourier transform of h(x) respectively by H (s) and $H^{+}(s)$

$$H^{-}(s, y) = \frac{1}{\sqrt{2\pi}}\int_{-\infty}^{0} h(x,y)e^{isx}dx \tag{5.50}$$

$$H^{+}(s, y) = \frac{1}{\sqrt{2\pi}}\int_{0}^{+\infty} h(x,y)e^{isx}dx \tag{5.51}$$

Introduce the displacement discontinuities [[u]] and [[v]] and and the corresponding left Fourier transforms [[U]], [[V]]. Displacement is continuous for $x > 0$ so that [[U+]] and [[V+]] are zero. From the field equations for auxiliary fields ϕ, ψ, and the boundary conditions on the crack one obtains

$$\Sigma_{yy}^{+}(s, y=0) + \Sigma_{yy}^{-}(s, y=0) = 2\mu(s^2 - \frac{\omega^2}{c_p^2})^{-1/2}\frac{c_s^2}{\omega^2}$$
$$\times\left\{(s^2 - \frac{\omega^2}{2c_s^2})^2 - s^2(s^2 - \frac{\omega^2}{c_p^2})^{1/2}(s^2 - \frac{\omega^2}{c_s^2})^{1/2}\right\}[[V^{-}]]. \tag{5.52}$$

$$\Sigma_{xy}^{+}(s, y=0) + \underline{\Sigma}_{xy}^{-}(s, y=0) = 2\mu(s^2 - \frac{\omega^2}{\varsigma^2})^{-1/2} \frac{c_s^2}{\omega^2} \times$$

$$\times \left\{ (s^2 - \frac{\omega^2}{2c_s^2})^2 - s^2(s^2 - \frac{\omega^2}{c_p^2})^{1/2}(s^2 - \frac{\omega^2}{c_s^2})^{1/2} \right\} [[U^{-}]] \qquad (5.53)$$

The underlined quantities in Eqs. (5.52) and (5.53) are known from incident fields. These equations are typically of the general form of equations which can be solved by the Wiener-Hopf technique. That is to find unknown functions $F^{+}(s)$ regular and non zero in $\tau_1 < \tau$ and $G^{-}(s)$ regular and non zero in $\tau < \tau_2$ satisfying ($s = \tau + i\eta$)

$$A(s)F^{+}(s) + B(s)G^{-}(s) + C(s) = 0 \qquad (5.54)$$

in the strip $\tau_1 < \tau < \tau_2$, $-\infty < \eta < +\infty$. The key and difficult step of the WH-method is that to find a function E(s) such that the ratio B/A can be *factorized* as the ratio of functions $E^{+}(s)$, $E^{-}(s)$ as $B(s)/A(s) = E^{+}(s)/E^{-}(s)$. Here A = 1 in Eqs. (5.52) and (5.53). Once $E^{+}(s)$ has been found, the function $f(s) = C(s)/E^{+}(s)$ can by splitted into $f(s) = D^{+}(s) + D^{-}(s)$ using Cauchy's integrals for $\tau < c < \tau < d < \tau_2$

$$D^{+}(s) = \frac{1}{2i\pi} \int_{-\infty+ic}^{+\infty+ic} \frac{f(\xi)}{\xi - s} d\xi, \qquad \frac{G^{-}(s)}{E^{-}(s)} + D^{-}(s) = -P(s) \qquad (5.55)$$

Thus by the continuation theorem, Eq. (5.54) for unknown $F^{+}(s)$ and $G^{-}(s)$ becomes

$$\frac{F^{+}(s)}{E^{+}(s)} + D^{+}(s) = P(s), \quad \frac{G^{-}(s)}{E^{-}(s)} + D^{-}(s) = -P(s) \qquad (5.56)$$

where P(s) is a polynomial of degree less than the integral part of min (*p, q*), which can be determined by examining conditions at infinity in the physical problem. Now we consider Eq. (5.52) for determining the unknowns $\Sigma_{yy}^{+}(s, y = 0)$ and $[V^{-}]$ or Eq. (5.53) for the unknowns $\Sigma_{xy}^{+}(s, y = 0)$ and $[U^{-}]$. We need the factorization of the bracket {.} of (5.52) or (5.53) as

$$\left\{ (s^2 - \frac{\omega^2}{2c_s^2})^2 - s^2(s^2 - \frac{\omega^2}{c_p^2})^{1/2}(s^2 - \frac{\omega^2}{c_s^2})^{1/2} \right\} =$$

$$= \omega^2 (\frac{1}{c_s^2} - \frac{1}{c_p^2})(\frac{1}{c_R^2} - s^2)^2 S^{+}(s) S\ (s) \qquad (5.57)$$

$$S^{\pm}(s) = \frac{1}{4}\exp\left\{-\frac{1}{\pi}\arctan\int_{\omega/c_p}^{\omega/c_s} 4\,\frac{\xi^2(\xi^2 - \omega^2 c_p^{\,2})^{1/2}(\omega^2 c_s^{-2} - \xi^2)^{1/2}}{(2\xi^2 - \omega^2 c_s^{-2})^2}\frac{d\xi}{\xi \pm s}\right\} \tag{5.58}$$

Factorization (5.58) given by Kostrov (1975) solves the Wiener-Hopf problem for unknowns $\Sigma_{yy}^{+}(s, y = 0)$ and $[V^{-}]$ in Eq. (5.51) and $\Sigma_{xy}^{+}(s, y = 0)$ and $[U^{-}]$ in Eq. (5.53). Since the left and the right Fourier transforms are known, the stresses are completly determined by the inverse Fourier transforms of $\Sigma_{yy}(s, y = 0)$, $\Sigma_{xy}(s, y = 0)$.

Applications

Applications of the Wiener-Hopf technique have been given by Achenbach (1980) for the simpler problem of scattering of a SH-wave $u_3(x,t)$ by a crack. A plane incident wave

$u_3^{(in)}(\mathbf{x}, t) = UH(ct + x_2)$

of amplitude U impinges the semi-infinite crack $x_2 = 0$, $x_1 < 0$, H(.): Heaviside function. The method of solution is based on Fourier's transform and the Wiener-Hopf techniques discussed above

$$u_3(\mathbf{x}, t) = u_3^{(in)}(\mathbf{x}, t) + w(\mathbf{x}, t), \qquad w(\mathbf{x}, t) = \frac{1}{2\pi}\int_{\mathbb{R}} \phi(\omega, \mathbf{x})\exp(-i\omega ct)d\omega$$

$$\phi(\mathbf{x}, \omega) = \mp\frac{U}{2\pi}\int_C \frac{-i}{\omega\gamma\sqrt{\gamma - 1}}\exp(\mp\omega x_2\sqrt{\gamma^2 - 1} - i\omega\, x_1)d\gamma$$

(with +sign for $x_2 > 0$, –sign for $x_2 > 0$). Branch cuts are made at $\gamma = 1$ in the upper complex half-plane, and at $\gamma = -1$ in the lower half-plane. The contour C goes along the real axis from $-\infty$ to $+\infty$ and has to be indented *above* at $\gamma = -1$ by a vanishing semi circle described clockwise and *below* at $\gamma = 1$. Fig. 5.3 shows schematically how antiplane shear wave is reflected at the crack surface S^{+}, with twice the incident wave amplitude, while the wave vanishes at the hidden surface S^{-}, except some perturbed region near the crack tip, as if the crack is an opaque screen for incident wave. The feature is similar for in-plane shear wave parallel to the crack surface, but more complex because of scattered fields radiated from the crack tip with speeds c_1, c_2.

The screen effect justifies some approximations made in the next Chapter in order to solve to crack detection problems.

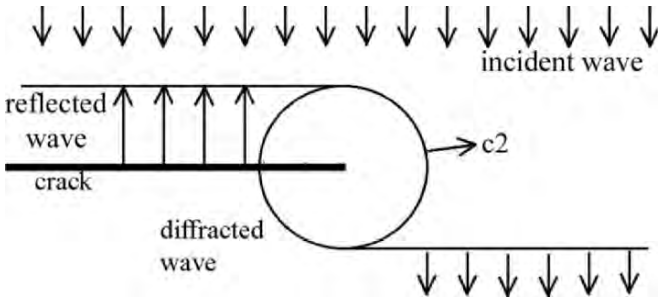

Figure 5.3: Waves fronts generated by incident inplane shear wave parallel to the semi-infinite crack; Reflected wave and diffracted waves propagation speeds with speeds c_1, c_2

5.6 Path-independent integrals

5.6.1 Path-independent integrals for moving cracks

A path-independent integral has been given by Freund (1972) and interpreted as the *energy flux* to the moving crack tip

$$F = \lim_{\eta \to 0} \int_{\Gamma_\eta} \left[\left(W + \frac{1}{2} \rho \dot{\mathbf{u}}.\dot{\mathbf{u}} \right) n_1 - \mathbf{n}.\boldsymbol{\sigma}.\mathbf{u}_{,1} \right] ds \tag{5.59}$$

Crack parameter F coincides with the energy release rate G in isothermal evolution. The path-independency property means only that the geometry of the contour Γ_η can be chosen arbitrarily. However, when the size η goes to zero, the integrant of F is singular as O(1/r) and, even if the bracket in (5.59) is integrable, the applicability of F in numerical computations may not be easy. It is well known that numerical solutions by finite elements methods are inaccurate in the crack tip region.

Therefore, a path-independent integral based on an arbitrary large contour and involving more regular functions, should be of interest for numerical computations. Many authors proposed the use of the following path-indepedndent integral, (Kishimoto et al, 1980)

$$J = \int_\Gamma ((W + \frac{1}{2} \rho \dot{\mathbf{u}}.\dot{\mathbf{u}}) n_1 - \mathbf{n}.\boldsymbol{\sigma}.\partial_1 \mathbf{u}) ds + \int_{A(\Gamma)} \rho \ddot{\mathbf{u}}.\partial_1 \mathbf{u} \, dA \tag{5.60}$$

The area A(Γ), enclosed by the contour Γ , moves with the same velocity da/dt. The second area integral is *divergent* in plane strain or anti-plane strain, because $\rho\partial_t\partial_t\mathbf{u}.\partial_1\mathbf{u} \cong O(1/r^2)$ has a non integrable singularity in the domain A(Γ). Thus J-integral given in (5.60) does not have a physical meaning. Considering that the singular part of $\rho\partial_t\partial_t\mathbf{u}.\partial_1\mathbf{u}$ is $O(1/r^2)$, the integral over A(Γ) outside the circle C_η, with centre on the moving crack tip and radius η, diverges as ln(η) as $\eta \to 0$,

$$\int_{A(\Gamma)-C_\eta} \rho\ddot{\mathbf{u}}.\mathbf{u}_{,1}dA \cong C\ln(\eta)$$

In order to overcome this difficulty, a mixed path and area integral over a moving path Γ is proposed in (Bui, 1977)

$$J = \int_\Gamma ((W - \tfrac{1}{2}\rho\dot{\mathbf{u}}.\dot{\mathbf{u}})n_1 - \mathbf{n}.\boldsymbol{\sigma}.\partial_1\mathbf{u} - \rho\dot{\mathbf{u}}.\partial_1\mathbf{u}\dot{a}n_1)ds + \frac{d}{dt}\int_{A(\Gamma)}\rho\dot{\mathbf{u}}.\partial_1\mathbf{u}dA \quad (5.61)$$

Even if there is an area integral A(Γ), J is independent of Γ. The path independency property of J results from a conservation law, (Fletcher, 1976)

$$\mathrm{div}[(W - \tfrac{1}{2}\rho\dot{\mathbf{u}}^2)I - \acute{}\mathrm{gra}^{\,t}\mathbf{u}).\boldsymbol{\sigma}] + \frac{\partial}{\partial t}(\rho\dot{\mathbf{u}}.\mathrm{gradu}) = 0 \quad (5.62)$$

and from the convected differentiation of the integral over moving domain $A(\Gamma)\backslash C_\eta$ with the crack speed.

Term $\rho\partial_t\mathbf{u}.\partial_1\mathbf{u}$ in the second integral of (5.61), is singular as O(1/r), thus is locally integrable in the area domain. Once the convergent area integral has been evaluated, the time derivative is applied to the result (The operators d/dt and $\int_A$ cannot be interchanged). The integral (5.62) can be evaluated by standard numerical methods, since the area integral is weakly singular. The important result is that J^{dyn} is exactly the isothermal energy release rate $G = J^{dyn}$.

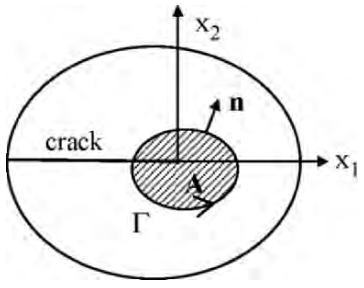

Figure 5.4: Path contour Γ and dashed area A(Γ) for J^{dyn}-integral

There is another path-independent integral, proposed by Nilsson (1973) for stationary crack, based on time Laplace's transform of fields, $a(\mathbf{x}, t) \rightarrow \hat{a}(\mathbf{x}, p)$

$$J^{(N)} = \int_{\Gamma} [\{W(\hat{\varepsilon}) + \tfrac{1}{2} p^2 \rho \hat{\mathbf{u}}.\hat{\mathbf{u}}\} n_1 \; - \mathbf{n}.\hat{\sigma}.\partial_1 \hat{\mathbf{u}}] ds \tag{5.63}$$

where transformed fields are written with a hat. The square root of $J^{(N)}(p)$ in pur mode I, or mode II, or mode III, is the Laplace transform of the corresponding $J(t)^{1/2}$. Nilsson's integral requires the mechanical fields be defined on *infinite* duration $[0, \infty]$.

5.6.2 A path-independent integral for crack initiation

Path-independent integrals are applications of conservation laws to computational Fracture Mechanics. To obtain accurate results on SIF, from numerical results which are generally inexact near the crack tip, one considers path-independent integrals which depend on the far-field, or depend weakly on the singular fields near the crack tip, like the J^{dyn} integral.

A pure line integral can be derived by considering new class of conservation laws in Elastodynamics which are related not to derivative of energy, but rather to *duality* between the actual fields and the dual (or adjoint) fields. Consider the actual dynamic field $\mathbf{u}(\mathbf{x}, t)$ of the solid, at rest at negative time, which satisfies the following equations in Ω

$$\mathrm{div}\,\sigma(\mathbf{u}) \; - \rho \frac{\partial}{\partial t} \dot{\mathbf{u}} = 0 \tag{5.64}$$

$$\mathbf{u} = \mathbf{0}, \;\; \dot{\mathbf{u}} = \mathbf{0}, \; (t \leq 0) \tag{5.65}$$

with some boundary conditions and initial condistions. The notation $\sigma(\mathbf{u})$ stands for $\mathbf{L}.\varepsilon(\mathbf{u})$. Let us introduce an adjoint field in the form $\mathbf{v}(\mathbf{x},t;\tau)$ satisfies the following equations in Ω:

$$\mathrm{div}\,\sigma(\mathbf{v}) \; - \rho \frac{\partial}{\partial t} \dot{\mathbf{v}} = 0 \tag{5.66}$$

$$\mathbf{v} = \mathbf{0}, \;\; \dot{\mathbf{v}} = \mathbf{0} \;\; (t \geq \tau) \tag{5.67}$$

with some boundary conditions. The adjoint field depends on time. Combining Eqs. (5.64), (5.66) and using the symmetry property of the elastic moduli tensor L, we obtain

$$\mathrm{div}\{\sigma(\mathbf{u}).\mathbf{v} - \sigma(\mathbf{v}).\mathbf{u}\} - \frac{\partial}{\partial t}(\mathbf{v}.\dot{\mathbf{u}} - \mathbf{u}.\dot{\mathbf{v}}) = 0 \tag{5.68}$$

Upon integrating the result (5.68) over the *finite* time interval $[0, \tau]$ and taking into account the initial condition on **u**, Eq. (5.65) and the final conditions on **v**, Eq. (5.67), we obtain the classical Conservation laws (from which the well-known reciprocity theorem of Elastodynamics is derived, (Willis, 1965))

$$\mathrm{div}\left\{\int_0^\tau (\sigma(\mathbf{u}).\mathbf{v} - \sigma(\mathbf{v}).\mathbf{u})dt\right\} = 0 \tag{5.69}$$

5.6.3 Inverse problems in dynamic fracture

Conservation law (5.69) provides us a powerful method to solve some inverse problems in Fracture Mechanics:

Problem 1. Determine the dynamic stress intensity factor of a stationary crack, by measurements of *both* stress vector **T** and velocity $\partial_t\mathbf{u}$ on the external boundary, without using the finite element methods. This is an identification problem for stress intensity factor rather than an inverse problem, since the datum **T**(x, t) is the only sufficient one to solve the well-posed forward problem. If the datum **T**(x, t) is a self equilibrated stress field, the solution to the Neumann boundary problem provides $\partial_t\mathbf{u}$ and the dynamic stress intensity factor. However, the knowledge of both boundary data **T** and $\partial_t\mathbf{u}$ bypasses the solution and can determine directly the SIF. This problem has important applications in experimental mechanics specially for experimentators who do not have (or are not familar with) softwares for numerical computations in dynamic problems.

Problem 2. Find the dynamic SIF of a *hidden* crack in the body, from measurements **T**, $\partial_t\mathbf{u}$ on the external boundary. We need to determine first the crack. The determination of the hidden crack is a true ill-posed inverse problem, which will be considered in Chap. 11. Having obtained the crack, we then calculate the SIF by using classical numerical methods.

In Chap. 11, we will show that global conservation law (5.69) has applications in the evaluation of materials, to detect flaws in solids, or a fault in the earthquake inverse problem.

Usually, the earthquake inverse problem is solved by geometric optimization methods with asumptions on physical earthquake mechanisms. Novel methods based on the conservation law (5.69) will bypass the assumptions on the geometry and physical mechanisms of the fault.

5.7 An experimental method for dynamic toughness

This section gives the solution to the identification Problem 1, for a given crack in two-dimensional problem. We introduce an auxiliary elasto-dynamic field $\mathbf{w}(\mathbf{x}, t;a)$ for the same solid with a fixed crack of length a, satisfying the same dynamic Eqs. (5.64), (5.65) but with different boundary conditions, and being regular at the crack tip as $\mathbf{w} \cong O(\sqrt{r})$. Define the adjoint field **v** as

$$\mathbf{v}(\mathbf{x}, t; a, \tau) \equiv \frac{\partial}{\partial a} w(\mathbf{x}, \tau - t; a) \tag{5.70}$$

The singularity of the field (5.70) is just what we want for an adjoint field. In fact, in the neighbourhood of the crack tip, the auxiliary field **w** depends on the crack length through the combinaison $((x_1 - a)^2 + x_2^2)^{1/2}$ and thus the adjoint field **v** admits the right singularity as $O(r^{-1/2})$. The path-independent $H(\mathbf{u}, \mathbf{w})$-integral (or H-integral for short) is defined for the finite duration $[0, t_1]$ of an experiment by (Bui and Maigre, 1988; Maigre, 1990)

$$H(\tau) = \frac{1}{2} \int_\Gamma \int_0^\tau \{\mathbf{n}.\sigma(\mathbf{u}).\mathbf{v} - \mathbf{n}.\sigma(\mathbf{v}).\mathbf{u}\} ds dt, \tau \in [0, t_1] \tag{5.71}$$

Γ is an arbitrary path surrounding the crack tip, with each end point on opposite crack faces, along which $\sigma(\mathbf{u}).\mathbf{n} = \sigma(\mathbf{v}).\mathbf{n} = \mathbf{0}$. The path-independency property of H follows from the last free conditions. The H-integral method has some advantage over other methods based on Laplace's transforms. The finiteness of the duration of experiments precludes us from using Laplace's transform of signals or functions in Nilsson's integral which need to be measured or defined over infinite time interval. Let $K_\alpha(u)$ and $K_\alpha(w)$ be the SIF of the fields **u** and **w** respectively. For stationary crack, no difference is made between kinematic SIF and dynamic SIF.

On consideration of the contour Γ along the exterior boundary S of the solid, it is obvious that integral $H(\tau)$ can be evaluated from the data $\sigma(\mathbf{u}).\mathbf{n}$ and **u** on S and from the known expression of the adjoint field **v**. The corresponding integral is thus a datum denoted by $H^d(\tau)$.

One the other hand, a small contour around the crack tip enables us to evaluate $H(\tau)$-integral with the stress-intensity factors of both fields. It is then easy to prove the relation (Maigre, 1990; Bui and Maigre, 1988)

$$\frac{1 - \nu^2}{E}(K_I^u * K_I^w + K_{II}^u * K_{II}^w) = H^d(\tau) \tag{5.72}$$

where the symbol (∗) indicates a time-convolution. Now, considering adequate choice of auxiliary fields, symmetrical field ($K_{II}^{w} = 0$) or anti-symmetrical one ($K_{I}^{w} = 0$), one can calculate separately each mode K_{I}^{u} or K_{II}^{u} by an *inverse time-convolution.* The auxiliary field **w** can be either exact analytical solution (for instance the solution of the problem of diffraction of plane waves by a semi-infinite crack) or numerical solution or the actual field itself. In the first two cases (analytical or numerical **w**), Eq. (5.72) provides a linear time convolution equation to determine the dynamic SIF from experimental data, without solving numerically the elastodynamic equation. In the third case (**w** = **u**), for symmetrical geometry and loading, Eq. (5.72) is a quadratic time convolution equation which can be solved for K_{I}^{u}. The quadratic deconvolution method has been validated numerically by finite element methods on the example shown in Figure 5.5, with opposite impulse applied to the specimen. The H-integral (5.68) for **w** = **u**, is denoted by H(**u**, **u**), where surface fields **u**, σ(**u**)**.n** are obtained by the finite elements method.

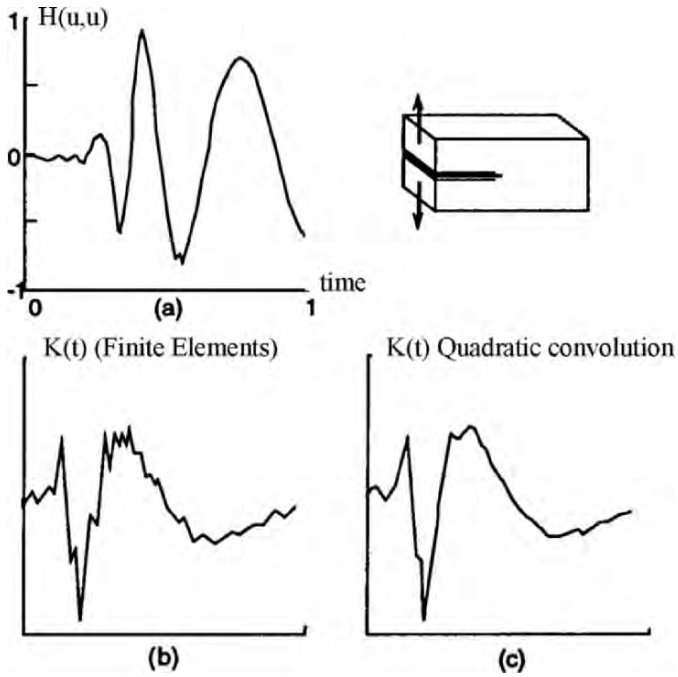

Figure 5.5: (a) Calculated H(**u**, **u**)-integral in the specimen under impulse loading; (b) Dynamic SIF by Finite Elements Methods; (c) $K_I(t)$ by quadratic inverse time- convolution, (Bui and Maigre, 1988)

Fig. 5.5 (a) shows the time evolution of the H-integral. The SIF obtained by the finite elements method is shown in Fig. 5.5 (b) and the SIF derived from inverse time-convolution in given in Fig. 5.5 (c). The agreement between different numerical approaches is quite good. The effectiveness of the adjoint field method to determine the dynamic SIF *experimentally*, with analyses not based on the Finite Elements Methods but on the inverse time-convolution method, has been demonstrated in the works of Bui et al (1992), Rittel et al (1992) related to experiments on metals, plexiglass, rock, glass etc. In experiments, it is easier to load a structure by a compressive force than by a traction force. For this purpose, a specimen called CCS (Compact Compressive Specimen) is machined according to the geometry shown in Fig. 5.6. The experimental setup consists of Kolsky-Hopkinson bars and software for signals analysis. Strain gages are used to detect the onset of propagation, that is the initiation point (In). It should be noted that impact compressive load acting on one side of the specimen induces a slight dissymmetry, or a mixed mode fracture, with a small ratio K_{II}/K_I about 10%. The amount of K_{II} can be determined by the inverse time-convolution with an adjoint field in mode II.

5.8 Identification of energies in dynamic fracture

Now let us generalize to moving crack the inverse energetic problem considered in Chap. 2 for stationary crack. Additional datum is the crack length history a(t), which can be measured in two-dimensional problems

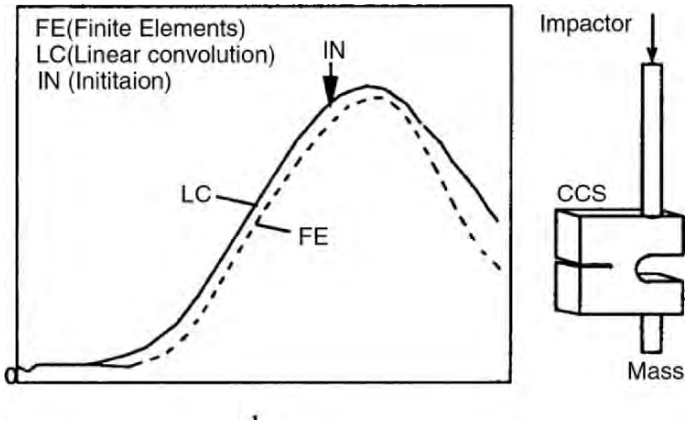

Figure 5.6: Dynamic SIF function of time in Compact Compression Specimen (CCS) under impactor; LC: Linear convolution; FE : Finite elements solution; IN: Crack initiation, (H. Maigre, 1990; Rittel et al, 1992)

by either a high speed camera or rupture gages. Moreover for plates, lateral in-plane surfaces are accessible to experiments to determine the crack opening displacement, thence the kinematic factor $K_I^u(t)$. Optical methods like caustics (Theocaris and Papadopoulos, 1984) can provide the dynamic stress intensity factor $K_I^\sigma(t)$ too. The other data are the traction vector $\mathbf{T}(\mathbf{x},t)$ and the velocity $\dot{\mathbf{u}}(\mathbf{x},t)$ on the external boundary of the solid S_{ext}. The energetic identification problem consists in the determination of elastic strain energy, kinetic energy and fracture energy. Thus we need three independent equations.

This identification problem has been solved by Bui and de Langre (1988) as follows. Since crack propagates, for velocity less than 60% of the Rayleigh wave velocoty c_R, there is practically no distinction between kinematic and dynamic Stress Intensity Factors. Otherwise, these SIF in mode I are linked by the universal relationship (5.20). Therefore, we already get the first equation giving the total fracture energy

$$W_R(t) = \frac{1-\nu^2}{E}\int_0^t \dot{a}(\tau) K_I^{(u)}(\tau) K_I^{(\sigma)}(\tau) d\tau \tag{5.73}$$

The second equation is provided by the balance equation of energy

$$W_{elast}(t) + W_{kin}(t) + W_R(t) = \int_{S_{ext}} \int_0^t \mathbf{T}(\mathbf{x},\tau).\dot{\mathbf{u}}(\mathbf{x},\tau) dS_x d\tau \tag{5.74}$$

Finally the third equation is given by the generalization of Brun's theorem to crack propagation, (Bui and de Langre, 1988)

$$W_{kin}(t) - W_R(t) = \tfrac{1}{2}\int_{S_{ext}} \{\int_0^t - \int_t^{2t}\} \mathbf{T}(\mathbf{x},2t-\tau).\dot{\mathbf{u}}(\mathbf{x},\tau) dS_x d\tau$$

$$+ \frac{1-\nu^2}{E}\int_t^{2t} \dot{a}(t) K_I^{(\sigma)}(2t-\tau) K_I^{(u)}(\tau) d\tau \tag{5.75}$$

In the second term of the right hand side of Eq. (5.75) only the time interval [t, 2t] is considered because the corresponding integral over [0, t] vanishes identically (See the proof in an Exercice)

Chapter 6

Three-Dimensional Crack Problems

Closed-form solutions in 2D fracture mechanics has been derived by using complex variables and Muskhelishvili's method of solutions. In 3D fracture mechanics, the power tool to solve crack problems is provided by boundary integral equation methods. This chapter is devoted to a review of mathematical methods for studying three-dimensional crack problems.

6.1. Fundamental tensors in elastostatics

Let us denote the elastic operator by L so that equilibrium equation in elastostatics, in the presence of a volumic force $\mathbf{f}$ can be written as

$$L\,\mathbf{u} := \mu \operatorname{div}\operatorname{grad}\mathbf{u} + \frac{\mu}{1-2\nu}\operatorname{div}\mathbf{u} = -\mathbf{f} \quad \text{in } \Omega \tag{6.1}$$

Unless stated otherwise, we assume that the boundary of the solid domain $\partial\Omega$ is a regular surface(*) having a normal $\mathbf{n}$ at each point.

Stress vector is derived from displacement $\mathbf{u}$ by applying the stress operator $T^{\mathrm{n}} : \mathbf{u} \to T^{\mathrm{n}}\mathbf{u} \equiv \sigma(\mathbf{u}).\mathbf{n}$

$$T^{\mathrm{n}} := 2\mu\frac{\partial}{\partial \mathrm{n}} + \lambda\,\mathbf{n}.\operatorname{div} + \mu\,\mathbf{n}\wedge \mathrm{r}\mathfrak{o}\mathrm{t} \tag{6.2}$$

6.1.1 The Kelvin-Somigliana tensor

The first fundamental tensor in elasticity is the Kelvin-Somigliana tensor associated to a point force, $\mathbf{f} = \delta_3(\mathbf{x} - \mathbf{y})\mathbf{e}^{\mathrm{k}}$, which satisfies

---

(*) Generally for Lyapounov's surface of index $0 < \mathrm{q} \le 1$. For instance $=1$ for the surface $y_3 - k(y_1^2 + y_2^2) = 0$; $\mathrm{q} = 1/2$ for $y_3 - k(y_1^2 + y_2^2)^{3/4} = 0$; $\mathrm{q} = 0$ for the conical surface $y_3 - k(y_1^2 + y_2^2)^{1/2} = 0$ whose vertex $\mathbf{y} = \mathbf{0}$ has undefined normal vector.

$$L\,\mathbf{V}^k(\mathbf{x},\mathbf{y}) = -\delta_3(\mathbf{x}-\mathbf{y})\mathbf{e}^k \tag{6.3}$$

The components of the Kelvin-Somigliana tensor $V_i^k(\mathbf{x},\mathbf{y})$ are given by the following formula

$$V_i^k(\mathbf{x},\mathbf{y}) = \frac{1}{16\pi\ (1-\nu)}\left\{(3-4\nu)\delta_{ik} + \frac{(x_i-y_i)(x_k-y_k)}{|\mathbf{x}-\mathbf{y}|^2}\right\}\frac{1}{|\mathbf{x}-\mathbf{y}|} \tag{6.4}$$

where $|\mathbf{x}-\mathbf{y}|=\{(x_i-y_i)(x_i-y_i)\}^{1/2}$ is the Euclidian distance between **x** and **y**. Traction vector $T^{n_x}\mathbf{V}^k(\mathbf{x},\mathbf{y})$ on an area element of normal $\mathbf{n}_x$ at point **x** is given by

$$T^{n_x}\mathbf{V}^k(\mathbf{x},\mathbf{y}) = -\frac{1-2\nu}{8\pi(1-\nu)|\mathbf{x}-\mathbf{y}|^3}\Big\{-(x_k-y_k)\mathbf{n} + (x_h-y_h)n_h\mathbf{e}^k + n_k(\mathbf{x}-\mathbf{y}) +$$

$$+\frac{3}{(1-2\nu)|\mathbf{x}-\mathbf{y}|^2}(x_k - y_k)(x_h-y_h)n_h(\mathbf{x}-\mathbf{y})\Big\} \tag{6.5}$$

6.1.2 The Kupradze-Bashelishvili tensor

This fundamental tensor is associated to a plane P(y) or P_y, with normal $\mathbf{n}_y$ at **y**, and defined by the set of vectors $\{\mathbf{B}^1(\mathbf{x},\mathbf{y};\mathbf{n}_y);\mathbf{B}^2(\mathbf{x},\mathbf{y};\mathbf{n}_y);\mathbf{B}^3(\mathbf{x},\mathbf{y};\mathbf{n}_y)\}$ which satisfies the elastic equilibrium equation

$$L\,\mathbf{B}^k(\mathbf{x},\mathbf{y};\mathbf{n}_y) = 0,\ \mathbf{x}\notin P_y \text{ (for fixed } \mathbf{y}\in P_y) \tag{6.6}$$

and boundary condition

$$\mathbf{B}^k(\mathbf{x},\mathbf{y};\mathbf{n}_y) = 0\,,\ \mathbf{x},\mathbf{y}\in P_y \text{ and } \mathbf{x}\neq\mathbf{y} \tag{6.7}$$

The components of $\mathbf{B}^k(\mathbf{x},\mathbf{y};\mathbf{n}_y)$ are

$$B_i^k(\mathbf{x},\mathbf{y};\mathbf{n}_y) = \frac{1-2\nu}{2\pi\ (3-4\nu)}\left\{2\mu\delta_{ik} + \frac{3\mu}{1-2\nu}\frac{(x_i-y_i)(x_k-y_k)}{|\mathbf{x}-\mathbf{y}|^2}\right\}\frac{\partial}{\partial n_y}\left(\frac{1}{|\mathbf{x}-\mathbf{y}|}\right) \tag{6.8}$$

Remark that $B_i^k(\mathbf{x},\mathbf{y};\mathbf{n}_y) = B_k^i(\mathbf{x},\mathbf{y};\mathbf{n}_y)$. To investigate the physical nature of the Kupradze-Bashelishvili tensor, let us consider a point **z** on P_y and a

scalar function f(**y**) whose compact support contains **z**. First we multiply Eq. (6.6) by f(**y**) and then integrate the result over the plane P(y). Second by taking the limits as $\mathbf{x} \to \mathbf{z}^{\pm}$ from both side of the plane, (+) sign in the normal side, we obtain

$$\lim_{\mathbf{x}\to\mathbf{z}^{\pm}} \int_{P(y)} \mathbf{B}^{k}(\mathbf{x},\mathbf{y};\mathbf{n}_{y}) f(\mathbf{y}) dS_{y} = \pm f(\mathbf{z})\mathbf{e}^{k} \tag{6.9}$$

The above equation shows that the vectors defined by

$$\mathbf{B}^{k}(\mathbf{z}^{\pm},\mathbf{y};\mathbf{n}_{y}) = \pm\mathbf{e}^{k}\delta_{P(y)}(\mathbf{y}-\mathbf{z}) \tag{6.10}$$

are opposite Dirac delta distributions. Physically the k-component of Kupradze-Bashelishvili's tensor is a dislocation dipole, in the $\mathbf{e}^{k}$ direction, which has important applications in 3D crack problems since it describes the discontinuity of displacement fields, Kupradze (1963).

6.2. Fundamental theorems in elastostatics

Two boundary-value problems in elastostatics, the Neumann and the Dirichlet problems with boundary conditions, respectively

$\sigma(\mathbf{y}).\mathbf{n} = \mathbf{T}^{d}(\mathbf{y})$, $\mathbf{y} \in \partial\Omega$, (Neumann problem)

$\mathbf{u}^{d}(\mathbf{y})$, $\mathbf{y} \in \partial\Omega$, (Dirichlet problem)

have been solved in a closed-form by Pham (1967). Pham's methods of solutions are based on boundary integral equations methods. The surface $\partial\Omega$ of a bounded solid must be sufficiently regular for ensuring that a unique normal vector **n** exists at any point of the boundary. The boundary of a cube does not have a regular surface because of vertices and wedges, but a worm cube like a dice in Las Vegas casinos does have. The regularity of the solid boundary can be relaxed if one considers that a part $\partial\Omega_{\eta}$ of this regular boundary, depending on a small parameter η, tends towards singular surfaces like vertices and wedges when $\eta \to 0$. This is why exact solutions in 3D elasticity theory, which are seldom, are of great interest in fracture mechanics. This section is devoted to the presentation of Pham's results. It should be noted that no equivalent results have been proved for mixed boundary value problems, with data $\mathbf{T}^{d}(\mathbf{y})$, $\mathbf{y} \in \partial\Omega_{T}$ and $\mathbf{u}^{d}(\mathbf{y})$, $\mathbf{y} \in \partial\Omega_{u}$, even if the coupled integral equations of the mixed boundary-value problems can be easily derived and solved numerically.

6.2.1 Solution of the Neumann boundary value problem

Traction vector being prescribed on the surface $\partial\Omega$, it is then appropriate to make use of the Kelvin-Somigliana tensor $\mathbf{V}^k(\mathbf{x}, \mathbf{y})$ which, for $\mathbf{z} \in \partial\Omega$ and $\mathbf{x} \in \Omega$, satisfies $L\mathbf{V}^k(\mathbf{x}, \mathbf{y}) = 0$. For any displacement field in three-dimensional elasticity, satisfying the elastic equilibrium equation without body force, one has the first representation formula by a *single layer* potential

$$S_i(\mathbf{x}) = 2\int_{\partial\Omega} {}^{k}_{i}(\mathbf{x}, \mathbf{z})\psi_k(\mathbf{z})dS_z \tag{6.11}$$

with a vectorial density function $\psi(\mathbf{z})$ defined on $\partial\Omega$. The simple layer potential (6.11) is continuous across $\partial\Omega$, but the corresponding stresses with a component along the normal should be discontinuous. More precisely, the current elastic problem can be considered as an *interior* problem, associated to $\Omega \equiv \Omega^-$. The limit of $T^{n_x}\mathbf{S}(\mathbf{x})$ as $\mathbf{x} \to \mathbf{y}^- \in \partial\Omega$ is given by

$$T^{n_y}\mathbf{S}(\mathbf{y}\ ) = \psi(\mathbf{y}) + 2(pv)\int_{\partial\Omega}\psi_k(\mathbf{z})T^{n_y}\mathbf{V}^k(\mathbf{y},\mathbf{z})dS_z \tag{6.12}$$

For $\mathbf{x} \to \mathbf{y}^+ \in \partial\Omega$ one has

$$T^{n_y}\mathbf{S}(\mathbf{y}^+) = -\psi(\mathbf{y}) + 2(pv)\int_{\partial\Omega}\psi_k(\mathbf{z})T^{n_y}\mathbf{V}^k(\mathbf{y},\mathbf{z})dS_z \tag{6.13}$$

Eqs. (6.12) and (6.13) are similar to Plemelj's formulae in plane elasticity.

The Neumann boundary value problem for $\Omega \equiv \Omega^-$ is solved by Eq. (6.11) which involves a vectorial density $\psi(\mathbf{y})$ satisfying the boundary integral equation

$$\psi(\mathbf{y}) + 2(\mathrm{pv})\int_{\partial\Omega}\psi_k(\mathbf{z}\,T^{n_y}\mathbf{V}^{\kappa\prime}\mathbf{y}\ \mathbf{z})dS_z = \mathbf{T}^{\alpha}(\mathbf{y})$$

or in terms of components

$$\psi_i(\mathbf{y}) + 2(\mathrm{pv})\int_{\partial\Omega}\psi_k(\mathbf{z})\{T^{n_y}\mathbf{V}^k(\mathbf{y},\mathbf{z})\}_i dS_z = \mathrm{T}_i^{\mathrm{d}}(\mathbf{y}) \tag{6.14}$$

According to Pham (1967) the solution of Eq. (6.14) is given by the strongly convergent series

$$\psi(\mathbf{y}) = \mathbf{h}^{(0)}(\mathbf{y}) + \mathbf{h}^{(1)}(\mathbf{y}) + \mathbf{h}^{(2)}(\mathbf{y}) + \ldots + \mathbf{h}^{(N)}(\mathbf{y}) + \ldots \tag{6.15}$$

where

$$\mathbf{h}^{(0)}(\mathbf{y}) = \mathbf{T}^{\mathrm{d}}(\mathbf{y})$$

$$\mathbf{h}^{(1)}(\mathbf{y}) = -2(\mathrm{pv})\int_{\partial\Omega}\left\{T^{\mathrm{n_y}}\mathbf{V}^{\mathrm{k}}(\mathbf{y},\mathbf{z})\right\}\mathrm{h}_{\mathrm{k}}^{(0)}(\mathbf{z})dS_z$$

.....

$$\mathbf{h}^{(\mathrm{N})}(\mathbf{y}) = -2(\mathrm{pv})\int_{\partial\Omega}\left\{T^{\mathrm{n_y}}\mathbf{V}^{\mathrm{k}}(\mathbf{y},\mathbf{z})\right\}\mathrm{h}_{\mathrm{k}}^{(\mathrm{N}-1)}(\mathbf{z})dS_z$$

Series (6.15) converges absolutely and uniformly in the space $C(\partial\Omega)$ of continuous functions on $\partial\Omega$. This has been proved by Pham (1967) under the compatibility condition for $\mathbf{T}^{\mathrm{d}}(\mathbf{y})$, $\mathbf{y} \in \partial\Omega$, which is nothing but the orthogonality condition

$$\int_{\partial\Omega}\mathbf{T}^{\mathrm{d}}(\mathbf{y}).\,\mathbf{f}(\mathbf{y})dS_{\mathrm{y}} = 0 \tag{6.16}$$

between $\mathbf{T}^{\mathrm{d}}(\mathbf{y})$ and the general solution $\mathbf{f}(\mathbf{y})$ of the homogeneous adjoint equation

$$\mathrm{f}_{\mathrm{i}}(\mathbf{y}) + 2(\mathrm{pv})\int_{\partial\Omega}\mathrm{f}_{\mathrm{k}}(\mathbf{z})\left[T^{\mathrm{n_z}}\,\mathbf{V}^{\mathrm{i}}(\mathbf{z},\,\mathbf{y})\right]_{\mathrm{k}}\,dS_z = 0 \tag{6.17}$$

Kernel in Eq. (6.17) is the transposed one of Eq. (6.14) where variables $\mathbf{y}$ and $\mathbf{z}$ are interchanged $[T^{\mathrm{n_y}}\mathbf{V}^{\mathrm{k}}(\mathbf{y},\mathbf{z})]_{\mathrm{i}} \rightarrow [T^{\mathrm{n_z}}\mathbf{V}^{\mathrm{i}}(\mathbf{z},\mathbf{y})]_{\mathrm{k}}$. It turns out that, as shown in Sect. 6.2.3, the general solution of (6.17) is the rigid displacement field $\mathbf{f}(\mathbf{y}) = \mathbf{a} + \mathbf{b} \wedge \mathbf{y}$, so that Eq. (6.16) simply expresses the equilibrium condition of prescribed datum $\mathbf{T}^{\mathrm{d}}(\mathbf{y})$.

It should be noted that in solving crack problems for a bounded solid subject to tractions on its external surface, one first considers the same boundary value problem for an uncracked body. The series (6.15) solves a three-dimensional problem in elasticity by a simple calculation of integrals, without using the finite element method and associated softwares. Then one searches the solution of the auxiliary problem with opposite traction vectors on the crack surfaces.

6.2.2 Solution of the Dirichlet boundary value problem

There is a second representation formula of displacement satisfying the elastic equilibrium equation without body force by a *double layer* potential

$$\mathrm{D}_{\mathrm{i}}(\mathbf{x}) = \int_{\partial\Omega}\mathrm{B}_{\mathrm{i}}^{\mathrm{k}}(\mathbf{x},\,\mathbf{z};\mathbf{n}_z)\phi_{\mathrm{k}}(\mathbf{z})dS_z \tag{6.18}$$

with kernel given by Kupradze-Bashelishvili's tensor $B_i^k(\mathbf{x},\mathbf{z};\mathbf{n}_z)$ and a vectorial density $\phi(\mathbf{z})$ defined on the surface. According to Eq. (6.10), the fundamental property of Eq. (6.18) is the discontinuity relation

$$\mathbf{D}(\mathbf{x}^+) - \mathbf{D}(\mathbf{x}\ ) = 2\boldsymbol{\phi}(\mathbf{z}) \tag{6.19}$$

so that $\mathbf{D}(\mathbf{x})$ could be considered as the displacement of an infinite solid with a surface crack along $\partial\Omega$. For the interior problem considered here, the density for solving the Dirichlet boundary value problem in $\Omega \equiv \Omega^-$ of the integral equation obtained from Eq. (6.18) by a limiting process $\mathbf{x} \to \mathbf{y}^-$

$$\boldsymbol{\phi}_i(\mathbf{y}) + (pv)\int_{\partial\Omega} B_i^k(\mathbf{y},\mathbf{z};\mathbf{n}_z)\boldsymbol{\phi}_k(\mathbf{z})dS_z = u_i^d(\mathbf{y}),\ (\mathbf{y} \in \partial\Omega) \tag{6.20}$$

According to Pham's work, the solution to Eq. (6.20) is given by the absolutely and uniformly convergent series in $C(\partial\Omega)$ the space of continuous functions

$$\boldsymbol{\phi}(\mathbf{y}) = \mathbf{g}^{(0)}(\mathbf{y}) + \mathbf{g}^{(1)}(\mathbf{y}) + \mathbf{g}^{(2)}(\mathbf{y}) + ... + \mathbf{g}^{(N)}(\mathbf{y}) + ... \tag{6.21}$$

where

$$\mathbf{g}^{(0)}(\mathbf{y}) = -\frac{1}{2}\mathbf{u}^d(\mathbf{y})$$

$$\mathbf{g}^{(1)}(\mathbf{y}) = \tfrac{1}{2}\left\{\mathbf{g}^{(0)}(\mathbf{y}) + (\mathrm{pv})\int_{\partial\Omega} B^k(\mathbf{y},\mathbf{z};\mathbf{n}_z).\mathbf{g}^{(0)}(\mathbf{z})dS_z\right\}$$

....

$$\mathbf{g}^{(N)}(\mathbf{y}) = \tfrac{1}{2}\left\{\mathbf{g}^{(N-1)}(\mathbf{y}) + (\mathrm{pv})\int_{\partial\Omega} B^k(\mathbf{y},\mathbf{z};\mathbf{n}_z).\mathbf{g}^{(N-1)}(\mathbf{z})dS_z\right\}$$

The series (6.15) and (6.16) provide the solutions to quasi-static three-dimensional elasticity, by a simple calculation of integrals. This makes it possible to solve a three-dimensional elastic problem on a laptop without a finite element method program.

Remarks. A mixed boundary value problem in three-dimensional elasticity could be formulated by considering both potentials (6.11) and (6.18), with unknowns $\psi(\mathbf{z})$ defined on $\partial\Omega_T$ and $\phi(\mathbf{z})$ defined on $\partial\Omega_u$. The coupled equations for $\psi(\mathbf{z})$ and $\phi(\mathbf{z})$ are

$$T^{n_y}\left\{\mathbf{S}(\mathbf{y}^-) + \mathbf{D}(\mathbf{y}^-)\right\} = \mathbf{T}^d(\mathbf{y}) \ \text{ on } \partial\Omega_T \tag{6.22}$$

$$\{\mathbf{S}(\mathbf{y}^-) + \mathbf{D}(\mathbf{y}^-)\} = \mathbf{u}^d(\mathbf{y}) \quad \text{on } \partial\Omega_u \tag{6.23}$$

It is found that a unique solution of the latter system of equations, for the densities $\psi(\mathbf{z})$ defined on $\partial\Omega_T$ and $\phi(\mathbf{z})$ defined on $\partial\Omega_u$, exists while computed numerically, but no constructive iterative solutions are known. There is no proof of the existence of solution either.

6.2.3 Direct methods using Kelvin-Somigliana's tensor

These methods are based on the Betti-Somigliana reciprocal theorem in elasticity, which considers two independent fields, on the one hand, the current field $\{\mathbf{u}(\mathbf{x}), T^{n_z}\mathbf{u}(\mathbf{z}), \mathbf{f} = \mathbf{0}\}$ with no body force, on the other hand, the Betti-Somigliana's tensor fields $\{\mathbf{V}^k(\mathbf{z},\mathbf{y}), T^{n_z}\mathbf{V}^k(\mathbf{z},\mathbf{y}), \mathbf{f} = \delta_3(\mathbf{z}-\mathbf{y})\mathbf{e}^k\}$. The reciprocal theorem is written as

$$u_k(\mathbf{y}) = \int_{\partial\Omega} \{\mathbf{V}^k(\mathbf{z},\mathbf{y}) \,.\, T^{n_z}\mathbf{u}(\mathbf{z}) - \mathbf{u}(\mathbf{z}) \,.\, T^{n_z}\mathbf{V}^k(\mathbf{z},\mathbf{y})\} dS_z \tag{6.24}$$

For simplicity, recalling the normal $\mathbf{n}_z$ in the traction vector at the first argument $\mathbf{z}$, we set the notations

$$T_i(\mathbf{z}) = \mathbf{e}^i \,.\, T^{n_z}\mathbf{u}(\mathbf{z})$$

$$T_{ik}(\mathbf{z},\mathbf{y}) = \mathbf{e}^i \,.\, T^{n_z}\mathbf{V}^k(\mathbf{z},\mathbf{y})$$

so that Eq. (6.24) can be re-written as

$$u_k(\mathbf{y}) = \int_{\partial\Omega} \{V_i^k(\mathbf{z},\mathbf{y})\ {}_i(\mathbf{z}) - u_i(\mathbf{z})\ {}_{ik}(\mathbf{z},\mathbf{y})\} dS_z\,, (\mathbf{y} \in \Omega^-) \tag{6.25}$$

Remark that for $\mathbf{y}$ outside $\partial\Omega$ ($\mathbf{y} \in \Omega^+$) one has

$$0 = \int_{\partial\Omega} \{V_i^k(\mathbf{z},\mathbf{y})\ {}_i(\mathbf{z}) - u_i(\mathbf{z})\ {}_{ik}(\mathbf{z},\mathbf{y})\} dS_z\,, (\mathbf{y} \in \Omega^+) \tag{6.26}$$

Now, for any $\mathbf{y}$ inside Ω^-, we can calculate the stress tensor σ_{hk} by appropriate differentiation of Eq. (6.25) and application of the moduli tensor to obtain stress components in the form

$$\sigma_{hk}(\mathbf{y}) = \int_{\partial\Omega} \{W_i^{kh}(\mathbf{z},\mathbf{y})\ {}_i(\mathbf{z}) - u_i(\mathbf{z}) Z_{ikh}(\mathbf{z},\mathbf{y})\} dS_z \tag{6.27}$$

with some kernels W and Z. If stress $T_i(\mathbf{z})$ is known on the whole surface, taking the limit of Eq. (6.24) as $\mathbf{y} \to \mathbf{x} \in \partial\Omega^-$ one obtains the boundary integral equation for the unknown $u_k(\mathbf{x})$ on $\partial\Omega$. By assuming that surface $\partial\Omega$

is regular (Lyapounov's surface) the BIE for Neumann's problem is ($T(\mathbf{z})= T^d(\mathbf{z})$)

$$\frac{1}{2}u_k(\mathbf{x}) = (pv)\int_{\partial\Omega}\{V_i^k(\mathbf{z},\mathbf{x})\ _i(\mathbf{z}) - u_i(\mathbf{z})\ _{ik}(\mathbf{z},\mathbf{x})\}\,dS_z\ (\mathbf{x}\in\partial\Omega\ ) \tag{6.28}$$

Remark that $T_{ik}(\mathbf{z}, \mathbf{y}) \neq T_{ki}(\mathbf{z}, \mathbf{y})$, so that the system of integral equations based on Eq. (6.28) is unsymmetric.

The Dirichlet boundary value problem is more difficult to solve with direct methods, because Eq. (6.25) with $\mathbf{u}(\mathbf{x})$ prescribed on the whole surface is a Fredholm integral equation of the *first kind* for the unknown $T_i(\mathbf{z})$. This is a rather ill-posed problem. It should be noted that the same Dirichlet boundary value problem, based on the indirect method (6.20) makes use of the symmetric kernel

$$B_i^k(\mathbf{x},\mathbf{y};\mathbf{n}_y) = B_k^i(\mathbf{x},\mathbf{y};\mathbf{n}_y)$$

and that Eq. (6.20) is a well-posed problem, being the Fredholm integral equation of the *second kind*.

To overcome difficulties in solving the Dirichlet problem with Eq. (6.28), one generally adds a complementary equation defined as the limit of Eq. (6.27) as $\mathbf{y} \to \mathbf{x}\in\partial\Omega^-$. A new difficulty arises in the presence of the kernel Z which involves second derivatives of the tensor V and thus divergent integrals which exist only in the Hadamard *finite-part* sense, so that direct methods based on Somigliana's representation requires regularization methods for dealing with hyper-singular integrals. The readers interested in the last subject, which is very technical, can refer to (Bonnet, 1999). Examples of finite-part integrals are given in Sect. 6.7.2.

Remarks.
Eq. (6.28) has a particular solution

$$\mathbf{w}(\mathbf{y}) = \mathbf{a} + \mathbf{b}\wedge\mathbf{y}$$

as a family of rigid body displacement field for which the stress vanishes:

$$T_i(\mathbf{z}) = \mathbf{e}^i.\,T^{n_z}\mathbf{w}(\mathbf{z}) = 0$$

$$\tfrac{1}{2}w_k(\mathbf{y}) = (pv)\int_{\partial\Omega} - w_i(\mathbf{z})\{T^{n_z}\mathbf{V}^k(\mathbf{z},\mathbf{y})\}_i\,dS_z$$

This is nothing but the homogeneous adjoint Eq. (6.17) whose solutions are the rigid body displacement fields.

6.3. A planar crack in an infinite elastic medium

This problem is the analogue of a 2D problem for a central crack of finite length in infinite plane of Chap. 3. We now derive an integral equation for the planar crack S of arbitrary shape. The surface S consists of two faces $S^{\pm}$. We denote the normal to the lower face S^- by **n**. To solve the auxiliary problem, we assume that the solution of a bounded solid subject to loadings on its surface has been solved previously by methods presented in Sect. 6.2. If the crack size is small compare with the solid size, a model of a finite crack S in an infinite elastic medium is good for applications.

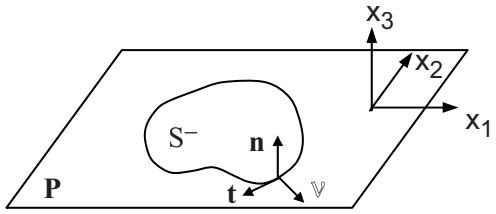

Figure 6.1: A planar crack S in an infinite elastic medium. The normal to the lower crack face is **n**. Binormal and tangent vectors to the crack front are respectively **n** and **t**. The lower face S^- is loaded by pressure $p = -T_3$ and shears T_1, T_2

6.3.1 The symmetric opening mode I

The solution is searched in the form $\mathbf{u}(\mathbf{x}) = \mathbf{S}(\mathbf{x}) + \mathbf{D}(\mathbf{x})$ which combines a single layer potential **S** and a double layer potential **D** with unknown densities $\psi = (\psi_1, \psi_2, 0)$, $\phi = (0, 0, \phi_3)$ respectively. The latter choice is suggested by the discontinuity relation

$$[[u_3]] = 2\phi_3 \tag{6.29}$$

so that density ϕ_3 is physically the crack opening displacement of the upper face under pressure $p = T_3$ on S^+ ($p = -T_3$ on S), with T_3 being the stress on plane P for the uncracked solid. The normal **n** being along $\mathbf{e}^3$, it is easy to calcultate $T^{\mathrm{n}}\mathbf{S}$. The stress vector $T^{\mathrm{n}}\mathbf{D}$ is much more difficult to calculate because it requires a regularization procedure for handling hyper-singular integrals (divergent integrals). In what follows, we shall omit the details of calculations given in (Bui, 1975, 1977) and we give only results which are quite simple (see examples of the regularization of hyper-singular integrals in Sect. 6.7.2). Conditions $\sigma_{31} = \sigma_{32} = 0$ on S^- can be written as

$$\psi_1(z_1, z_2) - \frac{2\mu^2}{\lambda + 3\mu}\frac{\partial \phi_3}{\partial z_1} = 0 \tag{6.30}$$

$$\psi_2(z_1, z_2) - \frac{2\mu^2}{\lambda + 3\mu}\frac{\partial \phi_3}{\partial z_2} = 0 \tag{6.31}$$

Therefore, the displacement field of auxiliary problem can be expressed by means of density ϕ_3

$$u_i(\mathbf{x}) = \int_S B_i^3(\mathbf{x}, \mathbf{z}, \mathbf{n}_y)\phi_3(\mathbf{z})\, dS_z + \frac{4\mu^2}{\lambda + 3\mu}\int_S V_i^\alpha \frac{\partial \phi_3}{\partial z_\alpha}\, dS_z \tag{6.32}$$

with $\mathbf{z} = (z_1, z_2, 0)$. Normal stress σ_{33} can be written as, (Bui, 1977)

$$\frac{\mu(\lambda + \mu)}{\pi(\lambda + 2\mu)}(\text{pv})\int_S \frac{\partial(1/|\mathbf{z} - \mathbf{y}|)}{\partial y_a}\frac{\partial \phi_3}{\partial z_\alpha}\phi_3(\mathbf{z})\, dS_z = T_3(\mathbf{y}) \tag{6.33}$$

This is an integral equation for determining the density ϕ_3, subject to $\phi_3(\mathbf{y}) = 0$ along the crack front $\mathbf{y} \in \partial S$. Eq. (6.33) has been derived by Kossecka (1971) in her 3D dislocations theory, and also by Weaver (1977) using a direct method based on Somigliana's fundamental tensor. The above mentionned works were given for opening mode I. Now we extend the representation $\mathbf{u}(\mathbf{x}) = \mathbf{S}(\mathbf{x}) + \mathbf{D}(\mathbf{x})$ to shear modes, where $[[u_3]] = 0$.

6.3.2 The shear modes

The shear modes are characterized by discontinuites

$$[[u_1]] = 2\phi_1(x_1, x_2) \tag{6.34}$$

$$[[u_2]] = 2\phi_2(x_1, x_2) \tag{6.35}$$

We search a solution which satisfies the additional condition $\sigma_{33} = 0$ on the crack, so that a general solution could be obtained by the superposition of opening mode I and shear modes II and III. Therefore, it is necessary to introduce a single layer potential $\mathbf{S}(\mathbf{x})$ and a double layer potential $\mathbf{D}(\mathbf{x})$ with respective densities

$$\psi = (0, 0, \psi_3) \tag{6.36}$$

and

$$\phi = (\phi_1, \phi_2, 0) \tag{6.37}$$

Expliciting the condition $\sigma_{33}(\mathbf{S} + \mathbf{D}) = 0$ on the crack, it can be shown that

$$\psi_3(z_1, z_2) + \frac{2\mu^2}{\lambda + 3\mu}\left(\frac{\partial \phi_1}{\partial z_1} + \frac{\partial \phi_1}{\partial z_1}\right) = 0 \tag{6.38}$$

Therefore, displacement fields of the auxiliary problem for shear modes can also be expressed by means of density ϕ only. Explicit shear stresses on the crack S are given by

$$\frac{\lambda\mu}{2\pi(\lambda + 2\mu)}(\mathrm{pv})\int_S \frac{\partial(1/|\mathbf{z}-\mathbf{y}|)}{\partial y_1}\left(\frac{\partial \phi_1}{\partial z_1} + \frac{\partial \phi_2}{\partial z_2}\right)dS_z +$$

$$+ \frac{\mu}{2\pi}(\mathrm{pv})\int_S \frac{\partial(1/|\mathbf{z}-\mathbf{y}|)}{\partial y_\alpha}\frac{\partial \phi_1}{\partial z_\alpha}\,dS_z = T_1(\mathbf{y}) \tag{6.39}$$

$$\frac{\lambda\mu}{2\pi(\lambda + 2\mu)}(\mathrm{pv})\int_S \frac{\partial(1/|\mathbf{z}-\mathbf{y}|)}{\partial y_2}\left(\frac{\partial \phi_1}{\partial z_1} + \frac{\partial \phi_2}{\partial z_2}\right)dS_z +$$

$$+ \frac{\mu}{2\pi}(\mathrm{pv})\int_S \frac{\partial(1/|\mathbf{z}-\mathbf{y}|)}{\partial y_\alpha}\frac{\partial \phi_2}{\partial z_\alpha}\,dS_z = T_2(\mathbf{y}) \tag{6.40}$$

It should be noted that Eqs. (6.39) and (6.40) are *coupled* while the opening mode I, Eq. (6.33), is uncoupled from the shear modes.

6.4. A planar crack in a bounded elastic medium

The problem of an equilibrium crack in a bounded solid whose external boundary S_{ext} is subject to loadings is now investigated.

We shall establish the equations for the case of a stress free crack and for mixed boundary value problems which can be used for numerical computations.

This Section investigates the nature of the stress singularities near the crack front ∂S.

Solution is searched in terms of a single layer potentials $\mathbf{S}(\mathbf{x}; \psi)$ with density $\psi = (\psi_1, \psi_2, \psi_3)$ on S, a double layer potential $\mathbf{D}(\mathbf{x}; \phi)$ with density $\phi = (\phi_1, \phi_2, \phi_3)$ on S and a double layer potential $\Delta(\mathbf{x}; \zeta)$ with density $\zeta = (\zeta_1, \zeta_2, \zeta_3)$ defined on S_{ext}.

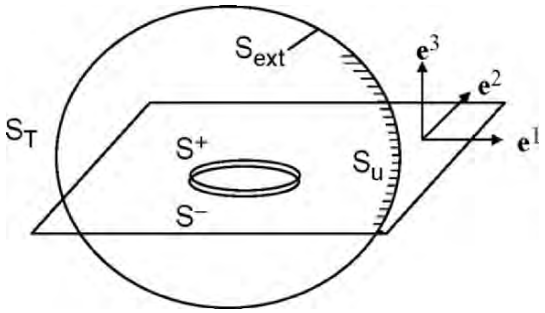

Figure 6.2: A finite planar crack S, with faces $S^{\pm}$, in a bounded elastic solid, subject to traction vector on S_T and displacement vector on S_u. A double layer potential of density is defined on the external surface S_{ext}. Single and double layer potentials are defined on the stress free crack

On the crack, densities ψ and ϕ are not independent since we assume that Eqs. (6.30), (6.31) and (6.38) still hold, so that $\phi = (\phi_1, \phi_2, \phi_3)$, are true unknowns on the crack, which are directly related to crack discontinuities. The unknowns densities $\phi = (\phi_1, \phi_2, \phi_3)$, $\zeta = (\zeta_1, \zeta_2, \zeta_3)$ will be determined by the stress free conditions on S and the boundary conditions on $S_{ext} = S_T \cup S_u$.
The double layer potential Δ is defined by the integral over S_{ext} with kernel B and density ζ

$$\Delta_i(\mathbf{x};\zeta) = \int_{S_{ext}} B_i^k(\mathbf{x}, \mathbf{z}; \mathbf{n}_z)\zeta_k(\mathbf{z})dS_z \tag{6.41}$$

The single layer potential **S** over the crack is

$$S_i(\mathbf{x};\phi) = \frac{4\mu^2}{\lambda + 3\mu}\int_S V_i^{\alpha}(\mathbf{x}, \mathbf{z})\frac{\partial\phi_3}{\partial z_\alpha}dS_z + \\ + \frac{4\mu^2}{\lambda+3\mu}\int_S V_i^3(\mathbf{x}, \mathbf{z})\{\frac{\partial\phi_1}{\partial z_1} + \frac{\partial\phi_2}{\partial z_2}\}dS_z \tag{6.42}$$

The double layer potential **D** over the crack is

$$D_i(\mathbf{x};\phi) = \int_S B_i^k(\mathbf{x}, \mathbf{z}; \mathbf{n}_z)\phi_k(\mathbf{z})dS_z \tag{6.43}$$

The stress free conditions on S are written as

$$\frac{\lambda\mu}{2\pi(\lambda + 2\mu)}(\mathrm{pv})\int_S \frac{\partial(1/|\mathbf{z}-\mathbf{y}|)}{\partial y_1}(\frac{\partial\phi_1}{\partial z_1} + \frac{\partial\phi_2}{\partial z_2})dS_z +$$

$$+\frac{\mu}{2\pi}(\mathrm{pv})\int_S \frac{\partial(1/|\mathbf{z}\quad \mathbf{y}|)}{\partial \mathrm{y}_\alpha}\frac{\partial \phi_1}{\partial \mathrm{z}_\alpha}\,dS_z + T^{\mathbf{e}1}\Delta(\mathbf{y};\zeta) = 0\,,\ (\mathbf{y}\in \mathrm{S}^-) \quad (6.44)$$

$$\frac{\lambda\mu}{2\pi(\lambda+2\mu)}(\mathrm{pv})\int_S \frac{\partial(1/|\mathbf{z}-\mathbf{y}|)}{\partial \mathrm{y}_2}\left(\frac{\partial \phi_1}{\partial \mathrm{z}_1} + \frac{\partial \phi_2}{\partial \mathrm{z}_2}\right)dS_z$$

$$+\frac{\mu}{2\pi}(\mathrm{pv})\int_S \frac{\partial(1/|\mathbf{z}-\mathbf{y}|)}{\partial \mathrm{y}_\alpha}\frac{\partial \phi_2}{\partial \mathrm{z}_\alpha}\,dS_z + T^{\mathbf{e}2}\Delta(\mathbf{y};\zeta) = 0,\quad (\mathbf{y}\in \mathrm{S}^-) \quad (6.45)$$

$$\frac{\mu(\lambda+\mu)}{\pi(\lambda+2\mu)}(\mathrm{pv})\int_S \frac{\partial(1/|\mathbf{z}-\mathbf{y}|)}{\partial \mathrm{y}_a}\frac{\partial \phi_3}{\partial \mathrm{z}_\alpha}\phi_3(\mathbf{z})\,dS_z + T^{\mathbf{e}3}\Delta(\mathbf{y};\zeta) = 0,\ (\mathbf{y}\in \mathrm{S}^-) \quad (6.46)$$

The boundary conditions on S_u are (I = 1, 2, 3)

$$-\zeta_{\mathrm{i}}(\mathbf{y}) + (\mathrm{pv})\int_{\mathrm{S_{ext}}} \mathrm{B}_{\mathrm{i}}^{\mathrm{k}}(\mathbf{y},\,\mathbf{z};\mathbf{n}_z)\zeta_{\mathrm{k}}(\mathbf{z})dS_z + S_{\mathrm{i}}(\mathbf{y};\phi)$$

$$+\,\mathrm{D}_{\mathrm{i}}(\mathbf{y};\phi) = \mathrm{u}_{\mathrm{i}}^{\mathrm{d}}(\mathbf{y}),(\mathbf{y}\in \mathrm{S_u}) \quad (6.47)$$

The boundary conditions on S_T are

$$T^{\mathrm{ny}}\left\{\mathbf{S}(\mathbf{y};\phi) + \mathbf{D}(\mathbf{y};\phi) + \Delta(\mathbf{y}\ ;\zeta)\right\} = \mathbf{T}^{\mathrm{d}}(\mathbf{y}),(\mathbf{y}\in \mathrm{S_T}) \quad (6.48)$$

Eqs. (6.44)-(6.48) are the coupled linear system of integral equations for vectorial densities ϕ on S and ζ on S_{ext}.

It is out of the scope of this chapter to derive the solution to Eqs. (6.44)-(6.48), even by a numerical method. In what follows, we'll use these equations for singularity analyses of the stress fields at points outside S, near the crack front ∂S.

6.4.1 Singularity analysis

To do so, let us disregard the terms $T^{\mathbf{e}1}\triangle^{\mathrm{k}}(\mathbf{y};\zeta)$, $T^{\mathbf{e}2}\triangle^{\mathrm{k}}(\mathbf{y};\zeta)$, $T^{\mathbf{e}3}\triangle^{\mathrm{k}}(\mathbf{y};\zeta)$ of Eqs. (6.44)-(6.46), which are regular at the crack front ∂S. We are left with the asymptotic analysis for $|\mathbf{y}-\mathbf{z}| \to 0$, $\mathbf{z}\in \mathrm{S}$, $\mathbf{y}\in \mathrm{P}$ (the crack plane) and $\mathbf{y}\notin \mathrm{S}$ of the reduced system of homogeneous Eqs. (6.33), (6.39), (6.40). These equations are identical to the ones for a planar crack in an *infinite* elastic medium. Moreover, considering the near crack front solution we as-

sume the following asymptotics at each point $\mathbf{y}_0 \in \partial S$ (the point of P *outside* the crack is denoted by $\mathbf{y}'$ and the point of P *inside* the crack by $\mathbf{y}$)

$$\sigma_{33}(\mathbf{y}') \cong \mathrm{K_I}(\mathbf{y}_0)/\sqrt{2\pi\rho(\mathbf{y}',\mathbf{y}'_0)} \tag{6.49}$$

$$\sigma_{3\nu}(\mathbf{y}') \cong \mathrm{K_{II}}(\mathbf{y}_0)/\sqrt{2\pi\rho(\mathbf{y}',\mathbf{y}'_0)} \tag{6.50}$$

$$\sigma_{3t}(\mathbf{y}') \cong \mathrm{K_{III}}(\mathbf{y}_0)/\sqrt{2\pi\rho(\mathbf{y}',\mathbf{y}'_0)} \tag{6.51}$$

where $\mathbf{n}$ (or $\mathbf{e}^3$), $\mathbb{v}$, $\mathbf{t}$ are local basis vectors at the crack front ∂S, Fig. 6.2 and $\mathrm{K_i}$ (i = I, II, III) are the stress intensity factors, $\mathbf{y}_0'$ is the projection of $\mathbf{y}'$ on the tangent Ot to the crack front at $\mathbf{y}_0$. Consider the opening mode I. Magnifying the coordinates at point $\mathbf{y}_0$, crack front becomes the straight line $x_\nu = 0$, while the crack itself S becomes the half-plane $x_\nu < 0$. The crack opening displacement ϕ_3 near the crack front can be written as

$$\phi_3(\mathbf{y}) \cong C_{\mathrm{I}}(\mathbf{y}_0)\frac{1}{\sqrt{2\pi}}\sqrt{\rho(\mathbf{y},\mathbf{y}'_0)} \tag{6.52}$$

where $\mathbf{y}_0'$ is the projection of $\mathbf{y}$ on the tangent Ot to the crack front at $\mathbf{y}_0$. The stress $\sigma_{33}(\mathbf{y}')$ at $\mathbf{y}'$ near the crack front corresponding to (6.52) is

$$\sigma_{33}(\mathbf{y}') = \frac{\mu(\lambda+\mu)}{\pi(\lambda+2\mu)}(pv)\int_{x_\nu<0}\frac{\partial(1/|\mathbf{z}-\mathbf{y}'|)}{\partial y'_\alpha}\frac{\partial\phi_3}{\partial z_\alpha}\phi_3(\mathbf{z})\,dS_z \tag{6.53}$$

This is exactly the asymptotic singular stress field outside the crack for $\rho(\mathbf{y}',\mathbf{y}_0') \to 0$.

Substituting Eq. (6.52) into (6.53) we then obtain

$$\sigma_{33}(\mathbf{y}') = \frac{\mu(\lambda+\mu)}{(\lambda+2\mu)}\mathrm{C_I}(\mathbf{y}_0)\frac{1}{\sqrt{2\pi\rho(\mathbf{y}',\mathbf{y}'_0)}} \tag{6.54}$$

Comparing Eqs.(6.54) and (6.49) we obtain

$$\mathrm{K_I}(\mathbf{y}_0) = \frac{\mu(\lambda+\mu)}{\lambda+2\mu}\mathrm{C_I}(\mathbf{y}_0) \tag{6.55}$$

Therefore the crack opening discontinuity has the asymptotics

$$[\![\mathrm{u_3}]\!] = 2\phi_3 \cong \mathrm{K_I}(\mathbf{y}_0)\frac{4(1-\nu)}{\mu}\sqrt{\frac{\rho(\mathbf{y},\mathbf{y}'_0)}{2\pi}}\ ,\ (\rho(\mathbf{y},\mathbf{y}'_0)\to 0) \tag{6.56}$$

A comparison between Eq. (6.56) and Eq. (1.53) Chap. 1 shows that it is the same formula for the *plane strain* case $\kappa = 3 - 4\nu$.

Remarks. Results (6.54)-(6.56) derived by Bui (1975) using Kupradze's potentials have been first given by Bueckner (1973) using the Boussinesq-Papkovivch potentials with the Newtonian scalar density f(**y**). Bueckner derived the normal stress as

$$\sigma_{33}(x_1,x_2) = -\frac{\mu(\lambda+\mu)}{\pi(\lambda+2\mu)}\left(\frac{\partial^2}{\partial x_1^2} + \frac{\partial^2}{\partial x_2^2}\right)\int_S f(\mathbf{y})\frac{1}{|\mathbf{y}-\mathbf{x}|}dS_y \tag{6.57}$$

and proved that f is the opening displacement u_3. In fact further analyses show that Eqs. (6.57) and (6.33) express the same normal stress. They are different forms of the *finite part* of a divergent integral which arises when the Laplacian operator $(\partial^2/\partial x_1^2 + \partial^2/\partial x_2^2)$ is wrongly interchanged with the integral operator.

We do not conclude that any regular point of the crack front is strictly in plane strain state $\varepsilon_{tt} = 0$. As a matter of fact, in a three-dimensional crack problem ε_{tt} is non singular, plane strain state is rather a particular case of the asymptotics (6.56). Exact solutions for particular cases (half plane crack, circular crack) confirm the asymptotics (6.56).

The analysis of shear modes, Eqs. (6.44), (6.45) yields similar results

$$[\![u_\nu]\!] = 2\phi_\nu \cong K_{II}(\mathbf{y}_0)\frac{4(1-\nu)}{\mu}\sqrt{\frac{\rho(\mathbf{y},\mathbf{y}_0')}{2\pi}},\ (\rho(\mathbf{y},\mathbf{y}_0') \to 0) \tag{6.58}$$

$$[\![u_t]\!] = 2\phi_t \cong K_{III}(\mathbf{y}_0)\frac{4}{\mu}\sqrt{\frac{\rho(\mathbf{y},\mathbf{y}_0')}{2\pi}} \tag{6.59}$$

6.4.2 Solutions to some crack problems

We consider some useful solutions to three-dimensional crack problems, given in (Sneddon, 1969; Kassir and Sih, 1960).

Circular crack under constant pressure

This solution has been obtained by Sneddon (1969), using Hankel's transform of elastic equilibrium equations. With the notations of Sect. 6.4, the solution for constant pressure p on a circular crack of radius a in an infinite elastic medium is

$$\phi_3(\mathbf{z}) = \frac{p(\lambda+2\mu)}{\pi\mu(\lambda+\mu)}\sqrt{a^2-|\mathbf{z}|^2}$$

It can be verified that $\phi_3(\mathbf{z})$ Eq. (6.59) satisfies Eq. (6.33) with $T_3 = -p$. The stress intensity factor is

$$K_I = 2p\sqrt{\frac{a}{\pi}} \tag{6.60}$$

Circular crack under arbitrary pressure

One assumes that normal stress can be expressed in Fourier's series as

$$T_3(r,\theta) = -p_0 \sum_{m\geq 0} k_m(r)\cos(m\theta) \tag{6.61}$$

By introducing functions $g_m(t)$ and $w_m(r)$ related to $k_m(r)$ as

$$g_m(t) = \int_0^1 k_m(tu)\frac{u^{m+1}}{\sqrt{1-u^2}}du,$$

$$w_m(r) = \frac{2}{\pi}r^m\int_0^1 g_m(t)\frac{t^{-m+1}}{\sqrt{t^2-r^2}}dt$$

Muki (1960) obtained the solution

$$\phi_3(r,\theta) = \frac{1-\nu}{\mu}p_0 a\sum_{m\geq 0} w_m(r)\cos(m\theta) \tag{6.62}$$

Using kinematic definition of SIF, Eq. (6.56), one finds the stress intensity factor along the circular crack

$$K_I(\theta) = 2p_0\sqrt{\frac{a}{\pi}}\sum_{m\geq 0} g_m(1)\cos(m\theta) \tag{6.63}$$

Circular crack under opposite concentrated loads

The unit point force load on S^+ at point $\mathbf{B} = (b, 0)$ $(b < a)$ in polar coordinates is

$T_3 = \delta(r - b)\delta(\theta)$,

with periodic Dirac distribution $\delta(\theta)$ being expanded in Fourier series as

$$\delta(\theta) = \frac{1}{2\pi} + \frac{1}{\pi}\sum_{m=1}^{\infty} \cos(m\theta)$$

Therefore functions $k_m(r)$, $g_m(t)$ are given by

$$k_0(r) = \frac{1}{2\pi ab}\,\delta(r - \frac{b}{a})$$

$$k_m(r) = \frac{1}{\pi ab}\,\delta(r \quad \frac{b}{a}),\ m = 1, 2, \ldots$$

$$g_m(t) = \frac{1}{\pi a^2 t}\,(\frac{b}{at})^m\,(1 - \frac{b^2}{a^2 t^2})^{1/2}$$

The stress intensity factor along the circle is given by

$$K_I(\theta) = 2F(\pi a)^{-3/2}(1 - \frac{b^2}{a^2})^{-1/2}\left(\frac{1}{2} + \sum_{m=1}^{\infty}\frac{b^m}{a^m}\cos(m\theta)\right) \tag{6.64}$$

It should be noted that the last terms between parenthesis can be written as

$$\frac{1}{2} + \sum_{m=1}^{\infty}\frac{b^m}{a^m}\cos(m\theta) \equiv \frac{a^2 - b^2}{a^2 + b^2 - 2ab\cos\theta)} \equiv \frac{a^2 - b^2}{\rho^2(A,B)}$$

Finally, stress intensity factor in mode I at the point A on the crack front, due to opposite unit point force at B, is given by

$$K_I(A; B) = \frac{(a^2 - b\ )^{1/2}}{\pi^{3/2}\sqrt{a}}\frac{1}{\rho^2(A,B)} \tag{6.65}$$

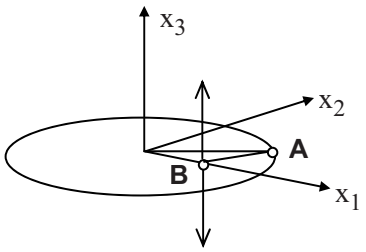

Figure 6.3: Opposite concentrated loads at B on a circular crack of radius a

Half-planar crack under opposite concentrated loads

Kassir and Sih (1960) solved this crack problem using the Papkovich-Neuber potentials.

The crack front is along Ox_2, the normal is along Ox_3.

Let us consider the mode I for deriving the stress intensity factor from the solution (6.65) of the problem of a circular crack of radius a subjected to a pair of opposite normal point forces, by taking some limiting process as the radius a goes to infinity. Let the shortest distance between the load point B and the circle be ξ. We take new coordinates for Fig. 6.3 so that B = (–ξ, 0, 0)and consider a transformed geometry of the circular crack by fixing ξ and letting $a \to \infty$. In this limiting process, the circular crack becomes a half-planar crack tangent to Ox_2, the stress intensity factor (6.65) for the load R becomes

$$\frac{(a^2 - b\ )^{1/2}}{\pi^{3/2}\sqrt{a}}\ \frac{R}{\rho^2(A,B)} \to \frac{R\sqrt{2\xi}}{\pi^{3/2}}\ \frac{1}{\xi\ \ + x_2^2(A)}$$

$$K_I(A) = \frac{R\sqrt{2\xi}}{\pi^{3/2}\xi^{3/2}}\ \frac{1}{1 + x_2^2(A)/\xi^2} \tag{6.66}$$

This formula is in agreement with Kassir and Sih's result. For shear modes II and III, the results are

$$K_{II}(A) = \frac{4P\sqrt{2}}{\pi^{3/2}\xi^{3/2}}\ \frac{\nu}{(2-\nu)}\ \frac{x_2(A)/\xi}{\{1 + x_2^2(A)/\xi^2\}^2}$$

$$+ \frac{Q\sqrt{2}}{\pi^{3/2}\xi^{1/2}}\ \frac{1}{\{1 + (x_2^2(A)/\xi^2\}}\left(1 + \frac{2\nu}{2-\nu}\ \frac{(1\ \ x_2^2(A)/\xi^2)}{(1 + x_2^2(A)/\xi^2)}\right) \tag{6.67}$$

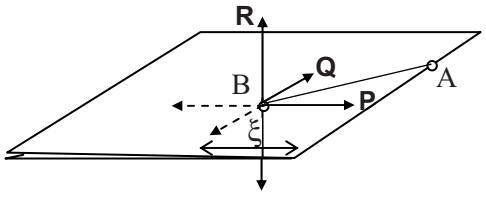

Figure 6.4: Point force load on a half planar crack (Kassir and Sih, 1960)

$$K_{III}(A)=\frac{P\sqrt{2}}{\pi^{3/2}\xi^{3/2}}\frac{1}{(1+x_2^2(A)/\xi^2)}\left(1-\frac{2\nu}{2-\nu}\frac{(1-x_2^2(A)/\xi^2)}{(1+x_2^2(A)/\xi^2)}\right)+$$

$$-\frac{4Q\sqrt{2}}{\pi^{3/2}\xi^{3/2}}\frac{\nu}{(2-\nu)}\frac{x_2(A)/\xi}{\{1+(x_2^2(A)/\xi^2\}^2} \qquad (6.67)$$

6.5. The angular crack in an infinite elastic medium

The planar crack geometry S is defined by points $M(\rho, \theta, x_3= 0)$ in cylindrical coordinates, $0 < \rho < \infty$, $-\gamma < \theta < +\gamma$, $x_3 = 0$. The vertex $\rho = 0$ is a singular point of the crack front. We focus on the nature of the singularity near the vertex $\rho = 0$. The stress singularity at regular points A of the line crack front $\theta = \pm\gamma$ is already known, that is, for instance in mode I, the stress or the displacement ϕ_3 are characterized by the stress intensity factor $K_I(s)$, where $s = |OA|$. Intuitively when A approaches the vertex, function $K_I(s)$ is expected to vanish or to go to infinity according to whether the angle 2γ is acute ($\gamma < \pi/2$) or obtuse ($\pi/2 < \gamma$)..This is because of observations of fatigue crack propagation, which show that acute vertex crack point does not propagate while obtuse vertex point has a rapid crack propagation.

Mathematically, the crack opening near the vertex has the asymptotics $\phi_3(r, ..\theta) \cong \rho^{\alpha}..\theta.$, in polar coordinates.

To determine the eigenvalues α and the eigenfunctions $g(\theta)$, avoiding the complexity of the eigenvalue problems by classical approaches in three dimensions, we consider the homogeneous integral Eq. (6.33) of the crack

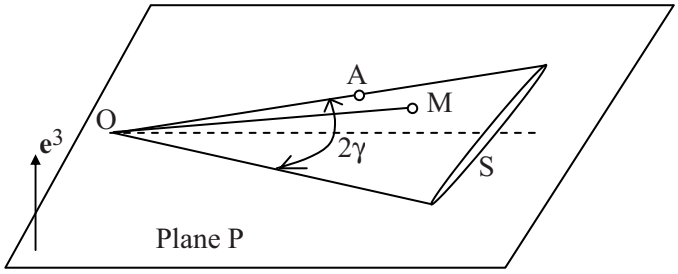

Figure. 6.5: The angular crack with acute vertex ($2\gamma < \pi$) or obtuse vertex ($\pi < 2\gamma$). The crack opening has the asymptotics $\phi_3(...\theta) \cong \rho^{\alpha}g.\theta.$ near the vertex O

opening displacement in mode I

$$(\mathrm{pv})\int_S \frac{\partial(1/|\mathbf{z}-\mathbf{y}|)}{\partial y_\alpha}\frac{\partial \phi_3(\mathbf{z})}{\partial z_\alpha}\, dS_z = 0 \tag{6.68}$$

It can be shown that the above equation can be written in the following form

$$-\phi_3(\mathbf{y})\int_{P\setminus S}\frac{1}{|\mathbf{z}-\mathbf{y}|^3}dS_z + (\mathrm{pv})\int_S \frac{\phi_3(\mathbf{z})-\phi_3(\mathbf{y})}{|\mathbf{z}-\mathbf{y}|^3}dS_z = 0 \tag{6.69}$$

Inserting $\phi_3(..\theta) \cong \rho^\alpha..\theta.$ in Eq. (6.69) we obtain

$$g(\theta)\frac{2\sin\gamma}{\cos\theta-\cos\gamma}$$

$$-(\mathrm{pv})\int_S \frac{\{x^\alpha g(u)-g(\theta)\}\,x\,dx\,du}{[(x\cos u-\cos\theta)^2+(x\sin u-\sin\theta)^2]^{3/2}} = 0 \tag{6.70}$$

It can be verified that eigenfunction $g(\theta)$ is explicitly given by

$$g(\theta) = (\cos\theta - \cos\gamma)^{1/2} \tag{6.71}$$

It should be noted that for $\gamma = \pi/2$, Eq. (6.71) agrees with the well known eigenfunction $g(\theta) = \cos\theta$ for a straight crack front. We remark that the inverse of $g(\theta)$ is the angular function $(\cos\theta - \cos\gamma)^{-1/2}$ which appears in the

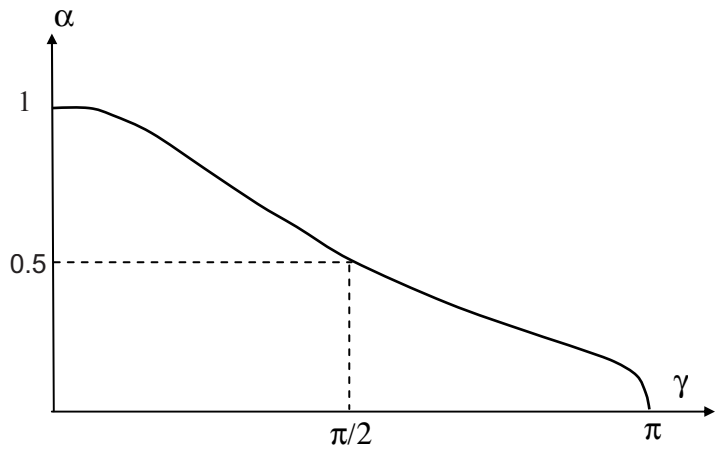

Figure 6.6: Eigenvalue α is a function of the angle γ. Value $\alpha = 0.5$ for $\gamma = \pi$

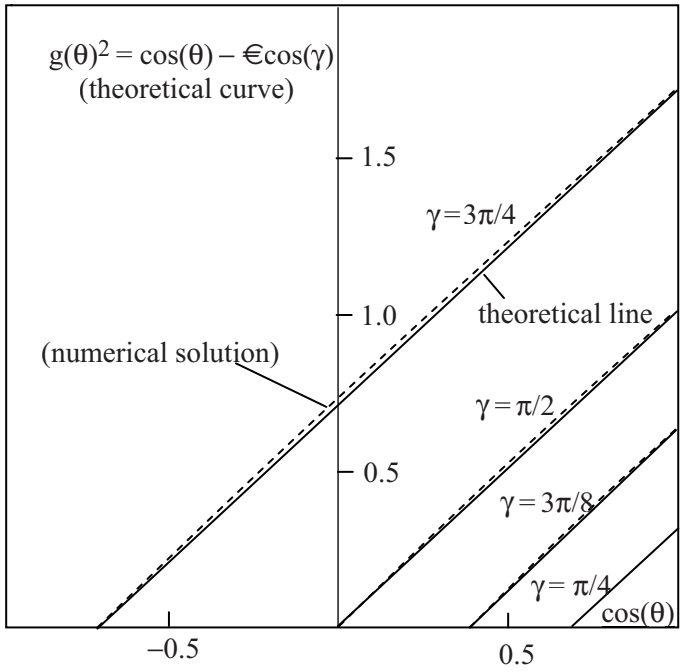

Figure 6.7: Analytical eigenfunction $g^2(\theta)$ versus $\cos(\theta)$ for different angles γ Numerical solutions of equation (6.70) are plotted in dotted lines

solution of a flat angular punch, of angle 2γ, on an elastic half plane, given by Rvatchev (1959), Solomon and Zamfirescu (1968). The eigenvalue α is then determined numerically as a function of γ. Fig. 6.6 shows that $1/2 < \alpha$ for $\gamma < \pi/2$ and $\alpha < 1/2$ for $\pi/2 < \gamma$. Since the normal stress outside the crack behaves like $\sigma \cong \rho^{\alpha(\gamma)-1}(\cos\theta - \cos\gamma)^{-1/2}$ the stress intensity factor $K_I(s)$ for $s \to 0$, as expected, is equal to either zero or infinity according to whether the angle 2γ is either acute ($\alpha > 1/2$) or obtuse ($\alpha < 1/2$).

6.6. The edge crack in an elastic half-space

The problem of an orthogonal edge crack at the free surface of an elastic half-space is now discussed. This problem has been worked out by many authors, for instance Benthem (1976), Bazant and Estenssoro (1979). Benthem (1976) considered the case of a crack front edge which ends orthogonally at the free surface $x_2 = 0$. The crack S is on the plane $x_2 = 0$. Bazant and Estenssoro (1979) considered the more general case of inclined

crack front edge (with the angle γ) and inclined crack plane. Displacement near the terminal point is searched in the form $u_i = \rho^{\lambda} f_i(\theta,\varphi)$ with spherical coordinates and the pole at the terminal point. The above mentionned works make use of standard procedure for determining eigenvalues λ of interest for applications and eigen-functions from linear elastic equilibrium equations. It turns out that for orthogonal crack, the eigenvalue λ in the range 0.5-0.6 depends on Poisson's ratio. For instance, with $\nu = 0.3$, Benthem's numerical solution is $\lambda = 0.5477$. Thus, defining $r = \rho\sin\varphi$ as the distance to the crack front ($\varphi = 0$) and $s = \rho\cos\varphi$ as the distance to the free surface ($\varphi = \pi/2$), one gets the stress intensity factor in mode I as

$$K_I(s) \cong s^{0.5477-0.5} = O(s^{0.0477}).$$

A power function with so small an exponent rapidly decreases to zero as the distance to the free surface s tends to zero.

This phenomenon is called a boundary *layer effect* and explains why the plane stress solution, discussed in Chap. 3, cannot be an exact solution of crack problem for thin plate, but is rather an approximate one, with K_I being some average $\langle K_I(s) \rangle$ through the thickness.

Bazant and Estenssoro (1979) did not consider orthogonal crack front. They introduced rather an angle γ between the crack front and the crack lips and obtained the value $\gamma = 101°$, for $\nu = 0.3$, for which $K_I(s = 0)$ is finite. Observations in fatigue crack of metals show slightly higher angles, Figs. 6.8 and 6.9.

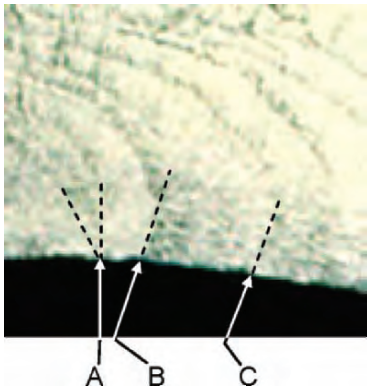

Figure 6.8: A view of fatigue arrest marks on steel, showing the fixed terminal point (A) for inclined crack fronts with angle $\gamma \leq 90°$ and moving terminal points (B) with angle $\gamma \cong 102°$ and (C) with nearly the same angle $\gamma \cong 100°$ indicated by arrows (Courtesy of René Labbens)

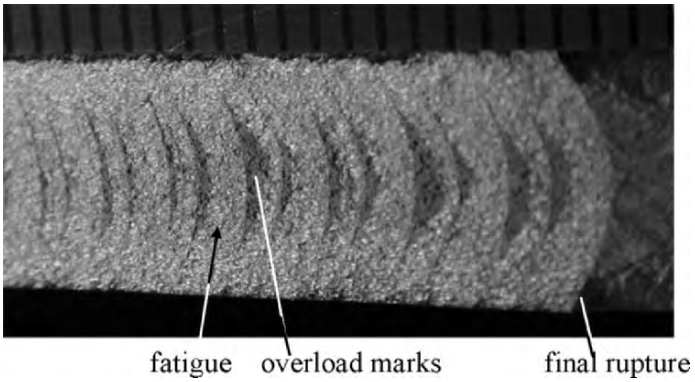

Figure 6.9: Three-dimensional nature of fatigue crack propagation in aluminium (in light); brittle propagation by overloads with different amplitudes (in dark); the last overload results in the final brittle fracture (Courtesy of Louis Anquez and Marta Dragon-Louiset, Dassault-Aviation)

.

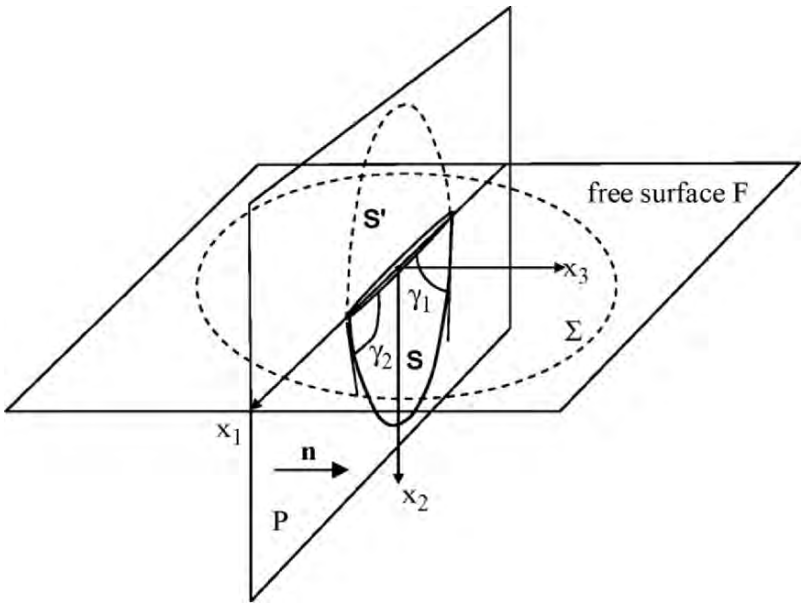

Figure 6.10: A edge crack S in a half-space, with the crack front terminating at angles γ_1, γ_2 at the free surface. The union of S and its mirror image S' are considered as a unique crack SS' in an infinite elastic body. An orthogonal stress free crack Σ in infinite body can be considered as the stress free surface of an infinite half space when its size is very large. The system of cracks in an infinite medium SS' and Σ can be analyzed by the coupled boundary integral equations

show higher angles, Fig. 6.9. Now we show how Bazant and Estenssoro's problem of an orthogonal edge crack can be re-formulated by boundary integral equations defined on *bounded* surfaces. We do not remake Bazant and Estenssoro's analysis based on an eigenvalue problem for an unbounded edge crack.

The main aim of this sub-section is to propose an integral equations method to solve the auxiliary problem of an (finite) edge crack S of arbitrary shape which is orthogonal to the free surface F and subjected to opposite stress vectors on $S^{\pm}$.

The representation of the solution by means of single and double layer potentials is not unique. Therefore we can consider an infinite elastic body with a system of two orthogonal cracks, on the one hand, a surface crack Σ lying on the plane F, on the other hand, an edge crack S together with its mirror crack S' lying on the orthogonal plane P. Two crossed cracks in an infinite elastic body are able to model an edge crack at a stress free surface when Σ is very large. The angles of the edge crack fronts at terminal points can be different γ_1, γ_2.

Single layer and double layer potentials on $S \cup S'$

The solution is searched in the form $\mathbf{u}(\mathbf{x})^{(1)} + \mathbf{u}(\mathbf{x})^{(2)}$, with subscript (1) for the contribution from S and S', and (2) from Σ. The first contribution is $\mathbf{u}(\mathbf{x})^{(1)} = \mathbf{S}(\mathbf{x}) + \mathbf{D}(\mathbf{x})$ which combines a single layer potential **S** and a double layer potential **D** with unknown densities $\psi = (\psi_1, \psi_2, 0)$, $\phi = (0, 0, \phi_3)$ respectively

$$S_i(\mathbf{x}) = 2 \int_{S \cup S'} {}^{k}_{i}(\mathbf{x}, \mathbf{z}) \psi_k(\mathbf{z}) dS_z \tag{6.72}$$

$$D_i(\mathbf{x}) = \int_{S \cup S'} B_i^k(\mathbf{x}, \mathbf{z}; \mathbf{n}_z) \phi_k(\mathbf{z}) dS_z \tag{6.73}$$

where densities ψ and ϕ are related by

$$\psi(z_1, z_2) \; - \frac{2\mu^2}{\lambda + 3\mu} \operatorname{grad}\phi_3(z_1, z_2) = 0 \tag{6.74}$$

Single layer and double layer potentials on Σ

The second contribution is due to Σ , $\mathbf{u}(\mathbf{x})^{(2)} = \Gamma(\mathbf{x}) + \Delta(\mathbf{x})$ which combines a single layer potential Γ and a double layer potential Δ with unknown densities $\alpha = (\alpha_1, 0, \alpha_3)$, $\beta = (0, \beta_2, 0)$ respectively

$$\Gamma_i(\mathbf{x}) = 2\int_\Sigma {}^{k}_{i}(\mathbf{x},\ \mathbf{y})\alpha_k(\mathbf{y})dS_y \tag{6.75}$$

$$\Delta_i(\mathbf{x}) = \int_\Sigma B_i^k(\mathbf{x},\mathbf{y};\mathbf{n}_y)\beta_k(\mathbf{y})dS_y \tag{6.76}$$

where densities α and β are related by

$$\alpha(y_1, y_2) \qquad \frac{2\mu^2}{\lambda+3\mu}\,\mathrm{grad}\beta_2(y_1, y_2) = 0 \tag{6.77}$$

Coupled integral equations

We combine different potentials to obtain the displacement field of the edge crack

$$\mathbf{u}(\mathbf{x}) = \mathbf{S}(\mathbf{x}) + \mathbf{D}(\mathbf{x}) + \Gamma(\mathbf{x}) + \Delta(\mathbf{x})$$

Displacement $\mathbf{u}(\mathbf{x})$ is completely determined by the unknown discontinuities

$[[u_3]] = 2\phi_3$ on $S\cup S'$

$[[u_2]] = 2\beta_2$ on Σ

To determine these unknowns, calculating the normal stresses T_3 on $S\cup S'$ and T_2 on Σ we then obtain the coupled integral equations

$$\mathbf{e}^3 \cdot T^{n_t}(\Delta+\Gamma) + \frac{\mu(\lambda+\mu)}{\pi(\lambda+2\mu)}(\mathrm{pv})\int_{S\cup S'}\frac{\partial}{\partial n_\alpha}\left(\frac{1}{|\mathbf{t}-\mathbf{z}|}\right)\frac{\partial\phi_3}{\partial z_\alpha}dS_z = T_3^d(\mathbf{t}) \tag{6.78}$$

$(\mathbf{t}\in S\cup S',\ \mathbf{t}\notin\Sigma)$

$$\frac{\mu(\lambda+\mu)}{\pi(\lambda+2\mu)}(\mathrm{pv})\int_\Sigma\frac{\partial}{\partial n_\alpha}\left(\frac{1}{|\mathbf{p}-\mathbf{z}|}\right)\frac{\partial\phi_3}{\partial z_\alpha}dS_z + \mathbf{e}^2\cdot T^{n_p}(\mathbf{S}+\mathbf{D}) = 0 \tag{6.79}$$

$(\mathbf{p}\in\Sigma,\ \mathbf{p}\notin S\cup S')$

It should be noted that, unlike 3D finite elements methods, where the vector field of displacement is to be determined in unbounded 3D space, the method proposed in Eqs. (6.78)-(6.79) is based on two scalar unknowns ϕ_3 and β_2 defined on bounded surfaces respectively SS' et Σ.

6.7. On some mathematical methods for BIE in 3D

For applications to scatterng of elastic waves in the frequency domain, let us remind some results of B.I.E methods, particularly indirect formulations analogous to the ones discussed in previous sections, for a regular domain not containing cracks.
A crack may be rather considered as a flat cavity with small thickness whose surface is smooth enough so that a normal vector is assumed to exist at each point.

6.7.1 The Kupradze elastic potential theory

The elastic potentials are those considered in Kupradze (1963), with kernels $\mathbf{V}^{(\omega)k}(\mathbf{x}, \mathbf{y})$ and $T^{\mathbf{n}_x}\mathbf{V}^{(\omega)k}(\mathbf{x}, \mathbf{y})$, where $\mathbf{V}^{(\omega)}$ is the fundamental Stokes tensor, which satisfies

$$L + \rho\omega^2)\mathbf{V}^{(\omega)k}(\mathbf{x}, \mathbf{y}) + \mathbf{e}^k\delta(\mathbf{x} - \mathbf{y}) = \mathbf{0}, \quad \mathbf{x} \in \mathbb{R}^3 \tag{6.80}$$

Components $\mathbf{V}^{(\omega)k}$ are

$$V_i^{(\omega)k}(\mathbf{x}, \mathbf{y}) = \frac{1}{4\pi\mu}\left\{\delta_{ik}H(k_2 r) + \frac{1}{k_2^2}\frac{\partial}{\partial y_i}\frac{\partial}{\partial y_k}\{H(k_2 r) - H(k_1 r)\}\right\} \tag{6.81}$$

with $k_1 = \sqrt{\rho\omega^2/(\lambda + 2\mu)}$, $k_2 = \sqrt{\rho\omega^2/\mu}$, $H(kr)(1/r)\exp(ikr)$.

The bounded solid Ω is denoted here by Ω_i (instead of Ω) and its complementary domain is Ω_e, the boundaries are denoted respectively by S_i and S_e (interior boundary of Ω_e). Consider first two fields **u** and **v** satisfying the time harmonic equations

$(L + \rho\omega^2)\mathbf{u} + \mathbf{g} = \mathbf{0}$ in Ω_i (or Ω_e)

$(L + \rho\omega^2)\mathbf{v} + \mathbf{f} = \mathbf{0}$ in Ω_i (or Ω_e)

Betti's reciprocal formulae hold for interior problems

$$\int_{\Omega_i}(\mathbf{u}.\mathbf{f} - \mathbf{v}.\mathbf{g})d\Omega + \int_{S_i}\{\mathbf{u}.T^n(\mathbf{v}) - \mathbf{v}.T^n(\mathbf{u})\}dS = \mathbf{0}$$

as well as for exterior problems (normal vectors on the cavity S_e and on S_i are opposite)

$$\int_{\Omega_i} (\mathbf{u}.\mathbf{f} - \mathbf{v}.\mathbf{g}) d\Omega + \int_{S_e} \{\mathbf{u}.T^n(\mathbf{v}) - \mathbf{v}.T^n(\mathbf{u})\} dS = \mathbf{0}$$

with the condition that the second integral over the sphere at infinity vanishes. Such conditions are satisfied by the *radiation* conditions

$$T^y \mathbf{u}^p - i\rho \; c_p \mathbf{u}^p = O(1/|\mathbf{y}|)$$

$$T^y \mathbf{u}^s - i\rho\omega c_s \mathbf{u}^s = O(1/|\mathbf{y}|)$$

for dilatational waves $\mathbf{u}^p$ and shear waves $\mathbf{u}^s$

$$\mathbf{u} = \mathbf{u}^p + \mathbf{u}^s$$

$$(1/k_1^2)\text{grad div } \mathbf{u}^p + \mathbf{u}^p = 0, \quad \text{rot } \mathbf{u}^p = 0,$$

$$(1/k_1^2)\text{grad div } \mathbf{u}^s + \mathbf{u}^s = 0, \quad \text{div } \mathbf{u}^s = 0$$

One introduces the single layer potential $\mathbf{S}^{(\omega)}(\mathbf{x})$ and the double layer potential $\mathbf{W}^{(\omega)}(\mathbf{x})$

$$\mathbf{S}^{(\omega)}(\mathbf{x}) = 2\int \mathbf{V}^{(\omega)}(\mathbf{y}, \mathbf{x}).\Phi(\mathbf{y}) dS_y, \quad \mathbf{x} \text{ in } \Omega_i \text{ (or } \Omega_e) \tag{6.82}$$

$$\mathbf{W}^{(\omega)}(\mathbf{x}) = 2\int [T^{n_y}\mathbf{V}(\mathbf{y}, \mathbf{x})]^\tau.\Psi(\mathbf{y}) dS_y \quad \mathbf{x} \text{ in } \Omega_i \text{ (or } \Omega_e) \tag{6.83}$$

These vectors satisfy the homogeneous equation

$$(L + \rho\omega^2)\mathbf{u} = \mathbf{0} \qquad \text{in } \Omega_i \text{ or } \Omega_e.$$

Neumann problems

For prescribed traction vectors $\mathbf{t}^d$ on S_i or S_e, the Neumann problems are

- Interior problem N_i:

$$+\Phi(\mathbf{y}) + 2(\text{pv})\int_{\partial\Omega} \Phi(\mathbf{z}).T^{n_y}\mathbf{V}^{(\omega)}(\mathbf{y}, \mathbf{z}) dS_z = \mathbf{t}^d(\mathbf{y}), \; \mathbf{y} \text{ in } S_i \tag{6.84}$$

• Exterior problem N_e:

$$-\Phi(\mathbf{y}) + 2(\text{pv}) \int_{\partial\Omega} \Phi(\mathbf{z}).T^{n_y}\mathbf{V}^{(\omega)}(\mathbf{y},\mathbf{z})dS_z = \mathbf{t}^d(\mathbf{y}),\ \mathbf{y} \text{ in } S_e \tag{6.85}$$

Dirichlet problems

For prescribed displacement $\mathbf{u}^d$ on S_i or S_e, the Dirichlet problems are

• Interior problem D_i:

$$-\Psi(\mathbf{y}) + 2(\text{pv}) \int_{S_i} [T^{n_z}\mathbf{V}^{(\omega)}(\mathbf{z},\mathbf{y})]^{\tau}.\Psi(\mathbf{z})dS_z = \mathbf{u}^d(\mathbf{y}),\ \mathbf{y} \text{ in } S_i \tag{6.86}$$

• Exterior problem D_e:

$$+\Psi(\mathbf{y}) + 2(\text{pv}) \int_{\partial\Omega} T^{n_z}\mathbf{V}^{(\omega)}(\mathbf{z},\mathbf{y}).\Psi(\mathbf{z})dS_z = \mathbf{u}^a(\mathbf{y}),\ \mathbf{y} \text{ in } S_e \tag{6.87}$$

Interior and exterior problems are adjoint problems. More precisely, on the one hand, problems (N_e) and (D_i) are adjoint systems of equations, on the other hand, problems (N_i) and (D_e) are adjoint systems of equations, with kernel $K(\mathbf{y}, \mathbf{z})$ and its transposed one $[K(\mathbf{z}, \mathbf{y})]^{\tau}$, with the interchange of variables $\mathbf{z}$, $\mathbf{y}$.

According to Kupradze's works, these equations can be studied by Fredholm's theory of integral equations of the second kind which is applicable to singular integral equations (6.84)-(6.87). If ω is not the eigenfrequency of the homogeneous equation (D_i) then a unique solution to Eq. (6.85) of problem (N_e) exists. To solve the case where ω is one eigenfrequency of the homogeneous equation (D_i), avoiding the difficulties arising in *spurious* frequencies in numerical solutions, some authors make use of a combinaison of single and double layer potentials, (Ha-Duong, 1979).

6.7.2 On the regularization of hypersingular integrals

Stress calculations of the double layer potentials $\mathbf{D}$, $\mathbb{A}$, $\mathbf{W}^{(\omega)}$ for field points $\mathbf{x} \in \Omega$, tending to a surface point $\mathbf{x} \to \mathbf{y} \in \partial\Omega$ involve hyper-singular integrals, or divergent integrals, when differentiations are wrongly made *inside* the integral symbol. To make sense to such illegal operations, Hadamard introduced the notion of *finite-part* of divergent integral.

Consider an integral $I(\mathbf{x})$ on the plane P, which exists in the principal value sense, that is $I(\mathbf{x}) = \lim_{\varepsilon \to 0} \int_{P \setminus C(x,\varepsilon)} f(\mathbf{x}, \mathbf{y})dS_y := \text{v.p.} \int_P f(\mathbf{x}, \mathbf{y})dS_y$.

The notation (pv) is somewhat ambiguous since it does not indicate explicitly the dependency of the symbol integral upon two hidden variables, **x** and ε appearing in the circular zone C(**x**, ε) with vanishing radius ε centred at **x** to be removed from P. Since I(**x**) is a pv-integral, the function f(**x**, **y**) has at least the singularity O(1/|**y** – **x**|^2) because otherwise a singularity O(1/|**y** – **x**|^m), m < 2, should be integrable in the plane P.

Hadamard's finite-part of divergent integrals

Considering the above mentioned (pv)-integral I(**x**), we may calculate its partial derivative ∂I(**x**)/∂x$_k$ as the integral

$$(\partial / \partial x_k) \int_{P \setminus C(x,\varepsilon)} f(\mathbf{x}, \mathbf{y}) dS \tag{6.88}$$

not as the integral

$$J_k(x) := \int_{P \setminus C(x,\varepsilon)} \frac{\partial}{\partial x_k} f(\mathbf{x}, \mathbf{y}) dS_y \tag{6.89}$$

which is divergent as ε → 0. More precisely $J_k(x)$ diverges as some power of 1/ε, for instance J$_k$(x) → C/ε^n. According to Hadamard's definition, the singular part (sp) of the divergent integral is (sp)J$_k$(x) = C/ε^n and its finite part is (fp)J$_k$(x): = J$_k$(x) – C/ε^n. In the literature the finite-part of a divergent integral is denoted by

$$(\mathrm{fp}) \int_P \frac{\partial}{\partial x_k} f(\mathbf{x}, \mathbf{y}) dS_y \quad \text{or} = \int_P \frac{\partial}{\partial x_k} f(\mathbf{x}, \mathbf{y}) dS_y$$

Converted differentiation of a pv-integral

Considering again the above mentioned (pv)-integral I(**x**), we can calculate its partial derivative ∂I(**x**)/∂x$_k$ as the convected differentiation of an integral over a changing domain P\C(**x**, ε) since x$_k$ is changing in the differentiation. Thus we may write for fixed ε

$$\frac{\partial}{\partial x_k} \int_{P \setminus C(x,\varepsilon)} f(\mathbf{x}, \mathbf{y}) dS_y = \int_{P \setminus C(x,\varepsilon)} \frac{\partial}{\partial x_k} f(\mathbf{x}, \mathbf{y}) dS_y - \int_{|y-x|=\varepsilon} f(\mathbf{x}, \mathbf{y}) n_k ds_y \tag{6.90}$$

with n$_k$ = (y$_k$ – x$_k$)/|**y** – **x**| being the outward normal to C. For a function f singular as O(1/|**y** – **x**|^2) the second term in the right hand side of (6.90) is singular as 0(1/ε) as ε → 0 so that we recover the divergent integral *minus*

its singular part defined by the integral over the circle $|\mathbf{y}-\mathbf{x}|=\varepsilon$, exactly as in Hadamard's definition.

Let us illustrate the concept of finite part integral by considering Bueckner's integral where f(y) is extended to the whole plane P by letting $f \equiv 0$ outside the crack S

$$B(\mathbf{x}) = \left(\frac{\partial^2}{\partial x_1^2} + \frac{\partial^2}{\partial x_2^2}\right) \int_P f(\mathbf{y}) \frac{1}{|\mathbf{y}-\mathbf{x}|} dS_y .$$

The first partial derivative of the Newtonian potential exists in the pv-sense as

$$I_k(\mathbf{x}) = \frac{\partial}{\partial x_k} \int_P f(\mathbf{y}) \frac{1}{|\mathbf{y}-\mathbf{x}|} dS_y = (pv) \int_P \frac{\partial}{\partial x_k} f(\mathbf{y}) \frac{1}{|\mathbf{y}-\mathbf{x}|} dS_y$$

The second derivative of $I_k(\mathbf{x})$ is

$$\frac{\partial}{\partial x_k} \frac{\partial}{\partial x_k} \int_P f(\mathbf{y}) \frac{1}{|\mathbf{y}-\mathbf{x}|} dS_y = \frac{\partial}{\partial x_k} (pv) \int_P \frac{\partial}{\partial x_k} f(\mathbf{y}) \frac{1}{|\mathbf{y}-\mathbf{x}|} dS_y \tag{6.91}$$

The integral (with summation on k)

$$\int_{P \setminus C(x,\varepsilon)} \frac{\partial}{\partial x_k} \frac{\partial}{\partial x_k} f(\mathbf{y}) \frac{1}{|\mathbf{y}-\mathbf{x}|} dS_y = \int_{P \setminus C(x,\varepsilon)} f(\mathbf{y}) \frac{1}{|\mathbf{y}-\mathbf{x}|^3} dS_y$$

diverges as $2\pi f(\mathbf{x})/\varepsilon$. Thus the fp-integral (6.91) is equal to

$$(fp) \int_{P \setminus C(x,\varepsilon)} \frac{\partial}{\partial x_k} \frac{\partial}{\partial x_k} f(\mathbf{y}) \frac{1}{|\mathbf{y}-\mathbf{x}|} dS_y \coloneqq \int_{P \setminus C(x,\varepsilon)} f(\mathbf{y}) \frac{1}{|\mathbf{y}-\mathbf{x}|^3} dS_y - f(\mathbf{x}) \frac{2\pi}{\varepsilon} \tag{6.92}$$

Noticing that

$$f(\mathbf{x}) \frac{2\pi}{\varepsilon} = \int_{P \setminus C(x,\varepsilon)} f(\mathbf{x}) \frac{1}{|\mathbf{y}-\mathbf{x}|^3} dS_y$$

we may write Eq. (6.92) as

$$(fp) \int_{P \setminus C(x,\varepsilon)} \frac{\partial}{\partial x_k} \frac{\partial}{\partial x_k} f(\mathbf{y}) \frac{1}{|\mathbf{y}-\mathbf{x}|} dS_y = \int_{P \setminus C(x,\varepsilon)} \{f(\mathbf{y}) \quad f(\mathbf{x})\} \frac{1}{|\mathbf{y}-\mathbf{x}|^3} dS_y \tag{6.93}$$

The right hand side of (6.93) is called a *first order* regularization of the divergent integral, given by Bui (1975). A *second order* regularization

proposed by Leblond (1986), and Guiggiani et al (1992) should be interesting for numerical computations.

It is given by the ordinary integral

$$(\mathrm{fp})\int_{\mathrm{P}\setminus\mathrm{C}(\mathrm{x},\varepsilon)} \frac{\partial}{\partial \mathrm{x}_\mathrm{k}} \frac{\partial}{\partial \mathrm{x}_\mathrm{k}} \mathrm{f}(\mathbf{y}) \frac{1}{|\mathbf{y}-\mathbf{x}|} dS_\mathrm{y} =$$

$$= \int_{\mathrm{P}\setminus\mathrm{C}(\mathrm{x},\varepsilon)} \{\mathrm{f}(\mathbf{y}) - f(\mathbf{x}) - (\mathrm{y}_\mathrm{k} - \mathrm{x}_\mathrm{k}) \frac{\partial \mathrm{f}(\mathbf{x})}{\partial \mathrm{x}_\mathrm{k}}\} \frac{1}{|\mathbf{y}-\mathbf{x}|^3} dS_y \qquad (6.94)$$

where the zero-valued term

$$-\int_{\mathrm{P}\setminus\mathrm{C}(\mathrm{x},\varepsilon)} (\mathrm{y}_\mathrm{k} - \mathrm{x}_\mathrm{k}) \frac{\partial \mathrm{f}(\mathbf{x})}{\partial \mathrm{x}_\mathrm{k}} \frac{1}{|\mathbf{y}-\mathbf{x}|^3} dS_y = 0.$$

has been added to (6.93). Finally, an integration by parts of the right hand side of (6.93) yields the formula, see Eq. (6.33)

$$(\mathrm{fp})\int_{P\setminus C(x,\varepsilon)} \frac{\partial}{\partial \mathrm{x}_\mathrm{k}} \frac{\partial}{\partial \mathrm{x}_\mathrm{k}} \mathrm{f}(\mathbf{y}) \frac{1}{|\mathbf{y}-\mathbf{x}|} dS_\mathrm{y} = (\mathrm{pv})\int_{P\setminus C(x,\varepsilon)} \frac{\partial}{\partial \mathrm{y}_\alpha} \mathrm{f}(\mathbf{y}) \frac{\partial}{\partial \mathrm{y}_\alpha} \frac{1}{|\mathbf{y}-\mathbf{x}|} dS_y$$

6.7.3 Other regularization methods

There are regularization methods which are based on a completely different approach to solve the equilibrium equations of elasticity. So far, elastic potentials approaches to BIE have been considered with unsymmetric system of equations. We mention now two approaches dealing with regular kernels and symmetric system of equations. The first one is the variational method proposed by Nedelec (1982) who proposed to lower the strength of the singularity by a double integration. Nedelec's method will be presented in the more general case of frictional contact in fracture mechanics. The second method is based on conjugate functions in the sense of Tonti's diagram in elasticity, as proposed by Bui (1992), which provides a posteriori *error estimate*. In contrast with classical BIE methods, both approaches yield regular and symmetric kernels.

Frictionless contact problems in fracture mechanics

Consider a crack S inside a bounded solid Ω, with external boundary S_{ext} and internal boundaries $S^{\pm}$.

To describe a crack discontinuity, it is thus convenient to introduce the double layer potential

$$\mathbf{u}(\mathbf{x}) = 2\int_{\partial\Omega} [T^{n_y} \mathbf{V}(\mathbf{y}, \mathbf{x})]^{\mathrm{T}} . \Psi(\mathbf{y}) dS_y \qquad \mathbf{x} \text{ in } \Omega \tag{6.95}$$

with vectorial density $\Psi(\mathbf{y})$ defined over $\partial\Omega \equiv S \cup S_{ext}$. The density on S is the crack discontinuity $[[\mathbf{u}]]$ which may be constrained by the contact condition $[[u_n]] \geq 0$. As in previous crack problems, we consider the auxiliary problem in which only opposite traction vectors $\pm\mathbf{t}^d$ are prescribed on $S^{\pm}$ (no traction on S_{ext}). In the absence of contact constraints, the variational formulation to crack problems has been given by Nedelec (1982). Let the symmetric bilinear form $a(\Psi, \Phi)$ and the linear form $b(\Psi)$ be defined as

$$a(\Psi, \Phi) = \int_S \sigma(\mathbf{u}(\Psi)) : \varepsilon(\mathbf{v}(\Phi)) dS \tag{6.96}$$

$$b(\Phi) = \int_S \mathbf{t}^d(\mathbf{y}) . \Phi(\mathbf{y}) dS_y \tag{6.97}$$

where $\mathbf{v}(\Phi)$ is the displacement field defined by the double layer potential with density Φ. The symmetric and positive definite form $a(.,.)$ is given by

$$a(\Psi, \Phi) = \int_S \int_S [\mathbf{n}(\mathbf{x}), \nabla_x \Psi_i, \mathbf{e}^r] \, G^{ik}_{rs}(\mathbf{x}, \mathbf{y}) \, [\mathbf{n}(\mathbf{y}), \nabla_y \Phi_k, \mathbf{e}^s] \, dS_x dS_y \tag{6.98}$$

where $[\mathbf{a}, \mathbf{b}, \mathbf{c}] \equiv (\mathbf{a} \times \mathbf{b}).\mathbf{c}$, $G^{ik}{}_{rs}(\mathbf{x}, \mathbf{y})$ are the r, s components of the second order tensor $\mathbf{G}^{ik}(\mathbf{x}, \mathbf{y})$ which is regular and symmetric, whose expression is given by Nedelec (1982) as

$$\mathbf{G}^{ik}(\mathbf{x}, \mathbf{y}) = -\frac{\partial^2}{\partial x_q \partial y_p} B^{kh}_{ij}(\mathbf{x} - \mathbf{y}) (\mathbf{e}^q \times \mathbf{e}^j) \otimes (\mathbf{e}^p \times \mathbf{e}^h)$$

$$B^{kh}_{ij}(\mathbf{z}) = \frac{\mu(\lambda+\mu)}{720\pi(\lambda+\mu)} \frac{\partial^4}{\partial z_i \partial z_j \partial z_k \partial z_h} |\mathbf{z}|^5 +$$

$$+ \frac{\lambda\mu}{48\pi(\lambda+2\mu)} \left(\delta_{kh} \frac{\partial^2}{\partial z_i \partial z_j} |\mathbf{z}|^3 + \delta_{ij} \frac{\partial^2}{\partial z_k \partial z_h} |\mathbf{z}|^3 \right) +$$

$$+ \frac{\mu}{96\pi} \left(\delta_{jh} \frac{\partial^2}{\partial z_i \partial z_k} |\mathbf{z}|^3 + \delta_{ih} \frac{\partial^2}{\partial z_j \partial z_k} |\mathbf{z}|^3 + \delta_{ik} \frac{\partial^2}{\partial z_j \partial z_h} |\mathbf{z}|^3 + \delta_{jk} \frac{\partial^2}{\partial z_i \partial z_h} |\mathbf{z}|^3 \right) +$$

$$+ \frac{\mu}{8\pi} (\delta_{ik} \delta_{jh} + \delta_{ih} \delta_{jk}) |\mathbf{z}| + \frac{\lambda\mu}{4\pi(\lambda+2\mu)} \delta_{ij} \delta_{kh} |\mathbf{z}| \tag{6.99}$$

Nedelec's variational formulation for non contact problems reads

$$a(\Psi, \Phi) - b(\Phi) = 0 \qquad \forall \Phi \in K$$

K being the space of continuously differentiable vector functions satisfying $\Phi = \mathbf{0}$ on the crack front ∂S. In frictionless contact problems, considering the subspace K^+ of functions satisfying the constraints $[[u_n]] \geq 0$ on S, we obtain the *variational boundary integral inequation*

$$a(\Psi, \Phi - \Psi) - b(\Phi - \Psi) \geq 0 \qquad \forall \Phi \in K^+ \tag{6.100}$$

The solution of the variational inequation provides both displacement field and contact zone. The reader will find mathematical analyses of variational inequations in (Ekeland and Temam, 1974).

Formulation of time harmonic elasticity by conjugate functions

The symmetric formulation of BIE in Nedelec's approach is provided by the symmetry of the bilinear form $a(\Psi, \Phi)$. Conjugate functions methods introduce a symmetry in the system of equations as shown in Tonti's diagram of elasticity, Chap. 1. The kinematic approach, called a *primal* formulation, begins with the Helmholtz scalar potential φ and vectorial potential $\mathbf{H}$

$$(\varphi, \mathbf{H}) \rightarrow \mathbf{u} = \nabla\varphi + \mathrm{curl}\mathbf{H} \rightarrow \{\varepsilon = D^*\mathbf{u}, \mathbf{v} = \partial_t \mathbf{u}\} \rightarrow \{\sigma = L\varepsilon, \mathbf{p} = \rho\mathbf{v}\} \rightarrow$$

$$\partial_t \mathbf{p} + D\sigma = 0$$

For time harmonic elasticity the *equation of motion*, $\partial_t \mathbf{p} + D\sigma = 0$, can be written as

$$(L + \rho\ ^2)(\nabla\varphi + \mathrm{curl}\mathbf{H}) = 0 \tag{6.101}$$

It can be splitted into two equations

$$\{(\lambda + 2\mu)\mathrm{div\ grad} + \rho\ ^2\}\varphi = 0 \tag{6.102}$$

$$\{\mu\mathrm{div\ grad} + \rho\ ^2\}\mathbf{H} = \mathbf{0} \tag{6.103}$$

The dynamic approach, called a *dual* formulation, starts from a second order dynamic tensor Z, which may be conveniently derived from a vectorial field Θ

$$\Theta \rightarrow Z = LD^*\Theta \rightarrow \{\sigma = \partial_t LD^*\Theta,\ \mathbf{p} = -DLD^*\Theta\}$$

so that the equation of motion is identically satisfied.

Continuing the dynamic diagram, we are led to

$$\{\sigma = \partial_t L D^* \Theta,\ \mathbf{p} = -D L D^* \Theta\} \rightarrow \{\varepsilon = L^{-1}.\sigma,\ v = \mathbf{p}/\rho\} \rightarrow\ -D^*\mathbf{v} + \partial_t \varepsilon = 0$$

For time harmonic elasticity the *compatibility* condition $-D^*\mathbf{v} + \partial_t \varepsilon = 0$, can be satisfied by the equation

$$(L + \rho\omega^2)\Theta\ = \mathbf{0} \tag{6.104}$$

Eqs. (6.102), (6.103), (6.104), together with boundary conditions on displacements or stress vectors, are the governing equations for the conjugate functions φ, $\mathbf{H}$, Θ.

We are now in a position to formulate the Variational Boundary Integral Equation (VBIE) for time harmonic elasticity. Let us consider the boundary integral

$$a(\varphi, \mathbf{H}, \Theta, \varphi^*, \mathbf{H}^*, \Theta^*) =$$

$$= \int_{\partial\Omega} (\nabla\varphi + \text{curl}\ \mathbf{H} - i\omega\Theta)(\nabla\overline{\varphi}^* + \text{curl}\ \overline{\mathbf{H}}^* - i\omega\overline{\Theta}^*)dS \tag{6.105}$$

It is obvious that the constitutive laws $\mathbf{p} = \rho\mathbf{v}$ and $\sigma = L.\varepsilon$ can be written respectively as

$$\nabla\varphi + \text{curl}\mathbf{H} - i\omega\Theta = \mathbf{0}\ \ \text{in}\ \Omega \tag{6.106}$$

$$LD^*(\nabla\varphi + \text{curl}\mathbf{H} - i\omega\Theta) = \mathbf{0} \text{....in}\ \Omega$$

Thus the only equation to be condidered for constitutive law making a link between conjugate functions φ, $\mathbf{H}$, Θ, is Eq. (6.106). Let $\mathbf{Y} = \nabla\varphi + \text{curl}\mathbf{H} - i\omega\Theta$. Combining Eqs. (6.101) and (6.104) we get

$$(L + \rho\omega^2)\mathbf{Y} = \mathbf{0}\ \ \text{in}\ \Omega.$$

If ω is not an eigenfrequency of the homogeneous equations $(L + \rho\omega^2)\mathbf{Y} = \mathbf{0}$ in Ω, and $\mathbf{Y} = \mathbf{0}$ on $\partial\Omega$, using uniqueness argument we obtain $\mathbf{Y} \equiv \mathbf{0}$ in Ω. Thus, to solve time harmonic elasticity it is sufficient to impose the boundary condition $\nabla\varphi + \text{curl}\mathbf{H} - i\omega\Theta\ = \mathbf{0}$ on $\partial\Omega$. We thus obtain the variational boundary integral equation

$$a\ \varphi, \mathbf{H}. \Theta:\ \varphi^*. \mathbf{H}^*. \Theta^*) = 0\ ,\ \ \forall(\varphi^*, \mathbf{H}^*, \Theta.^*) \in E \tag{6.107}$$

with the bilinear positive hermitian form

$$a(\varphi, \mathbf{H}, \Theta; \varphi^*, \mathbf{H}^*, \Theta^*) \equiv \int_{\partial\Omega} (\nabla\varphi + curl\mathbf{H} - i\omega\Theta)(\nabla\overline{\varphi^*} + curl\overline{\mathbf{H}^*} + i\omega\overline{\Theta^*})dS$$

and $E = \{\varphi, \mathbf{H}, \Theta\}$ being the set of conjugate functions satisfying

$$\{(\lambda + 2\mu)\text{div grad} + \rho\omega^2\}\varphi = 0 \quad \text{in } \Omega \tag{6.108}$$

$$\{\mu\text{div grad} + \rho\omega^2\}\mathbf{H} = \mathbf{0} \quad \text{in } \Omega \tag{6.109}$$

$$(L + \rho\omega^2)\Theta = \mathbf{0} \quad \text{in } \Omega \tag{6.110}$$

such that $(\varphi, \mathbf{H})$ satisfied, for instance, the boundary condition, $\nabla\varphi + \text{curl}\mathbf{H} = \mathbf{u}^d$ on $\partial\Omega$. Eq. (6.107) is the variational form of the so-called *error in constitutive law* introduced by Ladeveze (1975). A zero error of the constitutive law means that $\{\varphi, \mathbf{H}, \Theta\}$ is an exact solution. The associated quadratic form gives a global *a posteriori* error of numerical solutions. It should be emphasized that, unlike formulation (6.98) with a double integral, the VBIE, Eq. (6.107), involves a simple integral.

6.8. An integral equation in elasto-plasticity

To solve non-linear elastic-plastic problems in fracture mechanics, one can formulate the rate problem by integral equations. Unlike elastic problems which can be solved by *boundary* integral equations, elastic-plastic problems involve *domain* integrals. The reason is that equilibrium equation written as $\text{div}(L.\partial_t\varepsilon - L.\partial_t\varepsilon^p) = \mathbf{0}$, is that of elasticity for the rate problem $\partial_t\mathbf{u}$ with the body force $\text{div}(-L.\partial_t\varepsilon^p)$ in P, being in equilibrium with the traction vector $L.\partial_t\varepsilon^p.\mathbf{n}$ on ∂P. Thus plastic rate in some loading region P and displacement rate satisfy the equation

$$\dot{u}_i(\mathbf{x}) = \dot{u}_i^0(\mathbf{x}) + \int_P V_i^h(\mathbf{x}, \mathbf{y})\dot{f}_h(\mathbf{y})dS_y + \int_{\partial P} V_i^h(\mathbf{x}, \mathbf{y})\dot{T}_h(\mathbf{y})dS_y$$

where $\dot{u}_i^0(\mathbf{x})$ is solution of the rate problem in elasticity, and $\dot{f}_i = -2\mu\dot{\varepsilon}^p_{ij,j}$, $\dot{T}_i = 2\mu\dot{\varepsilon}^p_{ij}n_j$.

Thus the strain rate is given by

$$\dot{\varepsilon}_{ij}(\mathbf{x}) = \dot{\varepsilon}_i^0(\mathbf{x}) - 2\mu\int_P^{(sym)} \frac{\partial}{\partial x_j} V_i^h(\mathbf{x}, \mathbf{y})\dot{\varepsilon}^p_{hk,k}(\mathbf{y})dS_y + \\ + 2\mu\int_{\partial P}^{(sym)} \frac{\partial}{\partial x_j} V_i^h(\mathbf{x}, \mathbf{y})\dot{\varepsilon}^p_{hk}(\mathbf{y})n_k dS_y \tag{6.112}$$

where (sym) means the symmetrization of indices (i,j). Eq. (6.112) exists in the ordinary sense in 3D. Without changing the result when P is replaced by $P\backslash B(\mathbf{x},\eta)$ with a spherical ball B centred at $\mathbf{x}$ of small radius η,

then integrate the equation by parts, and taking account of terms over the sphere ∂B, we obtain

$$\dot{\varepsilon}_{ij}(\mathbf{x}) = \dot{\varepsilon}^0_i(\mathbf{x}) + 2\mu \int_{P\setminus B}^{(sym)} \frac{\partial}{\partial x_j}\frac{\partial}{\partial y_k} V^h_i(\mathbf{x},\mathbf{y})\dot{\varepsilon}^p_{hk}(\mathbf{y})dS_y +$$

$$+2\mu \int_{\partial B}^{(sym)} \frac{\partial}{\partial x_j} V^h_i(\mathbf{x},\mathbf{y})\dot{\varepsilon}^p_{hk}(\mathbf{y})\nu_k dS_y - 2\mu \int_B^{(sym)} \frac{\partial}{\partial \xi_j} V^h_i(\mathbf{x},\mathbf{y})\dot{\varepsilon}^p_{hk,k}(\mathbf{y})dS_y \quad (6.113)$$

It may be convenient to set the notation

$$V^h_{(i,j)}(\mathbf{x},\mathbf{y}) := \tfrac{1}{2}\{\partial V^h_i(\mathbf{x},\mathbf{y})/\partial x_j + \partial V^h_j(\mathbf{x},\mathbf{y})/\partial x_i\}$$

for symmetrization of indices (i,j). We also set the notation

$$V^{(h,k)}_{(i,j)}(\mathbf{x},\mathbf{y})\dot{\varepsilon}^p_{hk} := \tfrac{1}{2}\{\frac{\partial}{\partial y_k} V^h_{(i,j)}(\mathbf{x},\mathbf{y})\dot{\varepsilon}^p_{hk} + \frac{\partial}{\partial y_h} V^k_{(i,j)}(\mathbf{x},\mathbf{y})\dot{\varepsilon}^p_{kh}\},$$

$$V^{(h,k)}_{(i,j)}(\mathbf{x},\mathbf{y}) = V^{(i,j)}_{(h,k)}(\mathbf{y},\mathbf{x})$$

The kernel of the domain integral in Eq. (6.113) is symmetric. Assuming that the plastic rate is continuously differentiable, the limits of 2nd and 3rd terms in the right hand side of Eq. (6.113), as $\eta \to 0$, are given by

$$\lim_{\eta\to 0} 2\mu \int_{\partial B} V^h_{(i,j)}(\mathbf{x},\mathbf{y})\dot{\varepsilon}^p_{hk}(\mathbf{y})\nu_k dS_y = \frac{8-10\nu}{15(1-\nu)}\dot{\varepsilon}^p_{hk}(\mathbf{x}) \equiv \beta\,\dot{\varepsilon}^p_{hk}(\mathbf{x}) \quad (6.114)$$

$$\lim_{\eta\to 0} 2\mu \int_B V^h_{(i,j)}(\mathbf{x},\mathbf{y})\dot{\varepsilon}^p_{hk,k}(\mathbf{y})dS_y = 0 \quad (6.115)$$

We are led to a domain integral equation in the pv-sense with an extraneous term $\beta\,\dot{\varepsilon}^p_{hk}(\mathbf{x})$

$$\dot{\varepsilon}_{ij}(\mathbf{x}) = \dot{\varepsilon}^0_{ij}(\mathbf{x}) + 2\mu(\mathrm{pv})\int_P V^{(h,k)}_{(i,j)}(\mathbf{x},\mathbf{y})\dot{\varepsilon}^p_{hk}(\mathbf{y})dS_y + \beta\,\dot{\varepsilon}^p_{ik}(\mathbf{x}),\ \mathbf{x}\in P \quad (6.116)$$

Remarks

Some works are not aware of the fact that $\partial \mathbf{V}_i(\mathbf{x},\mathbf{y})/\partial x_j$ is singular as $|\mathbf{y}-\mathbf{x}|^{-2}$, so that $\partial^2 \mathbf{V}_i(\mathbf{x},\mathbf{y})/\partial x_j \partial x_k \cong O(|\mathbf{y}-\mathbf{x}|^{-3})$ is not integrable; the first integral of Eq. (6.112) upon an integration by parts formally yields a divergent integral

$$2\mu \int_P^{(sym)} \frac{\partial}{\partial x_j} \frac{\partial}{\partial y_k} V_i^h(\mathbf{x}, \mathbf{y}) \dot{\varepsilon}_{hk}^p(\mathbf{y}) dS_y \quad \text{(divergent integral)}$$

Precisely the Hadamard finite part of this divergent integral is

$$2\mu (\mathrm{pv}) \int_P^{(sym)} \frac{\partial}{\partial x_j} \frac{\partial}{\partial y_k} V_i^h(\mathbf{x}, \mathbf{y}) \dot{\varepsilon}_{hk}^p(\mathbf{y}) dS_y + \beta \dot{\varepsilon}_{hk}^p(\mathbf{x}) .$$

The existence of the pv-integral in (6.115) is ensured by the necessary and sufficient condition (6.115). Result (6.116) was first published in (Bui and Dangvan, 1970) and also in (Bui, 1978).

An integral inequation in perfect plasticity

Using Eq. (6.116), we now derive an *integral inequation* for perfect plasticity, with the V. Misès criterion $s_{ij}s_{ij} = k^2$. The plastic rate is proportional to the stress deviator, with the multiplier rate $\dot{\lambda}\ \mathbf{x}) \geq 0$

$$\dot{\varepsilon}_{ij}^p(\mathbf{x}) = \dot{\lambda}(\mathbf{x}) s_{ij}(\mathbf{x}) , \ \mathbf{x} \in \mathrm{P} \text{ (loading region)}$$

$$\dot{\varepsilon}_{ij}^p(\mathbf{x}) = 0 , \ \mathbf{x} \in \Omega \backslash \mathrm{P} \text{ (unloading or elastic region).}$$

Substituting $\partial_t \varepsilon = \mathbf{M} . \partial_t \sigma + \partial_t \varepsilon^p$ and $\partial_t \varepsilon^p(\mathbf{x}) = (\partial_t \lambda) s(\mathbf{x})$ in Eq. (6.116), taking account of $s : \partial_t \sigma = 0$ in P and multiplying the result by $s(\mathbf{x})$ we get a symmetric kernel integral equation for the multiplier

$$(1-\beta) k^2 \dot{\lambda}(\mathbf{x}) - 2\mu (\mathrm{pv}) \int_P s_{ij}(\mathbf{x}) V_{(i,j)}^{(h,k)}(\mathbf{x}, \mathbf{y}) s_{hk}(\mathbf{y}) \dot{\lambda}(\mathbf{y}) dS_y - \\ - s_{ij} \dot{\varepsilon}_{ij}^0(\mathbf{x}) = 0 , \ \mathbf{x} \in \mathrm{P} \qquad (6.117)$$

In the elastic unloading zone E, the inequality $s : \partial_t \sigma = s : \partial_t s < 0$ or equivalently the inequality $s : \partial_t \varepsilon^e < 0$ holds. Thus, Eq. (6.116) yields

$$\dot{\varepsilon}_{ij}^e(\mathbf{x}) = (\beta - 1) \dot{\varepsilon}_{ij}^p(\mathbf{x}) + (\mathrm{pv}) 2\mu \int_P V_{(i,j)}^{(h,k)}(\mathbf{x}, \mathbf{y}) \varepsilon_{hk}^p(\mathbf{y}) dS_y + \dot{\varepsilon}_{ij}^0(\mathbf{x})$$

Since $\dot{\lambda}(\mathbf{x}) = 0$ or $\dot{\varepsilon}_{ij}^p(\mathbf{x}) = 0$ in E, we obtain the inequality

$$-(\mathrm{pv}) 2\mu \int_P s_{ij}(\mathbf{x}) V_{(i,j)}^{(h,k)}(\mathbf{x}, \mathbf{y}) s_{hk} \dot{\lambda}(\mathbf{y}) dS_y - s_{ij} \dot{\varepsilon}_{ij}^0 > 0, \quad \mathbf{x} \in \mathrm{E} \qquad (6.118)$$

Formally, writing Eq. (6.117) and inequality (6.118) with operator A, we obtain the system of *integral inequation* for the rate problem of elastoplasticity, $Az - d = 0$ in P, $Az - d > 0$ in E (Bui and Dang Van, 1970).

Chapter 7

Non Linear Fracture Mechanics

7.1 Introduction

Microscopic and macroscopic observations of fractured specimens in ductile materials show evidence of the presence of cavities of various shapes and sizes, from about 5μm to 100μm. Some of them are present before loadings, others are created during the whole process of deformation and fracture.

Decohesion around an existing inclusion, for instance in 304 stainless steel, results in a cavity which keeps the inclusion imprisoned in its inside. In further loading only the matrix with a cavity can deform with a free inclusion inside. This mechanism induces small porosity measured by a densitometer – theoretically a zero porosity – since the undeformed inclusion still participates to the density measurement while it does not contribute to the strength of the material. After rupture, the broken surface shows a series of characteristic cups, sometimes with an imprisoned inclusion inside, but most of the inclusions have been removed from the material in the machining of specimens, Fig. 7.1. Cavities of this type shall be referred to as the population of cavities (a). The analysis of a cavity (a) can be done within the small strain assumption.

There is another mechanism of the cavity formation referred to as the cavity population (b). This consists in the growth of an existing *small* cavity – theoretically of a vanishing radius – in a very highly stressed zone, as observed in many works. Thompson (1984) observed pinholes initiated at the grain boundaries under shear. According to Moussy (1985), cavities are created by a microspopic *instability* in the presence of very high stress gradient, Fig. 7.2. Obsviously, under very high stress, the mechanisms are associated with a bifurcation phenomenon which implies a *finite* deformation analysis, as shown in a further analysis to understand cavitations in solids. Two features – low porosity measured from cavities of the type (a) and high porosity of population (b) not necessarily uniformly distributed in the medium – are reported in the literature.

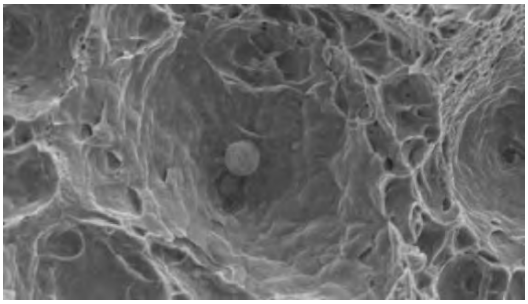

Figure 7.1: An spherical inclusion left inside a cup revealed in ductile rupture of aluminium (Courtesy of B. Tanguy and T.Q Luu, 2005, ENSMP Paris)

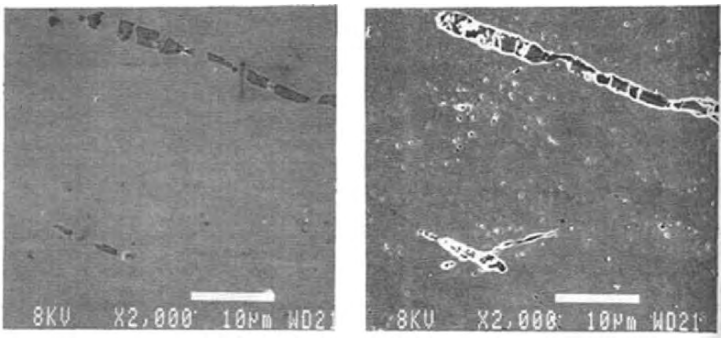

Figure 7.2: Cavities and microcavities unrevealed by mechanical burnishing (left) and revealed by ionic burnishing (right) in steel (F. Moussy, 1985, in Plastic Instability, Considère Symposium, Presses ENPC, Paris)

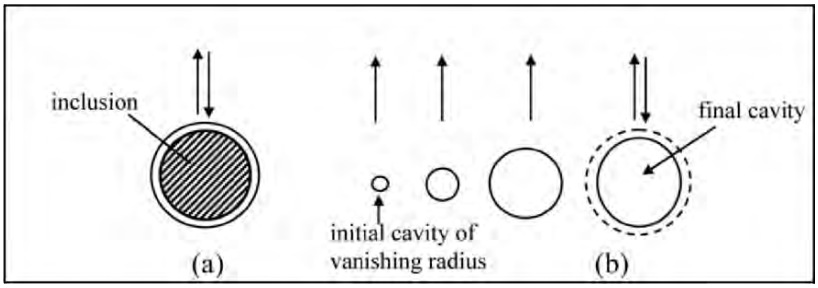

Figure 7.3: Population of cavities (a) formed by decohesion at inclusion; Growth of population (b) of microspopic cavities of vanishing radius in a highly stress zone, in *finite* elasto-plasticity, resulting in a larger cavity after elastic unloading

The cavity formation at two levels (a) and (b) has been first suggested by Pineau (1981), Fig. 7.3. However, despite the high porosity of population (b), cavities of type (b) are too small to be observed experimentally since they can be masked by a machining process. Both types of cavity populations contribute to the overall porosity, which is generally small, about 0.1 to 0.5%, as observed in experiments. On the other hand most theoretical porosity description using classical models of cavity growth in plasticity or viscoplaticity is of many order higher, 5% or more (Moussy, 1985, p. 266). For instance Brown and Embury (1973) give a simple criterion for coalescence of two parallel neighbouring cavities when their elongated height equals the remaining ligament between them, which would correspond to 15%. Thompson and Handcock (1984) proposed a model which gives a porosity about 5% at the formation of a crack. It is likely that both arguments hold true : measurements of the porosity of population (b) are un-der-estimated and existing models of cavity growth based on the small strain condition lead to an over-estimated porosity.

From a theoretical point of view, it is important to analyse the behavior of plastic materials containing cavities, particularly to know how an existing cavity grows and how it can grow at a microscopic point of the matrix. As far as we know, there are many unsolved problems such as the coalescence of cavities, which are not considered in this chapter.

7.2 Ductile fracture

Ductile fracture is a particular damage theory developed for metal plasticity, which is characterized by the nucleation and the growth of cavities. Unlike brittle fracture which deals with the mechanics of a crack, ductile fracture studies the macroscopic elasto-plastic behavior of materials in the presence of porosity. Classical plasticity theory deals with slips in crystals which imply plastic incompressibility. Ductile fracture damage involves the dilatance of the material under positive mean stress so that the void volume f or the density ρ is the pertinent internal variable associated with its conjugate mean stress σ_m. Plastic strain in the material matrix is still the internal variable associated with the deviatoric stress. Moreover, ductile fracture of metals is observed after a large strain of the specimen so that it requires, in principle, a finite strain analysis.

Among theories making use of the finite strain analysis, the most important one is provided by the model of Rousselier (1981). Another approach is given by an early work of Gurson (1977) which is based on the limit analysis of a rigid-perfectly plastic sphere containing an internal spherical

void and on a homogenization theory of a two-phases body, consisting of a rigid perfectly plastic medium and a population of cavities.

7.2.1 Rousselier's model

Let us first follow the works of Mandel (1971), Rousselier (1981), Stolz (1987) to set the general formulation of materials in finite strain. Then we present Rousselier's model of ductile fracture as the natural consequence of the finite strain formulation.

Introduce the configuration (0) of a representative volume element in its natural and undeformed state, the current configuration (c) of the same material at time t under Cauchy stress σ and the relaxed one (r) deduced from (c) by an unloading. F is the gradient of the transformation (0) $\rightarrow$ (c), P the gradient of the transformation (0) $\rightarrow$ (r), and E the gradient of the transformation (r) $\rightarrow$ (c), then F=EP (*).
The gradient of the velocity is

$$grad\,\mathbf{v} \equiv D + \Omega = \frac{d'\mathrm{F}}{d't}\,\mathrm{F}^{-1} \tag{7.1}$$

where the deformation rate D and the spin Ω are the symmetric and unsymmetric parts of *grad* **v** respectively, and *d'/d'*t is any convected derivative, Jaumann derivative or Mandel derivative relative to the rotation of the director frame which is related to crystal orientation.

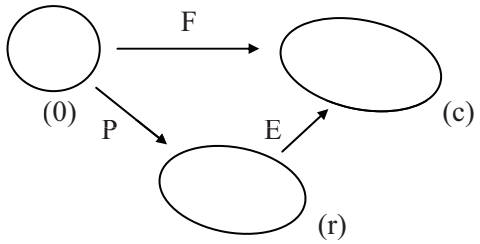

Figure 7.4: Natural (0), current (c) and relaxed (r) configurations. Gradients of transformations F, E, P

*In terms of matrice notation, one writes $F_{ij} = E_{ik}P_{kj}$ or F = E.P (a simple contraction of indices) or simply F = EP in operator notations if there is no ambiguity.

Let Δ^e be the Green elastic deformation tensor $\Delta^e := (E^t.E - I)/2$ and $\varphi(\Delta^e, \alpha_i)$ be specific free energy, function of Δ^e and of internal variables α_i characterizing strain hardening, strain-softening, damage like porosity. Introduce the densities

$$\rho = \frac{1}{\det F}.\ \rho_r = \frac{1}{\det P} \tag{7.2}$$

and the Kirchhoff stress π relative to the configuration (r)

$$E.\frac{\pi}{\rho_r}.E^t = \frac{\sigma}{\rho} \tag{7.3}$$

The dissipation rate $\Phi \geq 0$ is defined by

$$\Phi := \frac{\mathrm{tr}(\sigma.D)}{\rho} - \frac{d'}{d't}\varphi \geq 0 \tag{7.4}$$

which can be written as

$$\Phi = \Sigma : D^p - (\frac{\partial \varphi}{\partial \Delta^e} - \frac{\pi}{\rho_r}) : \frac{d'}{d't}\Delta^e - \frac{\partial \varphi}{\partial \alpha_i}\frac{d'\alpha_i}{d't} \geq 0 \tag{7.5}$$

The second term vanishes because the transformation (r) $\rightarrow$ (c) is reversible, thus

$$\frac{\pi}{\rho_r} = \frac{\partial \varphi}{\partial \Delta^e} \tag{7.6}$$

Introduce the generalized forces in the sense of (Halphen and Nguyen, 1975)

$$\Sigma = E^t.\frac{\sigma}{\rho}.(E^t)^{-1}, \qquad A_i = -\frac{\partial \varphi}{\partial \alpha_i} \tag{7.7}$$

which are the conjugates of the plastic deformation rate D^p and the internal rates $(d'/d't)\alpha_i$. The second principle reads

$$\Phi := \frac{\sigma : D^p}{\rho} + A_i \frac{d'\alpha_i}{d't} \geq 0 \tag{7.8}$$

Now, assume that there exists a convex single plastic potential $F(\Sigma, A_i)$ such that

$$D^p = \lambda \frac{\partial F}{\partial \Sigma}, \qquad \frac{d'}{d't} \alpha_i = \lambda \frac{\partial F}{\partial A_i} \tag{7.9}$$

with $\lambda \geq 0$, if , $F = \dot{F} = 0$, $\lambda = 0$ otherwise.

Now, consider the configuration (r) so that the elastic transformation is symmetric (pure deformation) and assume that the elastic deformation ε^e is small in comparison with unity. Thus the following relations hold

$$E = I + \Delta^e \cong I + \varepsilon^e \tag{7.10}$$

$$\rho \cong \rho_r \tag{7.11}$$

$$\sigma = \pi \tag{7.12}$$

$$\Sigma = \frac{\sigma}{\rho} = \frac{\partial \varphi}{\partial \varepsilon^e} \tag{7.13}$$

$$D^p = \lambda \frac{\partial F}{\partial (\sigma / \rho)}, \qquad \frac{d'}{d't} \alpha_i = \lambda \frac{\partial F}{\partial A_i} \tag{7.14}$$

The following forms of the specific energy and the plastic potential are used in Rousselier's model (we recall: $s_{ij}e_{ij} = tr(s.e) = s:e$)

$$\varphi(\varepsilon^e, \alpha, \beta) = \frac{1}{2} \varepsilon^e .L. \varepsilon^e + \varphi_1(\alpha) + \varphi_2(\beta) \tag{7.15}$$

Internal parameter β is denoted by ω in the damage theory of Lemaitre and Chaboche (1985). Since $\sigma = \rho \partial \varphi / \partial \varepsilon^e = \rho L.\varepsilon^e$, Lemaitre and Chaboche's theory is recovered by considering $\beta = 1 - \rho$ and the effective stress $\sigma/(1 - \omega)$ in their elastic law $\sigma/(1 - \omega) = L.\varepsilon^e$.

The plastic potential of the V. Mises type is given by

$$F(\frac{\sigma}{\rho}, A, B) := \left[J_2(\frac{\sigma}{\rho}) \right]^{\frac{1}{2}} + \frac{A}{\sqrt{3}} + B g(\frac{\sigma_m}{\rho}) \tag{7.16}$$

where

$$A = -d\varphi_1/d\alpha \ , \ B = -d\varphi_2/d\beta. \tag{7.17}$$

Let us decompose the deformation rate $D^p = D_d^p + D_m^p$ into deviatoric part D_d^p and spherical part D_m^p and the stress σ into deviatoric part s and spherical part σ_m. Hence one obtains

$$D_d^p = \lambda \frac{s}{2[J_2(\sigma)]^{1/2}} \text{ (deviatoric part)} \tag{7.18}$$

$$D_m^p = \lambda \frac{B}{3} g'(\frac{\sigma_m}{\rho}) \text{ (spherical part)} \tag{7.19}$$

$$\dot{\alpha} = \lambda \frac{\partial F}{\partial A} = \frac{\lambda}{\sqrt{3}} \tag{7.20}$$

$$\dot{\beta} = \lambda \frac{\partial F}{\partial B} = \lambda g(\frac{\sigma_m}{\rho}) \tag{7.21}$$

The equivalent deformation rate is

$$D_{eq}^p = (\tfrac{2}{3} D_{ij}^p D_{ij}^p)^{1/2} = \frac{\lambda}{\sqrt{3}} = \dot{\alpha} \tag{7.22}$$

Therefore internal parameter α is nothing but the cumulated plastic strain

$$\alpha = \int D_{eq}^p dt \tag{7.23}$$

Now, the damage parameter β is function of the mass density ($\beta = \beta(\rho)$), hence $\partial\beta(\rho)/\partial t = \beta'(\rho)\partial\rho/\partial t$. Now, considering the mass conservation law $\partial_t\rho + \rho \mathrm{div}\mathbf{v} = 0$ and remarking that

$$div\mathbf{v} = 3D_m \cong 3D_m^p = \lambda B g'(\frac{\sigma_m}{\rho}) = \dot{\beta} B \frac{g'(\sigma_m/\rho)}{g(\sigma_m/\rho)}$$

(D_m is the spherical part of D) one gets

$$\frac{1}{\rho B \beta'(\rho)} = -\frac{g'(\sigma_m/\rho)}{g(\sigma_m/\rho)} \tag{7.24}$$

The left hand side is a function of ρ while the right hand side is a function of σ_m/ρ. Both functions equal a *constant* C/σ_0 and thus

$$g(\frac{\sigma_m}{\rho}) \equiv D \exp(\frac{C\sigma_m}{\rho\sigma_0}) \tag{7.25}$$

$$C\rho\beta'(\rho)\varphi'_2(\beta(\rho)) = \sigma_0 \tag{7.26}$$

Eq. (7.25) is the fundamental result of Rousselier's theory on the exponential dependence of the damage rate on the spherical mean stress $\partial_t\beta = \lambda\exp(C\sigma_m/\rho\sigma_0)$. In contrast with other theories based on micromechanical model of cavity expansion, Rousselier's model is a consequence of the general framework of finite strain.

Eq. (7.26) shows that function $\beta(\rho)$ can be chosen to make a best fit with experiments and also to ensure the possible lost of stability of the material in the Drücker sense. Nguyen and Bui (1974) showed that stability implies

$$\dot{\sigma} : \dot{\varepsilon}^p = \lambda^2 \frac{\partial F}{\partial A_i} \frac{\partial^2 \varphi}{\partial \alpha_i \partial \alpha_j} \frac{\partial F}{\partial A_j} \geq 0 \tag{7.27}$$

In this model, the second derivative of the matrix $\partial^2\varphi/\partial\alpha_i\partial\alpha_j$ has two components $\partial^2\varphi/\partial\alpha_i\partial\alpha_j = \varphi_1''(\alpha) + \varphi_2''(\beta)$, the first one $\varphi_1''(\alpha)$ is strictly positive if strain hardening is assumed in the matrix material and the second one $\varphi_2''(\beta)$ is related to the void fraction. The choice of models is subjected to condition $\varphi_2''(\beta) < 0$ which makes it possible to have a structural instability. A simple choice is

$$\beta = 1-\rho \quad \Rightarrow \quad \varphi_2(\beta) = (\sigma_0 / C)\ln(1-\beta) \Rightarrow \varphi_2''(\beta) < 0 \tag{7.27}$$

Rousselier indicates other possible choices based on the void volume fraction f

$$\beta = f - f_0 \tag{7.28}$$

$$\beta = f - f_0 \quad \Rightarrow \quad \varphi_2(\beta) = \frac{\sigma_0}{C}\ln(1 - f_0 - \beta) \quad \Rightarrow \quad \varphi_2''(\beta) < 0 \tag{7.29}$$

Another choice is suggested by the model of Rice and Tracey (1969) of the growth of a spherical void of radius R_0

$$\frac{\dot{R}_0}{R_0} = 0.283 d_{eq}^p \exp\left(\frac{3\sigma_m}{\sigma_0}\right) \tag{7.30}$$

The ratio $\dot{R}_0/R_0 = \dot{R}/R$ is linked to $\dot{f}/f$ by

$$\frac{\dot{f}}{f(1-f)} = 3\frac{\dot{R}}{R}$$

Therefore functions $\beta(f)$ and $\varphi_2(\beta)$ are

$$\beta = \ln\frac{f(1-f_0)}{f_0(1-f)} \;\Rightarrow\; \varphi_2(\beta) = \ln(1-f_0+f_0\exp\beta) \;\Rightarrow\; \varphi_2'(\beta) < 0 \tag{7.31}$$

With these functions the yield criterion F=0 becomes ($1/\sqrt{3} = 0.577$)

$$\frac{\sigma_{eq}}{\rho} + 0.577\sigma_0 f\exp(\frac{3\sigma_m}{2\rho\sigma_0}) - \varphi_1'(\alpha) = 0 \tag{7.32}$$

Gurson's model discussed below leads to the yield stress

$$\sigma_{eq}^2 + 2\sigma_0^2 f\cosh(\frac{3\sigma_m}{\sigma_0}) - (1+f^2)\sigma_0^2 = 0 \tag{7.33}$$

For small damage, approximate form of Eq. (7.33)

$$\sigma_{eq} + 0.5\sigma_0 f\exp(\frac{3\sigma_m}{\sigma_0}) - \sigma_0 = 0 \tag{7.34}$$

is quite similar to Rousselier's model, with coefficient 0.5 instead of 0.577.

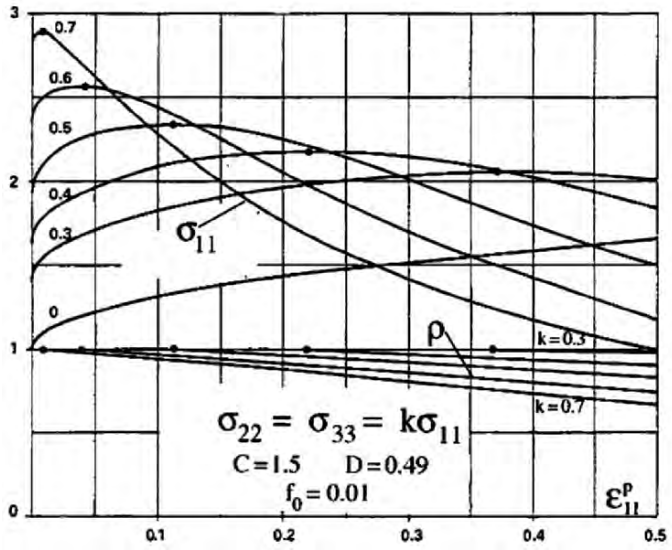

Figure 7.5: Triaxial tension test (unit yield stress) for different factor k in the range [0, 0.7]. The maximum stress σ_{11} before the occuring of softening is found for plastic strain less than 15%, for lateral stresses factor k > 0.5. Values of density ρ are given for k in the range [0.3, 0.7], Rousselier (1980)

An application of Rousselier's model to a triaxial tension test is shown in Fig. 7.5 (unit yield stress). The maximum stress σ_{11} before softening is reached for plastic strain less than 15%, for a lateral stresses factor $k > 0.5$.

7.2.2 The micromechanics of plasticity

Before introducing Gurson's model, let us consider the homogenization of a porous material Ω including voids ω, with boundary $\partial\Omega$ which is aimed at the application of the limit analysis of Plasticity theory to the problem considered (Hill, 1967; Mandel, 1964).

The volume fraction of the voids is $f = \omega/\Omega$. Microscopic quantities are denoted by small letters, macroscopic ones are in capital letters. The porous solid is subjected to a homogeneous macroscopic strain rate (tensor) D, that is the boundary velocity field is

$$\mathbf{V}(\mathbf{x}) = \mathbf{D}.\mathbf{x} \quad (\forall \mathbf{x} \in \partial\Omega) \tag{7.34}$$

Any continuous and continuously differential velocity C^1 field $\mathbf{v}(\mathbf{x})$ satisfying the boundary condition $\mathbf{v}(\mathbf{x}) = \mathbf{V}(\mathbf{x})$ $(\mathbf{x} \in \partial\Omega)$ is called a kinematically admissible field of the set KA. Such field is defined on the sound material.

One considers its C^1 continuation inside the voids and thus defines $\mathbf{v} \in$ KA in the whole domain Ω. There is no body force and the surface of cavities $\partial\omega$ is stress free. Upon considering Hill-Mandel theorems in the theory of crystal aggregates one obtains the general following results ($<\bullet>_\Omega$ denotes the mean value on domain Ω and $<\bullet>_{\Omega\setminus\omega}$ the mean value on the matrix $\Omega\setminus\omega$)

$$\Sigma := <\sigma(\mathbf{x})>_\Omega = (1-f)<\sigma(\mathbf{x})>_{\Omega\setminus\omega} \text{ (definition)} \tag{7.35}$$

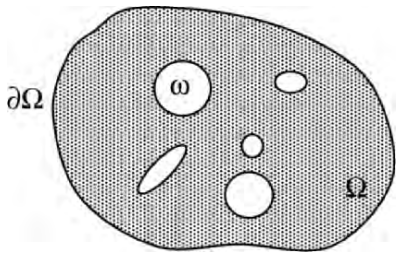

Figure 7.6: The Representative Volume Element of a porous material Ω containg cavities, of total volume ω

$$\mathbf{D} = \langle \mathbf{d}(\mathbf{x}) \rangle_{\Omega} \tag{7.36}$$

$$\Sigma : \mathbf{D} = \langle \sigma(\mathbf{x}) : \mathbf{d}(\mathbf{x}) \rangle_{\Omega} = (1-f) \langle \sigma(\mathbf{x}) : \mathbf{d}(\mathbf{x}) \rangle_{\Omega \setminus \omega} \tag{7.37}$$

The RVE is said *macroscopically homogeneous* in the Hill-Mandel sense when the following conditions are satisfied. For any d'($\mathbf{x}$) kinematically admissible with the homogeneous field D', $\mathbf{v}'(\mathbf{x}) = \mathbf{D}'.\mathbf{x}$ ($\mathbf{x} \in \Omega \cup \omega$), and for any $\sigma(\mathbf{x})$ statically admissible with the homogeneous stress field Σ, $\sigma(\mathbf{x}).\mathbf{n}(\mathbf{x}) = \Sigma.\mathbf{n}(\mathbf{x})$ on $\partial\Omega$ or $\mathbf{0}$ on $\partial\omega$ respectively, Eqs. (7.35)-(7.37) hold for the microscopic fields $\sigma(\mathbf{x})$, d'($\mathbf{x}$) in Ω. This is always true for any pair of non related fields d'($\mathbf{x}$), $\sigma(\mathbf{x})$. Macrohomogeneity implies intuitively that in a *rea'* process, kinematic boundary condition $\mathbf{v}'(\mathbf{x}) = \mathbf{D}'.\mathbf{x}$ ($\mathbf{x} \in \partial\Omega$) results in the boundary stress $\sigma'.\mathbf{n}$ which must not fluctuate too much from a homogeneous state. Conversely, static boundary condition $\sigma.\mathbf{n} = \Sigma.\mathbf{n}$ on $\partial\Omega$ results in the measured boundary velocity field $\mathbf{v}(\mathbf{x})$ which must not deviate too much from a homogeneous boundary field. Can such a condition be satisfied in the periodic homogenization of cells? Suppose that the cell is a cube which contains *one* spherical cavity very close to one of its faces and that homogeneous stress condition is assumed on the boundary of the cell. The macroscopic homogeneity in the Hill-Mandel sense does not hold. The deformation of the cube face close to the cavity is more important than those of other faces so that the overall deformation of the cube is far from a homogeneous state. Macroscopic homogeneity in periodic cells is obtained when there are many small cavities randomly distributed in the cell.

Having introduced basic notations and mechanical fields at both microscopic and macroscopic levels, let us consider the plastic criterion at the microscopic level defined $f(\sigma(\mathbf{x})) \leq 0$ which is a convex C^m in the stress σ-space and let us show how to derive the macroscopic plastic criterion $F(\Sigma) \leq 0$ in the stress Σ-space. To do so, we consider the case of an elastic-plastic matrix and assume the usual symmetry of the moduli tensor. According to Hill's maximum principle of the plasticity theory, the following inequality holds for any x in $\Omega \setminus \omega$:

$$(\sigma(\mathbf{x}) - \sigma^*(\mathbf{x})) : \mathbf{d}^p(\mathbf{x}) \geq 0 \tag{7.38}$$

for any $\sigma(\mathbf{x})$, $\sigma^*(\mathbf{x})$ such that $f(\sigma(\mathbf{x})) = 0$ and $f(\sigma^*(\mathbf{x})) \leq 0$. The stress $\sigma(\mathbf{x})$ is on the yield surface ∂C^m, while the stress $\sigma^*(\mathbf{x})$ belongs to the convex C^m, both stresses are in equilibrium with Σ, that is $\mathrm{div}(\sigma) = \mathrm{div}(\sigma^*) = 0$ and $\sigma(\mathbf{x}).\mathbf{n}(\mathbf{x}) = \sigma^*(\mathbf{x}).\mathbf{n}(\mathbf{x}) = \Sigma.\mathbf{n}(\mathbf{x})$ on $\partial\Omega$. For brevity, the stress field $\sigma^*(\mathbf{x})$ statically admissible with Σ and plastically admissible, $\sigma^*(\mathbf{x}) \in C^m$, is called the SPA field. Since the variation from $\sigma(\mathbf{x})$ to $\sigma^*(\mathbf{x})$ is purely elastic, by introducing Mandel's localization 4th order tensor $\mathbf{A}(\mathbf{x})$, which gives

a purely elastic stress $\tau(\mathbf{x})$ for the applied stress Σ to the body : $\tau(\mathbf{x}) = A(\mathbf{x}).\Sigma$, we have

$$\sigma(\mathbf{x}) - \sigma^*(\mathbf{x}) = A(x).(\Sigma - \Sigma^*) \tag{7.39}$$

Now, making use of Mandel's homogenization formula for the plastic strain rate $D^p = <A^\tau(\mathbf{x}).d^p(\mathbf{x})>_\Omega$ where A^τ is the transposed tensor of A, we obtain

$$<(\sigma(\mathbf{x}) - \sigma^*(\mathbf{x})):d^p(\mathbf{x})>_\Omega = <A(\mathbf{x})_{ijhk}(\Sigma - \Sigma^*)_{hk}d^p(\mathbf{x})_{ij}>_\Omega$$

$$= < (\Sigma - \Sigma^*)_{hk}A^t(\mathbf{x})_{hkij}d^p(\mathbf{x})_{ij}>_\Omega = (\Sigma - \Sigma^*):<A^t(\mathbf{x}).d^p(\mathbf{x})>_\Omega$$

$$\equiv (\Sigma - \Sigma^*):D^p \geq 0 \tag{7.40}$$

The parallel is completly established between (7.38) and (7.40) which is the maximum principle of plasticity in the macroscopic level.

The result (7.40) derived under the general condition of non negligible elastic strain is due to Mandel (1964) and Bui (1969)(*). It remains to define the macroscopic convex of plasticity C^M.

Now we neglect the elastic strain rate at both levels so that $^p \equiv d$, $D^p \equiv D$. The function $d^p(\mathbf{x}) \rightarrow \sigma(\mathbf{x}):d^p(\mathbf{x}) \equiv \pi(d^p)$ is called the plastic dissipation defined, according to (7.38), by

$$\pi(d^p) \coloneqq \max_{\sigma^* \in C} \sigma^*.d^p \tag{7.41}$$

Owing to the convexity of C^m, $\pi(d^p)$ is linear in d^p since $d^p \rightarrow \lambda d^p$ implies
$\pi(d^p) \rightarrow \lambda\pi(d^p)$, for any scalar λ. For any D, let us define the function $P(D^p)$ called the macroscopic dissipation

$$P(D^p) \coloneqq \min_{\mathbf{v}(\mathbf{x})=D^p.\mathbf{x}} <\pi(d(\mathbf{v}))>_\Omega = (1-f) \min_{\mathbf{v}(\mathbf{x})=D^p.\mathbf{x}} <\pi(d(\mathbf{v}))>_{\Omega-\omega} \tag{7.42}$$

Function $P(D^p)$ is a *linear form* of D^p, because the change by a scalar factor $D^p \rightarrow \lambda D^p$ implies the changes $\mathbf{v}(\mathbf{x}) \equiv D^p.\mathbf{x} \rightarrow \lambda\mathbf{v}(\mathbf{x})$, $d^p \rightarrow \lambda d^p$ and $\pi(d^p) \rightarrow \lambda\pi(d^p)$. Any linear form $P(D^p)$ is defined by its expression $P(D^p) = a_{ij}D^p_{ij}$ with symmetric (a_{ij}) so that a_{ij} can be identified with Σ_{ij}. Therefore $P(D^p)$ is identified with $\Sigma:D^p$ for some Σ, $P(D^p) \equiv \Sigma:D^p$.

*Bui (1969) found two other formulae, for elastic strain rate $D^e = <A^t(\mathbf{x}).d^e(\mathbf{x})>_\Omega$ and for the total strain rate $D = <A^t(\mathbf{x}).d(\mathbf{x})>_\Omega$ which is also equal to $D = <d(\mathbf{x})>_\Omega$. Thus Mandel's formula $D^p = <A^t(\mathbf{x}).d^p(\mathbf{x})>_\Omega$ is infered by substraction.

Now from (7.40) it is clear that the stress Σ^* belongs to the macroscopic convex C^M defined by its convex hull

$$\Sigma^* : D^p \leq P(D^p) \text{ for any } D^p \tag{7.43}$$

The convex C^M is approached by the c-family of hyperplane $\Sigma_{ij} D^p_{ij} = c$, in the stress-space where c is the constant value given by the right hand side of (7.42) (c is constant parameterized by D^p and the convex C^m) with normal D^p. The convex hull determines the convex C^M from the outside.

Elastic-plastic microstructure

We now relax the assumption of negligible elastic strain to prove that, even in perfect plasticity and contrary to common belief, there is generally a difference between microscopic and macroscopic plastic dissipations

$$<\sigma(\mathbf{x}) : d^p(\mathbf{x})>_\Omega \ (\neq \Sigma : D^p) \tag{7.44}$$

for $f(\sigma) = 0$, $d^p(\mathbf{x}) = \lambda \partial f/\partial \sigma$. In elasto-plasticity, the field $d^p(\mathbf{x})$ is *not* a kinematical one, but $d(\mathbf{x}) = d^e(\mathbf{x}) + d^p(\mathbf{x})$ is an element of KA. From the yield criterion, upon differentiating $f(\sigma)$ we obtain

$$\dot{\sigma} : \lambda \frac{\partial f}{\partial \sigma} = 0 \quad \Rightarrow \quad \dot{\sigma}(\mathbf{x}) : d^p(\mathbf{x}) = 0 \tag{7.45}$$

Now, let us consider a particular proportional loading such that ε^p and d^p are proportional at any point in Ω and any time $\varepsilon^p = \gamma d^p$

$$\dot{\sigma}(\mathbf{x}) : \varepsilon^p(\mathbf{x}) = \dot{\sigma}(\mathbf{x}) : \gamma d^p(\mathbf{x}) = 0 \tag{7.46}$$

On the other hand (E is the macroscopic strain corresponding to $\varepsilon(\mathbf{x})$)

$$\Sigma : D - \dot{\Sigma} : E = < \sigma : d >_\Omega - < \dot{\sigma} : \varepsilon >_\Omega =$$

$$< \sigma : d^p >_\Omega + < \sigma : d^e >_\Omega - < \dot{\sigma} : \varepsilon^p >_\Omega - < \dot{\sigma} : \varepsilon^e >_\Omega$$

By virtue of the elastic moduli tensor symmetry

$$< \dot{\sigma} : \varepsilon^e >_\Omega = < \sigma : d^e >_\Omega$$

Taking into account of (7.46) we obtain

$$\Sigma : D - \dot{\Sigma} : E = < \sigma : d^p >_\Omega = (1 - f) < \sigma : d^p >_{\Omega - \omega} \tag{7.47}$$

The total macroscopic plastic dissipation, in the presence of elasticity, is less than the plastic work

$$W^p = \int_0^t \Sigma_{ij} D_{ij}^p dt \quad > \quad \int_0^t < \sigma_{ij}\, d_{ij}^p >_\Omega \, dt \tag{7.48}$$

Physically, this means that macroscopic elastic unloading does not completely release the residual stress of a polycrystal. A part of the elastic strain energy is blocked inside crystals. Experiments on heat dissipation in plasticity have been performed by Bui (1965) confirming quantitatively the inequality (7.48).

7.2.3 Gurson's model

Gurson considered the limit analysis of a hollow incompressible sphere of external radius b and internal radius a. We shall follow the presentation of Gurson's model given recently by Leblond (2003) which has the merit of simplicity. The approximate velocity field to be considered consists of two parts

$\mathbf{v}(\mathbf{x}) = \mathbf{v}^{(A)}(\mathbf{x}) + \mathbf{v}^{(B)}(\mathbf{x})$

with

$$\mathbf{v}(\mathbf{x})^{(A)} = \frac{\alpha}{r^2}\mathbf{e}^r \tag{7.49}$$

$$\mathbf{v}(\mathbf{x})^{(B)} = \beta.\mathbf{x} \tag{7.50}$$

Field (A) is radial and field (B) is deviatoric ($\mathrm{tr}\beta = 0$, $\beta = \beta^r$). Both fields have been used by Rice and Tracey (1969).

Since the field (A)+(B) is only an approximation, the macroscopic dissipation rate is majored by

$$P^+(D^p) = \frac{1}{\Omega}\int_a^b 4\pi r^2 < \pi(d(r)) >_{S^r} dr \tag{7.51}$$

where S^r is the surface of the sphere of radius r.
The integral is very difficult to calculate in explicit form. It will be not calculated in closed-form but as suggested by Leblond (2003), can be majored by a quantity which can be explicitly evaluated. Leblond observed that $P^+(D^p)$ itself can be majored by

$$P^{++}(D^p) = \frac{1}{\Omega}\int_a^b 4\pi r^2 \{< \pi^2(d(r)) >_{S^r}\}^{1/2} dr \tag{7.52}$$

Here the integrant is given by

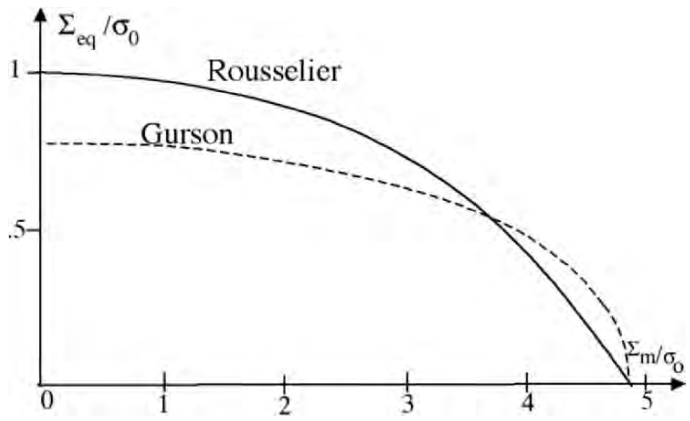

Figure 7.7: Comparison between Rousselier's model, Eq (7.32) and Gurson's one, Eq. (7.54), for porous plasticity, Σ_{eq}/σ_0 versus Σ_m/σ_0

$$< \pi^2 (d(r)) >_{S^r} = \sigma_0 (4 D_m^2 \frac{b^6}{r^6} + D_{eq}^2) \tag{7.53}$$

The calculation of $P^{++}(D^p)$ from expression (7.53) can be performed analytically (Leblond, 2003). The macroscopic yield criterion defined by the convex hull, which is necessarily larger than the exact convex C^M, can also be determined in closed-form

$$\frac{\Sigma_{eq}^2}{\sigma_0^2} + 2f \cosh\left(\frac{3\Sigma_m}{2\sigma_0}\right) - 1 - f^2 = 0 \tag{7.54}$$

This is the Gurson model of the yield function of porous plastic materials. The yield stress in tension is σ_0. Rousselier's model (7.32) and Gurson's one are compared in Fig. 7.7. Noticeable difference can be observed on the slope γ at point (Σ_m/σ_0, 0): finite slope in Rousselier's model, infinite slope in Gurson's theory.

7.2.4 Extension of porous plasticity models to aggregates

Gurson's model is strictly valid for a perfectly plastic matrix. The model has been generalized to a hardening matrix described by some law $\bar{\sigma} = g(\bar{\varepsilon})$ between equivalent mean stress and strain. Gurson assumed that his rigid-perfect plasticity model could be replaced by

$$\frac{\Sigma_{eq}^2}{\bar{\sigma}^2} + 2f\cosh\left(\frac{3\Sigma_m}{2\bar{\sigma}}\right) - 1 - f^2 = 0 \tag{7.55}$$

and that the flow law is given by the equivalent rate $\bar{\dot{\varepsilon}}$ in the sense of the conservation of plastic dissipation rate

$$(1-f)\bar{\sigma}:\bar{\dot{\varepsilon}} = \Sigma : D^p \tag{7.56}$$

We do not insist on different empirical modifications of Gurson's model, more or less justified for applications.

Now let us mention other promising generalisations of porous plasticity to polycrystalline aggregate which introduce non homogeneous matrix material in the microscale (Rousselier and Leclercq, 2005).

Because of the first term in (7.55) $\Sigma_{eq}^2/\bar{\sigma}^2$ .Gurson's model cannot adapt to stress additivity in the polycrystalline aggregate theory. Rousselier's model (7.32) which involves a linear term in σ_{eq} can do.

We first recall some self-consistent models analogous to the one introduced for isotropic crystals by Kröner (1961) and for anisotropic crystals by Bui (1969). The self-consistent theory of plasticity originated from a rigorous result on the theory of ellipsoidal or spherical inclusions by Eshelby (1957). For a spherical inclusion in a homogeneous plastic matrix, the stress and strain inside the inclusion are both uniform. They are called eigenstress and eigenstrain. If the plastic strain of the matrix is E^p, the plastic strain of the spherical inclusion is ε^p, then the stress in the inclusion is given by Eshelby-Kröner's formula, with $\beta = (8–10\nu)/15(1 – \nu)$ (roughly $\beta \cong 0.5$)

$$\sigma_{(i)} = \Sigma + 2\mu(1-\beta)(E^p - \varepsilon^p{}_{(i)}) \tag{7.57}$$

For the correction of anisotropy of the inclusion (i) with moduli $L^{(i)}$, embedded in an isotropic matrix of moduli L_0, Kröner's formula (7.57) is generalized by Bui (1969) as

$$\sigma_{(i)} = A^{(i)}.\{\Sigma + 2\mu(1-\beta)(E^p - \varepsilon^p)\} \tag{7.58}$$

Formula (7.58) bears a close resemblance to (7.39). The localization tensor $A^{(i)}$ is given by an exact formula for a spherical inclusion (i)

$$A^{(i)} = L^{(i)}.B^{(i)}.(L_0)^{-1} \tag{7.59}$$

where $B^{(i)}$ is given by

$$B^{(i)} = \{I + R.(L^{(i)} - L_0)\}^{-1} \tag{7.60}$$

$$R_{ijhk} = \frac{3\lambda_0 + 8\mu_0}{15\mu_0(\lambda_0 + 2\mu_0)} I_{ijhk} - \frac{\lambda_0 + \mu_0}{15\mu_0(\lambda_0 + 2\mu_0)} \delta_{ij}\delta_{hk} \tag{7.61}$$

Various other modifications of (7.57) are considered in order to take account of cumulated plastic strain in cyclic loadings (Cailletaud, 1987), or viscous relaxation stress (Berveiller and Zaoui, 1979). In the last reference Eq. (7.57) is modified as

$$\sigma_{(i)} = \Sigma + 2\mu(1-\beta)\alpha(E^p - \varepsilon^p(i)), \quad \frac{1}{\alpha} = 1 + \frac{J_2(E^p)\sqrt{3}}{J^2(\Sigma)} \tag{7.62}$$

Rousselier and Leclercq (2005) proposed an extension to volumetric deformations of damaged materials

$$\sigma_{(i)} = \Sigma + 2\mu(1-\beta)[\eta I_2 \otimes I_2 + \alpha I_4]_{\cdot}(E^p \quad \varepsilon^p{}_{(i)}) \tag{7.63}$$

with $1/\eta$ and $1/\alpha$ some adjustable affine functions of $(E^p)_{eq}$. The coupled Rousselier's model and polycrystalline aggregate contains two adjustable parameters D_1 and σ_1 (f_i: volume fraction of phase (i) in a sound material)

$$\frac{\Sigma_{eq}}{1-f} + D_1\sigma_1 f \exp\left(\frac{\Sigma_m}{\rho\sigma_1}\right) - \left(\sum_{i=1}^{N} f_i\sigma_{(i)}\right)_{eq} = 0 \tag{7.64}$$

As already noted, Rousselier's model accommodates the additivity of stress at the microscopic level, but not Gurson's model.

7.3 Bifurcation problems in plasticity

Experiments on the deformation of a sheet of metal with a circular hole, as shown in Fig. 4.5, indicate two features. The structure undergoes very large plastic deformation (images 1 to 16, triggered at every two seconds) then suddenly (between images 16 and 17) necking phenomena occurs at the internal cavity in the thickness direction before crack propagation. The following scenario is likely, as described by the schematic view of Fig. 7.7: thinning of the ligament by lateral necking, then crack initiation and propagation in the thin ligament. This explains the high temperature rise observed in experiments long time before crack propagation. When the ligament thinning becomes critical a crack appears then propagates. This process occurs very rapidly. Instability phenomena occur generally in the competition between the stabilizing effect of hardening of the material and the destabilizing effect due to a geometry change.

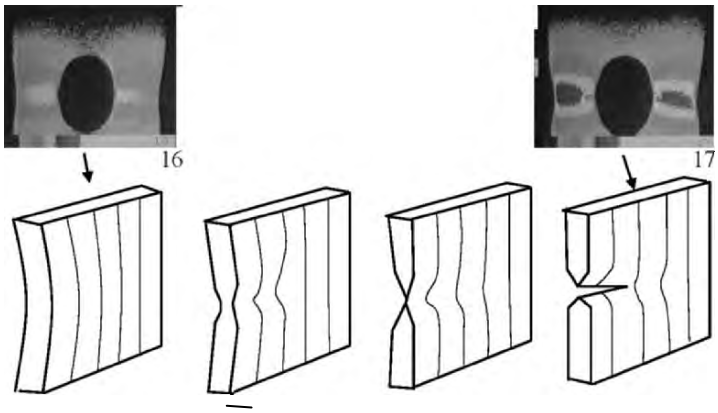

Figure 7.8: Two seconds separate images 16 and 17 of Fig. 4.5; first lateral necking thins down the ligament before in-plane necking takes place at the inner radius; then crack propagates in the thin ligament

Void damage introduces an additional destabilizing effect by increasing the softening part of the material constitutive law. Most instability analyses do not consider the material instability by void damage. Only in recent works void damage theories have been considered in instability analyses.

As far as we know, and also as pointed out by Nguyen (2000), there is no general bifurcation theory in plasticity or damage plasticity for describing all phenomena of instability. Only specific theories are known for particular cases.

The subject is very difficult, as illustrated by some further examples in Engineering mechanics and the Mechanics of materials. We do not consider here mathematical problems of instability (*) and bifurcation plasticity and damage. The readers can refer to the works by Hill (1958), Hutchinson (1973), Hutchinson and Budiansky (1974), Tvergaard and Needleman (1975), Rudnicky and Rice (1980), Triantafyllidis (1983),Petryk (1985), Benallal et al (1991). For a comprehensible and synthetic view on instability, we refer to Nguyen (2000).

Let us consider a mechanical system defined by its geometry, constitutive laws, initial conditions and loading conditions. The state variables of

(*) Instability and bifurcations are the rules in open biological systems Ω with the exchange of materials and energy, through its boundary $\partial\Omega$. They are essentially governed by chemical reactions, cell division, growth and death (apoptose), diffusion, gradient of concentration, kinematical constraints (leading to folds in the brain and fingerprints) and perhaps mechanical constraints too.

the system (current geometry, position or velocity of material points $\mathbf{y} \in \mathbb{R}^n$ in a finite dimensional space), satisfies a non-linear differential equation

$$\frac{d\mathbf{y}}{dt} = f(\mathbf{y}, \lambda) \tag{7.65}$$

where λ is some control variable. The control variable can be an initial geometry imperfection or the radius of a cavity in a *geometric instability* analysis or the width of a shear band in *a localized bifurcation* analysis, or the load function of time λ(t) in a *dynamic* instability analysis (Petryk, 1985, Nguyen, 2000).

Now let us mention some instability problems arising in Engineering mechanics and the Mechanics of materials.

1. **Necking in bars and sheets of metals**. The well known formula $\sigma = \partial\sigma/\partial\varepsilon$ of Considère (1985) determines the theoretical stress at necking of a tensile bar. Most theoretical analyses of necking predict so high a value of the critical load which would be far outside the range of practical interest (Miles, 1971). This is because critical load is sensitive to local imperfections. Moreover, there is uncertainty about the correct constitutive law to be considered for real experiments. Instabilities phenomena by necking, surface ondulations, are typically geometric instabilities.

2. **Shear band localizations**. This is a huge subject of great interest for applications in solids, structures and geomechanics, which cannot be overviewed in a few words. Let us mention the work by Benallal et al (1991) who gave the necessary and sufficient conditions for continuous localization (in a band) or discontinuous localization at the free surface. Localized shear band is associated with a plane of normal **n**, along direction **g** (**g.n** = 0). The discontinuous gradient of the velocity is of the form $[\nabla \mathbf{v}] = \mathbf{g} \otimes \mathbf{n}$. However, the nominal stress vector rate must be continuous $\dot{\theta}^{+}.\mathbf{n} = \dot{\theta}^{-}.\mathbf{n}$ or $\mathbf{n}.\mathrm{H}^{+}.\nabla\mathbf{v}^{+} = \mathbf{n}.\mathrm{H}^{-}.\nabla\mathbf{v}^{-}$. Generally, the modulus H is continuous (the same elastic or plastic loading, or elastic unloading at both sides) thus

$$(\mathbf{n}.\mathrm{H}.\mathbf{n}).\mathbf{g} = 0$$

The existence of localized shear discontinuity implies that $\det(\mathbf{n}.\mathrm{H}.\mathbf{n}) = 0$. The acoustic tensor **n**.H.**n** has been introduced by Mandel (1962), Hill (1962) in studies of accelerating waves in elasto-plastic solids.

3. **Cavitations in plasticity and viscoplasticity**. A spectacular phenomenon is observed in metal extrusion in high temperature, Fig. 7.8. There are chevron cavities periodically distributed along the extruded part of the bar. Let us consider a visco-plastic material domain Ω(t = 0) in dotted line in a steady state flow upstream the extruded section A. Pertinent

quantity like the longitudinal stress σ_{33} is time-independent and negative because of high pressure. At the extruded section, the drop of pressure and temperature make the flow strongly *time-dependent*. Suppose that the fundamental time-independent solution at negative time branches into a time T-periodic solution. If the maximum stress σ_{33} at $x_1 = A$, at time $t = t_A$ is positive and high enough for a crack to appear (crack is then moving out the extruded section), the decrease then the increase of the stress σ_{33} at $x_1 = A$, at time $t = t_A + T$ initiates a new crack and so on. The distance between cracks is VT where V is the velocity of the extruded metal. Time-periodic solution should result in a periodically spaced chevron cracks. This kind of instability is called the Hopf bifurcation, Fig. 7.9.

To understand the mathematics of such an instability, assume that the steady solution is described by some time independent relation $f(\mathbf{y}, \lambda) = 0$ or $\mathbf{y} = g(\lambda)$. Suppose that the gradient matrix $M = \partial f/\partial \mathbf{y}$ posseses a simple eigenvalue $s(\lambda) = \alpha(\lambda) + i\beta(\lambda)$ and

$\alpha(\lambda_A) = 0$, $\beta(\lambda_A) > 0$.

Other eigenvalues are assumed to have strictly negative real part. Then the fundamental branch $\mathbf{y} = g(\lambda)$ is stable up to $\lambda = \lambda_A$ corresponding to point A.

Now, we make another assumption, called the *transversality* condition (Iooss and Joseph, 1980)

$$\frac{\partial \alpha}{\partial \lambda}(\lambda_A) > 0 \tag{7.66}$$

then at $\lambda = \lambda_A + 0$ the real part of the considered eigenvalue $s(\lambda)$ gets through the imaginary axis with a strictly non zero real part value.

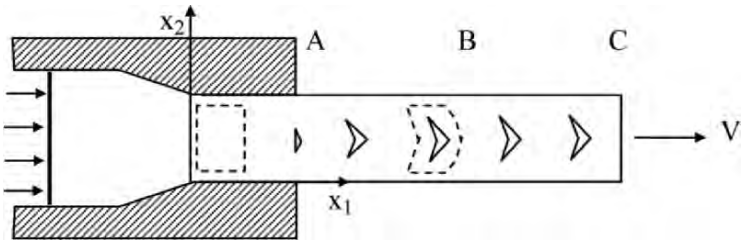

Figure 7.9: Hopf bifurcation into a periodic cracking in metal extrusion

The static curve $\mathbf{y} = g(\lambda)$ branches out into a time-periodic response, with an increasing amplitude from as $O(\lambda - \lambda_A)^{1/2}$ (Nguyen, 2000). This is the Hopf bifurcation.

Along BC, Eq. (7.65) is no longer valid since the temperature and the stress decrease to values sufficiently low for stress-strain law to become time-independent and periodic cracks to be frozen. For instance, metal in BC behaves like a plastic solid rather than a visco-plastic one at A.

Hopf's bifurcation(*) frequently occurs in fluids dynamics. For instance a steady state laminar viscous flow upstream becomes unstable downstream at the backward-facing step (Lesieur, 1997), Fig. 7.10. It is striking that features in Figs. 7.9 and 7.10 are quite similar, stable regime and unstable one with the increasing of amplitude, even if the mechanisms are different.

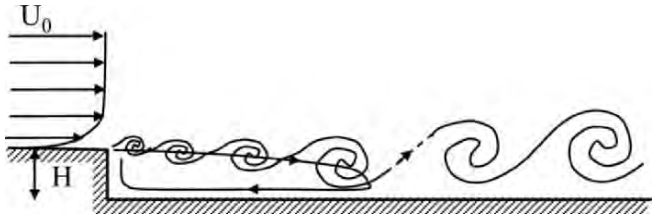

Figure 7.10: Schematic view of a backward-facing step flow (Permission of Marcel Lesieur, Turbulence in Fluids, 1997, Kluwer Acad. Publ./Springer-Verlag(**))

7.4 A finite strain theory of cavitation in solids

Cavitation in fluid is a common phenomenon which is explained by a phase change of fluid into vapor below some pressure. That is a volume of fluid is transformed into vapor. Unlike cavity formation around a solid inclusion, true cavitation in solids should be viewed as an intrinsic material and geometrical instability at some critical stress state. The appearance of a cavity from *nothing* (no defects in an homogeneous medium) for instance

(*)The following example is given in Iooss and Joseph (1980):
$dy_1/dt - (3\lambda-2\sigma)(y_1+2y_2)-y_1^2-2y_1y$, $dy/dt-(2\lambda-\sigma)(y_1+y_2)+y_1y+y_2^2$ where σ is a constant. The eigenvalues satisfy $s_1s_2=(2\lambda-\sigma)(2\sigma-3\lambda)>0$, for $\sigma/2<\lambda<2\sigma/3$ and $s_1+s_2-5\lambda-3\sigma-0$ for the bifurcation parameter $\lambda-3\sigma/5$, so that s_1--s_2 cross the imaginary axis.

(**)initiated from an inflection point in the velocity profile or Kelvin-Helmholtz's instability

in a two-dimensional problem, raises certain mathematical questions about the change of the solid domain topology, from a simple to a double connected one.

However physical considerations avoid such a difficulty because a continuum modelling of solids is nothing but an homogenization of a discontinuous medium where cavities already exist at the microscopic scale or at the atomic scale. Suppose that a stress concentration exists at a microscopic scale and results in the separation of atoms over certain large distance d, then the mean value of the stress over d is less than the initial mean stress. This happens in the coalescence of a series of small cavities into a microscopic crack. When the size of a microscopic cavity becomes of the same order of the RVE size – the Representative Volume Element of the homogenization theory – the macroscopic stress decreases and eventually vanishes. This is the process of a cavity formation from "nothing" at the macroscopic scale, which is physically the coalescence and growth of "existing" cracks and cavities at the microscopic scale. Here the change to topology is simply related to a scale change.

This process is different from the decohesion around an existing inclusion, resulting in a cavity which surrounds the imprisoned inclusion. In further loading of the material, the imprisoned inclusion remains undeformed while only the matrix undergoes deformattion.

Now, for studying the first mechanism of cavitation we will assume that a cavity of infinitesimal radius exists somewhere and will grow under favourable local stress conditions. Recent works related cavitation to bifurcation phenomenon in the framework of finite elasticity (Ball, 1982) or in rate-dependent solid, (Abeyaratne and Hou, 1989). The latter paper showed the following features in the radial traction of a sphere. Below certain stress value, the sphere with an infinitesimal cavity undergoes a homogeneous deformation. At certain critical stress, another solution exists with a non zero stress free cavity.

Let us recall the solution provided by Abeyaratne and Hou (1989) for an existing infinitesimal cavity, at the center of a spherical ball of unit radius a at time t = 0, i.e. a(0) = 1. Spherical symmetry and incompressibility are assumed. Consider a material point in one radial direction, at distance R ($0 \le R \le 1$) in the undeformed configuration. Its radial coordinate is r = f(R,t) in the current configuration at time t.

The deformation gradient tensor n spherical coordinates is

$$\mathbf{F} = \frac{\partial f}{\partial R}\mathbf{e}^R \otimes \mathbf{e}^R + \frac{f}{R}(\mathbf{e}^\theta \otimes \mathbf{e}^\theta + \mathbf{e}^\varphi \otimes \mathbf{e}^\varphi) \tag{7.67}$$

Incompressibility means $\det\mathbf{F} = 1$

$$\frac{f^2}{R^2}\frac{\partial f}{\partial R}=1 \tag{7.68}$$

Let b(t) and a(t) be the current cavity radius and the current external radius respectively. Eq. (7.68) leads to

$$r=f(R,t)=\{R^3+b^3(t)\}^{1/3} \tag{7.69}$$

$$a(t)=f(1,t)=\{1+b^3(t)\}^{1/3}$$

The current cavity b(t) radius has to be determined from the load T(t) with the initial condition for the cavity b(0)=0. The material velocity is

$$\mathbf{v}=\dot{r}(r,t)\mathbf{e}^r=\frac{b^2\dot{b}}{r^2}\mathbf{e}^r \tag{7.70}$$

and the strain rate tensor $\mathbf{D}=(\text{grad}\mathbf{v}+(\text{grad}\mathbf{v})^t)/2$ is

$$\mathbf{D}=\dot{\gamma}(r,t)\{-\sqrt{3}\mathbf{e}^r\otimes\mathbf{e}^r+\frac{1}{2\sqrt{3}}(\mathbf{e}^\theta\otimes\mathbf{e}^\theta+\mathbf{e}^\varphi\otimes\mathbf{e}^\varphi)\} \tag{7.71}$$

with the strain rate

$$\dot{\gamma}(r,t)=2\sqrt{3}\,\frac{\dot{r}(r,t)}{r} \tag{7.72}$$

and upon integrating the strain

$$\gamma(r,t)=2\sqrt{3}\,\ln\frac{r}{R}=\frac{2}{\sqrt{3}}\ln\frac{r^3}{r^3-b^3} \tag{7.73}$$

On the other hand, the Cauchy stress and the deviator of the Cauchy stress are respectively

$$\sigma=\sigma_{rr}\mathbf{e}^r\otimes\mathbf{e}^r+\sigma_{\theta\theta}(\mathbf{e}^\theta\otimes\mathbf{e}^\theta+\mathbf{e}^\varphi\otimes\mathbf{e}^\varphi) \tag{7.74}$$

$$\mathbf{s}=\tau\{-\frac{2}{\sqrt{3}}\mathbf{e}^r\otimes\mathbf{e}^r+\frac{1}{\sqrt{3}}(\mathbf{e}^\theta\otimes\mathbf{e}^\theta+\mathbf{e}^\varphi\otimes\mathbf{e}^\varphi)\} \tag{7.75}$$

with $\tau=(s_{\theta\theta}-s_{rr})/\sqrt{3}$. The equilibrium equation is written as

$$\frac{\partial\sigma_{rr}}{\partial r}-\frac{2\sqrt{3}}{r}\tau=0 \tag{7.76}$$

Abeyaratne and Hou (1989) considered the following constitutive law

$$\tau = g(\dot{\gamma}, \gamma) \equiv g_1(\gamma) + \mathrm{sgn}(\dot{\gamma})\left|\dot{\gamma}\right|^m g_2(\gamma) \tag{7.77}$$

where m>0 and $g_1(\gamma)$, $g_2(\gamma)$ are arbitrary non negative functions.
The boundary conditions are the stress free condition on the cavity and the traction T(t) at the outer radius a, for t≥0

$$\sigma_{rr}(b,\ t) = 0$$

$$\sigma_{rr}(a,\ t) = \frac{T(t)}{a^2} \tag{7.78}$$

7.4.1 Abeyaratne and Hou's Solution in finite elasticity

Upon integrating the equilibrium equation and using the boundary condition, one gets

$$T(t) = 2\{1 + b^3(t)\}^{2/3}\sqrt{3}\int_b^{(1+b^3)^{1/3}} g(\dot{\gamma}(r,t), \gamma(r,t))\frac{dr}{r} \tag{7.79}$$

$$\dot{\gamma}(r,\ t) = 2\sqrt{3}\ \frac{b^2(r,\ t)\,\dot{b}(r,\ t)}{r^3} \quad \text{and} \quad \gamma(r,t) = \frac{2}{\sqrt{3}}\ln\frac{r^3}{r^3 - b^3}$$

Inserting the latter expressions of $\dot{\gamma}$ (r,t) and γ (r,t) one gets an *implicit* differential equation, with b(0)=0, to determine the void evolution b(t) as a function of the load T(t). Now, using the constitutive equation (7.77), Eq. (7.79) can be written as

$$b^m T(t) = \frac{2}{\sqrt{3}}\{1 + b^3(t)\}^{2/3}\left\{\mathrm{sgn}(\dot{b})(2\sqrt{3}\left|\dot{b}\right|)^m \int_b^{1/(1+b^3)} g_2\left(\frac{2}{\sqrt{3}}\ln\frac{1}{u}\right)\frac{du}{(1-u)^{1-m}}\right.$$
$$\left. + b^m\int_b^{1/(1+b^3)} g_1\left(\frac{2}{\sqrt{3}}\ln\frac{1}{u}\right)\frac{du}{(1-u)}\right\} \tag{7.80}$$

Finite elasticity

In the case $g_2(\gamma)=0$, Eq. (7.80) has two solutions:

i) First solution b=0.

The infinitesimal cavity size remains unchanged for any load $T(t)<T_0$ given below.

ii) Second solution b(t) given implicitly by

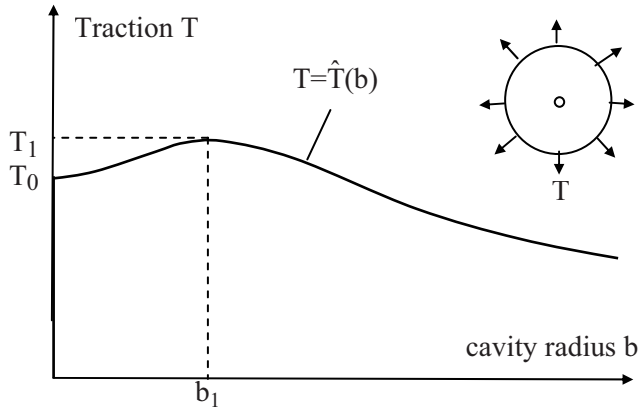

Figure 7.11: Bifurcation diagram in the cavitation of an existing infinitely small spherical cavity in finite elasticity, Abeyaratne and Hou (1989)

$$T(t)=\frac{2}{\sqrt{3}}\{1+b^3(t)\}^{2/3}\int_b^{1/(1+b^3)} g_1\left(\frac{2}{\sqrt{3}}\ln\frac{1}{u}\right)\frac{du}{(1-u)} \tag{7.81}$$

The cavitation solution is similar to Ball's result (1982). The right hand side of (7.81) is a function of b denoted by $\hat{T}(b)$. Fig. 7.11 shows the equilibrium curve $T=\hat{T}(b)$, which is the *post-bifurcation* state, starting from point $(0,T_0)$ where the critical stress T_0 is given by

$$T_0=\frac{2}{\sqrt{3}}\int_b^1 g_1\left(\frac{2}{\sqrt{3}}\ln\frac{1}{u}\right)\frac{du}{(1-u)} \tag{7.82}$$

The necessary and sufficient condition for this cavitation solution is that the right hand side of Eq. (7.82) be strictly positive. No equilibrium solution exists for load higher than T_1. Dynamic effects must be introduced for $T>T_1$. Load T_1 appears to be the ultimate load in the quasistatic deformation theory of plasticity, in finite strain condition.

7.4.2 Solution for a creeping material

In the case of creep, the constitutive law considered by Abeyaratne and Hou (1989) is

$$g(\dot{\gamma},\gamma)=\mu\gamma^n(1+\mathrm{sgn}(\dot{\gamma})|\dot{\gamma}|^m),\ n>1,\ m>0, \tag{7.83}$$

similar results have been obtained by Abeyaratne and Hou (1989). The equilibrium curve solution of the cavitation problem in finite elastiticity separates the plane (b,T) into two domains, contraction zone and expansion zone. Below the curve, points (b(t), T=cte) evolve towards the solution $b=0$.

The existence of the stable branch between 0 and b_1 which arrests the expansion or the unstable branch above b_1 which contracts existing cavities in its left hand side, will lower the porosity in comparison with theories based on small strain assumption, Fig. 7.12. Applications of this theory to ductile fracture is very promising. For cavities under certain size, say $b < b_{max} \cong 2b_1$ a threshold stress can be introduced, $T_{cr} \cong T_1$ (or T_0) so that theories of cavity growth in viscoplastic medium, as given in the literature, are good for $T > T_{cr}$, and that they give over-estimated prediction of porosity rate for $T < T_{cr}$.

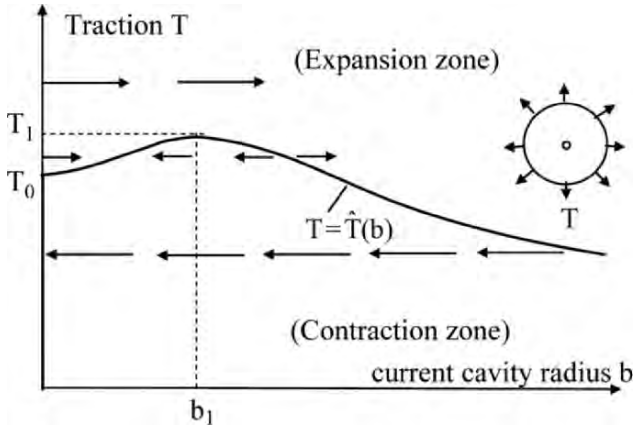

Figure 7.12: Stability analysis for a creeping matrial, $g_1(\gamma) = g_2(\gamma) = \mu\gamma^n$. Stable branch for small cavity at low load $T<T_0$. For load $T>T_1$, a vanishing radius cavity will grow indefinitely. In a pure creeping material, with $g_1(\gamma) = 0$, $g_2(\gamma) = \mu\gamma^n$, there is no contraction zone: the equilibrium state $b=0$ is unstable at all loads (Abeyaratne and Hou, 1989)

Chapter 8

The Fluid-Filled Crack

8.1 Introduction

There are many applications of fluid-filled crack problems, in engineering and materials science: fluid flows in pipes or structures, hydraulic fracturing of rocks for the oil industry, interaction between a fluid and a cracked solid. This chapter is devoted to these problems, for both static and dynamic fluids. It illustrates many concepts encountered in fluid-filled crack problems. Problems involving the interaction between solid mechanics, with a medium slightly perturbed with respect to its initial configuration, and fluid mechanics, with an Eulerian description of fluid flow, are not always easy to handle. The example of the Griffith crack in a two-dimensional linear elastic solid illustrates this difficulty. Near the crack tips, the crack opening displacement arising from the fluid pressure acting on the crack faces, cracks open near tips as $0(r^{1/2})$. The pressure p is applied on a crack in its *current* deformed configuration – the normal vector $\mathbf{n}$ approaches the unit vector $\mathbf{e}^1$ continuously at the right crack tip – while the stress, the strain and the displacement in the solid domain are measured in the *initial* undeformed configuration, with a fixed normal to the crack $\mathbf{n} = (0, \pm 1)$. Three possible models of fluid-filled cracks avoiding such difficulties which will be considered in this chapter:

i) The first model ignores the local action of the pressure and accounts only for its global effect. For instance in a closed pipe of mean radius R and small thickness e subjected to some pressure p, the radial stress at the interior radius is $\sigma_{rr} = -p$, axial stress is $\sigma_{zz} = p\,R/(2e)$, and the hoop stress is $\sigma_{\theta\theta} = pR/e$. The global stress is twice as high as the axial stress and much higher than the local stress σ_{rr}, which can be neglected.

ii) The second model considers a crack with *zero* toughness $K_{Ic} = 0$, so that $[[u_2]] = O(r^{3/2})$, (Detournay, 1999).

iii) The third model considers a fluid-filled crack with a *gap* (or lag) near the tip (Abe et al, 1976; Abou-Sayed et al, 1978; Bui, 1996).

8.2 The leak before break inverse problem

This problem arises in the context of maintenance operations of nuclear structures. Suppose that a pressurized pipe containing hot water leaks through some small longitudinal crack. The knowledge of the design geometry of the pipe, the crack geometry and the thermo-mechanical conditions yields a direct problem which consists in the determination of the fluid flow rate Q and the stress-intensity factor K_I. Nothing is basically new in this problem. The only possible novelties lie in the choice of fluid flow models, or in methods for solving the fluid flow rate problem for incomplete data with regard to either the loading, as shown in Fig. 8.1, or the crack shape. For instance, to determine the stratified interface between the liquid and the vapor, one has to deal with an inverse problem with data consisting of measured flux and temperature on the external surface of the pipe.

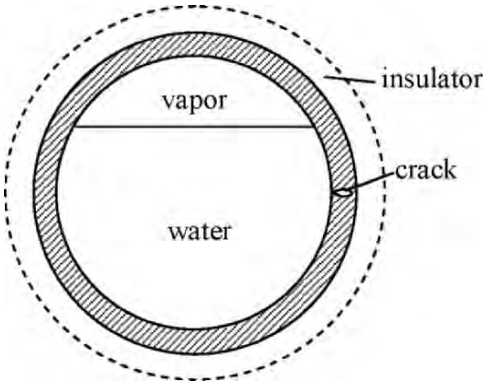

Figure 8.1: An inverse problem in Nuclear Engineering to determine a crack

Let us consider the former problem of a fluid flow occupying the whole pipe, in the presence of some insulator prohibiting any measurement from the outside, including that of the crack length. To determine the critical crack length before break, we have to solve an inverse problem, using the leakage rate of water as data for the inversion. This is the Leak Before Break (LBB) inverse problem in Nuclear Engineering. Given a physical model, solutions to direct problems yield a multi-parametric model of the fluid flow rate which can be compared to experiments, in order to determine the optimal solution with respect to the crack geometry.
Generally, no good solution exists in this problem of fitting theoretical and experimental results, because the physical model under consideration is

inadequate to describe the experiments. The main reason is that the experimental flow rate Q(a) behaves like some power law of the crack length. Models of the fluid flow rate yield some power law too, $Q = Ca^m$, the coefficient m here depending strongly on the physical model of fluid flow. To solve the LBB problem, one has to find the best possible *physical* models, describing laminar flow or turbulent flow or possibly both regimes in different fluid domains in the breach of the opening crack., rather than the best parameters of a given physical model as is usual in the parametric optimization of systems.

In what follows, we make a review of existing models of fluid flow through a longitudinal crack in a pipe and introduce some new ones. The first model is devoted to turbulent flow in the crack breach and the second one to a laminar flow.

8.2.1 Empirical models of fluid flow in a crack breach

The following characteristics are considered in models of fluid flow:

R : mean radius of the pipe; R_1, R_2 : internal and external radii

H : thickness

2a : longitudinal crack length

2b : maximal opening of the rectangular crack of dimensions 2a×h halfway through the thickness

E, ν : Young's modulus and Poisson's ratio respectively

R_e : Reynolds number, $\overline{U}$: mean velocity

Δp/h : pressure gradient through the pipe thickness.

The physical constants of the fluid are those of water at the temperature and pressure of interest. The mass per unit volume $\rho(=\rho_0)$ and the kinematic viscosity are considered as constant. Application of the pressure p results in an elliptic crack opening $v(x_1)$ and a minor axis is b(p,a) given by (in plane stress conditions)

$$v(x_1) = \frac{pR}{4h\mu}(\kappa+1)\sqrt{a^2 - x_1^2} \tag{8.1}$$

$$b(p,a) = \frac{2pRa}{hE} \tag{8.2}$$

Perfect fluid

The simplest possible model of fluid flow rate corresponds to a perfect fluid, the flow rate then follows from Bernoulli's classical theorem as

$$Q_0 = \pi a\, b(p,a)\left(\frac{2p}{r}\right)^{1/2} \tag{8.3}$$

Substituting (8.2) into (8.3) we obtain $Q_0 \propto a^2 p^{3/2}$.

A lubrication theory

A simple model of viscous flow is suggested by the lubrication theory for a laminar flow in a *constant* elliptical breach of area $S = \pi ab$.

The velocity profile is then parabolic, for a small ratio b/a, one gets the flow rate

$$Q_1 = \frac{\pi p a^3 b^3(p,a)}{4\rho\ h(a^2+b^2(p,a))} \cong \frac{\pi p a b^3(p,a)}{4\rho\ h} \tag{8.4}$$

Now let us mention some other turbulent flow models.

Classical turbulent flow models

Turbulent flow models are classical for circular tubes, but less so for other breach geometries. Most works considered some "equivalence" with a rectangular section, with the same cross-section, particularly in lubrication theory. Let us recall two models of fluid flow in pipes, which can be extended to the elliptical breach considered in the leak before break problem:

i) Turbulent flow along a smooth wall,

ii) Turbulent flow along a rough wall.

Depending on the relative roughness d/R, or equivalently to the Reynolds number $R_e = 2RU/\eta$, different regimes can arise

- High Reynolds number or smooth surface ($d/R < 19.2\ (R_e)^{-7/8}$)

Introduce the pressure gradient $\lambda = 2pRL^{-1}(\rho U^2/2)^{-1}$. The relationship between R_e and λ reads

$$\lambda^{-1/2} = 0.85\ \mathrm{In}\ (\lambda^{1/2}R_e) - 0.8 \qquad \text{(V. Karman)} \tag{8.5}$$

$$\lambda^{-1/2} = 0.85\ \mathrm{In}\{2.5\lambda^{1/2}R_e + 0.27\ d/R\}. \text{ (Colebrook)} \tag{8.6}$$

- Low Reynold number or rough surface $d/R > 19.2\ (R_e)^{-7/8}$

The coefficient λ is independent of R_e and depends only on the relative roughness through the formula

$$\lambda = \lambda_0 = \{A\ \ln(d/R) + B\}^{-2} \tag{8.7}$$

where A and B are material constants.

Eqs. (8.6) and (8.7) cannot be used in nuclear vessels because d/R is inaccessible to experiments. Eq. (8.7) for a circular tube yields the following Darcy-Chézy formula, where C_1 is related to the nature of the solid surface

$$Q_2 = C_1 \left\{ p \frac{R^5}{L} \right\}^{1/2} \tag{8.8}$$

Turbulent flow with logarithmic velocity profile

Now we consider an adaptation of V. Karman's model for a circular tube to a flat cavity, whose surfaces are very close to each other. The idea consists in using the well known boundary layer solution for viscous flow near a planar wall, duly completed using a symmetry argument. Near the wall the fluid flow is laminar and the velocity is given by

$$U(y) = ky, \quad 0<y<\varepsilon \tag{8.9}$$

where y is the coordinate along the normal. Outside this boundary layer of thickness ε, the logarithmic profile solution is dominant (Landau and Lifschitz, 1971)

$$U(y) = \frac{\nu_0}{0.417} \ln \left(\frac{\nu_0 y}{\eta}\right) + \nu_0 \tag{8.10}$$

where ν_0 is some constant to be determined by choosing $k = (\nu_0)^2/\eta$ and $\varepsilon = \eta/\nu_0$, we ensure the continuity of the velocity between the laminar and turbulent zones. The logarithmic profile function is assumed to hold above the major axis of the ellipse $y = \bar{b} = \pi\beta/4$, while a symmetric profile solution is considered below the major axis. This kind of approximation has been considered in models of fluid flow in circular tubes. Here we use the same approximation to derive the mean velocity, in the presence of a boundary layer, as

$$\bar{U} = \frac{\nu_0}{0.417} \ln \left(\nu_0 \frac{\bar{b}}{\eta}\right) + \cdots \tag{8.11}$$

where the omitted terms are small, for large $\nu_0 \bar{b}/\eta$. It remains to establish the link between the pressure gradient p/h and the constant ν_0. For this, we write the equilibrium condition between the force at the input section $4pa\bar{b}$ and the viscous friction force on the lateral crack wall. The shear stress is $\tau = \rho\eta\partial U/\partial y = \rho(\nu_0)^2$ and the viscous resistance is thus $4ah\rho(\nu_0)^2$, so that

$$p = \rho h v_0^2 / \bar{b} \tag{8.12}$$

Eqs. (8.11) and (8.12) parametrically determine the pressure as a function of the mean velocity with the aid of the ancillary variable.

Finally the fluid flow rate is given by

$$Q_3 = 2.4\pi ab \left\{ p \frac{\bar{b}}{\rho h} \right\}^{1/2} \ln \left\{ \frac{\bar{b}}{\eta} (p \frac{\bar{b}}{\rho h})^{1/2} \right\} \tag{8.13}$$

where $\bar{b} = \pi b/4$ and $b = 2pRah/E$. Applicability of (8.13) requires that the argument of ln(·) be greater than 1. This model provides a relation between R_e and λ similar to Karman's solution for tubes

$$\lambda^{-1/2} = (1/0.83) \text{ In } (\lambda^{1/2} R_e) - 1.66 \tag{8.14}$$

$$\lambda = \frac{2p\bar{b}}{h} \left\{ \frac{1}{2} \rho^{-2} \right\}^{-1} \tag{8.15}$$

$$R_e = 2 \frac{\bar{b}\bar{U}}{\eta} \tag{8.16}$$

The main interest of Eq. (8.13) is that the expression of Q_3 does not depend on the roughness ratio d/R.

Experiments have been carried out on tubes with the following geometrical and physical constants.

$p = 10^7$ Pa (=100 bars), $R = 10^{-2}$(m), $h = 10^{-3}$(m)

$E = 2.10^{11}$(Pa), $\nu = 0.3$

$\rho = 7.25$ kg/m^3 (water at 300°C)

$\eta' = 1.38\ 10^{-7}$(m^{2}s^{-1}) (kinematic viscosity $\eta' = \eta/\rho$).

Experimental points (*: Experiments FC), Fig. 8.2, show a remarkable agreement with model (8.13) for a < 10mm corresponding to a flow rate of 200 *l*/hour. For a<10mm, model (8.13) gives higher results than experiments, which means that it is conservative for very small cracks. Designers appreciate this feature of the model. However, for large crack, it gives too low prediction and thus becomes non conservative.

Consider a leakage rate visible to the naked eye, corresponding to, say, 2a = 5mm. The best fit of experimental and theoretical curves, for model (8.3), is then achieved by defining $Q_0' = 0.3Q_0$.

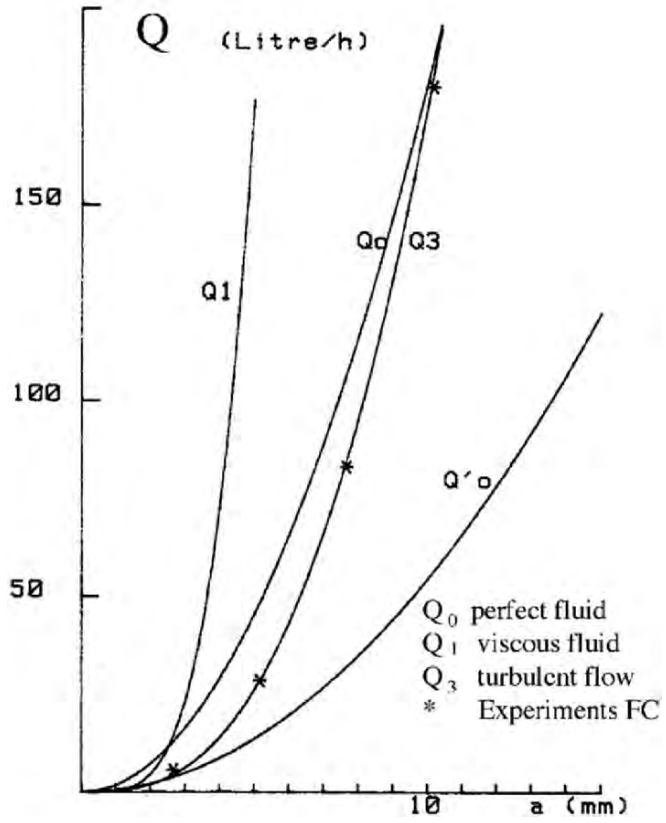

Figure 8.2: Fluid flow rate Q through a longitudinal crack of length 2a. Comparison between theories and experiments performed at FC Dept. (R&D, Electricité de France). Model (8.13) combines a boundary layer and a logarithmic profile velocity

8.2.2 Variable breach area

Generally, the breach of a longitudinal crack in a cylindrical shell is not constant. This is a consequence of the theory of cracked shells of Bergez and Radenkovic (1972). One of the principal curvatures of the breach surface vanishes (in the radial direction), so that the flow is either divergent (*bulging* effect) or convergent (*pinching* effect). According to Krent (1978), there are two flow regimes governed by his shell parameter β

$$\beta = a\frac{\left\{12(1-\nu^2)\right\}^{1/4}}{\sqrt{Rh}} \tag{8.17}$$

$\beta < 4.78$: Divergent flow (bulging effect). The radial stream lines emerge from a line Oz parallel to the cylinder axis OZ, Fig. 8.3 (a)
$\beta > 4.78$: Convergent flow (pinching effect). The radial stream lines converge to a line Oz parallel to the cylinder axis OZ, Fig. 8.3 (b).
The half-opening displacement $b(x_3)$ is an affine function of the coordinate x_3 (the coordinate through the thickness). Therefore we shall take account for the variation of the flow section, like in lubrication theory. However, in contrast to the lubrication theory which is based on the assumption of an unidimensional flow, we shall derive the exact solution for a *three-dimensiona'* fluid flow. The equation of the crack surface, in polar coordinates r, θ, z, is

$$f(\theta, z) = 0 \tag{8.18}$$

The section at r_m corresponding to the mid shell surface (r is the distance to the polar axis Oz, r_m corresponds to $x_3 = 0$), corresponding to the mid-surface of the shell, is the ellipse

$$\frac{z^2}{a^2} + \frac{r_m^2\theta}{b_0^2} - 1 = 0 \tag{8.19}$$

where $b_0 = b\ (x_3 = 0)$. Note that polar axis Oz is on the concave side of the shell for divergent flow and on the convex side for convergent flow. Let r_1, r_2 be the internal and external radii of divergent flow respectively (or the external and internal radii of convergent flow). Then

$$r_m = \frac{r_1 + r_2}{2} \tag{8.20}$$

Let $\alpha = b_0/r_m$ be the half angle of the breach at the center. Fluid particles move along radial lines, defined by the angle $\omega(z)$, $|\omega(z)| < \alpha$. On the wall, $f(\theta, z) = 0$ or $\theta = \pm\,\omega(z)$, and the fluid velocity is zero.

Mechanical aspects of the breach

When subject to the pressure p, or to the hoop stress $\sigma = pR/h$, crack opens proportionally to $x_3 = r - r_m$. The stress intensity factor is given by (Bergez and Radenkovic, 1972)

$$K_I(x_3) = \sigma\sqrt{\pi a}\left(K_{mm} + 2\,K_{bm}\frac{x_3}{h}\right) \tag{8.21}$$

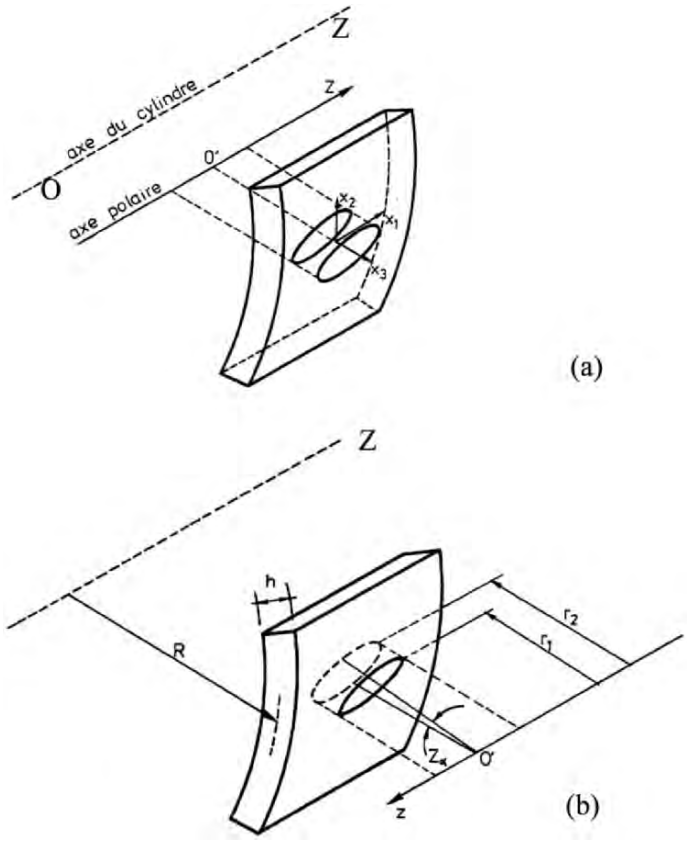

Figure 8.3: (a) Divergent flow for $\beta < 4.78$; Divergent flow (bulging); (b) Convergent flow (pinching) for $\beta > 4.78$. The breaches in either of two cases are ellipses with constant major axis 2a and variable minor axis $2b(x_3)$

The coefficients K_{mm}, K_{bm} here have been evaluated by Krent (1978) and are given in Tables A and B, as functions of R/h and β. These coefficients allow for r_1, r_2, b_0 and α to be calculated as

$$r_1 = \frac{h}{2} \left(\frac{K_{mm}}{K_{bm}} - 1 \right)$$

$$r_2 = \frac{h}{2} \left(\frac{K_{mm}}{K_{bm}} + 1 \right) \qquad \text{(divergent case } K_{bm} > 0) \qquad (8.22)$$

Table A. $K_{mm}(\beta)$

β	R/h = 10	R/h = 50
0.	–	–
0.25	1.017	1.015
0.50	1.063	1.058
0.75	1.129	1.121
1.00	1.00	1.201
1.5	1.409	1.396
2.0	1.635	1.620
3.0	2.121	2.102
4.0	2.615	2.595
5.0	3.102	3.079
6.0	3.577	3.552
7.0	4.042	4.014
8.0	4.497	4.464
9.0	4.944	4.905
10.0	5.387	5.340

Table B. $K_{bm}(\beta)$

β	R/h = 10	R/h = 50
0.	–	–
0.25	0.0264	0.0236
0.50	0.0611	0.0571
0.75	0.0933	0.0900
1.00	0.1211	0.1196
1.50	0.1610	0.1647
2.0	0.1807	0.1909
3.0	0.1673	0.1920
4.0	0.0949	0.1346
◄------(β = 4.78)------►		
5.0	−0.025	0.0292
6.0	−0.183	−0.115
7.0	−0.373	−0.292
8.0	−0.590	−0.496
9.0	−0.830	−0.723
10.0	−1.091	−0.971

$$r_1 = \frac{h}{2}\left(1 + \frac{K_{mm}}{K_{bm}}\right)$$
$$r_2 = \frac{h}{2}\left(1 - \frac{K_{mm}}{K_{bm}}\right) \qquad \text{(convergent case } K_{bm} < 0\text{)} \tag{8.23}$$

Solution of the three-dimensional fluid flow problem

Now, having specified the geometry of the cracked cylinder in its undeformed state, we investigate the laminar fluid flow through the breach. The hypothesis of laminar fluid flow is not applicable to "GV tubes" under normal service conditions which imply turbulent flow. Other applications should therefore be in one's mind when considering this model. We do not fix the breach shape yet. We shall determine instead the function $f(\theta,z)$ which characterizes the breach by Eq. (8.18). The radial velocity is searched in the form

$$U(r,\theta,z) = \frac{f(\theta,z)}{r} \tag{8.24}$$

The radial component of the term $(\nabla\mathbf{U}).\mathbf{U}$ of the Navier-Stokes equation is of order $O(U^2/r_m)$. On the other hand the viscous term of order $\eta'U/b^2$ with $U = 100ms^{1}$, $r_m = 10^{1}m$, $\eta' = 10^{-6}m^2s^{-1}$ and $b = 10^{-5}m$, is about 10 times larger. We do not adopt the simplified assumption of one dimensional incompresible fluid flow of lubrication theory since the velocity vector is radial and depends on all three coordinates r, θ, z. We look for a solution of the linearized equations

$$\frac{1}{\rho}\frac{\partial p}{\partial r} + \eta'\left(\frac{1}{r^3}\frac{\partial^2 f}{\partial\theta^2} + \frac{1}{r}\frac{\partial^2 f}{\partial z^2}\right) = 0$$

$$-\frac{1}{\rho r}\frac{\partial p}{\partial\theta} + 2\eta'\frac{1}{r^3}\frac{\partial f}{\partial\theta} = 0 \tag{8.25}$$

$$-\frac{1}{\rho}\frac{\partial p}{\partial z} = 0$$

with the following boundary conditions:

$p = p_0$ at the internal radius

$p = 0$ at the external radius

$f(\theta, z) = 0$ on the breach wall (adherence condition).

It remains to determine the domain of validity of Eq. (8.19) of the elliptic breach. Eliminating p in (8.25) we obtain

$$\frac{\partial^3 f}{\partial \theta^3} + 4\frac{\partial f}{\partial \theta} = 0$$
$$\frac{\partial^3 f}{\partial \theta \partial z^2} = 0 \tag{8.26}$$

A solution of (8.26) is

$$f(\theta, z) = A\cos(2\theta) + B\, z^2 + C \tag{8.27}$$

Let us take the following values for the constants A, B, and C

$$A = \frac{\gamma}{2\alpha^2}, \qquad B = -\frac{\gamma}{a^2}, \qquad C = \gamma\left(1 - \frac{1}{2\alpha^2}\right) \tag{8.28}$$

Then we obtain

$$f\ \theta, z) = \gamma\left\{\frac{1}{2\alpha^2}\cos(2\theta) - \frac{z^2}{a^2} + 1 - \frac{1}{2\alpha^2}\right\} \tag{8.29}$$

Formally, Eq. $f(\theta, z) = 0$ with function f given by (8.29) and Eq. (8.19) are different. Nevertheless, considering that the maximum angle of the breach is small, expanding the right hand side of (8.29) up to order θ^2, and remembering that $\alpha = b_0/r_m$ we obtain the *same* elliptical breach (8.19)

$$f\ \theta, z) = \gamma\left(-\frac{r_m^2\theta^2}{b_0^2} - \frac{z^2}{a^2} + 1\right) = 0 \tag{8.30}$$

This three-dimensional solution for the laminar flow through a longitudinal crack is exact. The velocity, pressure and flow rate easily follow from there.

8.3 Wear mechanics

This important topic in Engineering deals with the couplings between problems of contact with fracture and fluid mechanics. Inverse problems are implied by the analysis of the unknown properties of the interface between

solids in contact. A sliding wear contact between two elastic solids is typically a nonlinear problem. On the one hand, the contact problem itself is nonlinear even if there is no wear; on the other hand, the presence of torn particles changes the properties of the interface to some extent depending on the rate of detached particles and on their unknown mass density in the so-called *third-body* which is an aggregate film composed of solid particles and a lubricant fluid.

Most works on wear are restricted to the global description of wear, through the coefficient μ of Coulomb's friction law and the lubricant parameter $L = \eta V/p$ (where η is the fluid viscosity, V the relative velocity between sliding solids, p the pressure). Seldom references considered the couplings between the micro-mechanisms of detachment of particles feeding the third body and the macroscopic description of stress and strain in solids. Let us remind some experimental results.

Experiments on sliding contact and wear, as observed in Stribeck's curves, Fig. 8.4, provide a relation between $\mu = \tau/p$ (τ is the m ean shear stress) and L:

Regime (I), Coulomb's friction coefficient is constant when the solid surfaces are directly in contact; this notably occurs in the case of dry friction;

Regime (II) of instability;

Regime (III) of mild wear, called the *hydrodynamic* regime, where $\mu(L) \cong a + bL$, or for small a, $\mu(L) \cong bL$. The latter law means that $\mu = b\eta V/p$ is simply related to the laminar viscous fluid flow. The coefficient $b\eta$ is not considered in the above-mentioned paper as a constant but rather as a coefficient which evolves with the volume fraction φ of debris, $b\eta = f(\varphi)$.

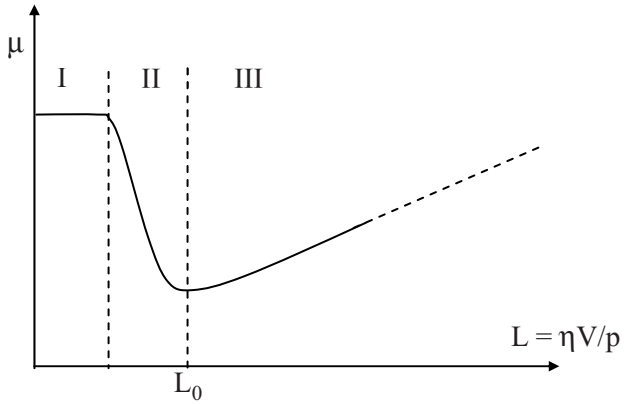

Figure 8.4: Stribeck's curve with friction coefficient $\mu = \tau/p$, lubricant coefficient $L = \eta V/p$, fluid viscosity η, relative velocity V, pressure p and shear τ

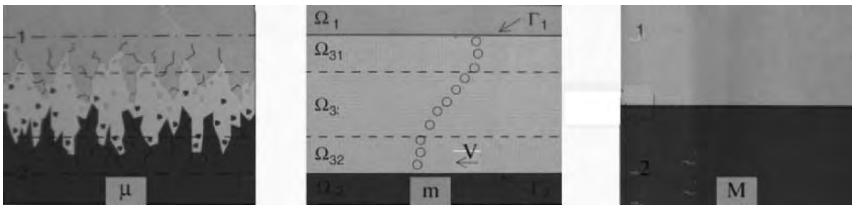

Figure 8.5: Micro description (μ) of solids Ω_1 and Ω_2 with adjacent damaged zones Ω_{31} and Ω_{32} where debris are produced by wear on their boundaries Γ_i; meso-scale description (m) of the homogenized third body Ω_3; macroscopic description (M) of the sliding contact between solids Ω_1 and Ω_2 with the volume fractions of debris as internal parameters (from, Dragon-Louiset, 2001)

The hydrodynamic regime of mild wear, in the presence of the third body, has been investigated by Dragon-Louiset (2001), Dragon-Louiset and Stolz (1999), in the framework of thermodynamics of irreversible processes. Consider the worn system shown in Fig. 8.5, consisting of two solids in sliding contact Ω_1 and Ω_2. Due to the tearing off of debris from either of two solids, one considers that the interface region is a mixture of debris dispersed in a viscous fluid. Let us consider a less general model than the one proposed by Dragon-Louiset (2001), by neglecting the intermediate zones Ω_{31} and Ω_{32}, and considering that the tearing off of debris occurs at the boundary Γ of Ω_2 denoted hereafter by Ω, and that the upper solid Ω_1 is undeformable.

8.3.1 Wear criterion and wear rate

The criterion of tearing off of particules adopted is similar to the usual one in fracture mechanics; it uses the energy-release rate, applicable to elastic-brittle materials. Let us define the function

$$g = \mathbf{n}.\sigma.\nabla\mathbf{u} - \rho\psi \quad \text{in the sound elastic zone } \Omega, \tag{8.31}$$

where $\mathbf{n}$ denotes the outward unit vector normal to the interface, σ the stresses, $\mathbf{u}$ the displacement vector, and ψ the free energy of the sound zone. Assuming the existence of some threshold energy g^s, the wear criterion reads

$$G(\sigma) \equiv g - g^3 - g^s < 0 \quad \text{(no wear)} \tag{8.32}$$

$$G(\sigma) \equiv g - g^3 - g^s \geq 0 \text{ (wear)} \tag{8.33}$$

The wear rate is assumed to be given a priori by the following macroscopic heuristic law

$$v = F(\sigma) \text{ when } G(\sigma) \geq 0 \tag{8.34}$$

Considerations of macroscopic stress and displacement at the boundary Γ to describe the wear mechanisms at a microsopic scale imply some kind of coupling between the two scales.

The rate of debris production depends on the macroscopic stress σ at the interface. The stress σ in Ω arises from the action of the rigid punch Ω_1 acting on the boundary of Ω. In the moving frame tied to the punch, the solid Ω slides with the velocity $-V$.

Let x, y (instead of x_1, x_2) denote the coordinates. The third body is made of a mixture of solid debris and fluid. The interface extends along Ox, $-a \leq x \leq a$, with a wake $x \leq -a$.

Let $e(x)$ be the thickness of the interface. The third body is characterized by the volume fractions of solid $\varphi_s(x)$ and the fluid $\varphi_f(x) = 1 - \varphi_s(x)$. Being a geometrical parameter, the volume fraction $\varphi_s(x)$ allows for the consideration of *stick* phenomena for high values of this parameter. For example, the shear flow becomes impossible for the compact hexagonal arrangement of circular debris of equal radius, with $\varphi_s(x) = 62\%$, (Dragon-Louiset, 2001).

One expects that the mechanical property of the mixture is governed by the internal parameter φ_s.

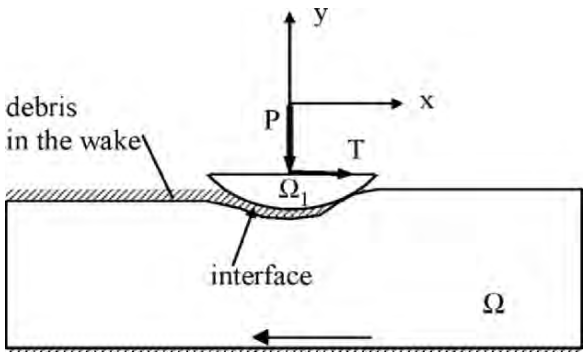

Figure 8.6: A punch sliding on an elastic half-plane and the third body interface. Moving coordinates are used to describe the solid-fluid-solid interaction. The debris are teared off from the solid Ω

8.3.2 Conservation of mass

The volume fraction of the solid is simply denoted by $\varphi \equiv \varphi_s$. The equations of conservation of mass of both phases can be written, in the steady state, in the form

$$\frac{\partial}{\partial x}\left[e(x)\varphi(x\ \rho_s v_x(x)\right] - \alpha\rho_s v(x) = 0 \text{ (solid)} \tag{8.35}$$

$$\frac{\partial}{\partial x}\left[e(x)(1-\varphi(x))\rho_f v_x(x)\right] = 0 \text{ (fluid)} \tag{8.36}$$

where $\alpha\rho_s v(x)$ is the source term arising from the tearing off of debris at the rate v(x), which feeds the interface through Γ; α represnts the proportion of debris which diffuses toward the third body, $(1-\alpha)$ the proportion of debris which are "imprisoned" by asperities and are removed from the contact zone witout modyfying the rheology of the third body, and ρ_s, ρ_f are the densities of the solid and the fluid, respectively. The relation between $\varphi(x)$ and v(x) (mean velocity $v_x(x) = -V/2$) reads

$$\varphi(x) = -\frac{2\alpha}{Ve(x)}\int_a^x v(u)du \quad (x \le a) \tag{8.37}$$

Considering a linear variation of the flow through the thickness, one gets

$$e(x) = \frac{e_0}{1-\varphi(x)} \tag{8.38}$$

Eqs. (8.37), (8.38) are equivalent forms of (8.35), (8.36) respectively. Provided that v(x) is known, Eqs. (8.37) and (8.38) yield the volume fraction of the solid $\varphi(x)$ as

$$\varphi(x) = \frac{A(x)}{1+A(x)}, \qquad A(x) = -\frac{2\alpha}{Ve_0}\int_a^x v(u)du \tag{8.39}$$

Equation $\varphi(x) \cong A(x)$ stands as a good approximation of the first Eq.(8.39).

8.3.3 Rheology of the third body

Because of the smallness of the ratio e_0/a, the behavior of the third body under compression can safely be represented by the following simple uniaxial stress strain law in the form

$$\mathrm{k}\ \varphi)\sigma_{yy} = \frac{c_1}{\mathrm{e(x)}}(\mathrm{u_y^+} - \mathrm{u_y^-}) \tag{8.40}$$

where k(φ) is the compliance of the layer e(x) and c_1 is constant. An explicit form of k(φ) can be derived from micromechanical considerations. For example, by making use of Reuss's model of the mixture solid/fluid based on additivity of strains, one gets

$$\mathrm{k}\ \varphi) = \frac{\varphi}{\mathrm{K}} + \frac{1-\varphi}{\mathrm{K_f}} \tag{8.41}$$

where K is the stiffness of the torn solid particles, K_f is the compressibility of the fluid, $K_f = \infty$ for the incompressible case considered by Dragon-Louiset (2001). Eq. (8.41) is rigorous in the limit of vanishingly small viscosity of the fluid. Stupkiewicz and Mróz (1999) used another approach to calculate the stiffness of the mixture, by averaging microscopic stresses. As a matter of fact, their model is based on additivity of stresses (Voigt model of the aggregate) and is somewhat of a "dual" model to that proposed by Dragon-Louiset (2001).

A second law describes the viscous behavior of the third body under shear stress. As suggested by experiments (the Stribeck curve) the shear stress $\sigma^-_{xy} = \sigma_{xy}$ can be assumed to be of the form

$$\sigma_{xy} = \mathrm{m}\ \varphi)\left(\frac{\mathrm{du_x^+}}{\mathrm{dt}} - \frac{\mathrm{du_x^-}}{\mathrm{dt}}\right) \cong \mathrm{m}\ \varphi)\mathrm{V} \tag{8.42}$$

where V is the relative velocity and $\mathrm{m}(\varphi) = \eta(\varphi)/\mathrm{e(x)}$ can be evaluated by a micromechanical model of dispersion of solid particles in a viscous fluid. The expression of the viscosity coefficient of the mixture η(φ) used in Dragon-Louiset's work corresponds to the Einstein mixture law given by $\eta(\varphi) = \eta_0(1 + 2.5\varphi)$ (see Landau and Lifchitz, 1971), so that

$$\mathrm{m}\ \varphi) \coloneqq \frac{\eta(\varphi)}{\mathrm{e}(\varphi)} = \frac{\eta_0(1+2.5\varphi)}{\mathrm{e}_0}(1-\varphi) \tag{8.43}$$

For small φ, Eq. (8.43) implies that the material constant m(φ) reads

$$\mathrm{m}\ \varphi) \cong \frac{\eta_0(1+1.5\varphi)}{\mathrm{e}_0} \tag{8.44}$$

Therefore, mechanical considerations show that the third body is neither a solid nor a fluid. It is rather a *hybrid* medium, being a solid in compression

and a fluid in shear. It is similar to a ball bearing which transmits high compressive axial forces while offering little viscous resistance to rotation.

The volume fraction of the solid $\varphi(x)$ is the internal parameter of the third body which can be determined by solving the coupled system of equations of the whole system (rigid punch + third body + solid half-plane Ω) for a given applied load.

8.3.4 The W-equation for a sliding punch on a half-plane

The general model of wear described in the preceding sections depends on the material constant g^s, the physical parameters defining the energy release rates g, g^3 of the solid Ω and the damaged zone respectively, the geometrical parameter of the thin layer e_0 and the macroscopic rate law of the tearing off of particles $F(\sigma)$. When these parameters are specified as well as the rate law F, the determination of the internal parameter $\varphi(x)$ in the particular system of a rigid circular punch of radius R with the profile $u^+_y(x) = \delta + (x - x_0)^2/2R$, sliding on an elastic half plane has been carried out by Dragon-Louiset (2001). The boundary integral equation method establishes an additional functional relationship between the gradients of the boundary displacements $\partial_x\{u_x(x, 0), u_y(x, 0)\}$ ∂x and the boundary stress $\{\sigma_{xy}(x, 0), \sigma_{yy}(x, 0)\}$ in the form known as Cauchin's equations (Bui, 1994). The necessary data are: the total force (compression P, shear T), the velocity V, and the boundary conditions

$$\{\sigma_{xy}(x, -a), \sigma_{yy}(x, -a)\} = 0,$$

$$\{\sigma_{xy}(x, +a), \sigma_{yy}(x, +a)\} = 0$$

$$\varphi(+a) = 0$$

The vertical displacement of the punch δ can be measured. The unknowns are the length 2a and centre x_0 of the contact zone.

It can be shown that the solution of the non-linear coupled system of equations provides the density of debris $\varphi(-a)$ at the downstream section which can be used to determine the lifetime of the composite structure.

The wear model developed here is truly a predictive one (Dragon-Louiset, 2001).

The readers can refer to this reference for details on the derivation of equations, given here without proof. The normal stress satisfies the equation.

$$\frac{\mathrm{d}}{\mathrm{dx}}\{\mathrm{k}(\varphi)(\mathrm{x})\sigma_{\mathrm{yy}}(\mathrm{x})\}+(pv)\frac{1}{\pi}\int_{-a}^{+a}\sigma_{\mathrm{yy}}(\mathrm{t})\frac{dt}{\mathrm{t}-\mathrm{x}}$$

$$=\frac{\mathrm{c}_1}{\mathrm{R}}(\mathrm{x}-\mathrm{x}_0)+\mathrm{c}_2\mathrm{m}\ \varphi)(\mathrm{x})\mathrm{V}:=\mathrm{b}(\mathrm{x}) \tag{8.45}$$

while the shear stress is given by

$$\mathrm{c}_2\sigma_{\mathrm{xy}}(\mathrm{x})\ =-\mathrm{c}_1\frac{\mathrm{d}}{\mathrm{dx}}\mathrm{u}_{\mathrm{y}}(\mathrm{x})+(\mathrm{pv})\frac{1}{\pi}\int_{-a}^{+a}\sigma_{\mathrm{yy}}(\mathrm{t})\frac{dt}{\mathrm{t}-\mathrm{x}} \tag{8.46}$$

For a trial value $\varphi^{(n)}(x)$ at iteration (n), Eq. (8.45) refered to as the W-equation, can be solved to yield σ_{yy} in closed-form, subject to the orthogonality condition for a bounded stress solution

$$\int_{-a}^{+a}\left[\frac{\mathrm{c}_1}{\mathrm{R}}(\mathrm{t}-\mathrm{x}_0)+\mathrm{c}_2\mathrm{m}(\varphi)(\mathrm{t})\mathrm{V}\right](\mathrm{a}^2-\mathrm{t}^2)^{-1/2}\frac{dt}{\mathrm{t}-\mathrm{x}}=0 \tag{8.47}$$

Instead of specifying the loads P and T, one can first specify the contact zone [–a,+a], then Eq. (8.47) yields $x_0(\varphi)$. Eq. (8.46) gives the shear stress, then subsequently v and the value $\varphi^{(n+1)}$ of φ at the next iteration are provided by $v = F(\sigma)$ and Eq. (8.39). Provided that the iterative scheme does converge, the solution $\varphi^{(\infty)}(x)$ provides the loads P and T through

$$\mathrm{P}=\int_{-a}^{+a}\sigma_{\mathrm{yy}}(\mathrm{t})dt \tag{8.48}$$

$$\mathrm{T}=\int_{-a}^{+a}\sigma_{\mathrm{xy}}(\mathrm{t})dt \tag{8.49}$$

In brief, the predictive wear model is based on a full coupling between different scales:

i) The micro-scale of the grains where the fracture mechanisms, the criterion of wear through the tearing off of particles and the production of debris are considered. These phenomena are governed by the macroscopic contact stress, as usual in fracture mechanics,

ii) The meso-scale of the multiphase flow of the mixture debris/fluid, subjected to compressive stress and shear. Homogenization of the third body yields an hybrid medium which is solid in compression and fluid in shear, where the volume fraction φ of debris plays the role of an internal parameter,

iii) The macro-scale of the sliding contact of solids in the presence of some hybrid solid/fluid interface. The solution for the macroscopic contact

stresses depends on the production of debris at the micro-scale (Dragon-Louiset, 2001)

8.3.5 Identification of constants

Now to solve the identification problem in wear mechanics it is reasonable to consider a simple model which depends on a limited number of constants. We consider a model of tearing off of debris of the form $v = C(g - g^s)_+^m$ which is similar to Paris's law in fatigue, with a threshold g^s such that $v = 0$ when $g - g^s < 0$. The unknowns of the model are the material constants C, m and the film thickness e_0. The controlled parameters of the model can be chosen in their experimental range of variation: different punch radii R, indentations δ and velocities V higher than some lower limit corresponding to Stribeck's lubricant parameter $L_0 < \eta V/p$. The richer the data, the better the identification of constants. Data which can be measured include the downstream worn mass $\rho_s e_0 \varphi(-a)$ per unit length and unit thickness of the punch, the normal stress P and the shear T. In theory, for rich enough data, the inverse problem of identificiation of the constants C, m, e_0 can be solved by considering the whole set of equations for the unknowns, using the classical least squares method.

8.4 Hydraulic fracturing of rocks

8.4.1. The physical problems

Crack propagation induced by a injection of a fluid into a bore hole is widely investigated for applications pertaining to hydraulic fracturing of rocks. Most works are based on the lubricant theory which makes the assumption of small flow channel 2w(r, t) in comparison with the crack size, one dimensional viscous incompressible fluid flow with the radial velocity u(r, z, t) and negligible inertial force as compared to the viscous force $\rho\partial^2 u/\partial t^2 \ll \eta\Delta u$ (η and $\eta' = \eta/\rho$ respectively dynamic and kinematic viscosity coefficients). There are two types of models, with or without a lag at the crack tip. Further insight on the physical and mechanical necessity of existence of some lag will be discussed. Let us show first an experimental existence of a lag in hydraulic fracturing of rocks by injected water in the bore. Fig. 8.8 clearly shows the fluid front and the fracture tip separated by a dry area (C.J. de Pater et al, 1999).

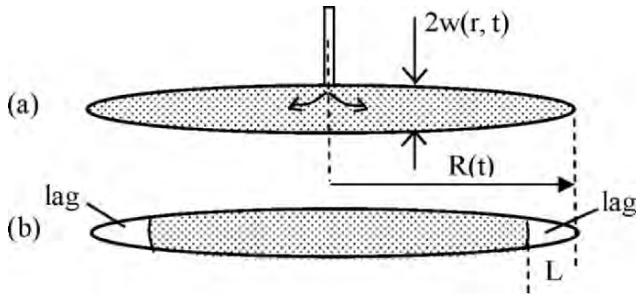

Figure 8.7: Radial fluid flow in a circular crack, under injected flow rate Q, pressure $p_0(0, t)$; (a) model without lag; (b) model with a lag at crack tip

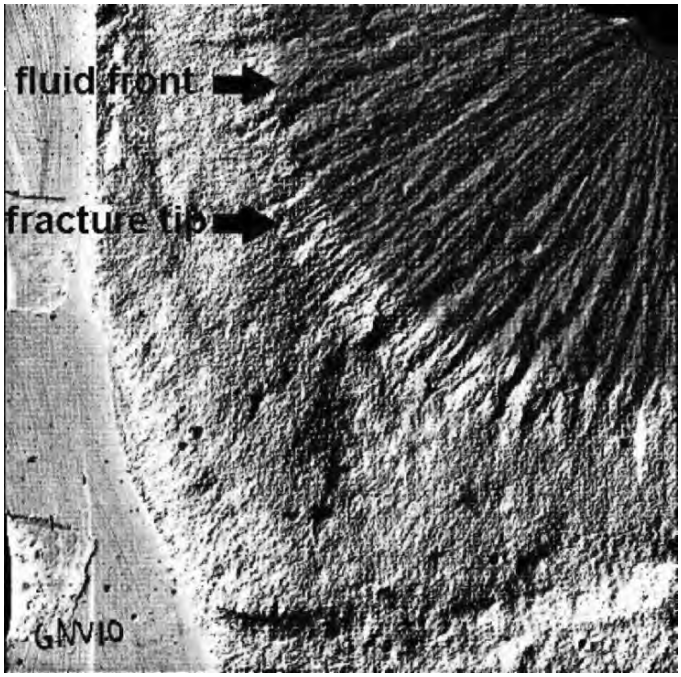

Figure 8.8: Hydraulic fracturing of rock by injected water in the bore (upper right). The radial pattern may be probably caused by dynamic effects; the fluid front and the fracture tip are clearly visible; the smooth surface beyond the fracture tip is typical of a brittle fracture (Courtesy of C.J de Pater, TU Delft University, see Van Dam et al, 1999)

The presence of a lag may affect the boundary condtions to be considered near the tip, and solve the problem of the appearance of singularities in many models of hydraulic fracturing without a lag.

8.4.2 Equations in hydraulic fracturing of rocks

The radial flow of an incompressible viscous fluid in the channel of width 2w(r, t) is governed by the linearized Navier-Stokes equations, where terms $\{\partial\mathbf{u}/\partial t + (\mathbf{u}.\text{grad}\mathbf{u})\mathbf{u}\}$ are negligible. The radial component of the velocity is denoted by $u_r = u(r, z, t)$, and $u_z = 0$. The field equations in the fluid domain read

$$\frac{1}{\rho\eta'}\frac{\partial p}{\partial z} = 0$$

(fluid dynamics) (8.50)

$$\frac{1}{\rho\eta'}\frac{\partial p}{\partial r} = \frac{\partial^2 u}{\partial r^2} + \frac{\partial u}{r\partial r} + \frac{\partial^2 u}{\partial z^2}$$

$$w(r, t) = \frac{4(1-\nu^2)}{\pi E}\int_r^{R(t)} \frac{\xi d\xi}{\sqrt{\xi^2 - r^2}} \int_0^1 yp\ \xi y, t) \frac{dy}{\sqrt{1-y^2}} \tag{8.51}$$

Eq. (8.51), for the opening of the fluid-filled crack, is used in lubrication theory to express the elastic fluid-crack interaction. The material constant of the material to be considered in brittle fracture is the toughness K_{Ic} which is related to w(r, t) near the tip r = R(t) through

$$\lim_{r\to R}\{(R-r)^{-1/2} w(r, t)\} = \frac{4(1-\nu^2)}{E} K_{Ic}\ \text{(fracture criterion)} \tag{8.52}$$

The quantity prescribed at the hole is either p the pressure

$$p(r = r_0, z) = p_0(t) \qquad \text{(boundary condition on p at the hole)} \tag{8.53}$$

or the rate flow

$$Q(r = r_0, t) = Q_0(t) \qquad \text{(boundary condition on Q at the hole)} \tag{8.54}$$

The flow rate at r, can be expressed in terms of the width w(r, t), using the condition of incompressibility condition of the fluid between the radii r and R(t).

$$Q(r,t) = 4\pi \int_r^{R(t)} y \frac{\partial w(y)}{\partial t} dy \tag{8.55}$$

Let us derive another equation which provides a direct link between the pressure gradient ∂p/∂r and Q. We look for a solution of the Navier-Stokes equations with a radial velocity of the form

$$u = \alpha(t)(z^2 - w^2)\frac{1}{r} \tag{8.56}$$

satisfying the adherence condition (more exactly the *no-slip* condition) on the walls u(r, z = w, t) = 0. The pressure does not depend on z. Eq. (8.50) is rewritten as

$$\frac{1}{\rho\eta'}\frac{\partial p}{\partial r} = \alpha\frac{z^2 - w^2}{r^3} + 2\alpha\frac{1}{r} \tag{8.57}$$

Since the hole has a nonzero radius r_0, the first term of the right hand side of Eq. (8.57) is negligible in comparison to the second one. With such an approximation, the mean velocity at the section of radius r, the flow rate, and the pressure gradient are given, respectively, by

$$\bar{u} = \frac{1}{2w}\int_{-w}^{+w} u(r, z)dz \cong \frac{2\alpha w^2}{3r} \tag{8.58}$$

$$Q = -\frac{8\alpha\ w^3}{3} \tag{8.59}$$

$$\frac{1}{\rho\eta'}\frac{\partial p}{\partial r} \cong \frac{2\alpha}{r} = -\frac{3Q}{4\pi r w^3} \tag{8.60}$$

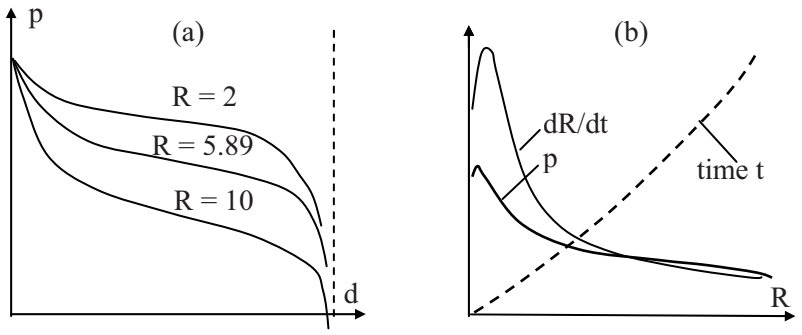

Figure 8.9: (a) Pressure p function of $d = (r - r_0)/(R - r_0)$, for different crack sizes; (b) dR/dt, pressure p and time t as function of R (Zazovskii, 1979)

No closed-form solution exists to the whole system of approximate Eqs. (8.50)-(8.60). Only numerical solutions and some asymptotic solution near the crack tip r = R have been worked out. For a stationary crack, R = Cte, it can be shown that the pressure has a negative singularity at the tip, s = (R – r), $p \cong O(s^{-1/2})$, (Abe et al, 1976). To avoid this strong singularity, Savitski and Detournay (2001) introduced a model involving a zero toughness model $K_{Ic} = 0$ and obtained a less singular behavior $p \cong O(s^{1/3})$. Zazovskii (1979) gave numerical solutions for the moving crack R(t) under the criterion (8.52) and obtained a negative, logarithmically divergent pressure $p \cong O(\ln(s))$. Zazovskii's numerical results are shown schematically in Fig. 8.9. It should be noted that all one-dimensional flow models without a lag yield a negative pressure at the crack tip, Fig. 8.9.a, which should imply the appearance of a cavitation. To introduce a lag, a simple model consists in introducing some characteristic length L, below which no fluid, in the macroscopic sense, can penetrate into the crack as suggested by Fig. 8.8. Another possibility has been exploited by Bui and Parnes (1982) who introduced a two-dimensional flow correction to models without a lag. This modified model avoids the singularity of the pressure.

8.5 Capillary phenomenon in fracture mechanics

Surface energy and surface tension of fluids as well as fluid-solid interactions are not only significant at the atomic scale, but at the macroscopic scale too: sap rises in trees, sand cohesion increases with humidity, bird feathers repel water etc. In material sciences, there is a well-known phenomenon reported by Rehbinder and Lichtman (1957): the resistance of some solids is drastically reduced by moisture. Also, experiments reported by Vutukuri (1974) have clearly evidenced an influence of liquids upon the tensile strength of rocks which possess natural microcracks.

The concept of surface tension acting along solid-fluid and fluid-vapor interfaces, while simple in the underlying physics, is a difficult one when dealing with applications requiring quantitative predictions. Problems involving fluid-filled cracks and moving fluid-solid interfaces are made more intricate by viscosity.

Let us consider for instance a three-phases system (oil + water + crack) with a fluid-filled crack. The structure of the moving fluid^1-fluid^2-solid interface has been analysed by Moffatt (1964), Dussan and Davis (1974). By observing the movement of honey drops placed on the fluid interface and on the solid, Dussan and Davis (1974) found that the adherence condition

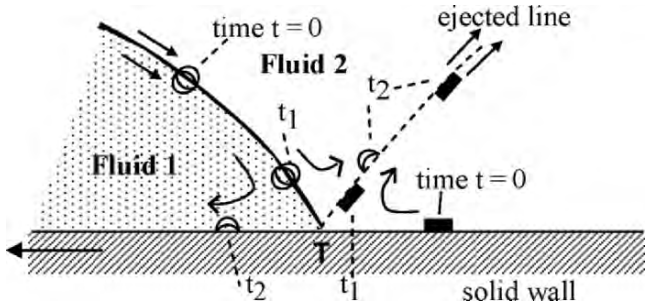

Figure 8.10: Fluid 1(water) is moving on a solid surface and pushing forward fluid 2 (oil); Drops of honey on the fluid-fluid and fluid-solid interfaces are observed at different times in the moving frame attached to the triple point T; an ejected line is observed in fluid 2; Particles of honey drops on the fluid interface move either on the ejected line or lay over the solid wall; Fluid 1 rolls on the solid while fluid 2 rolls off the solid at the triple point T, (Dussan and Davis, 1974)

is stronger than the *no-slip* condition actually observed in experiments. The adherence condition means that fluid particles can never leave the solid wall. Experiments show that this is not true. Fluid 1 is rolling *on* the rigid wall while fluid 2 is rolling *off* the triple point T at some angle. There is an "ejected" line or a "discontinuous" line of fluid 2 which consists of contiguous particles which have been separated in the past. No analyses have been carried out of the nature of singularities at the triple point, neither in the fluid domains nor in the elastic one.

Two consequences, however, can be drawn for the fluid-filled crack, in both statics and dynamics:

i) The fluid can roll on or off the solid wall, depending on a change of the pressure p or the mechanical load σ,

ii) In both statics and dynamics, the equilibrium between fluid and vapor or vacuum at their interface may be considered in the framework of surface force theories.

8.5.1 The equilibrium crack partially filled with a fluid

We first examine the two-dimensional problem of equilibrium of a crack partially filled with a non-wetting fluid. The fluid-solid system is defined by a surface tension α which is a characteristic parameter of the fluid. Also, the contact angle θ at the triple point depends on the whole system (fluid-solid-vacuum). The fluid pressure p is balanced by the surface force of the interface fluid-vacuum, given by Laplace-Young's law

$$p = \frac{\alpha}{R} \tag{8.61}$$

where R is the radius of curvature of the meniscus (zero pressure outside). In a three-dimensional model,

$$p = \alpha\left(\frac{1}{R_1} + \frac{1}{R_2}\right)$$

where $1/R_1$ and $1/R_2$ are the principal curvatures. Therefore, in a plane problem, the meniscus is a circle of radius $R \neq 0$. Fig. 8.11 shows the geometry of the fluid-vacuum-solid system near the opening crack tip. The maximum pressure corresponds to the critical radius R_c predicted by a brittle fracture theory with toughness K_{Ic}

$$R_c = \frac{4K_{Ic}^2(1-\nu^2)^2}{\pi E^2} \tag{8.62}$$

Even if such the pressure $p_c = \alpha/R_c$ can be ascribed to the fluid, there is always a thin layer of vapor or vacuum along the segment lying between the triple point B and the crack tip A, with a lag $|KA| \neq 0$. Since θ is constant

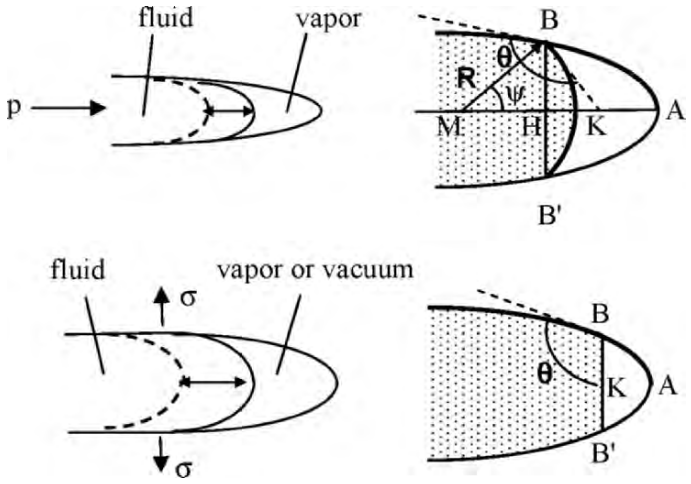

Figure 8.11: The moving fluid-solid-vapor (or vacuum) interface in the presence of surface force; the case of a circular convex meniscus ($\theta > \pi/2$) is considered in this figure; concave meniscus is possible for $\theta < \pi/2$ and high pressure of the vapor zone; fluid can roll on or off the crack surface at points B, B' under changing pressure or loads, without dissipation of energy in the fluid-solid interface

and the pressure p is non negative, a geometrical argument shows that point B cannot get closer to point A than a certain minimum distance.

This is an important feature for investigating the crack propagation because it allows for some relative slip to occur between a viscous fluid and a solid wall, in the near tip region BA. There must be no shear stress in this slip zone.

There are other physical and geometrical reasons for a lag to exist.

i) Let us consider some physical constants of rocks:

- Toughness, $K_{Ic} = 10^6\ Nm^{-3/2}$,
- Young's modulus, $E = 5.10^{10}\ Nm^{-2}$,
- Poisson's ratio, $\nu = 0.3$.

The radius of curvature at the critical load given by (8.62) is $R_c = 5 \times 10^{-10}$m or 5Å. This radius is equal to twice the size of the water molecule H_2O. At this scale a continuum model loses its meaning.

ii) Suppose that some viscous fluid is in contact with the crack wall at the crack tip A. Upon crack propagation, the "solid" points A^+ and A^- move in opposite directions upward and downward, so that the no-slip condition is violated at point K, in contact with $A^{\pm}$.

Equations of the equilibrium fluid-filled crack

Let b denote the value of x(B) or x(H) and v(b) the crack opening displacement at B. Let 2ψ denote the angle of the meniscus. The exact relationship between θ and ψ is

$$\theta = -\frac{\partial v}{\partial x} + \psi + \frac{\pi}{2} \tag{8.63}$$

where v(x) is the crack opening displacement. Since there is a lag, the gradient $\partial v/\partial x$ is regular near the crack tip and can be neglected in the small strain assumption in comparison to the remaining terms. Hence we obtain the following simpler relation which means that the fluid-filled crack problem becomes an uncoupled one

$$\theta = \psi + \frac{\pi}{2} \tag{8.64}$$

The fluid pressure is $p = \alpha/R$ with

$$R = \frac{v(b)}{\sin \psi)} \tag{8.65}$$

Now we derive the solution of the fluid-filled crack of length 2a subjected to some fluid pressure p acting on the interval $-b \le x \le b$ plus some remote uniform tension traction σ. The stress-intensity factor at the crack tip A is given by the following classical formula which can be found in many text-books

$$K_I = 2p\left(\frac{a}{\pi}\right)^{1/2} \arcsin\left(\frac{b}{a}\right) + \sigma\sqrt{a} \tag{8.66}$$

We need to derive the crack opening displacement *from* the knowledge of stress-intensity factor. We shall omit the details of the derivation given in (Bui, 1978). The crack profile v(x) is given by

$$v(x) = \frac{4a(1-\nu^2)}{\pi E}\left\{pF(x) + \sigma G(x)\right. \tag{8.67}$$

where

$$\begin{aligned} F(x) = {} & \sqrt{(1-x^2/a^2)}\arcsin(b/a) + \\ & + (b/2a)\ln\left|\frac{2\sqrt{(a^2-b^2)}\sqrt{(a^2-x^2)} + 2a^2 - b^2 - x^2}{(x^2-b^2)}\right| + \\ & + \frac{x}{2a}\log\left|\frac{2bx\sqrt{a^2-b^2}\sqrt{a^2-x^2} - a^2(x^2+b^2) + 2b^2x^2}{a^2(x^2-b^2)}\right| \end{aligned} \tag{8.68}$$

and

$$G(x) = \frac{\pi}{2}\sqrt{1-(x^2/a^2)} \tag{8.69}$$

Substituting Eqs. (8.65) and (8.67) in Eq. (8.61) we obtain a quadratic equation on p

$$F(b)p^2 + \sigma\, G(b)p - \gamma E^2 = 0 \tag{8.70}$$

where the dimensionless constant γ is given by

$$\gamma = \frac{\pi\alpha\sin(\psi)}{4aE(1-\nu^2)} \tag{8.71}$$

One would expect (8.70) at first sight to yield two possible solutions for the pressure. As a matter of fact, when $\gamma = 0$ there is no surface tension and

there is a trivial solution p = 0, so that only one solution of Eq. (8.70) is significant for the fluid-filled crack problem

$$p = \frac{1}{2F(b)}\left\{-\sigma G(b) + \sqrt{\sigma^2 G^2(b) + 4\gamma E^2 F(b)}\ \right\} \tag{8.71}$$

The solution (8.71) is real for $0 \le b < a$. Fig. 8.12 shows the dimensionless pressure $p/E\gamma^{1/2}$ versus the ratio b/a of the wet zone, for several remote loads $\Sigma = \sigma/E\gamma^{1/2}$.

When b approaches a, without reaching it (up to some b_{max}), the pressure increases according to

$$p \cong C\frac{1}{(1-(b/a))^4} \tag{8.72}$$

with $C = 2^{1/4}E(\gamma/\pi)^{1/2}$. However, the pressure cannot become singular because of the lag. To calculate the limit value b_{max} we express the geometrical condition $(x(A) - x(K)) > 0$, which yields the following implicit condition $(1\ \cos\psi)\alpha < p(b_{max})(a - b_{max})$. Using the asymptotics (8.72) the maximun size of the wet zone is

$$b_{max} = a - \{(1 - \cos\psi)^4\alpha^4\pi^2(2a)^{-1}E^{-4}\gamma^{-2}\}^{1/3} \tag{8.73}$$

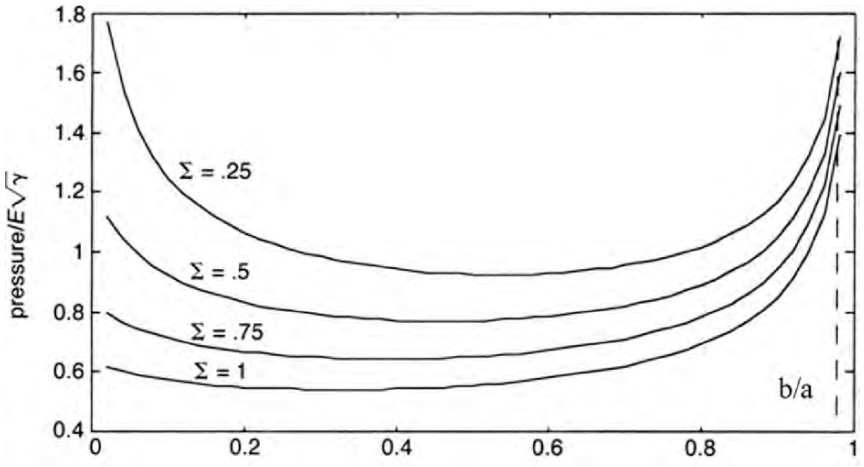

Figure 8.12: Pressure of the fluid occcupying the wet zone –b < x <b, as a function of b/a, for several values of the remote load Σ

8.5.2 Capillary stress intensity factor

The stress intensity factor is given by

$$K_I = \left[\sigma + \frac{2p}{\pi} \arcsin(\frac{b}{a}) \right] \sqrt{\pi a} \tag{8.74}$$

Therefore the toughness of a wet cracked body subjected to some remote tensile stress σ is lower than that for a dry material by the amount

$$K_I^0 = \frac{2p}{\pi} \arcsin(\frac{b}{a}) \sqrt{\pi a} \tag{8.75}$$

which is referred to as the *Capillary Stress Intensity Factor* by Bui (1996), Fig. 8.13.

This is nothing but the Rehbinder effect which is explained by a mechanical argument here. The lowering of the strength of the materials by moisture has been reported in the literature (Rehbinder and Lichtman, 1957, Eeckhout, 1976).

Previous interpretations of the Rehbinder phenomenon were generally based upon Van der Vaals's interaction forces and chemical interactions between fluid molecules and solid ones. Such an influence actually exists but it is not the only one. When a water molecule penetrates into the crack tip cavity in glass, a link is broken between some atom **Si** and the atom **O** of the bond ..-**Si**-**O**-**Si**-, another one is broken in H-**O**-H. Then two hydroxyls **O**H build new bonds with the silicium atoms in glass resulting in

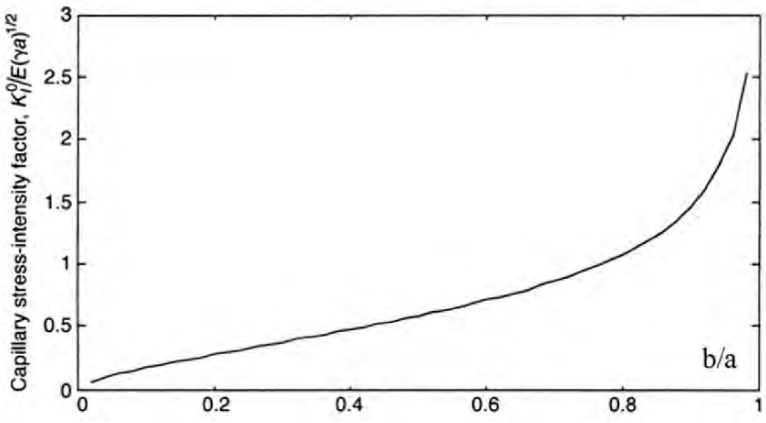

Figure 8.13: Capillary stress intensity factor existing prior to external loads

two separate –**Si**-**O**-H and H-**O**-**Si** and a new cavity or an additional crack length (Michalske and Bunker, 1988). This mechanism demands less energy than that required to directly break the bond **Si**-**O**-**Si**. However, the size of the water molecule (or other liquids) is comparable to that of the cavity so that there is little room for a chemical interaction under low applied stress, precisely because of a lag.

8.6 Viscous fluid flow solution near a moving crack tip

We consider a steady state propagation of a crack driven by some hydraulic pressure and analyse the structure of fluid flow near the moving crack tip moving at the velocity V. The geometry of the coupled fluid-solid system is shown in Fig. 8.14. Neglecting inertial forces, the near tip geometry is defined by the toughness K_{Ic} of the solid. The fluid is separated from the solid wall by a lag, with the surface tension α, the convex meniscus S, the contact angle θ. In the moving frame, the fluid flow at section C is that given by a lubrication theory, with a parabolic profile and a zero global flow rate. The equations of the coupled system have been given by Bui et al (2002).

8.6.1 Equations of the fluid-filled moving crack

Having in mind a numerical solution, we shall write the full set of non-linear equations.

♦Navier-Stokes equations

$$\text{div}\,\mathbf{v} = 0 \qquad \text{in } \Omega \tag{8.76}$$

$$(\mathbf{v}.\text{grad})\mathbf{v} + \frac{1}{\rho}\text{grad}\,p - \eta'\,\text{div}\,\text{grad}\mathbf{v} = \mathbf{0} \qquad \text{in } \Omega \tag{8.77}$$

$$v_x = \frac{3V}{2}\left(1 - \frac{y^2}{h^2}\right), \qquad v_y = 0, \quad \text{on CC' (width 2h)} \tag{8.78}$$

$$v_x = -V, \qquad v_y = -\frac{\partial w(x)}{\partial x} \quad \text{on BC, B'C'} \tag{8.79}$$

♦Parabolic profile wall y = w(x)

$$x = -\frac{y^2}{2R_c}, \tag{8.80}$$

$$R_c = \frac{4K_{Ic}^2(1-\nu^2)^2}{\pi E^2} \tag{8.81}$$

♦Capillary force (**n** is the unit outward normal to S)

$$\begin{aligned} &\sigma_{nt} = 0 \\ &\qquad\qquad \text{(on the meniscus S)} \\ &p = \alpha\, \mathrm{div}\mathbf{n}, \end{aligned} \tag{8.82}$$

♦Global equilibrium equation

$$K_{Ic} = f(p, \sigma_{yy}^{\infty}) \tag{8.83}$$

The first Eq. (8.82) indicates that there is no shear force $\sigma_{nt} = 0$ on the meniscus surface, due to the lag. In a fixed frame, the fluid rolls on the crack wall at point B. Eq. (8.83) provides the stress intensity factor for the applied load σ^{∞} and the internal fluid pressure p. This pressure can be either a given datum – for instance at the bore hole in hydraulic fracturin ; – or a value implicitly determined by the flow rate of injected fluid or by the fluid volume of fluid in the wet zone.

8.6.2 Numerical results

When solving the above mentionned non linear equations, the value $\theta = 2\pi$ has been considered in order to avoid singularities at points B and B'. In fact, the point force at the triple points of magnitude 2pv(b) is negligible in comparison to the total force acting on the crack 2pa. In other words, the surface force acting on the meniscus at the microscale of the crack tip region has only a long range effect.

The computer code N3S (Navier-Stokes in 3D) of Electricité de France has been used to find a solution with a very small lag. Instead of solving the coupled problem, we are solving an approximate uncoupled one whichies Eqs. (8.76)-(8.80) only, with fixed x(b) and constant p on the meniscus. The meshes used are not fine enough for condition (8.78) to be satisfied exactly and implicitly. A constant pressure is imposed on the meniscus KB, rather than that determined by condition (8.82). At the stagnation point K close to the crack tip A, the curvature does not vary significantly so that condition (8.82) or (8.61) is approximately satisfied for value

α inferred from the mean value pR. This "inverse" solution approach corresponds to the value K_{Ic} infered from (8.81) and to some remote stress σ.

The stream lines are typically the well known ones of a "fountain" flow. The pressure decreases smoothly to some finite value at the meniscus S.

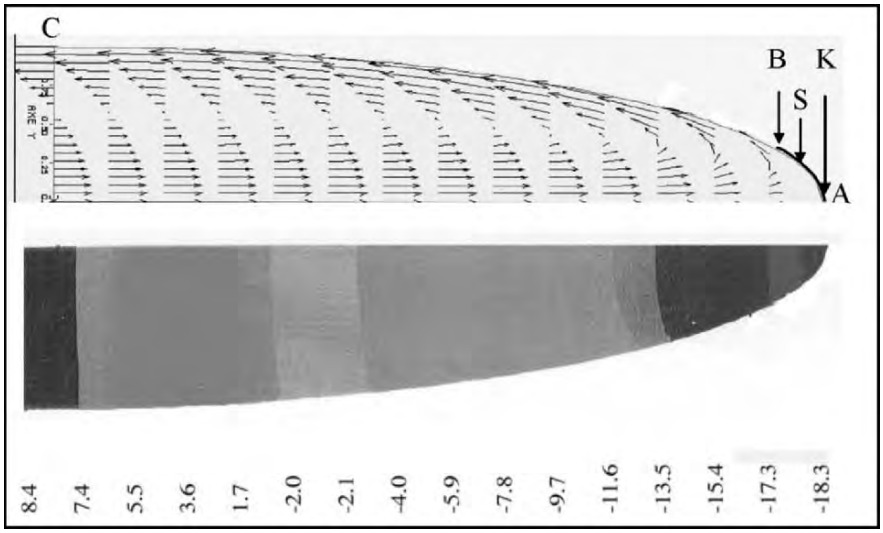

Figure 8.14: Stream lines of the "fountain" viscous fluid flow in the moving domain $|y| < w(x)$ of the opening crack with the velocity V: Fluid velocity is equal to ($v_x = -V$, $v_y = -\partial w/\partial x$) along BC; Constant pressure is imposed on AB (heavy line); parabolic flow of zero global flux is prescribed at section C; Pressure decreases smoothly from p = 8.4 at C to –18.3 at K; The fluid velocity vanishes at K while the velocity of the solid point A^+ is unbounded (Bui et al, 2002)

Chapter 9

Crack Detection by Scattering of Waves

9.1 Introduction

The assessment of structures is an important problem in Engineering Mechanics. Fracture Mechanics deals with the mechanical behavior of cracked solids or structures under applied loads. One assumes that the crack geometry and position as well as the boundary conditions on the crack are known. This is true for tunnel cracks through a thin wall, for which the crack geometry is known in a two-dimensional problem, or for edge cracks in a three-dimensional solid where the crack geometry is partially known. Except for these particular cases, the crack geometry in a solid is generally *unknown*. This is the case for a slide fault of an earthquake in seismic regions where both the release of shear stress and the fault geometry are unknown. The determination of the actual crack geometry in statics or dynamics poses many challenges for research nowadays, owing to the interest of the mathematician community for Engineering Problems (3 Journals on Inverse Problems have been created over the last decade). Mathematical works in inverse geometry problems have been developed for medical imaging and for the evaluation of materials. The term *Tomography* is used in classical method of inspection by X-rays, Single Photon Emission Computerized Tomography (SPECT), Positon Emission Tomography (PET), as well as in methods – called *generalized tomographie*s – which include Scatterings of acoustic and elastic waves in the frequency domain, method of Detection by Infra-Red emission, Mechanical testings, Vibration, Scatterings of waves in the time domain. The origin of these namings may be found in the use of ray theory of wave propagation. To scan a solid with ultra-sound devices, one gathers information from a source S (or the input) and a receiver R (the output). The pair SR acts as a X-ray line L in classical tomography. The only difference between these tomographies is lying in the physics of phenomena considered and the corresponding mathematics of the inverse problem.

Tomographic methods will be discussed in Chap. 10. In this chapter we will make a brief review of some classical methods to identify defects and cracks, by scatterings of acoustic and elastic waves. New methods of scatterings of waves to detect planar cracks and to solve the earthquake inverse problem in closed-form, in the time domain, will be specifically addressed in Chap. 11.

9.2 Scattering of acoustic waves

Applications of acoustic waves are found in Medical Imaging like the ultrasound scan, in Engineering for the evaluation of materials or the Non Destructive Testing (NDT) and in Geophysics for the detection of an oil reservoir. The scalar wave equation in the frequency domain is ($k = \omega/c$)

$$\text{div}\,\text{grad}\,\phi + k^2\phi = 0, \quad x \in \Omega \backslash \{s_0, r_0\} \tag{9.1}$$

outside the source s_0 and the receiver r_0. Genrally the domain considered is unbounded. This is not true in the medical imaging of a human body. It is not true for a real solid structure either. Nevertheless, it is well known that the medical diagnosis of malicious cells provides reliable information to radiologists and physicians.

To understand such a peculiar feature in acoustic scattering, we recall the principle of acoustic scan. Waves of frequency ω are generated by an emitter s_0 which is leant against the body, with a gel to make a better contact for a wave propagation.

Two methods exist: the receiver r_0 is located either at different stations (the "emitter-receiver" method) or at the same location at the source (the "transducer" method), with the same apparatus. In either of them, incident *plane* waves $\phi^{(in)}$ emitted by the remote source are diffracted by defects and diffracted waves $\phi^{(d)}$ propagating to the receiver r_0 or back to the tranducer, are travelling in an homogeneous medium considered *as* an infinite medium.

One assume that Eq. (9.1) holds in a human body outside malicious cells or in a sound solid outside cracks or inclusions. Thus it is assumed that the wavelength is small in comparison to the body or solid size. Therefore, the total field $\phi = \phi^{(in)} + \phi^{(d)}$ may be measured far from the inclusion. Waves are assumed to satisfy the radiation condition

$$\frac{\partial \phi}{\partial r} - ik\phi = O(1/r) \quad \text{at infinity} \tag{9.2}$$

The diffracted field $\phi^{(d)}(\mathbf{x})$ is related to the total field $\phi(\mathbf{x})$ on the surface of the inclusion S by an integral expression (for simplicity, the dependence on the frequency is omitted, except for the Green function), (Bonnet, 1999)

$$\phi^{(d)}(\mathbf{x}) = \int_S \{\phi(\mathbf{y})\frac{\partial}{\partial n_y}G^{\omega}(\mathbf{x},\mathbf{y}) - G^{\omega}(\mathbf{x},\mathbf{y})\frac{\partial}{\partial n_y}\phi(\mathbf{y})\}dS_y \quad x\in\Omega \tag{9.3}$$

where $G^{\omega}(\mathbf{x},\mathbf{y})$ is the Green function of the Helmhotlz equation corresponding to Eq. (9.1), where a Dirac delta source at $\mathbf{y}=\mathbf{x}$ has to be added $\mathrm{div}_y \mathrm{grad}_y G(\mathbf{x},\mathbf{y}) + k^2 G(\mathbf{x},\mathbf{y}) + \delta(\mathbf{y}-\mathbf{x}) = 0$. The domain Ω is outside the surface S. The Green function is given by

$$G^{(\omega)}(\mathbf{x},\mathbf{y}) = \frac{\exp(ik|\mathbf{x}-\mathbf{y}|)}{4\pi|\mathbf{x}-\mathbf{y}|} \tag{9.4}$$

To solve the exterior problem of waves scattering one needs some boundary condition which depends on the physics of the problem considered.

Finally, the model of an infinite medium with the incident plane waves are simple enough to make the data inversion possible, while realistically describing the main feature of the physics of wave propagation. This is a compromise between the physics and the mathematics of inverse problem.

9.2.1 Detection of a rigid inclusion

The boundary condition for a rigid inclusion is $\partial\phi/\partial n = 0$. From Eq. (9.3), the integral representation for the diffracted wave in Ω is given by

$$\phi^{(d)}(\mathbf{x}) = \int_S \phi(\mathbf{y})\frac{\partial}{\partial n_y}G^{\omega}(\mathbf{x},\mathbf{y})\,dS_y, \ (\mathbf{x}\in\Omega) \tag{9.5}$$

The diffracted wave at point $\mathbf{z}$ on S is given by

$$\phi^{(d)}(\mathbf{z}) = \frac{1}{2}\phi(\mathbf{z}) + (pv)\int_S \phi(\mathbf{y})\frac{\partial}{\partial n_y}G^{\omega}(\mathbf{z},\mathbf{y})\,dS_y \quad (z\in S) \tag{9.6}$$

In the scattering of waves, two assumptions are generally made:

i) The (pv)-integral term of Eq. (9.6) is negligible compared to $\phi(\mathbf{z})/2$, so that $\phi(\mathbf{z}) \cong 2\phi^{(d)}$, $\phi^{(in)}(\mathbf{z}) = \phi(\mathbf{z}) - \phi^{(d)}(\mathbf{z})) \cong \phi^{(d)}$ and $\phi(\mathbf{z}) \cong 2\phi^{(in)}(\mathbf{z})$. The assumption is known as the *Born approximation* in acoustic scattering

ii) The integral over S in Eq. (9.3) is limited to the surface S^+ illuminated by incident wave. This approximation is justified by the exact solution

of scattering of wave by a semi-infinite crack, provided by Achenbach (1980), where except for the crack tip region, the field at the *hidden* surface S^- is zero. Numerical solutions for a flat inclusion show the same features.

The diffracted field in the medium Ω, is thus expressed in terms of the incident field, approximately by

$$\phi^{(d)}(\mathbf{x}) \cong 2\int_{S+} \phi^{(in)}(\mathbf{y}) \frac{\partial}{\partial n_y} G^{\omega}(\mathbf{x},\mathbf{y}) dS_y, \ (\mathbf{x} \in \Omega) \tag{9.7}$$

These approximations lead to an exact inversion of diffracted data. The emitter is located at $\mathbf{x}$ far from the obstacle in the opposite direction. The same device emitter-receiver (called the transducer) is used for sending waves and receiving the backward diffracted signals. The illuminated surface S^+ is defined by $\mathbf{y}.\mathbf{x} > 0$, with $\mathbf{y}$ on the surface S, $\mathbf{x}$ at the receiver while the hidden surface S^- is defined by $\mathbf{y}.\mathbf{x} < 0$. Since the source point is far from the obstacle, we can express the incident field and its normal gradient on the inclusion approximately as ($\hat{\mathbf{x}} = \mathbf{x}/|\mathbf{x}|$)

$$\phi^{(in)}(\mathbf{y}) \cong G^{\omega}(\mathbf{x}, \mathbf{y}) \cong \frac{1}{4\pi|\mathbf{x}|} \exp(ik|\mathbf{x}|)\exp(-ik\mathbf{y}.\hat{\mathbf{x}}) S_y, \ (\mathbf{y} \in S^+) \tag{9.8}$$

$$\frac{\partial}{\partial n_y}\phi^{(in)}(\mathbf{y}) \cong -\frac{ik}{4\pi|\mathbf{x}|}\hat{\mathbf{x}}.\mathbf{n}(\mathbf{y})\exp(ik|\mathbf{x}|)\exp(-ik\mathbf{y}.\hat{\mathbf{x}}), \ (\mathbf{y} \in S^+) \tag{9.10}$$

Substituting $\partial \mathbf{G}^{\omega}(\mathbf{x},\mathbf{y})/\partial n_y \cong \partial\phi^{(in)}(\mathbf{y})/\partial n_y$, Eq. (9.10), and $\phi^{(in)}(\mathbf{y})$, Eq. (9.8) into Eq. (9.7) one arrives at the expression

$$\phi^{(d)}(\mathbf{x}) \cong -\frac{ik}{8\pi^2|\mathbf{x}|^2}\exp(2ik|\mathbf{x}|)\int_{y.x>0} xp(-2ik\mathbf{y}.\hat{\mathbf{x}})\hat{\mathbf{x}}.\mathbf{n}(\mathbf{y})dS_y \tag{9.11}$$

Now let us introduce the characteristic function $\varphi(\mathbf{x})$ of the inclusion, equals to 1 inside S, and zero outside. The technique of the transducer consists in collecting data for all possible orientations in the three-dimensional space, at fixed distance $|\mathbf{x}| = \delta$, in the whole range of frequencies. One measures the datum $\phi^{(d)}(\mathbf{x},\omega)$ at each frequency. By setting $\mathbf{K} = 2k\hat{\mathbf{x}}$ and $\omega = c|\mathbf{K}|/2$ we obtain the experimental datum $\Phi(\mathbf{K}) = \phi^{(d)}(\mathbf{K}\delta/|\mathbf{K}|; c|\mathbf{K}|/2)$. Since $\mathbf{K} = 2k\hat{\mathbf{x}}$, $k \in O_+$, $\hat{\mathbf{x}} \in S_2$ (unit sphere of dimension 2) vector $\mathbf{K}$ is a three-dimensional one, there is hope that the datum $\Phi(\mathbf{K})$ is rich enough for a volume occupied by the inclusion C (or the characteristic function $\varphi(\mathbf{x})$) to be determined. Eq. (9.11) can be written in the form

$$\phi^{(\mathrm{d})}(\mathbf{x};\omega)\exp(-2\mathrm{ik}|\mathbf{x}|) \cong -\frac{\mathrm{ik}}{8\pi^2|\mathbf{x}|^2}\int_{\mathbf{y}.\mathbf{x}>0}\exp(-2\mathrm{ik}\,\mathbf{y}.\hat{\mathbf{x}})\,\hat{\mathbf{x}}.\mathbf{n}(\mathbf{y})dS_y \quad (9.12)$$

Making the substitutions $\mathbf{x}\to -\mathbf{x}$ and $\mathbf{y}=-\mathbf{y}'$ into Eq. (9.12) and taking the complex conjugate (*), we then obtain

$$\left[\phi^{(\mathrm{d})}(-\mathbf{x};\omega)\exp(-2\mathrm{ik}|\mathbf{x}|)\right]^* \cong -\frac{\mathrm{ik}}{8\pi^2|\mathbf{x}|^2}\int_{\mathbf{y}'.\mathbf{x}<0}\exp(-2\mathrm{ik}\mathbf{y}'.\hat{\mathbf{x}})\,\hat{\mathbf{x}}.\mathbf{n}(\mathbf{y}')dS_{y'} \quad (9.13)$$

Noting that $S^+=\{\mathbf{y}.\mathbf{x}>0\}$ and $S^-=\{\mathbf{y}'.\mathbf{x}<0\}$ and adding (9.13) to (9.12) we obtain

$$\phi^{(\mathrm{d})}(\mathbf{x};\omega)\exp(-2\mathrm{ik}|\mathbf{x}|) + \left[\phi^{(\mathrm{d})}(-\mathbf{x};\omega)\exp(-2\mathrm{ik}|\mathbf{x}|)\right]^* \cong$$

$$\cong -\frac{\mathrm{ik}}{8\pi^2|\mathbf{x}|^2}\int_{S+\cup S-}\exp(-2\mathrm{ik}\,\mathbf{y}.\hat{\mathbf{x}})\,\mathbf{n}(\mathbf{y}).\hat{\mathbf{x}}\,dS_y$$

Finally introducing the characteristic function of C ($\varphi=1$ in C, $\varphi=0$ in Ω), we transform the above surface integral into a volume one over the infinite medium

$$\phi^{(\mathrm{d})}(\mathbf{x};\omega)\exp(-2\mathrm{ik}|\mathbf{x}|) + \left[\phi^{(\mathrm{d})}(-\mathbf{x};\omega)\exp(-2\mathrm{ik}|\mathbf{x}|)\right]^* \cong$$

$$-\frac{\mathrm{k}^2}{4\pi^2|\mathbf{x}|^2}\int_{\mathbb{R}^3}\varphi(\mathrm{y})\ \mathrm{xp}(-2\mathrm{ik}\mathbf{y}.\hat{\mathbf{x}})dV_y \quad (9.13)$$

The right hand side of Eq. (9.13) is the Fourier transform $F\varphi(\mathbf{K})$ of the unknown characteristic function $\varphi(\mathbf{y})$ thus ($\mathbf{K}=2\mathrm{k}\,\hat{\mathbf{x}}$)

$$F\varphi(\mathbf{K}) = -\frac{16\pi^2\delta^2}{\mathbf{K}^2}\left(\Phi(\mathbf{K})\exp(-\mathrm{i}|\mathbf{K}|\delta) + \{\Phi(-\mathbf{K})\exp(-\mathrm{i}|\mathbf{K}|\delta)\}^*\right) \quad (9.14)$$

Finally, the inverse Fourier transform of Equation (9.14) gives the characteristic function $\varphi(\mathbf{x})$ of the inclusion C

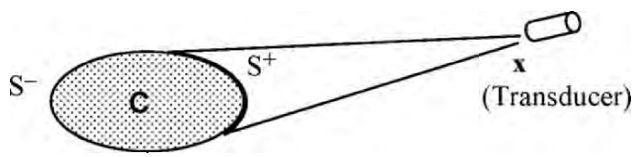

Figure 9.1: Point **y** of the illuminated part S^+ of the surface of the inclusion C satisfies **y.x** > 0, point **y'** of the hidden part S satisfies **y'.x** < 0

$$\varphi(\mathbf{y}) = -\frac{\delta^2}{\pi}\mathrm{Re}\left(\int_{\mathbb{R}^3}\frac{4}{\mathbf{K}^2}\Phi(\mathbf{K})\exp(-\mathrm{i}|\mathbf{K}|\delta)\exp(\mathrm{i}\mathbf{K}.\mathbf{y})d^3\mathbf{K}\right) \tag{9.15}$$

It is the well-known *Bojarski formula* which has important applications in ultrasound scan (Bojarski, 1981).

The analytical solution (9.15) is derived for an ideal experimental set-up which requires the whole spectrum ω and all directions of the transducer in the unit sphere S_2. Needless to say, one can only obtain approximate solutions from limited number of frequencies and directions of the transducer. For complete data, the explicit result (9.15) shows that the ultrasound inverse problem to detect an inclusion has a unique solution.

9.2.2 Detection of a flat cavity

We consider a plane incident wave of the form $\phi^{(\mathrm{in})}(\mathbf{y}) = \exp(\mathrm{ik}\mathbf{d}^0.\mathbf{y})$ with propagation vector $k\mathbf{d}^0$ in the direction $\mathbf{d}^0$ towards a flat cavity, whose thickness is assumed to be small. The flat cavity modellizes a crack in three-dimensions. Surface S^+ $\mathbf{n} = \mathbf{e}^3$) is illuminated by the incident wave. The crack plane is denoted by P and the characteristic function of S denoted by $\varphi(\mathbf{y})$. The boundary condition for a cavity is $\phi = 0$. The diffracted field at point $x \in \Omega$ (the infinite domain outside the cavity) is

$$\phi^{(\mathrm{d})}(\mathbf{x}) = -\int_{S^+} G^{\omega}(\mathbf{x},\mathbf{y})\frac{\partial}{\partial \mathrm{n}_y}\phi(\mathbf{y})dS_{\mathrm{y}}, \quad (\mathbf{x} \in \Omega) \tag{9.16}$$

The normal derivative at $\mathbf{x}$ near S^+, but not on the surface, is given by

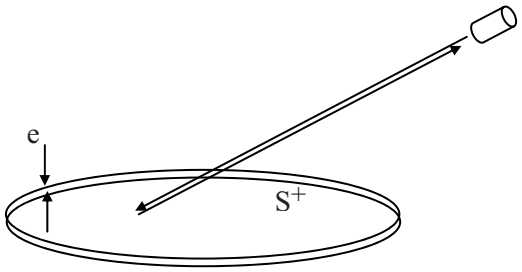

Figure 9.2: Flat cavity modelling a crack in three dimensional medium

$$\frac{\partial}{\partial \mathrm{n}_\mathrm{x}}\phi^{(\mathrm{d})}(\mathbf{x}) = \int_{\mathrm{S}+}\frac{\partial}{\partial \mathrm{n}_\mathrm{y}}G^{\omega}(\mathbf{x},\mathbf{y})\frac{\partial}{\partial \mathrm{n}_y}\phi(\mathbf{y})dS_\mathrm{y}, \quad (\mathbf{x}\in\Omega) \tag{9.17}$$

The limit as $\mathbf{x}\to\mathbf{z}$ on the surface is given by the principal value integral

$$\frac{\partial}{\partial \mathrm{n}_\mathrm{z}}\{\phi(\mathbf{z})-\phi^{(\mathrm{in})}(\mathbf{z})\} = \tfrac{1}{2}\frac{\partial}{\partial \mathrm{n}_\mathrm{z}}\phi(\mathbf{z}) + (\mathrm{pv})\int_{\mathrm{S}+}\frac{\partial}{\partial \mathrm{n}_y}G^{\omega}(\mathbf{z},\mathbf{y})\frac{\partial}{\partial \mathrm{n}_y}\phi(\mathbf{y})dS_\mathrm{y} \tag{9.18}$$

where $\mathbf{z}\in \mathrm{S}^+$. As before, the pv-integral is neglected in acoustic scattering models so that $\partial\phi/\partial \mathrm{n}_\mathrm{z} \cong 2\partial\phi^{(\mathrm{in})}/\partial \mathrm{n}_\mathrm{z}$ and

$$\phi^{(\mathrm{d})}(\mathbf{x}) = -\int_{\mathrm{S}+}2G^{\omega}(\mathbf{x},\mathbf{y})\frac{\partial}{\partial \mathrm{n}_y}\phi^{(\mathrm{in})}(\mathbf{y})dS_\mathrm{y}, \quad (\mathbf{x}\in\Omega) \tag{9.19}$$

The preceding reasoning given in Sect. 9.2.1 with the incident wave $\phi^{(\mathrm{in})}(\mathbf{y})=\exp(\mathrm{ik}\mathbf{d}^0.\mathbf{y})$ leads to ($\mathbf{x}\in\Omega$)

$$\phi^{(\mathrm{d})}(\mathbf{x}) = -\frac{\mathrm{ik}}{2\pi|\mathbf{x}|}\exp(\mathrm{ik}|\mathbf{x}|)(\mathbf{d}^0.\mathbf{e}^3)\int_{\mathrm{P}}\varphi(\mathbf{y})\exp(-2\mathrm{ik}\mathbf{y}.\mathbf{d}^0)d^2\mathbf{y}, \tag{9.20}$$

The characteristic function $\varphi(\mathrm{y}_1,\mathrm{y}_2)$ of S in the plane P of the flat cavity is extended to the characteristic function $\tilde{\varphi}(\mathrm{y}_1, \mathrm{y}_2, \mathrm{y}_3)$ of the flat cavity in the whole space by setting $\tilde{\varphi}(\mathrm{y}_1, \mathrm{y}_2,\mathrm{y}_3) \equiv \varphi(\mathrm{y}_1, \mathrm{y}_2) = 1$ for $0 < \mathrm{y}_3 < \mathrm{e}$ (small), $(\mathrm{y}_1, \mathrm{y}_2)\in \mathrm{S}$ and $\varphi(\mathrm{y}_1, \mathrm{y}_2, \mathrm{y}_3) = 0$ otherwise. Eq. (9.20) becomes

$$\phi^{(\mathrm{d})}(\mathbf{x}) \cong -\frac{\mathrm{ik}}{2\mathrm{e}\pi|\mathbf{x}|}\exp(\mathrm{ik}|\mathbf{x}|)(\mathbf{d}^0.\mathbf{e}^3)\int_{\mathbb{R}^3}\tilde{\varphi}(\mathbf{y})\exp(-2\mathrm{i}\ \mathbf{y}.\mathbf{d}^0)d^3\mathbf{y}, \quad (\mathbf{x}\in\Omega)$$

The normal $\mathbf{n}$ of the illuminated face S^+ is $\mathbf{n} = \mathbf{e}^3$. For a transducer, one has $\hat{\mathbf{x}} = -\mathbf{d}^0$. By letting $\mathbf{K} = 2\mathrm{k}\mathbf{d}^0$, we can write the above equation as

$$\phi^{(\mathrm{d})}(\mathbf{x};\mathrm{k}) \cong -\frac{\mathrm{iK}_3}{4\mathrm{e}\pi|\mathbf{x}|}\exp(\mathrm{ik}|\mathbf{x}|)\int_{\mathbb{R}^3}\tilde{\varphi}(\mathbf{y})\exp(-\mathrm{i}\mathbf{y}.\mathbf{K})d^3\mathbf{y}, \qquad (\mathbf{x}\in\Omega)$$

Measurements at large $|\mathbf{x}|$ from the cavity yield the *far field* F defined by

$$\mathrm{F}(\hat{\mathbf{x}};\mathrm{k}) = 4\pi|\mathbf{x}|\exp(-\mathrm{ik}|\mathbf{x}|)\ \phi^{(\mathrm{d})}(\mathbf{x};\mathrm{k}) \tag{9.21}$$

Therefore, the Fourier transform of the extended function $\tilde{\varphi}(\mathrm{y}_1, \mathrm{y}_2, \mathrm{y}_3)$, denoted by $\hat{\varphi}(\mathbf{K})$ is related to the far-field

$$\hat{\varphi}(\mathbf{K}) = \int_{\mathbb{R}^3} \tilde{\varphi}(\mathbf{y}) \exp(-\mathrm{i}\mathbf{K}.\mathbf{y}) d^3\mathbf{y} = \frac{\mathrm{ie}}{\mathrm{K}_3} \mathrm{F}(-\mathbf{K}/|\mathbf{K}|; \mathrm{k}) \tag{9.22}$$

To achieve the inversion, it is necessary that measurements of the far-field F are made for all the spectrum $\mathrm{k} > 0$ and all directions of incident waves $\mathbf{d}^0 \in \mathrm{S}_2$ (unit sphere, or a half-sphere) so that $\mathbf{K} = 2\mathrm{k}\mathbf{d}^0$ belongs to the three-dimensional space. In fact, measurements for the right hand side of Eq. (9.22) are made on the half space, $\mathrm{K}_3 < 0$, the extension to the upper half space $\mathrm{K}_3 > 0$ being made by a symmetrization. In practice one deals with a finite spectrum and a finite number of the transducers orientations. The quality of the inverted image depends on the richness of data. Nevertheless, the explicit formula (9.22), by an inverse Fourier transform, shows that the inverse problem considered has a unique solution.

9.2.3 Finite spectrum and finite number of incident waves

So far, the reconstruction of scatterer S has been based on the use of continuous spectrum $\mathrm{k} > 0$ and full observation directions $\hat{\mathbf{x}}$ in the unit sphere S_2. Born's approximation yields the remarkable result that the far-field $\mathrm{F}(\hat{\mathbf{x}}, \mathrm{k})$ gathered by the transducer contains sufficient informations to solve the inverse problem in closed-form. In practice, for instance in ultrasound scan, a finite number of transducer directions $\mathbf{d}^0 = -\hat{\mathbf{x}}$ and a finite range the spectrum or a finite number of frequencies are considered. In Geophysics, the number of natural sources like earthquake or artificial ones (for instance explosions to detect oil reservoir in the underground) are finite, as well as the number of recording stations on the ground.

Consider the inverse problem to detect a cavity C using Born's approximation and a finite number N of the transducer orientations and a finitenite number of frequencies M

$$\phi^{(\mathrm{in})}_{(\alpha)}(\mathbf{y}) = \exp(\mathrm{ik}_{(\beta)}\mathbf{d}^0_{(\alpha)}.\mathbf{y}), \ (\alpha = 1,..\mathrm{N}), \ (\beta = 1,..\mathrm{M})$$

The theoretical far-field depends implicitly of the cavity shape $\partial\mathrm{C}$ and is given by Eqs. (9.19), (9.21)

$$\mathrm{F}(\hat{\mathbf{x}}_{(\alpha)}; \mathrm{k}_{(\beta)}, \partial\mathrm{C}) = -4\pi |\mathbf{x}_{(\alpha)}| \exp(-\mathrm{ik}_{(\beta)} |\mathbf{x}_{(\alpha)}|) \times \int_{\partial\mathrm{C}} 2\mathrm{G}^{\omega}(\mathbf{x}_{(\alpha)}, \mathbf{y}) \frac{\partial}{\partial \mathrm{n}_y} \phi^{(\mathrm{in})}(\mathbf{y}; \mathrm{k}_{(\beta)}) dS_{\mathrm{y}} \tag{9.23}$$

The far-field measured is denoted by $F^{calcul}(\alpha, \beta)$.
To determine the cavity boundary ∂C one solves the *shape* optimization problem, with or without constraints on geometric parameters, (see Bonnet, 1999)

$$\min_{\partial C} \sum_{\alpha,\beta} \left\| F^{calcul}(\hat{\mathbf{x}}_{(\alpha)}; k_{(\beta)}, \partial C) - F^{meas}(\alpha, \beta) \right\|^2 \tag{9.24}$$

It is well known that the shape optimization problem is ill-posed. The presence of constraints on unknown parameters defining ∂C is then necessary to regularize the problem (9.24). Roughly speaking, regularization methods consist in choosing subspaces of functions to enforce the regulariry of the solution. For instance, in a two-dimensional problem, when the boundary ∂C is defined by the set of points $\{\mathbf{y}_1, \mathbf{y}_2, ..., \mathbf{y}_h\}$, optimal numerical solutions without constraints often present instabilities or oscillations: star shaped solution, "sea urchin" solution, dependence on the number h of elements, non uniqueness of the solution, local minima etc.

To avoid instabilities, one can consider *shape* parameters $\{p_1, p_2, .., p_m\}$ defining the geometry of guess model ∂C (circle, ellipse, rectangle etc..) in order to calculate the approximate far-field, (Kawabe, 1994). The nonlinear optimization problem (9.24) is then solved by a gradient method. Such a method implies a priori knowledge of the shape of the true cavity.

A more general method consists in parameterizing the curve ∂C by $\mathbf{y}(\theta) = (y_1(\theta)\ \ y_2(\theta))$ where $y(\theta)$ is 2π-periodic, twice continuously differentiable and $|\mathbf{y}'(\theta)| > 0$. Then the sensitivity analysis is performed by the use of Frechet differentiation of the far-field $F(\mathbf{y})$ with respect to $\mathbf{y}(\theta)$, (Kress and Zinn, 1992).

Another method to enforce the regularity of the solution to the geometric inverse problem, has been proposed by Colton and Monk (1985) to detect an unknown rigid scatterer with one incident plane wave propagating in the direction $\mathbf{d}^0$. One assumes that the receivers in different directions $\hat{\mathbf{x}}$ measure the far-field $F^{meas}(\hat{\mathbf{x}})$. The exact far-field for the true inclusion ∂C is given by

$$F(\hat{\mathbf{x}}; k, \mathbf{d}^0) = \frac{i\sqrt{2}}{4\sqrt{\pi k}} \exp(-\frac{i\pi}{4}) \int_{\partial C} \phi(\mathbf{y}) \frac{\partial}{\partial n_y} \exp(-i\mathbf{k}.\hat{\mathbf{x}}) dS_y \tag{9.25}$$

For clarity, let us denote the guess inclusion by D and define function $v(\mathbf{x})$ as

$$v(\mathbf{x}) = \int_{\hat{\mathbf{y}}=1} g(\hat{\mathbf{y}}) \exp(ik\mathbf{y}.\hat{\mathbf{x}}) dS_y$$

Function $v(\mathbf{x})$, $\mathbf{x} \in \mathbb{R}^2 \setminus \bar{D}$ is called *entire function* of the Herglotz type. If $v(\mathbf{x})$ satisfies the radiation condition and the Helmholtz equation of the exterior boundary value problem with a particular boundary condition

$$\operatorname{div}\operatorname{grad} v + k^2 v = 0, \qquad \mathbf{x} \in \mathbb{R}^2 \setminus \bar{D} \tag{9.26}$$

$$\frac{\partial v}{\partial n} = \frac{\partial}{\partial n}[H_0^{(1)}(k|\mathbf{y}|)]^* \quad \mathbf{y} \in \partial D \tag{9.27}$$

where $H_0^{(1)}(.)$ is the Hankel function of order zero and the first kind, then D is called *Herglotz domain*.

We will denote the density by $g(\hat{\mathbf{y}}; D)$.

Colton and Monk (1985) derived the following result

$$\int_{|\hat{\mathbf{x}}|=1} F(\hat{\mathbf{x}}; k, \mathbf{d}^0)[g(x; D)]^* dS_x + \sqrt{2/(\pi k)} \exp(-\frac{i\pi}{4}) = 0 \tag{9.28}$$

A Herglotz domain D, in two-dimensions and polar coordinates, possesses the property that its boundary $r = r(\theta)$ is very smooth. Thus the boundary condition (9.27) is considered as an efficient method to enforce the regularity of the numerical geometric solution. It is equivalent to the regularization technique of solving ill-posed inverse problems. It remains to enforce the boundary condition $F^{meas}(\hat{\mathbf{x}}) = F(\hat{\mathbf{x}}; k, \mathbf{d}^0)$ by substituting the far-field measurement in (9.28). Then the proposed method reads

$$\underset{D}{Min}\Big\{\Big[\int_{|\hat{\mathbf{x}}|=1} F^{meas}(\hat{\mathbf{x}}; k, \mathbf{d}^0)[g(\hat{\mathbf{x}}; D)]^* dS_x + \sqrt{2/\pi k)} \exp(\frac{i\pi}{4})\Big]^2 +$$

$$+ \int_{\partial D} \Big| \frac{\partial v(\mathbf{y}; D)}{\partial n} - \frac{\partial}{\partial n}[H_0^{(1)}(k|\mathbf{y}|)] \Big|^2 dS_y \Big\} \tag{9.29}$$

This method has been considered by Ding and Planchard (1989) for studying a circular scatterer for which the exact solution has been used for modelling the data $F^{meas}(\hat{\mathbf{x}})$.

Numerical tests based on (9.29) showed that two frequencies and three directions $\mathbf{d}^0_{(\alpha)}$ (N=3) recover the scatterer with good accuracy.

This result is similar to that obtained by Kawabe (1994).

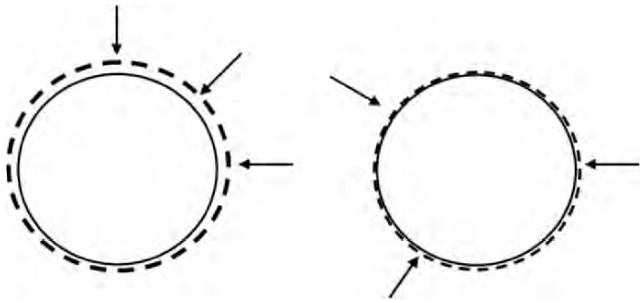

Figure 9.3: Reconstruction of a circular rigid inclusion using the method of Colton and Monk (1985), with two frequencies ω_1, ω_2, three directions N=3 of incident waves. (From unpublished works by Ding and Planchard, 1989, EDF)

9.3 Diffraction of elastic waves

The scattering of elastic waves aims at the inversion of data for volume defects in solids. To obtain reasonable models for the inversion, one makes use of similar assumptions: small defects, weak defects, infinite elastic medium, Born's approximation.

Born's approximation is related to the first order solution of the integral equation for the total elastic field **u**, while in acoustic scattering, the zero order solution has been used when we neglect the pv-integral in (9.6) and (9.18). Typically, as shown below, the total elastic field satisfies an integral equation of the type $\mathbf{u} = \mathbf{u}^{(in)} + B\mathbf{u}$. Formally, subjected to a convergence in suitable functional spaces, the solution **u** is given by the series $\mathbf{u} = (I-B)^{-1}\mathbf{u}^{(in)} = \mathbf{u}^{(in)} + B\mathbf{u}^{(in)} + B^2\mathbf{u}^{(in)}...$ with iterated integral operators B^N.

In Born's approximation, only the fisrt terms are considered for the solution $\mathbf{u} = \mathbf{u}^{(in)} + B\mathbf{u}^{(in)}$.

Consider a small defect in a solid structure, which is modelled by an infinite elastic medium. The defect, for instance a damaged zone, is an inclusion with a different elastic constants or with a change in the density. A plane incident wave impinges the defect in the $\mathbf{d}^0$ direction

$$\mathbf{u}^{(in)}(\mathbf{x},t) = \mathbf{A}\exp(i\mathbf{K}.\mathbf{x})\exp(-i\omega t) \tag{9.23}$$

where **A** and $\mathbf{d}^0$ are unit vectors, $\mathbf{K} = k\mathbf{d}^0$. For the incident P-wave $\mathbf{A}^{(P)} = \mathbf{d}^0$, for shear SH and SV waves we have $\mathbf{A}^{(S)} \perp \mathbf{d}^0$. Omitting the time factor, the diffracted wave is denoted by $\mathbf{u}^{(d)}(\mathbf{x})$. The total field satisfies the time harmonic equations

$$L_{ij}^{hk} u_{h,kj} + \rho\omega^2 u_i = 0 \quad (\text{in } \mathbb{R}^3 - \Omega) \tag{9.24}$$

$$L_{ij}^{(0)hk} u_{h,kj} + \rho^{(0)}\omega^2 u_i = 0 \text{ (in the inclusion } \Omega) \tag{9.25}$$

Let $\delta L = L - L^{(0)}$, $\delta\rho = \rho - \rho^{(0)}$, both vanish outside Ω and are constant inside Ω. Eqs. (9.24) and (9.25) can be written shortly as

$$L_{ij}^{hk} u_{h,kj} + \rho\omega^2 u_i + (\delta L_{ij}^{hk} u_{h,kj} + \omega^2 \delta\, u_i) = 0 \tag{9.26}$$

Introducing the Green function $G_{im}^{\omega}(\mathbf{x}, \mathbf{y})$ of the homogeneous medium, we express the general solution of (9.26) in the form,

$$u_i(\mathbf{x}) = u_i^{(in)}(\mathbf{x}) + \delta L_{mj}^{hk} \int_\Omega u_{h,k}(\mathbf{y}) G_{im,j}^{\omega}(\mathbf{x}, \mathbf{y}) d\Omega_y$$

$$+ \omega^2 \delta\rho \int_\Omega u_m(\mathbf{y}) G_{im}^{\omega}(\mathbf{x}, \mathbf{y}) d\Omega_y \equiv u_i^{(in)} + B_i \mathbf{u} \quad (x \in O^3) \tag{9.27}$$

where B_i are integral operators. Using Born's approximation, $\mathbf{u} = \mathbf{u}^{(in)} + B\mathbf{u}^{(in)}$ and the relation $\mathbf{u}^{(d)} = \mathbf{u} - \mathbf{u}^{(in)}$, we obtain the diffracted field as

$$u_i^{(d)}(\mathbf{x}) = \delta L_{mj}^{hk} \int_\Omega u_{h,k}^{(in)}(\mathbf{y}) G_{im,j}^{\omega}(\mathbf{x}, \mathbf{y}) d\Omega_y + \omega^2 \delta\rho \int_\Omega u_m^{(in)}(\mathbf{y}) G_{im}^{\omega}(\mathbf{x}, \mathbf{y}) d\Omega_y \tag{9.28}$$

We do not reproduce here the lengthy expressions of the Green tensor components, which can be found in textbooks, (see Achenbach, 1980; Bonnet, 1999). In fact, another assumption is generally made in scattering elastic waves, which greatly simplifies the expression for G : for *small* defects and for *large* distance between the defect (point **y**) and the receiver (point **x**), the approximate Green tensor components depend on $|\mathbf{x}-\mathbf{y}|$ and derivatives, which are estimated by means of the following expressions ($k = k_P$ or k_s)

$$1/|\mathbf{x}-\mathbf{y}| \cong 1/|\mathbf{x}|$$

$$|\mathbf{x}-\mathbf{y}| \cong |\mathbf{x}| - (\mathbf{y}.\hat{\mathbf{x}})$$

$$\frac{1}{|\mathbf{x}-\mathbf{y}|} \frac{\partial^2}{\partial y_i \partial y_j} \exp(ik|\mathbf{x}-\mathbf{y}|) \cong -\frac{k^2}{|\mathbf{x}|} \hat{x}_i \hat{y}_j \exp\{ik(|\mathbf{x}| - \hat{\mathbf{x}}.\mathbf{y})\}$$

It can be shown that the diffracted field (9.28) is given by

$$u_i^d(\mathbf{x}) = (\delta_{ij} - \hat{x}_i \hat{x}_j)\frac{1}{|\mathbf{x}|}\exp(ik_S|\mathbf{x}|)F_j(\hat{\mathbf{x}}, k_S, \mathbf{d}^0) +$$

$$+ \hat{x}_i \hat{x}_j \frac{1}{|\mathbf{x}|} u_i^d(\mathbf{x})\exp(ik_P|\mathbf{x}|)F_j(\hat{\mathbf{x}}; k_P, \mathbf{d}^0) \tag{9.29}$$

The far-field **F** defined on the unit sphere S_2 is given explicitly by

$$F_i(\hat{\mathbf{x}}; k, \mathbf{d}^0) = \frac{k^2\delta\rho}{4\pi\rho}\int_\Omega u_i^{(in)}(\mathbf{y})\exp(-ik\hat{\mathbf{x}}.\mathbf{y})d\Omega_y +$$

$$+ \frac{ik^3\delta\rho}{4\pi\rho\omega^2}\delta L_{hk}^{ij}\hat{x}_j \int_\Omega u_{h,k}^{(in)}(\mathbf{y})\exp(-ik\hat{\mathbf{x}}.\mathbf{y})d\Omega_y \ \hat{\mathbf{x}} \in S_2 \tag{9.30}$$

At fixed frequency, since the far-field is defined on the unit sphere, they are theoretically sufficient for the reconstruction of the surface $\partial\Omega$ of the defect. However, the inversion formula should not be simple to derive. Let us consider rather the possibility of collecting data in the whole spectrum, $k \in \mathbb{R}_+$ and from all directions $\hat{\mathbf{x}} \in S_2$ and show how to derive simply the volume defect Ω.

We consider the example of the reconstruction of defect due a constant change of density, while the elastic constant is homogeneous $\delta L = 0$. The contrary case of a constant change on elastic constants (the crack like defect) can be analysed in the same manner. We introduce the notations

$$\mathbf{X} = k\hat{\mathbf{x}}, \qquad M_i(\mathbf{X};\ k) \equiv 4\pi\rho F_i(\mathbf{X}/k;\ k,\ d^0)$$

Function **M(X;.)** of **X** in a three-dimensional space $(k > 0, \hat{\mathbf{x}} \in S_2)$ is known by experiments in which the emitter is fixed (incident P-wave $\mathbf{A} = \mathbf{d}$) and the receivers are in different directions $\hat{\mathbf{x}}$ of the 3D space. From Eq. (9.23) without the time factor and Eq. (9.30) we obtain

$$M_i(\mathbf{X};\ k) = A_i \int_{\mathbb{R}^3} \varphi(\mathbf{y})\exp\{i\mathbf{y}.(k\mathbf{d} - \mathbf{X})\}dy^3 \tag{9.31}$$

Since **F** is colinear with $\mathbf{u}^{(in)}$, Eq. (9.30) with $\delta L = 0$, **M** is colinear with $\mathbf{A} = \mathbf{d}$, we set $\mathbf{M} = m\mathbf{d}$. By a change of variables, we obtain the magnitude $m(\mathbf{X};k)$ of the far-field

$$m(k\mathbf{d} - \mathbf{X};\ k) = \int_{\mathbb{R}^3} \varphi(\mathbf{y})\exp(i\mathbf{y}.\mathbf{X})dy^3 \tag{9.32}$$

The Fourier transform of the characteristic function of the defect is known experimentally by the left hand side of (9.32). The conclusion is

that the far-field contains enough information which can be extracted in order to solve the inverse geometry problem. It should be noted that (9.31) indicates some compatibility between different components of the far-field data. If the data, measured components by components, are not compatible (noised data) each component $4\pi\rho F_i/d_i$ (no summation) provides independent estimations of the true defect. Needless to say, all the exact inversion formulas considered here suppose *exact* data or compatible data since they are obtained by solving forward problems

9.4 Non destructive testing of materials. A case study

This section briefly presents some experiments performed in real structures to detect cracks or defects in NDT using high frequency (Mhz), Nguyen (1992).

As discussed in Sect. 9.2, there are many conditions for solutions of scattering of waves in unbounded domain to be valid for bounded solids. Thus, it is necessary to make tests in real structures or specimens with a crack or hole in order to ensure the validity of both experimental set-ups and numerical solutions. The computations of the pressure in the time domain are performed in plane strain condition for a circular cylindrical cavity in order

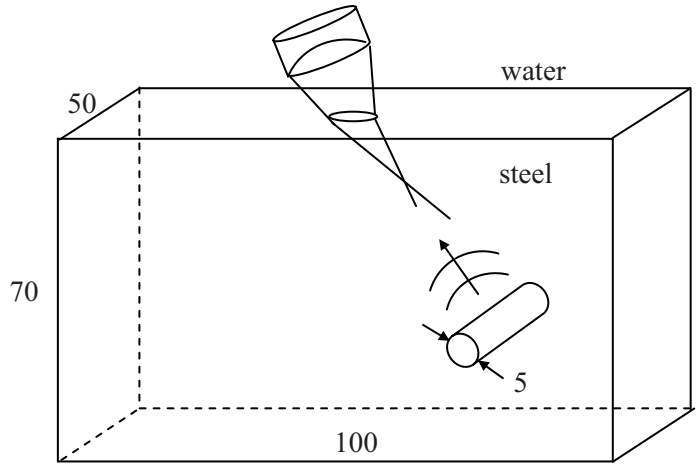

Figure 9.4: Geometry of the testing specimen in steel A42 (in cm). Focusing spherical transducer 2.25 Mhz operates in water. Measured p(t) at the interface

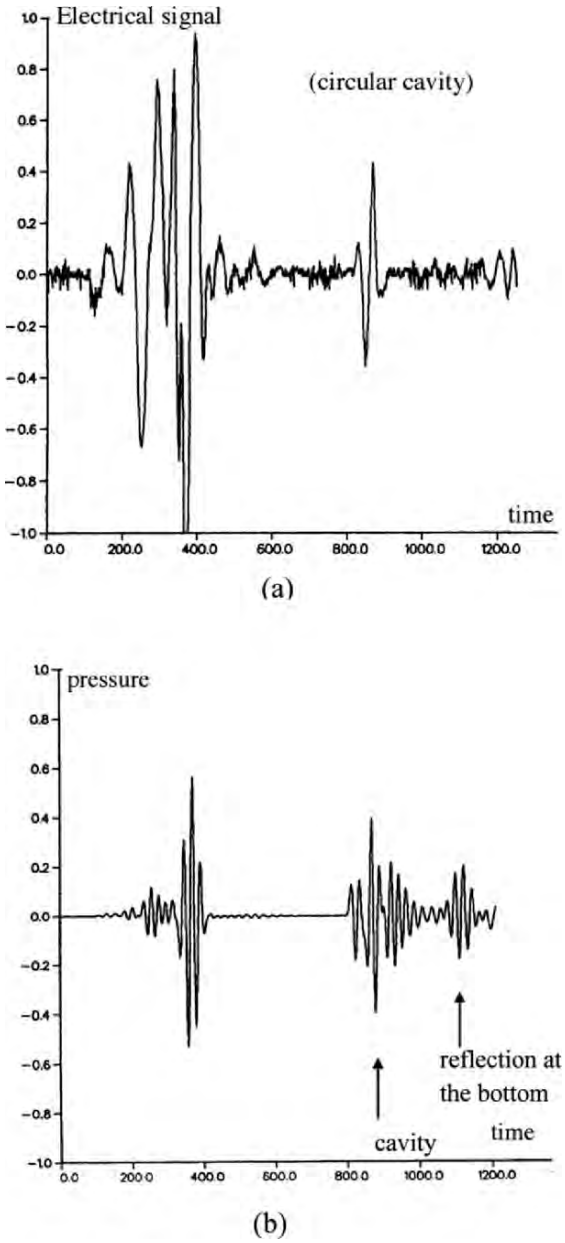

Figure 9.5: (a) Electrical signal of the transducer; High oscillations due to diffusion at the interface; Scattering waves by the cavity after a travel time; (b) Numerical computation of the water pressure p(t) at the interface, (From G. Nguyen's report EDF, 1992)

to determine the minimum size of the specimen for both valid measurements and numerical computations. Fig. 9.5 (a) shows the electrical signal of the transducer which may be sufficiently high for a transmitted wave to reach the solid medium. Most energy has been dissipated in water. The transducer also measures the reflected waves at the interface. Fig. 9.5 (b) gives the calculated acoustic pressure at the interface. A coupled fluid-solid interaction model has been used in the computations. The agreeement between theories and experiments for the location of the cavity is quite good for an engineering application.

9.5 Time reversal mirror (TRM)

This is a subject arising in medical imaging which has been recently developed, in theory as well as in experimental works and applications, since the seminal works of Prada and Fink (1994), Fink (1997), Fink and Prada (2001). Let us think about an inverse problem to determine the location of a stone in the bladder, then the mathematical solution to the inverse problem, and finally a medical treatment which consists in destroying the stone, mechanically by waves. An incredibly altogether complex operation to solve an inverse problem in fracture mechanics for the medical imaging and a treatment – is done by the well-known time reversal mirror.

Assume that a source at $\mathbf{x}_0$ (in $\Omega^+ = \{x_1 > 0\}$) emits a brief signal f(t) of compact support γ (for instance two impulses of amplitudes a_1, a_2 separated by an infinitesimal distance δ. The precursor is represented by a thin line, the other wave by a heavy line. The precursor amplitude a_1 is less than a_2 for an easier graphical display ($a < a_2$). Both waves propagate in a three-dimensional homogeneus medium. The plane S ($x_1 = 0$) consists of a two-dimensional array of small transducers which are electronically monitored so that they record, save data and magnify signals emitted backwards after some delay.

If the plane S immediately reflects waves backwards, one should have the picture shown in Fig. 9.6 Denote the incident wave in Ω^+ by $u^+(\mathbf{x},t) := f(ct - |\mathbf{x}-\mathbf{x}_0|)$, the reflected wave in Ω^+ emerges from the left with wave $u(\mathbf{x},t) := f(ct - |\mathbf{x}+\mathbf{x}_0|)$ as an emitted one at point $-\mathbf{x}_0$. The emerging wave $u^-(\mathbf{x},t)$ for $\mathbf{x}$ in Ω^+ is a divergent one.

Now suppose that the transducer records the signal $u^+(\mathbf{x}_S, t) := f(ct - \mathbf{x}_S - \mathbf{x}_0|)$ at point $\mathbf{x}_S$ on S during [0,T] and then sends it *back* to Ω^+ after a modification as $v(\mathbf{x}_S, t) = {}^-u(\mathbf{x}_S, T-t)$ with *reversal time*. That means the wave a_2 is first sent back to Ω^+, then followed by a_1 in the reversed order.

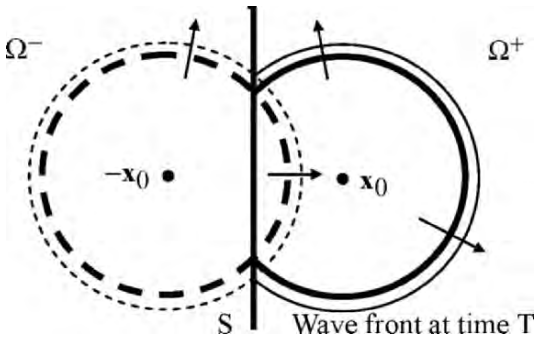

Figure 9.6: Divergent reflected wave $u^{-}(\mathbf{x},t)$ by $S(x_1 = 0)$; The gradient of the reflected wave $\partial u\ (\mathbf{x}_S,t)/\partial x_1$ is negative and at $\mathbf{x}_S = \mathbf{0}$ $\partial u\ (\mathbf{0},T)/\partial x_1 = (a_1 - a_2)/\delta < 0$

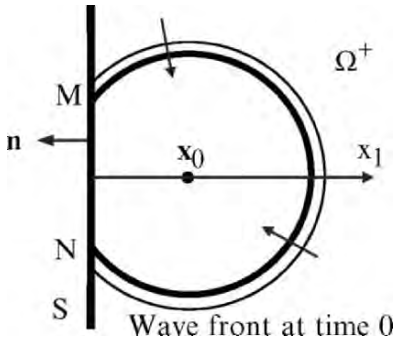

Figure 9.7: Time-reversed wave $v(\mathbf{x}, t)$ is convergent to the original scatterer $\mathbf{x}_0$; the gradient $\partial v(\mathbf{x}_S, t)/\partial x_1$ is positive on S. At time T/2 the wave is tangent to S at $\mathbf{x} = \mathbf{0}$ and $\partial v(\mathbf{0}, \frac{1}{2}T)/\partial x_1 = (a_2 - a_1)/\delta > 0$

The reverse time wave is a convergent one. Imagine that source signal $v(\mathbf{x}_S, t)$ has been electronically magnified by a large factor, thence the reversal time wave converges to the original scatterer (the bladder stone). Reversal time wave looks like a rewound movie playing backwards. In the inverse problem terminology, wave fronts of the time reversal mirror TRM are geometrical bounds of the unknown scatterer, for $t < T$. The smaller the time $(T - t)$ the better the bounds. The striking feature of TRM is that complex or random scatterers can be considered.

9.5.1 Experimental validation of TRM

We follow the works of Prada and Fink (1994) to describe their experimental setups for the validation of TRM. One transducer is used to emit a localized impulse which consists of three monochromatic waves, about $\delta/c \cong 1\mu s$. The spherical wave strikes a band B of randomly distributed scatterers which emit a broad band signal, called a *coda*, in both sides of the band B, about 200 μs. The signal is then used by a TRM to reconstruct the original source. One practically recovers a narrow band signal of the same order 1μs. The most striking result is that the more disordered the medium, the better the reconstruction of the source.

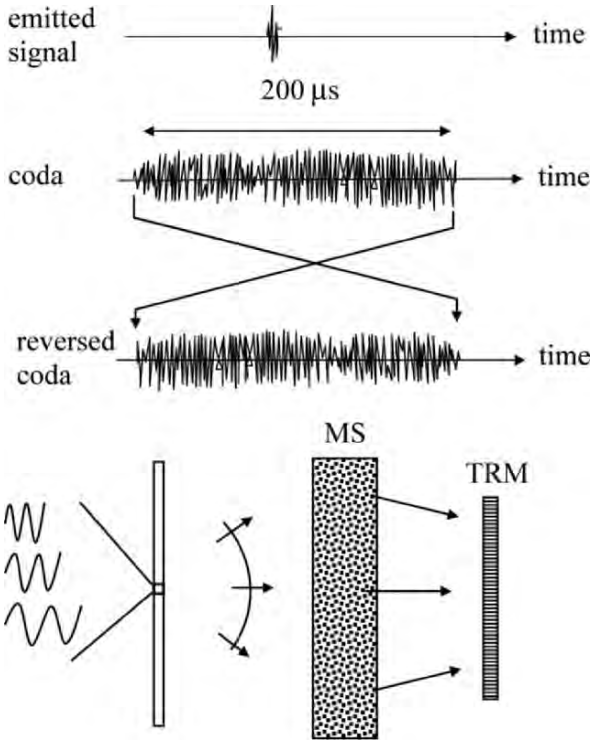

Figure 9.8: Localized signal emitted by a transducer consisting of 3 different frequencies; Multiple scattering by MS procudes a broad band signal; Wave received by TRM to reconstruct the initial source; The coda signal is recorded and then read in back slang to generate the reversed coda

9.5.2 The mathematics of time reversal mirror

As seen in Fig. 9.7, by taking the origin of time as the instant when direct wave reaches M and N, signal $v(\mathbf{x}_S, t)$ is thus known on $S\times[0,T]$ as well as the gradient $\partial v(\mathbf{x}_S,t)/\partial x_1$

$$\frac{\partial}{\partial x_1} v(\mathbf{x}_s, t) = \frac{\partial}{\partial x_1} u^-(\mathbf{x}_s, T - t) = \frac{\partial}{\partial x_1} f(c(T - t) - |\mathbf{x}_s + x_0|)$$

Now the unit normal to $\partial\Omega^+$ is directed on the left, Fig. 9.7, so that the normal gradient of the time-reversed field v is $\partial_n v(\mathbf{x}_S, t) = -\partial u^-(\mathbf{x}_S, T-t)/\partial x_1$.

Mathematically the time-reversed field $v(\mathbf{x}, t)$ satisfies the wave equation (without source term) and two boundary conditions on S

$$\text{div grad}\, v(\mathbf{x}, t) - \frac{1}{c^2}\frac{\partial^2 v(\mathbf{x}, t)}{\partial t^2} = 0 \text{ on } \Omega^+ \times [0, T]\ ^{(*)} \tag{9.33}$$

$$v(\mathbf{x}, t) = f(c(T-t) - |\mathbf{x} + \mathbf{x}_0|) \text{ on } S \times [0, T] \tag{9.34}$$

$$\frac{\partial v(\mathbf{x}, t)}{\partial n} = -\frac{\partial}{\partial x_1} f(c(T-t) - |\mathbf{x} + \mathbf{x}_0|) \tag{9.35}$$

Remark that $f \equiv 0$ on S outside the area hit by the incident wave (thus outside region MN). The problem (9.33)-(9.34) is unusual for a wave equation in the sense that there is *no* initial condition in Ω^+, but rather two superabundant data on S, the Dirichlet and the Neumann boundary conditions. Mathematically, this is a Cauchy problem for an hyperbolic equation which is known to be ill-posed. One efficient method is based on the so-called quasi-reversibility method of Lattès and Lions (1967), which has been generalized to hyperbolic equations by Klibanov and Timonov (2003) in order to solve Eqs. (9.33)-(9.34) without the ill-posedness of the original mathematical problem.

(*) More precisely the time interval $[0, T - \,]$

Chapter 10

Tomographic Evaluation of Materials

10.1 Introduction

Applications of X-ray in medical imaging are nowadays a means for diagnosis of tumors, fracture of bones. More powerful Gamma-ray tomography are used in material sciences for detecting metal forming defects, cavities, microcracks, inclusions, inserts etc. Fig. 10.1 shows an example of Gamma inspection to reveal defects in steel structure in highly stressed zone, Figure 10.2 reveals inserts inside ancient statue.

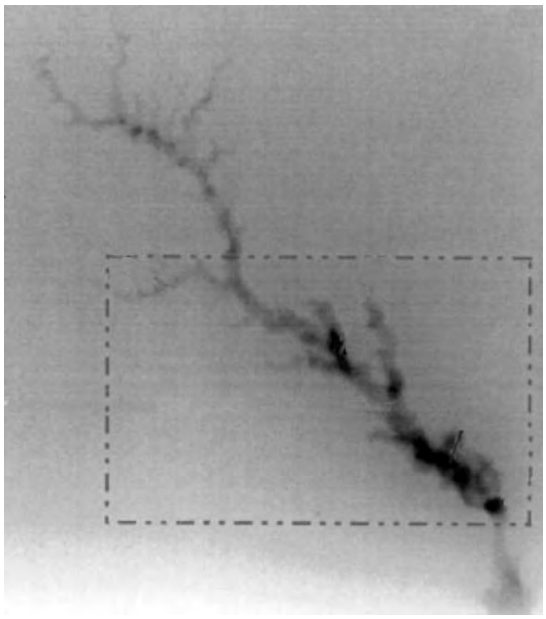

Figure 10.1: Gamma tomography revealing micro-crackings and cavities in stainless steel specimen; black zones are cavities (from Taheri, EDF/R&D document)

Figure 10.2: The Aphrodite statue of the Louvre Museum revealing metallic inserts (Permision Commissariat à l'Energie Atomique, CEA/DAMRI, Clefs Cea, N° 34 Hiver 1996-1997. La radioactivité)

In different techniques used in applications, the mathematical method of solution for data inversion is the same, namely Radon's transform and its inverse.

10.2 X-rays tomography

The principle of X-ray tomography is based on Radon's transform R. When a ray L passes through the body, its global attenuation m along the ray L can be measured experimentally. It is equal to the sum of unknown local attenuation density $\mu(x)$ along the ray L

$$m = \int_L \mu(\mathbf{x})dx := R\mu \tag{10.1}$$

Generally the local attenuation μ is considered as proportional to the unknown density ρ, so that Radon's transform and its inverse are key transforms for *structural* tomography, which determines the density map ρ(x).

In two-dimensional problems, the scalar μ depends on (x_1, x_2). The position of the ray L depends on two parameters, ρ and θ, defining the line L $(x_1\cos\theta + x_2\sin\theta - \rho = 0)$. The Radon transform is R: $\mu(x_1, x_2) \rightarrow m.\rho\ ,\ \theta)$. Classical X-ray Tomography does not consider diffusion or scattering (like the Compton scattering of electron). The body is perfectly transparent to rays which propagate without a deviation in homogeneous and free of defects zones.

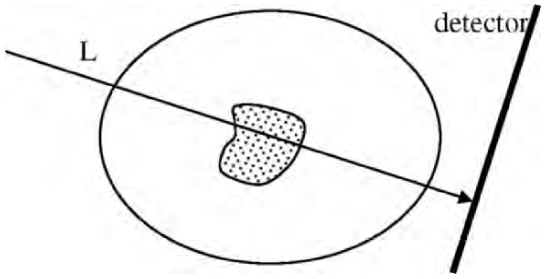

Figure 10.3: Structural tomography by X-rays. The detector measures the global attenuation m of the ray L passing through the body; the local attenuation is proportional to the density

10.2.1 Inverse Radon's transform

Let us extend μ(**x**), defined on the defect Ω, to the whole plane by setting

$\mu(x_1, x_2) = 0$ outside Ω

and denote the extended function by the same function μ(**x**). The object considered is scanned by parallel rays, making the angle $\theta + \pi/2$ with the Ox_1 axis, at the distance ρ from the origin of the coordinates. Introducing the Dirac delta function $\delta(x_1\cos\theta + x_2\sin\theta - \rho)$ we then express the global attenuation m along the ray as

$$m(\rho,\theta)=\int_{\mathbb{R}^2}\mu(x_1,x_2)\delta(x_1\cos\theta + x_2\sin\theta - \rho)dx_1dx_2 \tag{10.2}$$

Considering the partial Fourier transform m→M with respect to ρ with the corresponding Fourier variable K_ρ, we obtain

$$M(K_\rho,\theta)=\int_{-\infty}^{+\infty}\int_{\mathbb{R}^2}\mu(x_1,x_2)\delta(x_1\cos\theta + x_2\sin\theta-\rho)\exp(-i\rho K_\rho)dx_1dx_2d\rho \tag{10.3}$$

The latter equation can be written as

$$M(K_\rho,\theta)=\int_{\mathbb{R}^2}\mu(x_1,x_2)\exp(-iK_\rho(x_1\cos\theta + x_2\sin\theta))dx_1dx_2 \tag{10.4}$$

Expression (10.4) has the following physical meaning. Denote the Fourier transform with respect to the variable ρ by $F_{(\rho)}$

$$F_{(\rho)}:\ m(\rho,\theta)\rightarrow M(K_\rho,\theta)\equiv F_{(\rho)}m(\rho,\theta) \tag{10.5}$$

By varying ρ, with the angle θ held fixed, we get a "section" of the surface of the 2D Fourier transform of m, in the Fourier space (K_1, K_2), by putting $K_1 = K_\rho\cos\theta$ and $K_2 = K_\rho\sin\theta$. Now gathering the results obtained from different sections, for all angles θ, we obtain the transformed M in Cartesian coordinates (K_1, K_2),

$$M(K_\rho,\ \theta)\equiv M(K_1,K_2) \tag{10.6}$$

Therefore the inverse Radon transform is defined by the formula

$$\mu(x_1,x_2)\equiv F^{-1}_{(K_1)}F^{-1}_{(K_2)}\left(M(K_\rho,\theta)\right)= F^{-1}_{(K_1)}F^{-1}_{(K_2)}M(K_1,K_2) \tag{10.7}$$

which involves :

– a Fourier transform of the attenuation m(ρ,θ) with respect to ρ

– a change of variables $(K_\rho,\theta)\rightarrow(K_1,K_2)$

– and an inverse Fourier transform in the K-space.

It is worth mentioning some other properties of Radon's transform μ→Rμ. Consider the adjoint operator R* defined as

$$R^*:\ \psi(\rho,\theta)\ \rightarrow (R^*\psi)(x_1,x_2)\equiv\int_0^{2\pi}\psi(x_1\cos\theta + x_2\sin\theta,\ \theta)d\theta \tag{10.8}$$

For physical reasons, R is called the *projection* while R* is called the *back-projection*. Define the function B(ρ,θ)

$$B(\rho,\theta) := \frac{1}{2\pi}\int_{-\infty}^{+\infty}\exp(i\rho K_\rho)M(K_\rho,\theta)\left|K_\rho\right|dK_\rho \tag{10.9}$$

This function is not the inverse Fourier transform of M, but rather a weighted inverse Fourier transform, by the weight factor $|K_\rho|$. It can be shown that the solution μ is the back-projection of B

$$\mu(x_1,x_2) = \frac{1}{4\pi}R^*(B(\rho,\theta)) \tag{10.10}$$

B is also related to the Hilbert transform H

$$Hu(t) = \frac{1}{\pi}(pv)\int_{\mathbb{R}}\frac{u(s)ds}{t-s} \quad \text{(pv: principal value)}$$

by $B = HR\mu$, so that $\mu = (1/4\pi)R^*Hm$. The inverse Radon transform is $R^{-1} = (1/4\pi)R^*H$. These operators have important applications in medical imaging.

10.2.2 Example of crack detection

Let us consider the crack as a thin zone of some constant absorption with small thickness e, with length 2η and parallel to Ox_1. The presence of a discontinuity of the material may reflect the X-ray partially at both faces of the crack and thus causes equivalent absorption of the rays. The attenuation is given by

$m_\theta(\rho) = e/\cos\theta$, if $\rho_0 - \eta\cos\theta < \rho < \rho_0 + \eta\cos\theta$,

$m_\theta(\rho) = 0$, otherwise.

Hence

$$M(K_\rho,\theta) = \frac{2e}{K_\rho\cos\theta}\sin(\eta K_\rho\cos\theta)$$

or

$$M(K_1,K_2) = \frac{2e}{K_1}\sin(\eta K_1) \tag{10.11}$$

By the inverse Fourier transform, we obtain

$$F^{-1}_{(K_1)}F^{-1}_{(K_2)}M(K_1,K_2) = eC(x_1/\eta)\delta(x_2) \tag{10.12}$$

where C(t) = 0 if |t| > 0, C(t) = 1 if |t| < 0. Function C(t) is the characteristic function of the interval [−1,+1] and thus Eq. (10.12) yields the characteristic function of the thin cut in 2D.

10.3 Attenuated Radon transform

10.3.1 Functional tomography by SPECT and PET

More recently there have been some new methods in medecine imaging, for example the *functional* tomography which determines the distribution of sources of photons emitted by radionuclides absorbed by specific cells. The new methods make use of the so-called Attenuated Radon Transform, (Finch, 1986; Novikov, 2001; Natterer, 2001).

In material sciences, such a functional tomography can be used for investigating edge cracks or microcracks absorbing radioactive fluids which becomes sources of radionuclides.

In medical imaging, the *functional tomography* studies the activity of specific cells under investigation which emit photons from the radionuclides (^{133}Xenon, ^{18}Fluoro) absorbed by the cells. A collimator-detector measures the photons emitted at **x,** which travel along the line L of tissue parallel to the axis of the collimator-detector. The source f(**x**) of emitted photons is attenuated along the line segment L(**x**) from **x** to the collimator at the location **a** by the factor $\exp(-\int_{L(x)}\mu(\mathbf{s})ds)$. It can be shown that the exponential factor comes from the integration of Boltzman's transport equation of photons. The density map or the local attenuation μ(**x**) is already known from the structural tomography, by the Radon transform and its inverse. The unknown source f(**x**) may be determined by measurements of the photon intensity F captured by the collimator-receiver for different lines. The attenuated Radon transform of f(**x**) is the Novikov transform N: f→F

$$F = \int_L \exp\left(-\int_{L(x)} \mu(s)ds\right) f\,\rho\mathbf{k}^{\perp} + t\mathbf{k})dt \qquad (10.13)$$

k is the unit vector along L, $\mathbf{x} = \rho\mathbf{k}^{\perp} + t\mathbf{k}$, $\mathbf{k} = (\cos\theta, \sin\theta), \mathbf{k}^{\perp} = (-\sin\theta, \cos\theta)$, ρ the distance of L to the origin of coordinates, L(**x**) the part of L from the point $\mathbf{x} = \rho\mathbf{k}^{\perp} + t\mathbf{k}$ to the detector.

Solving Eq. (10.13) for f(**x**) is the subject of Single Photon Emission Computerized Tomography (SPECT).

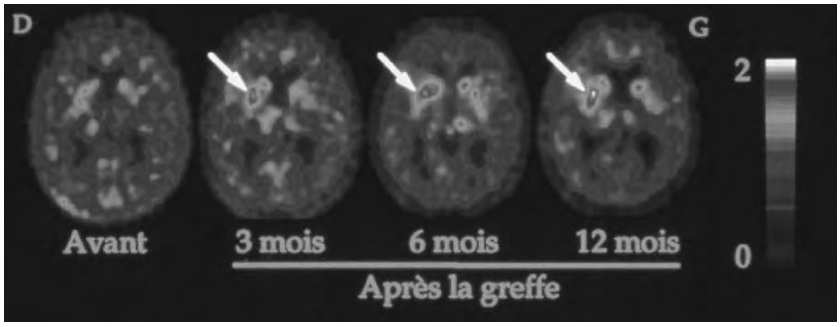

Figure 10.4: Positon Emission Tomography (PET). A functional tomography using ^{18}Fluoro-Deoxy-Glucose concentrated in living tissue absorbing glucose in the Parkinson desease : before, 3, 6, 12 monthes after the transplant of dopamine neurones, indicating the progressive fixing of ^{18}FDG and thence the viability of the transplant (permission of CEA/SHFJ Orsay, Ph. Remy, Clefs cea, N° 34 Winter 1996-1997)

Another method of medecine imaging called the Positon Emission Tomography (PET) considers the emission of a positon, which anhihilates immediately with a nearby electron to produce two photons γ emitted in opposite directions.

The experimental set-ups consist of two opposite collimator-receivers in the same line. The *simultaneous* measurements in opposite directions by the collimator-detectors give the intensity

$$F = \int_L \exp\{-\int_{L^+(x)} \mu(s)ds \; - \int_{L^-(x)} \mu(s)ds\} f(\rho\mathbf{k}^\perp + t\mathbf{k})dt$$

$$F = \exp(-\int_L \mu(s)ds) \int_L f(\rho\mathbf{k}^\perp + t\mathbf{k})dt \tag{10.14}$$

where $L = L^+(x) \cup L^-(x)$. Since the factor $\exp(-\int_L \mu(s)ds)$ is known from structural tomography, PET methods of solution are obtained by an inverse Radon's transform.

Methods based on emission of soft gamma rays (100k eV) and for soft materials, have applications in medical imaging, rather than in Engineering Mechanics. Nevertherless, to study damage in materials due to the neutrons of very high energy (>14 MeV) and radioactive elements produced in a fusion reactor (Tokamak, JET or ITER project), none but the neutron-tomography is able to detect defects in structures subjected to severe conditions.

10.3.2 Novikov's inversion formula

Eq. (10.13) for infinite line L is written with new variables (τ,ρ,θ) as

$$F(\rho, \theta) \equiv Nf(\rho, \theta) = \int_{-\infty}^{+\infty} \{ \exp(-\int_{t}^{\infty} \mu(s, \rho, \theta) ds) \} f(t, \rho, \theta) dt \qquad (10.15)$$

The breakthrough of inverting Eq. (10.15) was achieved by Novikov (2001) who gave the formula

$$f(x_1, x_2) = \frac{1}{4\pi} \left(\frac{\partial}{\partial x_1} - i \frac{\partial}{\partial x_2} \right) \int_{0}^{2\pi} \exp(i\theta) R(t, \rho, \theta) d\theta \qquad (10.16)$$

$$R(t, \rho, \theta) = \exp\left(\int_{t}^{\infty} \mu(s, \rho, \theta) ds \right) \times \left(\{ \exp(P^{-} F(\rho, \theta)) \} P^{-} \{ \exp(-P^{-} F(\rho, \theta)) \} \right.$$

$$\left. + \{ \exp(-P^{+} F(\rho, \theta)) \} P^{+} \{ \exp(P^{+} F(\rho, \theta)) \} \right) \times F(\rho, \theta) \qquad (10.17)$$

where $P^{\pm}$ are the projectors on the real axis

$$P^{\pm} f(\rho) = \pm \frac{1}{2} f(\rho) + (pv) \frac{1}{2i\pi} \int_{-\infty}^{+\infty} \frac{f(r)}{r - \rho} dr \qquad (10.18)$$

Novikov's inversion formulae (10.16)-(10.17) are explicit. There are also numerous iterative algorithms for inverting Eq. (10.15), in particular for constant attenuation μ, (Kunyansky, 2001).

10.4 Conical Radon's transform in Compton Scattering

Scattering of photons by the Compton effect, may considerably affects the image quality of the object in some cases. Classical tomographies, by Radon's transform or attenuated Radon transform, operate with *primary* γ photons which arrive at the collimator-detector without scattering. Here, the light arrives in the detector from primary photons and also from secondary low energy photons, scattered at various angles with the corresponding lost of energy. The higher the deviation angle, the higher the energy lost. The relation between energy lost E_0–E and the deviation angle θ, comes from the Compton single-scattering formula

$$E = E_0 \frac{1}{1 + \varepsilon(1 - \cos\theta)} \qquad (10.19)$$

where E_0 is the energy before scattering ($E_0 > E$), $\varepsilon = E_0/mc^2$, mc^2 the rest energy of the photon. Eventually, after scattering a photon can be scattered

again and again, by multiple scatterings. In what follows, only single-scatterings of photons are considered.

In applications to astrophysics, imaging of galactic sources of gamma rays of weak intensity, is considerably affected by absorption, deviation of light by Compton scattering effect. Up to now, most methods of imaging discard the scattered photons and operate only with the primary ones. It should be important that secondary photons can also be used for the reconstruction of the objects. To date mathematical and technical problems to use secondary photons have remained a major technical challenge in γ-rays imaging. Recently Nguyen and Truong (2002) established a new relation between the object radioactivity density and a series of images formed by single-scattered photons which are secondary photons parameterized by various angles of scattering. It appears that the transform can be viewed as a Compound Conical Radon Transform.

10.4.1 The conical Radon transform

The material of this section is adapted from the paper (Nguyen et al, 2004). Let g(**D**,θ) be the photon flux density at point **D** at the detector site plane.

Consider this quantity as describing a secondary emission imaging process since it is based on secondary emission by free nearby electrons of the surrounding medium. Photons of energy E are arriving at the detector point **D** from point **M**. Point **M** has deviated photons of energy E_0 at the site points **C** lying on the surface of a circular cone of angle θ, with the apex **M** and with the axis normal to the detector plane.

The unknown density function is f(**C**) at point **C** in the medium. The number of photons emitted in a solid angle $d\Omega_M$ around the site **M** by an elementary volume dv_C at point **C** is

$$\frac{1}{4\pi}\mathrm{f(C)}dv_C d\Omega_M$$

Noticing that

$$d\Omega_M = dS_M/\mathrm{r}^2(\mathbf{M},\mathbf{C})$$

with the Euclidian distance $\mathrm{r}(\mathbf{M},\mathbf{C}) := |\mathbf{M}-\mathbf{C}|$ between points **M** and **C**, the flux of photons at M from the volume dv_C in the direction **CM** is then given by

$$\frac{1}{4\pi}\mathrm{f}(\mathbf{C})dv_C \exp(-\mu\mathrm{r})\frac{1}{|\mathbf{M}-\mathbf{C}|^2}$$

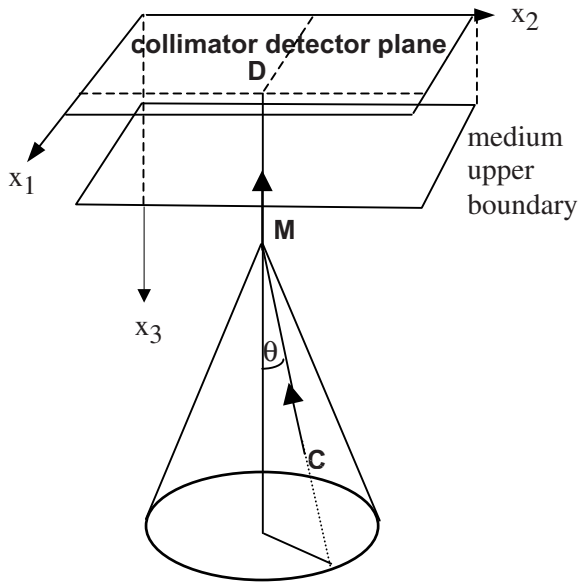

Figure 10.5: Geometry of the system for Conical Radon transform; Photons of energy E coming from **M** to **D** are issued from photons **C** of energy $E_0 \geq E$ on the cone scattered by electron **M** at angle θ

with the linear constant coefficient of absorption μ. The number of photons reaching the detector surface at **D** per unit time, per unit area (division by dS_M) is the flux density recorded at the detector plane, at the site **D**. This flux depends on the number $n_e(\mathbf{M})dv_M$ of free electrons, the distance from **M** to **D** and the probability P(θ) for a deflection by an angle θ (given by the Klein-Nishina probability)

$$\mathrm{P}\ \theta) = \frac{1}{[1+\varepsilon(1-\cos(\theta))]^2}\left[1 + \cos^2(\theta) + \frac{\varepsilon^2(1-\cos(\theta))^2}{1+\varepsilon(1-\cos(\theta))}\right]$$

When **M** is inside the medium, $M_3 > b_3$ (the location of the medium upper boundary is $x_3 - b_3$), the absorption has to be taken into account by the factor $\exp(-\mu(M_3 - b_3))$. When **M** is outside the medium the factor is 1. The recorded flux density is given by Nguyen and Truong (2002) as

$$\frac{1}{8\pi} f(C)dv_C \exp(-\mu r)\frac{n_e(M)dv_M}{|\mathbf{M}-\mathbf{C}|^2}\frac{r_e^2 P(\theta)}{|\mathbf{M}-\mathbf{D}|^2}\exp(-\mu(M_3 - b_3) \qquad (10.20)$$

The total number of photons recorded per unit time, per unit detector area at $\mathbf{D}=(D_1,D_2)$ is the flux (where, for convenience, the Dirac delta function in ¡^{2} has been introduced)

$$g(\mathbf{D},\theta)=\int dv_M \frac{1}{8\pi M_5^2}\delta(D_1-M_1)\delta(D_2-M_2)n_e(\mathbf{M})f(C)$$
$$\times \exp(-\mu(M_3-b_3)) \times \int f(\mathbf{C})\exp(-\mu r)\frac{n_e(M)dv_M}{|\mathbf{M}-\mathbf{C}|^2} r_e^2 P(\theta) \quad (10.21)$$

The conical Radon transform is defined by

$$T: f(\mathbf{C}) \rightarrow g(\mathbf{D},\theta) \quad (10.22)$$

The transform T maps a scalar function in a three-dimensional domain occupied by **C** to a function which is also defined in a three-dimensional domain {detector plane} × {angle θ range}. Let t = tan(θ) and denote the compound functions by using the same notation g(**D**, θ(t)) = g(**D**, t), $K(\theta) = n_e r_e^2 P(\theta)\sin(\theta)/8\pi$, K(t) = K(θ(t)) etc. The conical Radon transform can be rewritten as

$$g(\mathbf{D},t)=\int p(\mathbf{D},t;\mathbf{C})dv_C \quad , \mathbf{C}\in\mathbb{R}^3, \mathbf{D}\in\mathbb{R}^2, t\in[0,\infty] \quad (10.23)$$

The kernel p(**D**, t; **C**). is the image on the detector plane of secondary point source at site **C**.

For angle θ = 36° the amplitude of the image of single-scattered photons has the form of a mexican hat, Fig. 10.6, which is very far from the Gaussian shape generally considered in methods of imaging with primary photons. The energy lost at θ = 36° is –5%.

10.4.2 Nguyen and Truong's inversion formula

Recently Nguyen and Truong (2002) accomplished a feat of strenght in inverting the conical transform (10.22). It is out of the scope of this book to go into the details of the derivation of the inverse operator T^{-1}: g(**D**, θ)→ f(**C**). The transform itself is very complex, so its inverse should be complex too. Surprisingly, the inverse transform has a quite simple expression given in explicit form.

Consider the spatial Fourier transform of function:

$$F: g(D_1, D_2, t) \rightarrow G(u_1, u_2, t).$$

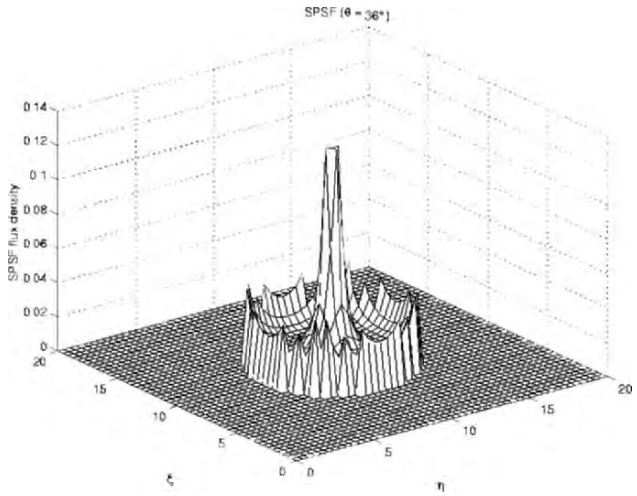

Figure 10.6: Kernel p(**D**, t; **C**). is the image of point source **C**, for angle θ = 36°

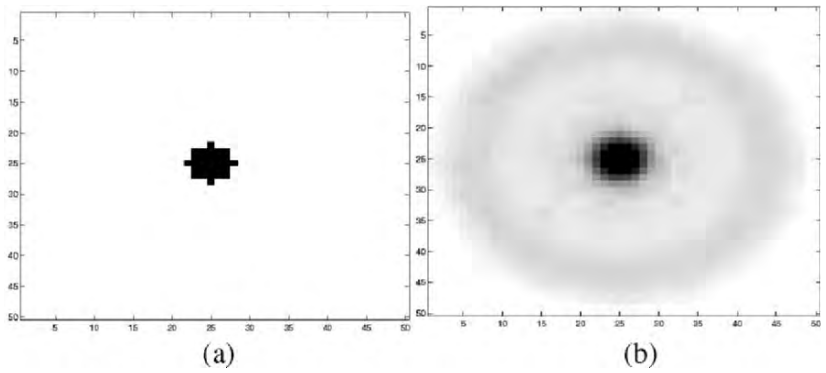

Figure 10.7: Polygonal disc (a) and its image by photons scattered at θ = 36° (b)

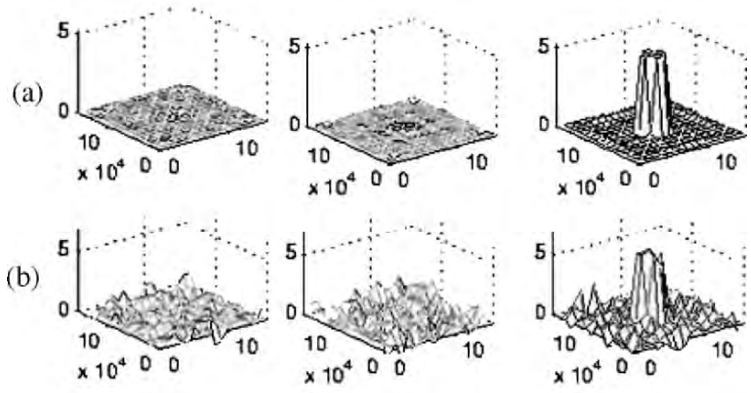

Figure 10.8: Reconstructed object at different times, using photons in the range $5° < \theta < 175°$, (a) in the absence of noise, (b) with noise (S/N = 9.7dB, RMSE = 8.9%), (permission Nguyen and Truong, Cergy PontoiseUniversity)

The inverse operator makes use of the inverse Fourier transform combined with a transform using Bessel functions

$$f(\mathbf{C}) = \int_{-\infty}^{\infty}\int_{-\infty}^{\infty} du_1 du_2 \exp\{-2i\pi[u_1C_1 + u_2C_2]\} 4\pi(C_3 - b_3)(u_1^2 + u_2^2) \times$$

$$\times \int_0^{\infty} t dt G(u_1, u_2, t) \frac{1}{K^*(t)} \{- J_0\left(2\pi t(C_3 - b_3)\sqrt{u_1^2 + u_2^2}\right) -$$

$$- (C_3 - b_3)\pi\sqrt{u_1^2 + u_2^2}) J_1\left(2\pi t(C_3 - b_3)\sqrt{u_1^2 + u_2^2}\right)\} \quad (10.23)$$

where $K^*(t) = 2K(t)/r_e^2$. A validation of the method has been given in (Nguyen and Truong, 2002) for a polygonal disc. Fig. 10.7 shows the original disc (a) and its image from the secondary photons scattered at $\theta = 36°$ (b).

To reconstruct the object, a series of images parameterized by θ in the range $5°<\theta<175°$ has been used under the following conditions: electron density in biological tissue $n_e = 3.5\times10^{23}$ electrons/cm^3, SPECT (Single Photon Emission Computed Tomography) γ-detector, ^{99}Technium radioisotope, model dimensions $16 \times 16 \times 16$, acquisition time per image 0.1s. Fig. 10.8 shows the reconstructed object at times 0.1, 0.2, 0.3s in the absence of noise (a) and with a noise (b)(S/N = 9.7dB, RMSE = 8.9%).

It should be noted that primary photons outside the range $0° < \theta < 5°$ are not recorded by classical SPECT because they miss the highly directional collimator-detector. Therefore, methods which consider altogether primary photons in the range $0 < \theta < 5°$ and secondary photons outside this range may be a challenge for γ emission imaging.

Chapter 11

The Reciprocity Gap Functional for Crack Detection

Recently there have arisen new methods for defect identification based on the so-called Reciprocity Gap functional (RG) which has the following physical meaning: when RG equals zero, there are no defects in the solids; the non zero value of RG indicates the presence of defects and provides a direct means for their identification. This theory orginates from the famous Calderon's work on distributed defects, who showed that *two* boundary values of the Dirichlet and Neumann type, determine the unknown volumetric defect in a linearized problem. The theory was extended to crack identification for the harmonic equation $\Delta u = 0$ in Ω, using two boundary data u and $\partial u/\partial n$ on $\partial\Omega$, on the external surface of the cracked body where measurements are possible. Andrieux and Ben-Abda (1992) extended the theory to determine the crack plane for the harmonic equation. Later, Andrieux et al (1999) solved the same identification problem in elasticity for the crack geometry. This chapter is devoted to inverse problems for crack identification in different cases ranging from elliptic equations, parabolic equations namely the heat diffusion equation with applications to crack identification using the Infra-Red camera technique and to hyperbolic equations. The latter topics concern transient acoustics, with applications for ultra-sound scan in the time domain (instead of the frequency domain in classical scatterings of waves) and transient elastodynamics, with applications for the earthquake problem

11.1 Distributed defect and crack

Calderon (1980) gave a nice method to identify a defect in a solid Ω, which affects for example the static heat conduction coefficient. This is done by changing the normalized conduction coefficient from 1 to $1 + k(\mathbf{x})$. The inverse problem of the static equation consists in determining $k(\mathbf{x})$

from boundary measurements, the surface temperature θ^d and the normal flux f^d. The temperature field satisfies the equations

$$-\mathrm{div}\{(1+k)\mathrm{grad}\,\theta\} = 0 \text{ in } \Omega \tag{11.1}$$

$$\partial_n\theta = f^d \text{ on } \partial\Omega \tag{11.2}$$

To solve the inverse problem, an adjoint field satisfying the equations in the domain Ω with another boundary condition is considered

$$-\mathrm{div}\{\mathrm{grad}\,\psi\} = 0 \text{ in } \Omega \tag{11.3}$$

$$\partial_n\psi = g \text{ on } \partial\Omega \tag{11.4}$$

Combine these equations to obtain

$$\int_\Omega k\,\mathrm{grad}\theta(k).\mathrm{grad}\,\psi d\Omega = \int_{\partial\Omega}\{\psi\partial_n\theta - \theta\partial_n\psi\}dS = \int_{\partial\Omega}\{\psi f^d - \theta^d\partial_n\psi\}dS \tag{11.5}$$

In Eq. (11.5) the field $\theta(k)$ solution of (11.1), (11.2) depends on k implicitly. The first integral of Eq. (11.5) is *nonlinear* in k. Calderon proposed a *first order* solution by considering small perturbation, so that the first order $k^{(1)}$ is solution of

$$\int_\Omega k^{(1)}\mathrm{grad}\phi.\mathrm{grad}\,\psi d\Omega = \int_{\partial\Omega}\{\psi f^d - \theta^d\partial_n\psi\}dS \tag{11.6}$$

where $\phi = \theta(k=0)$ satisfies the equation

$$-\mathrm{divgrad}\,\phi = 0 \text{ in } \Omega \tag{11.7}$$

$$\partial_n\phi = f^u \text{ on } \partial\Omega \tag{11.8}$$

Eq. (11.6) is not yet a Fredholm integral equation of the first kind. To obtain such an integral equation, Calderon introduced a y-family of adjoint fields or data $g(\mathbf{y})$, $f^u(\mathbf{y})$ so that (11.6) becomes a Fredholm equation of the fisrt kind with kernel $\mathrm{grad}\phi(\mathbf{x},\mathbf{y}).\mathrm{grad}\psi(\mathbf{x},\mathbf{y})$

$$\int_\Omega k^{(1)}(\mathbf{x})\mathrm{grad}\phi(\mathbf{x},\mathbf{y}).\mathrm{grad}\,\psi(\mathbf{x},\mathbf{y})d\Omega_x = \int_{\partial\Omega}\{\psi f^d(\mathbf{y}) - \theta^d(\mathbf{y})\partial_n\psi\}dS \tag{11.9}$$

A particular choice of adjoint fields allows the exact inversion of (11.9), (Calderon, 1980)

Now consider the inverse problem for crack identification using the same physics, with measurements of the surface temperature θ^d and the normal flux f^d. The temperature satisfies the harmonic equation in Ω and

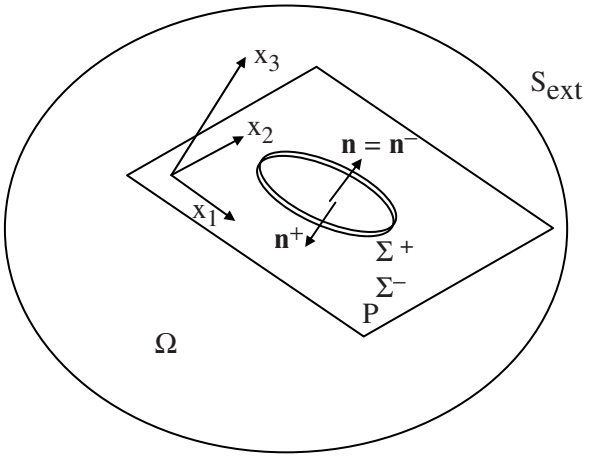

Figure 11.1: Geometry of the internal planar crack Σ to be identified; Two boundary data θ and ∂θ/∂n are measured on S_{ext}. No heat flux on the crack ∂θ/∂n = 0

boundary conditions $\partial\theta/\partial n = f^u$ on the external surface S and $\partial\theta/\partial n = 0$ on the internal crack faces $\Sigma^{\pm}$. Since there are two crack faces, we will consider the following notations. Let $\mathbf{n} = \mathbf{n}^-$, $\mathbf{n}^+ = -\mathbf{n}$. Introducing an adjoint field ψ in the *uncracked* domain occupying the same volume Ω and combining the equations for the current field and the adjoint field, we obtain

$$\int_{\Sigma}[[\theta]]\partial_n\psi\, dS = \int_S \{\psi\partial_n\theta - \theta\partial_n\psi\}\, dS \equiv \int_S \{\psi f^d - \theta^d\partial_n\psi\}\, dS \qquad (11.10)$$

The second integral is called the *Reciprocity Gap* functional RG, (Andrieux and Ben-Abda, 1992)

$$RG(\theta,\psi) := \int_S \{\psi\partial_n\theta - \theta\partial_n\psi\}\, dS$$

It is a bilinear form in (θ ,ψ) which becomes the linear form $R^d(\psi)$ defined by the third integral in (11.10) when the boundary data θ^d and f^d are considered

$$R^d(\psi) := \int_S \{\psi f^d \quad \theta^d\partial_n\psi\}\, dS$$

RG(θ, ψ) is also equal to the first integral over Σ. This is the consequence of a conservation law (or the reciprocal Betti identity). Eq. (11.10) written as $RG(\theta, \psi) = R\cdot(\psi)$, ∀ψ, is nothing but the variational form of the observation equation to find θ or to solve the inverse problem to determine Σ and

[[θ]]. Andrieux and Ben-Abda showed that a suitable choice of the adjoint field determines the solution explicitly. Consider the example of the following adjoint harmonic function $\psi = \sin(\omega x_1)\sinh(\omega x_2)$ to detect a line crack in two-dimensions, lying on the axis Ox_1. Let the jump $f = [[\theta]]$ be extended outside the crack by zero, so that $f(x_1)$ is an unknown function defined on the whole x_1-axis, whose support function is the line crack. The first integral of (11.10) is written as

$$\int_{-\infty}^{+\infty} f(x_1)\sin(\omega x_1)dx_1 = \int_S \{\psi f^d(\mathbf{x}) - \theta^d(\mathbf{x})\partial_n\psi\}\,dS \tag{11.11}$$

The right hand side of Eq. (11.11) is known from boundary data and from the given adjoint function, the left hand side of the equation is the Fourier transform $F(f(x_1))$ of the unknown function f. If the right hand side of Eq. (11.11), denoted by $R^d(\omega)$ is known for the whole spectrum ω, the function $f(x_1)$ is obtained by the inverse Fourier transform of the right hand side of Eq. (11.11), thus the support of the function $F^{-1}(R^d(\omega))$ gives the line crack. This method has been successfully extended to the harmonic equation in 3D, (Bannour et al, 1997). Let us remark that Eq. (11.10) written in the form

$$\int_\Sigma [[\theta]]\partial_n\psi\,dS = \int_S \{\psi f^d - \theta^d\partial_n\psi\}\,dS, \quad \forall\psi \tag{11.12}$$

bears a resemblance to a variational equation for linear problems. In fact, this is not exactly the case since the left hand side of the equation contains the unknown crack Σ. It is rather a *nonlinear* variational equation, with unknowns θ and Σ(θ). The notation Σ(θ) indicates that the crack Σ is related to the spatial support of the discontinuity [[θ]] . Eq. (11.12) establishes a duality between the current field θ and the adjoint field ψ.

11.2 Planar crack identification in quasi-static elasticity

The planar crack identification is based on the reciprocity gap RG(**u**, **v**) which gives the non linear equation, with unknowns Σ and [[**u**]]

$$\int_\Sigma [[\mathbf{u}]].\sigma[\mathbf{v}].\mathbf{n}\,dS = \int_S \{\mathbf{v}.\mathbf{T}^d - \mathbf{u}^d.\sigma[\mathbf{v}].\mathbf{n}\}\,dS := R^d(\mathbf{v}) \quad \text{(for any } \mathbf{v}) \tag{11.13}$$

where **u** is the actual displacement field and **v** is the adjoint field, continuous in Ω satisfying $\mathrm{div}\sigma[\mathbf{v}] = 0$. $R^d(\mathbf{v})$ is defined as the RG with boundary data. The method to solve this problem consists first in determining the crack plane P.

11.2.1 Determination of the normal to the crack plane

The cracked geometry is the same as that shown in Fig. 11.1, with the boundary data $\mathbf{u}^d$ (displacement instead of θ) and $\mathbf{T}^d$ (stress vector instead of the flux ∂θ/∂n). Since $\mathbf{n}$ can be factorized for a plane crack, Eq. (11.13) is written as

$$\mathbf{n}_\Sigma . \int_\Sigma \sigma[\mathbf{v}].[[\mathbf{u}]]dS = \int_S \{\mathbf{v}.\mathbf{T}^d \quad \mathbf{u}^d.\sigma[\mathbf{v}].\mathbf{n}\}\, dS, \forall \mathbf{v}$$

Andrieux et al (1999) showed that the normal $\mathbf{n}_\Sigma$ is explicitly determined by the (ij)-family of adjoint field $\mathbf{v}^{(ij)}$

$$v_k^{(ij)} = \frac{1}{2} M_{kh}^{mn} (\delta_{im}\delta_{jn} + \delta_{in}\delta_{jm}) \varkappa_h \tag{11.14}$$

with $M = L^{-1}$. The adjoint stress is constant. Let us give the solution without a proof (which can be easily checked). Consider the tensor

$$Q = \frac{1}{2}\{\mathbf{n} \otimes \int_\Sigma [[\mathbf{u}]]dS + \int_\Sigma [[\mathbf{u}]]dS \otimes \mathbf{n}\}$$

One verifies that $Q_{ij} = RG(\mathbf{u}, \mathbf{v}^{(ij)}) = R(\mathbf{v}^{(ij)})$ and

$$\left\| \int_\Sigma [[\mathbf{u}]]dS \right\| = \left\{ 2Q^2 - (tr(Q))^2 \right\}^{1/2} \tag{11.15}$$

$$\left\| \int_\Sigma [[\mathbf{u}^t]]dS \right\| = \left\{ 2Q^2 - 2(tr(Q))^2 \right\}^{1/2} \tag{11.16}$$

$$\int_\Sigma [[u_n]]dS = tr(Q) \tag{11.17}$$

where $[[\mathbf{u}^t]]$ is the tangential discontinuity. We assume that the norm of the integral in Eq. (11.15) is not equal zero, $2Q^2 - (trQ)^2 \neq 0$. Since Q is known from the boundary data, the latter condition can be checked in the choice of the loading. Define the unit vector

$$\mathbf{U} := \int_\Sigma [[\mathbf{u}]]dS \,/ \left\| \int_\Sigma [[\mathbf{u}]]dS \right\|$$

and consider the normalized $Q' = Q/\{2Q^2 - (trQ)^2\}^{1/2}$ which has two principal values $(1 + trQ')/2$ and $(1 - trQ')/2$, $(trQ' \leq 1)$. All possible vectors $\mathbf{U}$ and $\mathbf{n}$ can be chosen by permutations and changes on the sign of the components of vectors, in the basis of the eigenvectors $(\mathbf{q}^{(1)}, \mathbf{q}^{(2)}, \mathbf{q}^{(3)})$ of Q'

$$\left\{[\sqrt{\lambda_1},\ \sqrt{-\lambda_2},0],\ [\sqrt{\lambda_1},\ -\sqrt{-\lambda_2},0]\right\}$$

Two loading systems (a) and (b) are needed for determining the normal vector, parallel to the vector $\mathbf{q}^{(a)(3)} \wedge \mathbf{q}^{(b)(3)}$, thus the solution becomes $\mathbf{n} = \mathbf{q}^{(a)(3)} \wedge \mathbf{q}^{(b)(3)}/\|\mathbf{q}^{(a)(3)} \wedge \mathbf{q}^{(b)(3)}\|$.

11.2.2 Determination of the crack plane

Once the normal has been identified, we choose Ox_3 in the **n**-direction. The crack plane is defined by $x_3 - C = 0$. The constant C is obtained from $R^d(\mathbf{v}^{(\alpha)})$, with two adjoint fields $\alpha = 1$ or 2 such that $\sigma_{31}[\mathbf{v}^{(\alpha)}]$ and $\sigma_{32}[\mathbf{v}^{(\alpha)}]$ are linear in x_3

$$v_1^{(1)} = -x_1^2/2E \quad \nu x_2^2/2E + (2+\nu)x_3^2/2E,$$
$$v_2^{(1)} = \nu x_1 x_2/E, \qquad v_3^{(1)} = \nu x_1 x_3\ '/E \tag{11.18}$$
$$v_1^{(2)} = -x_2^2/2E - \nu x_1^2/2E + (2+\nu)x_3^2/2E,$$
$$v_2^{(1)} = \nu x_1 x_2/E, \qquad v_3^{(1)} = \nu x_2 x_3/E \tag{11.19}$$

These fields activate the tangential component $\int[[\mathbf{u}^t]]dS$. Eq. (11.13) gives the constant C by an equation in the form $pC + q = 0$, where p and q can be calculated explicitly, subject to the condition $|2Q^2 - 2(trQ)^2| > 0$ for the loading $\mathbf{T}^d$. The loading can be chosen so as to satisfy the latter condition which implies the former one – required for having **U** – because $|2Q^2 - (trQ)^2| > |2Q^2 - 2(trQ)^2| > 0$.

11.2.3 Determination of the crack shape

Since the crack Σ is known, Eq. (11.13) becomes a *linear* variational equation which can be solved by standard methods, with the basis function **v** satisfying the elastic equilibrium equations. A basis function of the Calderon type allows the derivation of explicit solution for the crack geometry.

Taking the origin and the basis vectors in the crack plane, we introduce a two-dimensional parameter $\mathbf{k} = (k_1, k_2, 0)$ and two complex vectors in $\mathbb{R}^3 + i\mathbb{R}^3$ depending on **k**, $\mathbf{Z}_{(k)} = (\mathbf{k} + i\|\mathbf{k}\|\mathbf{e}^3)$ and $\mathbf{Z}_{(k)}{}^* = (\mathbf{k} - i\|\mathbf{k}\|\mathbf{e}^3)$. Then we introduce two k-family of adjoint fields of the Calderon type

$$\mathbf{w}^+(\mathbf{x};\mathbf{k}) = \nabla_x \exp(-i\mathbf{Z}_{(k)}.\mathbf{x}) + \nabla_x \exp(-i\mathbf{Z}^*_{(k)}.\mathbf{x}) \tag{11.20}$$

$$\mathbf{w}^{-}(\mathbf{x};\mathbf{k}) = \nabla_x \exp(-i\mathbf{Z}_{(k)}.\mathbf{x}) - \nabla_x \exp(-i\mathbf{Z}^{*}_{(k)}.\mathbf{x}) \tag{11.21}$$

Note that the boundary value data $R^d(\mathbf{w}^+(\mathbf{k}))$ behaves like $O(\|\mathbf{k}|)$ as $\|\mathbf{k}\|\to 0$. Now assuming that $u_3 \neq 0$ on Σ in the crack problem, we make use of the RG functional, Eq. (11.13), to obtain

$$\mathrm{RG}(\mathbf{w}^+(\mathbf{k})) = \mathrm{R}^d(\mathbf{w}^+(\mathbf{k})) = \frac{2\mathrm{E}\|\mathbf{k}\|^2}{1+\nu} F_x[\![u_3]\!](\mathbf{k}) \tag{11.22}$$

$$F_x[\![u_3]\!](\mathbf{k}) = \frac{1+\nu}{2\mathrm{E}\|\mathbf{k}\|^2}\mathrm{R}^d(\mathbf{w}^+(\mathbf{k})) \tag{11.23}$$

Since $R^d(\mathbf{w}^+(\mathbf{k})) \cong O(\|\mathbf{k}\|$, as $\|\mathbf{k}\|\to 0$, the Fourier transform $F_x[[u_3]]$, having a simple pole at $\mathbf{k} = \mathbf{0}$, is invertible and therefore gives the normal displacement jump and its support Σ. In the earthquake inverse problem, there is no crack opening $[[u_3]] = 0$. We shall make use of Eq. (11.21) which is related to the tangential displacement discontinuity

$$\mathrm{RG}(\mathbf{w}^-(\mathbf{k})) = \mathrm{R}^d(\mathbf{w}^-(\mathbf{k})) = -\frac{2i\mathrm{E}\|\mathbf{k}\|}{1+\nu}\mathbf{k}.F_x[\![\mathbf{u}^t]\!](\mathbf{k}) \tag{11.24}$$

which can be writtten as

$$ik_1 F_x[\![u_1]\!](\mathbf{k}) + ik_2 F_x[\![u_2]\!](\mathbf{k}) = -\frac{1+\nu}{2\mathrm{E}\|\mathbf{k}\|}\mathrm{R}^d(\mathbf{w}^-(\mathbf{k})) \tag{11.25}$$

The left hand side of Eq. (11.25) is nothing but the Fourier transform of $\mathrm{div}[[\mathbf{u}^t]]$, whose support function is the crack geometry Σ.

11.3 The instantaneous RG functional

Consider a bounded elastic solid Ω subject to loading $\mathbf{T}^{\pm} = \sigma[\mathbf{u}].\mathbf{n}^{\pm}$ on its craks faces $\Sigma^{\pm}$ (this happens in earthquake where $\mathbf{T}^{\pm}$ is the shear stress released by fault slips). The stress vector on S_{ext} is zero. The field $\mathbf{u}(\mathbf{y}, t)$ satisfies $\mathrm{div}\sigma[\mathbf{u}] - c^{-2}\partial_t\partial_t\mathbf{u} = 0$. Introduce a rapid elastodynamic auxiliary field satisfying the elastodynamic equation in the uncracked body Ω_0 having the same external boundary S. The auxiliary field $\mathbf{v}$ is taken as a plane shear wave $\mathbf{k}$, with amplitude a, propagating in the $\mathbf{p}$ direction ($\mathbf{p}\perp\mathbf{k}$) in the fictitious infinite medium, (obtained by extending Ω to infinity)

$$\mathbf{v}(\mathbf{x}, t) = a\mathbf{k}H^{\delta}(t - \mathbf{x}.\mathbf{p}/c_s - \tau) \tag{11.26}$$

The associated stress fields correspond to a travelling impulse stress wave $\sigma[\mathbf{v}](x,t)$ propagating in the **p** direction towards the solid, τ is a parameter defining the initial wave front and $H^{\delta}(.)$ is the regularized function which gives the down step Heaviside function for $\delta \to 0$.

Suppose that τ is chosen in such a way that the support of function $\mathbf{v}(\mathbf{x},t)$ does not contain the crack for any time $t > 0$. Thus the RG functional involving $S1 \cup S2$ vanishes identically. By changing τ, RG begins to take a non zero value when the wave front is in contact with the crack front.

More precisely, the RG functional can be written as

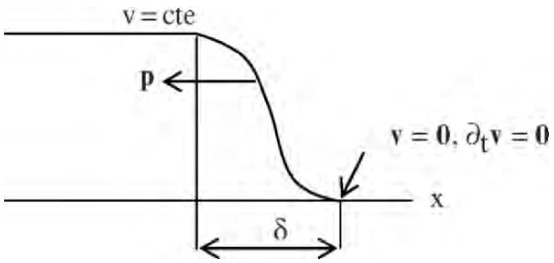

Figure 11.2: The moving impulse in direction **p** with a sharp front

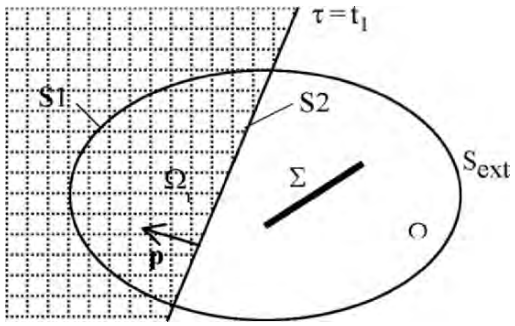

Figure 11.3: Travelling plane impulse wave **p**; Ω_1 is the part of Ω behind the wave at time t_1; S1 is the part of the external boundary S_{ext} behind the wave; S2 is the wave front inside Ω; The crack Σ at time t_1 is in front of the wave

$$\int_0^{t_1}\int_{\Omega_1}\{\mathbf{u}.\mathrm{div}\,\sigma[\mathbf{v}]-\mathbf{v}.\mathrm{div}\,\sigma[\mathbf{u}]\}d\Omega dt \equiv \int_0^{t_1}\int_{S1\cup S2}\{\mathbf{n}.\sigma[\mathbf{v}].\mathbf{u}-\mathbf{n}.\sigma[\mathbf{u}].\mathbf{v}\}dSdt \tag{11.27}$$

The contribution to the latter integral from S2 is zero because $\mathbf{v} = \mathbf{0}$ and $\sigma(\mathbf{v}).\mathbf{n} = \mathbf{0}$ on the front wave. The contribution from S1 can be evaluated at the axis ($\mathbf{p}$, $\mathbf{k}$, $\mathbf{j}$). The non-zero stress component $\sigma(\mathbf{v}).\mathbf{n}$ is the Dirac time impulse function $\sigma_{kp} = -(a\mu/c_s)\delta(t - x_p/c_s - \tau)$ and the contribution from $\sigma(\mathbf{u}).\mathbf{n}$ does not exist in the model. Therefore

$$\int_0^{t_1}\int_{\Omega_1}\{\mathbf{u}.\mathrm{div}\sigma[\mathbf{v}]-\mathbf{v}.\mathrm{div}\,\sigma[\mathbf{u}]\}d\Omega dt \equiv \int_{S1}\{\mathbf{n}.\sigma[\mathbf{v}].\mathbf{u}\}dS \tag{11.28}$$

where $\sigma[\mathbf{v}] = -(a\mu/c_s)(\mathbf{k}\otimes\mathbf{p} + \mathbf{p}\otimes\mathbf{k})$. The left hand side of Equation (11.28) is rewritten as

$$\int_0^{t_1}\int_{\Omega_1}\rho\{\mathbf{u}.\ddot{\mathbf{v}}-\mathbf{v}.\ddot{\mathbf{u}}\}d\Omega dt = \int_{\Omega_1}\rho\{\mathbf{u}.\dot{\mathbf{v}}-\mathbf{v}.\dot{\mathbf{u}}\}\Big|_0^{t_1}dS \tag{11.29}$$

It vanishes because at $t = 0$ one has $\mathbf{u} = \mathbf{0}$, $\partial\mathbf{u}/\partial t = \mathbf{0}$ and at $t = t_1$ one has $\mathbf{v} = \mathbf{0}$, $\partial\mathbf{v}/\partial t = \mathbf{0}$.

Therefore the instantaneous RGF defined by the right hand side of Eq. (11.27) vanishes as along as the wave does not intersect the crack. When it does, we have RGF ≠ 0 as shown in Fig. 11.4 where the plot of RGF(t) is given for two opposite waves $\pm\mathbf{p}$, (Bui et al, 2004). After the arrival time $t_1(\mathbf{p})$, the contribution to the instantaneous RGF from the crack increases.

The two-dimensional graphic plot of different positions of waves $\mathbf{p}$ approaching the line crack, at different time increments δt is given in Fig. 11.5. The convex hull becomes smaller and smaller when the waves approache the crack (represented by the heavy line). We stop plotting the RGF at time $t_1(\mathbf{p})$ such that $\mathrm{RGF}(t_1 + \delta t) = \varepsilon$ with small ε and $\mathrm{RGF}(t_1) = 0$.

The arrival time $t_1(\mathbf{p})$ can be experimentally determined since $\mathbf{u}$ can be measured from the recording of the acceleration on the stress free surface of the body. The difference with analysis by classical scattering of waves is noticeable in that bounded solids are considered instead of infinite medium. The method does not apply to concave shaped surface crack.

In the case of a planar crack, the crack plane is simply determined by two auxiliary waves of opposite propagation vectors. The function $F(\mathbf{p}) = 2\Delta - c_s\{t_1(\mathbf{p})\} + t_1(-\mathbf{p})\}$ measures the distance between the locations of auxiliary wave fronts at their arrival times. The location of the crack plane and its normal are determined by the zero $\mathbf{p}_0$ of the function F, $F(\mathbf{p}_0) = 0$, $\mathbf{n} = \pm\mathbf{p}_0$.

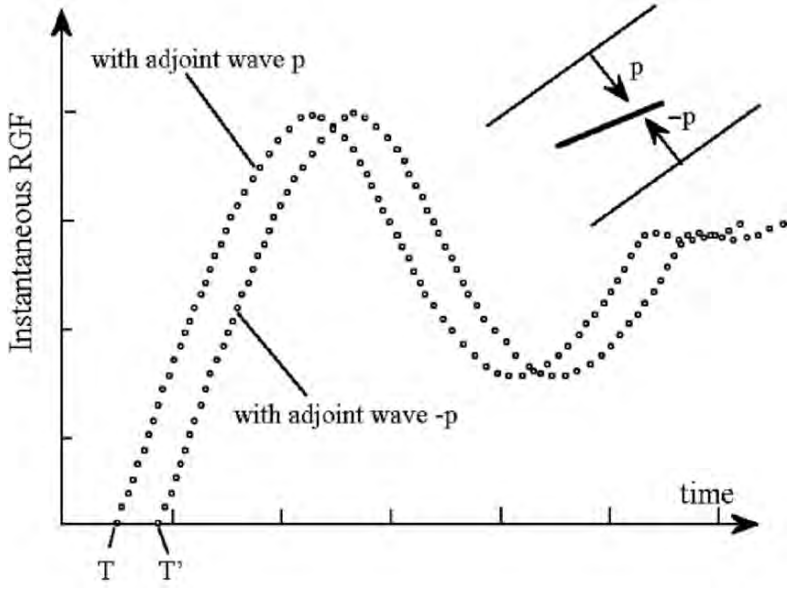

Figure 11.4: The instantaneous RGF(t) for opposite waves propagation vectors. Arrival times $T = t_1(\mathbf{p})$, $T' = t_1(-\mathbf{p})$ are used to determine the center of the crack

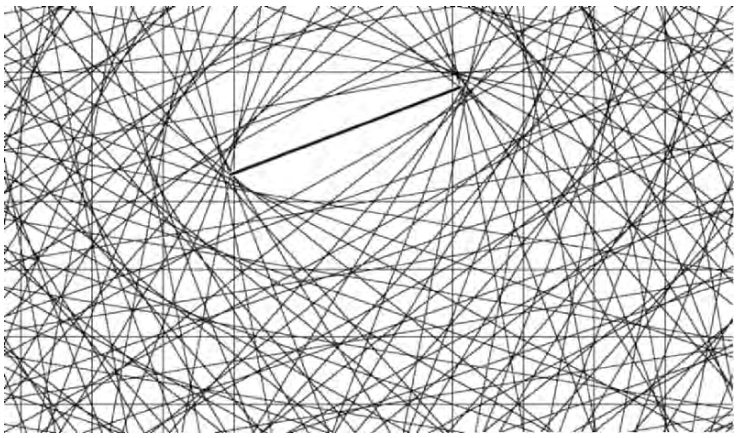

Figure 11.5: Convex hull containing the crack defined by the instantaneous RG functionals for different propagation vectors

There are other methods to determine the crack plane, as illustrated in further examples.

11.4 Inverse problem for the heat diffusion equation

Recent techniques in the evaluation of materials makes use of an Infra-Red camera, which records the surface temperature field $u(\mathbf{x}, t)$ of the body, subject of a impulse of heat flux. This method is very efficient for subsurface cracks or delaminations in laminar composites. Physically, the subsurface crack parallel to the free surface acts as an insulated screen for heat diffusion, so that the temperature measured is higher in the cracked zone than in the sound one. The technique is used in industrial applications yet without a mathematical analysis for the inversion. The mathematical background of this technique is based on the inverse geometry problem for the transient heat diffusion equation. Most works are devoted to the steady state problem for which the heat equation reduces to an elliptic equation, see Sect. 11.1. Friedman and Vogelius (1989), Andrieux and Ben-Abda (1992) solved exactly the corresponding inverse geometry problem. In what follows we consider the transient heat diffusion equation to solve the inverse problem for crack detection, proposed by Ben-Abda and Bui (2003).

Let us consider the parabolic heat diffusion equation for the current temperature field $u(\mathbf{x}, t)$ with normalized quantities

$$\mathrm{div}\,\mathrm{grad}u - \frac{\partial u}{\partial t} = 0, \quad \text{in } (\Omega \backslash \Sigma) \times [0, T] \tag{11.30}$$

$$u(\mathbf{x}, t) = 0, \quad t \le 0 \tag{11.31}$$

$$u = u^d, \quad \text{on } S_{ext} \times [0, T] \tag{11.32}$$

$$\frac{\partial u}{\partial n} = 0 \quad \text{on the fixed crack } \Sigma \tag{11.33}$$

The forward problem, Eqs. (11/30) - (11.33), for a *given* crack Σ is a well-posed one. The inverse problem consists in the determination of the crack Σ from the surface datum $u = u^d$ and the additional flux

$$\frac{\partial u}{\partial n} = \Phi^d \quad \text{on } S_{ext} \times [0, T] \tag{11.34}$$

To solve the inverse problem, we introduce the *adjoint* (or dual) function w(**x**, t) solution of the *backward* diffusion equation (time reversal)

$$\mathrm{div}\,\mathrm{grad}w + \frac{\partial w}{\partial t} = 0 \qquad \text{in } (\Omega\backslash\Sigma)\times[0,\,T] \tag{11.35}$$

$w(x, t) \equiv 0, \quad t > T$

The Reciprocity Gap functional defined by the bilinear form on the external surface S, is linear in w and linear in u (u and $\partial_n u$ are data on S).

$$RG(u,w) := \int_0^T \int_S \{u\partial_n w - w\partial_n u\}\, dSdt \tag{11.36}$$

It equals the internal "pseudo" bilinear form on Σ, linear in w and linear in u if and only if Σ is known (As a matter of fact, $\Sigma \equiv \mathrm{support}[[u]]$ is unknown, so that we must have to determine first the crack plane P)

$$RG(u,w) = \int_0^T \int_\Sigma [[u]]\partial_n w\; dSdt \tag{11.37}$$

Substituting the boundary data into Eq. (11.36), we obtain the linear form $w \rightarrow R(w)$

$$RG(u,\,w) = \int_0^T \int_\Sigma [[u]]\frac{\partial w}{\partial n}\, dSdt = \int_0^T \int_S \{u^d \frac{\partial w}{\partial n} - w\Phi^d\}\, dSdt := R(w) \tag{11.38}$$

The equation RG(u, w) = R(w) for any w in some space W, is the variational form of the observation equation which must be established in any inverse problem and generally solved by computational methods. In classical methods to solve inverse geometric problem, the crack Σ should be pameterized by geometrical constants to be determined s_1, s_2, ..s_N. The forward problem is first solved for fixed s_1, s_2, ..s_N. The surface flux $\Phi(s_1, s_2, ..s_N)$ has to be fitted to the experimental data. The optimization problem $\mathrm{Min}\{\|\Phi(s_1, s_2, ..s_N - \Phi^d\|\}$ in $\mathbb{R}^n$ is very ill-posed and cannot be solved without regularization techniques, (Chap. 12). In other words, the approximate variational problem RG(u,w) = R(w), in a finite dimensional space, is ill-conditionned. Therefore it is of great importance to derive exact inversion formulae, similar to the ones given in Tomography or Scattering of waves.

11.4.1 Solution for the crack plane location

The crack plane can be determined as follows. Consider an adjoint function w(**x**, t; **p**) depending on a family of unit vectors **p**, through the scalar argument y = **x.p** and let the RG functional, Eq. (11.38), be denoted by R(**p**). Eq. (11.37) becomes

$$\int_0^T \int_\Sigma [[u]].\frac{\partial w}{\partial n}\, dSdt = n_i p_i \int_0^T \int_\Sigma [[u]]\, w'(\mathbf{x}.\mathbf{p}, t) dSdt = R(\mathbf{p}) \tag{11.39}$$

where w' denotes the partial derivative of w with respect to the first argument y = **x.p.** We obtain an equation in the form $n_i p_i = R(\mathbf{p})/a(\mathbf{p})$ (the term a(**p**) does not vanish since the RG is not identically zero). Notice that an adjoint function in the form

$$w(\mathbf{x}, t, \mathbf{p}) = \frac{1}{\sqrt{4\pi(T-t)}} \exp\{-\frac{(x_i p_i)^2}{4(T-t)}\} \quad \text{for } t < T \tag{11.40}$$

$w(x, t; \mathbf{p}) = 0 \quad \text{for } t > T$

is solution of the backward heat diffusion equation. Considering R(**p**) as a function of **p** given by Eq. (11.38) we can determine (by computers) the zeros of this function, says $\mathbf{p}^1$, $R(\mathbf{p}^1) = 0$. Necessarily, from Eq. (11.39) the vector $\mathbf{p}^1$ lies in the crack plane ($\mathbf{n}.\mathbf{p}^1 = 0$) so that the zeros of R(**p**) are not unique.

Another independent vector $\mathbf{p}^2$ which is the zero of R(**p**) = 0 gives the normal $\mathbf{n} = \mathbf{p}^1 \times \mathbf{p}^2$.

Having determined the normal **n**, we take Ox_3 in the **n** direction so that the crack plane equation is $x_3 - C = 0$. To determine the constant C, we choose the b-family of adjoint field independent of x_1, x_2

$$w^{(b)}(\mathbf{x}, t) = \frac{1}{\sqrt{4\pi(T-t)}} \exp\{-\frac{(x_3 - b)^2}{4(T \quad t)}\} \quad \text{for } t < T \tag{11.41}$$

the corresponding RG functional is given by

$$RG(w^{(b)}) = \frac{1}{2}(b - C) \int_0^T \int_\Sigma [[u]] \sqrt{4\pi}(T-t)^{3/2} \exp\{-\frac{(C-b)^2}{4(T-t)}\} dSdt \tag{11.42}$$

Therefore the solution to the crack plane location is given the simple zero of the function $b \to RG(w^{(b)})$. Remark that the determination of the zeros of $RG(w^{(b)}) = R(w^{(b)})$ considered as a function of b, can be simply made by computers since the expression of $R(w^{(b)})$ is known explicitly. Now, the crack plane being determined, the "pseudo" bilinear form RG(u, w) becomes a true bilinear form in u, w.

11.4.2 Solution for the crack shape

The crack geometry can be determined by the same method as that given in the problem of Scattering of waves in infinite medium, perhaps more simply, by solving Eq. (38) with an adequate adjoint function w of the Fourier type. Introduce a 2D parameter $\mathbf{s} = (s_1, s_2, 0)$, a real positive scalar $q > 0$ and define

$$w^{(s,\,q)}(\mathbf{x},\,t) = \exp(iqt)\exp(-i\mathbf{s}.\mathbf{x})\exp\{x_3(s_1^2 + s_2^2 - iq)^{1/2}\} \tag{11.43}$$

Let the time Fourier transform of [[u]] be

$$F_t[[u]] := U(\mathbf{x};\,q) = \int_0^\infty [[u]]\exp(iqt)dt$$

As functions of $\mathbf{x}$ in the crack plane P, [[u]] and U have the *same* spatial support. We extend the definition of [[u]] outside the crack surface Σ bet letting $[[u]] \equiv 0$ for $\mathbf{x} \notin \Sigma$. Using the RG functional, expliciting $\partial w^{(\mathbf{s},q)}/\partial x_3$, we then obtain

$$\int_P U(\mathbf{x},\,q)\exp(-i\mathbf{s}\,.\,\mathbf{x})dS_x = \frac{1}{\sqrt{s_1^2 + s_2^2 - iq}}\int_0^\infty \int_S (u^d\partial_n w - \Phi^d w)dSdt \equiv F^{(q)}(\mathbf{s}) \tag{11.44}$$

One wonders whether $F^{(q)}(\mathbf{s})$, given by the double integral (11.44) with the boundary data integral over S, is the spatial Fourier transform F_x of some *compact* support function of $\mathbf{x}$. Such a compact support S nothing but the crack geometry. If this is true, the inverse Fourier transform of $F^{(q)}(\mathbf{s})$ solves the inverse geometry problem, that is $(F_x)^{-1}F^{(q)}(\mathbf{s}) = U(\mathbf{x}, q)$.

To show this, let us notice that for fixed $q > 0$, the right hand side of Eq. (11.48) denoted by $F^{(q)}(\mathbf{s})$ is a smooth function of $\mathbf{s}$ since $(s_1^2 + s_2^2 - iq)$ does not vanish. Denote by F(z) the complex extension of $F^{(q)}(\mathbf{s})$ to the complex hyperplane $\mathbb{C}^2$: $z = (z_1, z_2)$, $z_1 = s_1 + iv_1$, $z_2 = s_2 + iv_2$. The singularities of F(z) do not meet the real axes.

Observing that the solid is bounded (embedded in a sphere or radius a) we obtain the majoration for large $|z| = (|z_1|^2 + |z_2|^2)^{1/2}$

$F(z)| \le C\,|z|\exp\{a(|z_1| + |z_2|)\}\exp\{a(|z_1|^2 + z_2|^2)^{1/2}\} \le C\exp\{2a(|z_1|^2 + |z_2|^2)^{1/2}\}$

Such a majoration shows that F(z) is a function of the *exponential k-type*, $|F(z)| \le C\exp\{k(z|\}$, $k = 2a$, and therefore belongs to the space of Schwartz's tempered distribution $S'(s_1, s_2)$. According to the Wiener-Paley theorem, the exponential k-type function F(**s**) for real z, is the 2D spatial Fourier transform of a *compact* support function U(**x**, q) and suppU = supp[[u]]. The proof is complete. This solution to the inverse heat diffusion problem, to determine a planar crack in three-dimensions, has been given by Ben Abda and Bui (2003).

The method used is the same as that considered in statics for the scalar harmonic equation, (Andrieux and Ben Abda, 1992), in quasitatic elasticity (Andrieux and Ben Abda, 1996; Andrieux et al, 1999). In the next sections, we shall consider the transient inverse problems in acoustics and elastodynamics, for the crack detection in three-dimensional solid, which are of the hyperbolic type. Methods developped below are applicable to the earthquake inverse problem.

11.5 Inverse acoustic scattering of a crack in time domain

Most studies of inverse acoustic scattering of a crack like defect assumed very particular conditions: infinite medium, incident plane wave, analysis in the frequency domain. Here we consider bounded solid, arbitrary dynamic loading conditions on the boundary of the solid, and analysis in the time domain. The explicit solution for the inverse scattering, derived in (Bui et al, 1999) is based on the RG functional method similar to the one discussed in preceding sections. Consider the scalar acoustic wave equation with normalized constants and with, for pure mathematical reasons, a small damping term which will be set to zero in a limiting process $\varepsilon > 0$, $\varepsilon \to 0^+$ so that physically we are still dealing with the same equation

$$L(u) \equiv \left(\frac{\partial^2}{\partial t^2} - \text{divgrad} + \varepsilon\frac{\partial}{\partial t}\right) u = 0 \quad \text{in } \Omega \times [0, \infty] \tag{11.45}$$

The initial conditions and the boundary conditions on the external surface S and on the crack Σ are

$$u(\mathbf{x}, t < 0) = 0, \qquad \frac{\partial u}{\partial t}(\mathbf{x}, t < 0) = 0 \tag{11.46}$$

$$\frac{\partial u}{\partial n}(\mathbf{x}, t>0)\big|_S = \Phi^d, \quad \frac{\partial u}{\partial n}(\mathbf{x}, t>0)\big|_\Sigma = 0 \tag{11.47}$$

We assume that the boundary conditions are such that the solution u^ε has some good behavior at large time

$$\lim_{t\to\infty} t^2|u^\varepsilon| = 0, \quad \lim_{t\to\infty} t^2|\partial_t u^\varepsilon| =) \tag{11.48}$$

In what follows, for simplicity, we omit the subscript ε in u^ε but still consider it in the equations. Introduce the adjoint function w in the uncracked solid which satisfies

$$L^*(w) \equiv (\frac{\partial^2}{\partial t^2} - \text{divgrad} - \varepsilon\partial_t)\, w =), \quad \text{in } \Omega\times[0,\infty[\tag{11.49}$$

with the change of sign in $\varepsilon\partial/\partial t$. No other conditions are needed for the boundary values of w in space and time. The reciprocity relationship is written as follows

$$\begin{aligned}\int_0^\infty \int_\Sigma [[u]]\, \partial_n w\, dS dt = & \int_0^\infty \int_\Omega u(\partial_t\partial_t - \text{divgrad} - \varepsilon\partial_t) w\, d\Omega dt + \\ & + \int_\Omega (w\partial_t u \quad w\partial_t u + \varepsilon uw)\Big|_0^\infty \, d\Omega + \\ & + \int_0^\infty \int_S (\partial_n w - w\partial_n u) dS dt\end{aligned} \tag{11.50}$$

The first integral in the right hand side of Eq. (11.50) vanishes, the second integral also vanishes at t = 0 and $t\to\infty$. Therefore, the RG functional is the bilinear form in (u, w) defined by the third integral in Eq. (50). It becomes the linear form $R^d(w)$ when the boundary value data are inserted into the integral. We thus obtain the observation equation in the variational form

$$\int_0^\infty \int_\Sigma [[u]]\, \partial_n w\, dS dt = \int_0^\infty \int_S (u^d \partial_n w - w\Phi^d)\, dS dt \doteq R^d(w) \tag{11.51}$$

The method to determine the normal to the crack plane is simpler than in §11.2. We take two adjoint plane waves of distinct propagation vectors $\mathbf{k}$ $(\varepsilon = 0)$ $w^{(k)}(\mathbf{x}, t) = g(\mathbf{x}.\mathbf{k} + t)$, with g(.) an arbitrary function. The first integral in Eq. (51) being proportional to $\mathbf{n}.\mathbf{k}$, the zeros of the second expression, which depends on $\mathbf{k}$, gives vectors $\mathbf{k}$ lying in the crack plane. Thus two independent zeros $\mathbf{k}^1$, $\mathbf{k}^2$ determine the normal by $\mathbf{n} = \mathbf{k}^1 \times \mathbf{k}^2$. We take Ox_3 along $\mathbf{n}$ to determine the location of the plane defined by $x_3 - b = 0$.

We simply plot the function $b \to R(w^{(b)})$ for $\varepsilon = 0$, with the function $w^{(b)}(\mathbf{x}, t) \equiv (x_3 - b)^2 + (t - T/2)^2$. Such adjoint wave function has been used in Alves and Ha-Duong (1999) to study diffracted far-field by planes waves impinging the crack, called the *analysing waves*. When the analyzing waves w are parallel to the crack plane, they cannot "see" the crack. It is equivalent to say that the RG functional is zero in this case.

To determine the crack geometry, we consider the wave $w^{(\mathbf{s}, q)}(\mathbf{x}, t)$ with parameters $\mathbf{s} = (s_1, s_2) \in \mathbb{R}^2$, q real and positive. Let $\mathbf{x} = (x_1, x_2, x_3)$, $\mathbf{x}' = (x_1, x_2, 0)$. We introduce the adjoint field

$$w^{(\mathbf{s}, q)}(\mathbf{x}, t) = \exp(iqt)\exp(-i\mathbf{s}.\mathbf{x}')\exp\{(|\mathbf{s}|^2 - q^2 - i0^+q)^{1/2}x_3\} \tag{11.52}$$

Let $F_t[[u]] \equiv U(\mathbf{x}'; q) = \int_0^\infty [[u(\mathbf{x}', t)]]\exp(iqt)dt$ be the time Fourier transform of the jump [[u]]. The reciprocity gap is written as

$$\int_P U(\mathbf{x}',q)\exp(-i\mathbf{s}.\mathbf{x}')dS_{x'} = \frac{1}{\sqrt{|\mathbf{s}|^2 - q^2 - i0^+}} \int_0^\infty \int_S (u^d \partial_n w - w\Phi^d)dSdt$$
$$\equiv h(\mathbf{s}; q) \tag{11.53}$$

The reason for the regularization term $\varepsilon > 0$ in physical equations now becomes clear. In the Fourier spaces, owing to the imaginary term $i0^+$, the function $\mathbf{s} \to h(\mathbf{s}; .)$ when extended to a distribution $h(z:.)$ on $z = (z_1, z_2) \in \mathbb{C}^2$, $z_1 = s_1 + iv_1$, $z_2 = s_2 + iv_2$ has *no* singularities in the real axes s_1, s_2. In other words, the function $h(\mathbf{s}; .)$ is regular in the $\mathbf{s}$-plane and can be analytically continued in the complex hyperplane z which has, as in the inverse heat diffusion case, the same majoration of the "exponential 2a-type" at infinity. We conclude that for q fixed, the function $\mathbf{s} \to h(\mathbf{s}; q)$ is the 2D Fourier transform $F_{x'}$ of a *compact* support function of $\mathbf{x}'$, which is nothing but the time dependent crack surface where $[[u(\mathbf{x}', t)]] \neq 0$.

11.6 Elastodynamic scattering of a crack in time domain

The inverse geometry problem for determining a crack in transient loading is solved by the same method as the one given in Sect. 11.5 for the scalar wave equation. Briefly, we shall give the solution, without repeating the reasoning. Since applications to inverse problems in seismology are expected, some boundary conditions may be different from the classical

ones. For example, the stress free condition $\mathbf{T} = \mathbf{0}$ does not hold in the fault faces (In seismology, the terminology "fault" is used rather than "crack").

In crack problems, the stress free condition $\sigma.\mathbf{n} = 0$ can be assumed on the crack face Σ. In the earthquake problem, one deals with a surface which varies with time $\Sigma(t)$. The solid at time $t = 0$ releases suddenly some unknown shear stress $\tau.\sigma.\mathbf{n}$, with τ tangent to the fault Σ. We assume that Σ is planar, but neither the fault plane nor its time dependent geometry are known. Solve this inverse geometry problem, from acceleration data measured on the free surface of the solid – the ground in geophysics – seems to be an unrealistic task. It should be noted that some natural boundary conditions are used in the earthquake analysis:

i) stress free condition $\sigma.\mathbf{n} = 0$ on the external surface,

ii) no normal discontinuity $[[u_n]] = 0$,

iii) continuity of the shear stress $\sigma_{n\tau}$ (and also the normal stress σ_{nn}) but the shear force acting on $\Sigma^{\pm}$ are opposite to each other, because of opposite normals.

11.6.1 The observation equation in elastodynamics

The consequence of the property iii) is very important, as explained below. The RG functional is defined by the integral over the external surface S

$$\mathrm{RG} := \int_0^{\infty} \int_S (\mathbf{u}.\sigma[\mathbf{v}].\mathbf{n} - \mathbf{v}.\sigma[\mathbf{u}].\mathbf{n}) dS dt \tag{11.54}$$

From the conservation law, we have the identity between integral (11.54) over S and the same one over $\Sigma^{\pm}$

$$\begin{aligned} &\int_0^{\infty} \int_S (\mathbf{u}.\sigma[\mathbf{v}].\mathbf{n} \quad \mathbf{v}.\sigma[\mathbf{u}].\mathbf{n}) dS dt \equiv \int_0^{\infty} \int_{\Sigma_-} [[\mathbf{u}]].\sigma[\mathbf{v}].\mathbf{n} dS dt \\ &- \int_0^{\infty} \int_{\Sigma_+} \{\mathbf{v}.\sigma[\mathbf{u}^+].\mathbf{n}^+ + \mathbf{v}.\sigma[\mathbf{u}^-].\mathbf{n}^-\} dS dt \end{aligned} \tag{11.55}$$

We set $\mathbf{n}^- = \mathbf{n}$, $\mathbf{n}^+ = -\mathbf{n}$ on the crack. The double integral of $\mathbf{u}.\sigma[\mathbf{v}].\mathbf{n}$ over $\Sigma^{\pm}$ has been condensed into the first integral in the right hand side of (11.54). The double integral of $-\mathbf{v}.\sigma[\mathbf{u}].\mathbf{n}$ over $\Sigma^{\pm}$ is given by the second integral in the right hand side of (11.55). Now taking into account the property iii), $\sigma[\mathbf{u}^+] = \sigma[\mathbf{u}^-]$, we see that the third integral, which already vanishes in a stress free crack problem, vanishes in the earthquake problem too. Therefore in transient elastodynamics we obtain the *same* formula for the observation equation in (a stress free) crack and earthquake inverse problems (shear stress release on a fault)

$$\int_0^\infty \int_\Sigma [[\mathbf{u}]].\sigma[\mathbf{v}].\mathbf{n}\,dSdt = \int_0^\infty \int_S \{\mathbf{u}.\sigma[\mathbf{v}].\mathbf{n} - \mathbf{v}.\sigma[\mathbf{u}].\mathbf{n}\}\,dSdt := \mathrm{RG}(\mathrm{v}) \quad (11.56)$$

We denote the boundary value on S of the reciprocity functional by $R^d(v)$ when $\mathbf{u}$ and $\sigma[\mathbf{u}]$ are given data. Eq. (56) means that the total work done by the adjoint stress field on the fault slip is equal to the work done by the adjoint stress field on the actual displacement. This expected result shows that, without the knowledge of the whole history of data $\mathbf{u}^d(\mathbf{x}', t)$, $\mathbf{x}' \in S$, $t \in [0, \infty]$ the geometry inversion is impossible.

Eq. (11.56) does not indicate how to choose the adjoint fields $\mathbf{v}$ to reveal the geometry of the fault (normal $\mathbf{n}$, fault plane location, support of the jump $[[u]]$), and the jump $[[u]]$ itself. In classical approach with the control (or optimization) of the fault geometry and mechanisms, in order to get a best fit with experimental data, one solves a series of forwards problems which need the modelling of the true process governing the slip fault.

Here, the observation equation (56) *bypasses* the physical process (fault process) $\rightarrow$ (data) but the difficulty remains on the adequate choice of adjoint fields $\mathbf{v}$. Once the solution $[[u_t]]$ of Eq. (56) has been found, $[[u_t]]$ on Σ together with $\mathbf{u}(\mathbf{x}, t)$ on S can be used as the Dirichlet boundary data to solve an initial boundary value problem for the stress, the energy and the seismic moments etc. We summarize the equations of the elastodynamic inverse problem for crack detection:

Current field

$$\mathrm{div}\sigma[\mathbf{u}] - \rho\,\partial^2\mathbf{u}/\partial t^2 + \varepsilon\partial\mathbf{u}/\partial t = 0 \quad (\varepsilon \rightarrow 0^+) \quad \text{in } (\Omega - \Sigma) \times [0, \infty] \qquad (11.57)$$

$$\sigma[\mathbf{u}] = \mathrm{L}.\ldots.(\mathbf{u}), \qquad \sigma[\mathbf{u}].\mathbf{n} = \mathrm{T}^d \quad \text{on S}, \qquad [[\mathbf{u}.\mathbf{n}]] = 0 \quad \text{on } \Sigma,$$

$$\mathbf{u} = 0,\ \partial\mathbf{u}/\partial t = 0 \quad \text{for } t \le 0, \qquad t^2\,\mathbf{u}| \rightarrow 0, \quad t^2|\partial\mathbf{u}/\partial t| \rightarrow 0 \qquad \text{for } t \rightarrow \infty$$

Adjoint field

$$\mathrm{div}\sigma[\mathbf{v}] - \rho\,\partial^2\mathbf{v}/\partial t^2 - \varepsilon\partial\mathbf{v}/\partial t = 0 \quad (\varepsilon \rightarrow 0^+) \quad \text{in } (\Omega - \Sigma) \times [0, \infty] \qquad (11.58)$$

$$\sigma[\mathbf{v}] = \mathrm{L}.\ldots.(\mathbf{v}), \qquad [[\mathbf{v}]] = \mathbf{0} \quad \text{on } \Sigma,$$

Neither time conditions at infinity nor boundary conditions on S are demanded for the adjoint field.

RF functional

$$\int_0^\infty \int_\Sigma [[\mathbf{u}]].\sigma[\mathbf{v}].\mathbf{n}dSdt \equiv \int_0^\infty \int_S (\mathbf{u}.\sigma[\mathbf{v}].\mathbf{n} - \mathbf{v}.\ \sigma[\mathbf{u}].\mathbf{n})dSdt := \mathrm{R}(\mathbf{u},\mathbf{v})$$

$$\int_0^\infty \int_\Sigma [[\mathbf{u}]].\sigma[\mathbf{v}].\mathbf{n}dSdt = \int_0^\infty \int_S (\mathbf{u}^d.\sigma[\mathbf{v}].\mathbf{n} - \mathbf{v}.\ \mathbf{T}^d)dSdt := \mathrm{R}^{\mathrm{d}}(\mathbf{v}) \quad (11.59)$$

Measurements on the external surface are $\mathbf{u}^{\mathrm{d}}$, $\mathbf{T}^{\mathrm{d}}$ on S. For a bounded solid, the solution is obtained by the use of a P-wave adjoint function.

11.6.2 Solution

We do not repeat the reasoning of Sect. 11.5 to determine the crack plane Ox3, which is obtained by considering adjoint plane waves (analyzing waves)

$$\mathbf{v}^{(\mathbf{s},q)}(\mathbf{x}, t) = \mathrm{grad}\ \phi(\mathbf{x}, t; \mathbf{s}, q)$$

$$\phi(\mathbf{x}, t; \mathbf{s}, q) = \exp(iqt-\varepsilon t)\exp(i\mathbf{s}.\mathbf{x})\exp[x_3\{|\mathbf{s}|^2 + (iq-\varepsilon)^2/c_p^2\}^{1/2}] \quad (\varepsilon\to 0^+)$$

$$F_x\{is_1F_t[[u_1]]+is_2F_t[[u_2]]\} \equiv F_x\{F_t\mathrm{div}[[\mathbf{u}]]\}$$

$$= \frac{1}{2\mu}\mathrm{R}^{\mathrm{d}}(\mathbf{v}^{(\mathbf{s},q)})\{|\mathbf{s}|^2-(q+i\varepsilon)^2/c_p^2\}^{-1/2}$$

$$\mathrm{div}[[\mathbf{u}]] = \frac{1}{2\mu}(F_t)^{-1}(F_x)^{-1}\mathrm{R}^{\mathrm{d}}(\mathbf{v}^{(\mathbf{s},q)})\{|\mathbf{s}|^2-(q+i\varepsilon)^2/c_p^2\}^{-1/2} \quad (\varepsilon\to 0^+)$$

$$\Sigma(t) = \mathrm{Supp}\{\mathrm{div}[[\mathbf{u}]]\}$$

Box 1. P-wave adjoint field $\mathbf{v}^{(\mathbf{s},q)}(\mathbf{x}, t)$ and solutionΣ (t) in the plane $x_3 = 0$

$$\mathbf{w}^{(\mathbf{s},q)}(\mathbf{x}, t) = \mathrm{curl}\ \psi(\mathbf{x}, t; \mathbf{s}, q)$$

$$\psi(\mathbf{x}, t; \mathbf{s}, q) = \exp(iqt-\varepsilon t)\exp(i\mathbf{s}.\mathbf{x})\exp[x_3\{|\mathbf{s}|^2+(iq-\varepsilon)^2/c_s^2\}^{1/2}]$$

$$[[\mathbf{u}^\perp]] = ([[u_2]], -[[u_1]], 0),$$

$$\mathrm{div}[[\mathbf{u}^\perp]] = \frac{1}{2\mu}(F_t)^{-1}(F_x)^{-1}\mathrm{R}^{\mathrm{d}}(\mathbf{w}^{(\mathbf{s},q)})\{|\mathbf{s}|^2-(q+i\varepsilon)^2/c_p^2\}^{-1/2} \quad (\varepsilon\to 0^+)$$

$$\Sigma(t) = \mathrm{Supp}\{\mathrm{div}[[\mathbf{u}^\perp]]\}$$

Box 2. S-wave adjoint field $\mathbf{w}^{(\mathbf{s},q)}(\mathbf{x}, t)$ and solution $\Sigma(t)$ in the plane $x_3 = 0$

and we only give the solution for the crack geometry Σ(t), without proof using two methods, as summarized in Boxes 1 and 2.

The solution in Box.1 implies that there is a crack opening mode I and that the loadings are such that shear modes exist too. For the eathquake inverse problem, pure shear slips already exist in the crack surface. Thus it is worth noting that another analysing plane S-wave is more suitable for the detection of shear slips, namely the adjoint field $\mathbf{w}^{(s,\,q)}(\mathbf{x}, t)$. The solution is summarized in Box 2, where $(F_t)^{-1}$ is the inverse time Fourier transform, $(F_x)^{-1}$ is the inverse in-plane spatial Fourier transform, (Bui et al, 2005).

11.7 The earthquake inverse problem and solution

The model disscussed in Sect. 11.6, based on the stress free surface is too simple to describe the actual earthquake in a seismic region. The stress free condition $\mathbf{T} = \sigma.\mathbf{n} = 0$ is fulfilled on the ground, but not on the underground half-sphere H, where displacement $\mathbf{u}(\mathbf{x}, t)$ and stress vector $\sigma(\mathbf{x}, t).\mathbf{n}$ are needed. As long as the sudden release of the shear stress on the fault Σ(t) at time $t > 0$ occurs elastically in some bounded region Ω of the earthquake site, we can derive an observation equation to study earthquake.

Consider Ω as an half-spherical elastic domain, with large radius compared with the fault size, but less than the crust depth. The fault is planar and located in the underground near the center of the half-sphere. Data on the ground consist of the measured acceleration $\partial^2\mathbf{u}/\partial t^2$ and the stress free condition $\mathbf{T} = \mathbf{0}$. Far from the seismic site, signals arriving at the half-sphere H can be considered as being emitted by a point source. In geophysics, one generally considers that the far-fields are well modellized as a point source at a half-space using measured data of the near-field and the far-field on

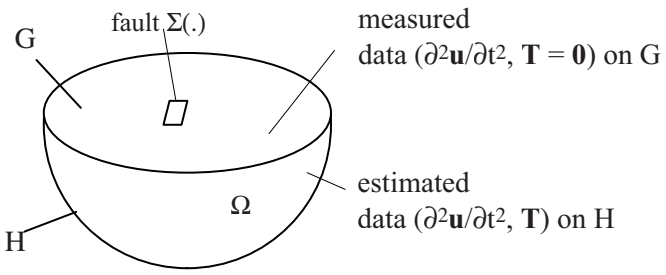

Figure 11.6: A model of the earthquake inversion to identify the moving fault Σ(t) from measured data on the ground and estimated data on the half-sphere H

the ground. The far-field measurements, for strong earthquake, at least of magnitude 6 or above, are related to volumic P and S waves and surface waves (Love and Rayleigh waves) propagating along the ground. They provide good global informations on the source, for instance its energy, radiation of energy, moments tensors m, Vallée (2003).

This would means that good informations on $\mathbf{u}(\mathbf{x}, t)$ and $\mathbf{T}(\mathbf{x}, t)$ are available on the half-sphere $\mathbf{x} \in H$ as the radiation by the point-source. Therefore, possible solutions to the earthquake inverse problem are provided by the following models.

Model based on RG and the ground data only

The solution $\Sigma(t)$ is given in Box 2, with the linear form $R^d(\mathbf{w}^{(s, q)})$ defined by the integral over $S \times [0, \infty]$ of Eq. (11.59), where $S = G \cup H$. In this model, the contribution to $R^d(\mathbf{w}^{(s, q)})$ from H is simply neglected. Only data on the ground G are used for the inversion. They are the free surface condition $\mathbf{T}(\mathbf{x}, t)=\mathbf{0}$ and the acceleration $\ddot{\mathbf{u}}(\mathbf{x}, t)$ on the ground. Unlike classical numerical methods, the RG functional method *bypasses* the assymptions on the fault released stress. It requires only the knowledge of the planar planar character of its geometry.

As a matter of fact, once the unknown $[[\mathbf{u}_t(\mathbf{x}, t)]]$ has been determined as well as the moving fault $\Sigma(t)$, the condition $[[\mathbf{u}_n(\mathbf{x}, t)]] = 0$ on $\Sigma(t)$, together with the data on the ground $\ddot{\mathbf{u}}(\mathbf{x}, t)$ and the stress free condition, are sufficient informations to solve the *forward* elastodynamic problem and to determine the released stress on the fault, hence the energy of the earthquake, its moments* $M_{ik} = \mu < [[u_i]] > A^{(k)}$.

Remark that in numerical models of the seismic source, for instance the finite element method, one uses the ground data for a best fitting of predicted seismic signals with observed signals and makes use of simple geometry such as: infinite medium, half-space. No boundary conditions other than the radiation condition of energy are imposed at infinity. In the finite element method, the boundary H is considered and modelled as an absorber.

Model based on the least square method

Numerical models of the seismic source, for instance the finite element method, make use of the near field data for a best fitting of predicted seismic signals with observed signals. These models consider simple geometries of the solid such as: infinite elastic medium, half-space. No boundary

---

* $< f_i >$ is the mean value f_i, $A^{(k)}$ the area of the slip on the plane, with normal **k,** seeAki and Richards (1980).

conditions other than the radiation condition of energy are imposed at infinity or on the half-sphere H, so that outgoing seismic waves do not contribute to the seismogram record on the ground. In the finite element method, the boundary H is modelled as a wave absorber which does not reflect waves.

The principle of inverse geometric methods in geophysics is the following one. Assume that the fault plane P, its moving shape $\Sigma(t)$, the unknown shear stress $\sigma_{tn}(\mathbf{x}, t)$ to be released on the fault, can be described by the set of N-dimensional parameter $\mathbf{p}$. Additional boundary data are the stress free condition $\mathbf{T}(\mathbf{x}, t) = 0$ on the ground and the absorption condition on H to satisfy the radiation condition. The solution to the forward elasto-dynamic problem determines the response $\ddot{\mathbf{u}}(\mathbf{x}, t; \mathbf{p})$ on the ground to be compared with the acceleration seismogram $\mathbf{a}(\mathbf{x}, t)$ at stations $\mathbf{x}$. The inverse seismic problem consists in finding the solution of

$$\min_{\mathbf{p}\in\mathbb{R}^N} \left\| \ddot{\mathbf{u}}(\mathbf{x}, t; \mathbf{p}) - \mathbf{a}(\mathbf{x}, t) \right\|^2 \tag{11.60}$$

The main difficulty of the least square method (11.60) as pointed out by many researchers concerns its ill-posedness. Equivalently, the determinant of the discretized linear system of equations is ill-conditionned (eigenvalues nearly zero), (Das and Suhadolc, 1996; Vallee, 2003). One important statement of the work (Das and Suhadolc, 1996) is that "even if the fitting of data seems to be quite good, the faulting process is poorly reproduced, so that in the real case, it would be difficult to know when one has obtained the correct solution". The reasons for that may be twofold: flat minimum of the functional to be minimized, existence of local minima. One difficulty has been pointed out, relating to the normal velocity $\varphi(\mathbf{x}, t)$ of the front, which must be well estimated or bounded by some values. In the inverse problems terminology, problem (11.60) must be solved either in subspaces defined by constraints on the boundedness of the velocity $\varphi(\mathbf{x}, t)$, or with regularized terms to be added to the square functional in order to enforce the regularity of solutions.

To illustrate the ill-posedness of problem (11.60), let us consider the simple example of a circular cavity of radius R_c centred at (α, β) in a square shaped two-dimensional elastic solid, in quasi-statics. Uniform normal tractions $\mathbf{T}^d$ are applied to the boundary and the corresponding displacement $\mathbf{u}^d(\mathbf{x}, t)$ is measured. To determine the unknown cavity, one can assume the simplest possible model of a guest circular cavity, so that the unknown parameters $\mathbf{p} = \{R, a, b\} \in \mathbb{R}^3$ consist of the center of the cavity (a, b) and its radius R. The least square method is based on the functional

$$F(a, b, R) = \left\| \mathbf{u}^{d}(\mathbf{x}) - u(\mathbf{x}; \mathbf{p}) \right\|^2 := \int_{\partial\Omega} \left| \mathbf{u}^{d}(\mathbf{x}) - \mathbf{u}(\mathbf{x}; \mathbf{p}) \right|^2 ds \tag{11.61}$$

Numerical methods by the finite element method, combined with a gradient adjoint functional, showed that the solution is not unique, because of flat minimum and local minima, Fig. 11.7, (Yao and Gong, 1994). Mathematically, the existence of spurious solutions and local minima in the preceding example can be understood as follows. Suppose that $R = R_c$ is fixed and $\alpha = \beta = 0$. The *exact* functional F(a, b) is a smooth surface with the unique minimum at $a = b = 0$, for which $F = 0$, Fig. 11.8a. Suppose that numerical errors result in an additional term with wave length comparable to the size of the solid, in the form $\varepsilon(1 - \cos(a + b)) > 0$, with $\varepsilon > 0$. Thus numerically F is the wavy function in Fig. 11.8b with local minima $F(a, b) > 0$.

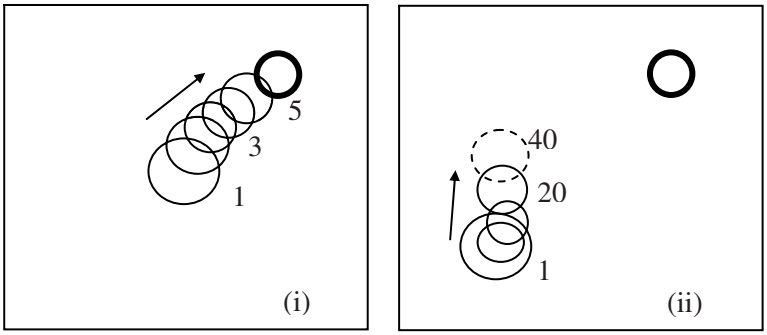

Figure 11.7: Numerical detection of a cavity in an elastic solid (heavy line): (i) Initial guess cavity (a, b) near the solution (α, β); iterated solutions converge; (ii) For (a, b) far from the solution, the iteration fails at a local minimum (in dotted line); (Yao and Gong, 1994)

Hybrid RG functional model and FEM model

The finite element method gives correct informations on the far-field, particularly for data on H. One can evaluate the far-field on r = R, by using a point source model, (Vallée, 2003).

The far field $\mathbf{u}^{F}(\mathbf{x}, t)$ can be obtained either by considering numerical solutions of forward problems or by rays theories or by using the impulse response function **K** of the half space – in practice, the response kernel **K** of the entire three-dimensional space is used – and the estimated point source γ, (Das and Kostrov, 1990)

$$\mathbf{u}^{F}(\mathbf{x}, t) = \int_0^t \int_F K(\mathbf{x}, \mathbf{y}, t, \tau).\gamma(\mathbf{y}, t) dS_y dt \tag{11.61}$$

where F is an estimate of the true fault Σ (F can be a point source). The far-field contains good information on global parameters of the earthquake. It gives data on H which can be used for the RG functional method. In return, the RG functional method provides detailed informations on the near fields, the moving fault geometry Σ(t) which can be useful for updating F, and the mechanisms of shear stress release for use in the FEM model. A coupling between two methods should be an alternative appoach to get a better solution to the seismic inverse problem.

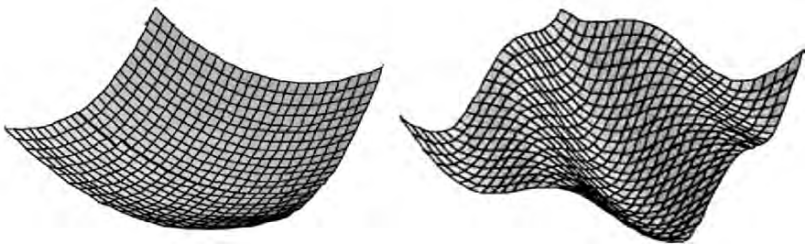

Figure 11.8: (a) Exact functional F(a, b) with the global minimum at the solution a = b = 0; (b) Numerical solution with two local minima $F(a_1, b_1) > 0$, $F(a_2, b_2) > 0$

Chapter 12

Methods of Solution to Inverse Problems

Inverse problems consist, in principle, in inverting the relation of *cause* (**z**) and *effect* which is considered as data (**d**) *accessible* to experiments. It is necessary that data are accessible to experiments, otherwise there is no significant inverse problem. Such a definition should give a status of inverse problems to any forward problems: for instance find the internal stress in an elastic solid (the cause) from measured boundary displacement (data), or find the internal displacement from measured stress vectors on the boundary. Both forward problems are well-posed ones, in the sense that the relation of cause and effect is well established by the equilibrium equations of elasticity which has good mathematical property for usual elastic body. There is only one condition for the second problem to have a solution, that is the stress vector on the boundary is a self equilibrated one in the absence of body force. Well-posed problem has a unique solution which depends continuously on the data. The main characteristics of inverse problems are twofold: first, the relation of cause to effect in real experiments is often not completely known, second, even when this relation is well established by some mapping A

$$\mathbf{z} \rightarrow A(\mathbf{z}) = \mathbf{d} \tag{12.1}$$

of metric space Z into D, the problem (12.1) is *ill-posed* (not well-posed).

12.1 The ill-posedness of the inverse problem

Let us reconsider the example of the earthquake inverse problem of the preceding chapter to get an inside into inverse problems. We assume that a model exists for the mapping A between the unknown $\mathbf{z}=\{\Sigma(t), \mathbb{T}(\mathbf{x}) \cdot\sigma(\mathbf{x},t)\cdot\mathbf{n}\}$, $\mathbf{x}\in\Sigma$ and the acceleration data $d^{meas}(\mathbf{x},t)$ on $[0,T]\times\partial\Omega$ ($\partial\Omega$ consists of the ground G and the internal half-sphere H).

A mapping A can be defined as the elastic response of the solid Ω to the shear stress τ **.σ.n** on Σ(t) and the stress free condition on ∂Ω. Solution to the earthquake inverse problem generally consists in the minimization

$$\underset{\mathbf{z}}{\text{Min}} \int_{\partial\Omega} \int_0^T \left\| d(\Sigma(t), \tau, \ \tau.\sigma.\mathbf{n}; t) - d^{meas}(t) \right\|^2 dtdS \tag{12.2}$$

where we have listed all arguments **z** of the predicted data d(Σ(t),τ, τ**.σ.n**;t) and the measured one $d^{meas}(t)$ on the ground. If data are only measured on the ground, missing data on the remaining part of the boundary make it impossible to solve the problem (12.2). Thus only an approximate solution can be expected. When data are known on the whole boundary G∪H, the solution exists and is unique only for *exact* data $d^{exact}(t)$, in the sense stated in the preceding chapter, that is

$$d^{exact}(t) \equiv A(\mathbf{z}).$$

for some **z**. Mathematically, data $d^{exact}(t)$ must belong to the domain D(A) of operator A. Finally in the ideal case of an exact data $d^{exact}(t)$, the least square method of fitting between approximate prediction and measured data uniformly distributes errors of the modelling on the whole space-time.

Needless to say, with approximate solution and noised data, one cannot expect a good solution. "Even if the fitting of data seems to be quite good, the faulting process is poorly reproduced, so that in the real case, it would be difficult to know when one has obtained the correct solution", as noted by Das and Suhadolc (1996). This is why a best fitting of the prediction to data does not guarantee that the solution is a correct one. This happens when the functional (12.2) has a flat minimum.

Consider again the earthquake problem and examine the kinematic approach actually considered in Geophysics which consists in modelling the displacement response on the ground **u**(**x**,t) from the unknown slip γ(**y**,t) on the unknown fault Σ(t), (Das and Kostrov, 1990)

$$u_k(\mathbf{x}, t) = \int_0^t d\tau \int_{\Sigma(\tau)} K_{ki}(\mathbf{x}, \mathbf{y}, t, \tau)\gamma_i(\mathbf{y}, \tau)dS_y \tag{12.3}$$

where K is the impulse response of the stress free solid ∂Ω (approximated by an infinite elastic medium). Even for known Σ(t), Eq. (12.3) to determine γ from measurement of **u** (after a double time integration of the data) is well known to be unstable. Moreover, no mathematical results exist for the equation with the unknowns **u** and Σ(t). Another form of Eq. (12.3) with the integration on the fault plane P is

$$u_k(\mathbf{x}, t) = \int_0^t d\tau \int_P K_{ki}(\mathbf{x}, \mathbf{y}, t, \tau)\gamma_i(\mathbf{y}, \tau)\phi(\mathbf{y}, \tau)dS_y \tag{12.4}$$

with the characteristic function $\phi(\mathbf{y},\tau)$ of $\Sigma(\tau)$ in the fault plane P. Even for known P, the simpler form equation (12.4) is *non linear*. Therefore, in order to effectively solve (12.4) one makes use of a priori assumptions on the geometry of $\Sigma(t)$, its velocity $\dot{\Sigma}(\tau)$, the slip direction etc. An a priori knowledge reduces the number of the unknowns. It is thus important to get such an information from the physics of the problem considered. Mathematically, one can also reduce the number of unknowns by considering subspaces, or by using non physical prior bounds such as minimum norm solution, smooth solution etc. The best method, however, is to get exact mathematical and physical constraints between solutions and data, as that provided by the RG functional method of Chap. 11, rather than artificial and non physical constraints.

12.2 General considerations on inverse problems

Consider two metric spaces, the space Z of unknown model parameters **z** and the space of observable quantitities or measured data **d**. The so-called observation equation is

$$A(\mathbf{z}) = \mathbf{d} \tag{12.5}$$

Fig. 12.1 shows a schematic view of spaces and mappings, $A(Z) \subset D$ is the range of A, **d** is a given data which generally does not belongs to A(Z), $\mathbf{d}^1 \in D$ is the nearest point $\mathbf{d}^1$ of minimum distance

$$\mathbf{d}^1 = \arg\min_{\mathbf{d}'} \rho(\mathbf{d}, \mathbf{d}') \tag{12.6}$$

$$\mathbf{d}^1 = \mathbf{P}_{A(Z)}(\mathbf{d}) \tag{12.7}$$

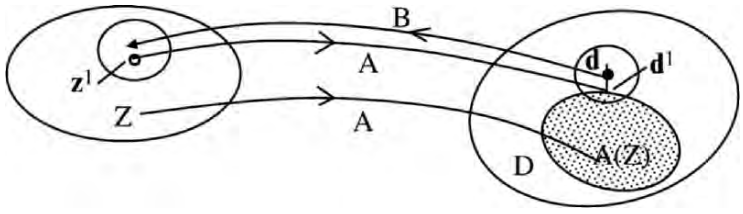

Figure 12.1: The model space Z and data space D: The quasi-solution $\mathbf{z}^1$ is such that $A(\mathbf{z}^1)$ is the projection $\mathbf{d}^1 = \mathbf{P}_{A(Z)}(\mathbf{d})$ of the data **d** on $A(Z) \subset D$

where $\mathbf{P}_{A(Z)}$ is the projector in A(Z). Any $\mathbf{z}^1$ such that $A(\mathbf{z}^1)=d^1$ is called a *quasi-solution* of Eq. (12.5). To construct such as solution, Tikhonov and Arsenine (1977) proposed to seek a mapping B of D into Z, such that $B(\mathbf{d})$ is a quasi solution $A(B(\mathbf{d}))=\mathbf{d}^1$ and that $B(\mathbf{d})$ is sufficiently regular and stable with respect to the perturbation of data. There is no guarantee for the uniqueness of the mapping B. In practice, the conditions for the solvability of (12.5) are

a) One has a priori knowledge of the subspace Z_1 of solutions for some class of regular data in A(Z). For instance one knows that the solution is near the point $\mathbf{z}^0$ (a priori information) belonging to Z_1,

b) The solution is unique in Z_1,

c) The solution is continuous in $\mathbf{d}\in A(Z_1)$.

Tikhonov and Arsenine (1977) proved another stronger result. For compact Z_1, under assumptions a) and b), there exists a continuous, monotonous and non decreasing function $\alpha(\varepsilon)$, $\alpha(0)=0$ such that

$$\rho(A\mathbf{z}^1, A\mathbf{z}^2)_D \le \varepsilon \;\Rightarrow\; \rho(\mathbf{z}^1, \mathbf{z}^2)_A \le \alpha(\varepsilon) \tag{12.8}$$

This inference means that condition c) is fulfilled as long as a) and b) are.

It is essential that some knowledge of subspace Z_1 exists. For instance, in the numerical inversion of seismic data, approximate solution is often stabilized by considering prior bounds on the fault velocity, such as constant velocity, knowledge on the planar nature of the fault – an assumption frequently used in Chap. 11 – physical constraints on the constant slip direction τ, neither back slip in the time interval considered nor variation of the slip direction etc. Artificial data, generated for an ideal fauting model with known $\Sigma(t)$ and shear release history, are used for testing the inversion procedure, (Das and Suhadolc, 1996). It is found that, if subspace Z_1 is too small, there appears a ghost solution together with the approximate one. This phenomenon should be linked to the existence of local minima of the flat least square functional (12.2).

12.3 Tikhonov's regularization

Non linear inverse problems can be linearized steps by steps by successive increments. Therefore, we will address first linear problems. We consider that Z and D are Hilbert spaces, with norms $\|.\|$ and $|.|$ respectively associated with scalar products $(\mathbf{z}^1, \mathbf{z}^2)_Z$ and $(\mathbf{d}^1, \mathbf{d}^2)_D$

$$\|\mathbf{z}\|^2 = (\mathbf{z}, \mathbf{z})_Z, \qquad |\mathbf{d}|^2 = (\mathbf{d}, \mathbf{d})_D \tag{12.9}$$

Theoretical observation equation is provided by a continuous linear operator A, with adjoint A*

$$(A\mathbf{z}^1, \mathbf{d}^2)_D = (\mathbf{z}^1, A^*\mathbf{d}^2)_Z \qquad \forall \mathbf{z}^1, \mathbf{d}^2 \tag{12.10}$$

If Hilbert spaces Z and D are not considered, see the remarks in the footnote(*). Let us introduce the prior information $\mathbf{z}^0$, a positive number $\beta > 0$, and define the closed convex subset

$$Z_1 = \{\mathbf{z}; \| \mathbf{z} - \mathbf{z}^0 \| \leq \beta\} \tag{12.11}$$

For given $\varepsilon > 0$ one seeks a solution in the convex $0 \leq \|A\mathbf{z} - \mathbf{d}\| < \varepsilon$. The regularized solution in the Tikhonov sense is given by *any* $\mathbf{z}$ belonging to the intersection S of the above convexes

$$S = \{\mathbf{z}; \| \mathbf{z} - \mathbf{z}^0 \| \leq \beta\} \cap \{\mathbf{z}; \|A\mathbf{z} - \mathbf{d}\| \leq \varepsilon\} \tag{12.12}$$

Indeed the set of solution S is either void, which means that no solution exists, or it is very large because of the arbitrariness of β, ε, $\mathbf{z}^0$. The solution is not unique.

When S is not void, one obvious solution is provided by the common centre $\mathbf{z}^1$ of two ellipsoids $E_1 \subset S \subset E_2$

$$E_1 : \frac{1}{\varepsilon^2} \|A\mathbf{z} - \mathbf{d}\|^2 + \frac{1}{\beta^2} \|\mathbf{z} - \mathbf{z}^0\|^2 \leq 1$$

$$E_2 : \frac{1}{\varepsilon^2} \|A\mathbf{z} - \mathbf{d}\|^2 + \frac{1}{\beta^2} \|\mathbf{z} - \mathbf{z}^0\|^2 \leq 2$$

$$\mathbf{z}^1 = \arg \min_{\mathbf{z}} \{\|A\mathbf{z} - \mathbf{d}\|^2 + \alpha \|\mathbf{z} - \mathbf{z}^0\|^2\} \tag{12.13}$$

where $\alpha = \varepsilon / \beta^2$ is the regularization Tikhonov's parameter, which represents a compromise between two contradictory choices: smallest residual but unstable solution and more stable one, close to the a priori knowledge $\mathbf{z}^0$ but with a higher residual, which may be far from the physics of the inverse problem. Among two choices, the second one $\|\mathbf{z} - \mathbf{z}^0\| \leq \beta$ is important

For general case, one considers normed spaces Z and D, normed dual spaces Z' and D', with dualities in Z and D, $\langle .,. \rangle_Z$ and $\langle .,. \rangle_D$ and transposed operator A^t linear from D' into Z', $\langle A\mathbf{z}, \mathbf{d}' \rangle_D = \langle \mathbf{z}, A^t\mathbf{d}' \rangle_Z$. Relationships with linear adjoint operator A linear from D into Z are obtained by introducing covariant operators C_Z and C_D and scalar products in Z and D, $.,.)_Z$ and $(.,.)_D$. One has: $Z' = C_Z^{-1}Z$, $D' = C_D^{-1}D$, and $A^* = C_Z A^t C_D^{-1}$. Hilbert spaces can be identified with their natural duals and adjoint operators are considered.

in practice. Very often one contents oneself with an approximate localization of a defect, or a crack in a structure, or a convex domain containing a tumor in the brain. The solution of (12.13) is parameterized by α

$$\mathbf{z}^{(\alpha)} = \mathbf{z}^0 + (A^*A + \alpha I)^{-1}A^*(\mathbf{d} - A\mathbf{z}^0)$$

For compact operator A, its inverse is unbounded, operator A*A is self-adjoint and compact. The eigenvalues of A*A are positive real, bounded and form a sequence of numbers converging to zero. The least square method without the additional term αI is ill-posed. The additional terms move the whole spectrum of A*A by a positive quantity α and thus ensures the invertibility of $(A^*A+\alpha I)$. For the continuity of the solution $\mathbf{z}^{(\alpha)}(\mathbf{d})$, and error estimates, see an Exercice.

12.3.1 Optimal choice of the regularization parameter

It raises the question about the choice of the regularizing parameter α. An optimal choice has been proposed by Kitagawa (1987). It is based on the use of Moore and Penrose's inverse operator $A_{MP}^{\ 1}$ such that $A_{MP}^{\ 1}Ad$ is a solution of $A\mathbf{z}-\mathbf{d}=\mathbf{0}$. Operator $(A_{MP}^{-1})A$ is the orthogonal projection on the set A*(D)

$$(A_{MP})^{-1}A = \mathbf{P}_{A^*(D)} \tag{12.14}$$

Let $z(\alpha')$ be the solution of the minimization problem (12.13) parameterized by the Tikhonov parameter α'. The optimal choice is determined by successive minimization problems (Kitagawa, 1987)

$$\mathbf{z}(\alpha') = \arg \min_{\mathbf{z}} \{|A\mathbf{z} \quad \mathbf{d}|^2 + \alpha' \|\mathbf{z} \quad \mathbf{z}^0\|^2\}$$

$$\alpha_{opt} = \arg \min_{\alpha'} \{\|A_{MP}^{-1}A\mathbf{d} - \mathbf{z}(\alpha')\|^2\} \tag{12.15}$$

Now, having introduced linear inverse problems, we consider the non linear case $A(\mathbf{z})-\mathbf{d}=\mathbf{0}$ and the minimization problem ($\alpha>0$)

$$\min_{\mathbf{z}} \{|A(\mathbf{z}) - \mathbf{d}|^2 + \alpha\|\mathbf{z} \quad \mathbf{z}^0\|^2\} \tag{12.16}$$

It is assumed that Fréchet's derivative $A'(\mathbf{z})$ exists and is defined by a tangent linear operator from Z to D

$$A(\mathbf{z}+\delta\mathbf{z}) - A(\mathbf{z}) = A'(\mathbf{z})\delta\mathbf{z} + o(\|\delta\mathbf{z}\|^2) \quad \forall\ \delta\mathbf{z} \tag{12.17}$$

The solution of (12.16) is then obtained by the multistage quadratic programming starting from the guest a priori knowledge $\mathbf{z}^0$,

$$\mathbf{z}^{n+1} = \mathbf{z}^n + \mathbf{s}^n$$

$$\mathbf{s}^n = \arg \min_{\mathbf{s}} \{\|A(\mathbf{z}^n) + A'(\mathbf{z}^n)\mathbf{s} - \mathbf{d}\|^2 + \alpha' \|\mathbf{z}^n + \mathbf{s} - \mathbf{z}^0\|^2\} \tag{12.18}$$

The gradient of the functional in (12.16) is

$$\mathbf{g}^n = 2A'(\mathbf{z}^n)*\{A(\mathbf{z}^n) + A'(\mathbf{z}^n)\mathbf{s} - \mathbf{d}\} + 2\alpha(\mathbf{z}^n + \mathbf{s} - \mathbf{z}^0) \tag{12.19}$$

The Hessian is positive

$$H^n = 2\{A'(\mathbf{z}^n)*A'(\mathbf{z}^n) + \alpha\} > 0 \tag{12.20}$$

12.3.2 Error estimate

One important point in mathematical works is to derive the error estimate with respect to the (yet unknown) exact solution $\mathbf{z}^{ex}$. There are some results reported in the literature for Inverse Problems in Hilbert's spaces settings. The main point is to make a comparison between the regularized solution $\mathbf{z}^{(\alpha)}(\mathbf{d})$ and the exact one $\mathbf{z}^{ex}$, even if this is not yet known.

What is the meaning of an « exact » solution ?
Let us introduce some terminologies. A pair $\{\mathbf{z}^{ex}, \mathbf{d}^{ex}\}$ is called *exact* or *compatible* if it satisfies the observation equation $A\mathbf{z}^{ex} = \mathbf{d}^{ex}$, $\mathbf{z}^{ex} \in Z$, $\mathbf{d}^{ex} \in D$.

Given data $\mathbf{d}$ may satisfy some *compatibility* condition for the existence of an unique *exact* solution in Z. However it is not always possible to write down explicitly the compatibility condition for exact $\mathbf{d}^{ex}$, even if precise informations on the physical nature of the problem are known. There is of course some exception (As an example, we keep in mind that the compatibility condition of the Neumann boundary data g, the normal gradient for the Laplace equation, is $\int g dS = 0$).

In practice, to obtain such a pair, one can take for example some $\mathbf{z}^{ex}$ and define $\mathbf{d}^{ex}$ as the direct image $A\mathbf{z}^{ex}$. Such a construction of the exact pair $\{\mathbf{z}^{ex}, \mathbf{d}^{ex}\}$ is based on the solution of forward problems which gives a compatible pair. The knowledge of an exact pair $\{\mathbf{z}, \mathbf{d}\}$, given by the solutions of forward problems, is useful to check the algorithm of approximate numerical solutions. One considers a model with known geometry, materials constants and boundary conditions for calculating $\{\mathbf{z}^{ex}, \mathbf{d}^{ex}\}$. Then one makes use of the numerical *artificial* data $\mathbf{d}^{ex}$ to recover the approximate numerical solution $\mathbf{z}^{(\alpha)}$ of the inverse problem. Another constructive solution

from given data $\mathbf{d}^{ex}$, consists in establishing an explicit formula giving the the solution $\mathbf{d}^{ex} = F(\mathbf{z}^{ex})$. Exact inverse solutions given in Chap. 12 fall in this category of constructive solutions.

The main result in error estimate is stated in the following theorem (Dang et al, 2000).

Theorem: Suppose that there exists $\mathbf{d}^1$ such that $\mathbf{z}^{ex} = A^*\mathbf{d}^1$. Then, the error $\|\mathbf{z}^{(\alpha)} - \mathbf{z}^{ex}\|$ is given by $\|\mathbf{z}^{(\alpha)} - \mathbf{z}^{ex}\| < \frac{1}{2}\alpha^{-1/2}(\|\mathbf{d} - \mathbf{d}^{ex}\| + \alpha\|\mathbf{d}^1\|)$.

The proof is given in an Exercice. The error estimate depends on both the regularisation parameter α which introduces some error on the modelling and the compatibility error on the datum $\|\mathbf{d} - \mathbf{d}^{ex}\|$ in comparison with the exact one. One gets the best possible error estimate by taking the regularization parameter $\alpha = k\varepsilon$ proportional to the datum error ε

$$\|\mathbf{d} - \mathbf{d}^{ex}\| < \varepsilon \Rightarrow \|\mathbf{z}^{(\alpha)} - \mathbf{z}^{ex}\| < \tfrac{1}{2}\, k^{-1/2}\varepsilon^{1/2}(1 + k\|\mathbf{d}^1\|)$$

12.4 Optimal control theory

Let us consider the example of elastic beam theory for determining the critical load P at buckling of a straight beam using the Optimal Control Theory. Let L be the beam length, $\phi(s)$ the rotation angle of the beam, $v = \phi'$ the curvature. The equilibrium state minimizes the potential energy J

$$\min_v J\ (v) = \int_0^L \{\tfrac{1}{2} EIv^2 - P(1 - \cos\phi)\}\, ds \tag{12.21}$$

Now we set the above problem in the framework of the Control Theory. To do so, we introduce a *time* like parameter, the arc length s. Find the *control* v(s) on the "time" interval [0, L] in order to minimize J(v) with the state equation

$$\frac{d\phi}{ds} = v \tag{12.22}$$

with "initial" condition

$$\phi(0) = 0 \text{ (clamped beam)} \tag{12.23}$$

and "terminal" condition

$$\phi'(L) = 0 \text{ (free moment)} \tag{12.24}$$

The solution of the control problem (12.21)-(12.24) in given in Appendix B.

Control Theory can be used for a variety of problems arising in Solids Mechanics and Fracture Mechanics. The first paper on this subject was due to Contensou (1946) who studied the better way to control the motion of a rigid body under the action of a rocket engine. Later, the theory and its applications to automatics derive largely from the works of Bellman (1957), Pontryagine (1959). Control Theory is then extended to partial derivative equations by Lions (1971). Here we shall rather look at applications to Solid Mechanics.

12.4.1 State equation and optimal control

We consider a control problem in finite dimensional space of a process characterized by $\mathbf{x}=(x_1(t),\ x_2(t),\ x_i(t),\ .x_n(t))$ governed by $\mathbf{v}(t)\in\mathbb{R}^m$. The *control* $\mathbf{v}(t)$ is assumed to be sectionally continuous in time, the state vector $\mathbf{x}(t)$ is continuous and sectionally differentiable in time and satisfies the differential equation

$$\frac{d\mathbf{x}}{dt}=\mathbf{f}(\mathbf{x},\mathbf{v},t)$$

$t\in[t_0,t_1]$, $\mathbf{x}\in\mathbb{R}^n$, $\mathbf{v}(t)$ in some subspace $V\subset\mathbb{R}^{'}$ with $\mathbf{f}$ continuous in $(\mathbf{x},\ \mathbf{v})$ and continuously differentiable in $\mathbf{x}$. The above equation describes a non autonomous system. However, by introducing a new coordinate $x_{n+1}\equiv t$, and an addition differential equation $(dx_{n+1}/dt=1)$ the vector $\mathbf{f}^*=(\mathbf{f},1)\in\mathbb{R}^{n+1}$ is a function of $(\mathbf{x}^*,\ \mathbf{v})$ which does not depend explicitly on time. Therefore one can restrict ourself to autonomous system $\mathbf{f}(\mathbf{x},\mathbf{v})$ (time independent)

$$\frac{d\mathbf{x}}{dt}=\mathbf{f}(\mathbf{x},\mathbf{v}) \tag{12.25}$$

One can fix either the initial condition

$$\mathbf{x}(t_0)=\mathbf{x}^0 \tag{12.26}$$

or the terminal condition

$$\mathbf{x}(t_1)=\mathbf{x}^1 \tag{12.27}$$

or both conditions. In a docking in space, condition (12.27) is used for relative coordinates $x_1(t_1)-x\ (t\ )-x\ (t\ )-0$ and velocities $\partial\, x_1(t_1)=\partial_t x\ (t_1)$

$=\partial_t x_3(t_1)=0$ Vector $\mathbf{x}\in \mathbb{R}^6$ thus represents the position and the velocity of a point in the phase space. One wishes to choose the optimal control $\mathbf{v}(t)$ to minimize the propellant or generally the cost function $J(\mathbf{v})$

$$J(\mathbf{v}) \quad g(\mathbf{x}(t_1), t_1) + \int_{t_0}^{t_1} L(\mathbf{x}(t), \mathbf{v}(t), t)dt \tag{12.28}$$

with given functions $g(\mathbf{x},\mathbf{v},t)$ and $L(\mathbf{x},\mathbf{v},t)$ under the constraint that some given function $\mathbf{h}(\mathbf{x},t)\in \mathbb{R}^q$ $(q<n)$ vanishes at terminal time t_1

$$\mathbf{h}(\mathbf{x}, t)\Big|_{t\ t_1} = \mathbf{0} \tag{12.29}$$

More general control problem involving state equation not governed by the differential equation (12.25), but by partial differential equations will be addressed further.

12.4.2 Adjoint system of equations

Here we consider the initial condition (12.26) for given $\mathbf{x}^0$ at given t_0 and terminal condition (12.29). One introduces the Lagrange multipliers $\lambda(t)\in \mathbb{R}^n$, μ (a constant vector of $\mathbb{R}^q$) for conditions (12.25) and (12.29) respectively and write (12.28) in the augmented form

$$J = \{\mathbf{g}+\boldsymbol{\mu}.\mathbf{h}\}_{|t\ t_1} + \int_{t_0}^{t_1} \{L(\mathbf{x}, \mathbf{v}, t) + \boldsymbol{\lambda}.(\mathbf{f}(x,v,t) \quad \dot{\mathbf{x}})\}dt \tag{12.30}$$

The Hamiltonian is defined as

$$H(\mathbf{x}, \lambda, t; \mathbf{v}) := L(\mathbf{x}, \mathbf{v}, t) + \lambda . \mathbf{f}(\mathbf{x}, \mathbf{v}, t) \tag{12.31}$$

Since $\mathbf{x}(t_0)=\mathbf{x}^0$, the change of the control $\delta\mathbf{v}$ modifies the path $\mathbf{x}(\mathbf{v},t)$ so that $d\mathbf{x}^1$ is related to $\delta\mathbf{x}^1$ (at constant t) and to $\dot{\mathbf{x}}^1 dt_1$ (at constant $\mathbf{v}$) by

$$d\mathbf{x}^1 = \delta\mathbf{x}^1 + \dot{\mathbf{x}}^1 dt_1$$

Upon substituting the latter expression in the differential dJ of Eq. (12.30), then integrating by parts and rearranging terms, we obtain

$$dJ = \{(\partial_t[g(\mathbf{x},t)+\mu.\mathbf{h}(\mathbf{x},t)] + L + \lambda(t).\mathbf{x}^1(t)\}\Big|_{t\ t_1} + \lambda(t).\delta\mathbf{x}\Big|_{t\ t_0} +$$

$$+ \{(\partial_x[g(\mathbf{x},t)+\mu.\mathbf{h}(\mathbf{x},t)] - \lambda(t)\}.\mathbf{x}\Big|_{t\ t_1} + \int_{t_0}^{t_1}\left(\frac{\partial H}{\partial \mathbf{x}} + \frac{d}{dt}\lambda\right).\delta\mathbf{x}dt$$

$$+ \quad \int_{t_0}^{t_1} \frac{\partial}{\partial \mathbf{v}} \mathrm{H}.\delta\mathbf{v}dt \tag{12.32}$$

Now we choose the adjoint state $\lambda(t)$ to cancel all terms in the right hand side of (12.32) except the last one so that

$$\mathrm{dJ} = \int_{t_0}^{t_1} \frac{\partial \mathrm{H}}{\partial \mathbf{v}}.\delta\mathbf{v}dt$$

Therefore, the adjoint state $\lambda(t)$ satisfies the adjoint system of equations

$$\frac{\mathrm{d}}{\mathrm{dt}}\lambda = -\frac{\partial \mathrm{H}}{\partial \mathbf{x}} \quad \text{(adjoint state equation)} \tag{12.33}$$

$$\lambda(t_1) = \mathrm{grad}[g(\mathbf{x},t)+\mu\,.\mathbf{h}(\mathbf{x},t)]\Big|_{t\ t_1} \quad \text{(terminal condition)} \tag{12.34}$$

$$\{\partial_t[g(\mathbf{x},t)+\mu\,.\mathbf{h}(\mathbf{x},t)] + \mathrm{L} + \lambda(t).\,\mathbf{f}(\mathbf{x},\mathbf{v},t)\}\Big|_{t\ t_1} = 0 \tag{12.35}$$

Eq. (12.35) is called the transversality condition. When no constraints on the control exist, the stationarity of J implies that

$$\frac{\partial \mathrm{H}}{\partial \mathbf{v}} = 0 \tag{12.36}$$

Since $\partial H/\partial\lambda=\mathbf{f}$, Eqs. (12.25) and (12.33) can be written in the Hamiltonian form

$$\frac{\mathrm{d}\mathbf{x}}{\mathrm{dt}} = \frac{\partial \mathrm{H}}{\partial \lambda}, \qquad \frac{\mathrm{d}}{\mathrm{dt}}\lambda = -\frac{\partial \mathrm{H}}{\partial \mathbf{x}}$$

Remark that if t_1 and $\mathbf{x}(t_1)$ are prescribed and that the constaints are on the intial state $\mathbf{k}(\mathbf{x},t=t_0)=\mathbf{0}$ ($\mathbf{k}\in\mathbb{R}^q$, $q<n$) one has to consider the intial condition for the adjoint state instead of Eq. (12.34) and the transversality condition at initial time instead of Eq. (12.35)

$$\lambda(t_0) = -\mathrm{grad}[g(\mathbf{x},t)+\mu\,.\mathbf{k}(\mathbf{x},t)]\Big|_{t\ t_0} \quad \text{(initial condition)} \tag{12.37}$$

$$\{-\partial_t[g(\mathbf{x},t)+\mu\,.\mathbf{k}(\mathbf{x},t)] + \mathrm{L} + \lambda\,.\,\mathbf{f}\}\Big|_{t\ t_1} \quad \text{(transversality cond.)} \tag{12.38}$$

Pontryagine's minimum principle

Consider the case where $g\equiv 0$, $\mathbf{h}\equiv\mathbf{0}$. The minimum principle states the necessary condition for a control $\mathbf{v}(t)$ and the corresponding state vector $\mathbf{x}(t)$ to

be optimal in the sense of minimum J. It is necessary that the adjoint state vector $\lambda(t)$ exists and that:
a) it satisfies the adjoint state equation (12.33), the terminal time condition (12.34), and the transversality condition (12.35).
b) for $t\in[t_0,t_1]$, the function $\mathbf{v}\rightarrow H(.,.,.;\mathbf{v})$ reaches its minimum M at $\mathbf{v}_{opt}$

$$M(\mathbf{x}(t),\lambda(t),t) := \min_{\mathbf{v}(t)} H(\mathbf{x}(t),\lambda(t),t;\mathbf{v}(t)) \tag{12.39}$$

We leave out difficult and complex questions related to the existence of an optimal path, (see Pontryagin et al, 1962).

Bellman's dynamic programming

Consider the case where $g\equiv 0$, $\mathbf{h}\equiv\mathbf{0}$ and a control problem in $\mathbb{R}$. The adjoint method provides the gradient of J, Eq. (12.32), with respect to the control v(t) as $\partial H/\partial v$ for an updtate of the actual control. The optimal path $x(t,v_{opt})$ is approached by successive pathes of different controls, then the optimal cost $J^0(v_{opt})$ is obtained by a limiting process. This appoach is quite general for control problems arising in inverse problems in finite or infinite dimensional spaces. In the finite dimension case, Bellman gives another method based on the minimum principle which gives directly the optimal path optimal cost by an integration along the optimal path $x(t,v_{opt})$.

Consider an optimal control problem

$$\min_{v[a,T]} J(x), \qquad J(x)=\int_a^T L(x,x')dt, \qquad x(a)=c$$

with the Lagrangian L(x,v) and x'=v (state equation). The optimal path between [a*,T] is indicated by arrows and the corresponding optimal cost is $J^0(c^*,a^*)$ for the optimal control $v_{opt}(t)$ over [a*,T], with $c^*=x(a^*)$. To obtain the optimal cost $J^0(c,a)$ for over a larger interval [a,T], we assume that $S=a^*-a$ is small and then consider a continuous control v(t)

$$v(t)=\begin{cases} w \text{ (constant) over } [a,a^*] \\ v_{opt}(t) \text{ over } [a^*,T] \end{cases}$$

Therefore

$$J^0(c,a)=\min_{v[a,T]}\left\{\int_a^{a^*} L(x,v)dt+\int_{a^*}^T L(x,v)dt\right\}$$

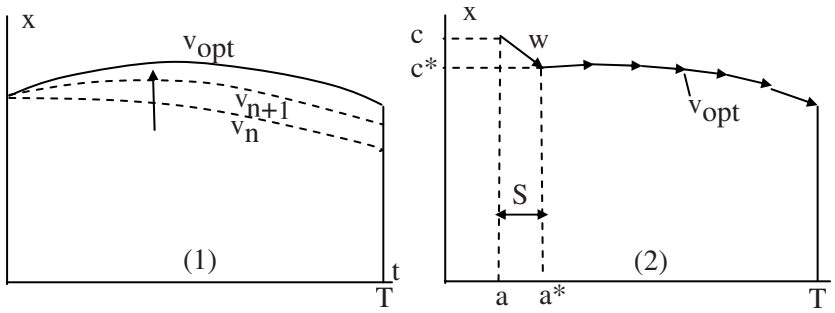

Figure 12.2: Control by the gradient approach (1) with the initial condition $x(0)=x^0$; Bellman's dynamic programming (2)

$$J^0(c,a) = \min_{v[\,a,T]} \left\{ SL(c,w) + J^0(c+wS, a+S) \right\} \tag{12.40}$$

To within $O(S^2)$, by expanding Eq. (12.40) one obtains Bellman's equation

$$\min_{v[\,a,T]} \left\{ L(c,v) + \frac{\partial J^0}{\partial c} v \right\} + \frac{\partial J^0}{\partial a} = 0 \tag{12.41}$$

with $J^0(c,T)=0$. Remark that $f(x,v)=v$, hence $H(x,\lambda,v)=L(x,v)+\lambda v$.
By the substitutions $c\to x$, $w\to v$, $a\to t$, and $\lambda\to\partial J^0/\partial x$, Eq. (12.41) can be written in the Bellman-Hamilton-Jacobi form

$$-\frac{\partial J^0}{\partial t} = \min_{v} H(x, \frac{\partial J^0}{\partial x}, v) \tag{12.42}$$

with boundary condition $J^0(c,T)=0$.

12.5 The dynamic system of quasi-static elasticity

Most inverse problems in solids mechanics are governed by elliptical equations: Laplace equation $\Delta u = \mathrm{div}\,\mathrm{grad}(u)=0$ or elasto-statics $\mathrm{div}\,\sigma[\mathbf{u}]=0$. Given two superabundant boundary data $u|_{\partial\Omega}$ and $\partial_n u|_{\partial\Omega}$, solve the Cauchy problem for Laplace's equation.

The Cauchy problem is a known subject. Recently methods of solution to Cauchy's problem have been used to detect flaws and cracks, (Bui, 1994).

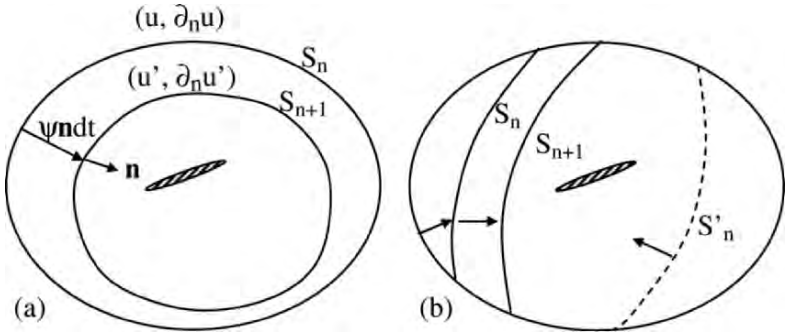

Figure 12.3: Propagation of fronts S_t with normal velocity $\psi(\mathbf{x})\mathbf{n}$. Solid domain behind the fronts is free of defects. Closed fronts in (a) and open fronts in (b)

The principle of defects detection is based on the formulation of quasi-static elasticity in the dynamic form (12.25). First, consider the anti-plane elastic problem governed by the harmonic equation $\Delta u=0$. Given the pair $(u,\partial_n u\equiv g^d)$ on S_0, more generally knowing $(u,\partial_n u)$ on S_n, find a new pair $(u', \partial_n u')$ on S_{n+1}, Fig. 12.3 (a) when the change $S_n \to S_{n+1}$ is controlled by some velocity field. This is the velocity field $\psi(\mathbf{x})$ given in Ω which defines by $\psi(\mathbf{x})\mathbf{n}dt$ the small change of S_n into S_{n+1} during the time interval dt. The propagation of fronts continues until we find a crack tip singularity or a discontinuity infered by the presence of cracks. Such regular fronts determine smaller and smaller domains containing cracks tips singularities or crack faces(*). Fronts S_n can be the open ones shown in Fig. 12.3 (b). By choosing different initial fronts S'_0 one can also approach the defects from the outside.

Let $\mathbf{z}=(u,\partial_n u)^\tau$ be the state vector defined for $\mathbf{x}\in S_t$ at time t. Its evolution is governed by some transfer matrix A of tangential operators, t being a time like parameter along orthogonal lines to fronts S_t

$$\frac{d\mathbf{z}}{dt} = A\,\mathbf{z} \tag{12.43}$$

Consider the example of Cauchy's problem for $\Delta u=0$ in the square domain

---

(*) A cavity defined by $\partial_n u=0$ cannot be determined by the reconstructed $u(\mathbf{x})$, but rather by the reconstructed conjugate function $v(\mathbf{x})$ such that $u+iv$ is analytical in the complex variable $z=x_1+ix_2$. Suppose that $|\nabla u(\mathbf{A})|=0$ at $\mathbf{x}=\mathbf{A}$. One sets $v(\mathbf{A})=0$.The cavity belongs to the set $\{\mathbf{x};\, v(\mathbf{x})=0\}$ of stream lines of potential flow.

$\Omega := \{\mathbf{x} |\ 0<x_1<1,\ 0<x_2<1\}$, with superabundant data

$u=1$ and $g=1$ on $x_2=0,\ 0<x_1<1$

and the homogeneous Neumann condition $\partial_n u - 0$ on $x_1 - 0$ or $x_1 - 1,\ 0<x_2<1$. The gradient g is the unknown on $x - 1,\ 0<x_1<1$. First, the Laplace equation $\partial_1\partial_1 u+\partial_2\partial_2 u=0$ is written in the dynamic form with fronts propagating in the Ox_2 direction $t\equiv x_2$:

$$\partial_2 u = g$$

$$\partial_2 g = \partial_2\partial_2 u = -\partial_1\partial_1 u$$

Hence the Laplace equation $\Delta u=0$ in two-dimensions is transformed into the dynamic equation (12.43) with the matrix operator

$$A = \begin{bmatrix} 0 & 1 \\ -\dfrac{\partial^2}{\partial x_1^2} & 0 \end{bmatrix} \tag{12.44}$$

In cylindrical coordinates, the time like variable is $t:=r$ and the harmonic equation becomes $d\mathbf{z}/dr=A\mathbf{z}$ with $\mathbf{z}=(u,\partial_r u)^\tau$ the matrix operator

$$A = \begin{bmatrix} 0 & 1 \\ -\dfrac{\partial^2}{r^2\partial\theta^2} & -\dfrac{1}{r} \end{bmatrix}$$

Further analyses show that operator A can be explicitly determined for general curvilinear coordinates, for $\Delta u=0$ and $div\sigma[\mathbf{u}]=0$ as well, Bui (1993). Cylindrical and spherical coordinates have been considered in (Zhong, 1995; Li and Recho, 2002).

Naively, one can attempt to integrate the Cauchy system (12.43) by the « time » integration ($t:=x_2$) with the « initial » conditions $\mathbf{z}_0(t)=(1,1)^\tau$ on $x_2=0$. Numerically, an explicit integration scheme blows up immediately after 2 or 3 steps. This illustrates the ill-posedness of Cauchy's problem. Hadamard showed that a perturbation of the data $u=1$ by a term $u(x_1,0)=1+\varepsilon\cos(2k\pi x_1)$ with small ε and large integer k leads to the exact solution $g(x_1,1)-1+2k\varepsilon\cos(2k\pi x_1)\cosh(2k\pi)$ which blows up when integer k is very large. Fig. 12.4(a) on the left shows the numerical result obtained in (Bui, 1993) for the initial data ($u=0,\ g=x_1^2$) on $S_0\subset\partial\Omega$ plus a random error 1%, just after one step increment $\delta t=0.02$. Fig. 12.4(b) on the right shows numerical result of the same problem after a regularization procedure based on the use of the smoothing operators described below.

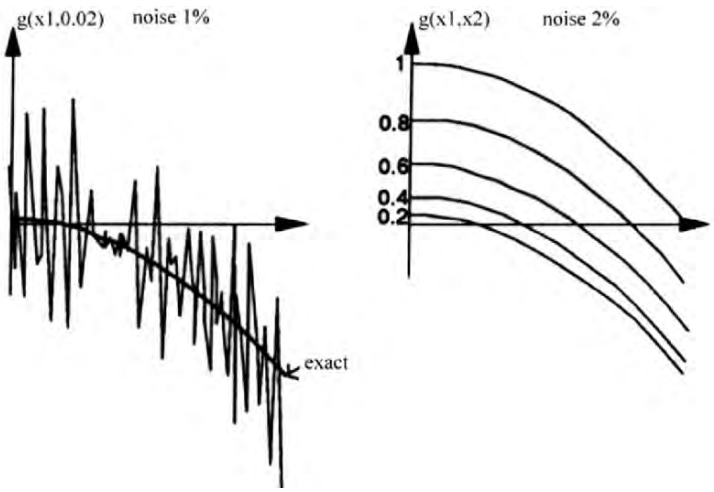

Figure 12.4: (a) Integration of the dynamic equation d**z**/dt = A**z** , without regularization; (b) with the regularization smoothing operator M, d**z**/dt = AM**z**, (Bui, 1993)

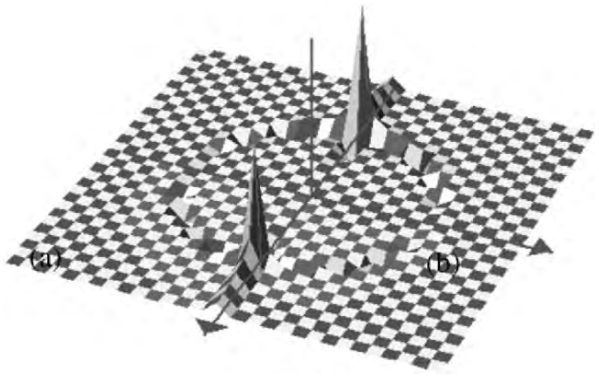

Figure 12.5: The level set v = 0 of the conjugate function v(**x**) corresponding to the cavity detection $\Delta u = 0$, $\partial_n u = 0$ on the boundary of the cavity

As another example, consider the reconstruction of a circular cavity defined by condition $\partial_n u = 0$ (see the footnote of Sect. 12.5). To determine graphically the level set v(**x**) = 0 of the reconstructed conjugate function, one may conveniently use the 3D-plot of $z = 1/v(\mathbf{x})$ if $|v(\mathbf{x})| > \varepsilon$, and $z = 1$ otherwise, Fig. 12.5.

12.5.1 Smoothing operators

A regularization procedure is required for obtaining stable solutions of Cauchy's problem considered the above examples. Mathematically, for given functions $x_1 \to u(.,x_1)$ one can define different smooth functions $x_1 \to Mu = \bar{u}(., x_1)$ by using smoothing operator M, which can be defined in different equivalent manners (Lorentz and Andrieux, 2003).

Since operator A involves second derivatives with respect to the spatial variable along the front $.{}_t$ (the spatial variable is x_1 in this example), we consider the space of smooth functions $\bar{u} \in H^2([0,1])$, $\bar{u}'(x_1=0) = \bar{u}'(x_1=1)=0$, such that the operator AM is bounded, $\|AM\mathbf{z}\| \le C'\|\mathbf{z}\|$ for some constant C' and for $\mathbf{z}=(\bar{u}, \partial_2 \bar{u})$.

Below the presentation of smoothing techniques of functions in [0, 1] follows the paper (Lorentz and Andrieux, 2003):

Differential equation:

$$\left.\begin{aligned} &M: u \to Mu := \bar{u} \quad \text{solution of} \\ &\bar{u} - k^2 \bar{u}'' + h^4 \bar{u}'''' = u \qquad \text{in } [0, 1] \\ &\bar{u}'(0) = \bar{u}'(1) = 0, \quad \bar{u}'''(0) = \bar{u}'''(1) = 0, \end{aligned}\right\} \tag{12.45}$$

where k and h is a characteristic length, small with respect to the interval [0,1] but large with respect to the wave length of the numerical oscillations of u.

Variational equation:

For given noised u, find $\bar{u} \in H^2([0,1])$, such that

$$\int_{[0,1]} [(\bar{u} - u)v + k^2 \bar{u}'v' + h^4 \bar{u}''v'']ds = 0, \qquad \forall\, v \in H^2([0,1]) \tag{12.46}$$

where v satisfies the boundary conditions (12.45). Test functions v satisfying (12.45) can be Fourier cosinus-functions of the form

$$v(x_1, x_2) = \sum_n a_n(x_2)\cos(n\pi x_1).$$

Minimisation of functional:

$$u \to \bar{u} = \text{Arg Min}_{V \in H^2} \int_{[0,1]} [(v-u)^2 + k^2(v')^2 + h^4 (v'')^2]ds \tag{12.47}$$

The first term alone corresponds to the usual least square approximation method. It can give a good result because of the smoothness of the space used H^2. However, better results are obtained with additional terms which correspond to the gradient penalties limiting higher order oscillations.

Convolution integral

$$\bar{u} \equiv Mu(x) = \int_{[0,1]} G(x, y)u(y)dy, \tag{12.48}$$

G(x; y): Green's function of the equation $G - k\,G'' + h^4 G'''' = \delta(x-y)$. Finally, the Cauchy problem consists in the integration of the differential equation with a bounded transfer operator AM, instead of unbounded A:

$$\frac{d}{dt}\mathbf{z} = AM\mathbf{z} \tag{12.49}$$

and taking into account the initial condition $\mathbf{z}(t=0)=(u^d, \partial_n u = g^d)^\tau$. At time t+dt, updated values of the vector $\mathbf{z}$ on S_{t+dt}, are given by $\mathbf{z}(t+dt) = \mathbf{z}(t)+AM\mathbf{z}(t)dt$. Since AM is bounded, we have the inequality, $\|AM\mathbf{z}\| \le C\|\mathbf{z}\|$ for $z=(\bar{u}, \partial_2 \bar{u})$ which guarantees the existence and uniqueness of the solution of Eq. (12.49) if the integration step is small.

12.5.2 Transfer matrix operator in elasticity

Front S_{t+dt} is derived from the precedent one S_t by displacing each point of S_t by vector $\psi(x)\mathbf{n}dt$, where $\mathbf{n}$ is the unit normal vector to the front, $\psi(x)$ is a positive and regular scalar field representing the normal «velocity». Therefore the « material » derivative of u is given by $du/dt = \psi g$. We have to complete the latter equation by the material derivative of g, that is to calculate dg/dt explicitly, via the transfer matrix $A(u,g;\psi)$.

Let us introduce the following notations for tangential operators along S

$$grad_s(.) := grad(.) - \mathbf{n}\partial_n(.) \quad \text{(tangential gradient)} \tag{12.50}$$

$$div_s(.) := div(.) - \mathbf{n} \cdot \partial_n(.) \quad \text{(tangential divergence)} \tag{12.51}$$

Now we remark that function u at any fixed point left behind the moving front S_t does not change its value $\partial u/\partial t = 0$. This *invariance* condition expresses the continuation of the same original function $u(\mathbf{x})$, which does not depend explicitly on the moving S(t).

Consider the evolution of fronts in Fig. 12.3 (b). Let Ω_t be the domain on the left of S_t, its boundary is $\partial\Omega_t = S_0 \cup S_t \cup S_\infty$. On S_0, $\partial_n u = g^d$ (inward

normal to Ω) is prescribed, on S the gradient $\partial_n u = g$ is known at time t, and we assume that $\partial_n u = 0$ on the complementary S_L .

Three cases can be considered :

i) The lateral boundary S_L does not exist,

ii) The lateral boundary S_L is orthogonal to Γ_t and $\partial_n u = 0$ on S_L,

iii) The lateral boundary S_L reduces to two fixed points (two-dimensional problem) or to a closed curve (three-dimensional problem).

These are natural conditions appearing in the following *rate variational problem* of elasticity. First consider the solution of the harmonic equation $\Delta u = 0$, more precisely the solution of the variational problem $a_t(u,v) = b_t(v)$ in Ω_t

$$\int_{\Omega_t} \text{grad}\, u . \text{grad}\, v \, d\Omega = \int_{S_t} g v \, dS - \int_{S_0} g^d v \, dS \,, \; \forall v \quad \text{(Problem P)} \tag{12.52}$$

where the test functions v are assumed to be independent of t. Sign (–) in the second integral in the right hand side of (12.52) is due to inward normal **n**. Consider the rate problem P' obtained by differentiating (12.52)

$$\frac{d}{dt} a_t(u,v) = \frac{d}{dt} b_t(v) \quad \text{(Problem P')} \tag{12.53}$$

On convected differentiation of the time dependent domain integral over Ω_t and integration by parts, together with the invariance condition $\partial u/\partial t = 0$, we obtain the formula, (Bonnet and Bui, 1989)

$$\begin{aligned} \frac{d}{dt} u &= \psi g \\ \frac{d}{dt} g &= - \, \text{div}_S(\psi \, \text{grad}_S u) - g \text{div}_S(\psi \mathbf{n}) \end{aligned} \tag{12.54}$$

The matrix of tangential operators is

$$A := \begin{bmatrix} 0 & \psi \\ \text{div}_S \psi \text{grad}_S & \text{div}_S(\psi \mathbf{n}) \end{bmatrix} \tag{12.55}$$

Field $\psi(\mathbf{x})$ which defines the magnitude of the velocity field on S_t can be arbitrarily chosen. Stream lines are parameterized by two coordinates on S_t and coordinate t describes the position of S_t along the stream lines. Matrix (12.55) is the generalization of (12.44) to curvilinear coordinates.

Now, to derive similar dynamic equations for three-dimensional elasticity, we consider the state vector $\mathbf{z} = (\mathbf{u}, \mathbf{T})^t$ with displacement **u** and stress vector $\mathbf{T} := \sigma[\mathbf{u}].\mathbf{n}$ on S_t. The above condition ii) for the *rate variational problem* (12.52) becomes $\mathbf{T} = \mathbf{0}$ on S_L. The variational problem of elasticity

$$\int_{\Omega_t} \text{grad}\,\mathbf{u}.\mathrm{L}.\text{grad}\,\mathbf{v}\,d\Omega = \int_{S_t} \mathbf{T}.\mathbf{v}\,dS - \int_{S_0} \mathbf{T}^{\mathrm{d}}.\mathbf{v}\,dS \quad \forall \mathbf{v} \quad \text{(Problem Q)} \tag{12.56}$$

where $\mathbf{v}$ is independent of t, as well as $\mathbf{T}^{\mathrm{d}}$. The invariance condition is $\partial\mathbf{u}/\partial t = \mathbf{0}$. The rate variational problem (Q') results from the convected differention of (12.56). It has been shown in (Bui, 1993) that the rate variational problem (Q') is

$$\int_{S_t} \psi\,\text{grad}\,\mathbf{u}.\mathrm{L}.\text{grad}\,\mathbf{v}\,d\Omega - \int_{S_t} \{\dot{\mathbf{T}} + \text{div}_S(\psi\mathbf{n})\mathbf{T}\}.\mathbf{v}\,dS - \int_{S_t} \psi\mathbf{T}.\frac{\partial \mathbf{v}}{\partial n}\,dS = 0\,, \forall \mathbf{v}$$

$$\dot{\mathbf{T}} = d\mathbf{T}/dt. \quad \text{(Problem Q')} \tag{12.57}$$

It can be shown that, the rate variational problem (Q') is equivalent to

$$\frac{dz}{dt} = \mathbf{L}(\mathbf{z}, \psi) \tag{12.58}$$

with components

$$\begin{aligned} \frac{d\mathbf{u}}{dt} &= \psi \mathrm{G}(\mathbf{u}, \mathbf{T}) \\ \frac{d\mathbf{T}}{dt} &= -\mathbf{T}\text{div}_S(\psi\mathbf{n}) - \text{div}_S\{\psi \mathrm{S}(\mathbf{u}, \mathbf{T})\} + \psi\left(\frac{1}{\mathrm{R}_1} + \frac{1}{\mathrm{R}_2}\right)\mathrm{S}(\mathbf{u}, \mathbf{T}).\mathbf{n} \end{aligned} \tag{12.59}$$

where $\mathrm{S}(\mathbf{u},\mathbf{T})$ is the stress tensor $\sigma = \mathrm{L}.\text{grad}\mathbf{u}$ as defined below, $\mathrm{G}(\mathbf{u},\mathbf{T})$ is the normal gradient $\partial\mathbf{u}/\partial n$ which has to be expressed in terms of state quantities $\mathbf{u}$, $\mathbf{T}$ defined on S_t only. In order to do so, we consider the constitutive law in local coordinates, (ξ_1, ξ_2) along S_t and t along the normal direction $\mathbf{n}$. Using (12.50) we obtain

$$\mathrm{G}(\mathbf{u},\mathbf{T}) = \{\frac{1}{2\mu}\mathbf{T}.\mathbf{e}^{\alpha} - \mathbf{e}^{\alpha}.(\text{grad}_S\mathbf{u})^{\text{sym}}.\mathbf{n}\}\mathbf{e}^{\alpha} +$$

$$+\frac{1}{\lambda + 2\mu}\{\mathbf{T}.\mathbf{n} - \lambda\,\text{tr}(\text{grad}_S\mathbf{u}) - 2\mu\mathbf{n}.(\text{grad}_S\mathbf{u})^{\text{sym}}.\mathbf{n}\}\mathbf{n} \tag{12.60}$$

Stress $\mathrm{S}(\mathbf{u}, \mathbf{T})$ has also to be expressed in terms of the state quantities $\mathbf{u}$, $\mathbf{T}$ only

$$\mathbf{S}(\mathbf{u}, \mathbf{T}) = \mathrm{L}.\{\text{grad}_S\mathbf{u} + \mathrm{G}(\mathbf{u}, \mathbf{T}) \otimes \mathbf{n}\} \tag{12.61}$$

Eqs. (12.58)-(12.61) are the *dynamic form* of Elasticity which depends on the control field $\psi(\mathbf{x})$, (Bui, 1993).

12.6 Quasi-reversibility method

A powerful method for solving Cauchy's problem is provided by the Quasi-reversibility method of Lattès and Lions (1967). Consider the Cauchy problem of the harmonic equation with two boundary data u^d and g^d given on a part of the boundary. There are no data on the complementary surface $\partial\Omega\backslash S_0$. There are no unknown defects either.

The QR method relies upon the use of a higher-order (4th order) partial differential equation defined herafter, depending on a small parameter ε, whose solution $u^{(\varepsilon)}$ is identical to the harmonic function u in the domain Ω, except in a layer of thickness 2ε along $\partial\Omega\backslash S_0$.

Let us consider a square domain $\Omega := \{\mathbf{x};\ 0<x_1<1,\ 0<x_2<1\}$. Consider $\Omega^\varepsilon := \{\mathbf{x};\ 0<x_2<1-2\varepsilon\}$, $C^\varepsilon := \{\mathbf{x}|\ 1-\varepsilon<x_2<1\}$. Ω^ε and Ω share the common boundary S_0. Cauchy's problem is equivalent to the problem of finding $u^{(\varepsilon)}$ solution of the problem :

$$\left.\begin{array}{ll} \Delta(M^{(\varepsilon)2}\,\Delta u^{(\varepsilon)}) = 0 & \text{in } \Omega^\varepsilon \\ u^{(\varepsilon)} = u^d \quad \text{and} \quad g^{(\varepsilon)} := \partial_n u^{(\varepsilon)} = g^d & \text{on } S_0. \end{array}\right\} \tag{12.62}$$

Function $M^{(\varepsilon)}(\mathbf{x})$ is a positive C^2 function defined in Ω .by

$$\left.\begin{array}{ll} M^{(\varepsilon)}(x_1, x_2) = 1 & \mathbf{x}\in\Omega^\varepsilon \\ M^{(\varepsilon)}(x_1, x_2) = 0 & \mathbf{x}\in C^\varepsilon \end{array}\right\} \tag{12.63}$$

and $M^{(\varepsilon)}(x_1, x_2)=0$ continuous for $1-2\varepsilon<x_2<1-\varepsilon$.
Since $M^{(\varepsilon)}(x_1,1)=0$, no other conditions are required for $u^{(\varepsilon)}$ and v on the boundary $x_2=1$.

The uniqueness of the solution $u^{(\varepsilon)}$ as well as the L^2-convergence $u^{(\varepsilon)}\to u$ are proved in (Lattès and Lions, 1967). Finally, the ill-posed Cauchy Problem is replaced by a well-posed one using a higher-order equation which makes use of two boundary data.

No explicit regularization procedures are needed because the functions space $H^2(\Omega)$ considered in the variational formulation of the fourth order equation (12.62) are implicitly more regular than the space $H^1(\Omega)$ considered

in the original variational problem of the second order equation. The variational problem consists in finding $u^{(\varepsilon)} \in H^2(\Omega)$ such that:

$$(M^{(\varepsilon)}\Delta u^{(\varepsilon)}, M^{(\varepsilon)}\Delta v) = 0, \quad \text{for any } v \in X^{(0)} \tag{12.64}$$

and $X^{(0)}$ being the set of test functions $v \in H^2(\Omega)$ satisfying $v=0$ and $\partial_n v=0$ on .. A better result can be obtained by using the penalty form of the variational equation

$$(M^{(\varepsilon)}\Delta u^{(\varepsilon)}, M^{(\varepsilon)}\Delta v)/\varepsilon^2 + (r^{(\varepsilon)}\text{gradu}^{(\varepsilon)}, r^{(\varepsilon)}\text{gradv}) = 0 \quad \forall v \in X^{(0)} \tag{12.65}$$

In the above equations the duality (.,.) means the integration over $\Omega^{(\varepsilon)}$ of the product of dual terms. The function $r^{(\varepsilon)}$ is defined by any continuous function such that

$r^{(\varepsilon)}=1$ for $x_2<1-\varepsilon$,

$r^{(\varepsilon)}=(1-x_2)/\varepsilon$ for $1-\varepsilon<x_2<1$.

The L^2-convergence $u^{(\varepsilon)} \rightarrow u$ to the solution u of the Cauchy problem is proved in (Lattès and Lions, 1967). The QR-method has been generalized to parabolic equation in (Lattes and Lions, 1967) and hyperbolic equation in (Klibanov and Timonov, 2003) for the mathematical treatment of time reversal.

12.7 Control of partial derivative equations

One consequence of damage in solids is the appearance of cavities and cracks at the microscopic scale. Damage reduces the elastic moduli L and the heat conduction coefficent k. To determine the damage field one can solve an inverse problem to determine the field $k(\mathbf{x})$ by use of the heat diffusion equation and the method of Control of partial derivative equations of Lions (1971).

12.7.1 Inverse problems in parabolic systems

Let us consider dimensionless quantities ($\rho c=1$, $k_0=1$) to solve the inverse problem : Find the heat conduction coefficient $k(\mathbf{x})$, from boundary measurements of the temperature θ and the flux $\partial_n\theta \equiv g$ during the time interval [0,T]. The forward problem is governed by equations

$$-\mathrm{div}\{k(\mathbf{x})\mathrm{grad}\,\theta\} + \frac{\partial\theta}{\partial t} = 0,\ \mathbf{x}\in\Omega \tag{12.66}$$

$$\theta(\mathbf{x},\ t\le 0) = 0,\quad \mathbf{x}\in\Omega \tag{12.67}$$

$$\partial_n\theta(\mathbf{x}',\ t) = g(\mathbf{x}',\ t)\ ,\ \mathbf{x}'\in\partial\Omega,\ t\in[0,\ T] \tag{12.68}$$

Let us consider a heat diffusion model with coefficient $h(\mathbf{x})$ which will be considered as the *control*. The corresponding temperature $u(\mathbf{x})$ satisfies the same boundary condition (12.68)

$$-\mathrm{div}\{h(\mathbf{x})\mathrm{grad}\,u\} + \frac{\partial u}{\partial t} = 0\ ,\ \mathbf{x}\in\Omega \tag{12.69}$$

$$u(\mathbf{x},\ t\le 0) = 0,\quad \mathbf{x}\in\Omega \tag{12.70}$$

$$\partial_n u(\mathbf{x}',\ t) = g(\mathbf{x}',\ t),\ \mathbf{x}'\in\partial\Omega,\ t\in[0,T] \tag{12.71}$$

The solution to the forward problem (12.69)-(12.71) is well-posed and is denoted by $u(\mathbf{x}, t;h)$. Now, in order to solve the inverse problem, one seeks the optimal control h which makes the best fitting between the predicted temperature $u(\mathbf{x}',t;h)$ and the measured one θ^d $(\mathbf{x}',t)$ at the boundary for any time in [0,T]. The functional to be minimized is the least square norm

$$\min_h J(u(h)):\quad \int_0^T\int_{\partial\Omega}\left|u(\mathbf{x}',t;h)\quad \theta^d(\mathbf{x}',t)\right|^2 dSdt \tag{12.72}$$

For numerical purposes, one needs to calculate the gradient of J with respect to the control, $\partial J/\partial h$. In direct *sensitive methods* in finite dimensional control space, $h=(h_1, h_2.., h_N)$ one should have to consider Eqs (12.69)-(12.71) for h+dh (h being calculated in the preceding step), thus to solve N direct problems. Now, let us show that Lions's adjoint method solves the sensitive problem of the gradient evaluation $\partial J/\partial h$ by considering *one* adjoint equation. Let us set the following notations:

$$a_h(u,v) \coloneqq \int_\Omega h\,\mathrm{grad}\,u.\,\mathrm{grad}\,v\,d\Omega \tag{12.73}$$

$$(u,v)_\Omega \coloneqq \int_\Omega u(\mathbf{x})v(\mathbf{x})\,d\Omega \tag{12.74}$$

$$(g,v)_{\partial\Omega}:\quad \int_{\partial\Omega} g(\mathbf{x}')v(\mathbf{x}')\,dS \tag{12.75}$$

The variational form of the problem (12.69)-(12.71) is

$$\int_0^T (\partial_t u, v)_\Omega dt + \int_0^T a_h(u, v)dt - \int_0^T (g, v)_{\partial\Omega} dt = 0, \quad \forall v \tag{12.76}$$

Thus the minimization problem (12.72) under constraints (12.69), (12.70), (12.71) or the variational constraint (12.76) can be solved by introducing Lagrange's multiplier $\lambda(\mathbf{x})$ and the Lagrangian L

$$L(u, h, \lambda) \triangleq J(u) + \int_0^T \{(\partial_t u, \lambda)_\Omega + a_h(u, \lambda) - (g, \lambda)_\Omega\} dt \tag{12.77}$$

If u is the solution of (12.76) then L=J. The minimum point of J(u) under specified constraints is the stationary point of the Lagrangian, $\delta L = 0$. Conversely the stationary Lagrangian, $\delta L = 0$ for any $\delta\lambda$, for fixed u and h, implies (12.76). Now consider the variations of both u and h and the corresponding change of L

$$\delta L = \frac{\partial L}{\partial u}\delta u + \frac{\partial L}{\partial h}\delta h$$

$$\frac{\partial L}{\partial u}\delta u \equiv \int_0^T (u - \theta, \delta u)_{\partial\Omega} dt + \int_0^T \{(\delta\partial_t u, \lambda)_\Omega + a_h(\delta u, \lambda)\} dt$$

$$\frac{\partial L}{\partial h}\delta h \equiv \int_0^T \int_\Omega \delta h \, \mathrm{grad}\, u . \mathrm{grad}\, \lambda \, d\Omega dt$$

One restrains the choice of λ by considering the one which cancels the variation $(\partial L/\partial u)\delta u$

$$\int_0^T (u - \theta, \delta u)_{\partial\Omega} dt + \int_0^T \{(\delta\partial_t u, \lambda)_\Omega + a_h(\delta u, \lambda)\} dt = 0 \tag{12.78}$$

One adds two additional conditions $\delta u(\mathbf{x}, 0) = 0$ and $\lambda(\mathbf{x}, t \geq 0) = 0$. On integrating (12.78) by parts, it is easily found that λ satisfies the adjoint equation

$$-\mathrm{div}\{h(\mathbf{x})\mathrm{grad}\,\lambda\} - \frac{\partial\lambda}{\partial t} = 0\,, \ \mathbf{x} \in \Omega \tag{12.79}$$

$$\lambda(\mathbf{x}, t \geq T) = 0, \quad \mathbf{x} \in \Omega \tag{12.80}$$

$$\partial_n \lambda(\mathbf{x}', t) = \theta(\mathbf{x}', t) - u(\mathbf{x}', t), \ \mathbf{x}' \in \partial\Omega, \ t \in [0, T] \tag{12.81}$$

Eq. (12.79) is the backward heat diffusion, which is a well-posed problem when solved backward from time t=T to t=0 (it is ill-posed when

solved forward from t=0 to T). With the adjoint field solution of (12.79)-(12.81) the variation of L or J is given by

$$\delta J = \int_0^T \int_\Omega \delta h \, \mathrm{grad}\, u . \mathrm{grad}\, \lambda \, d\Omega dt \tag{12.82}$$

This is the main result of adjoint equations methods, which provides the gradient of the functional J with respect to the control field h by solving *one* adjoint equation for the Lagrange multiplier field $\lambda(\mathbf{x},t)$.

12.7.2 Identification of materials

Inverse problems in elliptic systems, to determine the coefficient $k(\mathbf{x})$ in the steady state heat equation $\mathrm{div}(k(\mathbf{x})\mathrm{grad}\theta)=0$ or the moduli tensor $L(\mathbf{x})$ in the elastic equilibrium equation $\mathrm{div}(L(\mathbf{x})\mathrm{grad}\mathbf{u})=0$ are particular cases of the preceding model, without time derivative and time integration. For instance, the determination of the elastic moduli $L(\mathbf{x})$ from surface measurements of both displacement $\mathbf{u}(\mathbf{x})$ and traction vector $\mathbf{T}(\mathbf{x})$, can be done in a similar manner. To outline the main ideas, we refer to the works of Constantinescu (1995), Constantinescu and Tardieu (2000), Constantinescu and Verger (2002). One controls the elastic modulus tensor $M(\mathbf{x})$, so that the corresponding displacement $\mathbf{w}(\mathbf{x},M)$ under the same traction $\mathbf{T}(\mathbf{x})$ minimizes the functional J

$$\min_M J\ (w(M)) = \int_{\partial\Omega} \left| \mathbf{w}(\mathbf{x}';M) - \mathbf{u}(\mathbf{x}') \right|^2 dS_{x'} \tag{12.83}$$

Thus the model $\mathbf{w}(\mathbf{x}, M)$ satisfies the equilibrium equation

$$-\mathrm{div}\sigma[M\mathrm{grad}\mathbf{w}] = 0 \quad \text{in } \Omega$$

$$\mathbf{n}.\sigma[M\mathrm{grad}\mathbf{w}] = \mathbf{T} \text{ on } \partial\Omega$$

The adjoint displacement satisfies the equation

$$-\mathrm{div}\sigma[M\mathrm{grad}\lambda] = 0 \quad \text{in } \Omega$$

$$\mathbf{n}.\sigma[M\mathrm{grad}\lambda] = \mathbf{u} - \mathbf{w} \quad \text{on } \partial\Omega$$

and the variation δJ is

$$\delta J = \int_\Omega (\mathrm{grad}\ \mathbf{w})^{\mathrm{sym}} . \delta M . (\mathrm{grad}\lambda)^{\mathrm{sym}} \, d\Omega \tag{12.84}$$

Eq. (12.84) defines the gradient of J with respect M. Let us consider the representation of symmetric tensors in $\mathbb{R}^3 \otimes \mathbb{R}^3$ by vectors in $\mathbb{R}^6$ and the elastic moduli tensor δM by the 6×6 symmetric matrix

$$(\text{grad}\mathbf{w})^{\text{sym}}.\delta\mathbf{M}.(\text{grad}\lambda)^{\text{sym}} = \sum_{i,j=1}^{6} w'_i \delta M_{ij} \lambda'_j$$

It should be noted that the symmetry of the moduli elastic tensor allows the above term to be expressed as

$$w'_i \delta M_{ij} \lambda'_j = \delta M_{11} w'_1 \lambda'_1 + \delta M_{22} w'_2 \lambda'_2 + \delta M_{33} w'_3 \lambda'_3 +$$

$$\delta M_{12}(w'_1 \lambda'_2 + w'_2 \lambda'_1) + \delta M_{23}(w'_2 \lambda'_3 + w'_3 \lambda'_1) + \delta M_{31}(w'_3 \lambda'_1 + w'_1 \lambda'_3).$$

Therefore only 6 variations of the elastic moduli can be considered, not all 21 elastic moduli coefficients. Only inverse problems for a limited number of material symmetry can be inverted (2 coefficients for isotropy, 3 for cubic symmetry, 5 for hexagonal symmetry).

By taking δM_{ij} proportional to $-(\kappa\delta t)w'_i\lambda'_j$ one gets the controlled variation $\delta J/\delta t = -\kappa \int_\Omega |\text{grad}w|^2 |\text{grad}\lambda|^2 d\Omega$. In practice δM is an isotopic elastic modulus tensor, depending of two functions, Young modulus and Poisson coefficient corrections. More complex behaviors including elastoviscoplasticity are investigated by adjoint methods in (Constantinescu and Tardieu, 2000; Constantinescu and Verger, 2002).

12.8 Stochastic inversion methods

So far the focus has been on deterministic methods of inversion which do not involve uncertainty. It is worth mentionned two methods to solve some inverse problems, Tarantola's stochastic inversion method and Kalman's filter.

12.8.1. Tarentola's inversion method

The data **d**, the model parameters **z** are considered as random variables and the modelling A is a stochastic process making a link between Z and D, in finite dimensional spaces. Any *a priori* information on variables z is described by the probability density $\rho_Z(\mathbf{z})$, "before considerations of the correlation between **z** and **d**". Noised data are characterized by the probability density $f_D(\mathbf{d})$. The mapping z→d is defined by the joint probability density $f_A(\mathbf{z}, \mathbf{d})$ in the space $Z \times D$.

Tarentola (1987) proposed the solution **z** as the *a posteriori* information on the model "after taking into account the correlation between **z** and **d**", defined by the probability density

$$F(\mathbf{z}, \mathbf{d}) = \frac{f_D(\mathbf{d})\, {}_Z(\mathbf{z})\, {}_A(\mathbf{z}, \mathbf{d})}{\mu(\mathbf{z}, \mathbf{d})} \tag{12.85}$$

where $\mu(\mathbf{z}, \mathbf{d})$ is some normalizing factor. Thus the solution is given by

$$F_Z(\mathbf{z}) = \int_D F(\mathbf{z}, \mathbf{d}) d\mathbf{d} \tag{12.86}$$

Generally two assumptions have been made

i) $\mu(\mathbf{z}, \mathbf{d}) = \mu_Z(\mathbf{z})\, \mu_D(\mathbf{d})$

ii) $f_A(\mathbf{z}, \mathbf{d}) = f_A(\mathbf{z}|\mathbf{d})\mu_Z(\mathbf{z})$

Where $f_A(\mathbf{z}|\mathbf{d})$ is the *conditional* probabilty densitiy of **d** if **z** occurs is an occured event. Eq. (12.86) becomes

$$F_Z(\mathbf{z}) = {}_Z(\mathbf{z}) \int_D \frac{f_Z(\mathbf{z})\, {}_A(\mathbf{z}|\mathbf{d})}{D(\mathbf{d})} d\mathbf{d} \tag{12.87}$$

The Gaussian law is generally considered for the conditional probability density given by

$$f_A(\mathbf{z}, \mathbf{y}) = \frac{1}{\sqrt{(2\pi)^N \det(C)}} \exp\{-\frac{1}{2}(\mathbf{y} - A\mathbf{z}).C^{-1}(\mathbf{y} - A\mathbf{z})\} \tag{12.88}$$

where C is a covariance positive matrix

12.8.2. Kalman's filter

Some inverse problems involving a time-like parameter make use of Kamlan's filter, for instance in plasticity (Bittanti et al, 1984). Dynamic form equations of elasticity (12.43), (12.58) also involve a time-like parameter so that a linear multistage process (i=0,1,2..) can be considered

$$\mathbf{z}^{i+1} = \Phi^i \mathbf{z}^i + \Gamma^i \mathbf{w}^i \text{ (state equation)} \tag{12.89}$$

$$\mathbf{d}^{i+1} = A^i \mathbf{z}^i + \mathbf{v}^i \text{ (observation equation for measurements d)} \tag{12.90}$$

where $\mathbf{z}^i$ is the state vector at stage (i), $\mathbf{d}^i$ is the measurement, $A^i\mathbf{z}^i$ is the prediction, Φ^i , A^i, Γ^i, are matrices given by the discretized equations, $\mathbf{w}^i$ and $\mathbf{v}^i$ are respectively the error in modelling and in measurements. In addition to the above-mentionned equations, there are a priori informations about mean values and standard deviations:

$$E(\mathbf{z}^0)= \overline{\mathbf{z}}^0,\ E((\mathbf{z}^0 - \overline{\mathbf{z}}^0)(\mathbf{z}^0 - \overline{\mathbf{z}}^0)^t) = M^0$$

$$E(\mathbf{w}^i)= \overline{\mathbf{w}}^i,\ E((\mathbf{w}^i - \overline{\mathbf{w}}^i)(\mathbf{w}^k - \overline{\mathbf{w}}^k)^t) = Q^k\delta_{ik}$$

$$E(\mathbf{z}^0 - \overline{\mathbf{z}}^{0i})(\mathbf{w}^k - \overline{\mathbf{w}}^k)^t \text{ ..... (no correlation)}$$

$$E(\mathbf{v}^i(\mathbf{v}^k)^t = R_k\delta_{ik}$$

$$E((\mathbf{z}^0 - \overline{\mathbf{z}}^{0i})(\mathbf{v}^k)^t) = E((\mathbf{w}^0 - \overline{\mathbf{w}}^{0i})(\mathbf{v}^k)^t) = 0 \text{ (no correlations)}$$

The updated value $\hat{\mathbf{z}}^i$ is given by Kalman's formulae, (Kalman, 1963; Bryson and Ho, 1969),

$$\hat{\mathbf{z}}^0 = \overline{\mathbf{z}}^0$$

$$\hat{\mathbf{z}}^i = \overline{\mathbf{z}}^i + K^i(\mathbf{d}^i - A^i\mathbf{z}^i)$$

$$\overline{\mathbf{z}}^i = \Phi^{i-1}\hat{\mathbf{z}}^{i-1} + \Gamma^{i-1}\hat{\mathbf{w}}^{i-1}$$

$$K^i = P^i\,(A^i)^t\,(R^i)^{-1}$$

$$P^i = M^i\ -\ .^i(A^i)^t\,(A^i\,M^i\,A^i + R^i)^{-1}A^iM^i,$$

$$M^{i+1}\ = \Phi^i\,P^i\,(\Phi^i)^t + \Gamma^i\,Q^i\,(\Gamma^i)^t$$

12.9 Duality in solid mechanics and inverse problems

Let us make some concluding remarks on duality found in Part I as well as in Part II. In Chapter 1, it has been shown that Tonti's diagram in Physics reveals a profound symmetry or duality in Elasticity when the kinematics and the dynamics are considered together. The duality observed by Tonti (1975) in rods and beams theories has been worked out by Bui (1994) in Elasticity and Bossavit (1988) in Electromagnetics.

It is worth noticing that duality has been exploited long before in Mechanics through the *virtual power* principle, introduced by P. Germain who wrote "the Force is the dual of the mobility"

Virtual power is more general a principle than the derivative of energy, as illustrated by path-independent integrals J(**u**, **u**) and J(**u**, **u***). The last integral contains the J-integral as a particular case.

Duality is found in Mathematics to solve linear partial derivative equation, Au = f, by introducing an equivalent bilinear form a(u,v), u∈ H(Ω) and v∈ H'(Ω), where H and H' are some dual functional spaces. Let us mention some important dual spaces in Mathematics:

- Schwartz's spaces: $\mathscr{D}$ (indefinitely differentiable and compactly supported functions) and $\mathscr{D}'$ (Schwartz's distributions space);
- Schwartz's spaces: S (functions and derivatives of any order decreasing more rapidly than any power of 1/|**x**|) and S' (tempered distributions)
- Sobolev's dual spaces: $W^{m,p}(\Omega)$ and $W^{-m,p'}(\Omega)$, p'=p/(p−1) (p'=∞ if p=1).

Duality is also found in inverse problems. Applications of duality have been given by Constantinescu (1995), Nakamura and Uhlmann (1995), Ikehata (1999) to identify the elastic moduli field L(**x**) from two overdetermined boundary data, $\mathbf{u}^d(\mathbf{x})$ and $\mathbf{T}^d(\mathbf{x})$, $\mathbf{x} \in \partial\Omega$.

Constantinescu (1995) made use of the so-called "error in constitutive law". Dual variables ε and σ are considered as independent ones, the strain ε belonging to the kinematically admissible space KA such that $\mathbf{u}=\mathbf{u}^d$ on ∂Ω and the stress σ belonging to the statically admissible space SA such that $\sigma.\mathbf{n}=\mathbf{T}^d$ on ∂Ω. The inverse problem can be solved by one of the minimization problems, (Constantinescu, 1995)

$$\min_{L} \min_{\varepsilon\in KA,\sigma\in SA} \int_\Omega \left\| \varepsilon - L.\sigma \right\| d\Omega$$

$$\min_{L} \min_{\varepsilon\in KA,\sigma\in SA} \int_\Omega \left\| L^{-1/2}.\sigma - L^{1/2}.\varepsilon \right\| d\Omega$$

$$\min_{L} \min_{\varepsilon\in KA,\sigma\in SA} \int_\Omega (\sigma - L.\varepsilon) : {}^{-1} : (\sigma - L.\varepsilon) d\Omega$$

Cauchy's problems for the harmonic equation or the elastic equilibrum equation have been solved by duality in Sect. 12.5 where dual variables, displacement **u** and stress vector and **T** are treated at the same level in the *dynamical* system

$$\frac{d}{dt}\begin{bmatrix} \mathbf{u} \\ \mathbf{T} \end{bmatrix} = A(\mathbf{u}, \mathbf{T}, \psi)$$

This dynamic approach of Cauchy's problem is another illustration of duality in Elasticity, where the variational form $a_t(\mathbf{u},\mathbf{v})-b_t\,\mathbf{v})=0$ and its derivative $\frac{d}{dt}\,a_t(\mathbf{u},\mathbf{v})-\frac{d}{dt}\,b_t(\mathbf{v})=0$, have been considered to derive Eq. (11.63).

Nowhere else will we find a better use of duality than in Inverse problems. It is found that fields and adjoint fields are the key tools for solving inverse problems, sometimes in a closed-form. This is also illustrated by dual terminologies used in different topics:

- Tomography (projection and back projection),
- Scattering of waves (propagation and back propagation)
- Waves propagation and time reversal mirror
- Forward diffusion and back diffusion

Table. Duality in solid mechanics and inverse problems

Variables & functions	Action or results	Dual variables & conjugate fct.
Displacement **u**	Work	Force **f**, traction vector **T**
Virtual velocity **v***	Virtual power(1)	Force **f**, traction vector **T**
Deformation ε		Stress σ
Potential energy P		Complementary potential Q
Thermoelastic fields **u**, θ		Adjoint fields **u***, w*
..... α	Dissipation $A.\partial_t\alpha$	Generalized forces A
J-integral	Derivative of the energy –dW/da	Dual I-integral
J(u,u*)	Virtual power	
$(\mathbf{v},\varepsilon)^\tau = C\,\mathbf{u}$	Tonti's diagram	$C^*(\mathbf{p},\sigma)^\tau = (\mathbf{m},\mathbf{e})$
	Eq. of motion	$\mathbf{m}=\mathbf{0}$
	Equilibrium Ec	$\mathbf{e}=\mathbf{0}$
$S\left[\mathbf{v},\boldsymbol{\varepsilon}\right]^{\mathit{tr}}=[\eta,\zeta]^\tau$	Constitutive law	$S^*\left[Z,B\right]^{\mathit{tr}}=\left[\mathbf{p},\sigma\right]^{\mathit{tr}}$
η=0	C..... $v\leftrightarrow\dot{\varepsilon}$	
ζ=0	C..... of ε	
Projection	Tomography	Back projection
Propagation	Scattering of waves	Back propagation
Forward equations	RG functional	Time reversal mirror
Forward diffusion	RG functional	Backward diffusion
State equation	Control theory	Adjoint state equation
Primal problem	Convex analysis	Dual problem
Functional spaces :	Mathematical	Dual spaces :
$\mathscr{D}$, S	analysis	$\mathscr{D}'$, S'(Schwartz's spaces)
$H^{m,p}$		$H^{-m,p'}$(Sobolev's spaces)

Appendix A

Residual Stresses in Fracture Mechanics

The solid under consideration has been processed by metal forming, machining or subjected to repair operations (weld, burnishing etc.) or to accidents which result in irreversible deformations and residual stresses $\sigma^0(\mathbf{x})$ etc. Generally, the residual stresses, also called the *initial* stresses, are unknown and have to be determined by some techniques (X-rays, solution to well-defined inverse problems). They are originated from some initial plastic deformation. In this appendix, we will look for two problems: first to indicate the consequences of residual stresses in fracture mechanics, second to make a brief review on methods for identifying the residual stresses.

A.1. An approximate theory of residual stress

We recall that displacement and strain have been measured in the current configuration which is generally assumed to be stress free before the application of the loads. In this case, the stress-strain law in elasticity is $\sigma=\mathbf{L}.\varepsilon$. For an isotropic medium, the elastic law depends on Lamé's constant λ, μ. Now, the presence of initial stresses changes the elasticity law which becomes inhomogeneous and anisotropic since it depends on the intial stress distribution (Mandel, 1966) as

$$\sigma_{ij} = \lambda tr(\varepsilon)\delta_{ij} + 2\mu\varepsilon_{ij} + \{1 - tr(\varepsilon)\}\sigma^0_{ij}(\mathrm{x}) + \omega_{ik}(\mathbf{u})\sigma^0_{kj} - \sigma^0_{ik}\omega_{kj}(\mathbf{u}) \qquad \text{(A.1)}$$

where $\omega(\mathbf{u}) = (\nabla\mathbf{u} - \nabla^{\mathrm{T}}\mathbf{u})/2$ the skew-symmetric part of the gradient $\nabla\mathbf{u}$. The initial stress satisfies

$$\mathrm{div}(\sigma^0) = \mathbf{0} \text{ in } \Omega \text{ and } \sigma^0.\mathbf{n} = \mathbf{0} \text{ on } \partial\Omega. \qquad \text{(A.2)}$$

Only when σ^0 is small, of the same order as $O(\nabla\mathbf{u})$, that the linearized stress-strain law becomes isotropic for the stress difference $(\sigma - \sigma^0)$

$$\sigma_{ij} - \sigma_{ij}^{0}(\mathrm{x}) = \lambda tr(\varepsilon)\delta_{ij} + 2\mu\varepsilon_{ij} \tag{A.3}$$

Of course, this simplified theory is justified for an uncracked body, because of the smallness of the residual stress. But Eq. (A.3) becomes incorrect in the case of a cracked body because, prior to the applied mechanical loading which results in the stress $\sigma^M(\mathbf{x})$, the initial stress $\sigma^0(\mathbf{x})$ can be singular. Therefore we remind ourself of the approximate nature of Eq. (A.3) and of the neglected terms when dealing with residual stress-strain law. The reader can convince himself of the complexity of the residual stress theory in brittle fracture mechanics by investigating the asymptotic solution of the equilibrium crack with the stress-strain law (A.1), the condition (A.2) on the crack surfaces $F^{\pm}$, the stress-free condition $\sigma.\mathbf{n} = \mathbf{0}$ on $F^{\pm}$ and the initial stress field $\sigma^0(\mathbf{x}) = r^{-1/2}\mathbf{g}(\theta)$. One finds that the stress σ is more singular than the strain ε (*). Therefore, the square root singularity is no longer valid in the presence of singular initial stress. In what follows, even in case of singular initial stress, we will assume that the ratio $|\sigma^0|/(\lambda + 2\mu)$ is small enough to justify (A.3).

A.1.1. A theory of fracture with initial stresses

We assume that the stress-strain (A.3) holds for the uncracked solid Ω^0 with the initial stress $\sigma^0(\mathbf{x})$ and that the presence of the crack of length a releases elastically (no reversed plasticity) so that we are left with the residual stress $\sigma^R(\mathbf{x})$, prior to any mechanical load. The equation are

$$\mathrm{div}(\sigma^R(u^R(\mathbf{x})) = \mathbf{0} \text{ in } \Omega^t \tag{A.4}$$

$$\sigma^R.\mathbf{n} = \mathbf{0} \text{ on } F^{\pm} \text{ and } S_{ext}. \tag{A.5}$$

Let $\Sigma := (\sigma^R - \sigma^0) = L.(\varepsilon(u^R))$. The auxiliary stress Σ satisfies

$$\mathrm{div}\Sigma = \mathbf{0} \text{ in } \Omega^t \tag{A.6}$$

$$\Sigma..\mathbf{n} = -\sigma^0.\mathbf{n} \text{ on } F^{\pm} \text{ and } \Sigma..\mathbf{n} = \mathbf{0} \text{ on } S_{ext}. \tag{A.7}$$

(*) For the stress field $\sigma^0(\mathbf{x})$ equal to the singular solution in mode I, the asymptotic solution u_3 in anti-plane mode III can be easily derived. The strain ε_{3i} is singular as $\varepsilon_{3i} \cong O(^{-0.2})$ and the stress as $\sigma_{3i} \cong O(^{-0.7})$, the strain energy density is $W \cong O(r^{0.9})$ thus it is less singular than O(1/r). Therefore, there is a small zone around the crack tip where the full theory (A.1) is dominant, and outside this zone, the approximate theory (A.3) is quite good.

Now, the applied loading on the cracked solid is the traction vector **T** given on S_{ext}. The mechanical stress field arising from **T** is denoted by $\sigma^M = L.(\varepsilon(\mathbf{u}^M))$. In Eqs. (A.4)-(A-5) some surface components of the stress $\sigma^R(\mathbf{x})$ and the strain $\varepsilon(\mathbf{u}^R)$ can be measured by X-rays diffraction, namely the principal tangential strain $\varepsilon^R_{\zeta\zeta}$, $\varepsilon^R_{\eta\eta}$ along the external surface S_{ext}. The actual stress in the cracked solid is

$$\sigma = \sigma^R + \sigma^M \quad \text{or} \quad \sigma = \sigma^0 + \Sigma + \sigma^M \tag{A.8}$$

The intial stress σ^0 (or residual stress σ^R) acts as an internal loading while the applied stress **T** is the external loading to the cracked solid. Therefore, from the additivity of the stresses, we get the additivity of the stress-intensity factors of the fields Σ, σ^M, Fig. A.1.

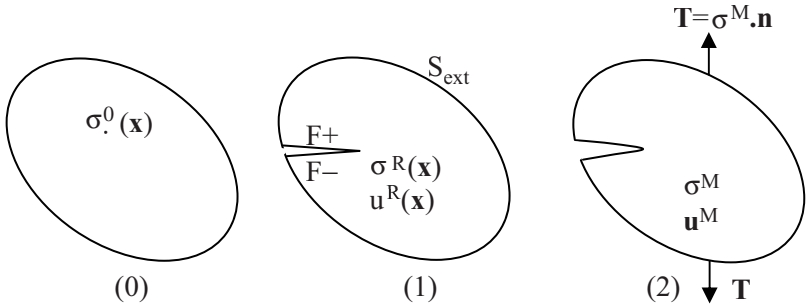

Figure A.1: Configuration (0) with initial stress $\sigma^0(\mathbf{x})$,σ^0 **x).n=0** on $\partial\Omega$; Configuration (1) with the residual stress $\sigma^R(\mathbf{x})$. after a crack propagation, $\sigma^R(\mathbf{x}).\mathbf{n}=\mathbf{0}$ on $F^{\pm}$ and $\sigma^R(\mathbf{x}).\mathbf{n}=\mathbf{0}$ on $\partial\Omega$; Solid (2) under the pure mechanical loading **T** and $\sigma^M(\mathbf{x}).\mathbf{n}=\mathbf{0}$ on $F^{\pm}$

A.1.2. Energy release rate

The strain energy calculated with the pre-stressed configuration $\sigma^0(\mathbf{x})$ can be shown to be

$$W_1 = \tfrac{1}{2}\int_{\Omega^0} (\Sigma + \sigma^M).L^{-1}.(\Sigma + \sigma^M)d\Omega + \int_{\Omega^0} \sigma^0 . \varepsilon(\mathbf{u})d\Omega \tag{A.9}$$

where $\mathbf{u}=\mathbf{u}^R+\mathbf{u}^M$. One can also consider the strain energy calculated with reference to the stress free configuration, for which the plastic strain responsible for the initial stress must be known

$$W_0 = \tfrac{1}{2}\int_{\Omega^0} (\sigma^0 + \Sigma + \sigma^M).L^{-1}.(\sigma^0 + \Sigma + \sigma^M)d\Omega \tag{A.10}$$

The relationship between W_1 and W_0 is

$$W_1 = W_0 - \tfrac{1}{2}\int_{\Omega^0} \sigma^0 . L^{-1} . \sigma^0 d\Omega \qquad (A.11)$$

The integral in Eq. (A.11) does not depend on the crack length so that the energy release rate can be calculated with either of the two expressions dW_1/da, dW_0/da. However, the choice (A.10) is not a good one since the strain $L^{-1}.(\tilde{\sigma}+\Sigma+\sigma^M)$ is not compatible. Finally, we note that the strain energy can be calculated in the pre-stressed configuration $\sigma^R(\mathbf{x})$ as

$$W_2 = \tfrac{1}{2}\int_{\Omega^0} (\sigma^R + \sigma^M).L^{-1}.(\sigma^R + \sigma^M) d\Omega + \int_{\Omega^0} \sigma^R . \varepsilon(\mathbf{u}) d\Omega \qquad (A.12)$$

The second integral of Eq. (A.12) vanishes because $\sigma^R(\mathbf{x})$ is a self-equilibrated stress field and $\varepsilon(\mathbf{u})$ is a kinematical field. Thus it remains to consider

$$W_2 = \tfrac{1}{2}\int_{\Omega^0} (\sigma^R + \sigma^M).L^{-1}.(\sigma^R + \sigma^M) d\Omega \qquad (A.12)$$

The evaluation of (A.12) yield the Irwin formula in mode I

$$G_2 = \frac{1-\nu^2}{E}(K_I^R + K_I^M)^2 \qquad (A.13)$$

A.2. Residual stress identification

A.2.1 Origin of the residual stresses

Residual stresses in solids arise from the manufacturing process of metals, from the solidification of melted metals to the machining operations on solid structures. There are complex thermo-mechanical and metallurgical transformations which cannot be easily modelized. Although the past history of the solid is unknown, we consider a fictituous stress-free reference configuration $C^{(\ )}$ together with successive configurations, $C^{(0)}$, $C^{(t)}$ and transformations

$$C^{(-)} \xrightarrow{\text{(manufacturing process)}} C^{0} \xrightarrow{\text{(mechanical loading)}} C^{(t)}$$

There are two methods for characterizing $C^{(0)}$: the first one consists in the modelling of the manufacturing process $C^{(\ )} \rightarrow C^{(0)}$ and the second considers either the initial stress field $\sigma^0(\mathbf{x})$ or the initial plastic strain $\varepsilon^{0p}(\mathbf{x})$ as unknowns, then determines some components of the surface stresses ex-

perimentally. No known methods exists for determining all components of the intial stress field $\sigma^0(\mathbf{x})$. Some inverse problems can be soved by the second method of identifying the plastic strain, by using informations on the overall deformation from $C^{(-)}$ to $C^{(0)}$, (see Bui, 1993).

A.2.2 Determination of the residual stresses

Non destructive methods

The distance d of to adjacent crystallographic plane in metals can be measured by X-rays inspection. Comparing d with the distance d_0 of the unstressed specimen, one obtains the principal *elastic* surface deformation which is related to $\Delta d=d-d_0$, even if there is some plasticity, because the plastic strain by slips of atomic lattice along slip planes do not change the inter-crystallographic distance. The X-ray method consists in measuring Bragg's optimal diffraction angle θ, with the wave length λ. The measured distance satifies Bragg's equation (n is an integer) $n\lambda-2d\sin\theta=0$. Therefore by measuring the variation of the Bragg diffraction angle, one obtains the elastic deformation

$$\Delta d/d_0=-\Delta\theta\cos\theta/\sin\theta \tag{A.14}$$

Another non destructive method is based on the stress analysis in different configurations $C^{(0)}$, $C^{(t)}$. In the presence of initial stresses, the Piola-Kirchhoff stress tensor satisfies the affine stress-strain law (in small strain)

$$\pi_{jk} = \pi_{jk}^{(0)} + L_{jklm}\varepsilon_{lm} \tag{A.15}$$

Now considering the relationship $\sigma(\det F)=F.\pi.F^{\tau}$ between Cauchy stress σ and Piola-Kirchhoff stress π (Sect. 1.1.3, Chap. 1) and upon linearization one gets the well-known formula, (Mandel, 1966)

$$\sigma_{jk} = (1-\mathrm{tr}\varepsilon)\sigma_{jk}^{(0)} + \frac{\partial u_j}{\partial x_h}\sigma_{hk}^{(0)} + \frac{\partial u_k}{\partial x_h}\sigma_{hj}^{(0)} + L_{jklm}\varepsilon_{lm} \tag{A.16}$$

where $\mathbf{u}(\mathbf{x})$ is the displacement measured between $C^{(0)}$ and $C^{(t)}$, under the assumption that the mechanical load does not introduce an additional plastic strain. Therefore, the variation of the stress $\Delta\sigma=\sigma-\sigma^{(0)}$ is a linear function of the gradient of displacement

$$\Delta\sigma = -(\mathrm{tr}\varepsilon)\sigma^{(0)} + \nabla\mathbf{u}\,.\sigma^{(0)} + \sigma^{(0)}.(\nabla\mathbf{u})^{\tau} + L.\varepsilon \tag{A.17}$$

Eq. (A.17) can be written in the form

$$\Delta\sigma = L^*.\varepsilon + \omega.\sigma^{(0)} - \sigma^{(0)}.\omega \tag{A.18}$$

Generally, the skew-symmetric tensor ω is small enough for neglecting the terms $\omega.\sigma^{(0)}$ and $\sigma^{(0)}.\omega$. Stress-strain law becomes

$$\Delta\sigma \cong L^*(\lambda, \mu, \sigma^{(0)}).\varepsilon \tag{A.19}$$

with the modified elastic moduli tensor L*, which depends on both Lamé's coefficients λ, μ, and the components of the initial stress tensor. An isotropic material becomes anisotropic and non homogeneous elastic medium. In practice, only surface stresses can be determined experimentally, for the principal stresses $\sigma^{(0)}_{11}$, $\sigma^{(0)}_{22}$, by assuming that these are sufficiently constant in some area for ultra-sonic measurements (the elastic wave velocities depend on elastic moduli, (Hayes and Rivlin, 1961).

Destructive methods

Let us mention briefly others experimental techniques for measurements of the residual stresses:
1. Boring hole in the solid for relaxing the stress and measurements of the elastic response
2. Cutting a thin structure and measurements of the three components of the strain induced by the operation, using strain gages.
3. Surface removing of the materials, layer by layer, by a mechanical or ionic burnishing, (Ballard and Constantinescu, 1994). Fig. A.2 shows the deformation of an aluminium bar after a mechanical cut along its symmetrical plane, compared to the initial one. This convinces us that initial stresses generally exist in a structure prior to the application of the loads.

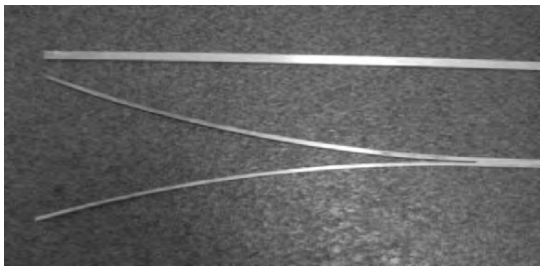

Figure A.2: Deformation of an aluminium bar, cut along its middle plane and compared to the original one (section:1cm^2)

Appendix B

Weak Interface Singularities

B.1 The Interface crack between dissimilar materials

Fracture Mechanics deal with the analysis of an existing crack in a structure. In a homogeneous linear elastic material, stress and strain have the well known square root singularity $0(1/\sqrt{r})$. Different singularities, corresponding to the pull-out and the push-in kinematics, respectively, have been found in the case of a frictional interface crack between an isotropic elastic medium and a rigid body, Chap. 3. The case of an inter ace crack between two different elastic media has been widely investigated in the literature, (Sih and Rice, 1964; Dundurs, 1969; Kassir and Bregman, 1972). The singular solution for a semi-infinite stress-free crack $x_1< 0$, $\sigma_{ij}(x_1<0,x_2=0)=0$ exhibits a strange oscillating behavior for the stress ahead the crack tip $x_1>0$, $x_2=0$

$$\sigma_{22} + i\sigma_{12}(\mathrm{r},\theta = 0) \cong \mathrm{K}\frac{1}{\sqrt{2\pi \mathrm{r}}}\mathrm{r}^{i\varepsilon} = \mathrm{K}\frac{1}{\sqrt{2\pi \mathrm{r}}}\{\cos(\varepsilon\ \ln r) + i\sin(\varepsilon\ \ln r)\} \quad \text{(B.1)}$$

with

$$\varepsilon = \frac{1}{2\pi}\ \ln\frac{(3-4\nu_1)\mu_2 + \mu_1}{(3-4\nu_2)\mu_1 + \mu_2} \quad \text{(B.2)}$$

The stress changes its sign an infinite number of times as r approaches zero. Moreover, the crack opening displacement $u_2(x_1<0,\ x_2=0^+)$ also changes its sign an infinite number of times, so that there is an overlapping of the two crack faces which violates the condition $[[u_2]]>0$. Let us consider the normal stress ahead the crack tip and assume that all quantities in (B.1) are dimensionless (the yield stress σ_0 of material (1) being the unit stress, the corresponding characteristic size $d_0=(K_{Ic}/\sigma_0 h)^2/2\pi$) about 1mm for metals). There are three intervals of particular interest: $[0,r_0]$, $[r_0,r_1]$, $[r_1,+\infty]$. For example, we take $\varepsilon=0.1$ and introduce r_0 and r_1 such that

$\varepsilon \ln r_0 = -\pi/2$ and $\varepsilon \ln r_1 = +\pi/2$. In the first interval, the stress changes its sign an infinite number of times. In the second interval, $[r_0, r_1]$, the stress $K(2\pi r)^{-1/2}\cos(\varepsilon \ln r)$ is non negative. Characteristic values corresponding to $\varepsilon = 0.1$ are $r_0 = \exp(-\pi/2\varepsilon) = 1.5\times10^{-7}$ and $r_1 = \exp(+\pi/2\varepsilon) = 6.6\times10^{6}$ or 6.6km. Therefore, the range of validity of the asymptotics (B.1) is $r_0 < r < r_1$. What happens in the first interval $[0, r_0]$?

Mathematically, the oscillating behavior has been singled out, the first time, by Abramov (1937) in the punch problem of an elastic half-plane. In the vicinity of the right corner A of the punch, a Dirichlet boundary condition (prescribed u_1 and u_2) is specified on the left of A, while the Neumann boundary (prescribed $\sigma_{12} = \sigma_{22} = 0$) is specified on the right of point A. Such discontinuity of the boundary conditions of different types causes an oscillating behavior of the solution.

Physically, the transition zone $[0, r_0]$ between two types of boundary conditions may be considered as a mean to "regularize" two kinds of incompatible boundary conditions.

Condensed matter physicists introduce long before the naming "frustration" to describe such an incompatibility which can be found in phase transition, interface solid/vapor etc. Nature does not like abrupt changes. It is likely that a self-organisation introduces some smooth transition between two regimes, two states, etc., via homogenization. An example of such a transition has been given in (Bui, 1993, p. 197) for a phase transition. A solid material can have two different states, S1 for stress magnitude less than γ_2, and S2 for stress magnitude higher than γ_1, such than $\gamma_1 < \gamma_2$. There is an overlapping zone (*) which allows the smooth transition between two states of the matter, in the homogeneized sense. The material in the transition consists of a *composite* of lamellar or dendritic or dispersed materials, composed of S1 and S2. The proportion of S1/S2 varies continuously from 1 to 0, (Silling, 1988; Bui, 1993).

In the interface solid mechanics, we introduce another manner of interpreting the oscillatory solution. Let us describe the behavior in the first interval in a "homogenized" sense.

This will imply some weak singularity (B.1). As a matter of fact, recalling that $\cos(\varepsilon \ln r_0) = 0$, the "mean normal stress" *over* the oscillating behavior interval $[0, r_0]$ is given by

$$\langle \sigma_{22}(r) \rangle = \frac{1}{r_0}\int_0^{r_0} \sigma_{22}\,dr = \frac{K}{\sqrt{2\pi}}\frac{1}{r_0}\,\mathrm{Re}\int_0^{r_0} r^{i\varepsilon-(1/2)}\,dr$$

(*) In the phase transformation liquid water $\leftrightarrow$ ice, normal temperature at the atmospheric pressure is $\gamma_2 = 0°C$, while temperature γ_1 at surfusion is below 0°C, at high pressure. The existing mixture (ice+water) is called the sorbet.

$$<\sigma_{22}(r)> = \frac{-K}{\sqrt{2\pi r_0}} \frac{\varepsilon}{(\varepsilon^2 + \frac{1}{4})} < 0 \qquad \text{(B.3)}$$

Therefore, we can define a homogeneous stress in the first interval which is a compressive one, while in the second interval it is given by the asymptotics (B.1) so that the stress is finite everywhere

$$\begin{aligned} \sigma_{22}(r) &= \frac{K}{\sqrt{2\pi r_0}} \frac{\varepsilon}{(\varepsilon^2 + \frac{1}{4})} \qquad 0<r<r_0 \\ \sigma_{22}(r) &= K \frac{1}{\sqrt{2\pi r}} \cos(\varepsilon \ln r) \quad \text{for } r_0<r \ (<r_1) \end{aligned} \qquad \text{(B.4)}$$

Comninou (1977) considered a different model with a frictionless contact zone C behind the crack tip. She obtained a singular *compressive* normal stress in C as $O(1/\sqrt{r})$ and a *finite* tensile stress ahead the crack tip. Her nice model avoids oscillatory solution and gives a finite stress everywhere. Despite different approaches, frictional contact crack or homogenized model, we recover the compressive zone at the crack tip beyond which the solution (B.1) is valid. Both models remove the oscillating behavior and give a physical sense to interface crack models.

Let us mention the solution for a circular crack of radius a, in mode I given by Kassir and Bregman (1972) (r=distance from the crack front)

$$_{zz}(r,z=0) = \frac{k}{\sqrt{2\pi r}} \cos(\varepsilon \ell n \frac{r}{r+2a})$$

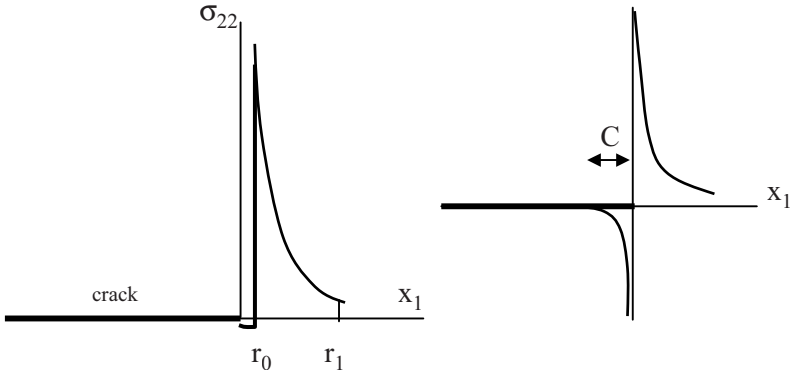

Figure B.1: The compressive stress zone $0<r<r_0$ in the homogenized model and the compressive contact stress zone C in Comninou's model

$$\sigma_{z\theta}(r,z=0)=\frac{k}{\sqrt{2\pi r}}\sin(\varepsilon l\, n\frac{r}{r+2a})$$

The oscillating behavior also occurs in a narrow zone near the crack front r/2a=1.5 10^{-7} where the homogenized stress is compressive.

B.2 Discontinuous Neumann boundary conditions

Consider the example of an elastic half-plane y<0, subjected to the constant pressure p on an interval of its boundary:

$\sigma_{xy} = 0$ and in $\sigma_{yy} = -p$ in $|x|<1$ and $\sigma_{xy} = \sigma_{yy} = 0$ in $|x|<1$. (B.5)

Remark that we cannot not specify stress conditions at points x=±1 because stresses are only defined on *open* sets and that precisely the Neumann boundary condition is discontinuous at these points. The solution of this problem (Flamant's problem) can be found in text book. Stress components at point M are obtained by integrating the solution of a point force along AB and given in Fig. B.2,

Let us examine the singularity near the tip x=+1, y=0, with the angle $\theta(M\cong A)=-\pi/2$, $\theta(M\cong B)=\theta_B$ measured at point B, $(2\theta\pm\sin2\theta)_{x=-1}\cong -\pi$ and $(\cos2\theta)_{x=-1}\cong -1$. Therefore, putting $r=|BM$, and $\theta|_{\xi=+1}=$ angle $(B\Delta,BM): =\theta_B$ we obtain the asymptotics near point B given by

$$\sigma_{xx}\cong(p/2\pi)(2\theta+\sin2\theta)_{x=+1}-(p/2\pi)(2\theta)_{x=-1}=(p/2\pi)\{2\theta_B+\sin2\theta_B+\pi\} \quad (B.6)$$

$$\sigma_{yy}\cong(p/2\pi)(2\theta-\sin2\theta)_{x=+1}-(p/2\pi)(2\theta)_{x=-1}=(p/2\pi)\{2\theta_B-\sin2\theta_B+\pi\} \quad (B.7)$$

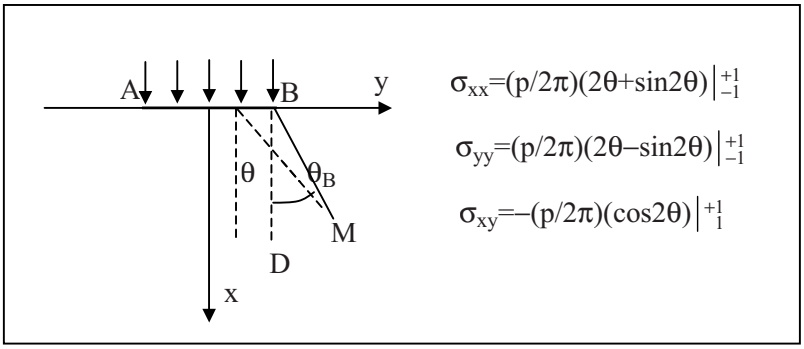

Figure B.2: Flamant's problem of an uniform pressure acting on a half-plane

$$\sigma_{xy} \cong -(p/2\pi)(\cos 2\theta)_{x=+1} + (p/2\pi)(\cos 2\theta)_{x=-1} = -(p/2\pi)\{2\cos^2\theta_B\} \qquad \text{(B.8)}$$

These functions do not depend on r and are bounded and discontinuous. Functions (B.6) and (B.8) shown in a three-dimensional surface plot, Fig. B.3, are named "thorn" singularity and "rasor blade" singularity, respectively. The naming "rasor blade" singularity of the shear stress is suggested by its sharped edge. Remark that without the term sin(2θ), functions (B.6) or (B.7) are similar to the screw dislocation field.

In the next section, the naming 'thorn" singularity will be justified by examples of interface problems arising in engineering applications.

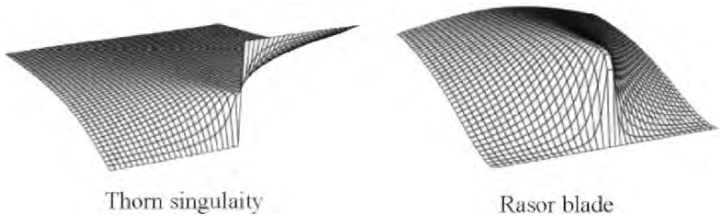

Figure B.3: The "thorn" singularity (B.6) and the "rasor blade" singularity (B.8)

B.3 Thermo-plastic discontinuity on a composite tube

Consider a long tube which consists of two parts which are welded at the section z=0. Both materials have the same elastic constant and different thermal expansion coefficients α.

Under an uniform heating of the tube, thermal stresses appear as the result of the mismatch between thermal strains, with the discontinuity [[αT]]. Such a discontinuity also arises in a homogeneous tube subjected to a thermal shock [[T]] ≠ 0. For this reason we shall consider the discontinuity [[αT]].

For small thichness, one usually considers that Love-Kirchhoff's shell solution provides a good solution for the longitudinal stress. According to Love-Kirchhoff's shell theory, the longitudinal stress $\sigma_{zz}(r,z)$ near z = 0 is antisymmetric in z, and thus is nearly zero in the transition zone. Measurements of residual stresses, by the hole techniques, show that very high values of the stress exist even at z = 0, Fig. B.4.

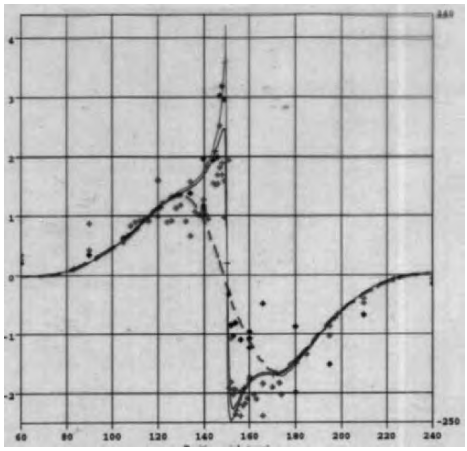

Figure B.4: Measurements of the residual longitudinal stress $\sigma_{zz}(r = r_e, z)$ by the hole techniques, Waeckel, Genette and Dupas (1998). The dotted line curve corresponds to the Love-Kirchhoff shell solution where $\sigma_{zz}(r=r_e, 0) = 0$. The continuous line is obtained by the FE method, with very fine meshes (100 times finer than the usual meshes in the shell solutions). The analytic solution of the boundary layer confirms the numerical FEM solution

This phenomenon is an illustration of the so-called localized effects (or boundary layer effect) in three-dimensional problems of junctions or interfaces which cannot be captured by a shell theory. A physical argument show how to deal with a thermal discontinuity. Imagine first that two halves of the tube are separated along the plane z = 0, so that each part can freely deforms without any stress. Second, apply normal pressure to the right half tube, with pressure p_e on the outer radius and pressure p_i on the inner radius, so as to make a perfect fit with the lelf half tube. Then weld the halves and release the pressures on the entire tube. The third operation induces a stress field singularity which is similar to the singular fields (B.6), (B.7), (B.8) of Flamant's problem. This is nothing but the thorn.

The thermal shock problem on a infinitely long tube, can be solved in closed-form, by considering the partial Fourier transform with respect to z, and solving the differental equation in r for the Love displacement function. We omit the details of the calculation and give here the result graphically, with the exact longitudinal stress discontinuity (a thorn singularity)

$$[\![\sigma_{zz}]\!] = \frac{E}{1-\nu}[\![\alpha T]\!] \tag{B.9}$$

Fig. B.5 shows the 3D surface $\sigma_{zz}(r,z)$ near the interface. It is observed that four thorn singularities appear at the junction between the interface and the free surfaces, $r=r_e$ and r_i.

Thorns are symmetric with respect to $x=(r-(r_e-r_i)/2)$ and antisymmetric with respect to z. The magnitude of the thorn stress is higher than twice the maximum Love-Kirchhoff stress. Such a high value explains the cracking sometimes observed at the interface (thermal striping). The maximum stress of LK theory is located at the characteristic shell distance δ which is 6 to 10 times the thorn size. Fig. B.6 shows a comparison between different theories for a thermal shock: Love-Kirchhoff shell solution (LK), finite element solution (FEM), and the exact solution.

The most interesting feature of the interface analysis with thorn singularity is that the same result holds for a plastic discontinuity $[[\varepsilon^p_{rr}]]\neq 0$ with the thorn in the longitudinal stress, exactly represented by the same figure B.5, with only the discontinuity relationship, (Bui and Taheri, 1989)

$$\left[\!\left[\sigma_{zz}\right]\!\right] = 2\mu\left[\!\left[\varepsilon^p_{rr}\right]\!\right] \tag{B.10}$$

Remark that the zz-component of the stress is related to the rr-component of the plastic deformation discontinuity. Fig. B.7 shows the thorns existing at the interface of a bi-tube (base metal and weld) which consists of the same elastic constants but different yield stresses for each material. The stress $\sigma_{zz}(r_i, z)$ is in continuous line, the stress at external radius is in dotted line. Thorn singularity analysis of plastic structures can be found in (Deperrois and Dang Van, 1990; Santacreu, 1994).

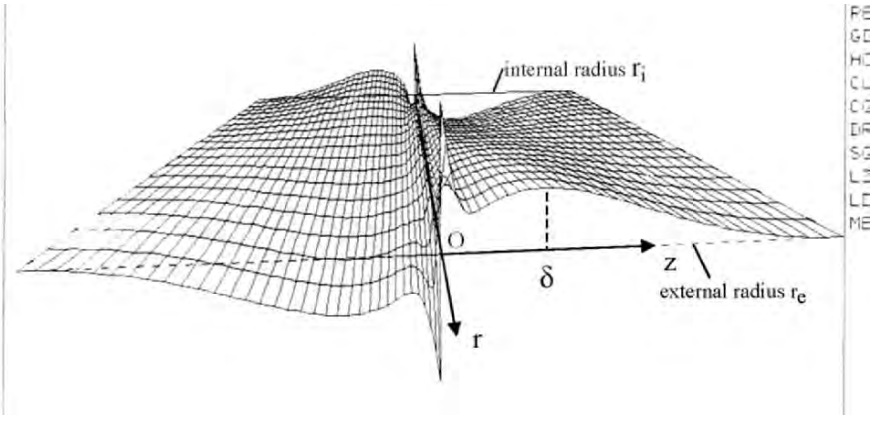

Figure B.5: The three-dimensional thorn singularities $\sigma_{zz}(r,z)$ at the interface z=0 with a discontinuous thermal strain $[[\alpha T]]$, (Bui and Taheri, 1989); Taheri, 1989)

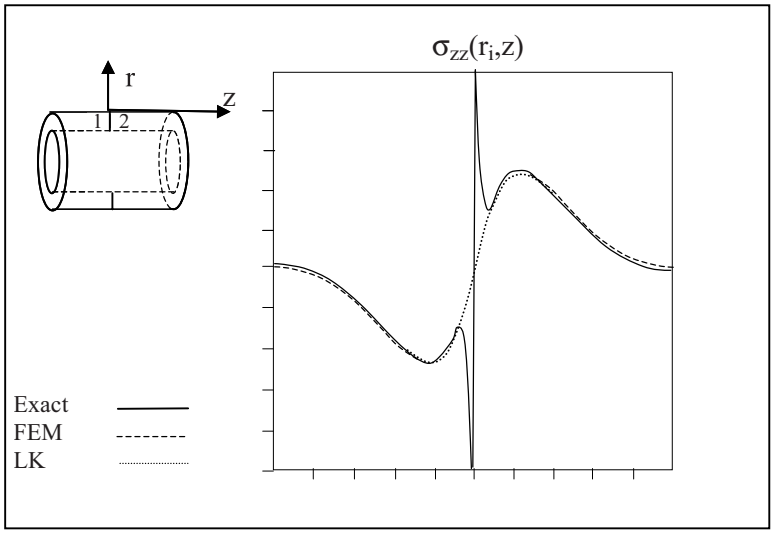

Figure B.6: The thorn singularities of the longitudinal stress $\sigma_{zz}(r_i,z)$ at internal radius in a bi-tube subjected to a thermal shock. Comparison between Love-Kirchhoff's shell solution (LK), finite element solution (FEM) and exact solution by Fourier's transform (Courtesy of S. Taheri, Electricité de France)

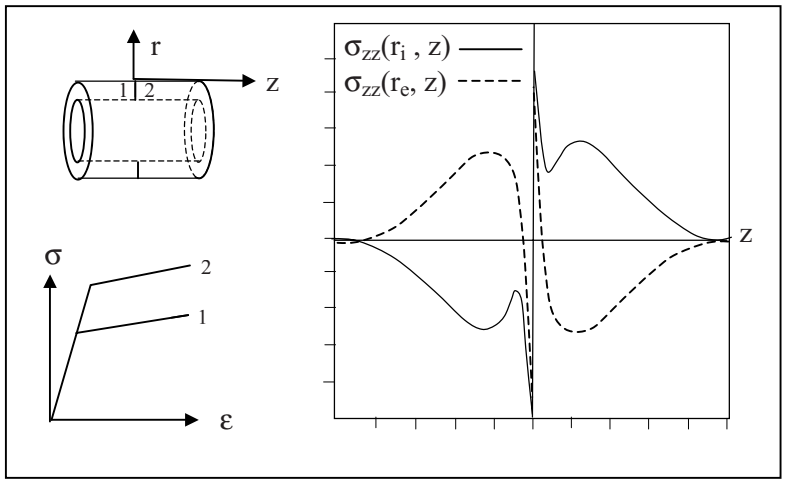

Figure B.7: Plastic shock on a bi-tube (base metal and weld) with the same elastic constants and different yield stresses (Courtesy of S. Taheri, Electricité de France)

Appendix C

Problems and Solutions

1. Mandel's plastic work formula

Consider an elastic-perfectly plastic material with V. Mises's criterion, in a monotonic loading.

1) Show that $\dot{\boldsymbol{\sigma}} : \boldsymbol{\varepsilon}^{\mathrm{p}} = 0$.

2) Show that the plastic work is given by

$$\mathrm{W_p} = \int_{\partial\Omega}\int_0^t (\mathbf{T}.\dot{\mathbf{u}} - \dot{\mathbf{T}}.\mathbf{u}) dS dt \ .$$

SOLUTION. In a monotonic loading, the plastic strain rate and plastic strain are proportional. The normality law implies $\dot{\varepsilon}^{\mathrm{p}} = \lambda \partial \mathrm{f} / \partial \boldsymbol{\sigma}$ and the yield criterion implies $(\partial \mathrm{f} / \partial \boldsymbol{\sigma}) : \dot{\boldsymbol{\sigma}} = 0$, thus $\dot{\boldsymbol{\sigma}} : \dot{\boldsymbol{\varepsilon}}^{\mathrm{p}} = 0$ then $\dot{\boldsymbol{\sigma}} : \boldsymbol{\varepsilon}^{\mathrm{p}} = 0$. The plastic work is given by

$$\begin{aligned}
\mathrm{W_p} &= \int_\Omega \int_0^t (\sigma : \dot{\varepsilon}^p) d\Omega dt \\
&= \int_\Omega \int_0^t (\sigma : (\dot{\varepsilon} - \dot{\varepsilon}^e) d\Omega dt = \int_\Omega \int_0^t \sigma : \dot{\varepsilon} d\Omega dt - \int_\Omega \int_0^t \dot{\sigma} : \varepsilon^e d\Omega dt \\
&= \int_\Omega \int_0^t (\sigma : \dot{\varepsilon} - \dot{\sigma} : \varepsilon^e - \dot{\sigma} : \varepsilon^p) d\Omega dt = \int_\Omega \int_0^t (\sigma : \dot{\varepsilon} - \dot{\sigma} : \varepsilon) d\Omega dt \\
&= \int_{\partial\Omega} \int_0^t (\mathbf{T}.\dot{\mathbf{u}} - \dot{\mathbf{T}}.\mathbf{u}) dS dt
\end{aligned}$$

2. Singularity of mode III

Consider the anti-plane loading, where the only non vanishing displacement component is $u_3(x_1,x_2)$.

Let μu_3 be the real part of f(z), ($z=x_1+ix_2$). Find the stress intensity factor K_{III} at the tip z=a in terms of potential f(z). SOLUTION: $K_{III}(a)= \lim_{z\to a} i(2\pi)^{1/2} f'(z)(z-a)^{1/2}$

3. Energy release rate

A sticky tape of thichness h, width w, Young modulus E is delaminated along a crack of length a. Show that the critical horizontal force at delamination is given by $F_c=2w(\gamma Eh)^{1/2}$.

SOLUTION: $G_c=2\gamma$ (per unit thickness). $G=(1/2w)Fdu/da$,
$u=aF/(Ewh) \Rightarrow F_c=2w(\gamma Eh)^{1/2}$

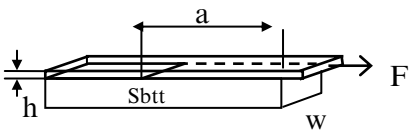

Figure C.1

4. Energy release rate

Consider the same problem with an inclined force F. For a delamination dx, calculate the work done by F, then the energy release rate G.

SOLUTION :

1. The work done by F is $W=F\times BC=Fdx(1\ \cos\theta)$.
2. $G=2\gamma=(1\ \cos\theta).F/w+F^2/(2hEw^2)$.

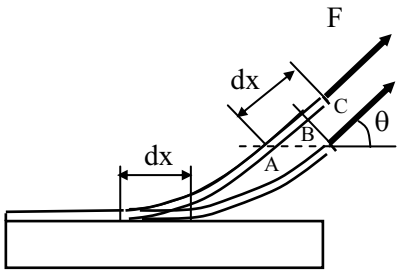

Figure C.2

5. Dual path-independent I-integral

One considers the stress energy density $U(\sigma)=(1/2)\sigma.M.\sigma$ such that $\varepsilon=\partial U/\partial\sigma$.

The dual path integral I is defined by

$$I \quad \int_\Gamma \{\ Un_1+\mathbf{u}(\sigma).\partial_1\sigma.\mathbf{n}\}ds\ .$$

1) Prove the path-independency property of the I-integral.
2) Show that I=J=G.

HINT: 2. Take the singular fields in mode I to calculate the I-integral and verify that $I=(1-\nu^2)K_I^2/E$ in plane strain.

6. Mode III edge crack in a band

Interpret the following function as the complex stress of some crack problem $f'(z) = -i\tau_{32}\sin(\pi z/2b)\{\sin^2(\pi a/2b)-\sin^2(\pi z/2b)\}$. Find the stress intensity factor.

SOLUTION: $K_{III} = \tau_{32}\sqrt{2b}\sqrt{\tan(\pi a/2b)}$

7. Left and right stress intensity factors

Consider a finite crack in an infinite medium, with the tips z = a and z = b>a. At point z=c, Two opposite normal point forces ±F are applied to points $z = c \pm i0$, a<c<b. Find the stress intensity factors at z = a and z = b.

SOLUTION:

$$K_I(a) = \frac{F\sqrt{2(b-c)}}{\sqrt{\pi}\sqrt{(b-a)(c-a)}},\quad K_I(b) = \frac{F\sqrt{2(c-a)}}{\sqrt{\pi}\sqrt{(b-a)(b-c)}}$$

8. Steady state propagation of brittle damage

Brittle damage is characterized by the vanishing stress tensor when $|\varepsilon|$ is larger than a threshold value ε_R.

During dt, the moving front BB' with velocity V releases the elastic strain energy of the shadowed area by $dD=Vdt\int_{BB'}Wdx_2$ which will be dissipated.

1. Calculate W.
2. Show that the rate of dissipation is the J-integral over BB'.

SOLUTION:

1. $W = \frac{1}{2}\sigma_{tt}\varepsilon_{tt} = \frac{1}{2}E\varepsilon_R^2$

2. On BB' the stress vector vanishes. $J=\int_{BB'}Wdx_2$ (JV=dD/dt).

Thus $J=hE\varepsilon_R^2$ (2h is the width of the damage zone).

Classical brittle fracture is consistent with the asymptotics $\varepsilon_R\to\infty$ and $h=J_{Ic}/\varepsilon_R\to 0$, if J_{Ic} is a constant material. This model illustrates a free boundary value problem in Fracture Mechanics to determine the unknown damage front BB'.

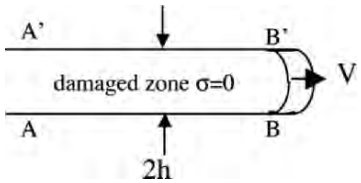

Figure C.3

9. Steady state propagation of damage in elastic-plastic material, with linear strain hardening

1) What is qualitatively the change with respect to the preceding model?

SOLUTION: There is a diffuse plastic dissipation in the active part of the solid, of global rate D_P , but no plastic dissipation in the wake plastic zone of elastic unloading, and a localized dissipation by fracture D_F through the release of elastic strain energy through BB'.

2) Assume that Neuber's criterion applies to the "notch" BB', that is BB'≅C/(σ.ε). Find the dissipation rate D_F by fracture over BB'.

SOLUTION: For large ε_R, the stress on BB' is of order $\eta\varepsilon_R$ where η is the constant hardening parameter. Thus,

$$\sigma_{tt} \cong \eta\varepsilon_R$$

$$2b \cong C / \sigma_{tt}\varepsilon_{tt} \cong \frac{C}{\eta\varepsilon_R^2}$$

$$W = \frac{1}{2E}\sigma_{tt}\sigma_{tt} \cong \frac{1}{2E}(\eta\varepsilon_R)^2$$

$$D_F = J = \frac{C}{\eta\varepsilon_R^2} W \cong \frac{C\eta}{2E}$$

The model is consistent with a constant critical value $J_{Ic}=C\eta/2E$.
But for a perfectly plastic material, the strain hardening vanishes $\eta=0$.
This is the Rice paradoxical result in perfect plasticity.

10. Steady state propagation of damage in elastic-plastic material, with parabolic strain hardening

Assume a uniaxial power law of the form σ≙ ε^n (n≠) and the Neuber estimation of the notch size as BB'≅C/(σ.ε). Find the dissipation rate by fracture D_F.

SOLUTION:

$2h \cong C/\sigma{:}\varepsilon = (C/A)\varepsilon_R^{-(n+1)}$

$W \cong O(\sigma^2) = O(\varepsilon_R^{2n})$

$D_F \cong O(hW) = O(\varepsilon_R^{n-1})$

Since $n<1$, for $\varepsilon_R\to\infty$ we obtain the asymptotics $D_F\to 0$.
The dissipation rate by fracture also vanishes in plasticity with a power law $\sigma=A\varepsilon^n$ $(n<1)$.

11. Separation of energy in dynamic fracture

Prove that $\int_{Crack}\int_0^t T_2(x_1, 2t-\tau)\dot{u}_2(x_1,\tau)dx_1 d\tau = 0$.

SOLUTION: The crack tip is moving with velocity da/dt. The stress component $T_2(x_1, 2t-\tau)$ associated with the crack tip position $a(2t-\tau)$ vanishes

for $x_1<a(2t-\tau)$, while the velocity $\dot{u}_2(x_1,\tau)$ associated with the crack opening at position $a(\tau)$ vanishes for $a(\tau)<x_1$.
For $0<\tau<t$, we have $t<2t-\tau$, thus $a(t)<a(2t-\tau)$. Therefore the intersection of the supports, $\mathrm{supp}(T_2(x_1,2t-\tau))$ and $\mathrm{supp}(\dot{u}_2(x_1,\tau))$, is void.
For $t<\tau<2t$, this intersection is not void. This is why Brun's theorem for a crack propagation is expressed by Eq. (6.75).

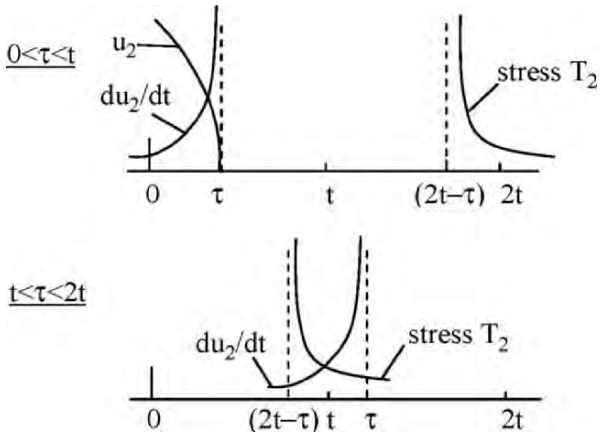

Figure C.4

12. Elastodynamics
Given $u(x_1,x_2,k)$, a solution of the steady-state wave equation $\Delta u+k^2u=0$, $k^2=\omega^2/c^2$ (with the time factor $\exp(-i\omega t)$), find a solution of the transient equation $\Delta u-c^{-2}\partial_t\partial_t u=0$.
SOLUTION: Replace k by (ip/c) and take the inverse Laplace transform to obtain the solution.

13. Dynamic J-integral
Prove the path-independency of dynamic J-integral.
HINT: Consider the Fletcher conservation law
$\mathrm{div}\left\{(W-\rho\dot{\mathbf{u}}^2/2)I-(\nabla\mathbf{u}).\sigma\right\}+\partial(\rho\dot{\mathbf{u}}.\nabla\mathbf{u})/\partial t=0$.

14. Homogenization in plasticity
Heterogeneous materials in the micro-scale are said to be macroscopically homogeneous in the Hill-Mandel sense, when $\Sigma=\langle\sigma(\mathbf{x})\rangle$ and $E^*=\langle\varepsilon^*(\mathbf{x})\rangle$ imply $\Sigma : E.=\langle\sigma(\mathbf{x}):\varepsilon.(\mathbf{x})\rangle$, for any statically admissible field $\sigma(\mathbf{x})$ in SA and any kinematically admissible field $\varepsilon.(\mathbf{x})$ in KA.

1) Explain why the plastic deformation $\varepsilon^p(\mathbf{x})$ generally does not satisfy the Hill-Mandel conditions, $E^p \neq <\varepsilon^p(\mathbf{x})>$ and $\Sigma : E^p \neq <\sigma(\mathbf{x}):\varepsilon^p(\mathbf{x})>$.

SOLUTION: The plastic strain field $\varepsilon^p(\mathbf{x})$ does not satisfy the compatibilty condition. Hill-Mandel's conditions do not apply to a non kinematical field.

2) Let $A(\mathbf{x})$ be the elastic concentration tensor $A(\mathbf{x})$: $\Sigma \rightarrow \sigma(\mathbf{x})$ giving the microscopic stress from the macroscopic one, in a *pure elastic* response. Suppose that L is isotropic. Prove the following identities (Bui, 1969)

$(E^e)_{ij} = <A_{hkij}(\varepsilon^e)_{hk}>$ (elastic strain $E^e = <A^\tau . \varepsilon^e>$)

$E = <A^\tau . \varepsilon> = <\varepsilon>$ (total strain)

SOLUTION: First of all, $A(\mathbf{x}).\Sigma$, being a stress field is an element of SA, thus $<A(\mathbf{x}).\Sigma> = <A(\mathbf{x})>.\Sigma$ for any Σ, hence $<A(\mathbf{x})> = I$ (identity)

Second, $L(\mathbf{x})^{-1}.A(\mathbf{x})$ being a strain field is an element of KA, admissible with the macroscopic strain L_0 [1], hence $<L(\mathbf{x})^{-1}.A(\mathbf{x})> = L_0^{-1}$.

Now, considering an arbitrary elasto-plastic strain field $\varepsilon'(\mathbf{x})$ admissible with E', with the corresponding stress $\sigma'(\mathbf{x})$ admissible with Σ' we obtain

$<\varepsilon'(\mathbf{x}).A(\mathbf{x})> = <\varepsilon'(\mathbf{x})>.<I> = <\varepsilon'(\mathbf{x})> = E'$ (total strain formula) (*)

Next, considering the elastic strain part $\varepsilon^{e'}(\mathbf{x})$ we obtain

$<\varepsilon^{e'}(\mathbf{x}).\ A(\mathbf{x})> = <\{L(\mathbf{x})^{\ 1}.\sigma'(\mathbf{x})\}.A(\mathbf{x})>$

Let $M(\mathbf{x}) = L(\mathbf{x})^{-1}$. The above equation is written as ($M = M^\tau$)

$<\varepsilon^{e'}(\mathbf{x})_{ij} A_{ijhk}(\mathbf{x})> = <\{M_{ijlm}(\mathbf{x})\sigma'_{lm}(\mathbf{x})\} A_{ijhk}(\mathbf{x})\} =$

$<\{M_{lmij}(\mathbf{x})A_{ijhk}(\mathbf{x})\}\sigma'_{lm}(\mathbf{x})\}> = <M_{lmij}(\mathbf{x})A_{ijhk}(\mathbf{x})> <\sigma'_{lm}(\mathbf{x})> =$

$(M_0)_{lmhk}\Sigma'_{lm} = E^{e'}$ (elastic strain formula) (**)

Mandel's formula is obtained by substracting Eq.(**) to Eq.(*).

15. Three-dimensional fracture

Consider a Compact Tension Specimen of the width w=2, with a straight crack front. Assume that the SIF is approximated by $k_I(s) = F(1-s^2)^{1/2}$, and that the crack propagation velocity is of the form $\varphi(s) = a_1 + a_2 s^2$.

1. Give the dissipation rate (2.80) explicitly.

SOLUTION: The crack radius is infinite.

$$D(\varphi) = 4\gamma a_1 + 4\beta |a_2| + \frac{4}{3}\gamma a_2 \leq 1,$$

with $a_1 \geq 0$, $a_1 + a_2 \geq 0$.

2. Find the solution to the crack propagation problem.

SOLUTION: The energy release rate is $G = \frac{4}{3} F^2 (a_1 + \frac{1}{5} a_2)$.

The primal problem

$$\max_{a_1, a_2} G$$

$$D(\varphi) \leq 1$$

is a linear programming in the convex domain shown in the next figure. Solutions (a_1, a_2) are on the vertices or the edges.

1rst case: $2\gamma/15>\beta$, the propagation mechanism is represented by the vertex C and the critical force is $F_c=\sqrt{\frac{15}{16}(\frac{8}{3}\gamma+4\beta)}$

2nd case: $2\gamma/15=\beta$, the solution is represented by any point on the edge BC, with the critical force $F_c=\sqrt{3\gamma}$

3rd case: $2\gamma/15<\beta$..τηε σολυτιον.is the vertex B.

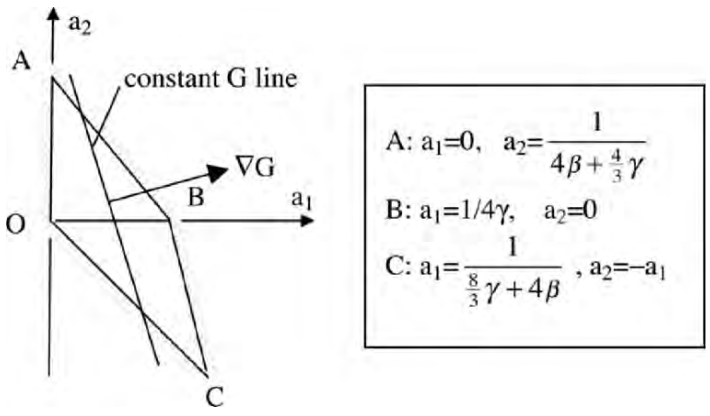

Figure C.5

16. Discontinuous solutions in elastic domain

Consider the axisymetric 2D elastic domain $\Omega_i=\{r_i<r<r_e\}$. The inner boundary is stress free $\sigma_{rr}(r_i)=0$, the traction at the external boundary is $\sigma_{rr}(r_e)=2\mu A(1/r_i^2-1/r_e^2)$. i) Find the stresses and compare with the solution for a circular domain *without* a cavity, for $A=ar_i^2$ (with constant a). Discuss the result for $r_i\to 0$. ii) Consider $A=A=ar_i^2$. Compare the total strain energies of Ω_i and Ω_0 (homogeneous solution for no cavity) by calculating $W(r_i)-W_0$.

SOLUTION: $\sigma_{rr}(r)=2\mu a(1-(r_i^2/r^2))$, $\sigma_{\theta\theta}(r)=2\mu a(1+(r_i^2/r^2))$.

The solution for the problem without a cavity is $\sigma_{rr}^0(r)=\sigma_{\theta\theta}^0(r)=2\mu a$, $\forall r$. The boundary value of the stresses are $\sigma_{rr}(r=r_i)=0$, $\sigma_{\theta\theta}(r=r_i)=4\mu a$, while at *fixed* $r\neq 0$, as $r_i\to 0$, the limits of the stresses are $\sigma_{rr}(r)\to 2\mu a$ and $\sigma_{\theta\theta}(r)\to 2\mu a$.

The energy difference vanishes $W(r_i)-W(0)\to 0$ as $r_i\to 0$. This solution is discontinuous at a point.

17. Francfort and Marigo's model

This is a free boundary value problem in Fracture Mechanics to determine an *unknown* crack X in an elastic solid. One assumes that the solution corresponds to the minimum of the total energy (Strain energy + Griffith's energy). Let us introduce the functional, depending on both the admissible field $\mathbf{u}\in$KA and the unknown X, $E(\mathbf{u},X)=\int_{\Omega\setminus X}W(\nabla\mathbf{u})d\Omega+a\text{Meas}(X)$, where a is fixed positive constant (equal to 2γ in the generalized Griffith model), and Meas(X) is some measure of the crack surface.

1) Give a physical meaning of each term.

2) Can we minimize each term of the functional? Give an interpretation of the minimization problem $\min_{X,\mathbf{u}\in KA} E(\mathbf{u},X)$.

SOLUTION: 1)The first term, for a given X, is the usual functional for solving the equilibrium crack problem. The problem $\min\int_{\Omega\setminus X}W(\nabla\mathbf{u})d\Omega$, ($\mathbf{u}\in$KA) for fixed X has a physical and mathematical sense since the functional is convex. The second term is the energy dissipated by fracture along surface X according to Griffith's model (constant surface energy).

2). Since X appears in the first term, the problem $\min_X$Meas(X) over X of the second term alone has no sense. Therefore the min-problem must be formulated globally over the whole set ($\mathbf{u}$,X) which involves a non convex functional. Solution to this problem is obtained via the notion of Γ-convergence of de Georgi et al (1989), (see Francfort and Marigo, 1998; Bourdin et al, 2000; Bilteryst and Marigo, 2003).

Additional remarks Let us consider scalar functions u (mode III, harmonic equation). For fixed X, the functional E(u,X) is convex in $u\in$KA. Schematically, the functional is shown in the figure below. The crack free problem is indicated in dotted line. If u_0 denotes the solution of the no-crack problem, then $E(u_0,X)>E(u_0,\varnothing)$, $\forall X$. This is simply explained by the fact that the difference is the positive second term aMeas(X). On the other hand $E(u_0,X)$ does not correspond to the solution of a cracked body, in the sense that X is not the minimizer. Under Dirichlet's boundary condition, the true elastic strain energy is lower than the one for an uncracked body. Therefore the solution u_∞ corresponds to the lowest minimum. Let us simply stress that physical considerations given in the above section suggest that a solution exists. Briefly, instead of specifying the set S_X of X and considering functions $u(\mathbf{x})\in$KA defining in $\Omega\setminus S_X$ one considers a larger set S_U of functions u in the same spatial domain Ω, $u(\mathbf{x})\in$KA, having discontinuities along surfaces X, for which Meas(X) is replaced by Meas(D_u), where D_u is the set of discontinuity of u.

The initial minimum problem becomes a *non convex* minimization problem $\min_{u\in S_u} E(\mathbf{u})=a\text{Meas}(D_u)+\int_\Omega W(\nabla\mathbf{u})d\Omega$.

Mathematically, one considers a sequence of functions $E_k(u)$ (k=1,2,3...): U→ O in a metric space U. The Γ-convergence (*) of this sequence to some function E(u) is considered. The minimizer of $E_k(u)$ over U is denoted by u_k and the minimum by $E_k(u_k)$. If the sequence of minimizers u_k converges to some u_∞, then u_∞ is the minimizer of E(u).

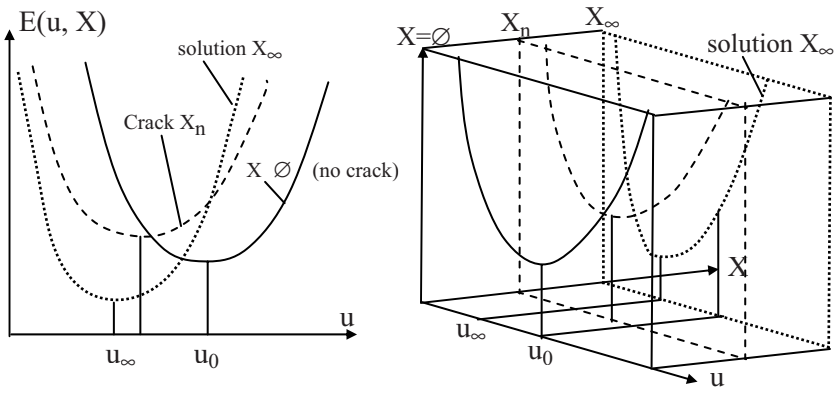

Figure C.6

18. Tikhonov's regularization. **Error estimate**
Suppose that there exists $\mathbf{d}^1$ such that the exact solution is $\mathbf{z}^{ex}=A*\mathbf{d}^1$, prove the error estimate $\|\mathbf{z}^{(\alpha)}-\mathbf{z}^{ex}\|< \frac{1}{2}\,\alpha^{-1/2}(\|\mathbf{d}-\mathbf{d}^{ex}\|+\alpha\|\mathbf{d}^1\|)$.

SOLUTION: The exact pair $(\mathbf{z}^{ex},\mathbf{d}^{ex})$ satisfies the variational equation
$(A\mathbf{z}^{ex}, A\mathbf{y})_D = (\mathbf{d}^{ex}, A\mathbf{y})_D \ \forall \mathbf{y}\in Z,$ (1)
The approximate quasi-solution $(\mathbf{z}^{(\alpha)},\mathbf{d})$ satisfies the equation
$(A\mathbf{z}^{(\alpha)}, A\mathbf{y})_D + \alpha(\mathbf{z}^{(\alpha)}, \mathbf{y})_Z = (\mathbf{d}, A\mathbf{y})_D \ \ \forall \mathbf{y}\in Z$
which can be written as:
$(A\mathbf{z}^{(\alpha)}, A\mathbf{y})_D + \alpha(\mathbf{z}^{(\alpha)}- \mathbf{z}^{ex}, \mathbf{y})_Z + \alpha(\mathbf{z}^{ex}, \mathbf{y})_Z = (\mathbf{d}, A\mathbf{y})_Z \ \ \forall \mathbf{y}\in Z$ (2)
Combining (1) and (2) we get:
$(A(\mathbf{z}^{(\alpha)}- \mathbf{z}^{ex}), A\mathbf{y})_D + \alpha(\mathbf{z}^{(\alpha)}- \mathbf{z}^{ex}, \mathbf{y})_Z + \alpha(\mathbf{z}^{ex}, \mathbf{y})_Z = (\mathbf{d}-\mathbf{d}^{ex}, A\mathbf{y})_D \ \ \forall \mathbf{y}\in Z$
By taking $\mathbf{y}= \mathbf{z}^{(\alpha)}- \mathbf{z}^{ex}$, we obtain
$\| A(\mathbf{z}^{(\alpha)}- \mathbf{z}^{ex})\|^2 + \alpha\|\mathbf{z}^{(\alpha)}-\mathbf{z}^{ex}\|^2 = \ (\mathbf{d}-\mathbf{d}^{ex}, A(\mathbf{z}^{(\alpha)}- \mathbf{z}^{ex}))_D -$
$-\alpha(\mathbf{z}^{ex}, \mathbf{z}^{(\alpha)}- \mathbf{z}^{ex})_Z$ (3)

(*) Γ-convergence: a sequence $E_k(u)$ converges to E(u), if and only if, for every $u\in U$, i) for every sequence $u_k\to u$, one has $E(u)\le \liminf_{k\to\infty}E_k(u_k)$; ii) there exists a sequence $u_{k'}\to u$ such that $\limsup_{k'\to\infty}E_{k'}(u_{k'})\le E(u)$.

The last term can be written as
$\alpha(\mathbf{z}^{ex}, \mathbf{z}^{(\alpha)}-\mathbf{z}^{ex})_Z = \alpha(A^*\mathbf{d}^1, \mathbf{z}^{(\alpha)}-\mathbf{z}^{ex})_Z = \alpha(\mathbf{d}^1, A(\mathbf{z}^{(\alpha)}-\mathbf{z}^{ex}))_D$
The left hand side of (3) is bounded by
$\| A(\mathbf{z}^{(\alpha)}-\mathbf{z}^{ex})\|^2 + \alpha\|\mathbf{z}^{(\alpha)}-\mathbf{z}^{ex}\|^2 \le \|\mathbf{d}-\mathbf{d}^{ex}\|.\|A(\mathbf{z}^{(\alpha)}-\mathbf{z}^{ex})\| +$
$+ \alpha\|\mathbf{d}^1\|.\|A(\mathbf{z}^{(\alpha)}-\mathbf{z}^{ex})| \le \|A(\mathbf{z}^{(\alpha)}-\mathbf{z}^{ex})\|.(\|\mathbf{d}-\mathbf{d}^{ex}\| + \alpha\|\mathbf{d}^1\|) \le$
$\le \|A(\mathbf{z}^{(\alpha)}-\mathbf{z}^{ex})\|^2 + \frac{1}{4}(\|\mathbf{d}-\mathbf{d}^{ex}\| + \alpha\|\mathbf{d}^1\|)^2 \quad \Rightarrow$
$\alpha\|\mathbf{z}^{(\alpha)}-\mathbf{z}^{ex}\|^2 \le \frac{1}{4}(\|\mathbf{d}-\mathbf{d}^{ex}\| + \alpha\|\mathbf{d}^1\|)^2 \Rightarrow \|\mathbf{z}^{(\alpha)}-\mathbf{z}^{ex}\| < \frac{1}{2}\alpha^{-1/2}(\|\mathbf{d}-\mathbf{d}^{ex}\| + \alpha\|\mathbf{d}^1\|)$

19. Tikhonov's regularization. **Continuity property**
Prove the majoration : $\| \mathbf{z}^{(\alpha)}(d) - \mathbf{u}^{(\alpha)}(d')\| \le \alpha^{-1}\|A\|.\|\mathbf{d}-\mathbf{d}'\|$,

SOLUTION: Consider two data **d**, **d**' and the corresponding solutions **z**, **z**'.
For convenience we simply write $\mathbf{z}=\mathbf{z}^{(\alpha)}(\mathbf{d})$ and $\mathbf{z}'=\mathbf{z}^{(\alpha)}(\mathbf{d}')$.
By substracting the corresponding bilinear forms one gets:
$(A(\mathbf{z}-\mathbf{z}'), A\mathbf{y})_D + \alpha(\mathbf{z}-\mathbf{z}', \mathbf{y})_D = (\mathbf{d}-\mathbf{d}', A\mathbf{y})_D \quad \forall \mathbf{y}\in Z$
$\Rightarrow (A^*A(\mathbf{z}-\mathbf{z}'), \mathbf{y})_Z + \alpha(\mathbf{z}-\mathbf{z}', \mathbf{y})_Z = (\mathbf{d}-\mathbf{d}', A\mathbf{y})_D \quad \forall \mathbf{y}\in Z$
Take $\mathbf{y} = \mathbf{z}-\mathbf{z}'$, one gets:
$\|A^*A\|.\|\mathbf{z}-\mathbf{z}'\|^2 + \alpha\|\mathbf{z}-\mathbf{z}'\|^2 \le \|A\|.\|\mathbf{d}-\mathbf{d}'\|.\|\mathbf{z}-\mathbf{z}'\| \Rightarrow$
$\Rightarrow \alpha\|\mathbf{z}-\mathbf{z}'\|^2 \le \|A\|\,\|\mathbf{d}-\mathbf{d}'\|.\|\mathbf{z}-\mathbf{z}'\| \Rightarrow \alpha\|\mathbf{z}-\mathbf{z}'\| \le \|A\|.\|\mathbf{d}-\mathbf{d}'\|$

20. Tikhonov's regularization. **Convergence property**
Show that $\| \mathbf{z}^{(\alpha)}(\mathbf{d}) - \mathbf{z}(\mathbf{d})\| \to 0$, as $\alpha \to 0$.

SOLUTION: $(A\mathbf{z}, A\mathbf{y})_D = (\mathbf{d}, A\mathbf{y})_D \quad \forall \mathbf{y}\in Z$
$(A\mathbf{z}^{(\alpha)}, A\mathbf{y})_D + \alpha(\mathbf{z}^{(\alpha)}, \mathbf{y})_Z = (\mathbf{d}, A\mathbf{y})_D \quad \forall \mathbf{y}\in Z$
$(A(\mathbf{z}^{(\alpha)}-\mathbf{z}), A\mathbf{y})_D + \alpha(\mathbf{z}^{(\alpha)}, \mathbf{y})_Z = 0 \quad \forall \mathbf{y}\in Z$
Take: $\mathbf{y} = \mathbf{z}^{(\alpha)}-\mathbf{z}$, one gets
$\|A(\mathbf{z}^{(\alpha)}-\mathbf{z})\|^2 + \alpha(\mathbf{z}^{(\alpha)}, \mathbf{z}^{(\alpha)}-\mathbf{z})_Z = 0 \Rightarrow \alpha(\mathbf{z}^{(\alpha)}, z^{(\alpha)}-\mathbf{z})_Z \le 0 \qquad (*)$
$\Rightarrow \|\mathbf{z}^{(\alpha)}\|^2 \le (\mathbf{z}^{(\alpha)}, \mathbf{z})_Z \le \|(\mathbf{z}^{(\alpha)}|.\|\mathbf{z}\| \Rightarrow \|\mathbf{z}^{(\alpha)}\| \le \|\mathbf{z}\|$
Since the sequence $\|\mathbf{z}^{(\alpha)}\|$ is bounded, there exists a subsequence converging weakly towards **z**, $(\mathbf{z}^{(\alpha)}-\mathbf{z}, \mathbf{y})_Z \to 0$, $\forall \mathbf{y}$. By taking $\mathbf{y}=\mathbf{z}$ we obtain :
$(\mathbf{z}^{(\alpha)}-\mathbf{z}, \mathbf{z})_Z \to 0 \qquad (*)$
Now consider:
$\|\mathbf{z}^{(\alpha)}-\mathbf{z}\|^2 = \underbrace{(\mathbf{z}^{(\alpha)}, \mathbf{z}^{(\alpha)}-\mathbf{z})_Z}_{\text{(negative)}} - (\mathbf{z}, \mathbf{z}^{(\alpha)}-\mathbf{z})_Z$
Using the inequality (*), the first term in the right hand side is negative. Thus one obtains
$\|\mathbf{z}^{(\alpha)}-\mathbf{z}\|^2 \le -(\mathbf{z}, \mathbf{z}^{(\alpha)}-\mathbf{z})_Z$
Therefore, according to Eq. (*), $\|\mathbf{z}^{(\alpha)}-\mathbf{z}\|^2 \le -(\mathbf{z}, \mathbf{z}^{(\alpha)}-\mathbf{z})_Z \to 0$ as $\alpha \to 0$, hence $\|\mathbf{z}^{(\alpha)}-\mathbf{z}\|^2 \to 0$. The sequence $\mathbf{z}^{(\alpha)}$ converges strongtly towards **z**.

21. Bifurcation Control of a beam

Solve the problem (12-21)-(12-24) of Sect. 12.4.

SOLUTION: The Hamiltonian is $H(\phi, \lambda; v)=\frac{1}{2}EIv^2-P(1-\cos\phi)+\lambda v$.

The adjoint state equation is

$$\frac{d\lambda}{ds}=-\frac{\partial H}{\partial \phi}=P\sin\phi$$

The optimality condition $\partial H/\partial v=0$ is written as

$EIv+\lambda=0$

By differentiating with respect to s, we obtain

$$EI\frac{dv}{ds}+\frac{d\lambda}{ds}=0$$

Since $v=\phi'$ we recover the classical equation $EI\phi''+P\sin\phi=0$, with $\phi(0)=0$, $\phi'(L)=0$. The solution is :

1. $\phi(s)\equiv 0$ for $L<\frac{\pi}{2}(EI/P)^{1/2}$ (straight beam)

2. $\phi(s)\neq 0$ for $L>\frac{\pi}{2}(EI/P)^{1/2}$ (buckled shaped beam).

23. The interface of a bi-material at a free surface (strong singularity)

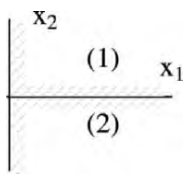

An interface of a bi-material intersects normally the free surface ($x_1=0$). Show that the stress singularity is (Zwiers, Ting and Spilker (1982):
$\sigma_{ij}\cong k^*r^{\delta}f_{ij}(\theta)+[\alpha_1+k\varepsilon_{33}\log r]h_{ij}^{(1)}(\theta)+\ldots$.

HINT: Search an asymptotic solution for displacement $\mathbf{u}\cong r^a(\log r)^b\mathbf{g}(\theta)$

References

Abe, H., Mura, T. and Keer, L.M. (1976). Growth of penny-shaped crack in hydraulic fracturing of rocks. J. Geophys. Res. 81(29), p. 5335.

Abou-Sayed, A., Brechtel, C. and Clifton, R. (1978). In-situ stress determination by hydrofracturing: a fracture mech approach. J. Geophys. Res. 83(6) pp. 2851-2862.

Abeyaratne, R. and Hou, H.S. (1989). Growth of an infinitesimal cavity in a rate-dependent solid. Trans ASME, 56, pp. 40-46.

Achenbach, J.D. and Bazant, Z.P. (1972). Elastodynamic near-tip stress and displacement fields for rapidly propagating cracks in orthotropic materials. J. Appl. Mech. 97, p. 183.

Achenbach, J.D. and Bazant, Z.P. (1975). J. Appl. Mech., 42, p. 183.

Achenbach, J.D. (1980). *Wave propagation in elastic solids*. North-Holland, Amsterdam (1980).

Achenbach, J.D., Sotitopoulos, D.A. and Zhu, H. (1987). Characterisation of cracks from ultrasonic scattering data. J. Non Destructive Evaluation, 54, p. 754.

Adler, L. and Achenbach, J.D. (1980). Elastic wave diffraction by elliptical cracks. Theory and Experiments. J. Non Destructive Evaluation, 1, 87 (1980).

Afanasev, E.E. and Cherepanov, G.P. (1973). Some dynamic problem of the theory of elasticity. P.M.M., 37(4), pp. 618-639.

Aki, K. and Richards, P.G. (1980). *Quantitative seismology, theory & methods*. *1*. W.H. Freeman and Cie. New York .

Alves, C.J.S. and Ha-Duong, T. (1999). On inverse scattering by screen. Inverse Problems 15, pp. 91-97.

Amestoy, M., Bui, H.D. and Dang Van, K. (1980). Analytic asymptotic solution of the kinked crack problem. In *Advances in Fracture Research*, D. Francois et al (Eds), pp. 107-113, Pergamon Press, Oxford, New York.

Andrieux, S. and Ben Abda, A. (1992). Identification de fissures planes par une donnée de bord unique: un procédé direct de localisation et d'identification. C. R. Acad. Sciences Paris, I (315), pp. 1323-1328.

Andrieux, S. and Ben Abda, A. (1996). Identification of planar cracks by complete overdetermined data inversion formulae. Inverse Problems, 12, pp. 553-563.

Andrieux, S., Bui, H.D. and Ben Abda, A. (1999). Reciprocity and crack identification. Inverse Problems, 15, pp. 59-65.

Audoly, B. (2000). Asymptotic study of the interface crack with friction. J. Mech. Phys. Solids, 10, pp. 1851-1864.

Bal, G. and Ryzhik, L. (1993). Time reversal and refocusing in random media. SIAM J. Appl. Math. 63, pp. 1475-1498.

Ball, J.M. (1982) Discontinuous equilibrium equations and cavitation in nonlinear elasticity. Phil. Trans. of Roy. Soc. London, A306, pp. 557-611.

Ballard, P. and Constantinescu, A. (1994). On the inversion of subsurface residual stresses from surface stress measurements. J. Mech. Phys. Solids, 42, pp. 1767-1788.

Bannour, T., Ben Abda, A. and Jaoua, M. (1997). A semi-explicit algorithm for the reconstruction of 3D planar cracks. Inverse Problems, 13, pp. 899-917.

Barenblatt, G.I. (1962). The mathematical theory of equilibrium cracks in brittel fracture. Advances in Appl. Mech. 7, pp. 55-129.

Bazant, Z.P. and Estenssoro, L.F. (1979). Surface singularity and crack propagation. Int. J. Solids & Struct., 15, pp. 405-426.

Bazant, Z.P. and Cedolin, L. (1991), Stability of structures: elastic, inelastic, fracture and damage theories. Oxford University Press, New York.

Ben Abda, A. and Bui, H.D. (2003). Planar cracks identification for the transient heat equation. Inverse and Ill-posed Problems, 11 (1), pp. 67-86.

Beinert, J. and Kalthoff, J.F. (1981). Experimental determination of dynamic stress intensity factors by shadow patterns. Experimental evaluation of SIC and SIF, Mech. Fract. 7, (Ed G.C. Sih) 281.

Bergez, D. and Radenkovic, D. (1972). La caractérisation des fissures dans les plaques fléchies et coques. C. R. Acad. Sciences, Paris, 275, pp. 221-224.

Bellman, R. (1957). *Dynamic programming*. Princeton Univ. Press, N.J.

Bellman, R. (1971). *Introduction to the mathematical theory of control process*. Acad. Press, New York, London.

Benallal, A. Billardon, R. and Geymonat, G. (1989). C.R. Acad. Sci., 308, II, pp. 893-898.

Benallal, A. Billardon, R. and Geymonat, G. (1991). Bifurcation and localization in rate-independent materials. In *Bifurcation and Stability of dissipative systems*. 1-44, CISM Course 327, Springer-Verlag, Wien, New-York.

Benthem, J.P. (1976). Three-dimensional state of stress at the vertex of a quarter infinite crack in a half-space. Euromech colloqium 77, Paris.

Berry, J.P. (1960). Some kinetic considerations of the Griffith criterion for fracture I and II. J. Mech. Phys. Solids, 8(3), pp. 194-206.

Berthier, Y., Vincent, L. and Godet, M. (1988). Velocity accommodation in fretting. Wear, 139, pp. 77-92.

Berveiller, M. and Zaoui, A. (1979). An extension of the self-consistent scheme to plastically flowing polycrystals. J. Mech. Phys. Solids, 26, pp. 325-344.

Bergez, D. and Radenkovic, D. (1972). C.R. Acad. Sci. Paris, 275, pp. 221-224.

Bilby, B.A. and Cardew, G.E. (1975). The crack with a kinked tip. Int. J. Fract., 11, pp. 708-712.

Bilteryst, F. and Marigo, J.J. (2003). An energy based analyss of the pull-out problem. European J. Mech. A/Solids, 22, pp. 55-69.

Biot, M.A. (1981) *New variational irreversible thermodynamics of physical-chemical continua.* Pergamon Press, Oxford.

Bittanti, S., Maier, G. and Nappi, A. (1984). Inverse problems in structural elasto-plasticity, a Kalman filter approach. In *Plasticity today*. Sawczuk and Bianchi G. (Eds.) Elsevier, p. 311.

Bojarski, N.N. (1981). Exact inverse scattering theory. Radio Sciences., 16, p. 1025.

Bojarski, N.N. (1983). Bistatic low frequency inverse scattering. J. Acoust. Soc. Am., 73, p. 733 (1983).

Bonnet, M. and Bui, H.D. (1989). Proc. 6th Japan Nat. Symp. on BEM, Tokyo, Jascome Publications, Tokyo, p. 179.

Bonnet, M. (1999). *Boundary Integral Equations Methods for Solids and Fluids*, John Wiley and Sons.

Bossavit, A. and Fremond, M. (1976). The frontal method based on mechanics and dynamic programming. Comp. Meth. Appl. Mech. Eng., 8, p. 153.

Bossavit, A. (1988). The computation of Eddy-currents in deformable conductors. in Applied Electromagnetics in Materials. K. Miya (Ed.), pp. 211-224, Pergamon Press, Oxford.

Bourdin, B., Francfort, G. and Marigo, J.J. (2000). Numerical experiments in revisited brittle fracture. J. Mech. Phys. Solids, 48, pp. 797-826.

Bowie, O.L. (1973). Solutions of plane crack problems by mapping techniques. Mech. of Fracture, 1, Noordhoff.

Brown, L.M. and Embury, J.D. (1973). Initiation and growth of voids at second phase particles. In 3rd Int. Conf. on Strength of metals.

Brun, L. (1969). Méthodes énergétiques dans les systèmes évolutifs linéaires; séparation des énergies. *J. Méca.*, 8, p. 125.

Bryson, A. and Ho, Y.C. (1969). *Applied optimal control*. Blaisdell Publ. Waltham, Toronto, London.

Bueckner, Hans F. (1973). Field singularities and related integral representations. In Mechanics of fracture 1. Methods of analysis ans solutions of crack problems. G.C. Sih (Ed.) Noordhoff Int. Publ. Leyden.

Bui, H.D. (1964). The hardening of metals. C. R. Acad. Sciences, Paris, 259, pp. 4509-451.

Bui, H.D. (1964). The hardening of metals. C. R. Acad. Sciences, Paris, 262, pp. 401-404.

Bui, H.D. (1965). Dissipation of energy in plasticity. Cahier Groupe Français de Rhéologie, 1, p. 15.

Bui, H.D. (1969). Study of the subsequent yield surfaces in metal hardenning and behavior laws of cubic metals. PhD thesis, University of Paris.

Bui, H.D. and Dang Van, K. (1970). On the rate boundary value problem in elasto-plasticity. Int. J. Solids & Structures, 6, pp. 183-193.

Bui, H.D., Zaoui, A. and Zarka, J. (1972). On the elastic-plastic and viscoplastic behavior of face-centered cubic metallic monocrystals and polycrystals. In *Foundations of Plasticity*, A. Sawczuk (Ed.). Noordoff Int. Publ. Leyden, pp. 51-75 (in French).

Bui, H.D. (1974). Dual path-independent integrals in the boundary-value problems of cracks. Eng. Fracture Mech., 6, pp. 287-296.

Bui, H.D. (1975). Application des potentiels élastiques à l'étude des fissures de forme arbitraire en milieu tridimensionel. C. R. Acad. Sci. Paris, 280, p. 1157.

Bui, H.D. (1977). Stress and Crack displacement intensity factors in Elastodynamics. Proc. 4th Int. Conf. Fract., 3, Waterloo, p. 91.

Bui, H.D. (1977). An integral equations method for solving the problem of a plane crack of arbitrary shape. J. Mech. Phys. Solids, 23, pp. 29-39.

Bui, H.D. (1978). *Brittle fracture mechanics*. Masson, Paris.

Bui, H.D. and Dang Van, K. (1978). Some remarks about the formulation of three-dimensional thermo-elastoplastic problems by integral equations. Int. J. Solids & Structures, 14, pp. 935-939.

Bui, H.D. and Putot, C. (1979). Singularities at the angular crack tip in three-dimensions. 4^{t} French National Cong. on Mechanics, Nancy, pp. 318-319.

Bui, H.D. and Putot, C. (1979). Integral equations formulation of the 3D edge crack at a free surface, C. R. Acad. Sciences, Paris, 288, A, p. 311.

Bui, H.D. and Dang Van, K. (1979). Generalization of the Griffith theory of fracture to a three-dimensional solid. J. Mecanique Appliquee, 3(2), p. 205.

Bui, H.D., Ehrlacher, A. and Nguyen, Q.S. (1980). Crack propagation in coupled thermo-elasticity. J. Meca. 19, pp. 697, Gauthier-Villars, Paris.

Bui, H.D. and Ehrlacher, A. (1981) Propagation of damage in elastic and plastic solid. In *Advances in Fracture Research*. D. Francois et al (Eds). Pergamon Press, Oxford, and New York, p. 353.

Bui, H.D., Ehrlacher, A. and Nguyen, Q.S. (1981). Experimental study of dissipation in crack propagation by infra-red thermography. C. R. Acad. Sciences Paris, 293(II), pp. 1015-1018.

Bui, H.D. (1984). A path-independent integral for mixed modes of fracture in linear thermo-elasticity. IUTAM Symposium on Fundamental of Deformation and Fracture. Sheffield, pp. 597, April 1984.

Bui, H.D. and Proix, J.M. (1984). Lois de conservation en thermoélasticité linéaire. C.R. Acad. Sci. Paris, II(298), p. 325.

Bui, H.D. (1987). Recent developments in fracture mechanics. In Fracture of non-metallic materials. K.P. Hermann and L.H. Larsson (Eds.) ECSC, EEC, EAEC, pp. 21-32.

Bui, H.D. and Maigre, H. (1988). Extraction of stress intensity factors from global mechanical quantities. C. R. Acad. Sci. Paris, 306(II), p. 1213.

Bui, H.D. and de Langre, E. (1988). Separation of energies in dynamic fracture. In *Theory and Applications*, Computational Mechanics'88, 1, S.N. Atluri and G. Yagawa (Eds) pp. 9i1-9i4.

Bui, H.D. and Taheri, S. (1989). The weak "Thorn" singularity in a bi-material junction in thermo-elasto-plasticity. C. R. Acad. Sciences, Paris, 309(II), pp. 1527-1533

Bui, H.D., Debruyne, G and Gao, Y.C. (1991) La singularité des champs en fond de fissure, Note HI.73/7270. Electricite de France.

Bui, H.D. (1992). On the variational boundary integral equations in elasto-dynamics with the use of conjugate functions. Journal of Elasticity, 28, p. 247

Bui, H.D., Maigre, H. and Rittel, D. (1992). A new approach to the experimental determination of the dynamic stress intensity factors. Int. J. Solids & Struct., 29, pp. 2881-2895.

Bui, H.D. (1994). *Inverse Problems in the Mechanics of Materials: an introduction*. CRC Press, Boca Raton. English translation from the French book, Eyrolles, Paris (1993).

Bui, H.D. (1996). Interaction between the Griffith crack and a fluid: theory of Rehbinder's effect. In Fracture: *A topological encyclopedia of current knowledge*, Chapter 6, G.P. Cherepanov (Ed.). Krieger, Melbourne.

Bui, H.D., Constantinescu, A. and Maigre, H. (1999). Inverse scattering of a planar crack in 3D acoustics: close form solution for a bounded solid. C. R. Acad. Sciences Paris, 327(II), pp. 971-976.

Bui, H.D. and Constantinescu, A. (2000). Spatial localization of the error of constitutive law for the identification of defects in elastic bodies. Arch. Mechanics, Warszawa, 52, pp. 511-522.

Bui, H.D., Dragon-Louiset, M. and Stolz, C. (2001). A thermodynamic analysis of wear. In *Handbook of materials Behavior Models*, J. Lemaitre (Ed.). Sect. 8.5, pp. 768-776. Academic Press.

Bui, H.D., Guyon, C. and Thomas, B. (2002). On viscous fluid flow near a moving crack, in *Continuum Thermomechanics*, G.A Maugin et al (Eds.) pp. 63, Kluwer Acad. Publ.

Bui, H.D., Constantinescu, A. and Maigre, H., (2004). Numerical identification of linear cracks in 2D elastodynamics using the instantaneous reciprocity gap. Inverse Problems, 20, pp. 993-1001.

Bui, H.D. and Oueslati, A. (2004). Exact solution of the problem of an interface crack between elastic and rigid bodies under frictional contact. C. R. Mecanique, 332, pp. 709-716.

Bui, H.D., Constantinescu, A. and Maigre, H., (2005). An exact inversion formula for determining a planar fault from boundary measurements. Inv. and Ill-posed Problems, 13, n°6, pp. 553-565.

Bui, H.D., Constantinescu, A. and Maigre, H. (2005). The reciprocity gap functional for identifying defects and cracks. In *Parameter identification of materials and structures*. Z. Mroz and G.E. Stavroulakis (Eds.). CISM Course and Lecture, n° 469, Springer, Wien, New York.

Bui, H.D. and Oueslati, A. (2005). The sliding interface crack with friction between elastic and rigid bodies. J. Mech. Phys. Solids, 53, pp. 1397-1421.

Bilteryst, F. and Marigo, J.J. (2003). An energy based analyss of the pull-out problem. European J. Mech. A/Solids, 22, pp. 55-69.

Cailletaud, G. (1987). Une approche micromécanique phénoménologique du comportement inélastique des métaux. Ph.D. Thesis, Paris Univ.

Calderon, A.P. (1980). On an inverse boundary problem. In *Seminar on numerical and applications to continuum physics* (W.H. Meyer and M.A. Raupp, Eds.) Brazilian Math. Soc., R. de Janeiro, pp. 65-73.

Chen, F.H.K. and Shield, R.R., (1977), Z.A.M.P, 28, p. 1.

Cherepanov, G.P. (1968). Int. J. Solids & Struct., 4, p. 811.

Cherepanov, G.P. (1979). *Mechanics of brittle fracture*. McGraw Hill, New York.

Chi-Sing, M. and Lu, W.Y. (1987). Towards an acousto-elastic theory for measurement of residual stress. J. Elasticity, 17(2), p. 159.

Colton, D. and Monk, R. (1985). A novel method for solving the inverse problem for time harmonic acoustic waves in the resonance region. SIAM, J. Appl. Math, 45, p. 1039.

Comninou, M. (1977). The interface crack. J. Appl. Mech. 44, pp. 631-636

Constantinescu, A. (1995). On the identification of elastic moduli from displacement-force boundary measurements. Int. J. Inverse Prob. Engineering, I, pp. 293-315.

Constantinescu, A. and Tardieu, N. (2000). Identification strategies for recovering material parameters from indentation experiments. In *Inverse Problems in Engineering*, M. Tanaka and G. Dulikravich (Eds) ISIP'2000, Elsevier.

Constantinescu, A. and Verger, L. (2002). Identification of a viscoplastic material behavior under anisothermal conditions. In: *Inverse problems and experiments design in thermal and mechanical engineering*, D. Petit, D.B. Ingham, Y. Jarn, and F. Plourde (Eds). Eurotherm Seminar 68, pp. 221-228, Edizioni ETS.

Contensou, P. (1946). Note sur la cinématique du mobile dirigé. Bulletin ATMA, pp. 45.

Dang Dinh Ang, Gorenflo, R., Le Khoi, V. and Dang, D.T. (2000). *Moment theory and some inverse problems in potential theory and heat conduction*. Springer, Berlin.

Dang Van, K. and Maitournam, H. (1993). Steady-state flow in classical plasticity: application to repeated rolling and sliding contact. J. Mech. Phys. Solids. 41, pp. 1691-1710.

Dang Van, K. (1999). Fatigue analysis by the multiscale approach. *High Cycle Metal Fatigue, From Theory to Applications*, CISM Courses and Lectures, 392, K. Dang Van and I.V. Papadopoulos (Eds.), Springer, pp. 57-88.

Das, S.P. and Kostrov, B.V. (1990). Inversion for seismic slip rate and distribution with stabilizing constraints : Applications to the 1986 Andeanov Islands earthquake. J. Geophys. Res., 95, pp. 6899-6913.

Das, S. and Suhadolc, P. (1996). On the inverse problem for earthquake rupture: The Haskell-type source model. Journal of Geophysical Research, 101(B3), pp. 5725-5738.

Dautray, R. and Lions, J.L. (1989). Mathematical analysis and numerical methods for science and technology. 1, p. 2. Springer-Verlag, Berlin.

De Giorgi, E., Carriero, M. and Leaci, A. (1989). Existence theorem for a minimum problem with free discontinuity set. Arch. Rat. Mech. Anal. 108, pp. 195-218.

Deng, X. (1994). An asmptotic analysis of stationary and moving cracks with frictional contact along bimaterial and in homogeneous solids. Int. J. Solids & Struct., 31, pp. 2407-2429.

Deperrois, A. and Dang Van; K. (1990). Inclusion de surface et singularité épine. C.R. Acad. Sci. Paris (311, pp. 1285-1290.

Destuynder, Ph. and Djaoua, M. (1981). Sur une interprétation de l'intégrale de Rice en théorie de la rupture fragile. Math. Meth. in Appl. Sci., 3, p. 70.

Detournay, E. (1999). Fluid and solid singularities at the tip of a fluid-driven fracture. In D. Durban and Z.R. Pearson (Eds.). *Non-linear singularities in deformation and flow*, pp. 27-42, Dordrecht, Kluwer Acad.

Devaney, A.J. (1982). Inversion formula for inverse scattering within the Born approximation. Optics Letter, 7, p. 11.

Ding, Y. and Planchard, J. (1989). Une méthode pour le problème inverse des ondes acoustiques en régime harmonique diffractées par une surface rigide en 2D. Report EDF/DER/HI-70.6545, Clamart, p. 1.

Dong, P. and Pan, J. (1990). Plane-strain mixed-mode near–tip fields in elastic perfectly plastic solids under small-scale yielding conditions. Int. J. Fracture, 45, pp. 243-262.

Dragon-Louiset, M. and Stolz, C. (1999). Approche thermodynamique des phénomènes d'usure de contact. C.R. Acad. Sciences Paris, 327(II), pp. 1275-1280.

Dragon-Louiset, M., Bui, H.D. and Stolz, C. (2000). On Prandtl's lifting equation arising in wear mechanics, Archiv of Mechanics, Warsaw. 52, pp. 547-567.

Dragon-Louiset, M. (2001). On a predictive macroscopic contact-sliding wear model based on micromechanical considerations. Int. J. Solids & Structures, 38, pp. 1624-1639.

Dudukalenko, V.V. and Romalis, N.B. (1973). Izv. An . SSR. MTT, 8(2), pp. 129-136.

Dugdale, D.S. (1960). Yielding of steel sheets containng slits. J. Mech. Phys. Solids, 8, pp. 100-104.

Dundurs, J. (1969). Mathematical theory of dislocations. ASME, NY, pp. 70-115.

Dussan, E. B. and Davis, S.H. (1974). On the motion of a fluid-fluid interface along a solid surface. In J. Fluid Mech., 65, p. 71.

Duvaut, G. and Lions, J.L. (1972). *Les inéquations en mécanique et en physique.* Dunod, Paris. (English translation: Inequations in physics and mechanics, Spinger-Verlag, Berlin, 1979).

Eeckhout, M.V. (1976). The mechanics of strength reduction due to moisture in coal mine shales, Int. J. Rocks Mech. Min. Sci., Geomech. Abstract. 13, p. 61.

Ehrlacher, A. (1985). Contribution à l'étude de l'endommagement brutal. Thèse Doctorat d'Etat, Université Paris VI.

Ekeland, I. and Temam, R. (1974). *Analyse convexe et problèmes variationels*. Dunod, Paris.

Eshelby, J.D. (1951). The force on an elastic singularity. Phil. Trans. Roy. Soc. London, A 244, pp. 87-112.

Eshelby, J.D. (1957). The determination of the elastic field of an ellipsoidal inclusion and related problems. Proc. Roy. Soc. Lond. A241, pp. 376-396.

Feraille-Fresnet, A. and Ehrlacher, A. (2000). Behavior of a wet crack submitted to heating up to high temperature. Mech. Mater., 32, pp. 471-484.

Feraille-Fresnet, A., Bui, D.D. and Ehrlacher, A. (2003). Hydrostatic interaction of a wetting fluid and a circular crack in an elastic material. Mech. Mater., 35, pp. 581-586.

Finch, D.V. (1986). Uniqueness for the attenuated x-ray transform in the physical range. Inverse Problem, 2, pp. 197-203.

Finch, D.V. (2003). The attenuated X-ray transform: recent developments. Inverse problems, 47, pp. 47-66.

Fink, M. (1997). Time reversed acoustics. Physics Today, 20, pp. 34-40.

Fink, M. and Prada, C. (2001). Acoustic time-reversal mirrors. Inverse Problems, 17, pp. R1-38.

Fletcher, D.C. (1976). Conservation laws in linear Elastodynamics. Arch. Rat. Mech. Anal., 60, p. 329.

Focas, A.S. and Marinakis, V. (2003). Reconstruction algorithm for the brain imaging techniques of PET and SPECT, Hermis-μπ, 4, pp. 45-62.

François, D., Pineau, A. and Zaoui, A. (1991). *Comportement mécanique des matériaux*, I. Hermès, Paris.

Francfort, G. and Marigo, J.J. (1998). Revisiting brittle fracture as an energy minimization problem. J. Mech. Phys. Solids. 46, pp. 1319-1342.

Freund, L.B. (1972). Energy flux into the tip of an extending crack in an elastic solid. J. Elast., 2., p. 341.

Freund, L.B. (1972). Crack propagation in an elastic solid subjected to general loading. II. Non uniform rate of extension, J. Mech. Phys. Solids, 20, pp. 141-152.

Freund, L.B. (1973). Crack propagation in an elastic solid subjected to general loading. III. Stress wave loading, J. Mech. Phys. Solids, 21, pp. 47-61.

Freund, L.B. and Rice, J.R. (1974). On the determination of elastodynamic crack tip stress fields. Int. J. Solids & Struct., 10, p. 411.

Freund, L.B. (1990). *Dynamic fracture mechanics*. Cambridge Monographs on Mechanics and Applied Mathematics. Cambridge University Press. NY.

Friedman, A. and Vogelius, M. (1989). Determining cracks by boundary measurements. Indiana Univ. Math. J., 38.

Gao, Y.C. (1980). Elastic-plastic fields at the tip of a crack before growing. Acta Mechanica Solida Sinica, 1, p. 69 (in Chinese).

Gao, Y.C. and Bui, H.D. (1995). Damage field near a stationary crack tip. Int. J. Solids & Structures, 32(14), pp. 1979-1987.

Garash, D. and Detournay, E. (1999). Similarity solution of a semi-infinite fluid-driven fracture in a linear elastic solid. Private communication.

Germain, P. (1962). *Mécanique des milieux continus*, Masson, Paris.

Germain, P. (1978). Duality and Convection in cintinuum mechanics. In *Trends in Applications to Mechanics*. G. Fichera (Ed.) pp. 107-128. Pitman, London.

Germain, P. (1973). The method of virtual power in continuum mechanics. Part II. In *Applications to continuum thermodynamics*. J.J.D. Domingos et al (Eds.), pp. 317-333, J. Wiley, New York.

Gill, P.E. and Murray, W. (1974). *Numerical methods for constraints optimization*. Academic Press, New York

Green, A.K. and Pratt, R.L. (1974). Eng. Fract. Mech., 6, p. 71.

Griffith, A.A. (1920). The phenomena of rupture and flow in solids. Phil. Trans. Roy. Soc. London, 221, pp. 16-98.

Guelfand, L.M. and Chilov, G.E., 1962. *Les distributions*, Dunod, Paris.

Guiggiani, M., Krishnasamy, G., Rudolphi, T.J. and Rizzo, F.J. (1992). ASME, J. Appl. Mech., 59, pp. 604-614.

Gurson, A.L. (1977). Continuum theory of ductile fracture by void nucleation and growth: Part I- Yield critaria and flow rules for porous ductile media. ASME J of Engng.Materials and Technology, 99, pp. 2-15.

Gurtin, M.E. (1979). Int. J. Fracture, 15, pp. 169.

Ha-Duong, T. (1979). La méthode de Schenck pour la résolution de problèmes de radiation acoustique. Bulletin DER/EDF, C(2), pp. 15-50.

Halphen, B. and Nguyen, Q.S. (1975). Sur les matériaux standards généralisés. J. Méca., 14, p. 39.

Haskell, N.A. (1984). Radiation pattern of surface waves from point sources in a multi-layered medium. Bulletin of Seismological Soc. of America, 54, p. 377.

Hayes, M. and Rivlin, R.S. (1961). Arch. Rat. Mech. Anal., 8, p. 358.

Hill, R. (1950). *The mathematical theory of plasticity*. Clarendon Press. Oxford.

Hill, R. (1958). A general theory of uniqueness and stability in elastic/ plastic solids. J. Mech. Phys. Solids, 6. pp. 236-249.

Hill, R. (1962). J. Mech. Phys. Solids, 10, pp. 1-16

Hill, R. (1967). The essential structures of constitutive laws of metals composites and polycrystals. J. Mech. Phys. Solids, 15, pp. 79-95.

de Hoop, A.T. and Stam, H.J. (1988). Time-domain reciprocity theorems for elastodynamic wave fields in solids with relaxation and their application to inverse problems. Wave Motion, 10, pp. 479-489.

Horgan, C.O. and Pence, T.J. (1989). Void nucleation in tensile dead-loading of a composite imcompressible nonlinearly elastic sphere. J. Elasticity, 21, pp. 61-82.

Horgan, C.O. and Polignone, D.A. (1995). Cavitation in nonlinearly elastic solids: a review. ASME, Appl. Mech. Rev., 48, pp. 471-485.

Hsu, D.K., Rose, J.H. and Thompson, D.O. (1984). Reconstruction of inclusions in solids using ultrasonic Born inversion. J. Appl. Phys., 55, p. 162.

Hui, C.Y. and Riedel, H. (1981). The asymptotic stress and strain feld near the tip of a growing crack under creep conditions. Int. J. Fract., 17, p. 409.

Hult and McClintock (1957). Elastic-plastic stress and strain distribution around sharp notches under repeated shear, Proc. 9th Int. Cong. Appl. Mech., 8, pp. 51-62.

Hutchinson, J.W. (1968). Singulat behavior at the end of a tensile crack in a hardening material. J. Mech. Phys. Solids, 16, pp. 13-31.

Hutchinson, J.W. (1973). Post-bifurcation behavior in the plastic range. J. Mech. Phys. Solids, 21, pp. 163-190.

Hutchinson, J.W. and Budiansky, B. (1974). Analytical and Numerical study of the effect of initial imperfections on the inelastic buckling of a cruciform column. IUTAM Symp. Buckling of Structures, pp. 98-105, Springer-Verlag, Cambridge.

Hudson, J.A. (1980). *The excitation and propagation of elastic waves*. Cambridge Univ. Press, Cambridge, NY.

Iooss, G. and Joseph, D.D. (1980). Elementary stability and bifurcation theory

Ishikawa, H., Kitagawa, H. and Okamura, H. (1979), Mechanical behavioir of materials, ICM 3, Cambridge, England, 3, p. 447.

Ikehata, M. (1998). Inversion for the linearized problem for an inverse boundary value problem in elastic prospection, SIAM J. Math. Anal., 50(6), p. 1635.

Kachanov, L.M. (1978). Crack growth under creep conditions. Ivz. An SSR Mekhanika Tverdogo Tela, 9(1), p. 57.

Kalthoff, J.F. (1985). On the measurement of dynamic fracture toughness: a review of recent works. Int. J. Fract., 27, p. 277.

Kassir, M.K. and Sih, G.C. (1960). *Three-dimensional crack problems*. Pergamon Press.

Kassir, M.K. and Bregman, A.M. (1972). J. Appl. Mech. 39, ASME 94 E, pp. 308-310.

Kawabe, H. (1994). The two dimensional inverse acoustic scattering for shape identification. In *Inverse Problems in Eng. Mech*. H.D. Bui and M. Tanaka (Eds.) pp. 33-39. Balkema/Rotterdam/Brookfield.

Kishimoto, K., Aoki, S. and Sakata, M. (1980). Dynamic stress intensity factor using J-integral and FE Methods. Eng. Fract. Mech., 13, p. 387.

Kitagawa, T. (1987). A deterministic approach to optimal regularization, the finite dimensional case. Japan J. Appl. Math., 4, p. 371

Klibanov, M.V. and Timonov, A. (2003). On the mathematical treatment of time reversal. Inverse Problems, 19, pp. 1299-1318.

Knowles, J.K. and Sternberg, E. (1972). Arch. Rat. Mech. Anal., 44, p. 187.

Kobayashi, A.S. (1978). Handbook on experimental Mech. Prentice Hall Inc., Englewood Cliffs.

Kohn, R.V. and Vogelius, M. (1985). Determining conductivity by boundary measurements. II. Interior results. Comm. Pure Appl. Math., 38, pp. 643-667.

Kohn, R.V. and Vogelius, M. (1987). Relaxation of a variational method for impedance computed tomography. Comm. Pure Appl. Math., 40, pp. 745-777.

Kolosov, G.V. (1909). On an application of complex function theory to a plane problem of the mathematical theory of elasticity. Yuriev.

Kostrov, B.V. (1975). On the crack propagation with variable velocity. Int. J. Fract., 11(1), pp. 47-56.

Krent, S. (1978). Int. J. Fracture. Vol 14, p. 123.

Kress, R. and Zinn, A. (1992). On the numerical solution of the three dimensional inverse obstacle scattering problem. J. Comp. Appl. Math., 42, pp. 49-61.

Kröner, E. (1961). Zur plastischen Verformung des Vielkristalls. Acta Metall., 9, pp. 155-161

Kunyansky, L.A. (2001). A new SPECT reconstruction algorithm based on the Novikov explicit inversion formula. Inverse problems, 17, pp. 293-306.

Kupradze, V.D. (1963). Dynamical problems in elasticity. *Progress in Solid Mechanics*. III, North Holland Publ.

Labourdette, R. and Baudin, G. (1981). An energy approach to three-dimensional fatigue crack growth problems. Report ONERA-TP-1981-16.

Ladevèze, P. (1975). Comparaison de modèles des milieux continus. Thèse Doctorat d'Etat, Univ. Paris 6.

Ladevèze, P. (1985). On the St-Venant principle in elasticity. In *Local effects in the analysis of structures*. Ladeveze P. (Ed.). Elsevier Sciences Publ., pp. 3-34.

Ladevèze, P. (1998). *Nonlinear computational structural methods: new approaches and non incremental methods of calculation*, Springer-Verlag, Berlin.

Landau, L. and Lifschitz, E. (1971). *Mécanique des fluides*. Ed. Mir, Moscou.

Langenberg, K.L. (1987). Applied inverse problems for acoustic, electromagnetic wave scattering. In *Basic methods of tomography and inverse problems* (Ed. P.C. Sabatier) Malvern Physics Series, Adam Hilger, Bristol, Philadelphia, p. 127.

Lattès, R. and Lions, J.L. (1967). *Méthode de quasi-réversibilité*. Dunod, Paris.

Laurentiev, M.M. (1967). *Some improperly posed problems of mathematical physics*. Springer-Verlag, Berlin, Heidelberg, New York.

Lazarus, V. (2003). Brittle fracture and fatigue propagation paths of 3D plane cracks under remote tensile loading. Int. J. Fracture, 112, pp. 23-46.

Leblond, J.B. (1986). C.R. Acad. Sci. Paris, II, 303, pp. 1521-1524.

Leblond, J.B. (2003). *Mécanique de la rupture fragile et ductile*. Hermès, Lavoisier, Paris.

Léger, A. and Potier-Ferry, M. (1988). Sur le flambage plastique. J. Méca. Théorique et Appliquée, 7, pp. 817-857.

Leguillon, D. and Sanchez-Palencia, E. (1987). Computation of singular solutions in elliptic problems and elasticity. Masson, Paris.

Lemaitre, J. and Chaboche, J.L. (1985). *Mécanique des matériaux solides*. Dunod, Paris.

Lesieur, M. (1997). Turbulence in Fluids. Kluwer Acad. Publ. Dordrecht/ Boston/London.

Li, J. (1997). Detrmination of the full elastic-plastic stress field of a tensile crack by a minimization of the complementary energy. Int. J. Fracture. 84, pp. 1-17.

Li, J, Zhang, X.B. and Recho, N. (1999). Fracture criterion study of a ductile crack under tensile loading. J. Th. and Appl. Mech., 37(4), pp. 779-798.

Lions, J.L. (1971). *Optimal control of systems governed by partal derivative equations*. Springer-Verlag, Berlin, Heidelberg, New York.

Lorentz, E. and Andrieux, S. (2003). Analysis of non-local models through energetic formulations. Int. J. Solids & Structures, 40, pp. 2905-2936.

Maigre, H. (1990). Contribution théorique à l'identification des grandeurs caractéristiques en mécanique de la rupture dynamique. Thèse de Doctorat, Ecole Polytechnique.

Maitournam, H., Pommier, B. and Thomas, J.J (2002). Détermination de la réponse asymptotique d'une structure anélastique sous chargement thermomécanique cyclique, C. R. Mecanique, 330, pp. 703-708.

Mandel, J., Habib, P. and Bui, H.D. (1962). Traction and torsion tests on metallic tubes and strings. Proc. Brown Univ. Symposium, pp. 97-117.

Mandel, J. (1962). J. de Mécanique, 1, 1962, pp. 3-30.

Mandel, J. (1964). Contribution théorique à l'étude de l'écrouissage et des lois de l'écoulement plastique. Proc. of the 11th Int. Congress on Appl. Mech. Munich, pp. 502-509.

Mandel, J. (1965). Energie élastique et travail dissipé dans les modèles rhéologiques. Cahier Groupe Français de Rhéologie, 1, p. 1.

Mandel, J. (1966). *Cours de Mécanique des milieux continus.* I, II, Gauthier-Villars, Paris.

Mandel, J. (1971). *Plasticité classique et viscoplasticité*. Cours CISM Springer-Verlag.

Mandel, J. (1978). Dissipativité normale et variables cachées. Mech. Res. Comm., 5, p. 225.

Maouche, N., Maitournam, H. and Dang Van, K (1997). On a new method of evaluation of the inelastic state due to moving contact. Wear, 203-204, pp. 139-147.

Marigo, J.J. (1989). Constitutive relation in plasticity, damage and fracture based on a work property. Nuclear Eng. Design, 114, p. 249.

Maugin, G.A. (1992). *The thermomechanics of plasticity and fracture*. Cambridge Univ. Press., Cambridge, New York, Melbourne, Sidney.

Maugis, D. and Barquins, M. (1980). Fracture mechanics and adherence of viscoelastic solids. in Adhesion and adsorption of polymers. Part A, L.H. Lee (Ed.), pp. 203-277.

Menikhes, L.D. and Tanana, V.P. (1998). On convergence of applications in the regularization method and the Tikhonov regularization method of the n-th order. Inv. and Ill-posed Problems, 6, pp. 243-262.

Meyer, G. (1996). La radioactivité à l'ouvrage. *Clefs CEA*, 34, pp. 46-50.

Michalske, T. and Bunker, B. (1988). La fracture du verre. In *Pour la Science*, pp. 52-59.

Miles, J.P. (1971). Bifurcation in plastic flow under uniaxial tension. J. Mech. Phys. Solids., 19, pp. 89-102.

Moffatt, H.K. (1964). Viscous and resistive eddies near a sharp corner. J. Fluid Mech., 18, pp. 1-18.

Moussy, F. (1985). in Plastic Instability, Considère Symposium, Presses ENPC, Paris, pp. 263-272.

Muskhelishvili, N.I. (1977). *Some basic problems of the mathematical problems of elasticity*. Noordhoff Int. Publ. Leyden.

Nakada, Y. (1965). Heat measurements in crystals. Phil. Mag., 11, p. 10

Nakamura, G. and Uhlmann, G. (1995). Inverse problem at the boundary of an elastic medium, SIAM J. Math. Anal.,, 26, 2, pp. 263-279.

Natterer, F. (2001). Inversion of the attenuated Radon transform. Inverse Problems, 17, pp. 113-119.

Nedelec, J.C. (1982). Integral equations wwith non integrable kernels. In *Integral equations and operator theory*, 5, pp. 562-572.

Nemat-Nasser, S., Sumi, Y. and Keer, L.M. (1980). Unstable growth of tensile crack in brittle solids. Int. J. Solids & Struct., 16, p. 1017.

Nemat-Nasser, S. and Hori, M. (1999). Micromechanics:Overall properties of heteegeneous materials. North-Holland, Amsterdam.

Nilsson, F. (1973). A path-independent integral for transient crack problems. Int. J. Solids & Struct., 9, p. 1107.

Nguyen, K., Mai, Faye, C., Eglin, L.L. and Truong, T.T. (2001). Apparent image formation by Compton scattered photons in gamma ray imaging. IEEE Signal Process. Letters, 8, p. 248.

Nguyen, K., Mai and Truong, T.T. (2002). On an integral transform and its inverse in nuclear imaging. Inverse Problems, 18, p. 265.

Nguyen, K., Mai and Truong, T.T. (2002). Exact inversion of a compound conical Radon transform and a novel nuclear imaging principle. C.R. Acad. Sci. Paris, 335(I), p. 213.

Nguyen, K., Mai, Truong, T.T., Bui, H.D. and Delarbre, J.L. (2004). A novel inverse problem in gamma-rays emission imaging. *Inverse Problems in Sciences and Engineering*, 12 (2), pp. 225-246.

Nguyen, Q.S and Bui, H.D. (1974) Sur les matéraux à écrouissage positif ou négatif. J. Mecanique, 13(2), pp. 321-342.

Nguyen, Q.S (1977). On the elastic-plastic initial-boundary value problem and its numerical integration. Int. J. Num. Meth. Engng., 11, pp. 817-832.

Nguyen, Q.S. (1981). A thermodynamic description of the running crack. IUTAM Symp. on 3D constitutive equations and ductile fracture, Dourdan, North-Holland, p. 315.

Nguyen, Q.S, Stolz, C and Debruyne, G. (1990). Energy method in fracture mechanics: stability, bifurcation and second variations. Eur. J. Mech. A/Solids, 2, p. 157.

Nguyen, G. (1992). Validation d'Ultson 2/ Comparaison Calculs-Mesures. Technical Notes N° HI-72/805, Electricite de France.

Nguyen, Q.S. (2000). *Stability and non linear solid mechanics*. Wiley & Son, London.

Noether, E. (1918). Invariant variationsprobleme. Gott. Nach. Math. Phys., 2, p. 235.

Novikov, R.G. (2001). An inversion formula for the attenuated x-ray transformation. Ark. Math. 40, pp.147-167. (Rapport de Recherche 00/05-3. Université de Nantes. Laboratoire de Mathématiques).

Novikov, R.G. (2001). Une formule d'inversion pour la transformation d'un rayonnement X atténué. C.R. Acad. Sci. Paris, 332(I), p. 1059.

Otsuka, K. (1981). Generalized J-integral and 3D fracture mechanics. Hiroshima Math. J., 11, p. 25.

Pecastaings, F. (1985). On a method to evaluate edge effects in elastic plates. In *Local effects in the analysis of structures*. Ladeveze P. (Ed.). Elsevier Sciences Publ., pp. 101-126.

Petryk, H. (1985). On energy criteria of plastic instability. In *Plastic instability. Proc. Considère Memorial*, ENPC Paris, pp. 215-226.

Pham, T.L. (1967). Potentiels elastiques, tenseurs de Green et de Neumann. J. Meca., 6(2), p. 211.

Pineau, A. (1981). In *Advances in Fracture Mechanics*, D. Francois et al (Eds.), Pergamon Press, 2, p. 635.

Pineau, A. (1992). Global and local approaches of fracture. Transferability of laboratory test results to components. In *Topics in Fracture and Fatigue*, Argon A.S (Ed.) Springer-Verlag, New-York, Berlin, Heidelberg, London, Paris.

Pinna, Ch. and Doquet, V. (1999). The preferred fatigue crack propagation mode in a M250 maraging steel loaded in shear. Fatigue Fract. Eng. Mater. Struct., 23, pp. 173-183.

Pontryagin, L. (1959). *Optimal control of processes*. (In Russian), Uspekhi Math Nauk, 14 (1), pp. 3-20.

Pontryagin, L., Boltiansky, V.G., Gamkrilidze, R.V. and Mischenko, E.F. (1962). The mathematical theory of optimal processes. Interscience Publ. Wiley, New-York.

Prada, C. and Fink, M. (1994). Eigenmodes of the time reversal operator: a solution to selective focusing in multiple target media. Wave Motion, 20, pp. 151-163.

Ravi-Chandar, K. and Knauss, W.G. (1984). An experimental investigation into dynamic fracture: I. Crack initiation and arrest. Int. J. Fract., 25, 247-263.

Rvatchev, V.L. (1957). On the pressure of a wedge shaped punch on an elastic half space. Prikl. Math. Mekh., 23.

Rehbinder P. and Lichtman, V. (1957). Effect of surface active media on strain and rupture of solids. Proc. 2nd Int. Cong. Surf., Act., 3, p. 563.

Rice, J.R. (1968). Mathematical analysis in the Mechanics of Fracture; in *Fracture*, H. Liebowitz (Ed.), p. 191, Acad. Press.

Rice, J.R. and Rosengren, G.F. (1968). Plane strain deformation near a crack tip in a power law hardening material. J. Mech. Phys. Solids, 16, p. 1.

Rice, J.R. and Tracey, D.M. (1969). On ductile enlargement of voids in triaxial stress states. J. Mech. Phys. Solids, 17, p. 201.

Rittel, D, Maigre, M. and Bui, H.D. (1992). A new method for dynamic fracture toughhness testing. Scripta Metallurgica et Materiala, 26, p. 1593.

Rousselier, G. (1981). Finite deformation constitutive relations including ductile fracture damage. In *Three-dimensional constitutive relations and ductile fracture.* Nemat-Nasser S. (Ed.). North-Holland, Amsterdam, p. 331.

Rousselier, G. and Leclercq, S. (2005). A simplified "polycrystalline" model for viscoplastic and damage finite elements analyses. Int. J. Plasticity (in press).

Rudnicky, J. and Rice, J.R. (1980). Int. J. Solids & Struct., 16. pp. 597-605.

Sabatier, P.C. (1987). *Basic methods of tomography and inverse problems*. Malvern Phys. Ser. Adam Hilger, Bristol, Philadelphia.

Saka, M., Abe, K. and Tanaka, M. (1986). Computational Mechanics, 1, pp. 11-19.

Salençon, J. (1977). Applications of the theory of plasticity in soil mechanics. Wiley and Sons, Chischester, New York, Brisbane, Toronto.

Santacreu, P.O. (1994). Sur la singularité épine engendrée par une discontinuité plastique. C. R. Acad. Sciences Paris, 318(II), pp. 1577-1582.

Savitski, A. and Detournay, E. (2001). Similarity solution of a penny-shaped fluid-driven fracture in a zero toughness linear elastic-solid. C.R. Acad. Sci. Paris, IIb(329), pp. 255-262.

Schwartz, L. 1978. *Théorie des distributions*, Hermann, Paris.

Sedov, A. and Schmerr, J.L.W. (1986). The time domain elasto-dynamic Kirchhoff approximation for cracks: the inverse problems. Waves Motion, 8, p. 15.

Sharma, S.M. and Aravas, N. (1991). Determination of higher order terms in asymptotic elastoplastic crack tip solution. J. Mech. Phys. Solids, 39, pp. 1043-1072.

Shih, C.F. (1974). Small-scale yielding analysis of mixed mode plane-strain crack problem. In *Fracture analysis*. ASTM STP 560.

Shockley, D.A., Kalthoff, J.F., Klemm, W. and Winkler, S. (1983). Simultaneous measurement of stress intensity and toughness for fast-running cracks in steel. Experimental Mechanics, 23, pp. 140-145.

Sidoroff, F. (1976). Variables internes en visco-élasticité et visco-plasticité. Thèse Doct. D'Etat, Univ. Paris VI.

Sih, G.C. and Rice, J.R. (1964). J. Appl. Mech., 31. ASME, 86 E, p. 477.

Sih, G.C. (1973). Handbook of stress intensity factors. Lehigh University.

Silling, A. (1988). Numerical study of lost of ellipticity near singularities in elastic material. J. Elasticity, 19, p. 213.

Sneddon, I.N. (1969). Transform solutions of crack problems in the theory of elasticity. Z.A.M.M, 49, p. 15.

Solomon, L. and Zamfirescu, I. (1965). Some approximate formulae and solutions in the contact problem for punches with aplane bounded non-elliptical basis. In Applications Th. of functions in continuum mechanics. 1.

Stolz, C. (1987). Anélasticité et stabilité. Ph.D Thesis, Paris Univ.

Stolz, C. (1991). Sur les équations générales de la dynamique des milieux continus anélastiques. C. R. Acad. Sciences Paris, II, p. 307.

Stolz, C. (2004). *Energy methods in non-linear mechanics*. AMAS, Lecture Notes 11, IPPT, Warsaw.

Stupkiewicz, S. and Mroz Z. (1999). A model of third body abrasive friction and wear in hot metal forming. Wear, 231, pp. 124-138.

Suo, X.Z. and Combescure, A. (1989). Sur une formulation mathématique de la dérivée seconde de l'énergie potentielle en théorie de la rupture fragile. C. R. Acad. Sciences Paris, 308(II), p. 1119.

Suo, X.Z. and Combescure, A. (1992). Eur. J. Mech. A/Solids, 11(5) pp. 609-624.

Suquet, P. (1982). *Plasticité et homogénéisation*. Ph.D Thesis. University P. & M. Curie, Paris.

Tarantola, A. (1987). *Inverse problem theory*. Elsevier, England.

Theocaris, P.S. and Papadopoulos, G.A. (1984). The influence of geometry of edge-cracked plates on K_I and K_{II} components of the SIF, studied by caustics. J.Phys. D: Appl. Phys., 17, pp. 2339-2349.

Thompson, R.D. and Hancock J.M. (1984). Int. J. Fracture, 24, pp. 209-228.

Tikhonov, A. and Arsenine, V. (1977). *Méthode de résolution de problèmes mal posés*. Editions Mir, Moscou.

Tonti, E. (1975). On the formal structure of physical theories. Cooperative Library Instituto di Polytechnico di Milano, Milano.

Triantafyllidis, N. (1983). On the bifurcation and post-bifurcation analysis of elastic-plastic solids under general prebifurcation conditions. J. Mech. Phys. Solids, 31, pp. 499-510.

Truong, T.T., Mai K., Nguyen, Bui H.D., and Daveau, C. (2002). Determination of the electronic density in a medium by an inverse method based on double-Compton scattering in transmission imaging. *Inverse Problems in Engineering: Theory and Practice*, II, H.R.B. Orlande (Ed.) (E-paper), pp. 304-412.

Tvergaard, V. and Needleman, A. (1975). On the buckling of elastic-plastic columns with asymmetric cross-sections. Int. J. Mech. Sci., 17, pp. 419-424.

Vallée, M. (2003). Etude cinématique de la rupture sismique en champ lointain: méthodes et résolution. Thèse Doctorat, Université de Grenoble.

Van Dam, C.J., De Pater, C.J. and Romijn, R. (1999). Reopening of dynamic fractures in laboratory experiments. In Cong. Int. Mecanique des roches, Paris, August, 1999, II, pp. 792-994.

Vutukuri, V.S. (1974). The effect of liquids on the tensile strength of limestone. Int. J. Rock Mech. Min. Sci. & Geomech. Abstr., 11, pp. 27-29.

Wadier, Y. (1994). *Contraintes résiduelles et mécanique de la rupture. Eléments d'analyse*. Note HI-74-93-089, Electricité de France.

Waeckel, F., Dupas, Ph. and Genette, P. (1998) Parcourir l'histoire d'un composant ou la détermination des contraintes résiduelles de soudage. Epure, DER/Electricité de France, N° 60, Octobre 1998, pp. 97-104.

Weaver, J. (1977). Three-dimensional crack analysis. Int. J. Solids & Struct., 13(4), pp. 321-330.

Weichert, R. and Schönert, K. (1974). On the temperature rise at the tip of a fast running crack. J. Mech. Phys. Solids, 22, p. 127.

Williams, M.L. (1957). On the stress distribution at the base of a staionary crack. J. Appl. Mech., 24, pp. 111-114.

Willis, J.R. (1965). Dislocations and inclusions, J. Mech. Phys. Solids, 13, p. 377.

Willis, J.R. (1967). J. Mech. Phys. Solids, 15(3), p. 151.

Willis, J.R. (1991). On methods for bounding the overall properties of nonlinear composites. J. Mech. Phys. Solids, 39, pp. 73-86.

Wilson, W.K. and Yu., I.W. (1979). Int. J. Fracture, 15(4), p. 377.

Wu, C.H. (1978). J. Appl. Mech., 45, pp. 553-558.

Yao, Z. and Gong, B. (1994). Defect identification using boundary element method. In Inverse problems in engineering mechanics. H.D. Bui, et al (Eds.), pp. 387-392.

Yoffe, E.H. (1951). The moving Griffith crack. Phil. Mag., 42, p. 739.

Zazovskii, A.F. (1979). Growth of coin-shaped crack produced by hydraulic fracture in an impermeable rock. Izv, An SSSR. Mekhanika Tverdogo Tela, 14(2), pp. 103-109.

Zener, C. and Rosakis, A.J. (1989). Dynamic fracture initiation and propagation in 4340 steel under impact loading. Int. J. Fracture, p. 30.

Zhong, W.X. (1995). A new systematic methodology in elasticity theory. Dalian Science & Technology University Press.

Zwiers, R.I., Ting, T.C.T. and Spilker, R.L. (1982). On the log singularities. J.Appl. Mech., 49, p. 561

Index

Mechanics

SOLID MECHANICS AND ITS APPLICATIONS

Series Editor: G.M.L. Gladwell

Aims and Scope of the Series

The fundamental questions arising in mechanics are: *Why?*, *How?*, and *How much?* The aim of this series is to provide lucid accounts written by authoritative researchers giving vision and insight in answering these questions on the subject of mechanics as it relates to solids. The scope of the series covers the entire spectrum of solid mechanics. Thus it includes the foundation of mechanics; variational formulations; computational mechanics; statics, kinematics and dynamics of rigid and elastic bodies; vibrations of solids and structures; dynamical systems and chaos; the theories of elasticity, plasticity and viscoelasticity; composite materials; rods, beams, shells and membranes; structural control and stability; soils, rocks and geomechanics; fracture; tribology; experimental mechanics; biomechanics and machine design.

1. R.T. Haftka, Z. Gürdal and M.P. Kamat: *Elements of Structural Optimization*. 2nd rev.ed., 1990 ISBN 0-7923-0608-2
2. J.J. Kalker: *Three-Dimensional Elastic Bodies in Rolling Contact.* 1990 ISBN 0-7923-0712-7
3. P. Karasudhi: *Foundations of Solid Mechanics.* 1991 ISBN 0-7923-0772-0
4. *Not published*
5. *Not published.*
6. J.F. Doyle: *Static and Dynamic Analysis of Structures.* With an Emphasis on Mechanics and Computer Matrix Methods. 1991 ISBN 0-7923-1124-8; Pb 0-7923-1208-2
7. O.O. Ochoa and J.N. Reddy: *Finite Element Analysis of Composite Laminates.* ISBN 0-7923-1125-6
8. M.H. Aliabadi and D.P. Rooke: *Numerical Fracture Mechanics.* ISBN 0-7923-1175-2
9. J. Angeles and C.S. López-Cajún: *Optimization of Cam Mechanisms.* 1991 ISBN 0-7923-1355-0
10. D.E. Grierson, A. Franchi and P. Riva (eds.): *Progress in Structural Engineering.* 1991 ISBN 0-7923-1396-8
11. R.T. Haftka and Z. Gürdal: *Elements of Structural Optimization.* 3rd rev. and exp. ed. 1992 ISBN 0-7923-1504-9; Pb 0-7923-1505-7
12. J.R. Barber: *Elasticity*. 1992 ISBN 0-7923-1609-6; Pb 0-7923-1610-X
13. H.S. Tzou and G.L. Anderson (eds.): *Intelligent Structural Systems.* 1992 ISBN 0-7923-1920-6
14. E.E. Gdoutos: *Fracture Mechanics.* An Introduction. 1993 ISBN 0-7923-1932-X
15. J.P. Ward: *Solid Mechanics*. An Introduction. 1992 ISBN 0-7923-1949-4
16. M. Farshad: *Design and Analysis of Shell Structures*. 1992 ISBN 0-7923-1950-8
17. H.S. Tzou and T. Fukuda (eds.): *Precision Sensors, Actuators and Systems*. 1992 ISBN 0-7923-2015-8
18. J.R. Vinson: *The Behavior of Shells Composed of Isotropic and Composite Materials*. 1993 ISBN 0-7923-2113-8
19. H.S. Tzou: *Piezoelectric Shells*. Distributed Sensing and Control of Continua. 1993 ISBN 0-7923-2186-3
20. W. Schiehlen (ed.): *Advanced Multibody System Dynamics*. Simulation and Software Tools. 1993 ISBN 0-7923-2192-8
21. C.-W. Lee: *Vibration Analysis of Rotors.* 1993 ISBN 0-7923-2300-9
22. D.R. Smith: *An Introduction to Continuum Mechanics.* 1993 ISBN 0-7923-2454-4
23. G.M.L. Gladwell: *Inverse Problems in Scattering*. An Introduction. 1993 ISBN 0-7923-2478-1

Mechanics

SOLID MECHANICS AND ITS APPLICATIONS

Series Editor: G.M.L. Gladwell

24. G. Prathap: *The Finite Element Method in Structural Mechanics*. 1993 ISBN 0-7923-2492-7
25. J. Herskovits (ed.): *Advances in Structural Optimization.* 1995 ISBN 0-7923-2510-9
26. M.A. González-Palacios and J. Angeles: *Cam Synthesis.* 1993 ISBN 0-7923-2536-2
27. W.S. Hall: *The Boundary Element Method.* 1993 ISBN 0-7923-2580-X
28. J. Angeles, G. Hommel and P. Kovács (eds.): *Computational Kinematics.* 1993 ISBN 0-7923-2585-0
29. A. Curnier: *Computational Methods in Solid Mechanics*. 1994 ISBN 0-7923-2761-6
30. D.A. Hills and D. Nowell: *Mechanics of Fretting Fatigue*. 1994 ISBN 0-7923-2866-3
31. B. Tabarrok and F.P.J. Rimrott: *Variational Methods and Complementary Formulations in Dynamics.* 1994 ISBN 0-7923-2923-6
32. E.H. Dowell (ed.), E.F. Crawley, H.C. Curtiss Jr., D.A. Peters, R. H. Scanlan and F. Sisto: *A Modern Course in Aeroelasticity*. Third Revised and Enlarged Edition. 1995 ISBN 0-7923-2788-8; Pb: 0-7923-2789-6
33. A. Preumont: *Random Vibration and Spectral Analysis.* 1994 ISBN 0-7923-3036-6
34. J.N. Reddy (ed.): *Mechanics of Composite Materials*. Selected works of Nicholas J. Pagano. 1994 ISBN 0-7923-3041-2
35. A.P.S. Selvadurai (ed.): *Mechanics of Poroelastic Media*. 1996 ISBN 0-7923-3329-2
36. Z. Mróz, D. Weichert, S. Dorosz (eds.): *Inelastic Behaviour of Structures under Variable Loads*. 1995 ISBN 0-7923-3397-7
37. R. Pyrz (ed.): *IUTAM Symposium on Microstructure-Property Interactions in Composite Materials.* Proceedings of the IUTAM Symposium held in Aalborg, Denmark. 1995 ISBN 0-7923-3427-2
38. M.I. Friswell and J.E. Mottershead: *Finite Element Model Updating in Structural Dynamics*. 1995 ISBN 0-7923-3431-0
39. D.F. Parker and A.H. England (eds.): *IUTAM Symposium on Anisotropy, Inhomogeneity and Nonlinearity in Solid Mechanics.* Proceedings of the IUTAM Symposium held in Nottingham, U.K. 1995 ISBN 0-7923-3594-5
40. J.-P. Merlet and B. Ravani (eds.): *Computational Kinematics '95*. 1995 ISBN 0-7923-3673-9
41. L.P. Lebedev, I.I. Vorovich and G.M.L. Gladwell: *Functional Analysis.* Applications in Mechanics and Inverse Problems. 1996 ISBN 0-7923-3849-9
42. J. Menčik: *Mechanics of Components with Treated or Coated Surfaces.* 1996 ISBN 0-7923-3700-X
43. D. Bestle and W. Schiehlen (eds.): *IUTAM Symposium on Optimization of Mechanical Systems.* Proceedings of the IUTAM Symposium held in Stuttgart, Germany. 1996 ISBN 0-7923-3830-8
44. D.A. Hills, P.A. Kelly, D.N. Dai and A.M. Korsunsky: *Solution of Crack Problems*. The Distributed Dislocation Technique. 1996 ISBN 0-7923-3848-0
45. V.A. Squire, R.J. Hosking, A.D. Kerr and P.J. Langhorne: *Moving Loads on Ice Plates*. 1996 ISBN 0-7923-3953-3
46. A. Pineau and A. Zaoui (eds.): *IUTAM Symposium on Micromechanics of Plasticity and Damage of Multiphase Materials*. Proceedings of the IUTAM Symposium held in Sèvres, Paris, France. 1996 ISBN 0-7923-4188-0
47. A. Naess and S. Krenk (eds.): *IUTAM Symposium on Advances in Nonlinear Stochastic Mechanics*. Proceedings of the IUTAM Symposium held in Trondheim, Norway. 1996 ISBN 0-7923-4193-7
48. D. Ieşan and A. Scalia: *Thermoelastic Deformations.* 1996 ISBN 0-7923-4230-5

Mechanics

SOLID MECHANICS AND ITS APPLICATIONS

Series Editor: G.M.L. Gladwell

49. J.R. Willis (ed.): *IUTAM Symposium on Nonlinear Analysis of Fracture*. Proceedings of the IUTAM Symposium held in Cambridge, U.K. 1997 ISBN 0-7923-4378-6
50. A. Preumont: *Vibration Control of Active Structures*. An Introduction. 1997 ISBN 0-7923-4392-1
51. G.P. Cherepanov: *Methods of Fracture Mechanics: Solid Matter Physics*. 1997 ISBN 0-7923-4408-1
52. D.H. van Campen (ed.): *IUTAM Symposium on Interaction between Dynamics and Control in Advanced Mechanical Systems.* Proceedings of the IUTAM Symposium held in Eindhoven, The Netherlands. 1997 ISBN 0-7923-4429-4
53. N.A. Fleck and A.C.F. Cocks (eds.): *IUTAM Symposium on Mechanics of Granular and Porous Materials.* Proceedings of the IUTAM Symposium held in Cambridge, U.K. 1997 ISBN 0-7923-4553-3
54. J. Roorda and N.K. Srivastava (eds.): *Trends in Structural Mechanics*. Theory, Practice, Education. 1997 ISBN 0-7923-4603-3
55. Yu.A. Mitropolskii and N. Van Dao: *Applied Asymptotic Methods in Nonlinear Oscillations*. 1997 ISBN 0-7923-4605-X
56. C. Guedes Soares (ed.): *Probabilistic Methods for Structural Design.* 1997 ISBN 0-7923-4670-X
57. D. François, A. Pineau and A. Zaoui: *Mechanical Behaviour of Materials.* Volume I: Elasticity and Plasticity. 1998 ISBN 0-7923-4894-X
58. D. François, A. Pineau and A. Zaoui: *Mechanical Behaviour of Materials.* Volume II: Viscoplasticity, Damage, Fracture and Contact Mechanics. 1998 ISBN 0-7923-4895-8
59. L.T. Tenek and J. Argyris: *Finite Element Analysis for Composite Structures.* 1998 ISBN 0-7923-4899-0
60. Y.A. Bahei-El-Din and G.J. Dvorak (eds.): *IUTAM Symposium on Transformation Problems in Composite and Active Materials*. Proceedings of the IUTAM Symposium held in Cairo, Egypt. 1998 ISBN 0-7923-5122-3
61. I.G. Goryacheva: *Contact Mechanics in Tribology*. 1998 ISBN 0-7923-5257-2
62. O.T. Bruhns and E. Stein (eds.): *IUTAM Symposium on Micro- and Macrostructural Aspects of Thermoplasticity*. Proceedings of the IUTAM Symposium held in Bochum, Germany. 1999 ISBN 0-7923-5265-3
63. F.C. Moon: *IUTAM Symposium on New Applications of Nonlinear and Chaotic Dynamics in Mechanics*. Proceedings of the IUTAM Symposium held in Ithaca, NY, USA. 1998 ISBN 0-7923-5276-9
64. R. Wang: *IUTAM Symposium on Rheology of Bodies with Defects*. Proceedings of the IUTAM Symposium held in Beijing, China. 1999 ISBN 0-7923-5297-1
65. Yu.I. Dimitrienko: *Thermomechanics of Composites under High Temperatures*. 1999 ISBN 0-7923-4899-0
66. P. Argoul, M. Frémond and Q.S. Nguyen (eds.): *IUTAM Symposium on Variations of Domains and Free-Boundary Problems in Solid Mechanics*. Proceedings of the IUTAM Symposium held in Paris, France. 1999 ISBN 0-7923-5450-8
67. F.J. Fahy and W.G. Price (eds.): *IUTAM Symposium on Statistical Energy Analysis*. Proceedings of the IUTAM Symposium held in Southampton, U.K. 1999 ISBN 0-7923-5457-5
68. H.A. Mang and F.G. Rammerstorfer (eds.): *IUTAM Symposium on Discretization Methods in Structural Mechanics.* Proceedings of the IUTAM Symposium held in Vienna, Austria. 1999 ISBN 0-7923-5591-1

Mechanics

SOLID MECHANICS AND ITS APPLICATIONS

Series Editor: G.M.L. Gladwell

69. P. Pedersen and M.P. Bendsøe (eds.): *IUTAM Symposium on Synthesis in Bio Solid Mechanics*. Proceedings of the IUTAM Symposium held in Copenhagen, Denmark. 1999 ISBN 0-7923-5615-2
70. S.K. Agrawal and B.C. Fabien: *Optimization of Dynamic Systems*. 1999 ISBN 0-7923-5681-0
71. A. Carpinteri: *Nonlinear Crack Models for Nonmetallic Materials*. 1999 ISBN 0-7923-5750-7
72. F. Pfeifer (ed.): *IUTAM Symposium on Unilateral Multibody Contacts*. Proceedings of the IUTAM Symposium held in Munich, Germany. 1999 ISBN 0-7923-6030-3
73. E. Lavendelis and M. Zakrzhevsky (eds.): *IUTAM/IFToMM Symposium on Synthesis of Non-linear Dynamical Systems*. Proceedings of the IUTAM/IFToMM Symposium held in Riga, Latvia. 2000 ISBN 0-7923-6106-7
74. J.-P. Merlet: *Parallel Robots*. 2000 ISBN 0-7923-6308-6
75. J.T. Pindera: *Techniques of Tomographic Isodyne Stress Analysis.* 2000 ISBN 0-7923-6388-4
76. G.A. Maugin, R. Drouot and F. Sidoroff (eds.): *Continuum Thermomechanics.* The Art and Science of Modelling Material Behaviour. 2000 ISBN 0-7923-6407-4
77. N. Van Dao and E.J. Kreuzer (eds.): *IUTAM Symposium on Recent Developments in Non-linear Oscillations of Mechanical Systems*. 2000 ISBN 0-7923-6470-8
78. S.D. Akbarov and A.N. Guz: *Mechanics of Curved Composites*. 2000 ISBN 0-7923-6477-5
79. M.B. Rubin: *Cosserat Theories: Shells, Rods and Points*. 2000 ISBN 0-7923-6489-9
80. S. Pellegrino and S.D. Guest (eds.): *IUTAM-IASS Symposium on Deployable Structures: Theory and Applications.* Proceedings of the IUTAM-IASS Symposium held in Cambridge, U.K., 6–9 September 1998. 2000 ISBN 0-7923-6516-X
81. A.D. Rosato and D.L. Blackmore (eds.): *IUTAM Symposium on Segregation in Granular Flows.* Proceedings of the IUTAM Symposium held in Cape May, NJ, U.S.A., June 5–10, 1999. 2000 ISBN 0-7923-6547-X
82. A. Lagarde (ed.): *IUTAM Symposium on Advanced Optical Methods and Applications in Solid Mechanics*. Proceedings of the IUTAM Symposium held in Futuroscope, Poitiers, France, August 31–September 4, 1998. 2000 ISBN 0-7923-6604-2
83. D. Weichert and G. Maier (eds.): *Inelastic Analysis of Structures under Variable Loads*. Theory and Engineering Applications. 2000 ISBN 0-7923-6645-X
84. T.-J. Chuang and J.W. Rudnicki (eds.): *Multiscale Deformation and Fracture in Materials and Structures*. The James R. Rice 60th Anniversary Volume. 2001 ISBN 0-7923-6718-9
85. S. Narayanan and R.N. Iyengar (eds.): *IUTAM Symposium on Nonlinearity and Stochastic Structural Dynamics.* Proceedings of the IUTAM Symposium held in Madras, Chennai, India, 4–8 January 1999 ISBN 0-7923-6733-2
86. S. Murakami and N. Ohno (eds.): *IUTAM Symposium on Creep in Structures*. Proceedings of the IUTAM Symposium held in Nagoya, Japan, 3-7 April 2000. 2001 ISBN 0-7923-6737-5
87. W. Ehlers (ed.): *IUTAM Symposium on Theoretical and Numerical Methods in Continuum Mechanics of Porous Materials.* Proceedings of the IUTAM Symposium held at the University of Stuttgart, Germany, September 5-10, 1999. 2001 ISBN 0-7923-6766-9
88. D. Durban, D. Givoli and J.G. Simmonds (eds.): *Advances in the Mechanis of Plates and Shells The Avinoam Libai Anniversary Volume*. 2001 ISBN 0-7923-6785-5
89. U. Gabbert and H.-S. Tzou (eds.): *IUTAM Symposium on Smart Structures and Structonic Systems*. Proceedings of the IUTAM Symposium held in Magdeburg, Germany, 26–29 September 2000. 2001 ISBN 0-7923-6968-8

Mechanics

SOLID MECHANICS AND ITS APPLICATIONS

Series Editor: G.M.L. Gladwell

90. Y. Ivanov, V. Cheshkov and M. Natova: *Polymer Composite Materials – Interface Phenomena & Processes*. 2001 ISBN 0-7923-7008-2
91. R.C. McPhedran, L.C. Botten and N.A. Nicorovici (eds.): *IUTAM Symposium on Mechanical and Electromagnetic Waves in Structured Media*. Proceedings of the IUTAM Symposium held in Sydney, NSW, Australia, 18-22 Januari 1999. 2001 ISBN 0-7923-7038-4
92. D.A. Sotiropoulos (ed.): *IUTAM Symposium on Mechanical Waves for Composite Structures Characterization*. Proceedings of the IUTAM Symposium held in Chania, Crete, Greece, June 14-17, 2000. 2001 ISBN 0-7923-7164-X
93. V.M. Alexandrov and D.A. Pozharskii: *Three-Dimensional Contact Problems*. 2001 ISBN 0-7923-7165-8
94. J.P. Dempsey and H.H. Shen (eds.): *IUTAM Symposium on Scaling Laws in Ice Mechanics and Ice Dynamics*. Proceedings of the IUTAM Symposium held in Fairbanks, Alaska, U.S.A., 13-16 June 2000. 2001 ISBN 1-4020-0171-1
95. U. Kirsch: *Design-Oriented Analysis of Structures*. A Unified Approach. 2002 ISBN 1-4020-0443-5
96. A. Preumont: *Vibration Control of Active Structures*. An Introduction (2^{nd} Edition). 2002 ISBN 1-4020-0496-6
97. B.L. Karihaloo (ed.): *IUTAM Symposium on Analytical and Computational Fracture Mechanics of Non-Homogeneous Materials.* Proceedings of the IUTAM Symposium held in Cardiff, U.K., 18-22 June 2001. 2002 ISBN 1-4020-0510-5
98. S.M. Han and H. Benaroya: *Nonlinear and Stochastic Dynamics of Compliant Offshore Structures*. 2002 ISBN 1-4020-0573-3
99. A.M. Linkov: *Boundary Integral Equations in Elasticity Theory*. 2002 ISBN 1-4020-0574-1
100. L.P. Lebedev, I.I. Vorovich and G.M.L. Gladwell: *Functional Analysis.* Applications in Mechanics and Inverse Problems (2^{nd} Edition). 2002 ISBN 1-4020-0667-5; Pb: 1-4020-0756-6
101. Q.P. Sun (ed.): *IUTAM Symposium on Mechanics of Martensitic Phase Transformation in Solids*. Proceedings of the IUTAM Symposium held in Hong Kong, China, 11-15 June 2001. 2002 ISBN 1-4020-0741-8
102. M.L. Munjal (ed.): *IUTAM Symposium on Designing for Quietness*. Proceedings of the IUTAM Symposium held in Bangkok, India, 12-14 December 2000. 2002 ISBN 1-4020-0765-5
103. J.A.C. Martins and M.D.P. Monteiro Marques (eds.): *Contact Mechanics*. Proceedings of the 3^{rd} Contact Mechanics International Symposium, Praia da Consolação, Peniche, Portugal, 17-21 June 2001. 2002 ISBN 1-4020-0811-2
104. H.R. Drew and S. Pellegrino (eds.): *New Approaches to Structural Mechanics, Shells and Biological Structures*. 2002 ISBN 1-4020-0862-7
105. J.R. Vinson and R.L. Sierakowski: *The Behavior of Structures Composed of Composite Materials*. Second Edition. 2002 ISBN 1-4020-0904-6
106. Not yet published.
107. J.R. Barber: *Elasticity*. Second Edition. 2002 ISBN Hb 1-4020-0964-X; Pb 1-4020-0966-6
108. C. Miehe (ed.): *IUTAM Symposium on Computational Mechanics of Solid Materials at Large Strains*. Proceedings of the IUTAM Symposium held in Stuttgart, Germany, 20-24 August 2001. 2003 ISBN 1-4020-1170-9

Mechanics

SOLID MECHANICS AND ITS APPLICATIONS

Series Editor: G.M.L. Gladwell

109. P. Ståhle and K.G. Sundin (eds.): *IUTAM Symposium on Field Analyses for Determination of Material Parameters – Experimental and Numerical Aspects.* Proceedings of the IUTAM Symposium held in Abisko National Park, Kiruna, Sweden, July 31 – August 4, 2000. 2003 ISBN 1-4020-1283-7
110. N. Sri Namachchivaya and Y.K. Lin (eds.): *IUTAM Symposium on Nonlinear Stochastic Dynamics.* Proceedings of the IUTAM Symposium held in Monticello, IL, USA, 26 – 30 August, 2000. 2003 ISBN 1-4020-1471-6
111. H. Sobieckzky (ed.): *IUTAM Symposium Transsonicum IV*. Proceedings of the IUTAM Symposium held in Göttingen, Germany, 2–6 September 2002, 2003 ISBN 1-4020-1608-5
112. J.-C. Samin and P. Fisette: *Symbolic Modeling of Multibody Systems*. 2003 ISBN 1-4020-1629-8
113. A.B. Movchan (ed.): *IUTAM Symposium on Asymptotics, Singularities and Homogenisation in Problems of Mechanics.* Proceedings of the IUTAM Symposium held in Liverpool, United Kingdom, 8-11 July 2002. 2003 ISBN 1-4020-1780-4
114. S. Ahzi, M. Cherkaoui, M.A. Khaleel, H.M. Zbib, M.A. Zikry and B. LaMatina (eds.): *IUTAM Symposium on Multiscale Modeling and Characterization of Elastic-Inelastic Behavior of Engineering Materials.* Proceedings of the IUTAM Symposium held in Marrakech, Morocco, 20-25 October 2002. 2004 ISBN 1-4020-1861-4
115. H. Kitagawa and Y. Shibutani (eds.): *IUTAM Symposium on Mesoscopic Dynamics of Fracture Process and Materials Strength.* Proceedings of the IUTAM Symposium held in Osaka, Japan, 6-11 July 2003. Volume in celebration of Professor Kitagawa's retirement. 2004 ISBN 1-4020-2037-6
116. E.H. Dowell, R.L. Clark, D. Cox, H.C. Curtiss, Jr., K.C. Hall, D.A. Peters, R.H. Scanlan, E. Simiu, F. Sisto and D. Tang: *A Modern Course in Aeroelasticity*. 4th Edition, 2004 ISBN 1-4020-2039-2
117. T. Burczyński and A. Osyczka (eds.): *IUTAM Symposium on Evolutionary Methods in Mechanics.* Proceedings of the IUTAM Symposium held in Cracow, Poland, 24-27 September 2002. 2004 ISBN 1-4020-2266-2
118. D. Ieşan: *Thermoelastic Models of Continua*. 2004 ISBN 1-4020-2309-X
119. G.M.L. Gladwell: *Inverse Problems in Vibration*. Second Edition. 2004 ISBN 1-4020-2670-6
120. J.R. Vinson: *Plate and Panel Structures of Isotropic, Composite and Piezoelectric Materials, Including Sandwich Construction*. 2005 ISBN 1-4020-3110-6
121. *Forthcoming*
122. G. Rega and F. Vestroni (eds.): *IUTAM Symposium on Chaotic Dynamics and Control of Systems and Processes in Mechanics*. Proceedings of the IUTAM Symposium held in Rome, Italy, 8–13 June 2003. 2005 ISBN 1-4020-3267-6
123. E.E. Gdoutos: *Fracture Mechanics. An Introduction. 2nd edition.* 2005 ISBN 1-4020-3267-6
124. M.D. Gilchrist (ed.): *IUTAM Symposium on Impact Biomechanics from Fundamental Insights to Applications*. 2005 ISBN 1-4020-3795-3
125. J.M. Huyghe, P.A.C. Raats and S. C. Cowin (eds.): *IUTAM Symposium on Physicochemical and Electromechanical Interactions in Porous Media*. 2005 ISBN 1-4020-3864-X
126. H. Ding, W. Chen and L. Zhang: *Elasticity of Transversely Isotropic Materials*. 2005 ISBN 1-4020-4033-4
127. W. Yang (ed): *IUTAM Symposium on Mechanics and Reliability of Actuating Materials.* Proceedings of the IUTAM Symposium held in Beijing, China, 1–3 September 2004. 2005 ISBN 1-4020-4131-6

Mechanics

SOLID MECHANICS AND ITS APPLICATIONS

Series Editor: G.M.L. Gladwell

128. J.-P. Merlet: *Parallel Robots.* 2006 ISBN 1-4020-4132-2
129. G.E.A. Meier and K.R. Sreenivasan (eds.): *IUTAM Symposium on One Hundred Years of Boundary Layer Research.* Proceedings of the IUTAM Symposium held at DLR-Göttingen, Germany, August 12–14, 2004. 2006 ISBN 1-4020-4149-7
130. H. Ulbrich and W. Günthner (eds.): *IUTAM Symposium on Vibration Control of Nonlinear Mechanisms and Structures.* 2006 ISBN 1-4020-4160-8
131. L. Librescu and O. Song: *Thin-Walled Composite Beams.* Theory and Application. 2006 ISBN 1-4020-3457-1
132. G. Ben-Dor, A. Dubinsky and T. Elperin: *Applied High-Speed Plate Penetration Dynamics*. 2006 ISBN 1-4020-3452-0
133. X. Markenscoff and A. Gupta (eds.): *Collected Works of J. D. Eshelby*. Mechanics and Defects and Heterogeneities. 2006 ISBN 1-4020-4416-X
134. R.W. Snidle and H.P. Evans (eds.): *IUTAM Symposium on Elastohydrodynamics and Microelastohydrodynamics*. Proceedings of the IUTAM Symposium held in Cardiff, UK, 1–3 September, 2004. 2006 ISBN 1-4020-4532-8
135. T. Sadowski (ed.): *IUTAM Symposium on Multiscale Modelling of Damage and Fracture Processes in Composite Materials*. Proceedings of the IUTAM Symposium held in Kazimierz Dolny, Poland, 23–27 May 2005. 2006 ISBN 1-4020-4565-4
136. A. Preumont: *Mechatronics*. Dynamics of Electromechanical and Piezoelectric Systems. 2006 ISBN 1-4020-4695-2
137. M.P. Bendsøe, N. Olhoff and O. Sigmund (eds.): *IUTAM Symposium on Topological Design Optimization of Structures, Machines and Materials*. Status and Perspectives. 2006 ISBN 1-4020-4729-0
138. A. Klarbring: *Models of Mechanics*. 2006 ISBN 1-4020-4834-3
139. H.D. Bui: *Fracture Mechanics*. Inverse Problems and Solutions. 2006 ISBN 1-4020-4836-X
140. M. Pandey, W.-C. Xie and L. Xu (eds.): *Advances in Engineering Structures, Mechanics and Construction*. Proceedings of an International Conference on Advances in Engineering Structures, Mechanics & Construction, held in Waterloo, Ontario, Canada, May 14–17, 2006. 2006 ISBN 1-4020-4890-4
141. G.Q. Zhang, W.D. van Driel and X. J. Fan: *Mechanics of Microelectronics*. 2006 ISBN 1-4020-4934-X
142. Q.P. Sun and P. Tong (eds.): *IUTAM Symposium on Size Effects on Material and Structural Behavior at Micron- and Nano-Scales*. Proceedings of the IUTAM Symposium held in Hong Kong, China, 31 May–4 June, 2004. 2006 ISBN 1-4020-4945-5